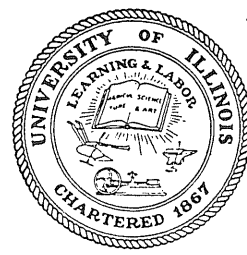


10
I 29A
No. 161

Copy 2

Fast Lab - Ship File



CIVIL ENGINEERING STUDIES

STRUCTURAL RESEARCH SERIES NO. 161

Matz Reference Room
Department of Civil Engineering
University of Illinois
Urbana, Illinois 61801

THE ENGINEERING BEHAVIOR OF STRUCTURAL METALS UNDER SLOW AND RAPID LOADING

By
J. M. MASSARD
and
R. A. COLLINS

Approved by
N. M. NEWMARK

Final Technical Report
to
OFFICE OF NAVAL RESEARCH
DEPARTMENT OF THE NAVY
Contract Nonr 1834(01)
Project NR-064-419

Matz Reference Room
Department of Civil Engineering
University of Illinois
Urbana, Illinois 61801

DEPARTMENT OF CIVIL ENGINEERING
UNIVERSITY OF ILLINOIS
URBANA, ILLINOIS
June 1958

THE ENGINEERING BEHAVIOR OF STRUCTURAL METALS
UNDER SLOW AND RAPID LOADING

by

J. M. Massard and R. A. Collins

Approved by

N. M. Newmark

Final Technical Report

to

Office of Naval Research
Contract Nonr-1834(01)
Project NR-064-419

Department of Civil Engineering
University of Illinois
Urbana, Illinois
October 1958

ABSTRACT

The purpose of this report is to describe an experimental investigation concerned with the behavior of a few structural metals under a range of stress conditions applied in times that correspond to the responses which might be excited in ship structures by underwater explosion or air blast loading, or in building structures by earthquake shock or the explosion of a large scale weapon. The engineering aspects of material behavior are emphasized.

The tests included uniaxial stress applied in either tension or compression, and flexural stress produced by third-point loading of small beams of rectangular section. The rise times of the loadings were varied from a few milliseconds to several minutes. An attempt is made to correlate the results obtained in the uniaxial stress tests with those obtained in flexure.

The applicability of the results of this investigation to the general problem of determining the behavior of structures under transient dynamic loadings producing extensive inelastic deformations is discussed briefly.

ACKNOWLEDGMENT

The investigation described in this report was performed by staff members of the University of Illinois in cooperation with the Office of Naval Research under Contract Nonr-1834(01), Project NR-064-419. The work was conducted in the Structural Research Laboratory of the Department of Civil Engineering under the general direction of Professor N. M. Newmark, Head of the Department. The project was under the supervision of Dr. J. M. Massard, Research Assistant Professor of Civil Engineering. The latter part of the work was the direct responsibility of R. A. Collins, Research Assistant in Civil Engineering. The instrumentation used throughout the investigation was, in general, the responsibility of V. J. McDonald, Research Associate Professor of Civil Engineering.

The initial development of the basic testing apparatus and the preliminary testing was done by Dr. Massard prior to the beginning of Contract Nonr-1834(01). For completeness, some of the results of other preliminary studies which predate the contract are included in this report. These were investigations described in Master's Theses submitted to the Graduate College of the University of Illinois by L. B. Smith and J. W. Storm. This early work was supported in part by funds obtained from the Bureau of Ships, Department of the Navy under Contract NObs 62250.

THE ENGINEERING BEHAVIOR OF STRUCTURAL METALS
UNDER SLOW AND RAPID LOADING

TABLE OF CONTENTS

	<u>Page</u>
ABSTRACT	ii
ACKNOWLEDGMENT	iii
LIST OF TABLES	vii
LIST OF FIGURES.	viii
1. GENERAL INTRODUCTION	1
1.1 Introduction.	1
1.2 Scope	2
2. RAPID LOADING AND STRAINING EQUIPMENT.	4
2.1 Introduction.	4
2.2 Description of Rapid Loading Apparatus.	4
2.3 Control of Loading Pulse.	5
2.4 Past Usage in Testing	6
2.5 Description of Slow Straining Unit.	6
2.6 Summary	6
3. UNIAXIAL STRESS TESTS.	8
3.1 Introduction.	8
3.2 Description of Testing Series	9
3.2.1 Types of Specimens	9
3.2.2 Manufacture of Specimens	10
3.2.3 Metallurgical Properties and Chemical Compositions	11

TABLE OF CONTENTS (Continued)

	<u>Page</u>
3.3 Description of Testing Procedures	12
3.3.1 Instrumentation.	12
3.3.2 Slow Tests	15
3.3.3 Machine Vibration Tests.	16
3.3.4 Residual Microstrain Determination	16
3.3.5 Rapid Tests.	17
3.3.6 Effective Gage Length.	19
3.4 Results of Uniaxial Tests	20
3.4.1 General Time Sensitive Behavior of the Various Metals Tested.	20
3.4.2 Results of Tension and Compression Tests	22
3.4.3 Results of Preliminary Reversed Stress Tests	23
3.5 Summary of Results for Uniaxial Stress Tests.	25
3.5.1 Summary of Results	25
3.5.2 General Significance of Results.	26
4. FLEXURE TESTS.	28
4.1 Introduction.	28
4.2 Description of Testing Series	28
4.2.1 Description of Specimens	28
4.2.2 Material Properties Under Uniaxial Stress.	29
4.3 Description of Testing Procedures	29
4.3.1 Testing Arrangement.	29
4.3.2 Instrumentation.	30
4.3.3 Description of Flexure Tests	31

TABLE OF CONTENTS (Continued)

	<u>Page</u>
4.4 Results of Flexure Tests.	32
4.4.1 Experimental Results	32
4.4.2 Correlation Study.	35
4.5 Summary of Results of Flexure Tests	37
4.5.1 Summary of Results	37
4.5.2 Significance of Results.	38
5. GENERAL SUMMARY.	39
5.1 General Summary	39
BIBLIOGRAPHY	41
APPENDIX -- DETERMINATION OF FLEXURAL RESISTANCE FROM BEAM DEFORMATION AND UNIAXIAL STRESS PROPERTIES	44

LIST OF TABLES

1. Summary of Uniaxial Testing Program
2. Uniaxial Specimen Designation Code
3. Results of Metallurgical Studies
4. Chemical Compositions of Specimen Steels
5. Summary of Uniaxial Stress Tests and Results

LIST OF FIGURES

1. Pressure Panel, and 20-Kip Pulse Loading Unit Arranged for Testing Uniaxial Tension Specimens
2. Schematic Representation of 20-Kip Pulse Loading Apparatus
3. 20-Kip Pulse Loading Unit
4. Some Loading Pulses that Can Be Produced
5. Pulse Loading Unit Being Used to Test Model Frame
6. 60-Kip Pulse Loading Unit in Frame for Testing Beam-Columns
7. 20-Kip Pulse Loading Unit and 20-Kip Straining Unit Connected in Series for Testing Tension-Compression Specimens: Shown with Pressure Control Panels
8. Schematic Representation of 20-Kip Straining Apparatus
9. Dimensions of Tensile Specimens
10. Connection of Tensile Specimen in Pulse Loading Machine
11. Dimensions of Specimens from Sheet Stock
12. Dimensions of Preliminary Tension-Compression Specimens
13. Dimensions of Tension-Compression Specimen and Manner of Connection
14. Metallographs of Specimen Materials
15. CRO Instruments, Pressure Panel, and Pulse Loading Unit Arranged for Testing Preliminary Tension-Compression Specimens
16. Hathaway Oscillographs and Associated Apparatus
17. Representative Oscillograms from Uniaxial Stress Tests
18. Slowly Cycled Stress-Residual Strain
19. Effective Gage Length -- Elongation
20. Representative Stress-Strain-Time Relation for Mild Steel
21. Stress-Strain and Strain-Time Relationships for Various Materials Tested in Tension and Compression

LIST OF FIGURES (Continued)

22. Upper Yield Stress-Elapsed Time to General Yielding
23. Upper Yield Stress Parameter-Elapsed Time to General Yielding
24. Upper Yield Stress Parameter-Elapsed Time to General Yielding (Various Rise Times of Load)
25. Lower Yield Stress-Rate of General Yielding
26. Lower Yield Stress Parameter-Rate of General Yielding
27. Upper Yield Stress Parameter-Secant Modulus
28. Nominal Stress-Elongation; Slow Loading with Reversal
29. Elongation-Time; Rapid Loading with Reversal
30. Stress-Elongation and Elongation-Time; Rapid Reversal from Static Stress
31. Over-all View of Flexural Testing Equipment
32. Arrangement for Testing Small Beams with Third Point Loading
33. View of Pure Flexure Region Instrumented
34. Instrumentation and Dimensions of Flexural Specimens
35. Deflection Gage Circuits
36. Stress-Strain, Delay Time, and Rate of General Yielding Data for Flexural Specimen Material
37. Recorded Data; BF Series
38. Recorded Data; BK Series
39. Recorded Data; BL Series
40. Moment-Curvature Relationships; BF Series
41. Moment-Curvature Relationships; BK Series
42. Moment-Curvature Relationships; BL Series
43. Assumed Moment-Curvature Relationships

LIST OF FIGURES

APPENDIXDETERMINATION OF FLEXURAL RESISTANCE FROM BEAM
DEFORMATION AND UNIAXIAL STRESS PROPERTIES

- A1. Typical Rapid Uniaxial Stress Test;
Applied Stress, Resulting Strain
- A2. Delayed Yielding and Rate of General Yielding Relationships
from Uniaxial Stress Tests of Beam Materials
- A3. Determination of Flexural Resistance from Beam Deformation
and Uniaxial Stress Properties

THE ENGINEERING BEHAVIOR OF STRUCTURAL METALS UNDER SLOW AND RAPID LOADING

1. GENERAL INTRODUCTION

1.1 Introduction

The purpose of the investigation which was conducted at the University of Illinois under Contract Nonr-1834(01) was to determine the time sensitive stress-deformation characteristics of the more commonly used structural metals, and the engineering significance of this information in the solution of problems concerned with the behavior of metal structures under transient dynamic loads producing extensive inelastic deformations.

The work which was done on the project can be divided arbitrarily into three related parts: (1) The testing of structural metals under uniaxial stress conditions which are produced slowly or rapidly, (2) the correlation of these behaviors with the ones obtained under conditions of slowly or rapidly applied flexural stress, (3) the development of the special testing apparatus required for the experimental work. These phases also form the major divisions of this report.

In the first part of the report is discussed the basic apparatus developed at the University of Illinois for use in the application of slow to rapid loads to uniaxially stressed coupons, small beams, or model frames. Since special fixtures and instrumentation were necessary for each type of test, only the basic apparatus will be discussed in this section. The details of the fixtures and instrumentation will be described in the other sections of the report which pertain to the actual testing programs; these are Sections 2 and 3 which describe respectively the uniaxial stress studies and the flexural stress studies.

The investigations conducted at the University of Illinois as a part of Contract Nonr-1834(01) were concerned with the engineering aspects of the behavior of the materials and structural elements under conditions of slow and rapid stressing. The metallurgical and fundamental physical nature of the deformation process was beyond the scope of this project. However, an attempt was made to classify the materials which were tested by evaluating and recording the metallurgical natures and the chemical compositions involved.

1.2 Scope

In the investigation described in this report small specimens of several sizes, shapes, and materials were tested at room temperature under stress conditions which for some steels included uniaxial tension, uniaxial compression, and flexure. These "stressings" were applied with a specially constructed machine that permitted independent control of the "rise" time of the loading, the maximum load, duration of the load, and the time of load decay. (This machine was designed not only for this investigation, but for general use as a pulse loading unit capable of applying a controlled load of 20,000 lb maximum to small structural elements in times as short as 0.005 seconds.)

In most of the tests, the loads were held at constant levels after application until the yielding process had been completed. The main variables of the experimental investigations were:

Uniaxial Tension

1. Rise time of load (0.005 second minimum to approximately 100 seconds.)
2. Maximum stress level
3. The type of steel (semi-killed, rimmed, low-alloy)

Uniaxial Compression-Tension

4. Manner of loading (tension, compression, and reverse loadings)

Some secondary variables of the uniaxial tests were:

- a. Manner of treatment (as-rolled, annealed before machining, annealed after machining.)
- b. Surface finish (as-machined, polished, notched)

Flexure

5. Level of maximum load

Using oscillographs and associated instrumentation having adequate response characteristics, records with respect to time were taken of the nominal specimen resisting stress, surface strains, and average elongation over the "gage" length of the specimen. From these records the relations between stress, strain, and time were determined for the various tests.

The results of the uniaxial tension and compression tests are presented and discussed in terms of (1) the time delay to the initiation of a significant amount of yielding, (2) the rate of general yielding where applicable, and (3) the general nature of the stress-strain-time behavior of the various metals tested.

In the slow and rapid flexural tests of small beams of rectangular section under third-point loading, enough information was obtained that the time dependent stress-strain behavior in the pure flexural region of the beam could be determined. An attempt is made to correlate this behavior with the information obtained from uniaxial tests of the same material.

2. RAPID LOADING AND STRAINING EQUIPMENT

2.1 Introduction

The equipment used for producing the loads and the deformations required during the course of the project consisted of two types; those in which nominal deformation was the quantity most nearly independent of the specimen behavior (standard hydraulic and screw-type universal testing machines and a specially constructed hydraulic actuator), and the slow and rapid pneumatic loading unit with which nominal loads that are nearly independent of specimen response could be produced. The pneumatic unit is hereafter called the pulse loading unit.

The Baldwin universal hydraulic testing machine which was used as the load standard in all dynamometer calibrations, was also used for many of the slow tests run at rates conforming to ASTM specification A 370-56T. However, in the later stages of the project, for convenience in use of the oscillographic equipment with which all slow and rapid tests were recorded, a hydraulic actuator system affording nominal straining control at slow rates of deformation was devised. This could be quickly connected in series with the pulse loading unit so that no change of either instrumentation connections or specimen fixtures was necessary in changing from slow straining tests to rapid loading tests.

2.2 Description of the Loading Apparatus

For the initial purposes of the investigation, a device that would produce a rapid loading pulse, that is, a pulse that is nearly independent of specimen response, was very desirable not only because such a device would permit producing the desired loading without the need of accurate knowledge of the specimen's response characteristics, but also because nearly identical loading pulses

could be applied easily to structural components, coupons, or frames having varying response characteristics. Other requirements were that the minimum rise and decay times of the loading pulse should not exceed approximately ten milliseconds, that both the magnitude and duration of the loading should be independently controllable, and that the maximum loading stroke should be at least four inches with an associated drop in load of not more than 50 per cent.

The 20-kip pulse loading device shown in Figs. 1, 2, and 3 was developed to satisfy these requirements. This unit is a piston device in which the load output is the result of differential pressure. Compressed nitrogen or helium is used as the pressure source. The rapid application and release of the load can be achieved through the use of solenoid triggered slide valves to obtain the timed pressure release from the two chambers of the device.

2.3 Control of Loading

The use of this device permits the application of a loading pulse that may begin from a static level ranging from 20 kips tension to 20 kips compression, undergo a rapid change of plus or minus 20 kips maximum (with the restriction that the prepulse load plus the dynamic change in load can not exceed the limits of plus or minus 20 kips), and then return rapidly to zero load. The duration of the peak load may be varied from a few milliseconds to many hours. The rise and decay times of the loading pulses are controllable by adjusting the size of the pressure release orifices. The minimum time for either rise or decay of the load is approximately six milliseconds. Using the adjustable orifices, it is possible to increase the time for rise or decay of the load to approximately half a second, and, of course, loadings at relatively slow rates can be achieved by the slow build-up of pressures in the chambers of the unit using the manual pressure supply system. A few possible loading pulses are shown in Fig. 4.

2.4 Past Usage in Testing

In the investigation described in this report the 20-kip pulse loading unit was used for the rapid uniaxial tension and compression tests, and also for the experiments involving rectangular beams under third-point loading. In addition to these investigations for which the testing arrangements are shown in Figs. 7 and 31, the loading unit was used also in a series of tests of small model frames under both slow and rapid loadings. The arrangement for these experiments is shown in Fig. 5.

Since the successful development of the 20 kip loading unit, machines of larger capacity based upon its design have been constructed at the University of Illinois. One of these machines is shown in Fig. 6. This machine has a capacity of plus or minus 60 kips and a minimum loading time of approximately 15 milliseconds under ordinary usage.

2.5 Description of the Slow Straining Unit

As was mentioned in the introduction to this section, a hydraulic actuator which can be connected in series with the 20-kip pulse loading unit was provided so that straining tests at slow rates could be performed conveniently without changing the instrumentation or the manner of specimen connection. A schematic diagram of this unit and the associated pressure control system is shown in Fig. 8. The entire testing arrangement is shown in Fig. 7.

2.6 Summary

A general purpose loading unit has been developed which permits control of the load pulse as follows:

- (a) The magnitude of the tensile or compressive load pulse can be varied from approximately 2000 to 20,000 pounds, corresponding to

main chamber pressures of 100 to 1000 psi. (100 psi is the lower limit of consistent operation.)

- (b) The time interval between the initiation of the load and the start of load release can be varied from a 0.007 second minimum to long hand-timed intervals.
- (c) The rise time of the load can be varied from a 0.005 second minimum to 1.5 seconds using the slide valves and variable orifices, or from a 5 second minimum to long times using the pressure regulators and/or needle valves to control pressure.
- (d) The decay time of the load is independently variable. The range possible is the same as that of the rise time since the two slide valve assemblies are identical.

For use in conjunction with this apparatus, an attachment for the control of slow straining rates has been provided. Therefore, in one location, apparatus is available with which slow tests may be run under either loading or straining control, and also with which rapid loading pulses can be applied.

3. UNIAXIAL STRESS TESTS

3.1 Introduction

During the past few decades much effort has been devoted to determining the behavior and the nature of the materials with which man builds. The more commonly used the material, the more extensive have been the investigations. Consequently, a great deal of information is available concerning the most commonly used structural metal, steel. However, the fact that steel is an alloy of iron and therefore can have greatly different properties has made the determination of its behavior in all its various forms a never ending task^{10, 15, 28, 40*}. As fast as new instrumentation capable of more accurate measurement or better time resolution has been developed investigators have attempted to extend their knowledge of materials. The development of the wire resistance strain gage and the common availability of oscillographic equipment useable in the microsecond range has led to the comparatively recent work of Davies, and Clark and Wood, et al., and has therefore resulted in the acquisition of new knowledge pertaining to the time sensitive behavior of metals.

While it is probable that no other materials have been the subject of as many investigations as structural steel and aluminum, little information is available about the stress-deformation characteristics of these metals in the range of strain rates corresponding to those that might be created in the members of typical structures by large dynamic forces, that is, strain rates increasing from "static" to about 1 in./in. per second. Furthermore, as regards iron alloys, the deformation characteristics are greatly affected by extremely small concentrations of the alloying elements and also by the form of their presence (as solutes or precipitates).

* Numbers refer to entries in the bibliography. The bibliography includes references for background information in addition to those references noted in the text.

In addition to these difficulties, no satisfactory theory based on chemical composition has been developed with which quantitative predictions of the time sensitive behavior of these metals can be made, although qualitatively many characteristics can be explained^{6, 16, 17, 29, 41}. Therefore, the time dependent stress-deformation characteristics of specific metals usually must be determined by experimental means.

The uniaxial stress tests described in this report were performed to obtain specific stress-strain-time information for a few of the more commonly used structural materials.

3.2 Description of Uniaxial Testing Series

3.2.1 Types of Specimens

The materials which were investigated included the following: rimmed steel from one inch bar stock in the as-rolled and annealed condition, semi-killed steel from one inch plate stock in the as-rolled condition, fully-killed steel, ASTM A-7 steel obtained from a 4M section, two low-alloy steels, a chrome-nickel steel, a steel meeting ASTM specification A-242, and USS T1 steel. In addition 60 61-T6 aluminum was tested. A summary of the materials tested is given in Table 1 and a description of the system used for specimen designation is presented in Table 2.

In the preliminary series, composed of specimens having an area of 0.100 sq in., the rimmed steel bar stock (RB) and the semi-killed steel plate stock (SP) were tested as-rolled (A), annealed after machining (B), and annealed before machining (C). In addition, some of the specimens of the preliminary series were tested polished smooth (S) and some with a small circumferential notch (N).

Following these tests it was decided to test these two steels as-rolled since metallurgical investigations revealed that the microstructures were quite uniform. These were the series called 2 MRBA, 2 SRBA, 2 SSPAL, and 2SSPAT.

The bar stock specimens were, of course, aligned axially with respect to the direction of rolling of the bar. The plate stock specimens were oriented with their longitudinal axes either parallel to the direction of mill rolling (L) or with their axes transverse to the direction of mill rolling (T).

The tests of the NS, NL, and NN series were not instrumented as completely as the others, in that only resisting stress-time and SR-4 gage strain-time information was recorded.

The dimensions of the various specimen types are given in Figs. 9, 11, 12, and 13. The form of the specimens varied from areas of 0.100 sq in. to 0.200 sq in. and in form from the gently curving profile illustrated in Fig. 9 to the profile shown in Fig. 13b which was developed for use in either tension or compression. Table 2 also provides a key to the profile used for the various series of tests.

3.2.2 Manufacture of Specimens

The specimens which were tested in the as-rolled condition were machined from band sawed blanks using a maximum depth of cut on each pass of no more than 0.02 in., which, under the oil coolant used, raised the specimen temperature to no more than 150 degrees F. The final cut to about 0.002 in. oversize for the specimen to be polished, was about 0.005 in. in depth. Following this cut, the specimens were polished by hand held emery cloth to the final dimensions and to a finish that varied from about 11 microinches r.m.s. to some 20 microinches r.m.s., with an average finish of about 15 microinches r.m.s. as indicated by a type PAC, serial 511 (Profilometer) manufactured by the Physicists Research Company, of Ann Arbor, Michigan.

The as-machined specimens were cut to the final dimension using a final pass of about 0.005 in. The surface roughness of these specimens varied from about 100 to 200 microinches r.m.s. with an average of about 150 microinches r.m.s.

As was mentioned in Section 3.2.1, a few of the preliminary series specimens were notched circumferentially (1N). These were "V" notches about 0.01 in. wide and 0.01 in. deep.

Following the pretest measurements of surface roughness and diameter, the SR-4 gages, if used, were applied to the gage section of the specimens. During this process the specimens were heated to about 180 degrees F for a period of some four hours. This may have aged the material somewhat with respect to the residual stresses resulting from the machining.

The procedure listed above, which is that followed in the preparation of the as-rolled specimens, was followed in preparing the "annealed before machining" specimens beginning, of course, with the annealed specimen blanks.

In the case of the "annealed after machining" specimens, the heat treatment, performed in an electric furnace by heating a tube containing the machined specimens sealed in an atmosphere of helium, was followed by the removal, by polishing, of the final 0.002 in. left by the machining process.

The NL, NN, and NHY specimens were prepared elsewhere and sent to the University for testing.

3.2.3 Metallurgical Properties and Chemical Compositions

In commenting upon the results of the metallurgical investigation performed by the Metallurgical Department of the University of Illinois on most of the steels used for the specimens described in this report, the authors refer the reader to the summary given in Table 3, and the metallographs of Fig. 14.

These studies did show that the steels were very uniform in their so-called as-rolled condition and that consequently for this reason the annealing and spherodizing were not necessary to obtain consistent results.

The almost complete decarburization of steel NS, and the broadly decarburized bands of steel NR should be noted. It is possible that this decarburization greatly affected the yield behavior of the materials as compared with that of the other steels.

The chemical compositions of the steels as determined in a check analysis by the R. W. Hunt Company of Chicago, are given in Table 4. Inadvertently the oxygen content of the steels was not requested; this is regrettable since this would probably be one of the more important differences between the rimmed and the semi-killed steels.

3.3 Description of Testing Procedures

3.3.1 Instrumentation

To record the data from the preliminary series of tests, the four channel cathode ray oscillograph shown in Fig. 15 was used. This equipment was virtually flat in response from some five cps to thirty kcs. The lower limit was imposed by the instability of the D.C. preamplifiers which caused significant drift in the traces over times as short as 0.1 or 0.2 seconds. For this reason, the equipment was not satisfactory for the recording of tests involving durations of several seconds.

On the basis of the records obtained with the CRO equipment, it was seen that the Hathaway magnetic oscillographic equipment available in the laboratory would have response characteristics adequate for the faithful recording of the resisting stresses and strains developed in the rapid load tests with the advantage of excellent long time stability that would permit use of the instrumentation for the recording of slow tests as well. Therefore, the magnetic oscillographic equipment, shown in Fig. 16, was used for the main series of tests. This equipment includes a Hathaway Type S-14C magnetic oscillograph, in which were used Type OC2,

Group 2-3 recording galvanometers. The Type MRC-18 Hathaway carrier strain amplifier system was modified using an external carrier oscillator and power supply which had characteristics superior to those of the original equipment. The usable upper frequency limit is about 450 cps, while the lower limit, as mentioned above, is D.C. A block diagram of the Hathaway equipment is shown in Fig. 34.

The phenomena recorded versus time for the preliminary testing series were the following: (1) the output of an SR-4 gage dynamometer recording the stress developed on the end of the specimen opposite that to which the load was applied; and (2) the output of two SR-4 strain gages attached diametrically opposite each other on a gage section of a specimen. On the 2RB, 2SP, NR, NHY, NL, and NN series the output from an extensometer connected across the gage length was recorded also. The dynamometer-specimen-extensometer arrangement used for most of these tests is shown in Fig. 10. In all other testing series, measurements included the output of the dynamometer as before, but strains were obtained from a dual range spring type extensometer connected across the specimen. This extensometer had two independent SR-4 bridges, the outputs of which were recorded with different sensitivities so that the entire range of strains could be resolved adequately.

The various dynamometer-instrumentation systems were calibrated "statically" versus the load measuring system in a 120,000-lb Baldwin universal hydraulic testing machine. In checking the accuracy of the dynamometer-oscillograph load measuring system, measurements from slow straining test oscillograms were compared with the load dial readings taken on the Baldwin machine at corresponding times. Usually the loads were within about 100 lb out of 10,000 lb with an occasional maximum error never greater than 300 lb. That is, the usual error was about ± 1 per cent (and usually lower) with a maximum error never observed to be greater than ± 3 per cent.

In the tests in which SR-4 gages were attached to the gage section of the specimen, bending could be determined. The percentages of bending ranged as high as 15 per cent in some few cases but generally were less than 5 per cent. The alignment procedure possible with the development of the uniaxial tension-compression fixtures was such that the percentages of bending were usually less than 5 per cent.

The extensometers that were used at various times throughout these investigations were all of the flat spring type shown in Figs. 10 and 13. This type of extensometer met requirements for range, sensitivity, dynamic characteristics, and simplicity. In these "transducers", flexural strains in the flat springs were measured with SR-4 gages connected as four arm bridges with all arms active, so that a strain magnification of four was obtained along with temperature compensation. The extensometer last used had two complete bridges of SR-4 gages on them so that two different sensitivities could be used to resolve the total range of specimen extension. Therefore, in these later tests SR-4 gages were not used on the specimens.

Just prior to each test, calibration traces were recorded on the oscillogram by shunting the respective bridges with precision resistors whose equivalence in terms of the quantities being measured had been determined earlier. Usually the complete dynamometer and extensometer-instrumentation channels were calibrated directly before and after every series of tests and, in some cases, in the middle of a long testing series.

It is believed that the total errors associated with measurement of nominal load are no more than ± 3 per cent, and that the total errors measured with the determination of extension between the points of attachment of the extensometers are no more than ± 5 per cent.

A major problem associated with interpretation of the results of the tests in which extension was measured across a reduced gage length is the determination of the effective gage length of the specimens throughout the entire range of deformation. The study which was made of this problem is reported in Section 3.3.6.

3.3.2 Slow Tests

From the summary of the testing, presented in Tables 5, it can be seen that slow tests, with two exceptions, were performed in the Baldwin universal testing machine, or the pulse-loading machine with or without the slow straining attachment. The equivalent elastic strain rates used for these tests were within those allowable under ASTM specification 370-56T. Since a rather complete summary of the conditions under which these tests were run is given in Table 5,* very little discussion is necessary in the text.

It is to be noted that slow tests of the RBA specimens which were tested in the Baldwin machine produced yielding at lower stresses than those which were tested in the pulse loading machine. However, no such difference in yield strength was obtained for specimens of the SPA series. The differences between these series of tests were the following: (1) the static specimens which were tested in the Baldwin machine were "pricked" on the gage area by the extensometer points (which might affect yielding behavior); (2) slightly different loading rates were used in

* In Table 5, the constants C , C_1 and C_2 are used within a test series to differentiate between the conditions under which each test was run. For the rapid tests, $C = \sigma_{uy} = \sigma_{ly}$.

In Table 5 and in the stress parameters used in this report:

σ_{uy} = upper yield stress
 σ_{uy}^* = upper yield stress in a slow straining test
 σ_{ly} = lower yield stress
 σ_{ly}^* = lower yield stress in a slow straining test
 $\sigma_{max} = \sigma_m$ = ultimate strength of a material

the two machines; and (3) the smoothness of application of loading between the two machines may have differed.

In Figs. 17a and 17b are shown photographic reproductions (about half size) of the type of oscillograms which were produced during the slow tests in the Baldwin machine as compared with the pulse loading machine.

3.3.3 Machine Vibration Tests

To determine whether any significant difference existed in the smoothness of the loadings produced by the three testing machines used (the Baldwin machine, the pulse loading machine, and a Riehle screw type testing machine), an attempt was made to measure the vibrations induced in the test specimens by operation of these testing machines. Within the sensitivity of the recording instrumentation no vibrations were evident in the loading produced by either the Baldwin machine or the pulse-loading machine. However, vibrations having an amplitude of some 30 or 40 microinches per inch of strain were apparent in the tests performed in the Riehle screw type machine.

3.3.4 Residual Microstrain Determination

Many metals, but not including mild steel, do not exhibit a perfectly linear relationship between applied stress and resulting strain or vice versa, even for relatively low values. Of course, the degree to which this holds true is somewhat dependent upon the sensitivity of measurement possible with the method used for observing stress and strain. While mild steel does have a nearly linear and almost perfectly elastic stress-strain relationship for relatively low levels, a departure from linearity and from elastic action does become evident at stress levels above something on the order of one-half of the nominal yield strength of the steel.

Some investigators^{35, 37} have suggested that a critical amount of inelastic "microstrain" may be necessary before a general yielding condition is initiated. (In this report the term microstrain will be applied to all inelastic straining preceding the development of the general yielding condition.) It follows, then, that a difference in the character of the microstraining which precedes general yielding would be related to the nature of the dynamic yielding behavior. However, as a matter of interest, a few cycled loadings were applied to a few specimens of the SRBA, MRBA, and SSPA series in the Baldwin hydraulic testing machine, the pulse-loading machine, and the Riehle screw type testing machine. The straining cycles, which had a "period" of about 2 minutes (during which about one minute was required for the straining and one minute for making the residual strain measurements), were of successively increasing magnitude culminating in the yielding of the specimen.

Preceding and following each cycle of straining, the SR-4 gages attached to the gage section of the specimen were "read" using a Baldwin Type L strain indicator. From these readings the residual strain resulting from each strain cycle was determined. The results which are presented in Fig. 18 indicate that in these tests general yielding was preceded by inelastic "microstrains" on the order of 20×10^{-6} in./in.

3.3.5 Rapid Uniaxial Tests

A description of the tests and the results are presented in Table 5. A study of these tables will reveal that in most of the rapid tests loads were applied rapidly to a constant level, and were held at these levels throughout the duration of the test until yielding had nearly stopped, usually some four or five seconds after its commencement. Following this the loads were released rapidly to zero. In most of the test series, identical specimens were tested at either the nominal "static" rates or with rise times of loadings on the order of 0.006

seconds. The tests were run at stress levels ranging between the static upper yield stress and the maximum strength of the specimen material so that a range of delay times and of rates of general yielding could be obtained.*

In the 2RB and 2SP series of tests, three rise times of loadings were used: 0.005 seconds, 0.10 seconds, and 0.50 seconds.

For the NR, PS, Q, K, T, and L series, the loads were applied to a few specimens in tension and to the others in compression. Only in the case of the NR series were the stresses reversed after the specimen had been initially yielded under a stress of the opposite sense.

As has been mentioned earlier, the phenomena recorded versus time for all series included nominal resistance and a measure of strain obtained with either SR-4 gages alone, SR-4 gages in combination with an extensometer, or a dual range extensometer.

Photographic reproductions, about one-half size, of oscillograms illustrating the loadings mentioned above and also typical results are shown in Figs. 17c to 17f.

Before each of these tests, as well as before each slow loading rate test, a small load (corresponding to a stress of no more than 10,000 psi) was applied as an aid in aligning the specimen with respect to the loading axis. If the SR-4 gages on the specimens so instrumented indicated a bending strain greater than about 5 per cent of the axial strain, the specimen was readjusted until the bending was less than that value. On the specimens not having SR-4 gages the small pretest load was applied and released to "settle" the specimen in its seat, a procedure

* In Table 5, the magnitudes of the rapid loads are listed under either σ_{uy} or σ_{ly} . These expressions for stress are equivalent in rapid tests.

which had produced satisfactory alignment of most specimens instrumented with SR-4 gages.

3.3.6 Effective Gage Length

As was mentioned earlier, a problem associated with use of the information obtained from the uniaxial stress investigation is that of relating extension determined from an extensometer attached across the shoulders of the reduced gage length of a specimen to the actual effective strain in the specimen. For small strains of an elastic specimen the effective gage length can be computed and is a constant times the actual gage length of the extensometer. However, when yielding occurs in the specimen, the effective gage length will change with the magnitude of that yielding. This has been indicated by a series of experiments designed to provide information concerning this matter. In Figs. 19 are shown the results of this investigation. Figs. 19a and 19b indicate that prior to the beginning of yielding, the effective gage length of a shouldered specimen of mild steel was approximately equal to the computed "elastic" value. As the specimen yielded, the effective gage length dropped rapidly to its lowest value which coincided with general yielding. As the specimen strain hardened, the value of the effective gage length increased. For specimens made of a material that exhibited no upper-lower yield point phenomena, the variation in effective gage length was less extreme and no increase of effective gage length with strain hardening was indicated. This is illustrated in Figs. 19c and 19d.

In the RB and SP series specimens the effective gage length after yielding had occurred was assumed to be constant. The value used was obtained by direct calibration during slow straining rate tests of the "static" specimens. For the PS, Q, K, T, and L materials, the effective gage length used was that determined from pilot tests of the same material. All strains as reported in this report are corrected for the effect of yielding upon the effective gage length.

3.4 Results of Uniaxial Tests

3.4.1 General Time Sensitive Behaviors of the Materials Tested

It is comparatively well known that metals having a body centered cubic lattice structure usually yield in a discontinuous manner under slow rates of straining. It has been shown that the same materials when subjected to rapid loading or straining yield in a manner indicating relatively large time sensitivity. Steel in the commonly used form is one of these materials, and therefore its yielding behavior differs considerably from that of a material such as aluminum 6061-T6.

It is a characteristic of mild and low-alloy steels that, under a slow relatively constant rate of nominal uniaxial straining at room temperatures, their resistance goes through four rather arbitrary stages: (1) the elastic range terminating in (2) microstraining followed by the development of the condition of (3) general yielding (in which the level of resistance is a function mainly of the rate of straining) which in turn is followed by the advent of (4) strain hardening and subsequent fracture. The four stages of the nominal resistance-deformation characteristics of these metals are quite evident in the slow straining rate tests, but, of course, are no less present in tests run under other conditions, such as slow constant rate of increase in nominal stress. Of the four stages mentioned, the middle two, microstraining and general yielding, are quite time sensitive; the elastic range is almost insensitive to time; and the range beyond the commencement of strain hardening is only slightly time sensitive.

The time sensitivity associated with what in this report is called the microstraining phenomena has been termed the "delayed yield" effect. This is perhaps best revealed under tests involving rapid stressing to a constant stress level such as were performed in this investigation using the 20-kip pulse loading machine.

In the materials studies presented in this report the time delay in yielding is defined arbitrarily as the interval between the time at which the stress first reached a value corresponding to the lowest upper yield stress obtained in a slow test, and the time at which yielding had become general enough that the apparent modulus (nominal stress/nominal strain) had dropped to about $2/3 E$. Delay time so defined has engineering significance in that it is related at one end to a stress level high enough to result in yielding under slow loading or deforming conditions, and at the other end to a parameter involving both stress and strain which has an arbitrary value indicative of an amount of yielding sufficient to mark the beginning of general yielding.

The rate of general yielding effect (usually termed somewhat ambiguously the strain rate effect) is most evident perhaps in tests performed at various constant rates of nominal strain, but it will also be apparent, of course, in tests in which nominal stress rather than nominal strain is the factor most nearly independent of specimen behavior. Such is the case in the "rapid loading to constant stress level" tests. After general yielding has begun (following the delay in yielding if present) the specimen will deform at a rate which is dependent upon the stress level being maintained by the pneumatic loading unit. Since the several tests are run at different constant stress levels, both delayed yield and rate of general yielding information can be obtained from a single test series.

For most mild steels the transition between the general yielding condition (flat yield region in the constant rate of straining test) and the region of strain hardening is somewhat more gradual than that between the other stages. (Of course, the "gradualness" is largely dependent upon the time resolution possible with the recording techniques used.) The tests run at the University of Illinois

on mild and low-alloy steels indicate that for a particular steel the transition begins at about the same total strain regardless of the rates involved.

In a rapid test to a constant stress level the straining finally ceases at a total strain which usually agrees well with that corresponding to the strain obtained at the same nominal stress under slow loading or deforming conditions.

For metals such as high-alloy steel, structural aluminum, etc., yielding under slow rates of straining is not a discontinuous process, and the behavior under rapid loading is not as time sensitive as is the case for mild steel. This is indicated in the results for the NHY, USS T-1, and 6061-T6 materials.

3.4.2 Results of Tension and Compression Tests

In Fig. 20 is presented in three dimensions the relation between stress, strain, and time as obtained from uniaxial tests of mild steel involving slow and rapid loading to constant stress levels. In this relationship the so-called delayed yield and rate of general yielding behavior are quite evident. Stress-strain and strain-time relationships representative of the materials tested are shown in Fig. 21. These contain the same information as is shown for one material in Fig. 20. The information which is presented in these figures is abstracted in the form of delayed yielding and rate of general yielding information where these phenomena were present, and in the form of various times required for yielding to progress to specified values of the nominal secant modulus (nominal stress/nominal strain) where delayed yielding and rate of general yielding behaviors were not pronounced. In Tables 5 are presented these values for all of the tests which were performed.

The delayed yielding and rate of general yielding behavior is presented respectively in Figs. 22, 23, 24, 25, and 26. In the first of the figures of each set the values are presented versus the nominal stress, and in the second and

third, versus a stress parameter involving, in the case of delayed yielding the static upper yield stress, and, in the case of rate of general yielding, the lower yield stress obtained under a rate of straining corresponding to approximately 10^{-3} in./in./sec. These basic values were obtained under slow straining of the specimen materials in conformance with ASTM Specification A370-56T, and therefore can serve as a basis for extrapolation of these results to other materials which are similar but which have values of upper and lower yield stress different from these obtained in this investigation.

There was little noticeable difference in the behavior of the materials which were tested under both initial tension and initial compression, that is, ASTM A-242 steel, USS T-1 steel, a fully-killed mild steel, and 6061-T6 aluminum. If the reader wishes to make further comparisons, he may obtain from Table 1 the information concerning the type of test and from both Table 5 and Figs. 22 through 26 the results which were obtained.

3.4.3 Results of Preliminary Reversed Stress Tests

As can be seen from Table 5u, a few tests were performed with a reversal of loading subsequent to initial testing. The material from which these specimens were made was the semi-killed plate stock used for the 2SSPA series, and the BF series flexure tests described in Section 4 of this report. The dimensions of the preliminary stress reversal specimens, the specimen profile, and the manner of attachment to the testing apparatus are shown in Fig. 12. There were several disadvantages in the use of this type of specimen, namely, the attachment of the extensometer to depressions punched into the surface of the specimen, the non-uniform diameter of the specimen, and the relative difficulty of attaining axially of the load. However, the results are nevertheless interesting, as can be seen from Figs. 28 through 30.

In Fig. 27 the relation between the upper yield stress parameter and the secant modulus (nominal stress/nominal strain) for the slow loading tests is shown. These curves indicate that yielding was rather gradual in these specimens and began at a stress which was considerably lower than that which was arbitrarily used as the upper yield stress of the material. In Fig. 28 is shown the effect of reversal of loading following slow yielding. This is the so-called Bauschinger effect; the fact that after having been yielded in one direction, subsequent reversal without aging will produce almost immediate inelastic behavior at relatively low strain with no evidence of an upper-lower yield behavior.

The results which were obtained in the four rapid stress reversal tests are shown in Fig. 29 in the form of strain-time relationships. In these tests a reversal of loading was applied within a minute or so of release of loading following yielding in the direction in which the loading was initially applied rapidly. Therefore, these were not rapid in the sense that the entire stress-time relationship including reversal was imposed within a very short period of time. However, the change of stress from the initial zero level to the constant stress levels indicated in the figures was rapid. Again a behavior which could be called the Bauschinger effect in rapid loading is evident in that no delay in yielding was apparent upon reversal of loading in a direction opposite to that used in initial yielding.

Because of the non-uniform diameter of the specimen profile used in these preliminary reversed loading tests and the consequent difficulty in relating extensometer deformation to unit strain, no attempt was made to interpret the results of the rapid reversed loading experiments in the form of rate of general yielding information.

In another series of stress reversal tests, an initial slow loading to a level below that which would cause general yielding was followed by a rapid reversal of loading to a level sufficient to cause yielding. As can be seen from Figs. 30, a delay in yielding was obtained in all of these tests, and this delay agreed well with the delay times obtained in the loadings of virgin material in the previously mentioned rapid tests.

3.5 Summary of Results for Uniaxial Stress Tests

3.5.1 Summary of Results

The results of the slow and rapid uniaxial stress tests which were performed on many materials in initial tension and initial compression, and on one material in complete stress reversal, have been presented in the form of tabulated results in Table 5 and in the various figures mentioned previously. In general terms the results can be summarized as follows.

(1) The metals tested which exhibited a pronounced upper-lower yield point behavior under conditions of slow straining, and had stress-strain relationships with discontinuities in slope, also exhibited the time sensitive behaviors termed delayed yielding and rate of general yielding (defined earlier in this report).

(2) In the only tests in which the rise times of rapid loadings were varied (from 0.006 sec to 0.5 sec), the comparisons of delay time as defined by a stress parameter involving the upper yield point indicated no particular sensitivity to the rise time of loading within the limits indicated above. This result can probably be attributed to the manner in which the elapsed time to general yielding was arbitrarily defined (the interval between the time at which the stress first reached the nominal static upper yield stress level and that at which general

yielding occurred as indicated by a value of stress/strain equal to 20×10^6 psi).

(3) Within the range of rapidity of loadings applied, that is, rise times greater than 0.006 seconds, the value of Young's modulus was constant. The so-called strain hardening region also was relatively insensitive to time effects. The major time sensitivity was associated with initial yielding and subsequent general yielding, the so-called delayed yielding and rate of general yielding behaviors mentioned previously. For the high strength alloys of steel, and for 6061-T6 aluminum for which static stress-strain relationships having no discontinuity of slope were obtained, no delayed yielding or rate of general yielding behavior was evident.

(4) The results of the very few preliminary experiments in slow and rapid reversal of loading indicate that the so-called Bauschinger effect which is commonly observed in slow reversal of stress, is also present in cases involving rapid stress reversal with a consequent absence of delayed yield behavior commonly found in virgin material. Because of the type of specimen used in these preliminary studies, no conclusions could be reached regarding the rate of general yielding behavior.

3.5.2 General Significance of Results

As can be seen from the results described above, the increased resistance which results from the time sensitive behaviors of mild steel arbitrarily termed the delayed yielding and rate of general yielding phenomena can approach values 50 per cent greater than the nominal yield values even for the relatively slow rates of straining which may be created in frame type civil engineering structures. in which the actual deformation of the major structural elements results from transfer of air blast or earthquake shock loading through the supports or outer shell.

In the case of many ship structures in which blast loading is applied directly, such as hull plating subjected to underwater explosion, the actual rates of strain-ing can be many times greater than 1 in./in./sec. In these cases it is to be expected that resistances at least as great as the nominal static ultimate strength may be obtained without yielding or may be supported by the rate of deformation. Therefore, estimates of the response of these structural elements based upon nominal resistances derived from static yield values with no increase for the time sensitive effects will be very greatly in error. (The error, however, will be on the safe side unless brittle fracture or fatigue is a consideration.)

4. SLOW AND RAPID FLEXURE TESTS

4.1 Introduction

Structural components undergoing flexure such as beams, plates, and columns, are major elements of almost any structure. Therefore, it is logical, as an intermediate step between the uniaxial stress investigation and application of these results to the behavior of large full-size structures, that flexural stress studies be made of the same materials which were tested under uniaxial stress conditions. Such an investigation is described in this section of the report.

In all, three sets of specimens were tested. These included a preliminary series, BF, made from the semi-killed plate stock designated SPA and PS, a series, BK, made from fully-killed steel K, and a less completely instrumented series, BL, made from 6061-T6 aluminum L.

Each of the series was composed of four specimens, one of which was subjected to a slow loading, while the other three were tested under rapid loading to a constant level.

Since the materials from which the flexure specimens were composed was also tested under conditions of uniaxial stress, a correlation of the two stress conditions was attempted.

The purpose of this section of the report is to describe these flexure tests, the conditions under which they were run, the results and their engineering significance.

4.2 Description of the Flexure Testing Series

4.2.1 Description of Flexure Specimens

The flexure specimens in all cases were small beams of rectangular section approximately 24 in. long. The depth of the section was very close to

2 in., while the thickness or width varied from approximately $2/3$ in. to approximately $7/8$ in. The specimens were band-sawed from the parent plate, then machined in a shaper to very near the final dimensions. Following this, the outer surfaces of the specimen were draw-filed and hand polished to the final dimensions. All of the materials were tested in the as-rolled condition, and the only treatment of any sort that they received other than normal handling was that during the application of SR-4 gages they may have been subjected to prolonged heat of no more than 180 degrees F.

4.2.2 Material Properties Under Uniaxial Stress

As was mentioned in the introduction of this section, uniaxial stress tests were made of the materials from which the flexure specimens were composed. The stress-strain relationships, typical of those which were obtained for these materials are shown in Figs. 36a, 36d, and 36g. In addition to these results, the delayed yield behavior and the rate of general yielding behavior of the two mild steels are shown in Figs. 36b, 36c, 36e, and 36f.

4.3 Description of the Testing Procedures

4.3.1 Flexure Testing Arrangement

Both the slow and rapid loading tests were performed in the apparatus shown in Fig. 32. This is an attachment designed specifically to adapt the 20-kip pulse loading unit for these flexure tests. The loads are applied to the underside of the beam at the third-points, thereby deforming the beam upward as is shown in the figure. The only feature of the testing arrangement that may not be clear from the photographs is the end reaction system. The major bearings in the arrangement are roller bearing assemblies which are attached to the machine frame by means of pins fixed on a 20-in. span. The reaction of the beam ends is transmitted to the outer race of the roller-bearing assembly through plates which are clamped to the

top and bottom of the beams by the bolts which are apparent in the figure. This end-reaction arrangement permits both translation and rotation at each end of the beam with the span length remaining fixed at 20 in. In other words, a change in length of the center line of the beam occurs during a test as the beam ends rotate and the beam deforms upward.

The loads which were applied to the specimen were measured by means of the two dynamometers visible in Fig. 32. The crossbar which can be seen in the photographs was provided to prevent flexure in the dynamometers.

4.3.2 Flexure Test Instrumentation

In these experiments measurements were made of the loads applied at the third-points of the beam, the acceleration of these loading points (except in the case of the aluminum specimens), the deflections at the third-points and at the center of the pure flexure region, and the strains on the outer fibers of the beam in the region of pure flexure. The relative locations of the loading points and the regions of strain measurement are shown in Fig. 34.

All phenomena were recorded on Hathaway magnetic oscillographs of the type mentioned in Section 3.3.1. The SR-4 gages used to measure the outer fiber strains on the specimen, and as the transducing elements in the dynamometers, were connected into four-arm bridge circuits as shown in Fig. 34. The accelerations were measured by means of an AMS-20A Hathaway accelerometer. It was fastened to the side of the loading beam as is evident in Fig. 32. The deflections were measured by means of the slide wire gages shown in the over-all view of the testing arrangement. The circuitry of the deflection measuring system is shown in Fig. 35.

Since two independent oscillographs were used for each test an interlocking timing system was necessary to permit correlation of the records. A timing

signal of 500 cps was recorded by one galvanometer in each oscillograph and the interlock was provided by a switch driven mechanically.

4.3.3 Description of Flexure Tests

As was mentioned in the introductory remarks, there were three series of flexure tests. The first of these was more or less preliminary in nature and, because of evident discrepancies, the results are somewhat questionable. This preliminary series, which has been designated BF, was composed of four tests. The first of these was run at a slow loading rate in the 20-kip pulse loading machine. In the other three, the loadings were applied in approximately 8 milliseconds after which a constant level was maintained until yielding had virtually ceased. Then the loading was released.

The second series designated BK, was tested using slightly different instrumentation. In an attempt to determine whether or not the distribution of strain throughout the depth of the beam section was linear, SR-4 gages were attached to the sides of the specimen at four depths through each half-depth of the beam. These gages may be clearly seen in Fig. 33. In addition, the curvatures in the region of pure flexure were determined for large deformations by means of spring steel curvature gages using SR-4 gages as the transducing elements. These were attached to the nominal center line of the beam on each side as is shown in Fig. 33. A different sensitivity was used in each of the two recording channels attached to the spring-steel curvature gages, so that the entire range of curvature was adequately defined. Deflections were measured only at the loading points in this particular series of tests. Again, as in the preliminary testing series, BF, the first test was performed at a slow rate. However, in this BK series the strain was controlled by means of a hydraulic jack attached to the lower end of the 20-kip pulse loading unit piston rod. This strain control resulted in a reasonably

constant rate of deformation throughout the duration of the test. The other three specimens of the BK series were tested with a load rapidly applied to a constant level. Three different levels of loads were used so that a range of possible delayed yield behavior and rate of general yielding behavior could be determined. Because of faulty film advance during the test of BK4, the records for this specimen were lost.

The last series of flexure specimens was composed of 6061-T6 aluminum. The instrumentation of this particular testing series included measurement of the loads at the third-points, the deflections at the loading points, the strain of the top and bottom fibers in the region of pure flexure, and the curvature in this same region. As with the other testing series, one test was performed slowly and the other three rapidly.

4.4 Results of Flexure Tests

4.4.1 Experimental Results of Flexure Tests

The data recorded in the three series of flexure tests are presented in Figs. 37, 38, and 39. The values of M_e and α_e for the flexural specimens are given in Figs. 36a, 36d, and 36g. Rate of curvature-time relationships for the rapid tests are also included since this information was obtained for use in computing the resisting moments for the sections.

It was planned to determine the resistance of a given beam by subtracting the inertia force as obtained from acceleration measurements at the loading point (and an assumed effective mass of the beam specimen system) from the applied load. However, the acceleration traces were not distinguishable in the region of initial loading. Therefore, the resistances were assumed to be the same as the applied load. The maximum error resulting from this approximation is estimated to be less than 2 per cent. Of course, for large deflections of the beam, a correction was

applied in determining resisting moment from the loads measured at the third-points of the beam.

The previously mentioned correction of resisting moment due to large deflections was made with the use of the loading point deflection gage information. The moment arm between the reaction and the loading point was increased by the factor secant ($\tan^{-1} m\Delta/6.67$); the reaction was taken as the dynamometer reading, a vertical force, increased by the same factor since the crossbar between the dynamometers produced a horizontal component of force acting at the loading points; and the moment arm was decreased by the factor tangent $\Delta/6.67$ since the loads were applied half the beam depth, or more, from the longitudinal centerline of the specimen. Actually, a more correct value for this latter factor was 1.8 times tangent $\Delta/6.67$ to account for the thickness of the loading blocks and the roller diameter. This larger correction would have decreased the indicated measured values of resisting moment ratio beyond $\alpha/\alpha_e = 30$ an additional 4 to 6 per cent with respect to what is now shown in Figs. 40a, 41a, and 42a.

Of primary interest to those concerned with the engineering behavior of materials subjected to flexure are the results presented in Figs. 40, 41, and 42. These are the relations between resisting moment and curvature obtained for the specimens tested. At any curvature the resistance obtained for the steel specimens tested rapidly was considerably larger than that obtained for the companion specimens tested slowly. This indicates that there is a time sensitivity associated with the behavior of mild steel in flexure.

In an earlier part of this report, Section 4.3.3, it was mentioned that the results of the BF Series were somewhat questionable since discrepancies were evident in the magnitudes of the measured resisting moments. These measured values were too high in the three regions which can be used for checking the data in both

slow and rapid tests; i.e., the elastic region ($\alpha/\alpha_e \leq 1$) where $M/M_e = \alpha/\alpha_e$, the general yield region ($1 \leq \alpha/\alpha_e \leq 10$) where M/M_e approaches 1.5, and the ultimate region ($\alpha/\alpha_e \cong 80$ for Series BF and BK) where $M/M_e = 1.5 \sigma_m^*/\sigma_{ly}^* = 2.9$ in these cases. Re-examination of the original data indicated that the load values assigned to the calibration shunt resistor used with both of the dynamometer channels did not correspond to the load equivalences of the dynamometers at dynamometer strains equal to the apparent strain output of the shunt resistor. This check indicated that the load equivalence of the shunt resistor was 88 to 91 per cent of the shunt value used originally in reducing the data. The original data were therefore reduced by a factor of 0.91. The adjusted data, shown in Figs. 37a and 37e, were used for all subsequent computations pertaining to this test series. Since this change cannot be substantiated, except by noting the reasonable agreement in the three regions of curvature as detailed above, the BF Series results must be considered questionable.

The measured resistances of the rapidly loaded BK specimens, Fig. 41a, indicate that for the particular rise times of load (4 to 10 milliseconds) possible with the machine-specimen system used, an upper limit of resistance was obtained, at least until the work hardening range of curvatures was entered. Specimen BK-3 was subjected to a potential load some 30 per cent greater than was BK-2, yet only at a curvature ratio of about 40 could specimen BK-3 provide sufficient resistance to oppose the acting force.

Mild steel beams were definitely time sensitive; but, the results of the rapid flexure tests of the BL series indicated that there was little, if any, time sensitive behavior of the aluminum members subjected to flexure. The resisting moment - curvature relationship for specimen BL-4 is the only indication of an increase in resistance with the rapidity of deformation of an aluminum beam.

However, this result is questionable since the measured resistance did not agree as well with theory as could be expected in the elastic region, an indication of possible inaccuracies in measurement. Since aluminum coupons stressed uniaxially did not exhibit a time dependent behavior, the lack of such behavior in aluminum flexural specimens was expected.

4.4.2 Correlation Study

An attempt was made to correlate the behavior of these small mild steel beams under flexure with the known uniaxial stress properties of the materials from which the beams were made. In the correlation associated with the preliminary series BF, it was necessary to assume that the distribution of strain was linear throughout the depth of the beam section and that the material behaved the same in both tension and compression. For the next series, BK, it had been determined that these assumptions were valid. Therefore, proceeding from the measured strains of the beams, the resistances in the region of pure flexure were computed using the measured values of the instantaneous strains and the known delayed yielding and rate of general yielding behaviors of the materials from which the beams were made. (The procedure used for analyzing the rapidly loaded specimens is described in the Appendix.) In the case of the slowly deformed specimens, BF-1, BK-1, and BL-1, the material stress-strain curves as determined from slow straining coupon tests were used together with the measured strains of the beams.

The results of the correlation studies are shown in Figs. 40, 41, and 42. The measured resistance of BF-1 generally exceeded the computed resistance, but, the opposite was true for specimen BK-1. The failure of measured resistance to be as great as computed resistance has been noted by other investigators of the inelastic behavior of members. The discrepancy has been blamed in part on the severe stress concentrations associated with the application of concentrated loads

to the specimens. The measured resistance curves for specimens BK-1 and BL-1 exhibit a rising characteristic at large curvatures which probably resulted from an inadequate correction for large deflections.

Figures 40 and 41 show the correlation, correct to within 0 to 15 per cent, for the rapidly loaded specimens when their resistance is computed using the delay time-strain rate procedure. It may be noted that the use of strain rate information alone was insufficient to predict the maximum resistance of the specimen before major yielding began, but that this deficiency was satisfied by the inclusion of delay time considerations. Since no uniaxial time dependent properties of these materials deformed into the range of strain hardening were determined, the correlation was continued with respect to curvature using only the available rate of general yielding data until the rate of curvature approached zero. At this limit, the existing resisting stress is theoretically σ_{ly}^* and the resisting moment is $1.5 M_e$. Actually, the beams had a much greater moment resisting capacity than these computations indicate, because the geometry of the specimen permitted strain hardening without local buckling.

The computations of the flexural resistance of the rapidly loaded beams described in this report agreed within an average of about 10 per cent with the measured resistance. However, the method of analysis presupposes the availability of the deformation-time function for the beam. In a practical problem the resistance and deformation functions, which are interrelated, are initially set arbitrarily before proceeding with the solution. Three common assumptions for beam resistance as a function of displacement are shown in Fig. 43. These are the following: (1) a resistance derived from a stress block (acting at any cross-section of the member) which is the elasto-plastic stress-strain curve for the beam material; (2) an elasto-plastic resistance function with an initial elastic slope

continued to the plastic moment ratio of $M/M_e = 1.5$; (3) an elasto-plastic resistance function with the initial elastic slope continued to a plastic moment ratio of something greater than 1.5 to account for the dynamic effects.

If the measured resistance of the rapidly loaded mild steel beams is interpreted in terms of the arbitrary resistance functions described above, the third method would most adequately predict the observed behavior if the fully plastic resistance is increased by 60 per cent for BF-2 and 40 per cent for BF-3 (probably high due to the questionably high dynamometer data), and 40 per cent for BK-2 and BK-3.

4.5 Summary of Results of Flexure Tests

4.5.1 Summary of Results

The major purpose of the flexure tests was to determine whether or not the resistance of material in flexure could be correlated with the stress-strain-time information obtained in slow and rapid uniaxial stress tests. Therefore, the results of the flexure tests are interpreted in such a manner that this comparison is relatively simple. Basic data which are representative of slow and rapid tests of each of the three materials tested are shown in Figs. 36. In Figures 40a, 41a, and 42a moment curvature relationships obtained from all of the flexure tests are shown.

As was mentioned earlier, the major purpose of the flexure tests was to determine whether or not the behavior of materials when subjected to slow and rapid flexure could be correlated with the behavior (as obtained from slow and rapid uniaxial stress tests) of the materials from which the beams were made. Therefore, the major result of the flexural test investigation is the comparison of beam resistances as determined from measured deformations of the beam specimens and knowledge of material properties with the behavior of the beams as measured directly

in each test. These comparisons are shown for each specimen in Figs. 40, 41, and 42, in which is presented (1) the measured moment curvature relationships, (2) the moment curvature relationship determined using measured deformation of the beam and material properties determined from slow and rapid uniaxial stress tests, and (3) the moment curvature relationship representing the elasto-plastic strain relationship which best represents the basic stress-strain relationship of the specimen material as obtained with slow straining rates. This comparison indicates that the behavior of the material under flexure can be explained within less than 10 per cent error by consideration of material properties as obtained in uniaxial stress tests. This explanation is in almost all cases more accurate than the commonly used elasto-plastic assumption.

4.5.2 Significance of Results

The results of the flexure tests have been correlated (within reasonable limits) with the uniaxial stress properties of the material from which the beams were made. This indicates that it should be possible to progress from the current knowledge of the behavior of structural metals under slow and rapid uniaxial stress to an explanation of the behavior of structures composed of elements such as beams, beam-columns, and medium thick plates when subjected to transient dynamic loadings producing extensive inelastic deformations.

5. GENERAL SUMMARY

5.1 General Summary

As was mentioned in the introduction of this report the primary purposes of the investigation were to determine the time sensitive stress deformation characteristics of several of the more commonly used structural metals, and to determine the engineering significance of this information as regards application in the solution of problems concerned with the behavior of metal structures when subjected to transient dynamic loads producing extensive inelastic deformation.

The work that has been done has included many tests of several of the more commonly used structural metals including mild steels of the rimmed, semi-killed, and fully-killed varieties as obtained from plate, bar, and rolled section stocks; a few of the commonly used alloys of steel; and one very commonly used structural aluminum. The tests have included slow and rapid applications of stress under uniaxial conditions and conditions of pure flexure. In addition, a very few reversed loadings were applied to one material.

The results indicate that in general those materials which have a pronounced upper lower yield point phenomena in slow straining rate tests (that is, a discontinuity in slope of the stress-strain relationship) also exhibit a time sensitive behavior in the region from initial inelasticity through general yielding, and a less significant time sensitive behavior in the region of strain hardening. The so-called elastic region is apparently insensitive to time effects for loadings applied in times no more rapid than a few milliseconds. The results pertaining to the time sensitivity where present have been arbitrarily presented in the form of delayed yield and rate of general yielding information. The results of the tests of materials which were not very time sensitive were presented in the form of

stress-strain and strain-time relationships, and in a few cases, as elapsed times to specific amounts of yielding as defined by various arbitrary selected values of the secant moduli (stress/strain).

A major purpose of the investigation, as was mentioned above, was to provide information which would indicate whether or not the results of uniaxial stress tests could be extended to flexural stress conditions. The results of the flexure tests which were performed in this investigation indicate that this can be done with less than 10 per cent error.

Therefore, in many cases it should be possible to apply the results of uniaxial stress tests in predicting the response of frame and plate type structures to transient dynamic loadings that produce extensive inelastic deformation.

BIBLIOGRAPHY

1. Belsheim, R. O., "Delayed-Yield Time Effects in Mild Steel under Oscillatory Axial Loads," Trans. A.S.M.E., Vol. 79, p. 1619, 1957.
2. Brown, A. F. C., and Vincent, N. D. C., "The Relation Between Stress and Strain in the Tensile Impact Test," Proc. Inst. Mech. Engre., Vol. 145, 1941, p. 126.
3. Brown, W. F. and Thompson, F. C., "Strength and Failure Characteristics of Metal Membranes in Circular Bulging," Trans. A.S.M.E., Vol. 71, p. 575.
4. Clark, D. S., and Wood, D. S., "The Time Delay for the Initiation of Plastic Deformation at Rapidly Applied Constant Stress," Proc. A.S.T.M., Vol. 49, p. 717, 1949.
5. Clark, D. S., "The Behavior of Metals Under Dynamic Loading," Trans. Am. Soc. for Metals, Vol. 46, p. 34, 1954.
6. Cottrell, A. H., and Bilby, B. A., "Dislocation Theory of Yielding and Strain Aging of Iron," Proc. Phys. Soc. (London), Vol. 62A, p. 49, 1949.
7. Crum, R. G. and Mavis, F. T., "Behavior of Certain Alloys Subjected to Dynamic Loading," A.S.T.M. Bulletin, No. 231, p. 88, July 1958.
8. Davis, E. A., "The Effect of the Speed of Stretching and the Rate of Loading on the Yielding of Mild Steel," Jour. App. Mech., Vol. 5, No. 4, p. A137, 1938.
9. Docherty, J. G., and Thorne, F. W., "The Phenomenon of Tensile (Yielding?) in Mild Steel and Iron," Engineering, Vol. 132, p. 295, 1939.
10. Edwards, C. A., Phillips, D. L., and Jones, H. N., "The Influence of Some Special Elements Upon the Strain Aging and Yield Point Characteristics of Some Low Carbon Steels," Jour. Iron and Steel Inst., Vol. 142, p. 199, 1940.
11. Fast, J. D., "Aging of Iron and Steel," Iron and Coal Trades Review, Vol. 160, p. 837, 1950.
12. Freudenthal, A. M., "The Inelastic Behavior of Engineering Materials and Structures," John Wiley and Sons, Inc., New York, 1950.
13. Galletly, G. D., Hosking, N. G. and Ofjord, A., "Behavior of Structural Elements Under Impulsive Loads III," Report to New England Division, Corps of Engineers, Dept. of the Army, 1951.
14. Goss, N. P., "Grain Displacement in Metal Stressed Below the Elastic Limit," Metal Progress, Vol. 61, p. 87, 1952.
15. Holden, A. N., and Hollomon, J. H., "Homogeneous Yielding of Carburized and Nitrided Single Iron Crystals," Trans. Amer. Inst. of Mining and Met. Engr., Vol. 185, p. 179, 1949.

BIBLIOGRAPHY (Cont'd)

16. Holden, A. N., "The Yielding Behavior of Iron Single Crystals, Jour. App. Phys., Vol. 22, p. 1290, 1951.
17. Holloman, J. H., and Zener, C., "Conditions of Fracture in Steel," Trans. Amer. Inst. Mining and Met. Engr., Vol. 158, p. 283, 1944.
18. Johnson, J. E., Wood, D. S. and Clark, D. S., "Dynamic Stress-Strain Relations for Annealed 2S Aluminum Under Compression Impact," Trans. A.S.M.E., Journal of App. Mech., Vol. 20, No. 4, p. 523, 1953.
19. Johnson, J. E., Wood, D. S. and Clark, D. S., "Delayed Yielding in Annealed Low-Carbon Steel Under Compression Impact," Proc. A.S.T.M., Vol. 53, p. 755, 1953.
20. Keyon, R. L., and Burns, R. S., "Aging in Iron and Steel," Age Hardening of Metals, Amer. Soc. of Metals, 1939.
21. Low, J. R., and Gensamer, M., "Aging and the Yield Point of Steel," Trans. Amer. Inst. of Mining and Met. Engr., Vol. 158, p. 207, 1944.
22. MacGregor, C. W., and Fisher, J. C., "Tension Tests at Constant True Strain Rates," Jour. App. Mech., Vol. 12, p. A217, 1945.
23. Manjoine, M. J., and Nadai, A., "High Speed Tension Tests at Elevated Temperatures," Proc. A.S.T.M., Vol. 40, p. 822, 1940.
24. Massard, J. M., "The Stress-Deformation Characteristics of Some Mild Steels Subjected to Various Rapid Uniaxial Stressings," Ph. D. Thesis, Univ. of Ill., 1955.
25. Mentel, T. J., "The Plastic Deformation Due to Impact of a Cantilever Beam with an Attached Tip Mass," Brown Univ., Tech. Rpt. 8 to USA Ord. Corps, ASTIA AD 91635, 1956.
26. Nadai, A., and Manjoine, M. J., "High Speed Tension Tests at Elevated Temperatures, Parts II and III," Jour. App. Mech., Vol. 8, p. A77, 1941.
27. Nadai, A., "Theory of Flow and Fracture of Solids," McGraw-Hill Book Company, Inc., New York, 1950.
28. Nabarro, F. R. N., "Mechanical Effects of Carbon in Iron," Report of Conference on Strength of Solids, Phys. Soc. (London), p. 38, 1948.
29. Nabarro, F. R. N., "Deformation of Crystals by the Motion of Single Ions," Report of Conference on Strength of Solids, Phys. Soc. (London), p. 75, 1948.
30. Prager, W., "Stress-Strain Laws of the Mathematical Theory of Plasticity -- A Survey of Recent Progress," Jour. App. Mech., Vol. 15, p. 226, 1948.

BIBLIOGRAPHY (Cont'd)

31. Rees, W. P., Hopkins, B. E., and Tipler, H. R., "Tensile and Impact Properties of Fe-Si, Fe-Ni, Fe-Cr, and Fe-Mo Alloys of High Purity," Jour. Iron and Steel Inst., Vol. 177, p. 93, 1954.
32. Schwartzbart, H., and Low, J. R., "The Yielding and Strain Aging of Carburized and Nitrided Single Crystals of Iron," Trans. Amer. Inst. Mining and Met. Engr., Vol. 185, p. 637, 1949.
33. Smith, L. B., "A Device to Permit Reversed Loading in the U. of I. 20-kip Pulse Loading Machine," M. S. Thesis, Univ. of Ill, 1955.
34. Storm, J. W., "A Device for the Rapid Loading of Small Beams in the University of Illinois 20-kip Pulse Loading Machine," M. S. Thesis, Univ. of Ill., 1955.
35. Taylor, D. B. C., "The Dynamic Straining of Metals Having Definite Yield Points," Jour. Mech. and Phys. of Solids, Vol. 3, p. 38, 1954.
36. Thielsch, H., "Strain Aging of Pressure Vessel Steels," Welding Journal, Welding Res. Supp., p. 283, 1951.
37. Vreeland, T. Jr., Wood, D. S., and Clark, D. S., "A Study of the Mechanism of the Delayed Yield Phenomena," Trans. A.S.M., Vol. 45, p. 620, 1953.
38. Wojcieszak, R. F. and Massard, J. M., "Slow and Rapid Lateral Loading Tests of Simply Supported Beam and Beam-Columns," Report to Dept. of the Air Force, Air Force Special Weapons Center, AFSWC-TR-56-21, 1957.
39. Wood, D. S., and Clark, D. S., "The Influence of Temperature Upon the Time Delay for Yielding in Annealed Mild Steel," Trans. A.S.M., Vol. 43, p. 571, 1951.
40. Wood, D. S., and Clark, D. S., "Delayed Yield in Annealed Steels of Very Low Carbon and Nitrogen Content," Trans. A.S.M., Vol. 44, p. 726, 1952.
41. Yokobori, T., "Delayed Yield and Strain Rate and Temperature Dependence of Yield Point in Iron," Jour. App. Phys., Vol. 25, p. 593, 1954.

APPENDIXDETERMINATION OF FLEXURAL RESISTANCE FROM BEAM DEFORMATION
AND UNIAXIAL STRESS PROPERTIES

As was mentioned in Section 4.4.2 the resisting moment corresponding to the curvature measured in the region of pure flexure was determined by computation using the deformation as determined either from SR-4 gages on the outer fiber of the beam or from the curvature gages applied to the sides of the beam, and three assumptions; (a) that the distribution of strain is linear through the depth of the beam section; (b) that the behavior of the beam material used is the same in both tension and compression; and (c) that the materials information obtained under conditions of uniaxial stress can be applied to the stress gradient conditions existing in the beam.

For single load applications, stress in mild steel is a single valued function of strain. Therefore, the procedure used in computing resisting moment from measured strains is straightforward. It consists of determining the strain distribution in the beam section at the time considered, finding the corresponding stress distribution by use of the comparable stress-strain relationship for the beam material, and computing the resisting moment from the stress distribution and consideration of the geometric properties of the beam section.

For the rapid tests, the procedure used to determine the resisting moment of a specimen section from the measured outer fiber strain or the strain as determined from the curvature gage is complicated by the fact that, under conditions of rapid loading, stress in the material is a function of not only strain, but also strain rate and time. However, by making one other major assumption in addition to those listed above, the desired resisting moment can be obtained. That assumption

is (d) that the stress-time characteristics of the beam material determined from the materials studied under a stress-time relationship that is applied rapidly and is thereafter maintained constant are applicable to the stress-time conditions probably existing in the beam specimens. (The validity of this assumption can be checked later by comparing the stress-time relationship computed for a given fiber in the beam with the stress-time function with which the materials were tested.)

The procedure used for determining the instantaneous resistance of the beam section to an imposed, measured straining is described in the following paragraph. This procedure requires the use of the measured strain-time information obtained for the beam section considered, and information similar to that contained in Figs. A1 and A2, which represent the inelastic time dependent and strain rate dependent behavior of one of the beam materials used.

By using the measured beam deformation as determined either from the SR-4 gages on the outer fiber or the curvature gage applied to the sides of the beam in conjunction with the information of Fig. A2, the times at which the various values of apparent modulus were reached could be determined as is shown in Fig. A3*. For each of these times the stress on the outer fiber could then be computed ($\sigma = \epsilon \cdot \sigma/\epsilon$) so that the stress-time history was known for the particular fiber considered from the initial straining through straining corresponding to $\sigma/\epsilon = 20 \times 10^6$ psi (Fig. A3). For strains beyond this value it was assumed that the instantaneous stress level could be determined from the measured strain rate through use of Fig. A2b. In this manner the stress-time relationship was determined for the particular fiber of the beam considered. This, of course, could be done for as many fibers through the depth of the section as desired (assuming that the

* The strain-delay time overlay used in Fig. A3a may be constructed from Fig. A2a since strain as well as stress may be related to delay time by means of the relationship σ/ϵ .

distribution of strain is linear with depth) so that instantaneous stress "blocks" and, in turn, instantaneous section resistances could be computed. For the BF and BL series flexure specimens the stress blocks were determined by consideration of strains at six locations through the half depth of the section. For the BK series specimens, in which four SR-4 gages were positioned through each half depth of the beam, a correlation of measured strains was made with the assumed linear distribution of strain mentioned in Section 4.4.2. This comparison indicated that the distribution of strain with depth was virtually linear. Therefore, as many individual strains were computed through the half depth of the beam for the BK specimens as were computed for the other flexure tests.

No "elapsed time to $\sigma/\epsilon = 30 \times 10^6$ psi" data for the BK material were available since no SR-4 strain gages were applied to the coupons and the extensometer was not capable of indicating the time at which the secant modulus first departed from a value of 30×10^6 psi. Therefore, in the analysis of this series of specimens the delay for time for $\sigma/\epsilon = 30 \times 10^6$ psi was taken as zero.

TABLE 1

SUMMARY OF UNIAXIAL TESTING PROGRAM

Series	Type of Material (As rolled and as machined except where noted)	Manner of Testing			
		Slow			Rapid
		Loaded	Strained	Cycled	Loaded
RB	Rimmed steel, ASTM A7	X	X	X	X
	Polished	X	X	X	X
	Notched		X		X
	Polished and annealed		X		X
	Notched and annealed				
SP	Semi-killed steel, ASTM A7				
	Polished	X	X	X	X
	Notched		X		X
	Polished and annealed		X		X
	Notched and annealed		X		X
NS	ASTM A7 steel	X	X		X
NR	ASTM A7 steel, annealed		X		X
NN	Low alloy steel		X		X
NL	Low alloy steel	X	X		X
NHY	Nickle-chromium steel		X		X
PS	Semi-killed steel, ASTM A7		X		X
K	Fully-killed steel, ASTM A7		X		X
Q	Low alloy steel, ASTM A242		X		X
T	USS T-1 steel		X		X
A,B	ASTM A7 steel, from rolled 4M section		X		X
L	6061-T6 structural aluminum		X		X

TABLE 2

UNIAXIAL SPECIMEN DESIGNATION CODE

Series RB, SP (Profile Fig. 9)

The numbers or letters in "digit" order are:

1. Specimen Area

1 = 0.100 sq.in. = 0.357 in. D.

2 = 0.200 sq.in. = 0.505 in. D.

2. Specimen Surface

S = Polished smooth (to about 15 μ in. r.m.s.)

M = As Machined (Surface roughness is about 150 μ in. r.m.s.)

N = Polished then notched about 0.01 in. deep

3. Type of Steel

R = Rimmed steel

S = Semi-killed steel

4. Stock Form of Metal

B = Hot rolled bar

P = Hot rolled plate

5. Treatment

A = As rolled

B = Annealed and spheroidized after machining (in Helium atmosphere)

2 1/2 hours at 1690°F.

23 hours at 1330°F.

C = Annealed and spheroidized before machining (in Helium atmosphere)

2 3/4 hours at 1690°F.

23 hours at 1310°F.

6. Identical Specimen Number

1 = first specimen of the type, etc.

Example: Specimen 1SRBA2 is a 0.357 in. D. polished specimen of rimmed steel obtained from hot rolled bar stock left as rolled and is the second specimen of this type.

Series NN, NS (Profile Fig. 11)

NL, NHY (Profile Fig. 9)

NR (Profile Fig. 12)

PS (Profile Fig. 13)

The series designation is suffixed to indicate the orientation of the coupon with respect to the direction of mill rolling of the parent material.

L = Longitudinal

T = Transverse

Series K, Q, T, L (Profile Fig. 13)

No suffix precedes or follows specimen number.

Series PSL-A, K-A (Profile Fig. 13)

A = Reduced gage section over full length of the specimen between threads

TABLE 3 RESULTS OF METALLURGICAL STUDIES

Steel Designation	Specimen Studied	Steel Stock and Treatment	Rockwell "B" Hardness ¹		Decarburization	Microstructure	A.S.T.M. Grain Size
			Surface	Center			
RBA	1SRBA ⁴	Rimmed Steel, Hot rolled 1" ϕ bar As rolled	73	80	---	Fine pearlite in an α matrix Some banding, showing slight directional properties	7
RBB	1NRBB ²	Rimmed Steel Hot rolled 1" ϕ bar Annealed, spheroidized ³	47	66	Surface Decarburized 0.015 to 0.020 inches deep	Coarse pearlite in an α matrix Extensive spheroidization of Fe_3C	-
RBC	1SRBC ⁴	Rimmed Steel Hot rolled 1" ϕ bar Annealed, spheroidized ⁴	62	72	No decarburization	Both coarse and fine pearlite in an α matrix. Some spheroidization of Fe_3C	-
SPA	1NSPA ⁴	Semi-killed Steel Hot rolled 1" plate As rolled	69	79	---	Fine pearlite in an α matrix Little or no directional properties	5
SPB	1NSPB ²	Semi-killed Steel Hot rolled 1" plate Annealed, spheroidized ³	58	66	No decarburization	Both fine and coarse pearlite in an α matrix. Some spheroidization of Fe_3C in the pearlite.	-
NS	T ⁴	Hot rolled 14 gage As rolled	68	45 ⁵	Decarburized total thickness of sheet	A few coarse Fe_3C particles in an α matrix. Some MnS inclusions in center.	-
NR	R ²	Hot rolled 1" plate Annealed, exact treatment unknown.	61	78	Decarburized in banded zones	Banded fine pearlite in an α matrix. Strongly directional properties.	-

1 Average of three readings

2 Readings taken on center of section used for metallurgical studies

3 Treated after machining but before polishing final 0.002 in. - 2 1/2 hr. at 1690°F., 23 hr. at 1330°F.

4 Treated before machining - 2 3/4 hr. at 1690°F., 23 hr. at 1310°F.

5 Specimen section was narrow and some yielding to sides may have occurred.

TABLE 4 CHEMICAL COMPOSITIONS OF SPECIMEN STEELS

Series	Specimen Checked	Description	Chemical Composition (Check Analysis)											
			C	Mn	P	S	Si	Cu	Ni	Cr	N	Al	Mo	V
RBA	2SRBA28	Rimmed steel Hot rolled, 1" ϕ bar	0.29	0.35	0.021	0.052	0.01	--	--	--	0.014	--	--	--
SPA	2SSPAL11	Semi-killed steel Hot rolled, 1" plate	0.27	0.51	0.033	0.036	0.03	--	--	--	0.013	--	--	--
NS	L4	Hot rolled 14 gage sheet	0.05	0.40	0.036	0.018	0.01	--	--	--	0.013	--	--	--
NR	R5	Hot rolled 1" plate Annealed	0.34	0.46	0.025	0.032	0.02	--	--	--	0.013	--	--	--
NN	NL11	Hot rolled 3/16" plate Low alloy	0.18	1.01	0.042	0.039	0.22	0.10	None	0.11	0.017	--	--	--
NL	LT1	Hot rolled 1" plate Low alloy	0.16	1.11	0.027	0.029	0.23	0.33	None	0.13	0.016	--	--	--
NHY	NHYL2		0.13	0.19	0.006	0.011	0.05	None	2.32	1.34	0.010	--	--	--
Q		Hot rolled 3/4" plate ASTM A-242	0.19	1.10	0.022	0.028	0.25	0.43	None	None	--	--	--	0.04
T		Hot rolled 3/4" plate U.S. steel "T-1"	0.11	0.84	0.036	0.015	0.28	0.32	0.99	0.50	--	0.09	0.53	0.025
K	*	Hot rolled 3/4" plate Fully killed steel	0.15	0.87	0.11	0.034	0.16	--	--	--	--	--	--	--

* Ladle Analysis

TABLE 5a SUMMARY OF UNIAXIAL STRESS TESTS AND RESULTS

Specimen	Type of Loading	Testing Machine Used	Bending, %	"Rise time" of load, sec.	Nominal Stress, ksi			Reduction in Area, %	Elongation in 2 in. gage, %	$\frac{\sigma_{uy} - \sigma_{uy}^*}{\sigma_{uy}^*}$	$\frac{\sigma_{uy} - \sigma_{uy}^*}{\sigma_{uy}^*}$	$\frac{\sigma_{uy} - \sigma_{uy}^*}{\sigma_{uy}^*}$	**Time to SR-4 Strain yield, Milliseconds	**Time to $\sigma/\epsilon = 20 \text{ Msi}$ Milliseconds	$\frac{\sigma_{ly} - \sigma_{ly}^*}{\sigma_{ly}^*}$	$\frac{\sigma_{ly} - \sigma_{ly}^*}{\sigma_{ly}^*}$	Rate of Yield at $\sigma = \sigma_{ly}^*$ in./in./sec.
					σ_{uy}	σ_{ly}	σ_{max}										
ISRBA1	Slow $\dot{\epsilon} = C_2$	Baldwin		150	49.4	37.4	63.2	57	34	0.08							
2	Rapid to $\sigma = C_1$	Pulse Ldg	0.9	0.006	52.8					0.15	0.42	88	113				
3	Slow $\dot{\epsilon} = C_2$	Baldwin		200	45.9*	37.0*	62.4*	62	40	0.00							
4	Rapid to $\sigma = C_1$	Pulse Ldg	3.4	0.006	57.4					0.25	0.70	31	49				
ISRBBI	Slow $\dot{\epsilon} = C_2$	Baldwin		80	26.8	21.5	53.8	49	35	0.10							
2	Rapid to $\sigma = C_1$	Pulse Ldg	3.3	0.006	27.9					0.14	0.12	1600					
3	Slow $\dot{\epsilon} = C_2$	Baldwin		80	24.4*	21.6*	54.0*	51	33	0.00							
4	Rapid to $\sigma = C_1$	Pulse Ldg	3.2	0.006	27.2					0.11	0.09	9000					
ISRBC1	Slow $\dot{\epsilon} = C_2$	Baldwin		60	26.0	25.0	58.3	47	34	0.00							
2	Rapid to $\sigma = C_1$	Pulse Ldg	1.6	0.006	31.4					0.21	0.17	240	368				
3	Slow $\dot{\epsilon} = C_2$	Baldwin		80	26.0*	23.4*	57.5*	47	31	0.00							
4	Rapid to $\sigma = C_1$	Pulse Ldg	5.3	0.006	43.0					0.66	0.53	3	12				
INRBA1	Slow $\dot{\epsilon} = C_2$	Baldwin		200	42.9*	35.5*	62.9*	38	36	0.00							
2	Rapid to $\sigma = C_1$	Pulse Ldg	4.0	0.006	53.0					0.23	0.50	16	38				
3	Slow $\dot{\epsilon} = C_2$	Baldwin		200	46.2	36.2	62.8	37	35	0.08							
4	Rapid to $\sigma = C_1$	Pulse Ldg	4.8	0.006	60.8					0.42	0.90	10	19				
INRBB1	Slow $\dot{\epsilon} = C_2$	Baldwin		160	25.8*	22.4*	54.1*	49	39	0.00							
2	Rapid to $\sigma = C_1$	Pulse Ldg	9.7	0.006	31.8					0.23	0.21	108	212				
3	Slow $\dot{\epsilon} = C_2$	Baldwin		160	26.2	21.4	54.6	47	36	0.02							
4	Rapid to $\sigma = C_1$	Pulse Ldg	8.5	0.006	44.5					0.72	0.66	3	12				

*Basic value used in stress parameter

**Time over static upper yield stress, σ_{uy}^*

***Extensometer point marks on gage section

TABLE 5b SUMMARY OF UNIAXIAL STRESS TESTS AND RESULTS

Specimen	Type of Loading	Testing Machine Used	Bending, %	"Rise time" of load, sec.	Nominal Stress, ksi			Reduction in Area, %	Elongation in 2 in. gage, %	$\frac{\sigma_{uy} - \sigma_{uy}^*}{\sigma_{uy}^*}$	$\frac{\sigma_{ly} - \sigma_{ly}^*}{\sigma_{ly}^*}$	**Time to SR-4 Strain yield, Milliseconds	**Time to $\sigma/\epsilon = 20 \text{ Msi}$ Milliseconds	$\frac{\sigma_{ly} - \sigma_{ly}^*}{\sigma_{ly}^*}$	$\frac{\sigma_{ly} - \sigma_{ly}^*}{\sigma_{ly}^*}$	Rate of Yield at $\sigma = \sigma_{ly}^*$ in./in./sec.
					σ_{uy}	σ_{ly}	σ_{max}									
ISSPA1	Slow $\dot{\epsilon} = C$	Baldwin		110	38.2	34.6	67.0	54	34	0.02						
2	Rapid to $\sigma = C_1$	Pulse Ldg	2.4	0.006	43.4					0.16	0.22	132	165			
3	Slow $\dot{\epsilon} = C$	Baldwin		250	37.5*	33.4*	63.7*	60	40	0.00						
4	Rapid to $\sigma = C_1$	Pulse Ldg	2.4	0.006	54.7					0.46	0.66	0	8			
ISSPBL	Slow $\dot{\epsilon} = C$	Baldwin		180	29.1	25.4	60.3	43	38	0.06						
2	Rapid to $\sigma = C_1$	Pulse Ldg	1.5	0.006	33.6					0.23	0.19	88	125			
3	Slow $\dot{\epsilon} = C$	Baldwin		170	27.4*	24.4*	60.4*	44	36	0.00						
4	Rapid to $\sigma = C_1$	Pulse Ldg	6.8	0.006	47.6					0.74	0.61	0	8			
INSPA1	Slow $\dot{\epsilon} = C$	Baldwin		100	32.0*		64.7*	51	34	0.00						
2	Rapid to $\sigma = C_1$	Pulse Ldg	0.4	0.006	43.4					0.36	0.35	44	88			
3	Slow $\dot{\epsilon} = C$	Baldwin		100	38.6	33.4	64.2	57	37	0.21						
4	Rapid to $\sigma = C_1$	Pulse Ldg	1.3	0.006	51.6					0.61	0.60	2	11			
INSPBL	Slow $\dot{\epsilon} = C$	Baldwin		200	29.2	25.2	59.4	35	34	0.11						
2	Rapid to $\sigma = C_1$	Pulse Ldg	1.5	0.006	35.0					0.34	0.26	72	133			
3	Slow $\dot{\epsilon} = C$	Baldwin		200	26.2*	24.4*	59.5*	38	34	0.00						
4	Rapid to $\sigma = C_1$	Pulse Ldg	0.4	0.006	44.4					0.69	0.55	3	11			

*Basic value used in stress parameter

**Time over static upper yield stress, σ_{uy}

***Extensometer point marks on gage section

TABLE 5c SUMMARY OF UNIAXIAL STRESS TESTS AND RESULTS

Specimen	Type of Loading	Testing Machine Used	Bending, %	"Rise time" of load, sec.	Nominal Stress, ksi			Reduction in Area, %	Elongation in 2 in. gage, %	$\frac{\sigma_{uy} - \sigma_{uy}^*}{\sigma_{uy}^*}$	$\frac{\sigma_{uy} - \sigma_{uy}^*}{\sigma_m^* - \sigma_{uy}^*}$	**Time to SR-4 Strain yield, Milliseconds	**Time to $\sigma/\epsilon = 20 \text{ Msi}$ Milliseconds	$\frac{\sigma_{ly} - \sigma_{ly}^*}{\sigma_{ly}^*}$	$\frac{\sigma_{ly} - \sigma_{ly}^*}{\sigma_m^* - \sigma_{ly}^*}$	Rate of Yield at $\sigma = \sigma_{ly}'$ in./in./sec.
					σ_{uy}	σ_{ly}	σ_{max}									
2MRBA 1	Slow	Pulse Ldg	2.6	15.5	52.6					0.08	0.27	4500		0.40	0.59	0.083
2	Rapid to $\sigma = C$	Pulse Ldg	3.2	0.006	51.5					0.06	0.19	1440	1575	0.37	0.54	0.13
3	Rapid to $\sigma = C$	Pulse Ldg	3.4	0.006	54.2					0.11	0.38	310	322	0.44	0.65	0.66
4	Rapid to $\sigma = C$	Pulse Ldg	1.1	0.006	56.8					0.17	0.56	85	87	0.51	0.75	1.08
5	Rapid to $\sigma = C$	Pulse Ldg	0.0	0.006	59.7					0.23	0.76	15	33	0.59	0.86	6.42
6	Rapid to $\sigma = C$	Pulse Ldg	1.8	0.160	50.4					0.03	0.12	1050	1077	0.34	0.50	0.13
7	Rapid to $\sigma = C$	Pulse Ldg	4.4	0.134	51.9					0.07	0.22	194	211	0.38	0.56	0.44
8	Rapid to $\sigma = C$	Pulse Ldg	0.9	0.153	56.4					0.16	0.53	115	134	0.50	0.74	1.10
9	Rapid to $\sigma = C$	Pulse Ldg	10.4	0.120	56.7					0.16	0.55	80	98	0.51	0.75	1.37
10***	Slow $\dot{\epsilon} = C_1$	Baldwin	2.7	68.0	43.1	37.5*	62.5	58	39	0.15	-0.39			0.00	0.00	0.00023
11	Rapid to $\sigma = C$	Pulse Ldg	0.6	0.742	52.2					0.07	0.24	3600	3703	0.39	0.57	0.15
12	Rapid to $\sigma = C$	Pulse Ldg	4.2	0.677	53.0					0.09	0.30	445	501	0.41	0.60	0.17
13	Rapid to $\sigma = C$	Pulse Ldg	0.0	0.560	55.5					0.14	0.47	380	404	0.48	0.70	0.59
14	Rapid to $\sigma = C$	Pulse Ldg	2.3	0.370	56.1					0.15	0.51	195	225	0.50	0.72	0.85
15	Slow	Pulse Ldg	0.8	17.8	51.5					0.06	0.19	3200		0.37	0.54	0.11
16	Slow	Pulse Ldg	2.5	21.5	52.2					0.07	0.24	2000		0.39	0.57	0.082
17	Cycled	Pulse Ldg	2.5		50.0					0.03						
18	Cycled	Baldwin	4.3		48.7*	39.0	63.2*	61	40							
2MRBA19	Cycled	Riehle	7.2		46.8	35.1	62.2	61	39	0.04	-0.13					

*Basic value used in stress parameter

**Time over static upper yield stress, σ_{uy}^*

***Extensometer point marks on gage section

TABLE 5a SUMMARY OF UNIAXIAL STRESS TESTS AND RESULTS

Specimen	Type of Loading	Testing Machine Used	Bending, %	"Rise time" of load, sec.	Nominal Stress, ksi			Reduction in Area, %	Elongation in 2 in. gage, %	$\frac{\sigma_{uy} - \sigma_{uy}^*}{\sigma_{uy}^*}$	$\frac{\sigma_{uy} - \sigma_{uy}^*}{\sigma_m^* - \sigma_{uy}^*}$	**Time to SR-4 Strain yield, Milliseconds	**Time to $\sigma/\epsilon = 20 \text{ Msi}$ Milliseconds	$\frac{\sigma_{ly} - \sigma_{ly}^*}{\sigma_{ly}^*}$	$\frac{\sigma_{ly} - \sigma_{ly}^*}{\sigma_m^* - \sigma_{ly}^*}$	Rate of Yield at $\sigma = \sigma_{ly}^*$ in./in./sec.
					σ_{uy}	σ_{ly}	σ_{max}									
2SRBA 1	Cycled	Pulse Ldg	2.1		50.2					0.00						
2	Rapid to $\sigma = C_1$	Pulse Ldg	0.3	0.006	56.9					0.14	0.50	1165	1212	0.46	0.74	0.14
3	Rapid to $\sigma = C_1$	Pulse Ldg	1.0	0.006	56.8					0.14	0.50	715	746	0.46	0.74	0.21
4	Rapid to $\sigma = C_1$	Pulse Ldg	5.7	0.006	56.9					0.14	0.50	775	789	0.46	0.74	0.24
5	Rapid to $\sigma = C_1$	Pulse Ldg	2.6	0.006	59.2					0.18	0.68	105	165	0.52	0.83	0.67
6	Rapid to $\sigma = C_1$	Pulse Ldg	3.8	0.20	54.4					0.09	0.32	1440	2290	0.39	0.64	0.18
7	Rapid to $\sigma = C_1$	Pulse Ldg	0.6	0.15	54.6					0.09	0.33	780	892	0.40	0.64	0.15
8	Rapid to $\sigma = C_1$	Pulse Ldg	0.0	0.14	57.2					0.14	0.53	950	974	0.47	0.75	0.47
9	Rapid to $\sigma = C_1$	Pulse Ldg	1.8	0.15	59.4					0.19	0.69	240	287	0.52	0.84	0.67
10***	Slow $\dot{\epsilon} = C_2$	Baldwin	11.5	90	44.6	40.1	63.9	60	40	-0.11				0.03	0.04	0.00026
11	Rapid to $\sigma = C_1$	Pulse Ldg	3.8	0.80	53.1					0.06	0.22	750	767	0.36	0.58	0.075
12	Rapid to $\sigma = C_1$	Pulse Ldg	4.6	0.70	53.3					0.07	0.23	4075	4190	0.37	0.59	0.12
13	Rapid to $\sigma = C_1$	Pulse Ldg	3.0	0.70	56.0					0.12	0.44	1000	1028	0.44	0.70	0.21
14	Rapid to $\sigma = C_1$	Pulse Ldg	4.3	0.70	57.8					0.16	0.57	680	692	0.48	0.78	0.24
15	Slow $\dot{\sigma} \neq C$	Pulse Ldg	5.7	20.5	53.8					0.08	0.27	4000		0.38	0.61	0.076
16	Slow $\dot{\sigma} = C$	Pulse Ldg	1.8	30.0	54.2					0.08	0.30	15000		0.39	0.63	0.045
17	Slow Increment	Pulse Ldg	2.5	22.0	48.3					-0.03				0.24	0.38	0.011
18	Slow Increment	Pulse Ldg	1.9	60+	53.1					0.06	0.22	4 min.		0.36	0.58	0.042
2SRBA19	Slow Increment	Pulse Ldg	0.7	60+	53.6					0.07	0.26	3 min.		0.37	0.60	0.029

*Basic value used in stress parameter

**Time over static upper yield stress, σ_{uy}^*

***Extensometer point marks on gage section

TABLE 5e SUMMARY OF UNIAXIAL STRESS TESTS AND RESULTS

Specimen	Type of Loading	Testing Machine Used	Bending, %	"Rise time" of load, sec.	Nominal Stress, ksi			Reduction in Area, %	Elongation in 2 in. gage, %	$\frac{\sigma_{uy} - \sigma_{uy}^*}{\sigma_{uy}^*}$	$\frac{\sigma_{uy}^* - \sigma_{uy}^*}{\sigma_{uy}^*}$	**Time to SR-4 Strain yield, Milliseconds	**Time to $\sigma/c = 20$ Msi Milliseconds	$\frac{\sigma_{ly} - \sigma_{ly}^*}{\sigma_{ly}^*}$	$\frac{\sigma_{ly}^* - \sigma_{ly}^*}{\sigma_{ly}^*}$	Rate of Yield at $\sigma = \sigma_{ly}^*$, in./in./sec.
					σ_{uy}	σ_{ly}	σ_{max}									
2SRBA20	Rapid to $\sigma = C_1$	Pulse Ldg	1.6	0.006	56.5					0.13	0.47	565	621	0.45	0.72	0.27
21	Rapid to $\sigma = C_1$	Pulse Ldg	4.7	0.006	58.8					0.18	0.65	110	130	0.51	0.82	0.65
22	Rapid to $\sigma = C_1$	Pulse Ldg	0.8	0.006	61.2					0.22	0.83	120	131	0.57	0.92	1.17
23	Rapid to $\sigma = C_1$	Pulse Ldg	3.6	0.006	60.2					0.20	0.75	125	135	0.54	0.88	1.85
24	Rapid to $\sigma = C_1$	Pulse Ldg	1.5	0.12	56.0					0.12	0.44	1030	1075	0.44	0.70	0.24
25	Rapid to $\sigma = C_1$	Pulse Ldg	1.6	0.12	57.6					0.15	0.56	85	94	0.48	0.77	0.69
26	Rapid to $\sigma = C_1$	Pulse Ldg	1.3	0.13	60.5					0.21	0.77	125	143	0.55	0.89	1.10
27	Rapid to $\sigma = C_1$	Pulse Ldg	1.3	0.12	60.4					0.21	0.77	150	172	0.55	0.88	1.14
28***	Slow $\dot{\epsilon} = C_2$	Baldwin	2.3	89	45.6	39.0	63.5	61	36	-0.11				0.00	0.00	0.00019
29	Rapid to $\sigma = C_1$	Pulse Ldg	1.4	0.55	56.0					0.12	0.44	390	435	0.44	0.70	0.32
30	Rapid to $\sigma = C_1$	Pulse Ldg	1.1	0.39	56.8					0.14	0.50	220	233	0.46	0.74	0.67
31	Rapid to $\sigma = C_1$	Pulse Ldg	0.6	0.35	57.4					0.15	0.54	180	184	0.47	0.76	0.82
32	Rapid to $\sigma = C_1$	Pulse Ldg	1.9	0.31	58.2					0.16	0.60	140	154	0.49	0.79	1.03
33	Slow $\dot{\epsilon} \neq C$	Pulse Ldg	1.2	26	52.2					0.04	0.15	2500		0.34	0.54	0.083
34	Slow $\dot{\epsilon} \neq C$	Pulse Ldg	0.0	16	51.5					0.03	0.10	1000		0.32	0.52	0.064
35	Cycled	Pulse Ldg	4.6		50.0					0.0						
2SRBA36	Cycled	Baldwin	0.9		50.2*	37.0	63.2*	61	38	0.0						

*Basic value used in stress parameter

**Time over static upper yield stress, σ_{uy}^*

***Extensometer point marks on gage section

TABLE 5f SUMMARY OF UNIAXIAL STRESS TESTS AND RESULTS

Specimen	Type of Loading	Testing Machine Used	Bending, %	"Rise time" of load, sec.	Nominal Stress, ksi			Reduction in Area, %	Elongation in 2 in. gage, %	$\frac{\sigma_{uy} - \sigma_{uy}^*}{\sigma_{uy}^*}$	$\frac{\sigma_{uy} - \sigma_{uy}^*}{\sigma_m^* - \sigma_{uy}^*}$	**Time to SR-4 Strain yield, Milliseconds	**Time to $\sigma/\epsilon = 20 \text{ Mei}$ Milliseconds	$\frac{\sigma_{ly} - \sigma_{ly}^*}{\sigma_{ly}^*}$	$\frac{\sigma_{ly} - \sigma_{ly}^*}{\sigma_m^* - \sigma_{ly}^*}$	Rate of Yield at $\sigma = \sigma_{ly}^*$ in./in./sec.
					σ_{uy}	σ_{ly}	σ_{max}									
2SSPAL1	Cycled	Riehle	4.3		37.0	31.5	63.9	56	43	-0.01						
2	Rapid to $\sigma = C_1$	Pulse Ldg	1.7	0.006	44.6					0.19	0.26	125	145	0.36	0.37	0.17
3	Rapid to $\sigma = C_1$	Pulse Ldg	4.5	0.006	50.9					0.36	0.49	12	21	0.56	0.57	1.87
4	Rapid to $\sigma = C_1$	Pulse Ldg	5.6	0.006	56.1					0.50	0.68	2	3	0.72	0.73	5.27
5	Rapid to $\sigma = C_1$	Pulse Ldg	7.4	0.006	40.0					0.07	0.09	370	453	0.22	0.23	0.068
6	Rapid to $\sigma = C_1$	Pulse Ldg	2.5	0.14	41.9					0.12	0.16	270	363	0.28	0.29	0.042
7	Rapid to $\sigma = C_1$	Pulse Ldg	2.2	0.13	46.1					0.23	0.32	105	130	0.41	0.42	0.32
8	Rapid to $\sigma = C_1$	Pulse Ldg	1.8	0.09	48.9					0.30	0.42	65	67	0.50	0.51	0.43
9	Rapid to $\sigma = C_1$	Pulse Ldg	0.9	0.13	40.4					0.08	0.11	850	926	0.24	0.24	0.016
10	Slow $\dot{\sigma} \neq C$	Pulse Ldg	4.1	22	38.7					0.03	0.04	6500		0.18	0.19	0.0063
11***	Slow $\dot{\epsilon} = C_2$	Baldwin	4.8	59	38.7	32.7*	64.5	56	36	0.03	0.04	2000		0.00	0.00	0.0002
12	Rapid to $\sigma = C_1$	Pulse Ldg	4.6	0.60	41.6					0.11	0.15	450	477	0.27	0.28	0.045
13	Rapid to $\sigma = C_1$	Pulse Ldg	0.0	0.40	44.8					0.19	0.27	250	268	0.37	0.38	0.34
14	Rapid to $\sigma = C_1$	Pulse Ldg	5.2	0.26	46.4					0.24	0.33	140	148	0.42	0.43	0.53
15	Rapid to $\sigma = C_1$	Pulse Ldg	2.9	0.60	40.8					0.09	0.12	1100	1140	0.25	0.25	0.020
16	Cycled	Pulse Ldg	5.8		37.2					-0.01						
2SSPAL17	Cycled	Baldwin	4.7		37.5*	34.5	64.7*	56	34	0.00						

*Basic value used in stress parameter
 **Time over static upper yield stress, σ_{uy}^*

***Extensometer point marks on gage section

TABLE 5g SUMMARY OF UNIAXIAL STRESS TESTS AND RESULTS

Specimen	Type of Loading	Testing Machine Used	Bending, %	"Rise time" of load, sec.	Nominal Stress, ksi			Reduction in Area, %	Elongation in 2 in. gage, %	$\frac{\sigma_{uy} - \sigma_{uy}^*}{\sigma_{uy}^*}$	$\frac{\sigma_{uy}^* - \sigma_{uy}^*}{\sigma_{uy}^* - \sigma_m^*}$	**Time to SR-4 Strain yield, Milliseconds	**Time to $\sigma/\epsilon = 20 \text{ Ms}$, Milliseconds	$\frac{\sigma_{ly} - \sigma_{ly}^*}{\sigma_{ly}^*}$	$\frac{\sigma_{ly}^* - \sigma_{ly}^*}{\sigma_m^* - \sigma_{ly}^*}$	Rate of Yield at $\sigma = \sigma_{ly}^*$, in./in./sec.
					σ_{uy}	σ_{ly}	σ_{max}									
2SSPAT 1	Cycled	Pulse Ldg	1.6		38.4					0.00	0.00					
2	Rapid to $\sigma = C_1$	Pulse Ldg	4.3	0.006	40.6					0.06	0.08	510	561	0.16	0.18	0.037
3	Rapid to $\sigma = C_1$	Pulse Ldg	1.7	0.006	45.0					0.17	0.24	125	138	0.29	0.32	0.38
4	Rapid to $\sigma = C_1$	Pulse Ldg	0.9	0.006	49.4					0.28	0.40	20	33	0.41	0.46	1.60
5	Rapid to $\sigma = C_1$	Pulse Ldg	4.0	0.006	53.2					0.39	0.54	5	10	0.52	0.58	4.46
6	Rapid to $\sigma = C_1$	Pulse Ldg	0.0	0.12	41.0					0.07	0.10	1210	1254	0.17	0.19	0.025
7	Rapid to $\sigma = C_1$	Pulse Ldg	3.1	0.13	41.6					0.08	0.12	340	377	0.19	0.21	0.075
8	Rapid to $\sigma = C_1$	Pulse Ldg	3.2	0.11	45.6					0.19	0.26	85	95	0.30	0.34	0.57
9	Rapid to $\sigma = C_1$	Pulse Ldg	3.3	0.080	48.5					0.26	0.37	45	53	0.39	0.43	1.30
10	Slow $\dot{\sigma} \neq C$	Pulse Ldg	0.0	18	38.5					0.00	0.00	4000		0.10	0.11	0.0078
11***	Slow $\dot{\epsilon} = C_2$	Baldwin	0.0	48	38.2*	35.0*	66.2*	48	38	0.00	0.00			0.00	0.00	0.00019
12	Rapid to $\sigma = C_1$	Pulse Ldg	0.6	0.54	40.2					0.05	0.07	400	617	0.15	0.22	0.032
13	Rapid to $\sigma = C_1$	Pulse Ldg	1.0	0.77	41.5					0.08	0.12	445	540	0.19	0.21	0.076
14	Rapid to $\sigma = C_1$	Pulse Ldg	3.7	0.35	43.9					0.14	0.20	170	202	0.25	0.29	0.25
2SSPAT15	Rapid to $\sigma = C_1$	Pulse Ldg	2.6	0.26	45.7					0.19	0.27	115	155	0.31	0.34	0.51

*Basic value used in stress parameter

***Extensometer point marks on gage section

**Time over static upper yield stress, σ_{uy}^*

TABLE 5b SUMMARY OF UNIAXIAL STRESS TESTS AND RESULTS

Specimen	Type of Loading	Testing Machine Used	Bending, %	"Rise time" of load, sec.	Nominal Stress, ksi			Reduction in Area, %	Elongation in 4 in. gage, %	$\frac{\sigma_{uy} - \sigma_{uy}^*}{\sigma_{uy}}$	$\frac{\sigma_{uy}^* - \sigma_{uy}^*}{\sigma_{uy}^*}$	**Time to SR-4 Strain yield, Milliseconds	**Time to $\sigma/\epsilon = 20 \times 10^6$ psi, Milliseconds	$\frac{\sigma_{ly} - \sigma_{ly}^*}{\sigma_{ly}^*}$	$\frac{\sigma_{ly}^* - \sigma_{ly}^*}{\sigma_{ly}^*}$	Rate of Yield at $\sigma = \sigma_{ly}^*$, in./in./sec.
					σ_{uy}	σ_{ly}	σ_{max}									
NST 9	Slow $\dot{\epsilon} = C_2$	Baldwin	6.8	100	38.2*	36.1*	46.3*	69		0.00						
10	Rapid to $\sigma = C$	Pulse Ldg	2.5	0.006	43.4					0.14	0.64	500	790			
11	Rapid to $\sigma = C$	Pulse Ldg	6.4	0.006	42.8					0.12	0.57	1120	1695			
12	Rapid to $\sigma = C$	Pulse Ldg	3.4	0.006	46.6					0.22	1.04	580	845			
13	Rapid to $\sigma = C$	Pulse Ldg	2.7	0.006	47.6					0.25	1.16	70	115			
NST 14	Slow $\dot{\sigma} \neq C$	Pulse Ldg	4.4	100	43.6					0.14	0.67					
NSL 10	Slow $\dot{\epsilon} = C_2$	Baldwin	16.1	90	34.6*	33.5*	46.1*	65		0.00						
11	Rapid to $\sigma = C$	Pulse Ldg	5.3	0.006	37.9					0.09	0.29	960	1195			
12	Rapid to $\sigma = C$	Pulse Ldg	0.4	0.006	39.9					0.15	0.46	580	975			
13	Rapid to $\sigma = C$	Pulse Ldg	2.1	0.006	43.0					0.24	0.73	70	85			
15	Slow $\dot{\sigma} \neq C$	Pulse Ldg	8.0	60	38.4					0.11	0.33					
NSL 16	Rapid to $\sigma = C$	Pulse Ldg	4.2	0.006	46.4					0.34	1.03	170	275			

*Basic value used in stress parameter

**Time over static upper yield stress, σ_{uy}^*

***Extensometer point marks on gage section

TABLE 5J

SUMMARY OF UNIAXIAL STRESS TESTS AND RESULTS

Specimen	Type of Loading	Testing Machine Used	Bending, %	"Rise time" of load, sec.	Nominal Stress, ksi			Reduction in Area, %	Elongation in 2 in. gage, %	$\frac{\sigma_{uy} - \sigma_{uy}^*}{\sigma_{uy}^*}$	$\frac{\sigma_{uy}^* - \sigma_m^*}{\sigma_m^*}$	**Time to SR-4 Strain yield, Milliseconds	**Time to $\sigma/\epsilon =$ Milliseconds	$\frac{\sigma_{ly} - \sigma_{ly}^*}{\sigma_{ly}^*}$	$\frac{\sigma_{ly}^* - \sigma_m^*}{\sigma_m^*}$	Rate of Yield at $\sigma = \sigma_{ly}^*$, in./in./sec.
					σ_{uy}	σ_{ly}	σ_{max}									
NNL 1	Slow $\dot{\epsilon} = C_2$	Baldwin		90	54.7	51.6	67.9	53	38	0.02				-0.02	-0.05	
2	Rapid to $\sigma = C_1$	Pulse Ldg	7.3	0.006	56.9					0.06	0.23	200		0.09	0.29	
3	Rapid to $\sigma = C_1$	Pulse Ldg	8.5	0.006	60.6					0.13	0.49	12		0.16	0.53	
4	Rapid to $\sigma = C_1$	Pulse Ldg	3.3	0.006	63.1					0.17	0.67	12		0.22	0.69	
5	Rapid to $\sigma = C_1$	Pulse Ldg	4.5	0.006	68.8					0.28	1.07	3		0.31	1.06	
6	Slow $\dot{\epsilon} = C_2$	Baldwin		90	53.7*	52.4*	67.8*	53	38	0.00	0.00			0.00	0.00	
7	Rapid to $\sigma = C$	Pulse Ldg	0.8	0.006	57.9					0.08	0.30	130		0.10	0.36	
8	Rapid to $\sigma = C$	Pulse Ldg	2.8	0.006	59.0					0.10	0.38	35		0.13	0.43	
9	Rapid to $\sigma = C$	Pulse Ldg	3.9	0.006	67.4					0.26	0.97	25		0.29	0.97	
10	Rapid to $\sigma = C$	Pulse Ldg	0.6	0.006	74.9					0.39	1.50	3		0.43	1.46	
11 #1	20 ms. Pulse	Pulse Ldg	3.7	0.006	59.9					0.12	0.44			0.14	0.49	
11 #2	Rapid to $\sigma = C_1$	Pulse Ldg	1.8	0.006	59.0					0.10	0.38	86		0.13	0.43	
NNL12	Slow $\dot{\epsilon} = C_2$	Baldwin		90	55.7	52.1	66.9	56	36	0.04				-0.01	-0.02	

*Basic value used in stress parameter

**Time over static upper yield stress, σ_{uy}^*

***Extensometer point marks on gage section

TABLE 5k SUMMARY OF UNIAXIAL STRESS TESTS AND RESULTS.

Specimen	Type of Loading	Testing Machine Used	Bending, %	"Rise time" of load, sec.	Nominal Stress, ksi			Reduction in Area, %	Elongation in 2 in. gage, %	$\frac{\sigma_{uy} - \sigma_{uy}^*}{\sigma_{uy}^*}$	$\frac{\sigma_{uy} - \sigma_{uy}^*}{\sigma_m^*}$	**Time to SR-4 Strain yield, Milliseconds	**Time to $\sigma/\epsilon =$ Milliseconds	$\frac{\sigma_{ly} - \sigma_{ly}^*}{\sigma_{ly}^*}$	$\frac{\sigma_{ly} - \sigma_{ly}^*}{\sigma_m^*}$	Rate of Yield at $\sigma = \sigma_{ly}'$ in./in./sec.
					σ_{uy}	σ_{ly}	σ_{max}									
NNT 1	Slow $\dot{\epsilon} = C_2$	Baldwin		90	53.1*	51.2*	66.9*	40	34	0.00				0.00	0.00	
2	Rapid to $\sigma = C_1$	Pulse Idg	1.4	0.006	54.8					0.03	0.12	550		0.07	0.23	
3	Rapid to $\sigma = C_1$	Pulse Idg	2.6	0.006	59.1					0.11	0.43	5700		0.15	0.50	
4	Rapid to $\sigma = C_1$	Pulse Idg	4.3	0.006	64.8					0.22	0.85	14		0.27	0.87	
5	Rapid to $\sigma = C_1$	Pulse Idg	0.9	0.006	70.5					0.33	1.26	4		0.38	1.23	
6	Slow $\dot{\epsilon} = C_2$	Baldwin		90	53.5	51.3	66.8	39	34	0.01				0.00	0.01	
7	Rapid to $\sigma = C_1$	Pulse Idg	5.2	0.006	57.9					0.09	0.35	160		0.13	0.43	
8	Rapid to $\sigma = C_1$	Pulse Idg	6.8	0.006	59.7					0.12	0.48	165		0.17	0.54	
9	Rapid to $\sigma = C_1$	Pulse Idg	2.5	0.006	68.4					0.29	1.11	15		0.34	1.10	
10	Rapid to $\sigma = C_1$	Pulse Idg	4.1	0.006	69.3					0.30	1.17	2		0.35	1.15	
11 #1	20 ms. Pulse	Pulse Idg	1.7	0.006	59.6					0.12	0.47			0.16	0.54	
11 #2	Rapid to $\sigma = C_1$	Pulse Idg	4.6	0.006	59.4					0.12	0.46	6		0.16	0.52	
NNT12	Slow $\dot{\epsilon} = C_2$	Baldwin		90	52.9	52.4	67.5	40	32	0.00				0.02	0.08	

*Basic value used in stress parameter

 **Time over static upper yield stress, σ_{uy}^*

***Extensometer point marks on gage section

TABLE 51 SUMMARY OF UNIAXIAL STRESS TESTS AND RESULTS

Specimen	Type of Loading	Testing Machine Used	Bending, %	"Rise time" of load, sec.	Nominal Stress, ksi			Reduction in Area, %	Elongation in 2 in. gage, %	$\frac{\sigma_{uy} - \sigma_{uy}^*}{\sigma_{uy}^*}$	$\frac{\sigma_{uy}^* - \sigma_m^*}{\sigma_m^*}$	**Time to SR-4 Strain yield, Milliseconds	**Time to $\sigma/\epsilon =$ Milliseconds	$\frac{\sigma_{ly} - \sigma_{ly}^*}{\sigma_{ly}^*}$	$\frac{\sigma_{ly}^* - \sigma_m^*}{\sigma_m^*}$	Rate of Yield at $\sigma = \sigma_{ly}$, in./in./sec
					σ_{uy}	σ_{ly}	σ_{max}									
NLL1	Slow $\dot{\epsilon} = C_2$	Baldwin		180	61.0	56.1	79.9	63	34	0.05				0.00	0.00	
2	Slow $\dot{\epsilon} = C_2$	Baldwin		180	57.9*	56.2*	79.9*	61	34	0.00				0.00	0.00	
3	Slow $\dot{\sigma} \neq C$	Pulse Ldg		20	60.4					0.04	0.11			0.07	0.18	
4	Rapid to $\sigma = C_1$	Pulse Ldg	0.7	0.005	70.1					0.21	0.55	80		0.25	0.59	
5	Rapid to $\sigma = C_1$	Pulse Ldg	1.0	0.005	67.9					0.17	0.45	1130		0.21	0.49	
6	Rapid to $\sigma = C_1$	Pulse Ldg	0.2	0.005	72.0					0.24	0.64	46		0.28	0.67	
7	Rapid to $\sigma = C_1$	Pulse Ldg	1.6	0.005	76.2					0.32	0.83	0		0.36	0.84	
NLL8	Rapid to $\sigma = C_1$	Pulse Ldg	0.9	0.005	79.0					0.36	0.96	0		0.41	0.96	
NLT1	Slow $\dot{\epsilon} = C_2$	Baldwin		180	57.8	54.7	77.8	62	35	0.03				0.00	0.00	
2	Slow $\dot{\epsilon} = C_2$	Baldwin		180	56.0*	54.7*	78.0*	60	35	0.00				0.00	0.00	
3	Slow $\dot{\sigma} \neq C$	Pulse Ldg		20	58.9					0.05	0.13			0.08	0.18	
4	Rapid to $\sigma = C_1$	Pulse Ldg	0.3	0.005	64.8					0.16	0.40	108		0.18	0.43	
5	Rapid to $\sigma = C_1$	Pulse Ldg	2.6	0.005	67.2					0.20	0.51	1150		0.23	0.54	
6	Rapid to $\sigma = C_1$	Pulse Ldg	2.5	0.005	71.5					0.28	0.70	13		0.31	0.72	
7	Rapid to $\sigma = C_1$	Pulse Ldg	3.2	0.005	77.2					0.38	0.96	1		0.41	0.97	
NLT8	Rapid to $\sigma = C_1$	Pulse Ldg	3.7	0.005	77.6					0.39	0.98	0.5		0.42	0.98	

*Basic value used in stress parameter

**Time over static upper yield stress, σ_{uy}

***Extensometer point marks on gage section

TABLE 5m SUMMARY OF UNIAXIAL STRESS TESTS AND RESULTS

Specimen	Type of Loading	Testing Machine Used	Bending, %	"Rise time" of load, sec.	Nominal Stress, ksi			Reduction in Area, %	Elongation in 2 in. gage, %	$\frac{\sigma_{uy} - \sigma_{uy}^*}{\sigma_{uy}^*}$	$\frac{\sigma_{uy}^* - \sigma_m^*}{\sigma_m^*}$	**Time to SR-4 Strain yield, Milliseconds	**Time to $\sigma/\epsilon = 20$ Msi Milliseconds	$\frac{\sigma_{ly} - \sigma_{ly}^*}{\sigma_{ly}^*}$	$\frac{\sigma_{ly}^* - \sigma_m^*}{\sigma_m^*}$	Rate of Yield at $\sigma = \sigma_{ly}^*$ in./in./sec.
					σ_{uy}	σ_{ly}	σ_{max}									
NHYL1***	Slow $\dot{\epsilon} = C_2$	Baldwin	0.5	250	80.2*		99.0*	75	26	0.00	0.00					
2	Rapid to $\sigma = C_1$	Pulse Ldg	1.2	0.006	86.0					0.07	0.31	0	30			
3	Rapid to $\sigma = C_1$	Pulse Ldg		0.006	86.2					0.07	0.32	0	2			
4	Rapid to $\sigma = C_1$	Pulse Ldg	15.6	0.006	90.4					0.13	0.54	0	3			
5	Rapid to $\sigma = C_1$	Pulse Ldg	3.7	0.006	90.3					0.13	0.54	0	3			
6	Rapid to $\sigma = C_1$	Pulse Ldg		0.006	91.9					0.15	0.62	0	0			
7	Rapid from $\sigma = 45$ ksi to $\sigma = C_1$	Pulse Ldg	2.6	0.006	83.6					0.04	0.18	0	6			
8	" "	Pulse Ldg	3.2	0.006	87.0					0.08	0.36	0	0			
9	" "	Pulse Ldg	1.1	0.006	88.6					0.10	0.45	0	3			
10	" "	Pulse Ldg	3.3	0.006	87.6					0.09	0.39	0	1			
11	" "	Pulse Ldg	4.1	0.006	91.2					0.14	0.58	0	1			
12***	Slow $\dot{\epsilon} = C_2$	Baldwin	5.3	150	80.3		96.8	75	27	0.00	0.00					
13	Rapid to $\sigma = C_1$	Pulse Ldg	14.3	0.006	83.7					0.04	0.19	0	0			
14	Rapid to $\sigma = C_1$	Pulse Ldg	4.3	0.006	84.0					0.05	0.20	0	2			
15	Rapid to $\sigma = C_1$	Pulse Ldg	0.5	0.006	88.5					0.10	0.44	0	3			
16	Rapid to $\sigma = C_1$	Pulse Ldg		0.006	90.2					0.12	0.53	0	0			
17	Rapid to $\sigma = C_1$	Pulse Ldg		0.006	92.5					0.15	0.65	0	0			

*Basic value used in stress parameter

 **Time over static upper yield stress, σ_{uy}^*

***Extensometer point marks on gage section

 1 Values at $\sigma/\epsilon = 20 \times 10^6$ psi

TABLE 5n

[illegible]

*Basic value used in stress parameter

Time over static upper yield stress, t_{uy}

***Extensometer point marks on gage section

1 Values at $\sigma/\epsilon = 20 \times 10^6$ psi

TABLE 50 SUMMARY OF UNIAXIAL STRESS TESTS AND RESULTS

Specimen	Type of Loading	Testing Machine Used	Bending, %	"Rise time" of load, sec.	Nominal Stress, ksi			Reduction in Area, %	Elongation in 2 in. gage, %	$\frac{\sigma_{uy} - \sigma_{uy}^*}{\sigma_{uy}^*}$	$\frac{\sigma_{uy} - \sigma_{uy}^*}{\sigma_m^* - \sigma_{uy}^*}$	**Time to SR-4 Strain yield, Milliseconds	**Time to $\sigma/\epsilon = 20 \text{ Msi}$, Milliseconds	$\frac{\sigma_{ly} - \sigma_{ly}^*}{\sigma_{ly}^*}$	$\frac{\sigma_{ly} - \sigma_{ly}^*}{\sigma_m^* - \sigma_{ly}^*}$	Rate of Yield at $\sigma = \sigma_{ly}$, in./in./sec.
					σ_{uy}	σ_{ly}	σ_{max}									
NHYT 1***	Slow $\dot{\epsilon} = C_2$	Baldwin	5.4	180	85.2		99.5	68	26	0.01	0.07					
2	Rapid to $\sigma = C_1$	Pulse Ldg	2.7	0.006	85.4					0.02	0.08	150	5395			
3	Rapid to $\sigma = C_1$	Pulse Ldg	1.0	0.006	86.4					0.03	0.14	0	15			
4	Rapid to $\sigma = C_1$	Pulse Ldg	1.9	0.006	88.8					0.06	0.29	50	126			
5	Rapid to $\sigma = C_1$	Pulse Ldg	0.5	0.006	88.5					0.05	0.27	0	2			
6	Rapid to $\sigma = C_1$	Pulse Ldg	1.8	0.006	91.0					0.08	0.43	0	0			
7	Rapid from $\sigma = 45 \text{ ksi}$ to $\sigma = C_1$	Pulse Ldg	0.9	0.006	85.0					0.01	0.06	200	482			
8	" "	Pulse Ldg	9.8	0.006	88.4					0.05	0.27	1200	1937			
9	" "	Pulse Ldg	0.2	0.006	89.2					0.06	0.31	0	9			
10	" "	Pulse Ldg	3.4	0.006	93.1					0.11	0.56	14	17			
11	" "	Pulse Ldg	0.2	0.006	95.9					0.14	0.73	1	7			
12***	Slow $\dot{\epsilon} = C_2$	Baldwin	3.0	150	84.1*		100.3*	69	25	0.00	0.00					
13	Rapid to $\sigma = C_1$	Pulse Ldg	0.7	0.006	86.8					0.03	0.17	0	70			
14	Rapid to $\sigma = C_1$	Pulse Ldg	0.3	0.006	88.1					0.05	0.25	14	1892			
15	Rapid to $\sigma = C_1$	Pulse Ldg	0.1	0.006	88.2					0.05	0.25	0	2			
16	Rapid to $\sigma = C_1$	Pulse Ldg	1.2	0.006	91.3					0.09	0.44	0	3			
17	Rapid to $\sigma = C_1$	Pulse Ldg		0.006	90.7					0.08	0.41	0	0			

*Basic value used in stress parameter
 **Time over static upper yield stress, σ_{uy}^*

***Extensometer point marks on gage section
 1 Values at $\sigma/\epsilon = 20 \times 10^6 \text{ psi}$

TABLE 5q SUMMARY OF UNIAXIAL STRESS TESTS AND RESULTS

Specimen ***	Type of Loading	Testing Machine Used	Bending, °	"Rise time" of load, sec.	Nominal Stress, ksi			Reduction in Area, %	Elongation in 2 in. gage, %	$\frac{\sigma_{uy} - \sigma_{uy}^*}{\sigma_{uy}^*}$	$\frac{\sigma_{uy}^* - \sigma_m^*}{\sigma_{uy}^*}$	**Time to SR-4 Strain yield, Milliseconds	**Time to $\sigma/\epsilon = 20$ Msi Milliseconds	$\frac{\sigma_{ly} - \sigma_{ly}^*}{\sigma_{ly}^*}$	$\frac{\sigma_{ly}^* - \sigma_m^*}{\sigma_{ly}^*}$	Rate of Yield at $\sigma = \sigma_{ly}^*$ in./in./sec.
					σ_{uy}	σ_{ly}	σ_{max}									
Group A1																
T-14M-1F	Slow $\dot{\epsilon} = C$	Baldwin	17.5	60	37.2	35.8	60.7	63	40							
T-14M-2F	Rapid to $\sigma = C_1$	Pulse Ldg	7.7	0.006	43.0					0.16	0.25	151	246	0.20	0.29	0.023
T-24M-1F	Slow $\dot{\epsilon} = C$	Baldwin	8.1	60	33.4	33.2	60.4	59	35							
T-24M-2F	Rapid to $\sigma = C_1$	Pulse Ldg	16.2	0.006	44.8					0.34	0.42	5	19	0.35	0.43	0.100
T-34M-1F	Slow $\dot{\epsilon} = C$	Baldwin	35.6	60	35.1	34.5	61.4	62	38							
T-34M-2F	Rapid to $\sigma = C_1$	Pulse Ldg	5.1	0.006	49.6					0.41	0.55	1	6	0.44	0.56	0.773
W-14M-1F	Slow $\dot{\epsilon} = C$	Baldwin	9.4	60	41.7	40.9	60.8	60	37							
W-14M-2F			No Records													
W-24M-1F	Slow $\dot{\epsilon} = C$	Baldwin	4.0	60	42.2	40.2	59.8	34								
W-24-2F			No Records													
B-14M-1F	Slow $\dot{\epsilon} = C$	Baldwin	16.4	60	36.0	35.1	60.3	61	42							
B-14M-2F			No Records													
B-24M-1F	Slow $\dot{\epsilon} = C$	Baldwin	2.5	60	34.0	33.2	60.4	58	40							
B-24M-2F			No Records													
B-34M-1F	Slow $\dot{\epsilon} = C$	Baldwin	12.8	60	36.2	35.1	61.2	58	36							
B-34M-2F			No Records													

*Basic value used in stress parameter
 **Time over static upper yield stress, σ_{uy}^*

***Extensometer point marks on gage section

TABLE 5r SUMMARY OF UNIAXIAL STRESS TESTS AND RESULTS

Specimen ***	Type of Loading	Testing Machine Used	Bending, %	"Rise time" of load, sec.	Nominal Stress, ksi			Reduction in Area, %	Elongation in 2 in. gage, %	$\frac{\sigma_{uy} - \sigma_{uy}^*}{\sigma_{uy}^*}$	$\frac{\sigma_{uy} - \sigma_{uy}^*}{\sigma_m^* - \sigma_{uy}^*}$	**Time to SR-4 Strain yield, Milliseconds	**Time to $\sigma/\epsilon = 20 \text{ Msi}$, Milliseconds	$\frac{\sigma_{ly} - \sigma_{ly}^*}{\sigma_{ly}^*}$	$\frac{\sigma_{ly} - \sigma_{ly}^*}{\sigma_m^* - \sigma_{ly}^*}$	Rate of Yield at $\sigma = \sigma_{ly}^*$, in./in./s.
					σ_{uy}	σ_{ly}	σ_{max}									
Group A2																
T-14M-1F	Slow $\dot{\epsilon} = C$	Baldwin			38.4	37.4	60.7	63	38							
T-14M-2F	Rapid to $\sigma = C_1$	Pulse Ldg	7.0	0.006	44.0					0.14	0.25	138	163	0.18	0.28	0.057
T-24M-1F	Slow $\dot{\epsilon} = C$	Baldwin			33.2	33.0	60.8	62	39							
T-24M-2F	Rapid to $\sigma = C_1$	Pulse Ldg	3.8	0.006	42.8					0.29	0.34	22	29	0.30	0.35	0.094
T-34M-1F	Slow $\dot{\epsilon} = C$	Baldwin			35.6	35.3	61.6	59	34							
T-34M-2F	Rapid to $\sigma = C_1$	Pulse Ldg	10.3	0.006	49.3					0.38	0.53	6	17	0.40	0.53	0.239
W-14M-1F	Slow $\dot{\epsilon} = C$	Baldwin			41.5	40.6	60.6	66	36							
W-14M-2F	Rapid to $\sigma = C_1$	Pulse Ldg	0.2	0.006	48.8					0.18	0.38	28	74	0.20	0.41	0.051
W-24M-1F	Slow $\dot{\epsilon} = C$	Baldwin			41.3	40.0	60.8	63	40							
W-24M-2F	Rapid to $\sigma = C_1$	Pulse Ldg	0.6	0.006	54.5					0.32	0.68	6	14	0.36	0.70	0.925
B-14M-1F	Slow $\dot{\epsilon} = C$	Baldwin			39.0	35.0	60.7	59	38							
B-14M-2F	Rapid to $\sigma = C_1$	Pulse Ldg		0.006	49.5					0.27	0.48	9	16	0.41	0.56	0.345
B-24M-1F	Slow $\dot{\epsilon} = C$	Baldwin			32.8	32.4	60.8	51	38							
B-24M-2F			No Records													
B-34M-1F	Slow $\dot{\epsilon} = C$	Baldwin			38.8	36.2	61.5	59	38							
B-34M-2F	Rapid to $\sigma = C_1$	Pulse Ldg	7.9	0.006	54.9					0.41	0.71	3	5	0.52	0.74	1.55

*Basic value used in stress parameter

**Time over static upper yield stress, σ_{uy}^*

***Extensometer point marks on gage section

TABLE 5a SUMMARY OF UNIAXIAL STRESS TESTS AND RESULTS

Specimen**	Type of Loading	Testing Machine Used	Bending, %	"Rise time" of load, sec.	Nominal Stress, ksi			Reduction in Area, %	Elongation in 2 in. gage, %	$\frac{\sigma_{uy}^* - \sigma_{uy}}{\sigma_{uy}^*}$	$\frac{\sigma_{uy}^* - \sigma_{uy}}{\sigma_m^* - \sigma_{uy}^*}$	*Time to SR-4 Strain yield, Milliseconds	**Time to $\sigma/\epsilon = 20 \text{ Msi}$ Milliseconds	$\frac{\sigma_{ly} - \sigma_{ly}^*}{\sigma_{ly}^*}$	$\frac{\sigma_{ly} - \sigma_{ly}^*}{\sigma_m^* - \sigma_{ly}^*}$	Rate of Yield at $\sigma = \sigma_{ly}^*$ in./in./sec.
					σ_{uy}	σ_{ly}	σ_{max}									
Group B1																
T-14M-1F	Slow $\dot{\epsilon} = C$	Baldwin	5.6		34.9	34.9	61.5	58	36							
T-14M-2F	Rapid to $\sigma = C_1$	Pulse Ldg	17.5	0.006	42.7					0.22	0.29	15	60	0.22	0.29	0.073
T-24M-1F	Slow $\dot{\epsilon} = C$	Baldwin			32.4	32.4	60.1	60	38							
T-24M-2F			No Records													
T-34M-1F	Slow $\dot{\epsilon} = C$	Baldwin			35.3	34.5	60.8	60	35							
T-34M-2F	Rapid to $\sigma = C_1$	Pulse Ldg	8.3	0.006	48.5					0.37	0.52	11	33	0.40	0.53	0.308
W-14M-1F	Slow $\dot{\epsilon} = C$	Baldwin			40.7	40.2	60.8	63	35							
W-14M-2F	Rapid to $\sigma = C_1$	Pulse Ldg	12.5	0.006	56.0					0.38	0.76	2	5	0.39	0.77	1.21
W-24M-1F	Slow $\dot{\epsilon} = C$	Baldwin			43.5	43.1	62.4	59	33							
W-24M-2F	Rapid to $\sigma = C_1$	Pulse Ldg	10.6	0.006	50.3					0.16	0.36	21	77	0.17	0.37	0.069
B-14M-1F	Slow $\dot{\epsilon} = C$	Baldwin			35.9	35.9	60.9	58	34							
B-14M-2F	Rapid to $\sigma = C_1$	Pulse Ldg	5.8	0.006	48.6					0.35	0.51	6	11	0.35	0.51	0.507
B-24M-1F	Slow $\dot{\epsilon} = C$	Baldwin			34.2	32.9	60.0	58	38							
B-24M-2F	Rapid to $\sigma = C_1$	Pulse Ldg	2.9	0.006	54.1					0.58	0.77	2	3	0.64	0.78	3.23
B-34M-1F	Slow $\dot{\epsilon} = C$	Baldwin	10.7		37.8	37.4	61.0	59	35							
B-34M-2F	Rapid to $\sigma = C_1$	Pulse Ldg	15.8	0.006	53.3					0.41	0.67	2	4	0.42	0.67	1.75

*Basic value used in stress parameter

**Time over static upper yield stress, σ_{uy}^*

***Extensometer point marks on gage section

TABLE 5t

SUMMARY OF UNIAXIAL STRESS TESTS AND RESULTS

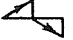
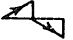

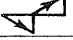
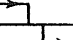
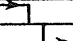
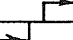
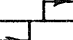


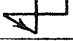
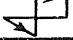
Specimen***	Type of Loading	Testing Machine Used	Bending, %	"Rise time" of load, sec.	Nominal Stress, ksi			Reduction in Area, %	Elongation in 2 in. gage, %	$\frac{\sigma_{uy} - \sigma_{uy}^*}{\sigma_{uy}^*}$	$\frac{\sigma_{uy} - \sigma_{uy}^*}{\sigma_m^* - \sigma_{uy}^*}$	**Time to SR-4 Strain yield, Milliseconds	**Time to $\sigma/c = 20$ Msi Milliseconds	$\frac{\sigma_{ly} - \sigma_{ly}^*}{\sigma_{ly}^*}$	$\frac{\sigma_{ly} - \sigma_{ly}^*}{\sigma_m^* - \sigma_{ly}^*}$	Rate of Yield at $\sigma = \sigma_{ly}$, in./in./sec.
					σ_{uy}	σ_{ly}	σ_{max}									
Group B2																
T-14M-1F	Slow $\dot{\epsilon} = C$	Baldwin			34.3	34.1	60.3	61	38							
T-14M-2F	Rapid to $\sigma = C_1$	Pulse Ldg	0.6	0.006	42.6					0.24	0.32	36	95	0.25	0.32	0.046
T-24M-1F	Slow $\dot{\epsilon} = C$	Baldwin			32.0	31.8	59.8	61	38							
T-24M-2F	Rapid to $\sigma = C_1$	Pulse Ldg	11.9	0.006	42.2					0.32	0.37	11	35	0.33	0.37	0.089
T-34M-1F	Slow $\dot{\epsilon} = C$	Baldwin			35.7	35.3	60.2	59	36							
T-34M-2F	Rapid to $\sigma = C_1$	Pulse Ldg	14.7	0.006	48.7					0.36	0.53	4	12	0.38	0.54	0.433
W-14M-1F	Slow $\dot{\epsilon} = C$	Baldwin			41.3	38.7	60.5	63	35							
W-14M-2F	Rapid to $\sigma = C_1$	Pulse Ldg	0.1	0.006	54.5					0.32	0.69	2	11	0.41	0.72	0.732
W-24M-1F	Slow $\dot{\epsilon} = C$	Baldwin			43.5	41.7	61.1	64	34							
W-24M-2F	Rapid to $\sigma = C_1$	Pulse Ldg	15.2	0.006	49.5					0.14	0.34	25	62	0.19	0.40	0.135
B-14M-1F	Slow $\dot{\epsilon} = C$	Baldwin			35.0	34.3	60.2	60	36							
B-14M-2F	Rapid to $\sigma = C_1$	Pulse Ldg	5.7	0.006	47.6					0.36	0.50	5	15	0.39	0.51	0.386
B-24M-1F	Slow $\dot{\epsilon} = C$	Baldwin			34.2	33.2	60.0	58	40							
B-24M-2F	Rapid to $\sigma = C_1$	Pulse Ldg	5.5	0.006	53.9					0.58	0.76	1	2	0.62	0.77	2.92
B-34M-1F	Slow $\dot{\epsilon} = C$	Baldwin			35.6	35.2	60.9	60	40							
B-34M-2F	Rapid to $\sigma = C_1$	Pulse Ldg	0.6	0.006	52.9					0.48	0.68	2	4	0.50	0.69	2.09

*Basic value used in stress parameter

**Time over static upper yield stress, σ_{uy}

***Extensometer point marks on gage section

TABLE 5u SUMMARY OF UNIAXIAL STRESS TESTS AND RESULTS

Specimen	Type of Loading (All 2 cycle)	Testing Machine Used	Bending, %	"Rise time" of load, sec.	Nominal Stress, ksi			Reduction in Area, %	Elongation in in. gage, %	$\frac{\sigma_{uy} - \sigma_{uy}^*}{\sigma_{uy}^*}$	$\frac{\sigma_{uy} - \sigma_{uy}^*}{\sigma_{uy}^*}$	$\frac{\sigma_{uy} - \sigma_{uy}^*}{\sigma_{uy}^*}$	**Time to SR-4 Strain yield, Milliseconds	**Time to $\sigma/\sigma = 20$ Msi Milliseconds	$\frac{\sigma_{ly} - \sigma_{ly}^*}{\sigma_{ly}^*}$	$\frac{\sigma_{ly} - \sigma_{ly}^*}{\sigma_{ly}^*}$	Rate of Yield at $\sigma = \sigma_{ly}$ in./in./sec.
					σ_{uy}	σ_{ly}	σ_{max}										
S.R.	Slow $\sigma = C_1$	Pulse Ldg			39.9*												
	Both Cycles																
1	Tension-Comp.		4.9		42.2												
2	Tension-Comp.		15.3		41.4												
3	Compression-Ten.		6.5		48.5												
4	Compression-Ten.		16.0		47.2												
D.R.	Rapid to $\sigma = C$	Pulse Ldg			39.9*												
	Both Cycles																
1	Tension-Comp.		5.6		44.0									690			
2	Tension-Comp.		8.5		46.0									400			
3	Compression-Ten.		1.0		44.0	Tens	****							120			
4	Compression-Ten.		3.7		49.3									130			
S.D.R.	Slow to $\sigma < \sigma_{uy}^*$	Pulse Ldg			39.9*												
	Rapid to $-\sigma = C$																
1	Tension-Comp.		3.3		43.6									1930			
2	Tension-Comp.		0.7		44.0									160			
3	Compression-Ten.		1.6		45.7									730			
4	Compression-Ten.		2.0		48.6									1180			

*Basic value used in stress parameter

**Time over static upper yield stress, σ_{uy}

***Extensometer point marks on gage section

****No yield following 48.4 ksi compression

TABLE 5v

SUMMARY OF UNIAXIAL STRESS TESTS AND RESULTS

Specimen	Type of Loading	Testing Machine Used	Bending, %	"Rise time" of load, sec.	Nominal Stress, ksi			Reduction in Area, %	Elongation in 1.875 in. gage, %	$\frac{\sigma_{uy} - \sigma_{uy}^*}{\sigma_{uy}^*}$	$\frac{\sigma_{ly} - \sigma_{ly}^*}{\sigma_{ly}^*}$	Time to SR-4 Strain yield, Milliseconds	Time to $\sigma/c = 20 \times 10^6$, Milliseconds	$\frac{\sigma_{ly} - \sigma_{ly}^*}{\sigma_{ly}^*}$	$\frac{\sigma_{ly} - \sigma_{ly}^*}{\sigma_{ly}^*}$	Rate of Yield at $\sigma = \sigma_{ly}^*$, in./in./sec.
					σ_{uy}	σ_{ly}	σ_{max}									
PSL 1	Slow $\delta = c_1$	Pulse Ldg	0.9	99.6		41.0	66.4*	56	25.6	0.01	0.02			0.23	0.23	0.032
	Tension															
2	Rapid to $\sigma = c$	Pulse Ldg	0.6	0.006		45.5				0.12	0.19		250	0.36	0.37	0.176
	Tension															
3	Rapid to $\sigma = c$	Pulse Ldg	3.4	0.006		51.5				0.27	0.42		17	0.54	0.55	2.43
	Tension															
4	Rapid to $\sigma = c$	Pulse Ldg	2.1	0.006		59.5				0.46	0.73		1	0.78	0.79	7.63
	Tension															
5	Rapid to $\sigma = c$	Pulse Ldg	7.3	0.006		42.5				0.06	0.09		545	0.27	0.28	0.045
	Compression															
6	Rapid to $\sigma = c$	Pulse Ldg	2.8	0.006		53.6				0.34	0.52		12	0.60	0.61	3.76
	Compression															
7	Rapid to $\sigma = c$	Pulse Ldg	3.2	0.006		65.0				0.62	0.95		1	0.95	0.96	11.65
	Compression															
8	Slow $\delta = c_1$	Pulse Ldg	6.1	82.0		40.0				0.00	0.00			0.20	0.20	0.014
	Compression															

*Basic value used in stress parameter

**Time over static upper yield stress, σ_{uy}^*

***Extensometer point marks on gage section

TABLE 5w

[illegible]

*Basic value used in stress parameter

Time over static upper yield stress, σ_{uy}^*

***Extensometer point marks on gage section

TABLE 5x. SUMMARY OF UNIAXIAL STRESS TESTS AND RESULTS

[illegible]

*Basic value used in stress parameter
**Time over static upper yield stress, σ_{uy}^*

***Extensometer point marks on page section

TABLE 5y

SUMMARY OF UNIAXIAL STRESS TESTS AND RESULTS

Specimen	Type of Loading	Testing Machine Used	Bending, %	"Rise time" of load, sec.	Nominal Stress, ksi			Reduction in Area, %	Elongation in 1.875 in. gage, %	$\frac{\sigma_{uy} - \sigma_{uy}^*}{\sigma_{uy}^*}$	$\frac{\sigma_{uy}^* - \sigma_{uy}^{**}}{\sigma_{uy}^{**} - \sigma_m^{**}}$	**Time to SR-4 Strain yield, Milliseconds	**Time to $\frac{\sigma}{\epsilon} = 20 \times 10^6$, Milliseconds	$\frac{\sigma_{ly} - \sigma_{ly}^*}{\sigma_{ly}^*}$	$\frac{\sigma_{ly}^* - \sigma_{ly}^{**}}{\sigma_m^{**} - \sigma_{ly}^{**}}$	Rate of Yield at $\sigma = \sigma_{ly}^*$, in./in./sec.
					σ_{uy}	σ_{ly}	σ_{max}									
PST 1	Slow $\delta = c_1$	Pulse Ldg	1.9	59.8		41.7	65.9	48	22.4	0.05	0.07			0.23	0.25	0.055
	Tension															
2	Rapid to $\sigma = c_1$	Pulse Ldg	3.7	0.006		42.8				0.07	0.11		348	0.27	0.29	0.375
	Tension															
3	Rapid to $\sigma = c$	Pulse Ldg	2.6	0.006		50.4				0.26	0.42		23	0.49	0.53	3.8
	Tension															
4	Rapid to $\sigma = c$	Pulse Ldg	3.7	0.006		57.8				0.45	0.71		1	0.71	0.76	19
	Tension															
5	Rapid to $\sigma = c$	Pulse Ldg	1.5	0.006		43.9				0.09	0.15		400	0.21	0.27	-
	Compression															
6	Rapid to $\sigma = c$	Pulse Ldg	0.9	0.006		54.5				0.36	0.57		14	0.51	0.63	3.25
	Compression															
7	Rapid to $\sigma = c$	Pulse Ldg	6.8	0.006		64.9				0.61	0.98		0	0.79	0.99	22.6
	Compression															
8	Slow $\delta = c_1$	Pulse Ldg	3.4	62.5		40.8				0.01	0.02			0.13	0.16	0.013
	Compression															

*Basic value used in stress parameter
 **Time over static upper yield stress, σ_{uy}^*

***Extensometer point marks on gage section

TABLE 5aa SUMMARY OF UNIAXIAL STRESS TESTS AND RESULTS

[illegible]

*Basic value used in stress parameter

**Time over static upper yield stress, σ_{uy}

***Extensometer point marks on gage section

TABLE 5bb SUMMARY OF UNIAXIAL STRESS TESTS AND RESULTS

[illegible]

*Basic value used in stress parameter

**Time over static upper yield stress, σ_{uy}

***Extensometer point marks on gage section

TABLE 5cc SUMMARY OF UNIAXIAL STRESS TESTS AND RESULTS

[illegible]

*Basic value used in stress parameter

Time over static upper yield stress, σ_{uy}^*

***Extensometer point marks on gage section

TABLE 5dd SUMMARY OF UNIAXIAL STRESS TESTS AND RESULTS

[illegible]

*Basic value used in stress parameter

Time over static upper yield stress, τ_{uy}

***Extensometer point marks on gage section

TABLE 5ee SUMMARY OF UNIAXIAL STRESS TESTS AND RESULTS

[illegible]

*Basic value used in stress parameter

**Time over static upper yield stress, σ_{uy}

***Extensometer point marks on gage section

TABLE 5ff SUMMARY OF UNIAXIAL STRESS TESTS AND RESULTS

Specimen	Type of Loading	Testing Machine Used	Bending, %	"Rise time" of load, sec.	Nominal Stress, ksi			Reduction in Area, %	Elongation in 1.875 in. gage, %	$\frac{\sigma_{uy} - \sigma_{uy}^*}{\sigma_{uy}^*}$	$\frac{\sigma_{uy} - \sigma_{uy}^*}{\sigma_m^* - \sigma_{uy}^*}$	**Time to SR-4 Strain yield, Milliseconds	**Time to $\sigma/\epsilon =$ Milliseconds	$\frac{\sigma_{ly} - \sigma_{ly}^*}{\sigma_{ly}^*}$	$\frac{\sigma_{ly} - \sigma_{ly}^*}{\sigma_m^* - \sigma_{ly}^*}$	Rate of Yield at $\sigma = \sigma_{ly}^*$ in./in./sec.
					σ_{uy}	σ_{ly}	σ_{max}									
	Tension	Pulse Ldg														
T 1	Slow $\dot{\epsilon} = c_1$		6.5	110	113.5*		130.1	89	18.9							
2	Rapid to $\sigma = c$			0.006	125.5									0.11	0.69	1.1
4	Rapid to $\sigma = c$			0.006	122.5									0.08	0.52	0.22
5	Rapid to $\sigma = c$			0.006	120.4									0.06	0.40	0.15
7	Rapid to $\sigma = c$			0.006	117.3									0.03	0.22	0.08
8	Slow $\dot{\epsilon} = c_1$		2.8	77	113.5		130.8*	89	18.4							
	Compression	Pulse Ldg														
T 9	Slow $\dot{\epsilon} = c_1$			69	120.0											
10	Rapid to $\sigma = c$			0.006	118.8									0.05	0.31	0.10
12	Rapid to $\sigma = c$			0.006	120.6									0.06	0.41	0.16
15	Rapid to $\sigma = c$			0.006	121.7									0.07	0.47	0.20
16	Slow $\dot{\epsilon} = c_1$			62	120.0											

*Basic value used in stress parameter

**Time over static upper yield stress, σ_{uy}^*

***Extensometer point marks on gage section

TABLE 5gg SUMMARY OF UNIAXIAL STRESS TESTS AND RESULTS

Specimen	Type of Loading	Testing Machine Used	Bending, %	"Rise time" of load, sec.	Nominal Stress, ksi			Reduction in Area, %	Elongation in 1.875 in. gage, %	$\frac{\sigma_{uy} - \sigma_{uy}^*}{\sigma_{uy}^*}$	$\frac{\sigma_{uy}^* - \sigma_{uy}}{\sigma_m^* - \sigma_{uy}^*}$	**Time to SR-4 Strain yield, Milliseconds	**Time to $\sigma/\epsilon =$ Milliseconds	$\frac{\sigma_{ly} - \sigma_{ly}^*}{\sigma_{ly}^*}$	$\frac{\sigma_{ly}^* - \sigma_{ly}}{\sigma_m^* - \sigma_{ly}^*}$	Rate of Yield at $\sigma = \sigma_{ly}$, in./in./sec.
					σ_{uy}	σ_{ly}	σ_{max}									
	Tension	Pulse Ldg														
L 1	Slow $\dot{\epsilon} = c_1$		1.0	49	42.5*		45.2	43	16.0							
2	Rapid to $\sigma = c$			0.006	44.7											
4	Rapid to $\sigma = c$			0.006	44.4											
5	Rapid to $\sigma = c$			0.006	43.1											
8	Slow $\dot{\epsilon} = c_1$		2.5	50	42.5*		45.4	42	15.4							
	Compression	Pulse Ldg														
L 9	Slow $\dot{\epsilon} = c_1$		4.9	81	41.0*											
10	Rapid to $\sigma = c$			0.007	41.3											
12	Rapid to $\sigma = c$			0.007	42.7											
13	Rapid to $\sigma = c$			0.007	46.1											
15	Rapid to $\sigma = c$			0.007	47.3											
16	Slow $\dot{\epsilon} = c_1$		9.9	82	41.0*											

*Basic value used in stress parameter

**Time over static upper yield stress, σ_{uy}^*

***Extensometer point marks on gage section

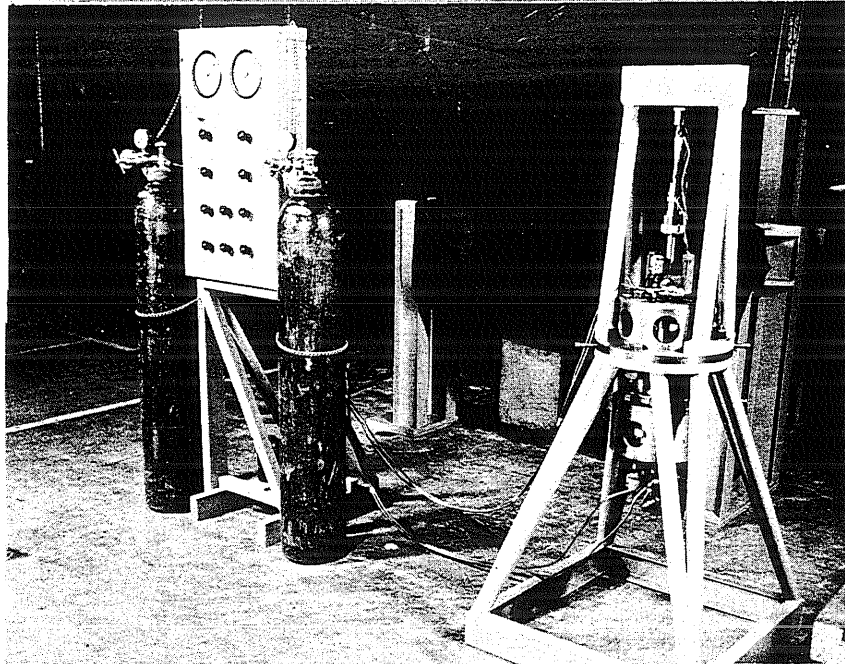


FIG. 1 PRESSURE PANEL, AND 20 KIP PULSE LOADING UNIT ARRANGED FOR TESTING UNIAXIAL TENSION SPECIMENS

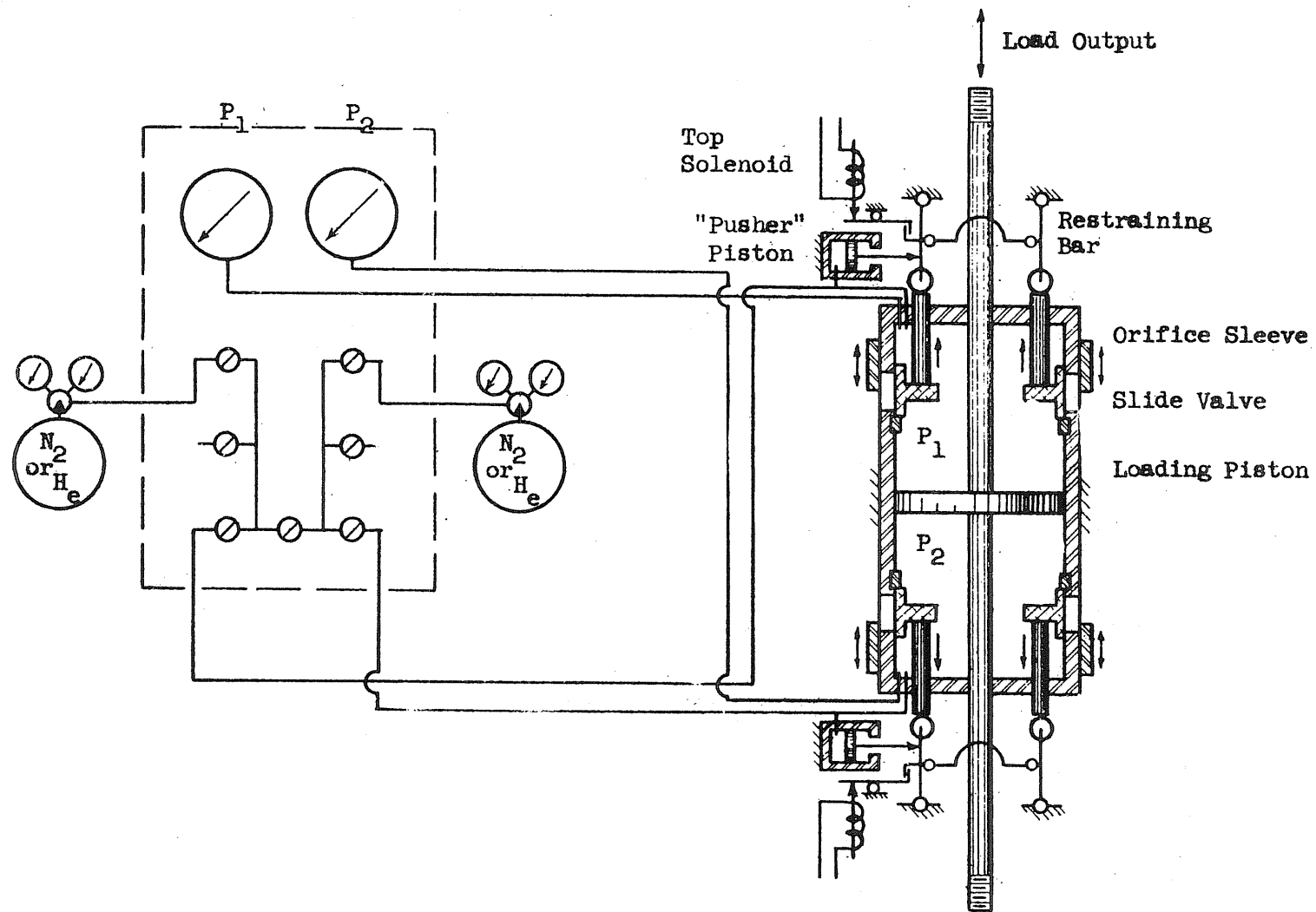


FIG. 2 SCHEMATIC REPRESENTATION OF 20 KIP PULSE LOADING APPARATUS

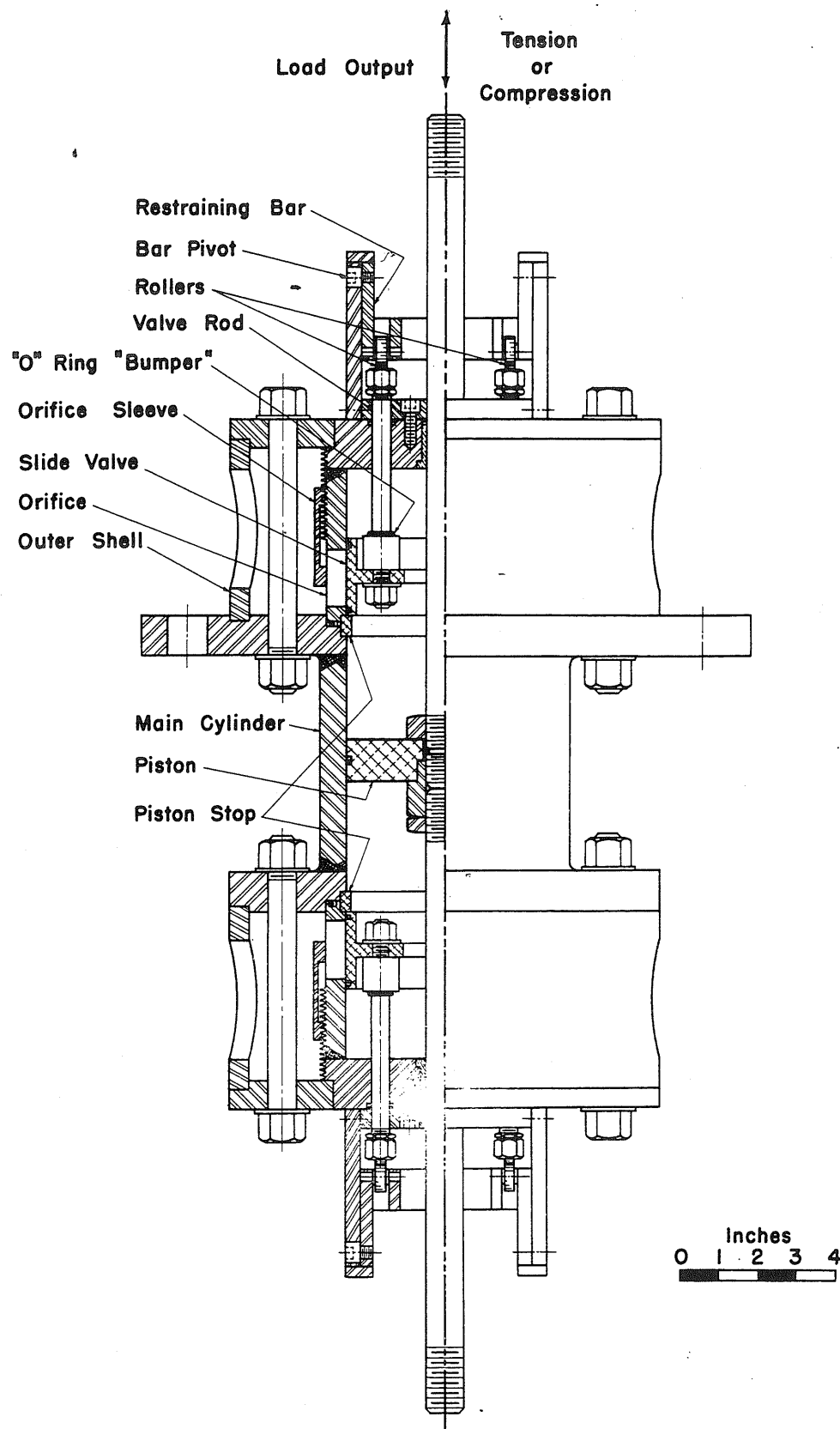


FIG. 3 20 KIP PULSE LOADING UNIT

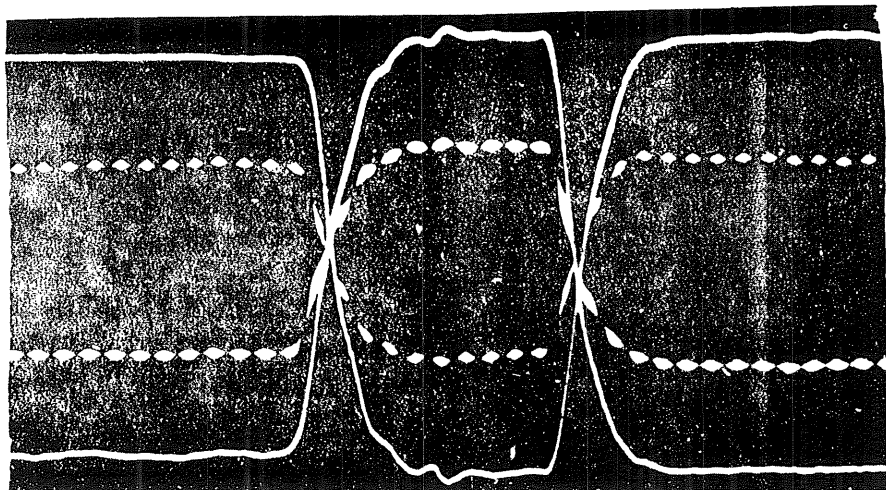


FIG. 4a 10,000 LB. PULSE - RAPID LOADING,
RAPID UNLOADING - 1000 CPS TIMING

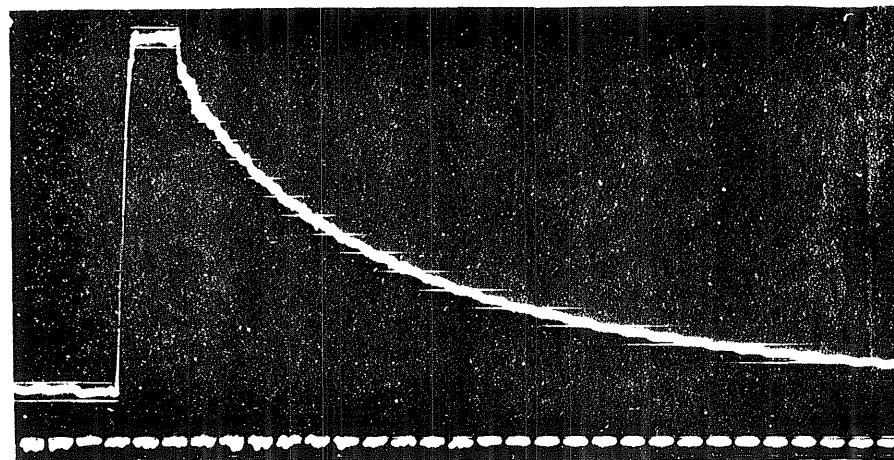


FIG. 4b 10,000 LB. PULSE - RAPID LOADING,
RELATIVELY SLOW UNLOADING - 60 CPS TIMING

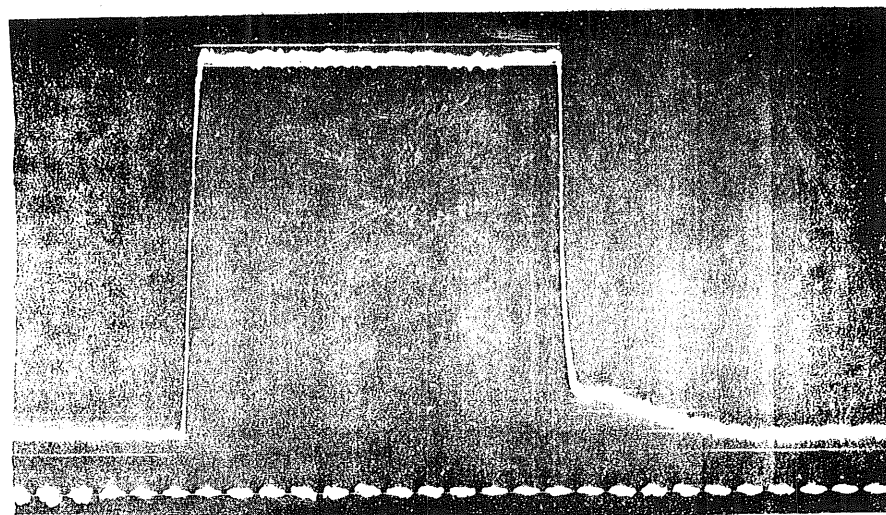


FIG. 4c 10,000 LB. PULSE - RAPID LOADING,
RAPID UNLOADING - 60 CPS TIMING

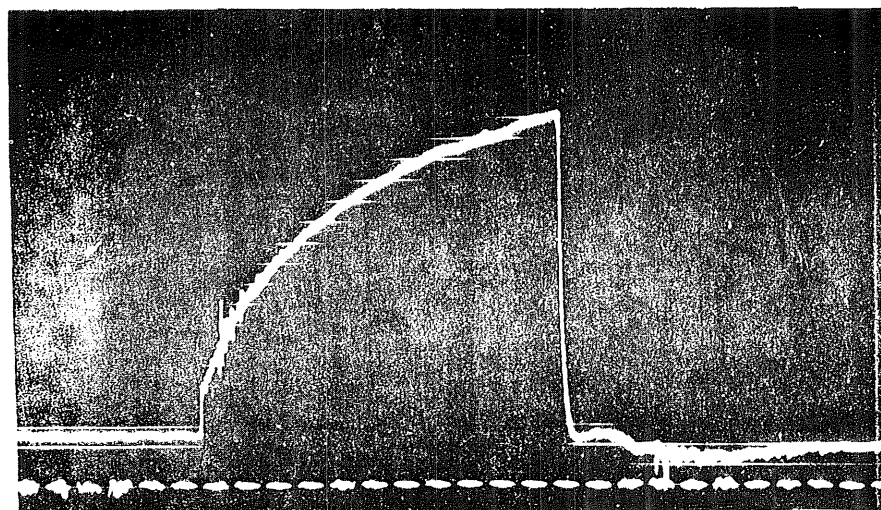


FIG. 4d 10,000 LB. PULSE - RELATIVELY SLOW LOADING,
RAPID UNLOADING - 60 CPS TIMING

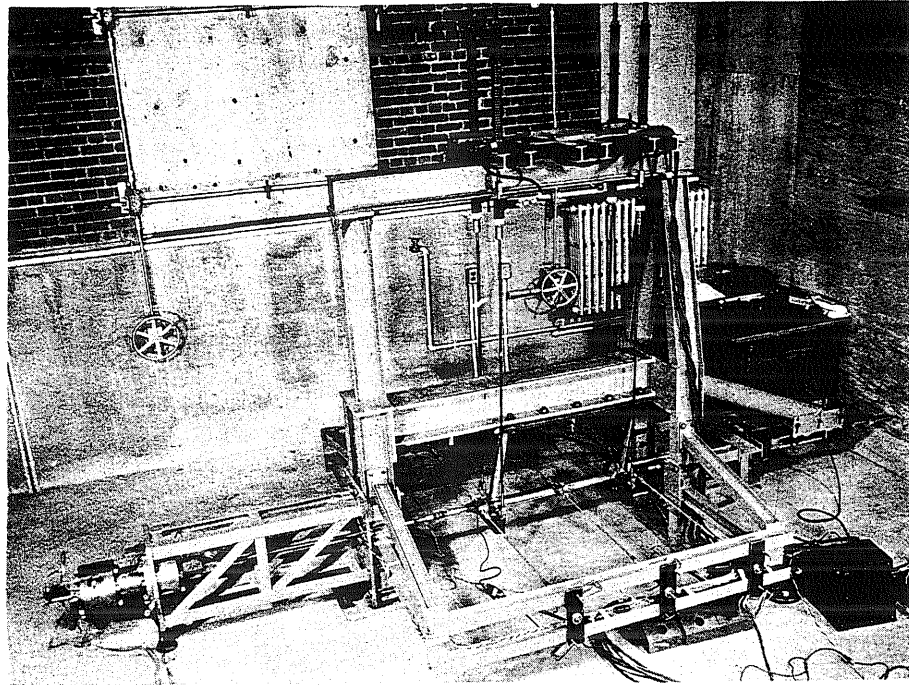


FIG. 5 PULSE LOADING UNIT BEING USED TO TEST MODEL FRAME
(Frame Shown After Testing)

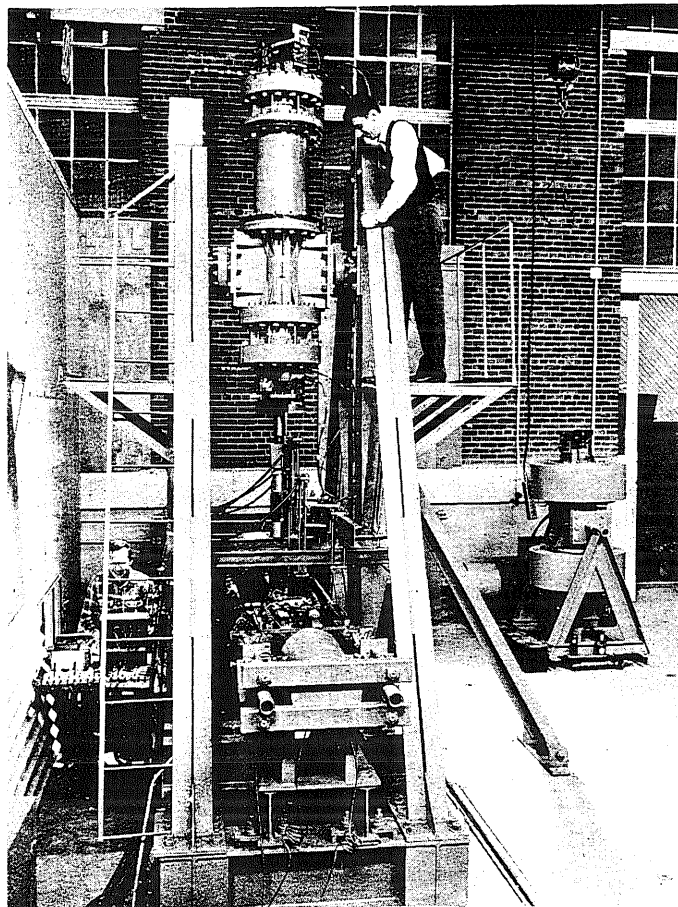


FIG. 6 60 KIP PULSE LOADING UNIT IN FRAME FOR TESTING BEAM-COLUMNS
(A 60 Kip Unit with Outer Chambers is in Background)

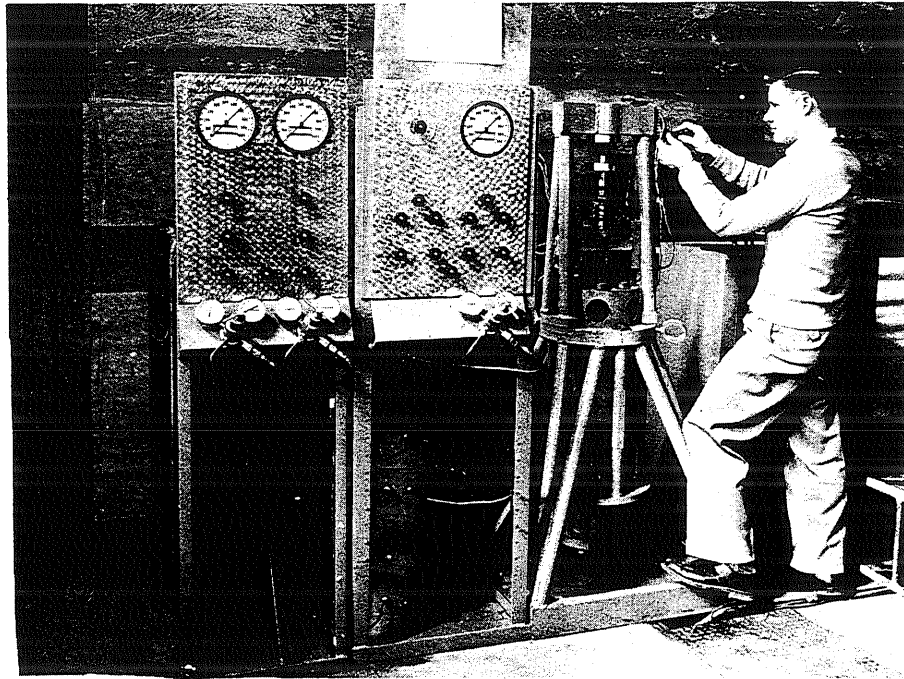


FIG. 7 20 KIP PULSE LOADING UNIT AND 20 KIP STRAINING UNIT CONNECTED
IN SERIES FOR TESTING TENSION-COMPRESSION SPECIMENS;
SHOWN WITH PRESSURE CONTROL PANELS

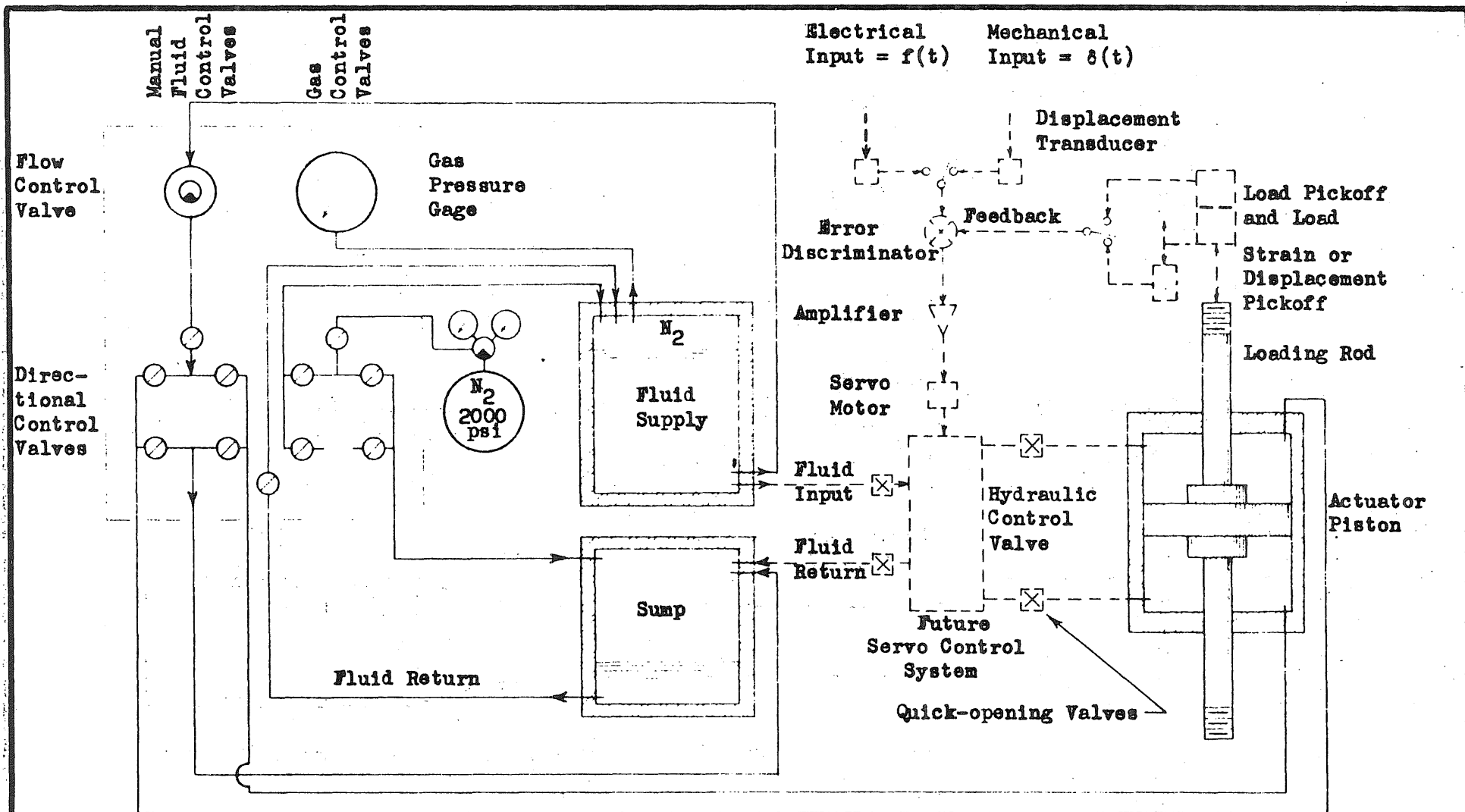


FIG. 8

SCHEMATIC REPRESENTATION OF 20 KIP STRAINING APPARATUS

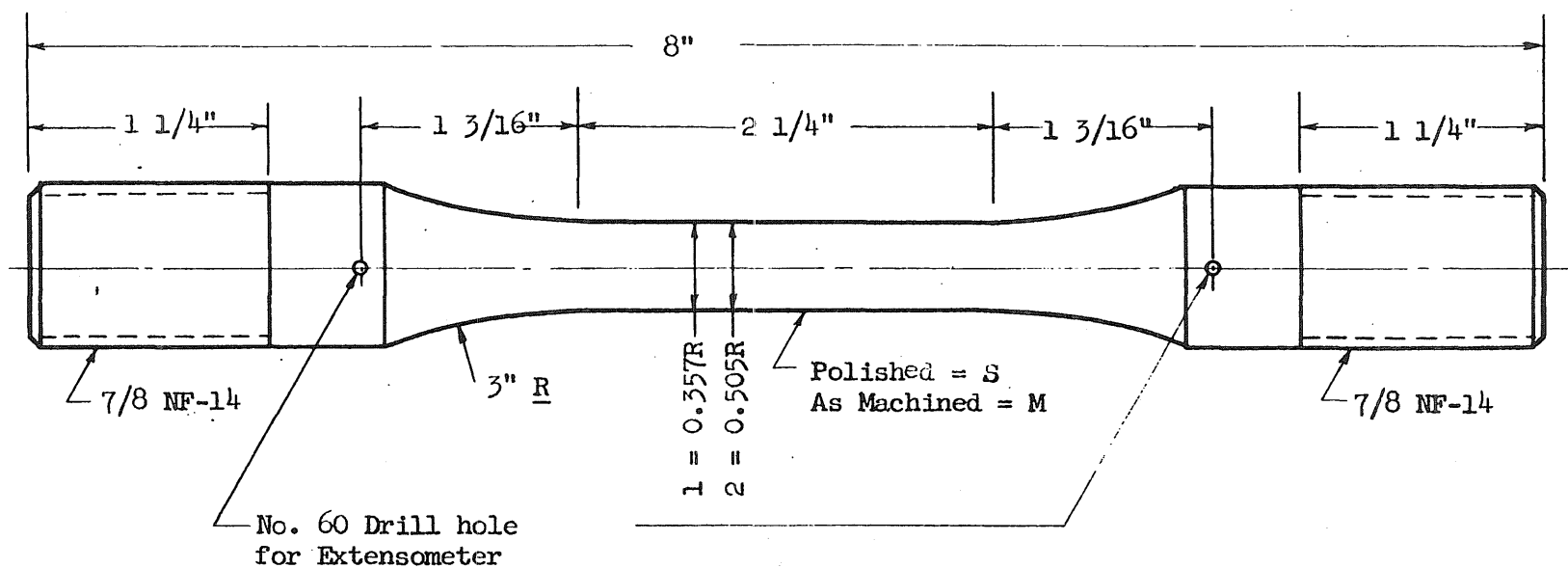


FIG. 9 DIMENSIONS OF TENSILE SPECIMENS
(Series RB, SP, NL, NHY)

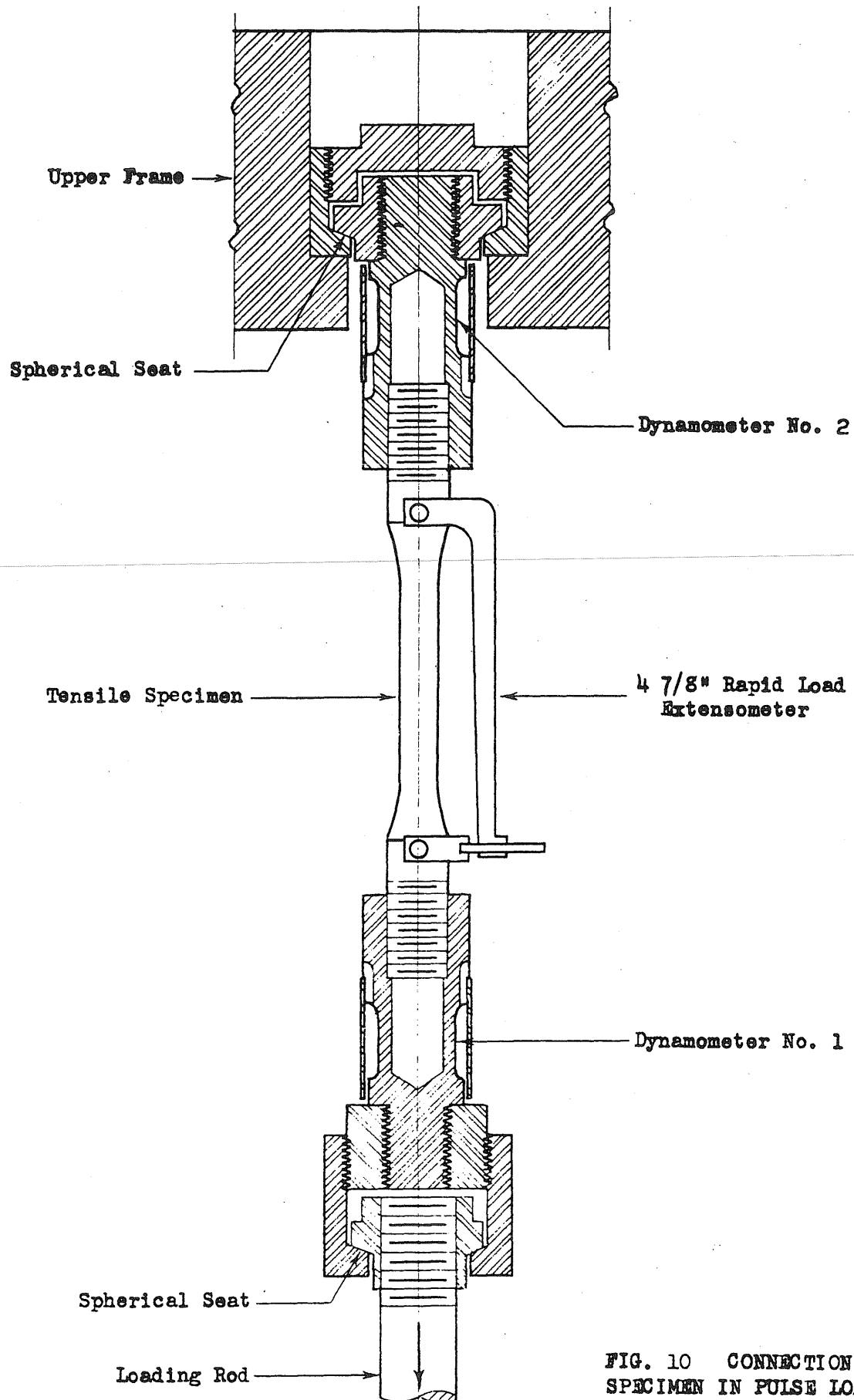
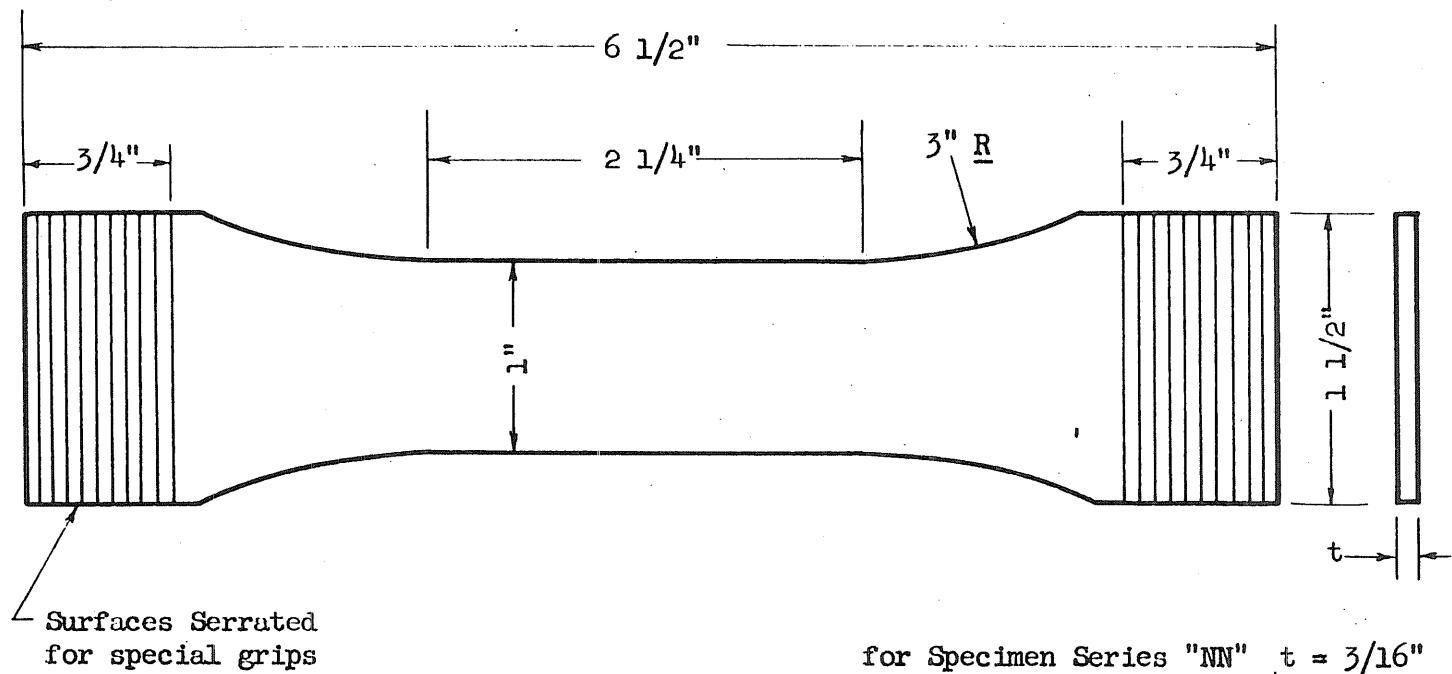


FIG. 10 CONNECTION OF TENSILE SPECIMEN IN PULSE LOADING MACHINE



for Specimen Series "NN" $t = \frac{3}{16}"$
 for Specimen Series "NS" $t = 0.071"$

FIG. 11 DIMENSIONS OF SPECIMENS FROM SHEET STOCK
 (Series NN, NS)

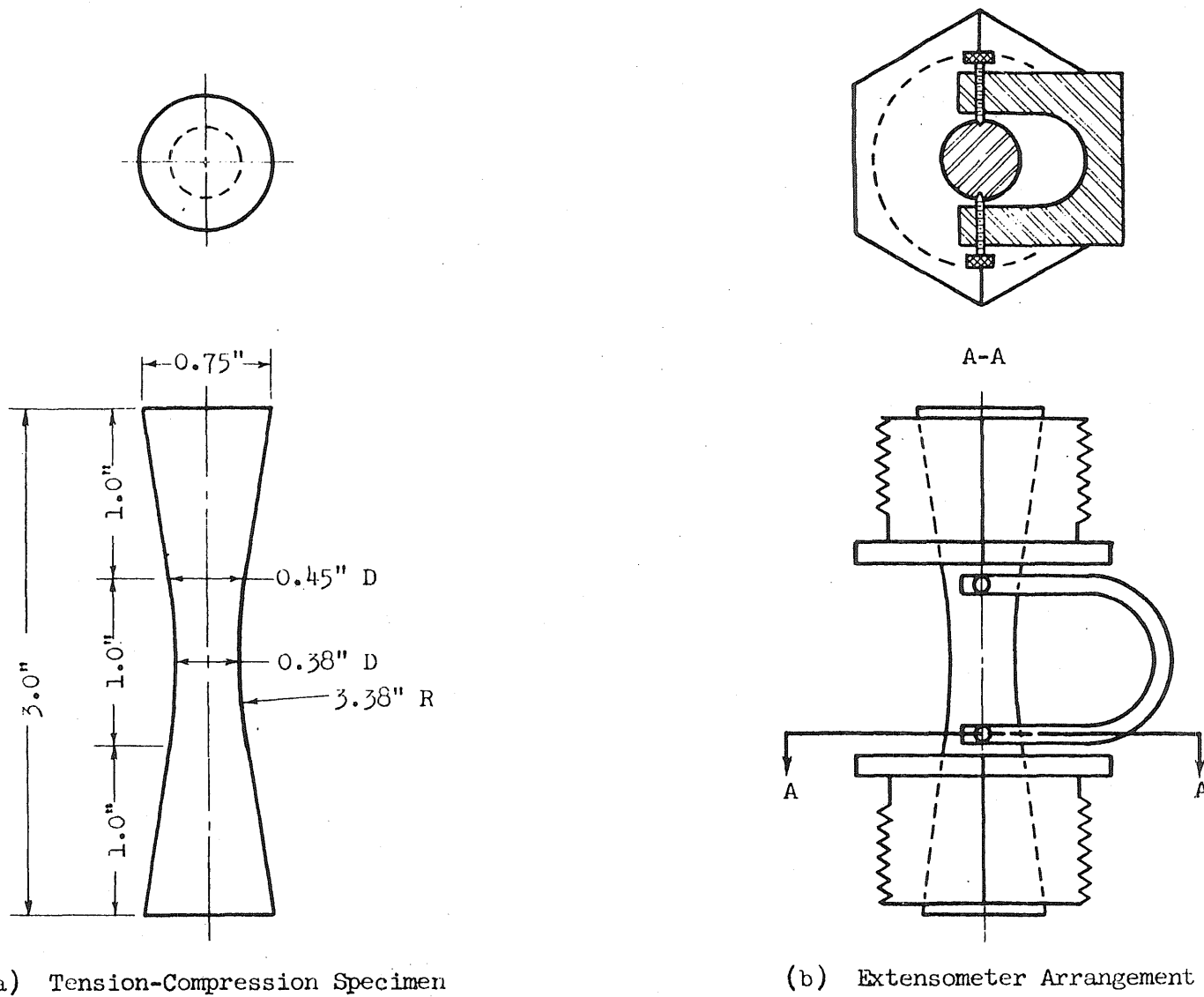


FIG. 12

DIMENSIONS OF PRELIMINARY TENSION-COMPRESSION SPECIMENS

(Series NR)

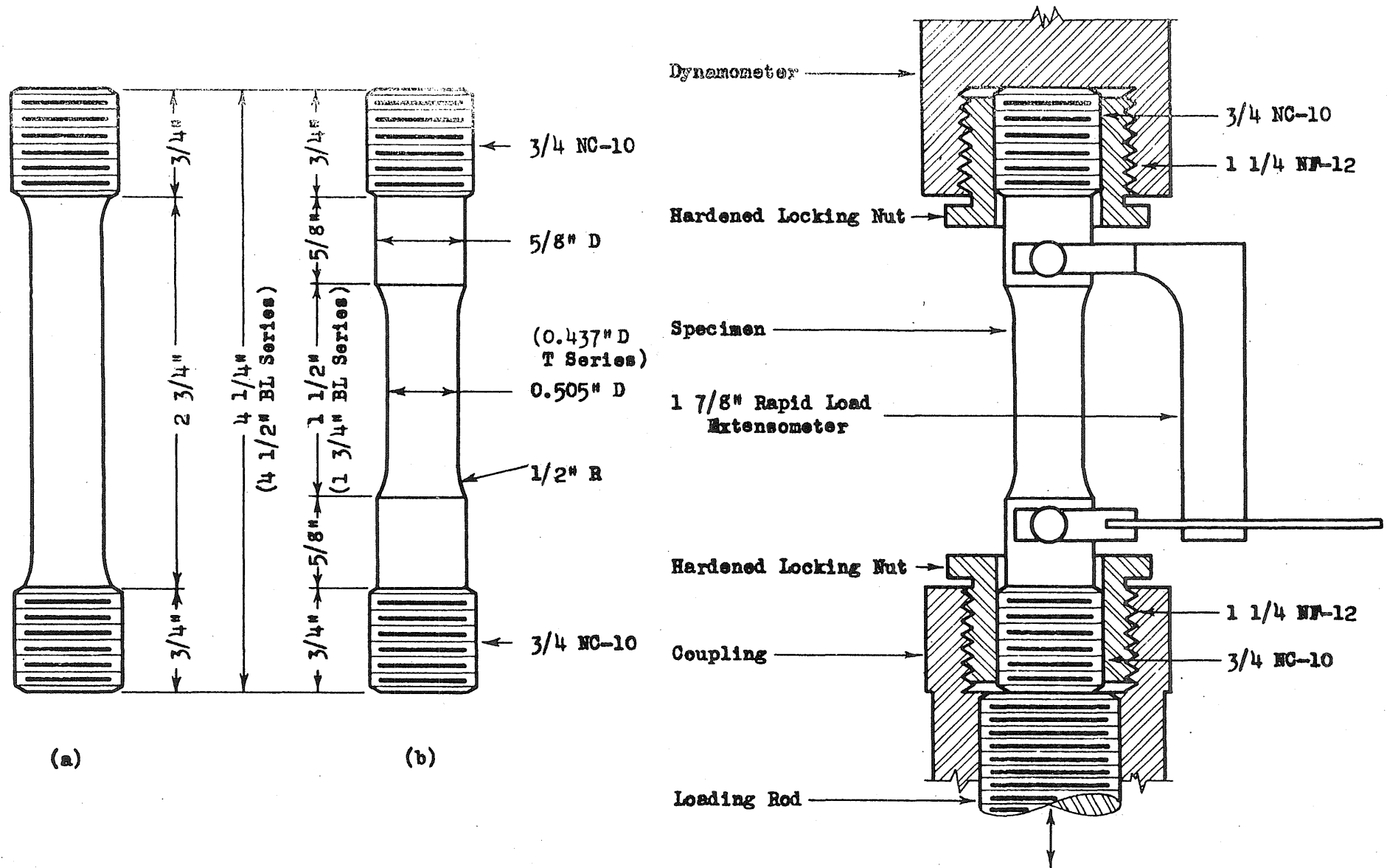


FIG. 13 DIMENSIONS OF TENSION-COMPRESSION SPECIMEN AND MANNER OF CONNECTION
(Series PSL-A, K-A; PS, K, Q, T, L)



FIG. 14a "RBA" STEEL, EDGE OF SPECIMEN 1SRBA⁴
(4% Picrol - 200X)



FIG. 14b "RBB" STEEL, EDGE OF SPECIMEN 1NRBB²
(4% Picrol - 200X)

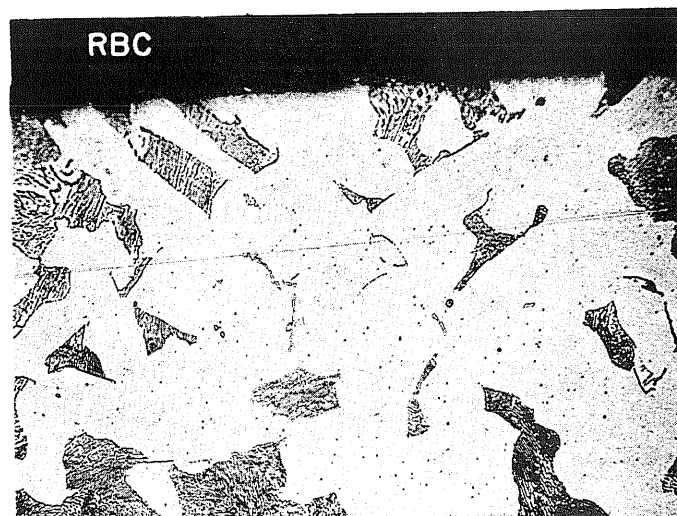


FIG. 14c "RBC" STEEL, EDGE OF SPECIMEN 1SRBC⁴
(4% Picrol - 200X)

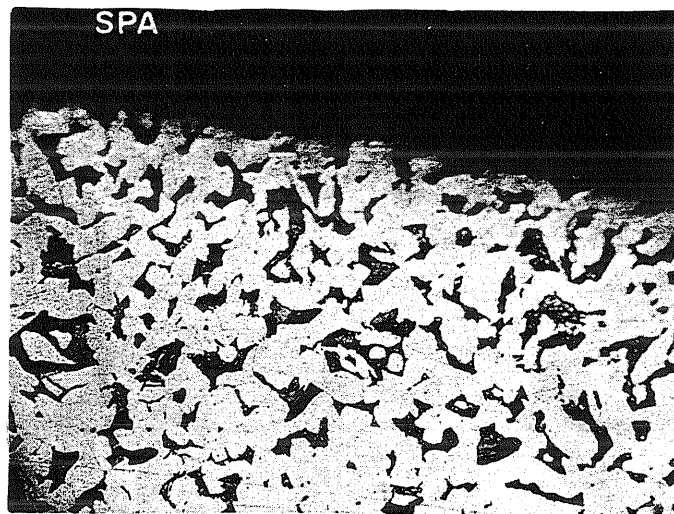


FIG. 14d "SPA" STEEL, EDGE OF SPECIMEN 1NSPA4
(4% Picrol - 200X)



FIG. 14e "SPB" STEEL, EDGE OF SPECIMEN 1NSPB2
(4% Picrol - 200X)

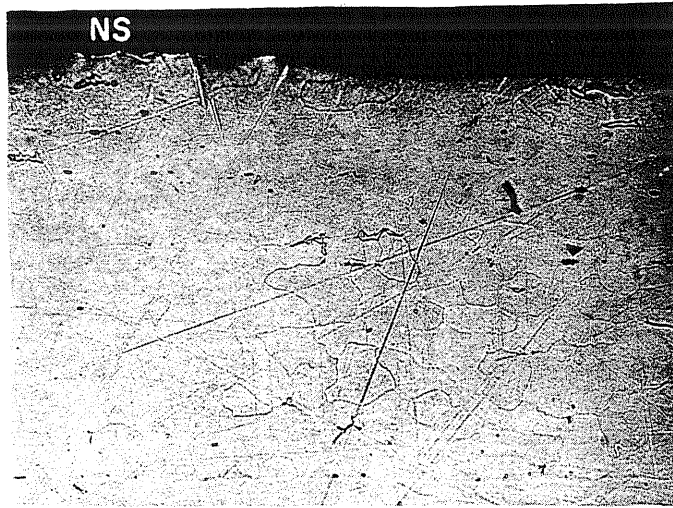


FIG. 14f "NS" STEEL, EDGE OF SPECIMEN NST4
(4% Picrol - 200X)

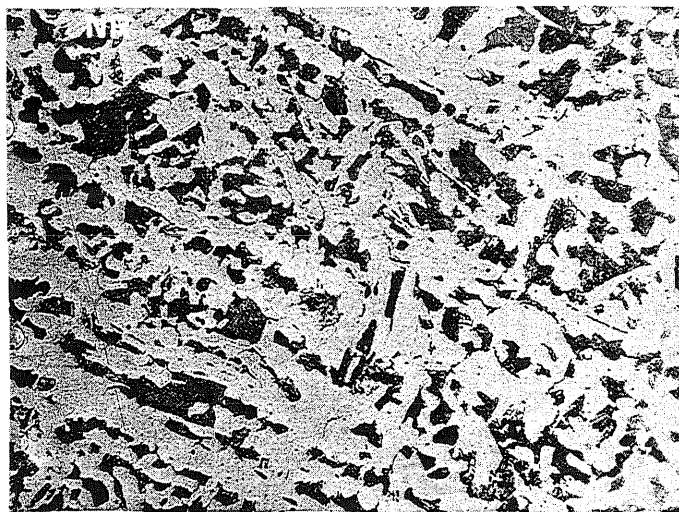


FIG. 14g "NR" STEEL, CENTER OF SPECIMEN NR2
(4% Picrol - 200X)

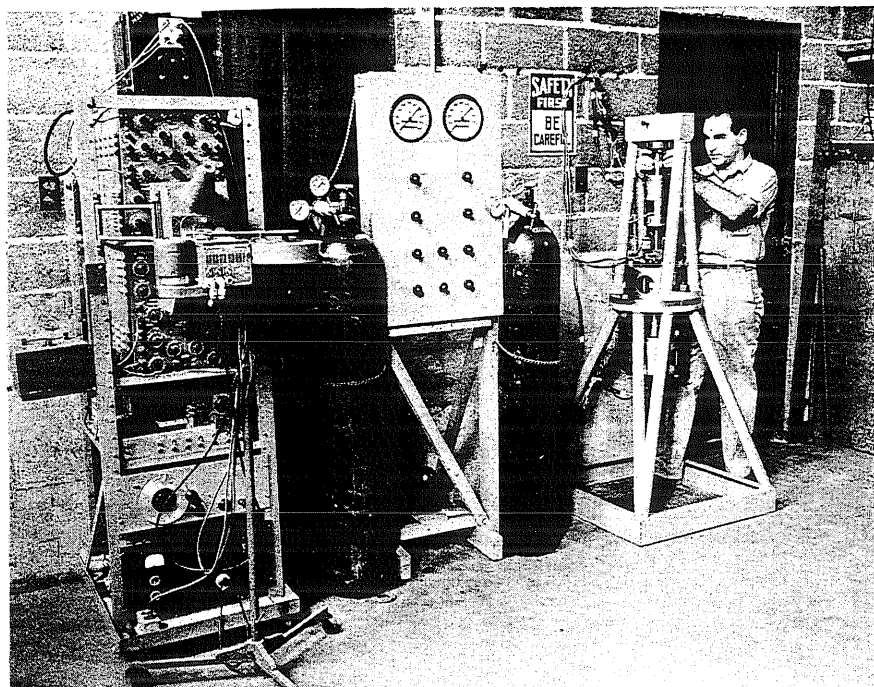


FIG. 15 CRO INSTRUMENTS, PRESSURE PANEL, AND 20 KIP PULSE LOADING UNIT ARRANGED FOR TESTING PRELIMINARY TENSION-COMPRESSION SPECIMENS

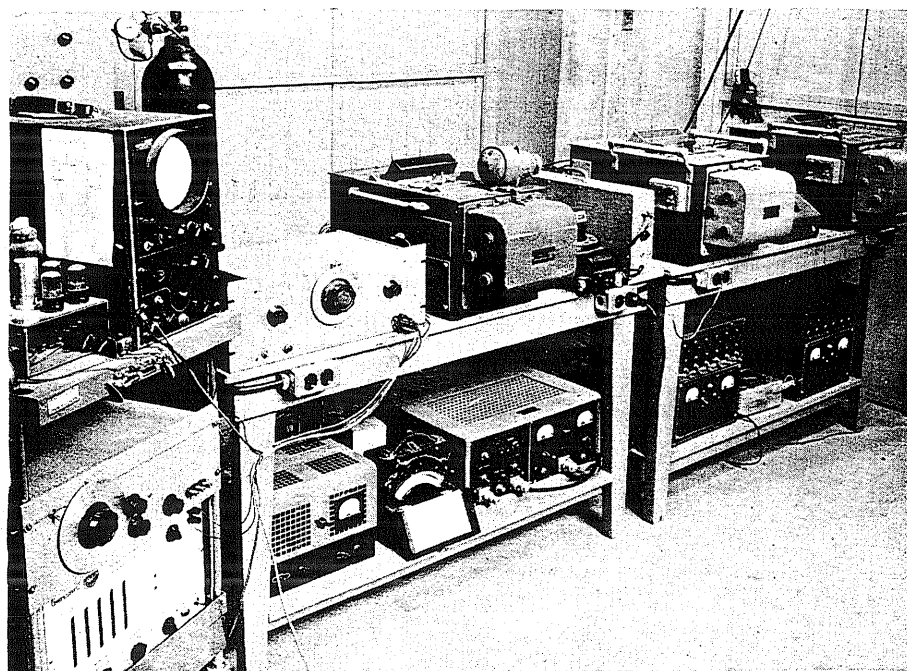


FIG. 16 HATHAWAY OSCILLOGRAPHS AND ASSOCIATED APPARATUS
(Two units used for flexure tests; one unit
used for rapid uniaxial stress tests)

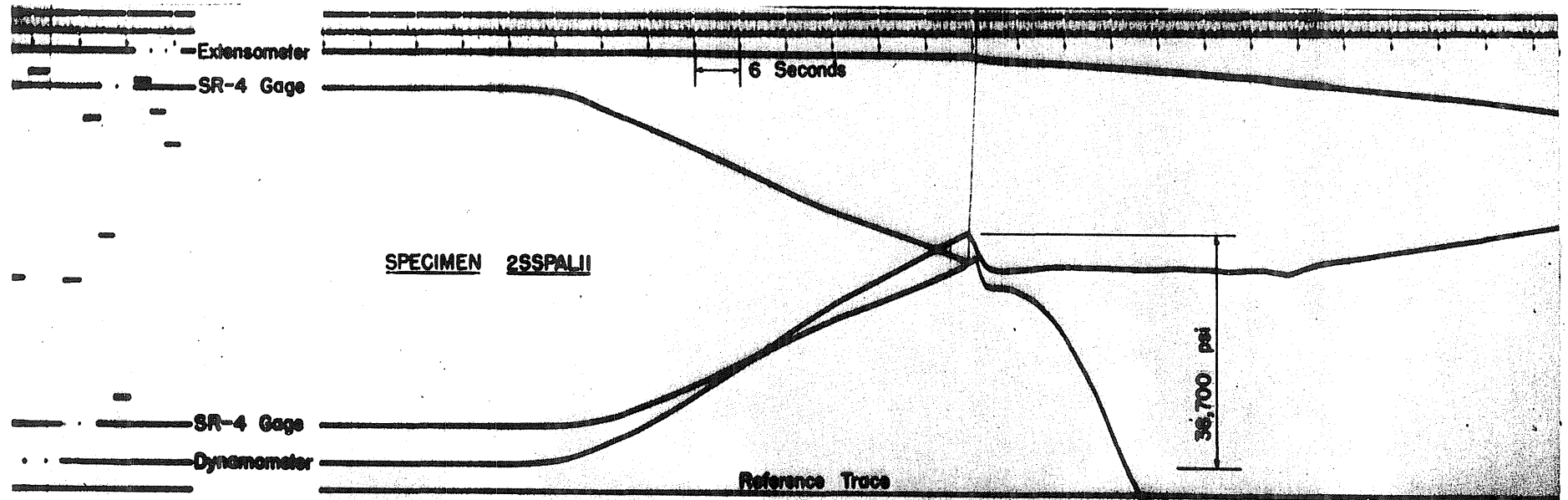


FIG. 17a OSCILLOGRAM (1/2 size) OF "SLOW" TEST IN BALDWIN MACHINE

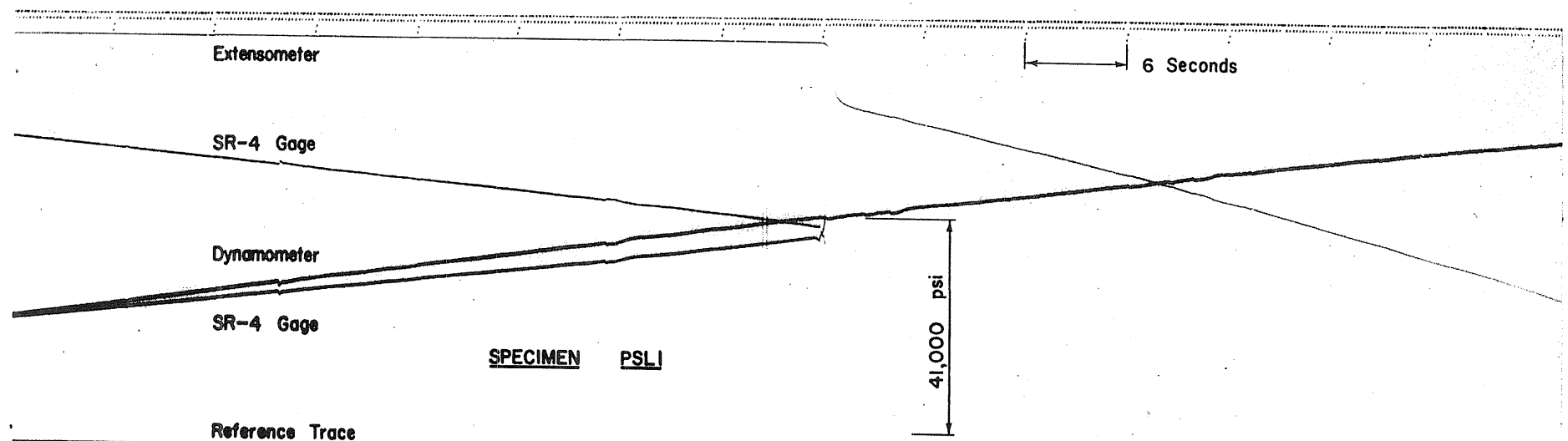


FIG. 17b OSCILLOGRAM (1/2 size) OF "SLOW" TEST IN PULSE LOADING MACHINE

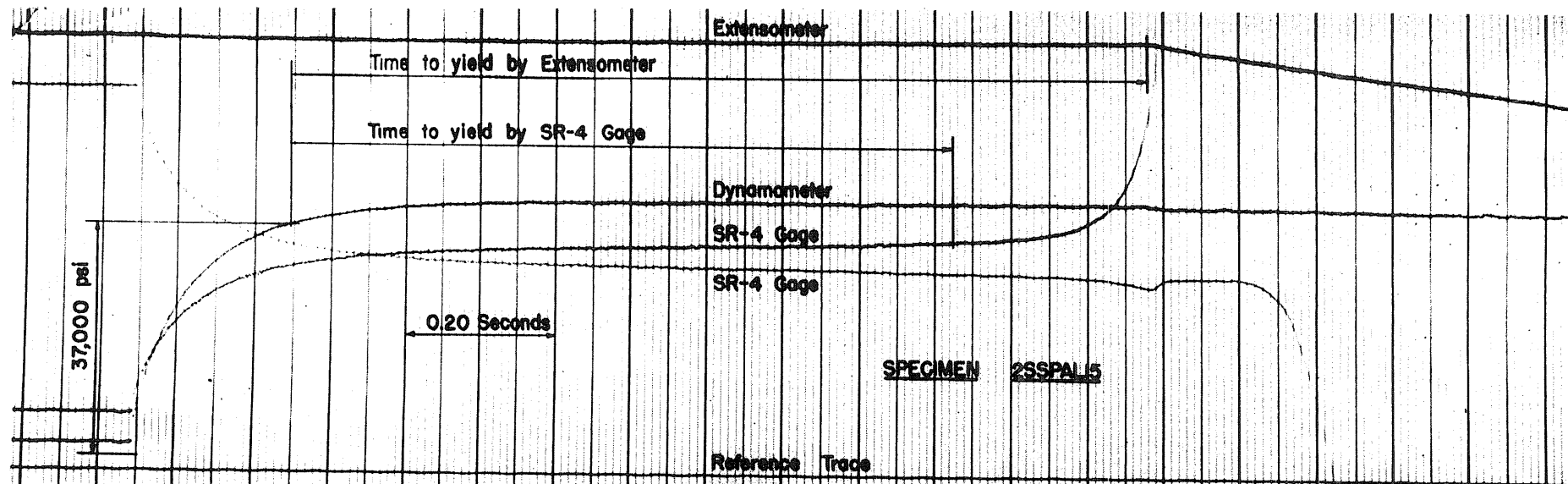


FIG. 17c OSCILLOGRAM (1/2 size) OF TEST FROM ZERO TO MAXIMUM LOAD IN ABOUT 0.5 SECONDS

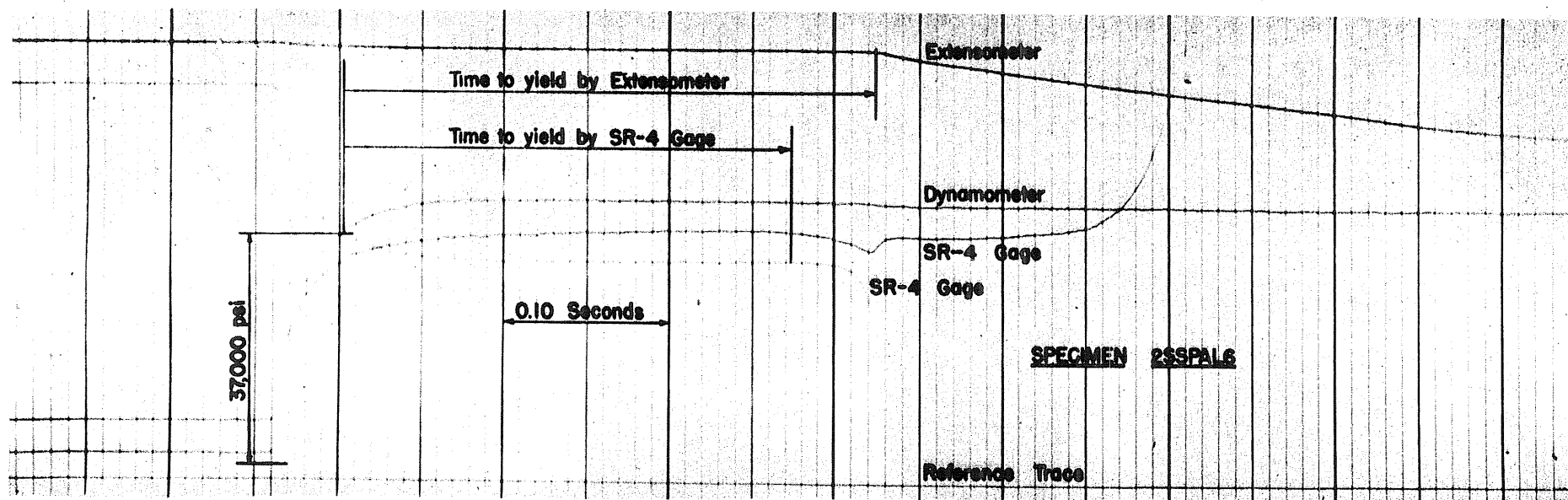


FIG. 17d OSCILLOGRAM (1/2 size) OF TEST FROM ZERO TO MAXIMUM LOAD IN ABOUT 0.10 SECONDS

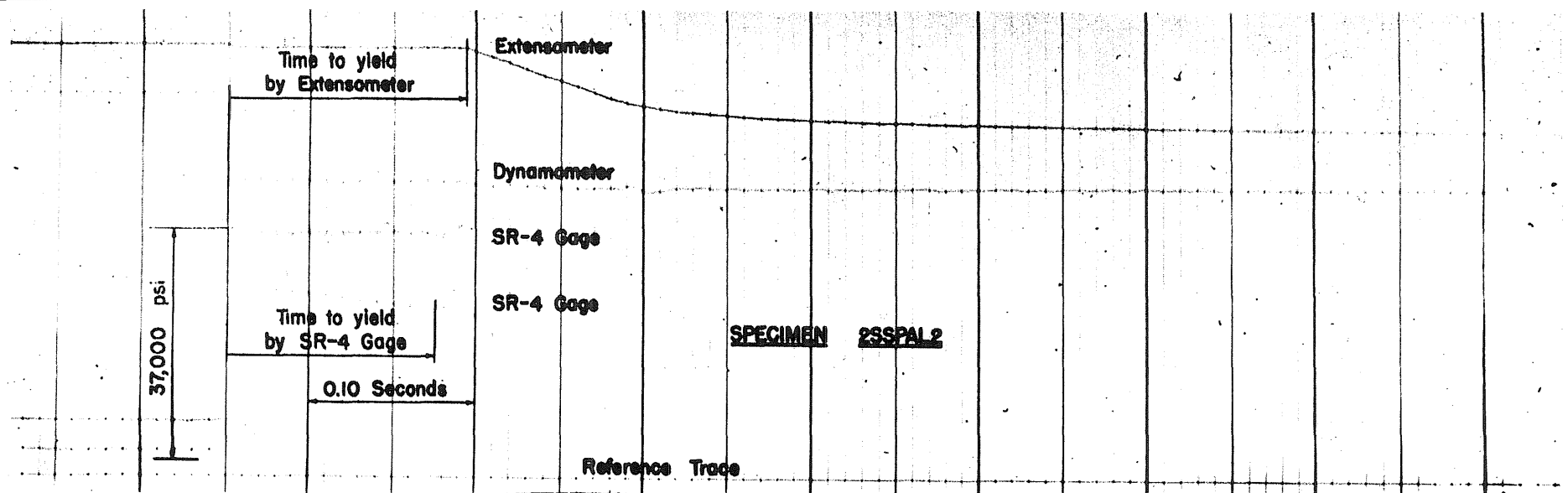


FIG. 17e OSCILLOGRAM (1/2 size) OF TEST FROM ZERO TO MAXIMUM LOAD IN ABOUT 0.005 SECONDS

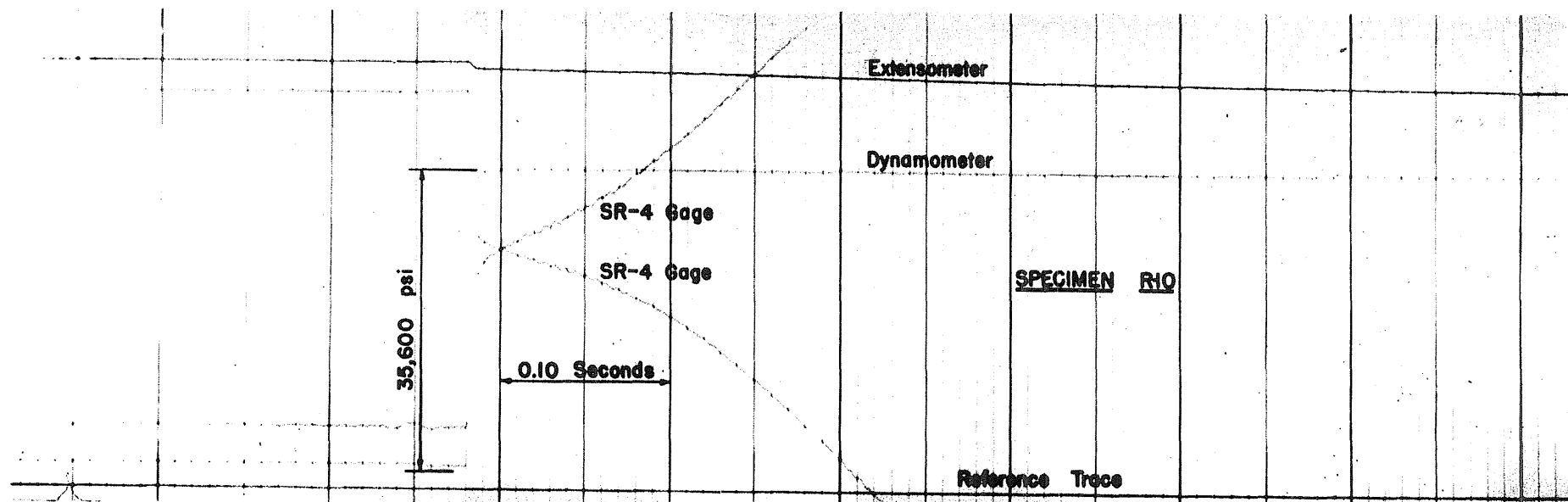
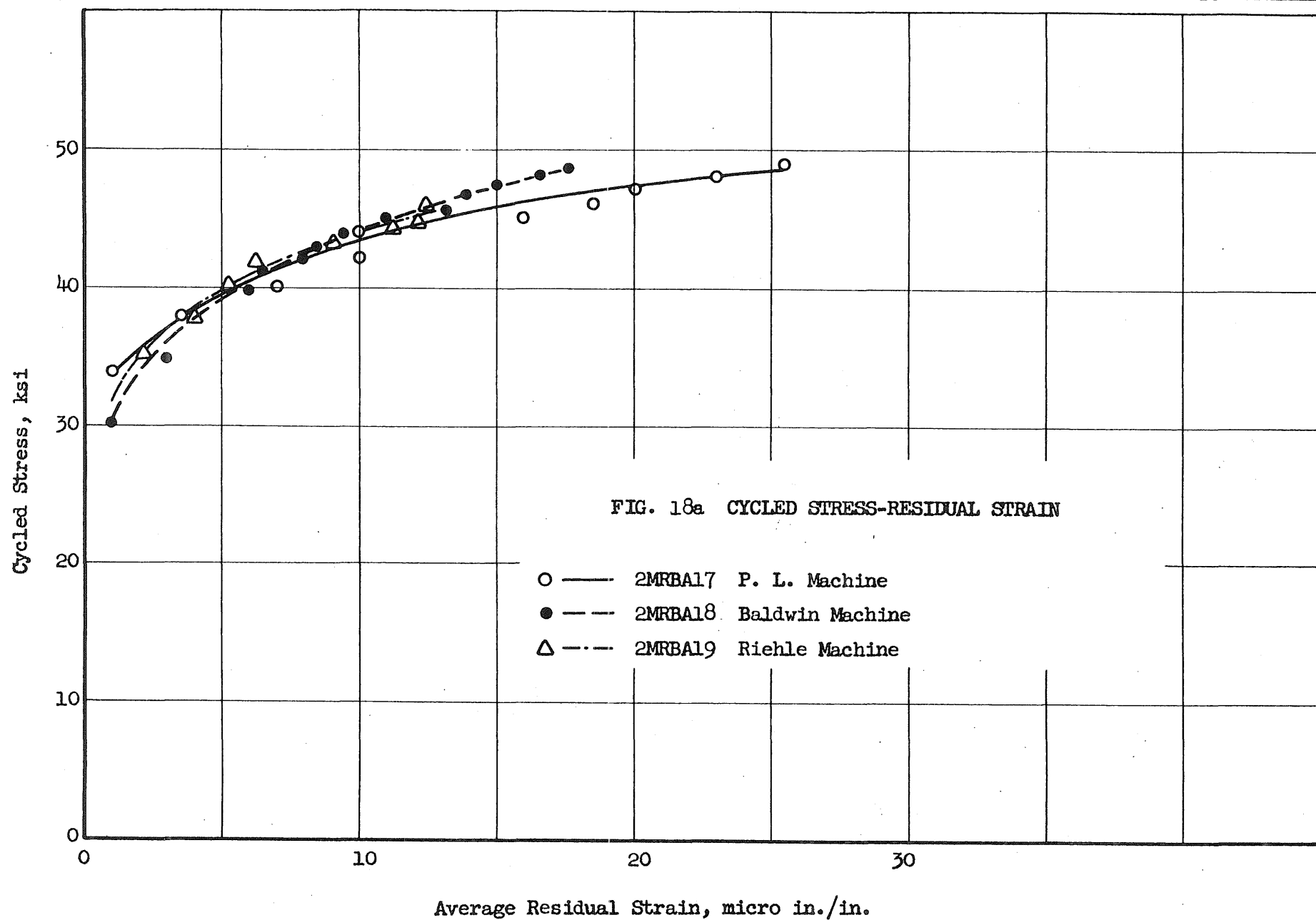
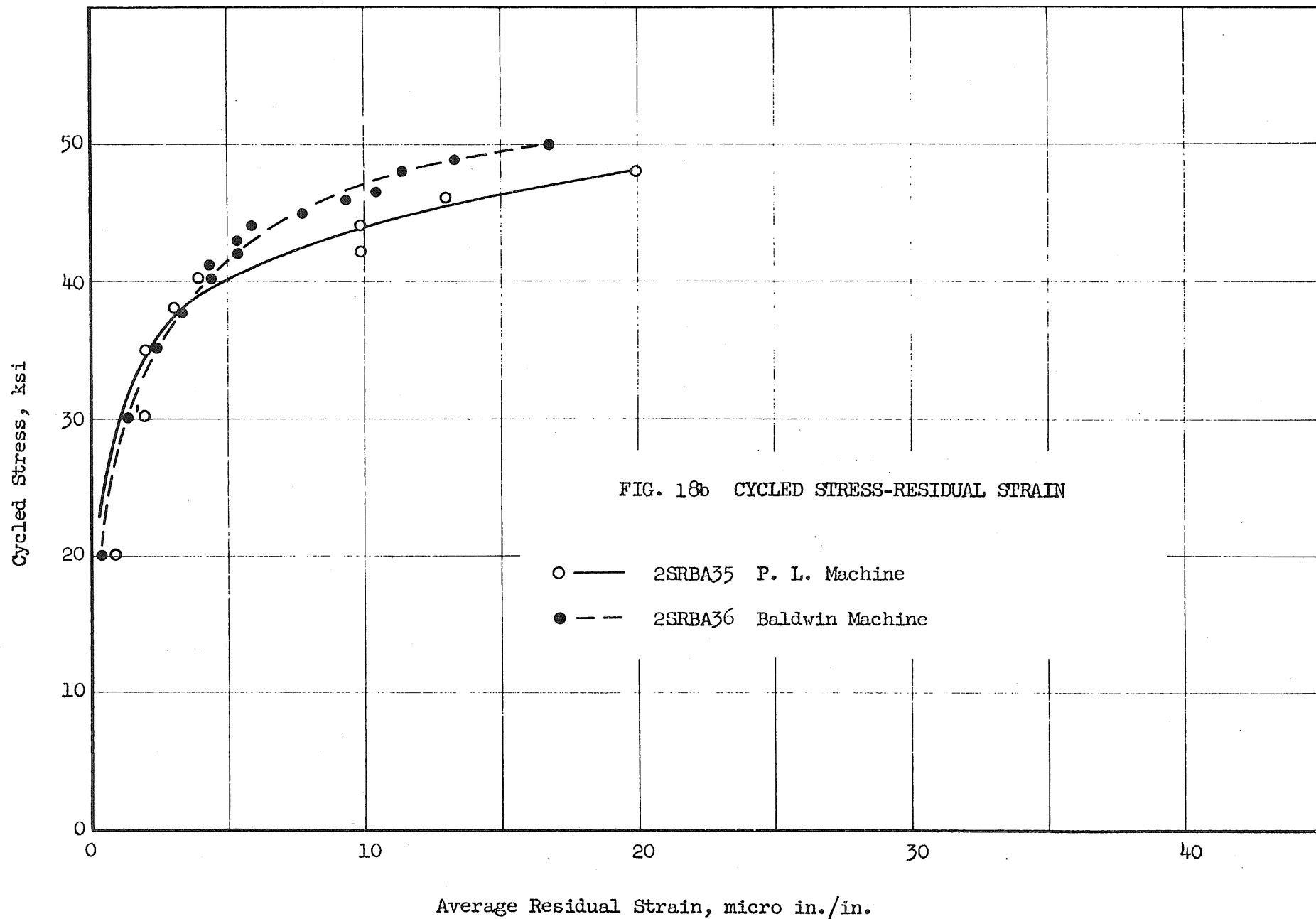
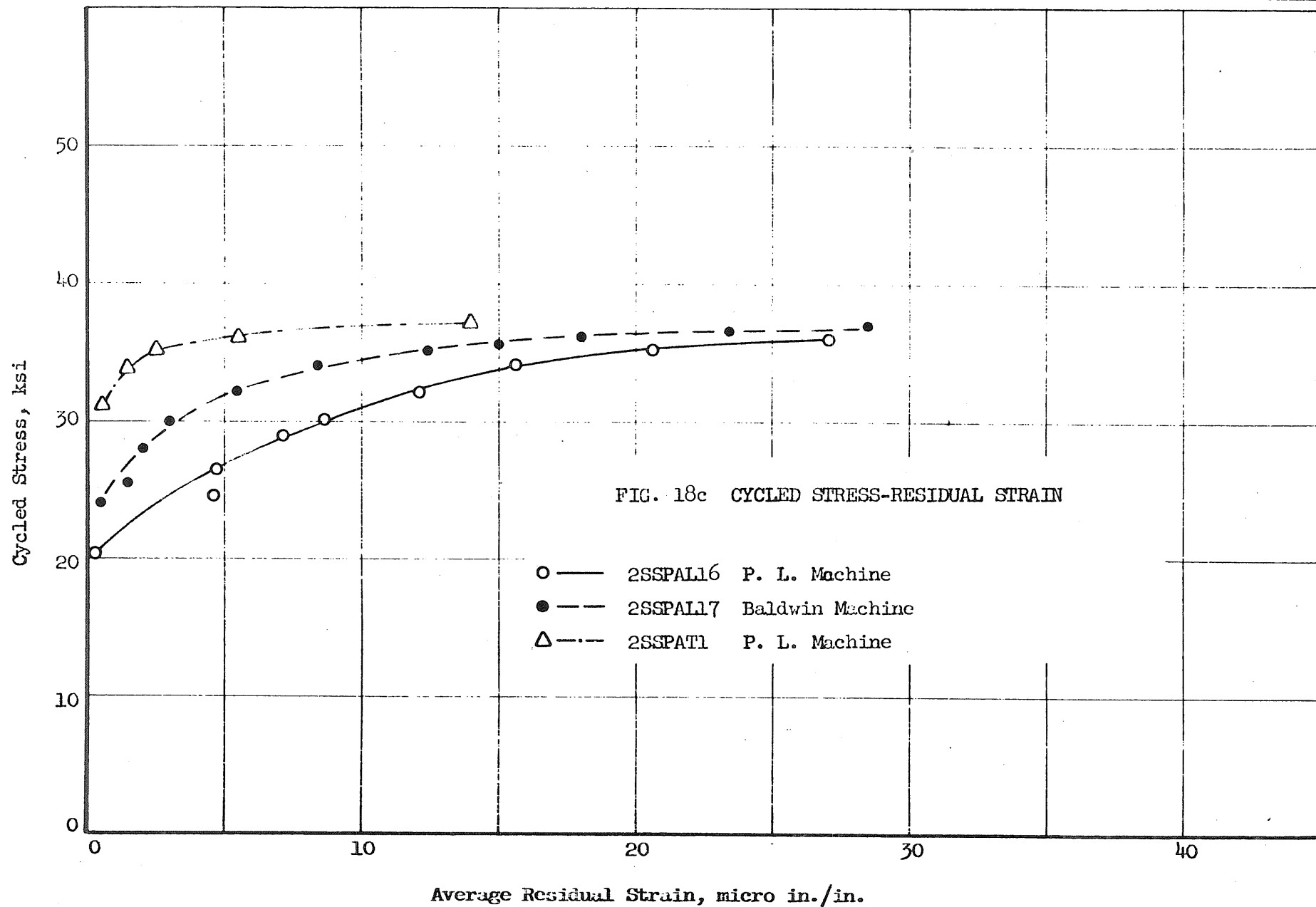


FIG. 17f OSCILLOGRAM (1/2 size) SHOWING GRADUAL YIELDING TYPICAL OF "NR" SPECIMEN SERIES







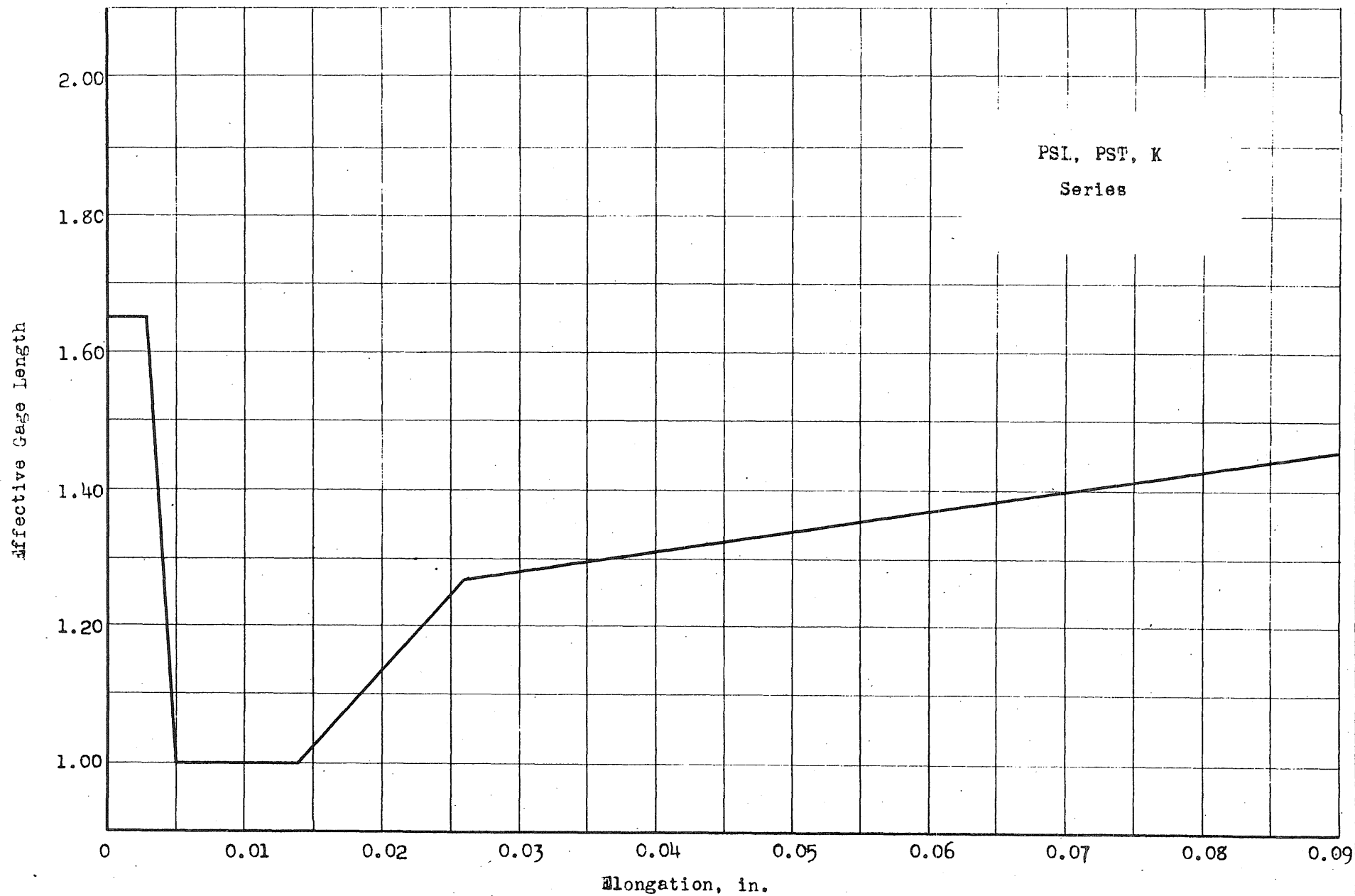


FIG. 19a EFFECTIVE GAGE LENGTH - ELONGATION

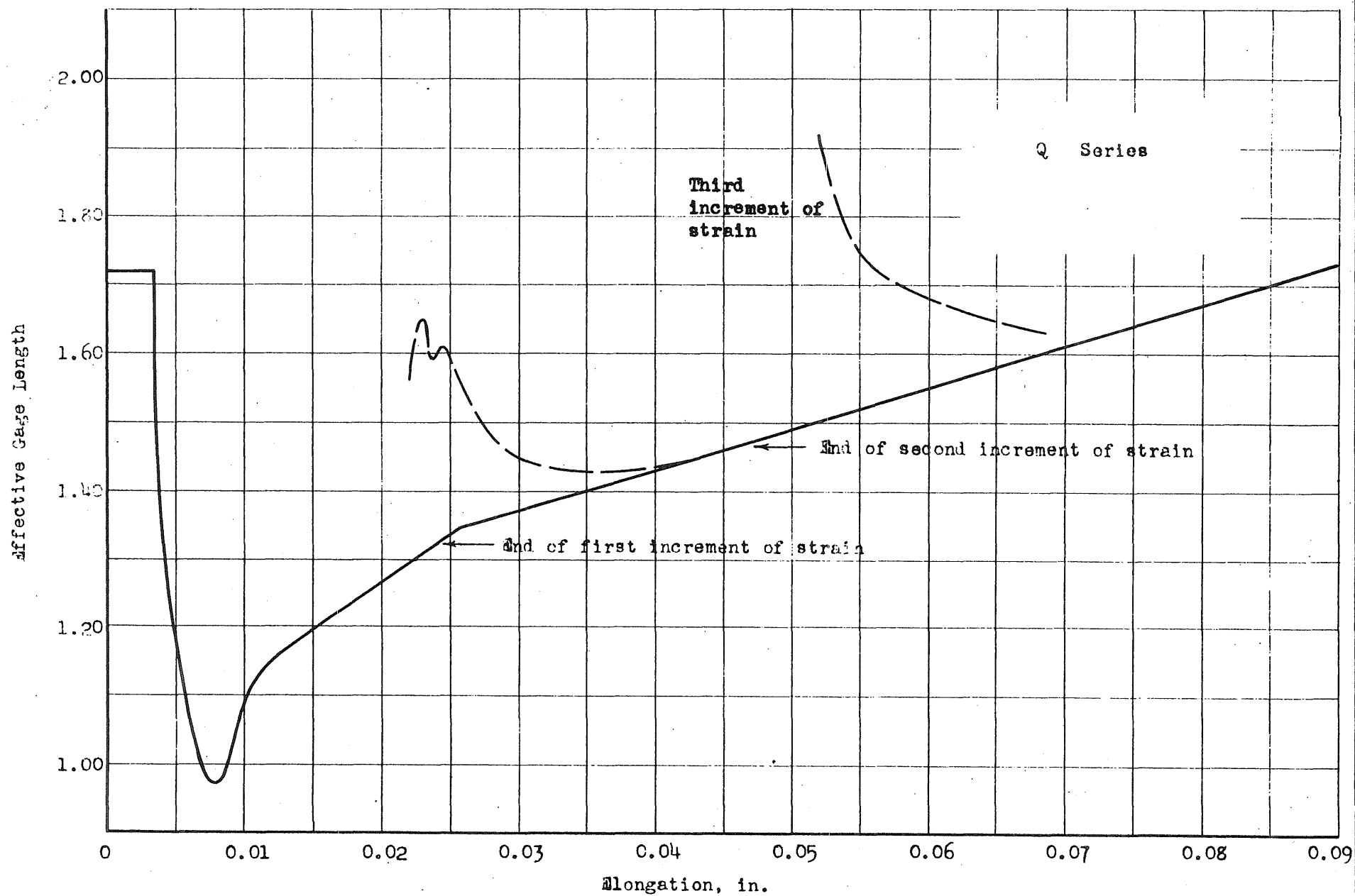


FIG. 19b EFFECTIVE GAGE LENGTH - ELONGATION

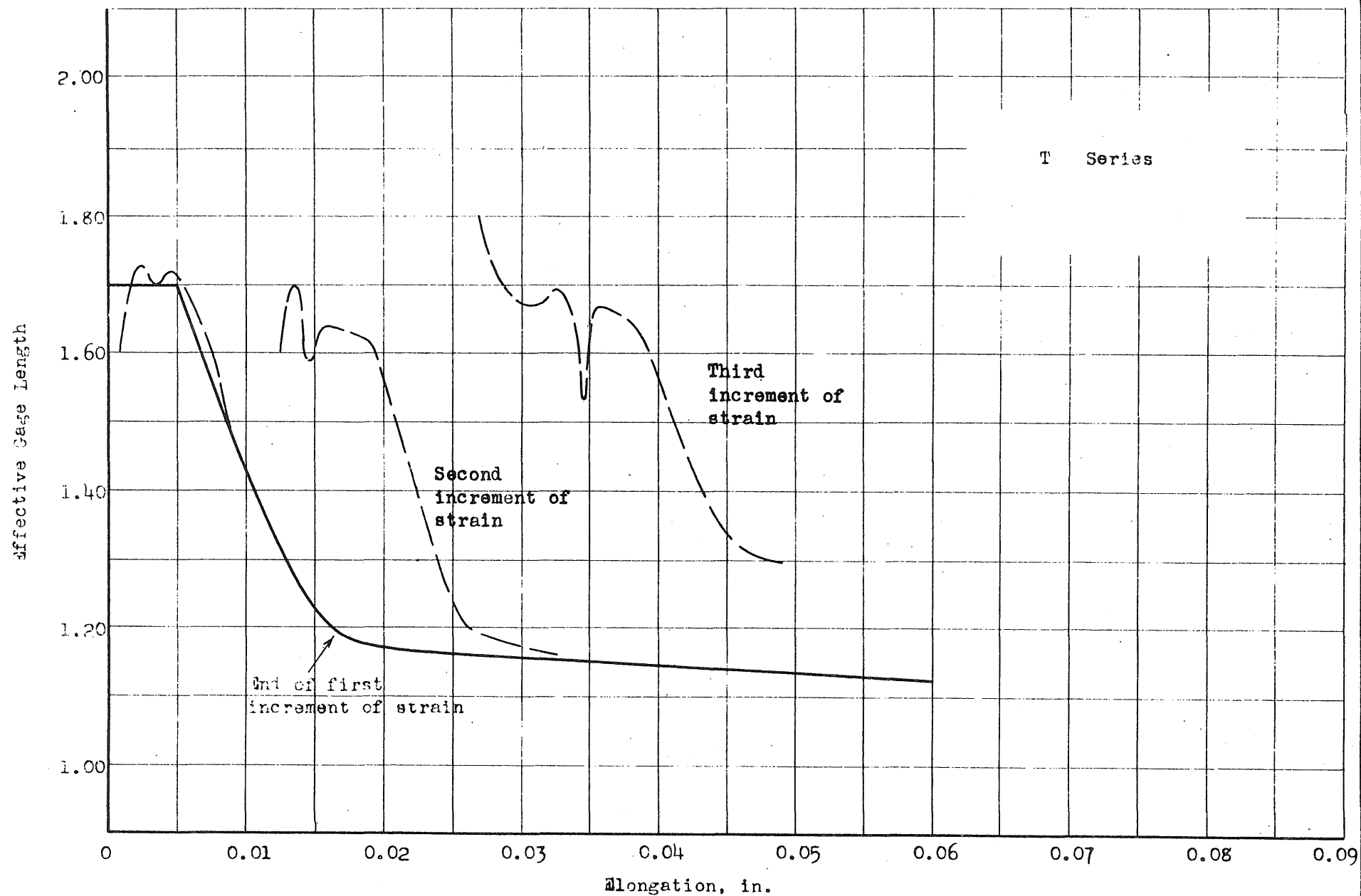
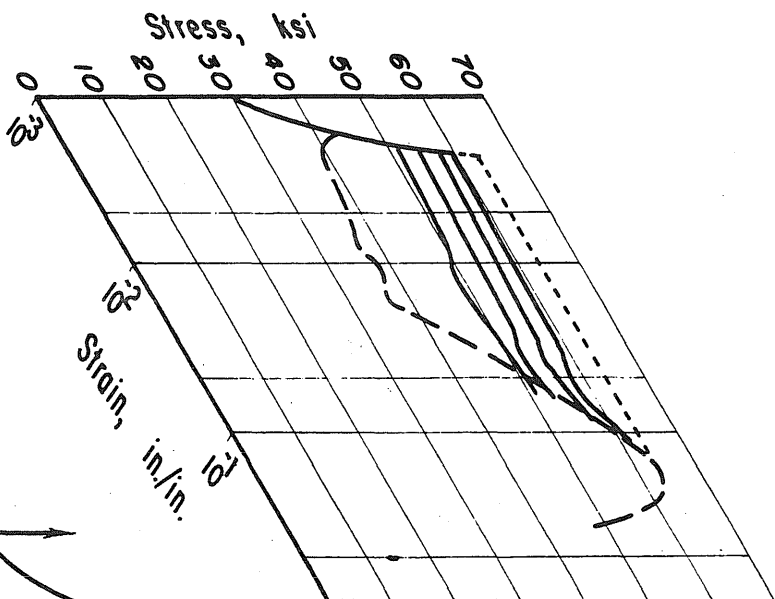


FIG. 19c EFFECTIVE GAGE LENGTH - ELONGATION



— Rapid Load to "Constant" Stress
(Elastic Strain Rate ≈ 0.3 in./in./sec.)
-- "Static" Tensile Test
(Strain Rate $\approx 4 \times 10^{-4}$ in./in./sec.)

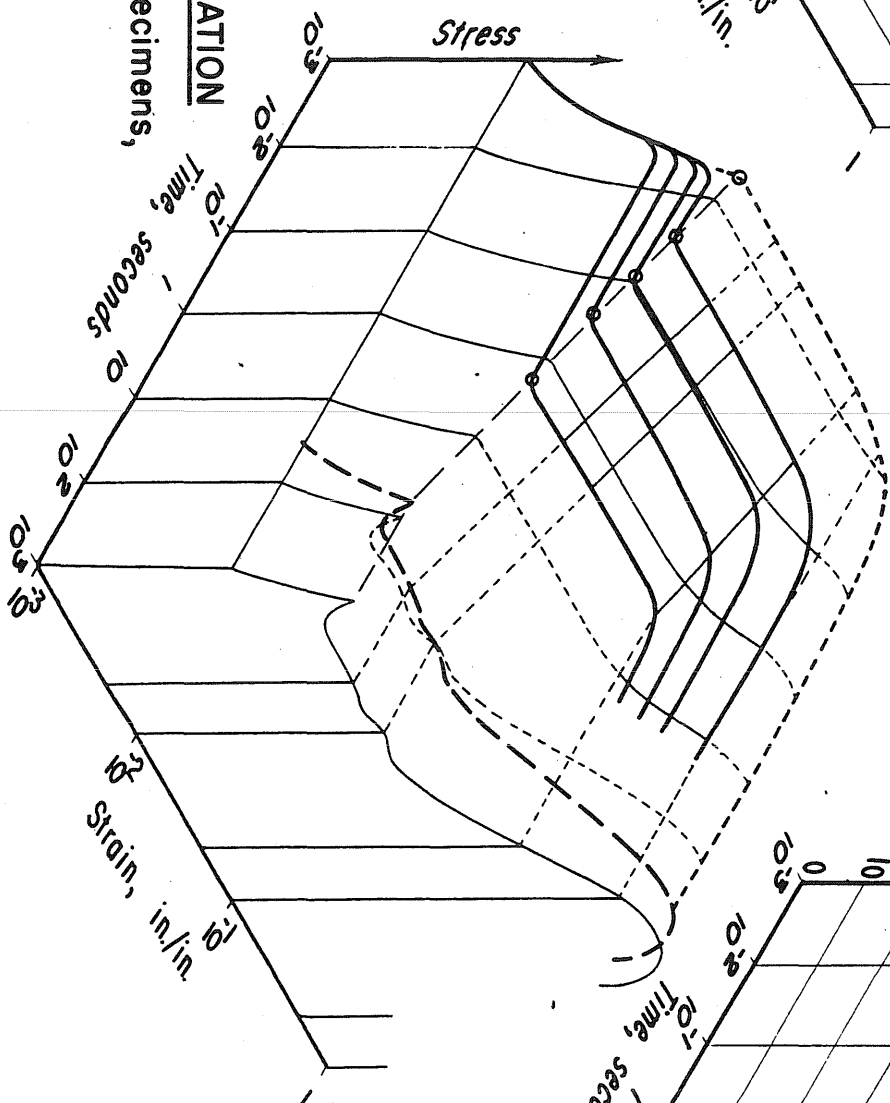
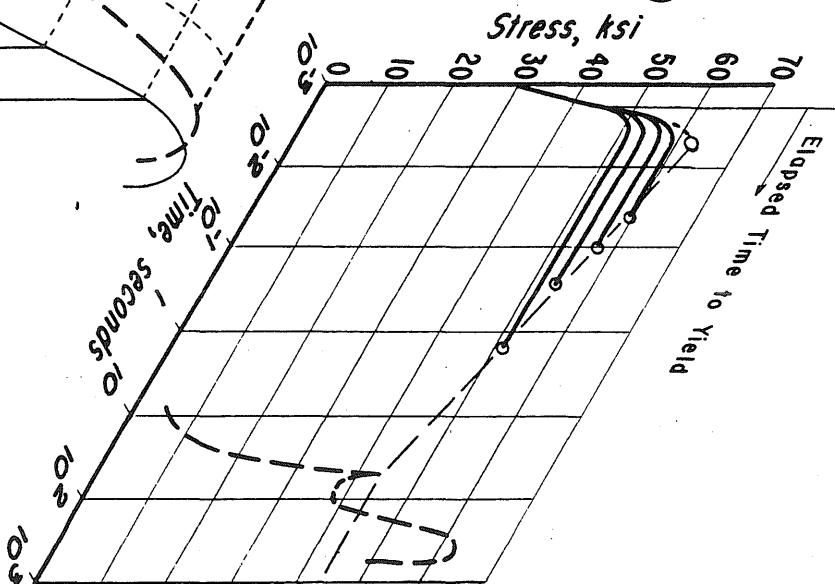


FIG. 20a REPRESENTATIVE
STRESS-STRAIN-TIME RELATION
Rimmed Steel Tensile Specimens,
0.505 D. x 2 in. Gage

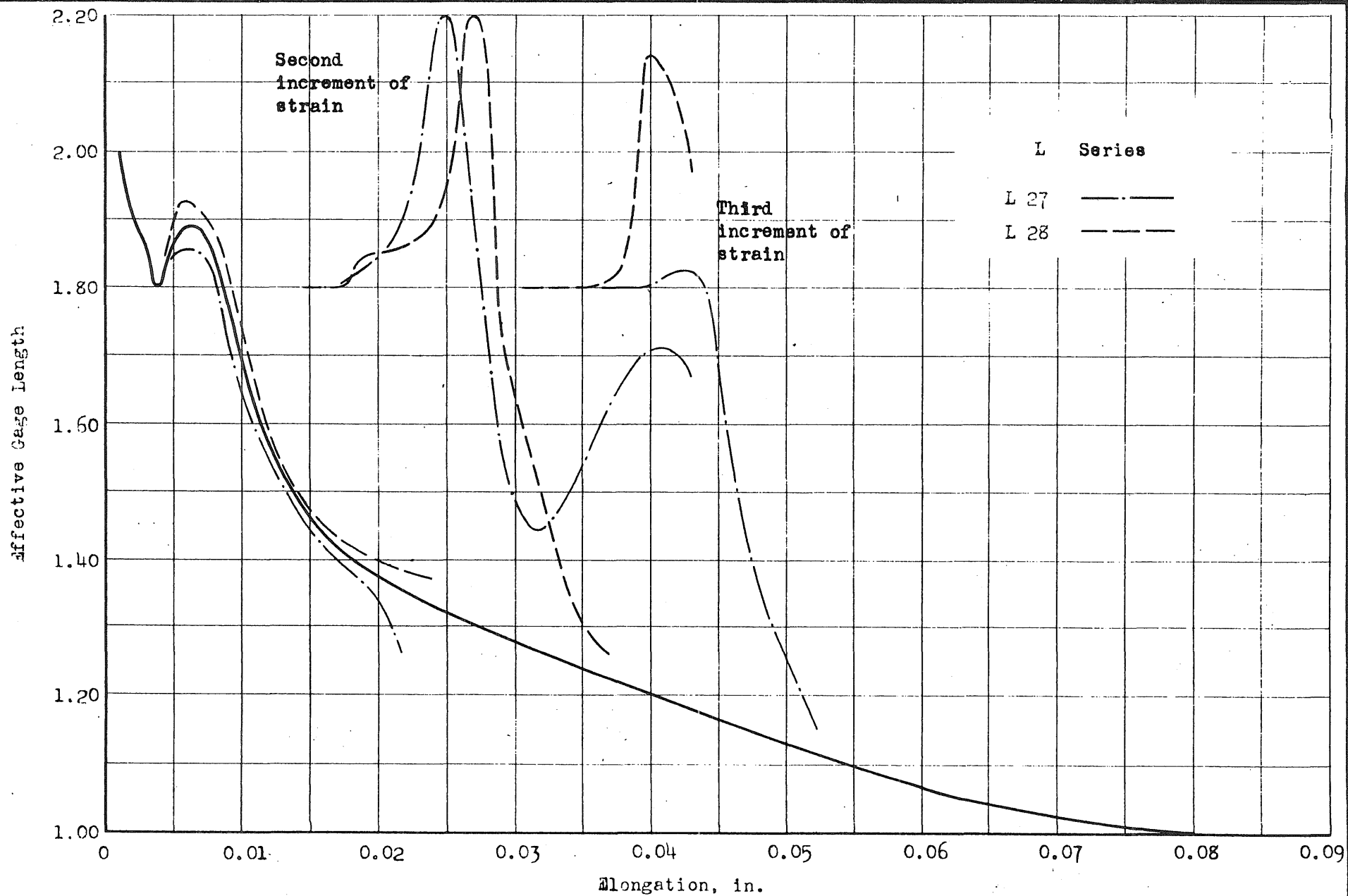


FIG. 19d EFFECTIVE GAGE LENGTH - ELONGATION

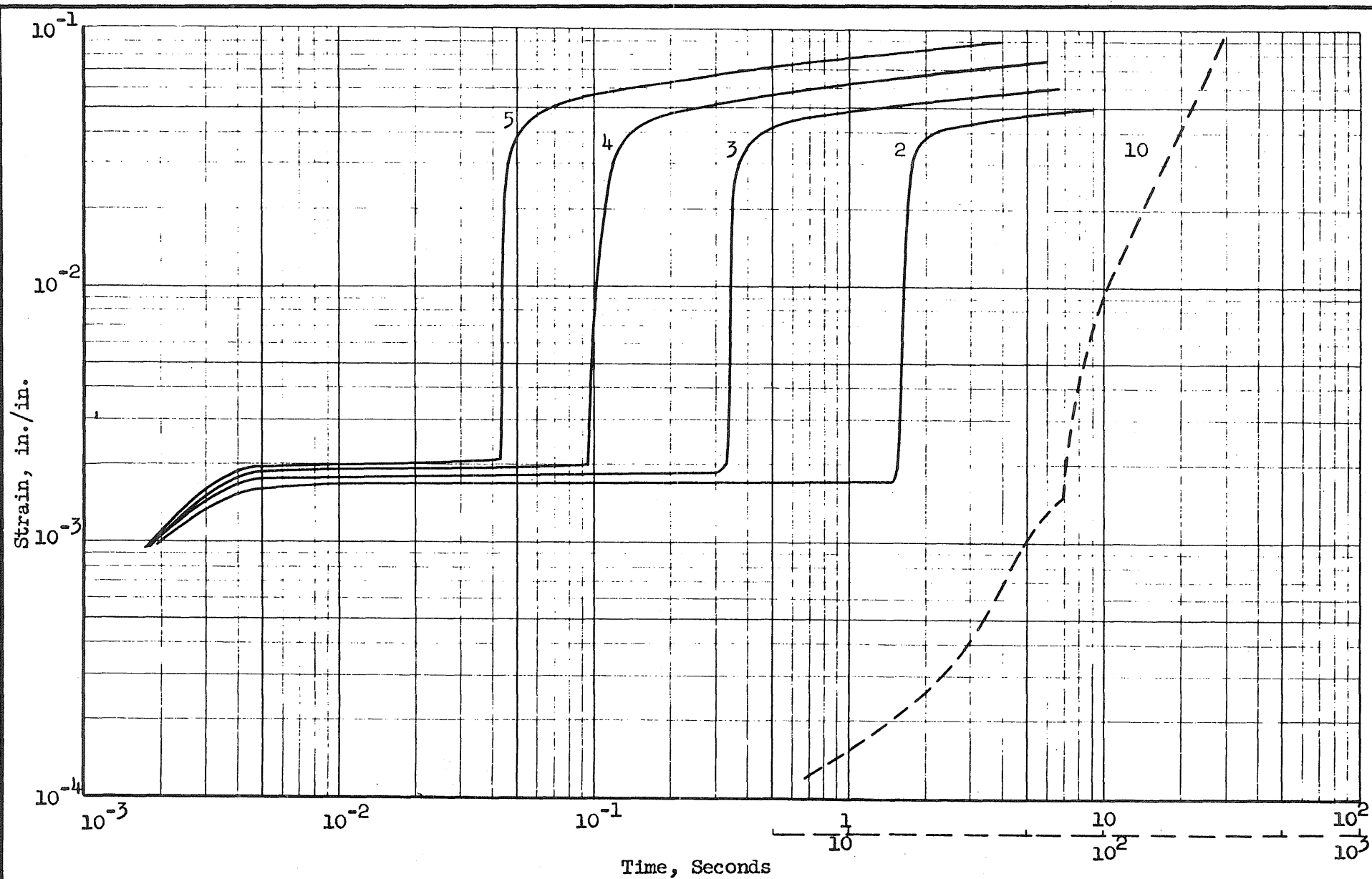
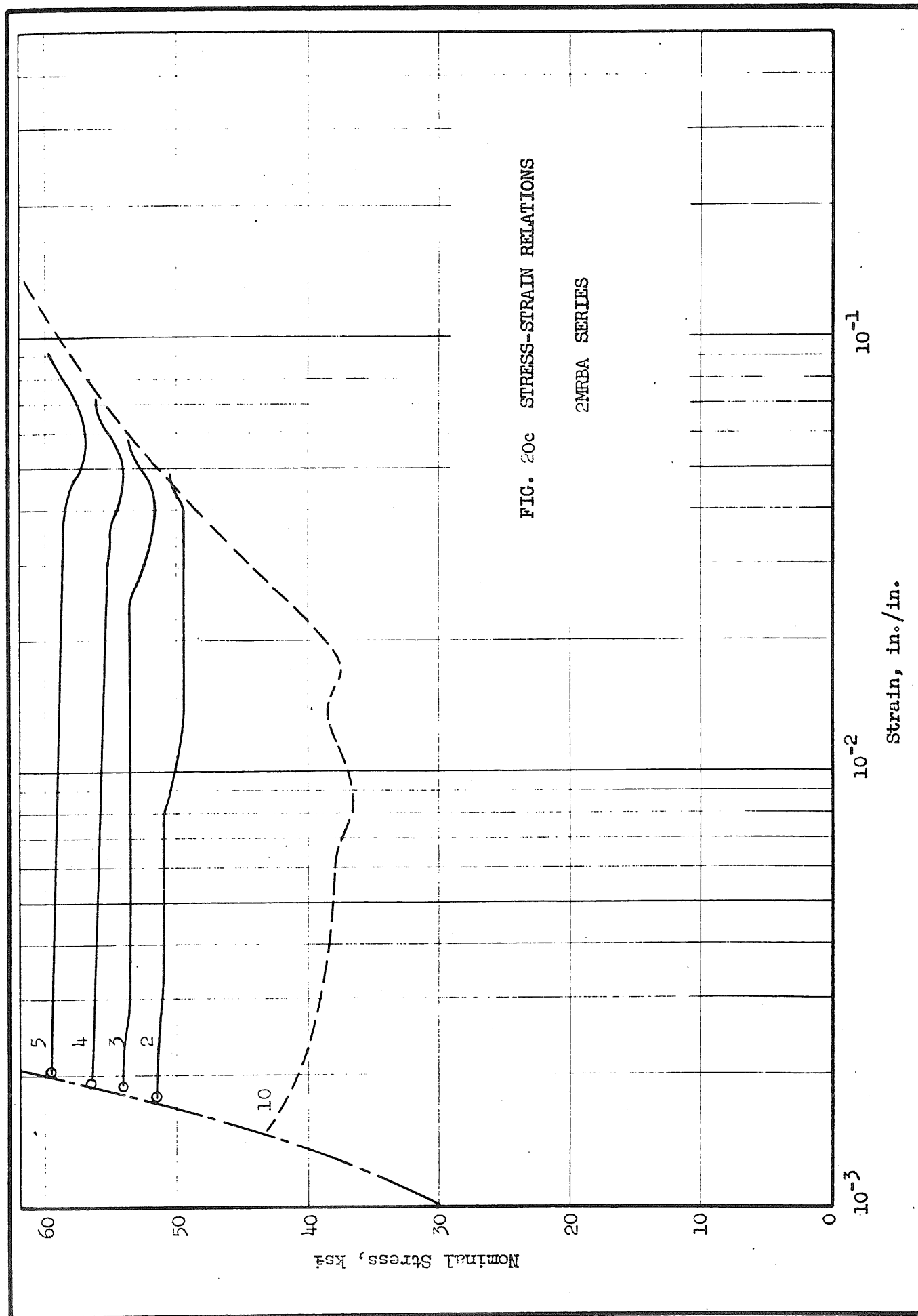


FIG. 20b STRAIN-TIME RELATION, 2MRBA SERIES



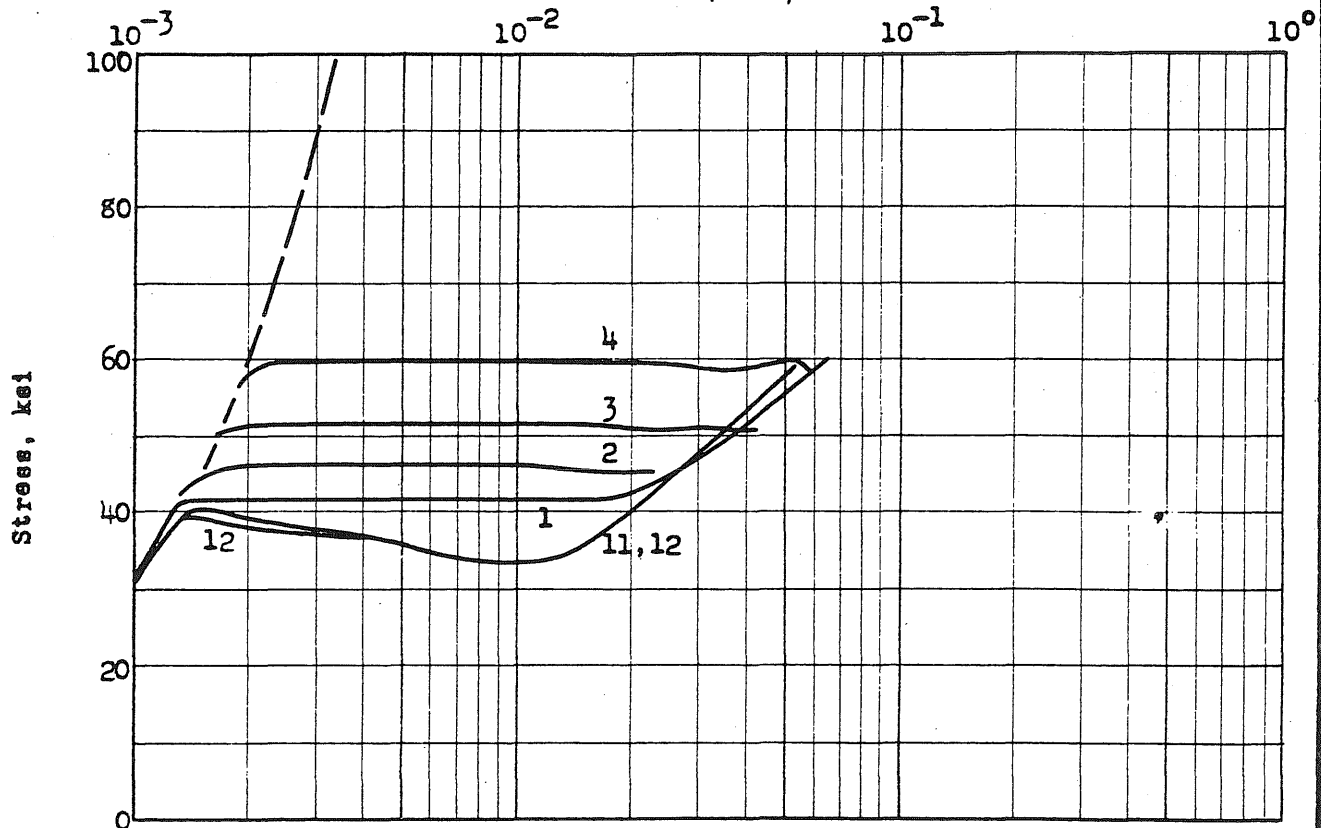
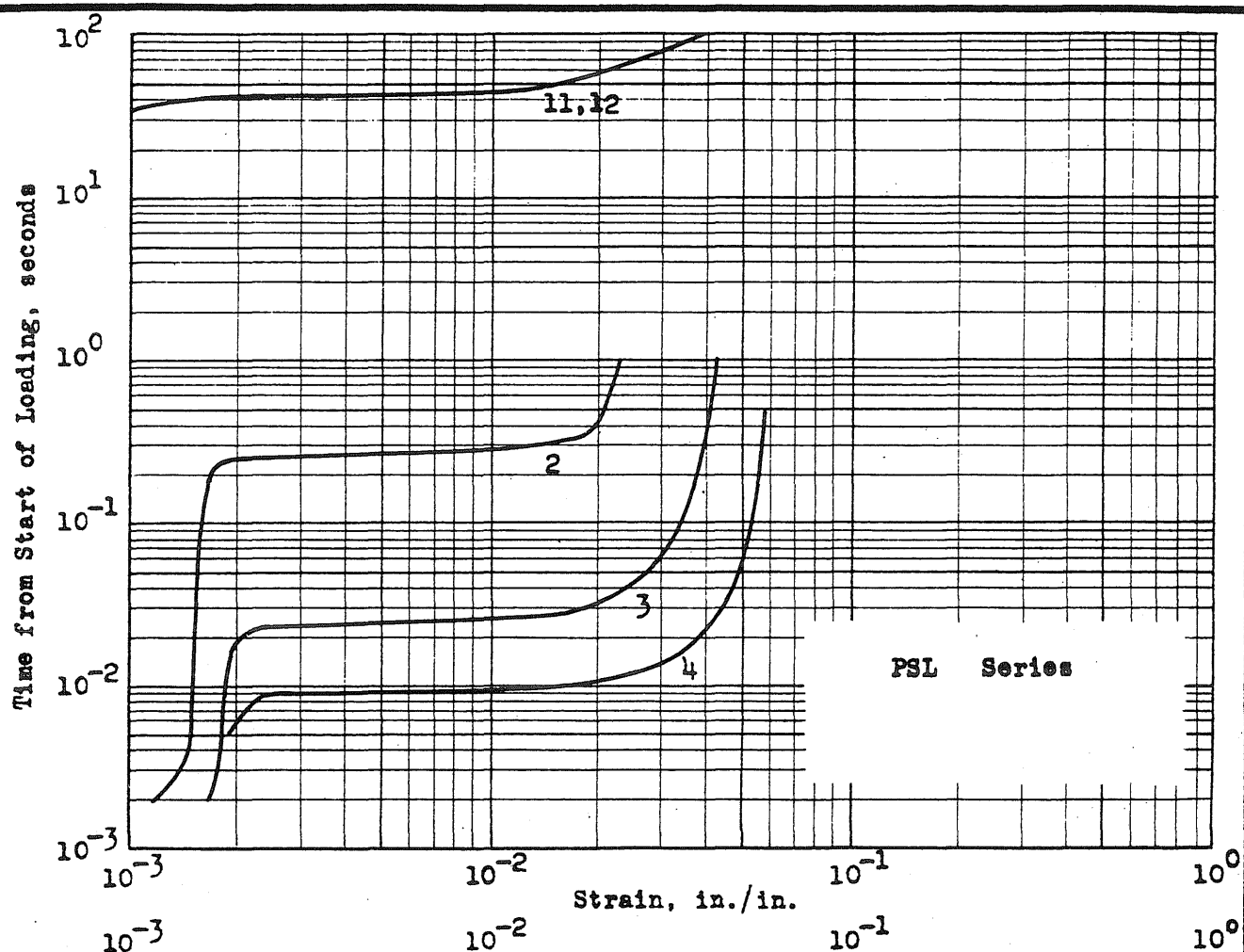


FIG. 21a STRESS-STRAIN AND STRAIN-TIME RELATIONSHIPS

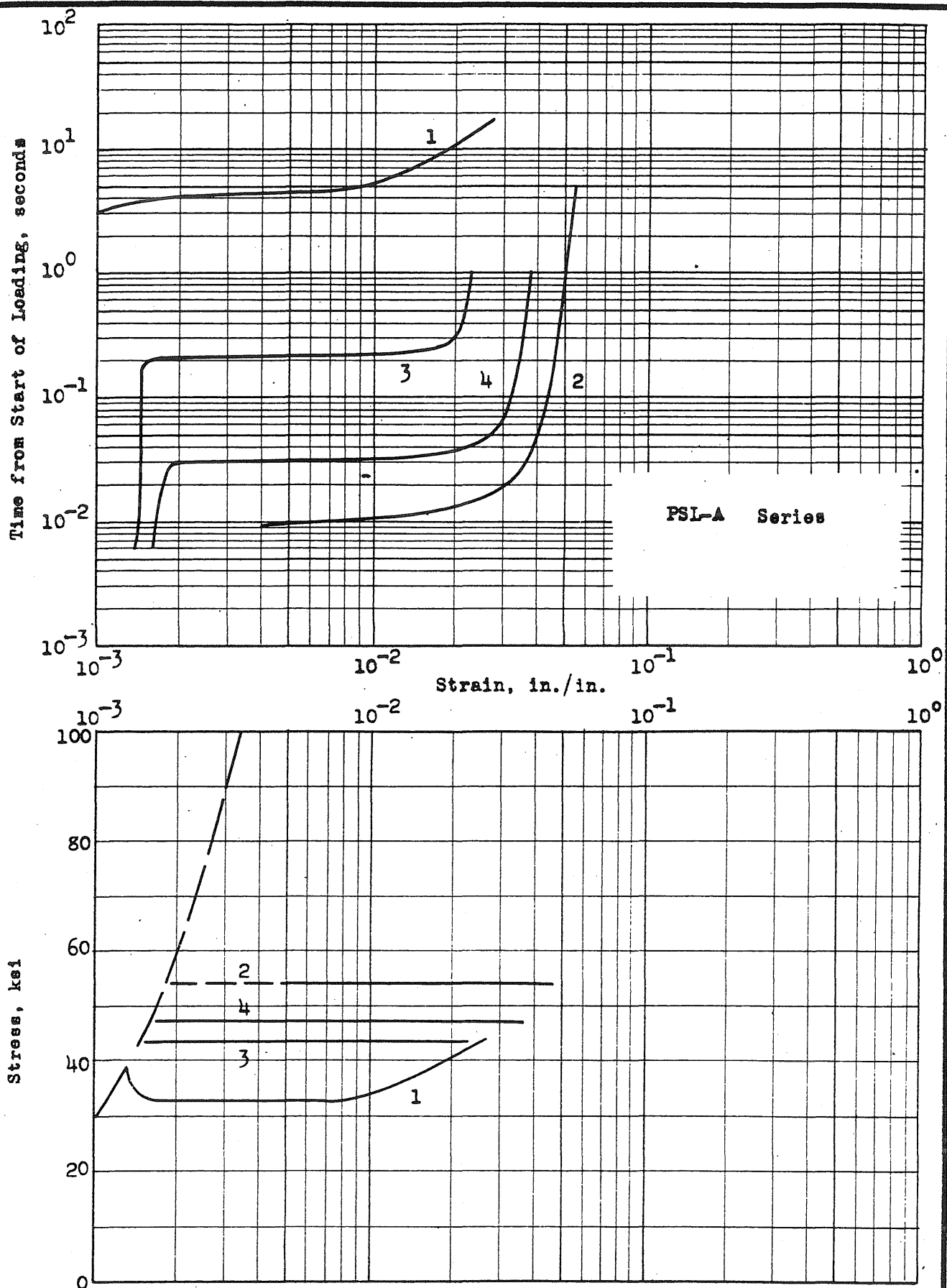


FIG. 21b STRESS-STRAIN AND STRAIN-TIME RELATIONSHIPS

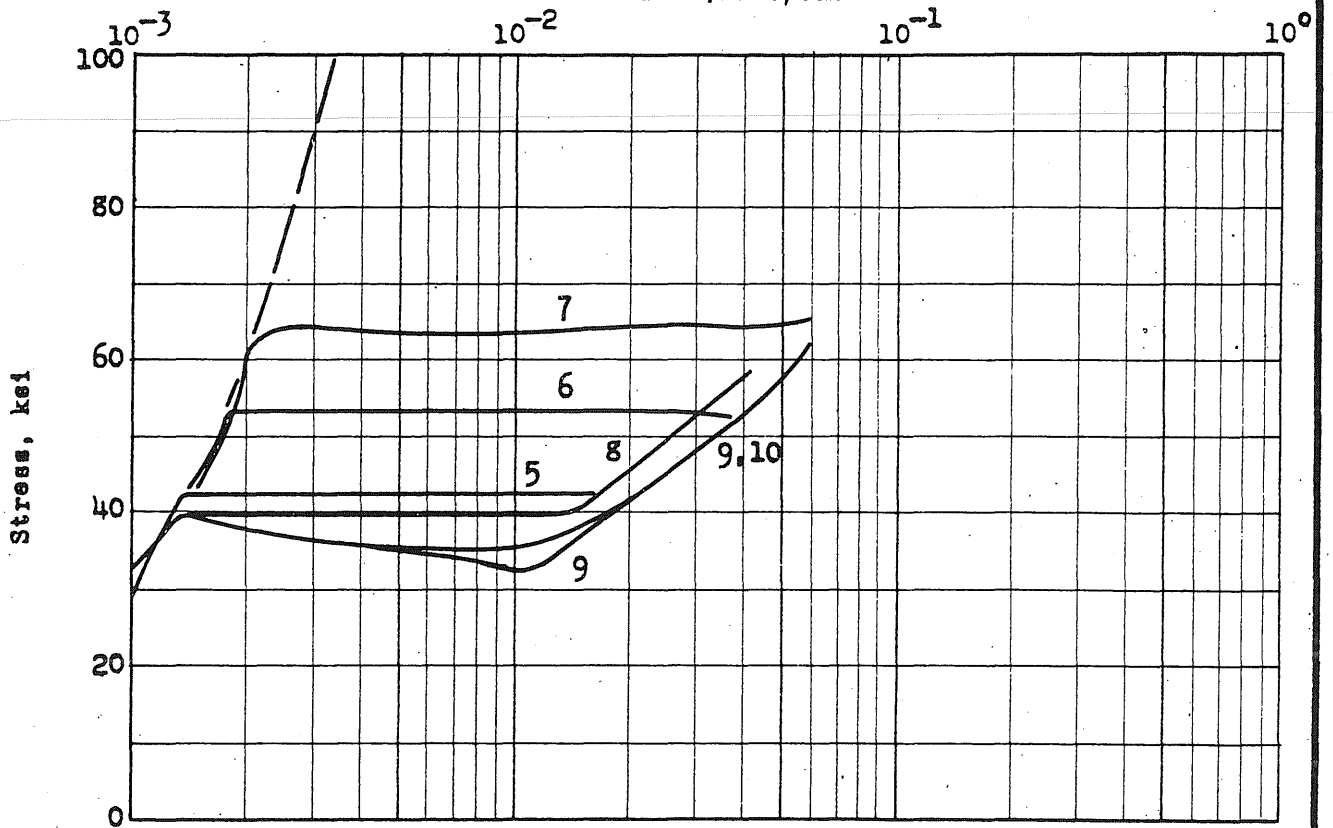
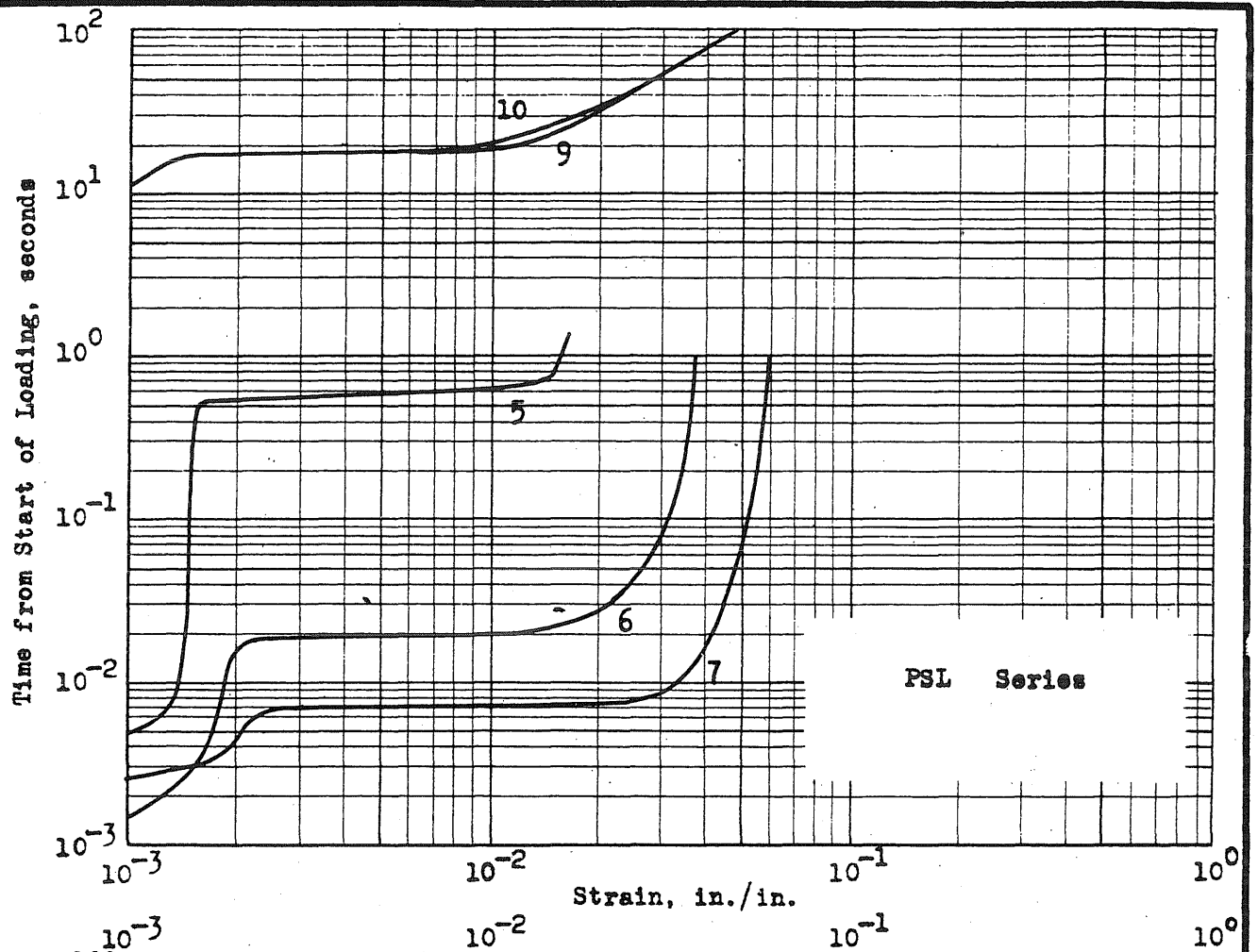


FIG.21c STRESS-STRAIN AND STRAIN-TIME RELATIONSHIPS

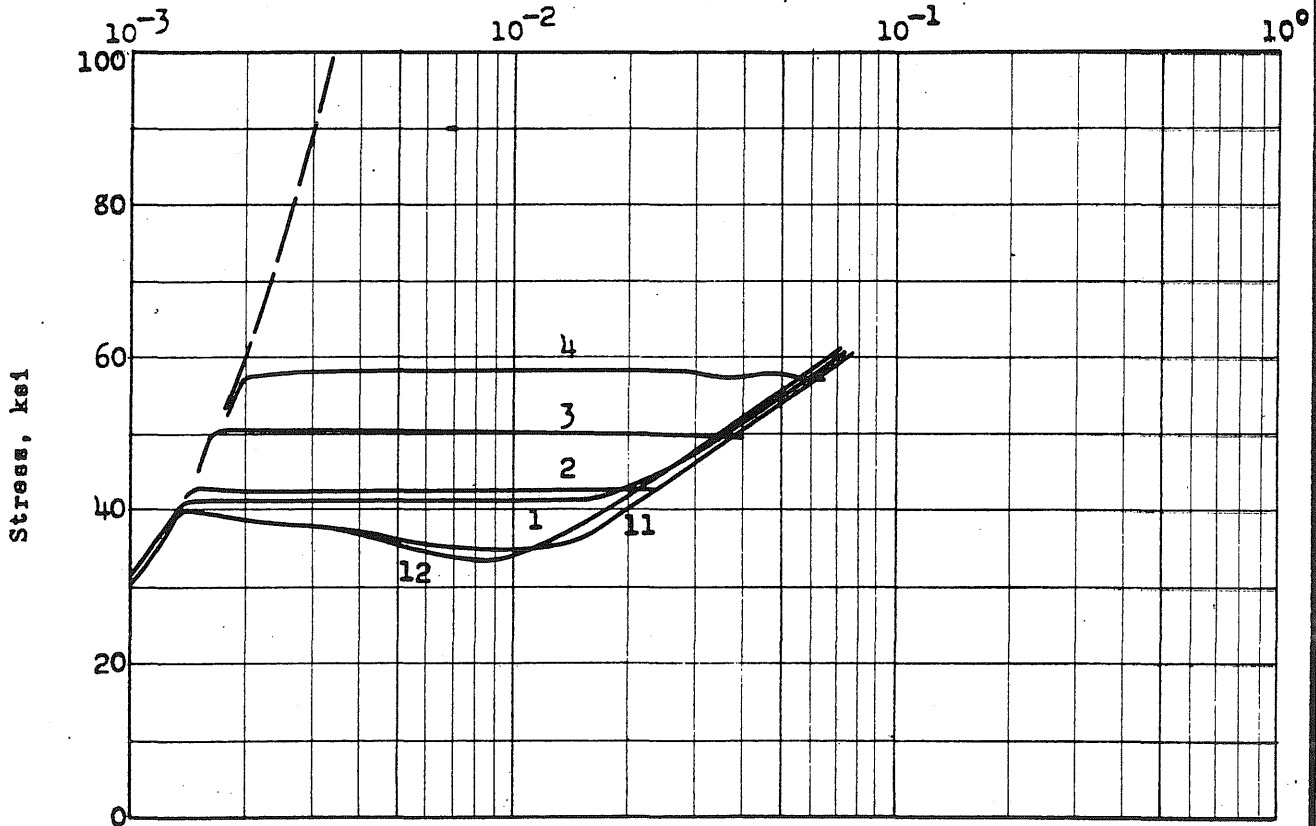
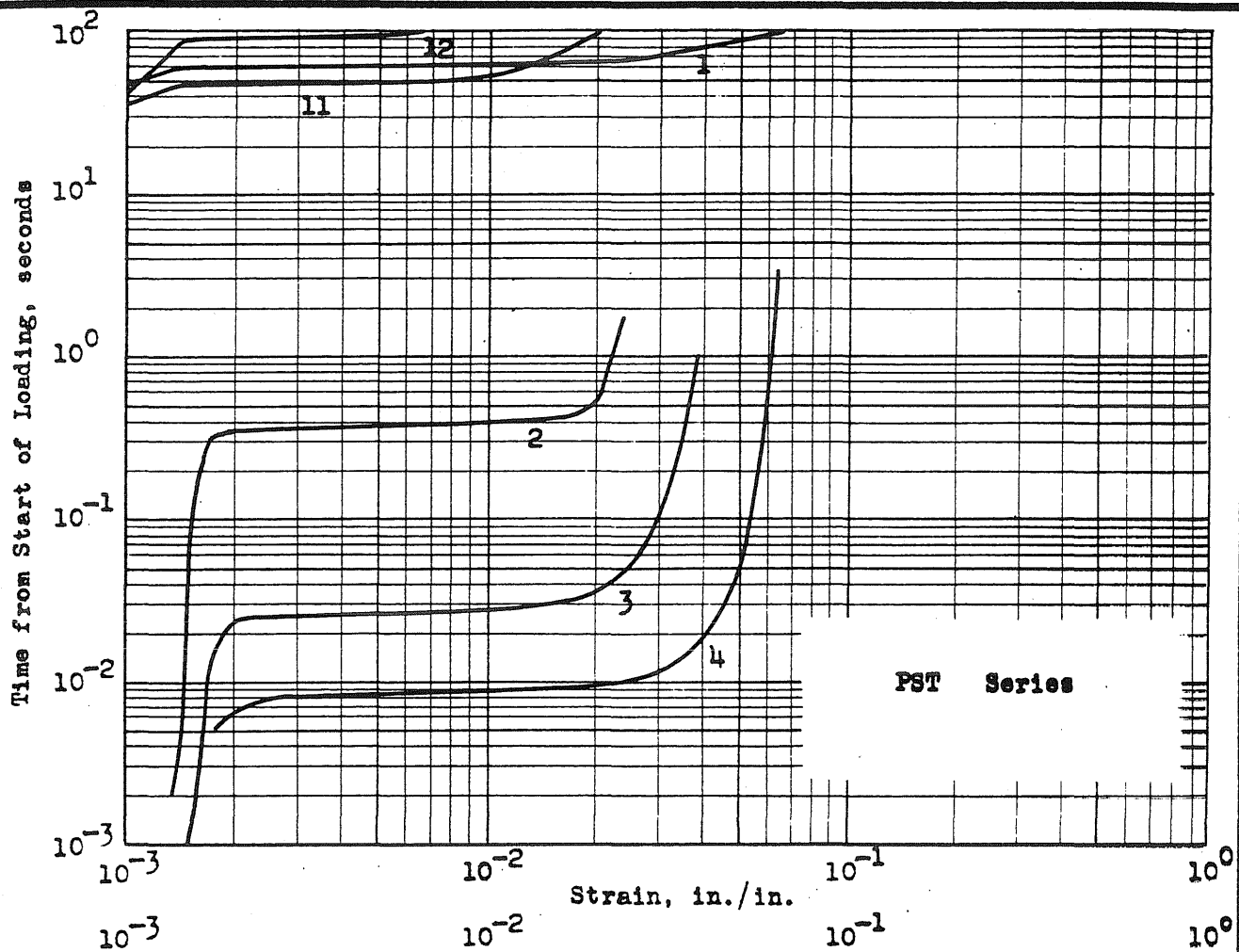


FIG. 21d STRESS-STRAIN AND STRAIN-TIME RELATIONSHIPS

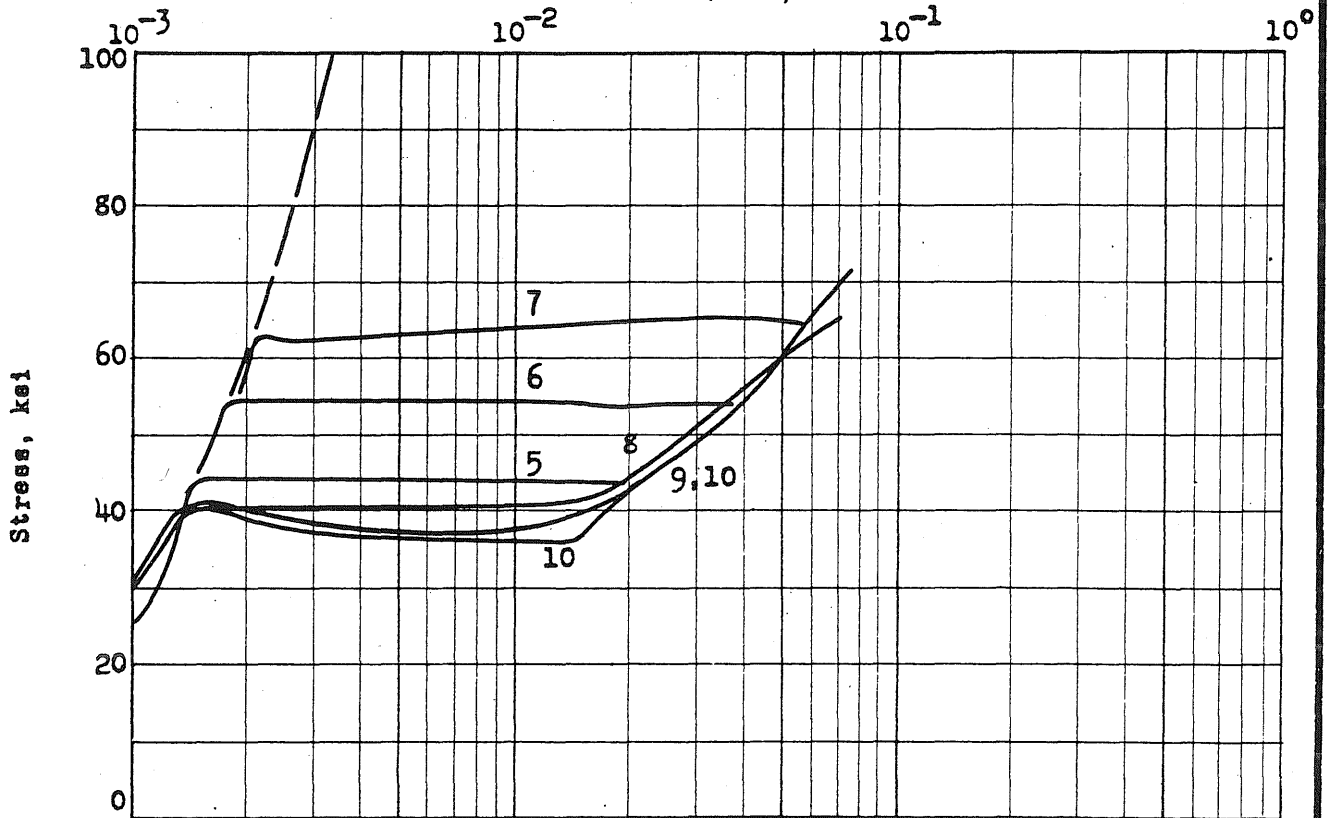
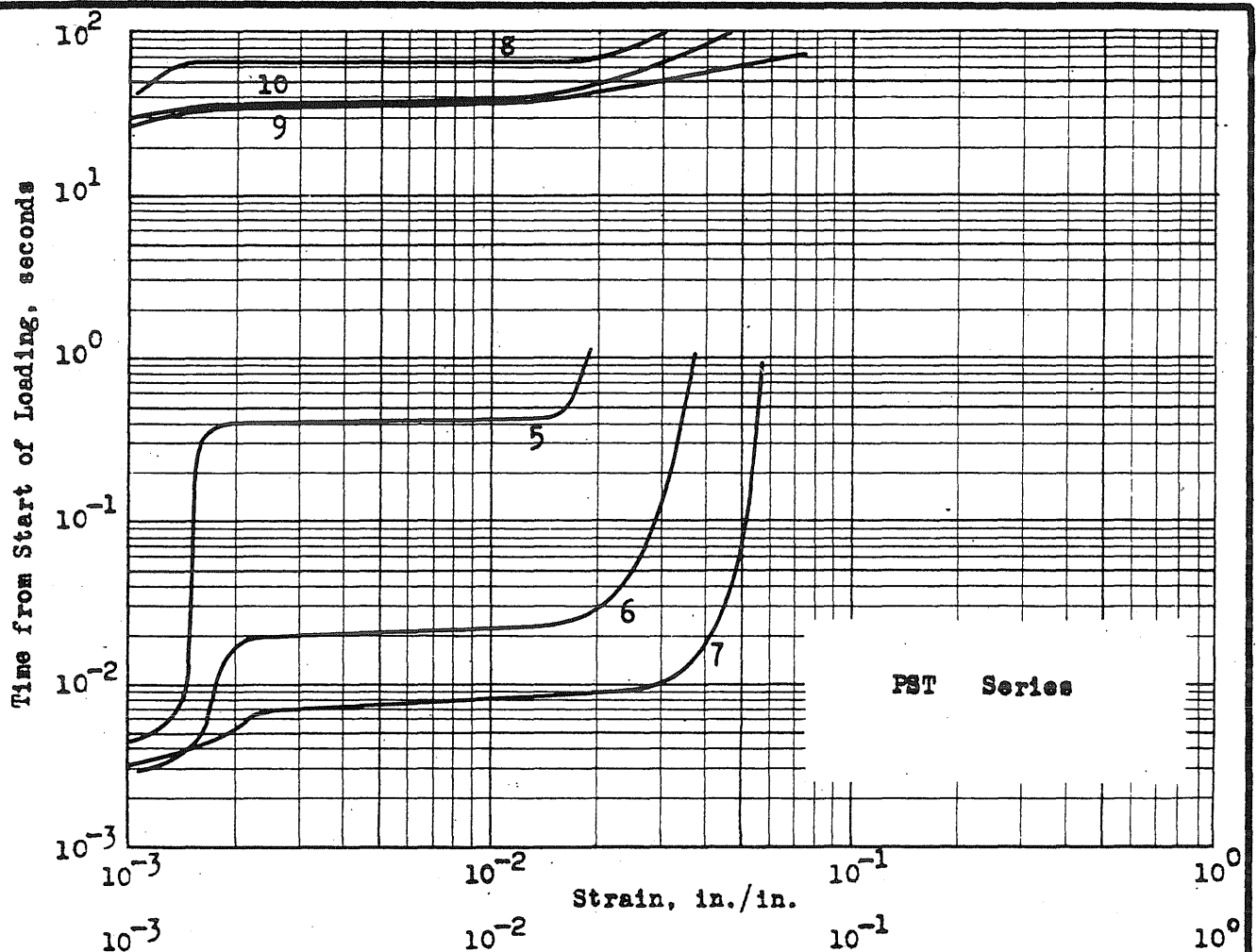


FIG. 21e STRESS-STRAIN AND STRAIN-TIME RELATIONSHIPS

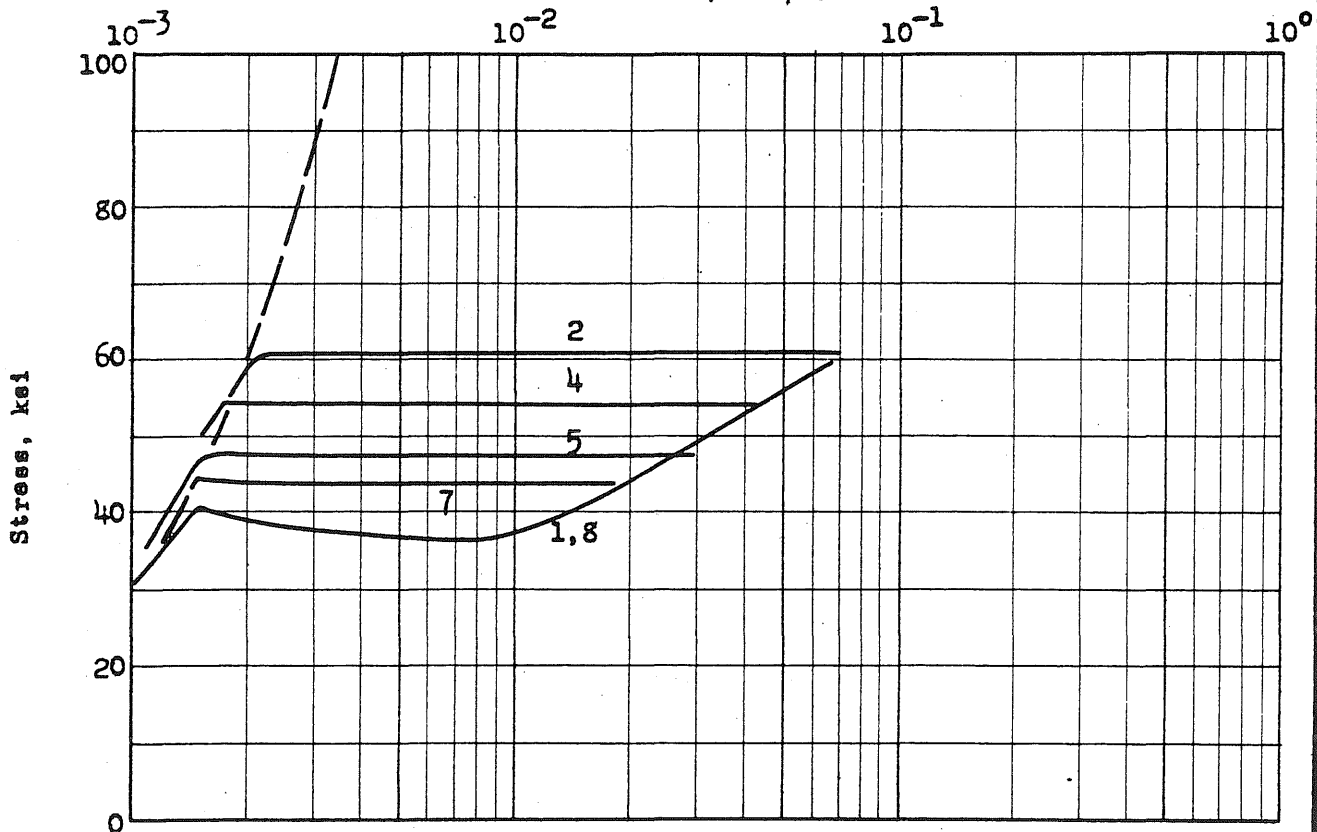
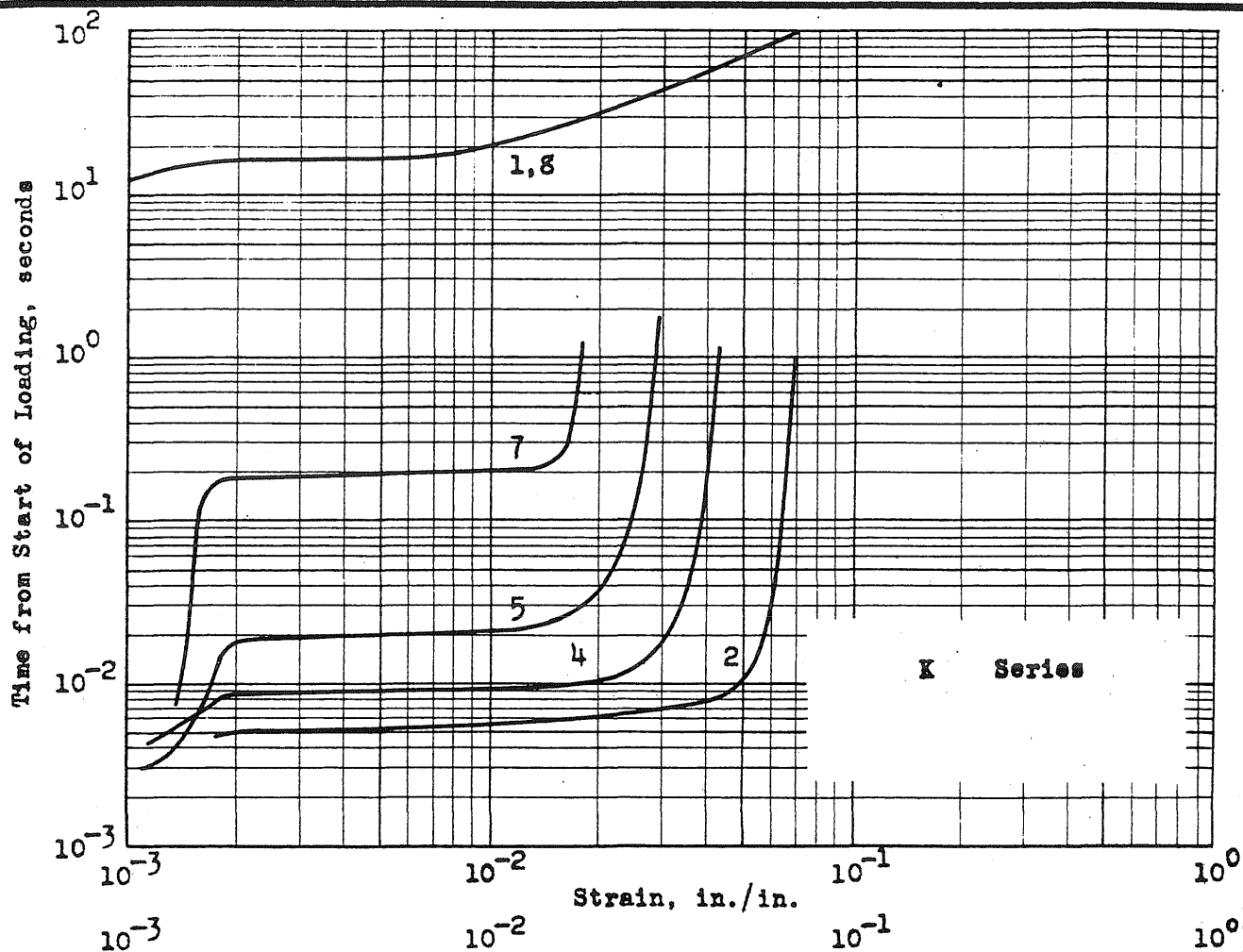


FIG. 21f STRESS-STRAIN AND STRAIN-TIME RELATIONSHIPS

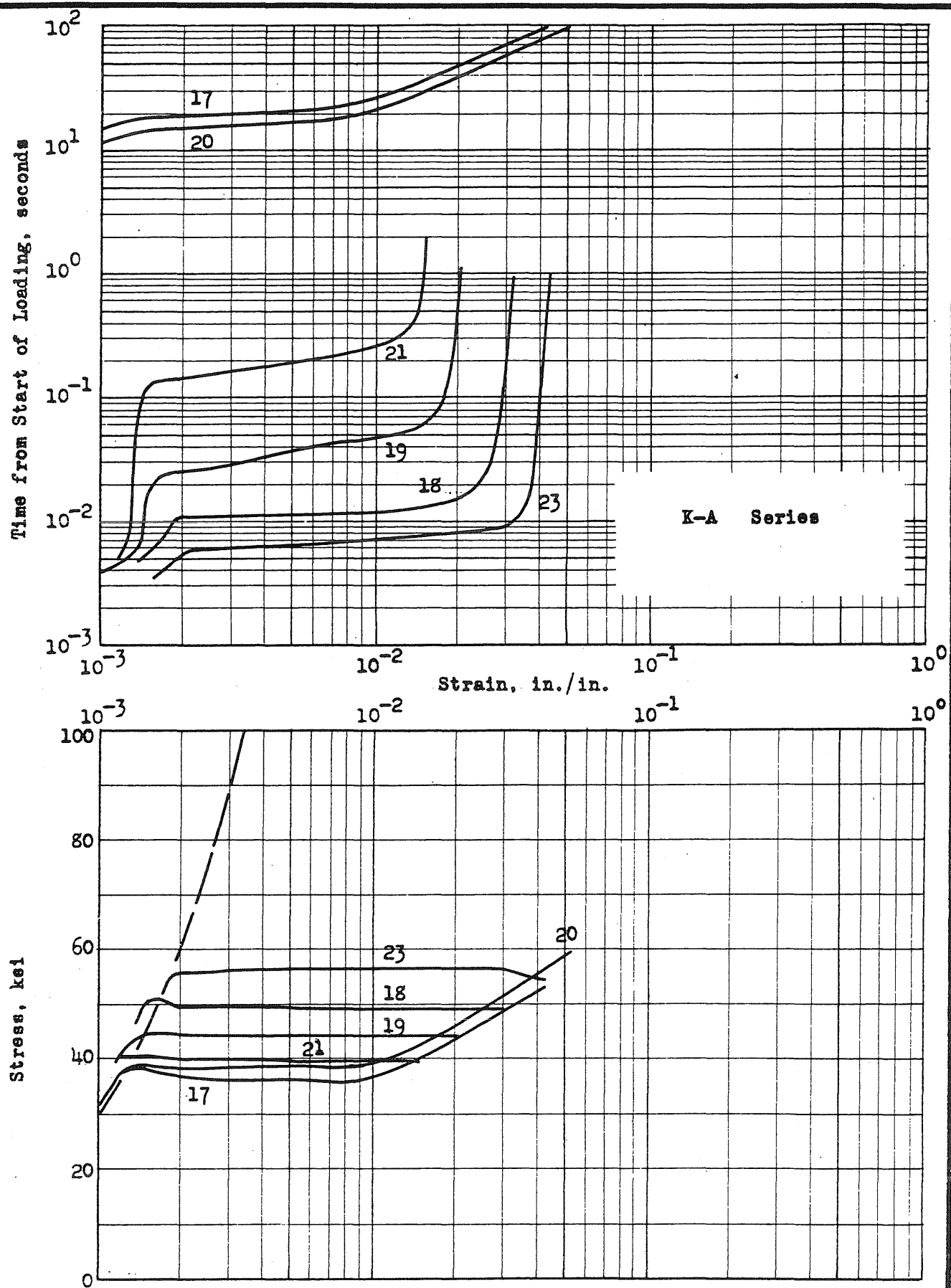


FIG. 21g. STRESS-STRAIN AND STRAIN-TIME RELATIONSHIPS

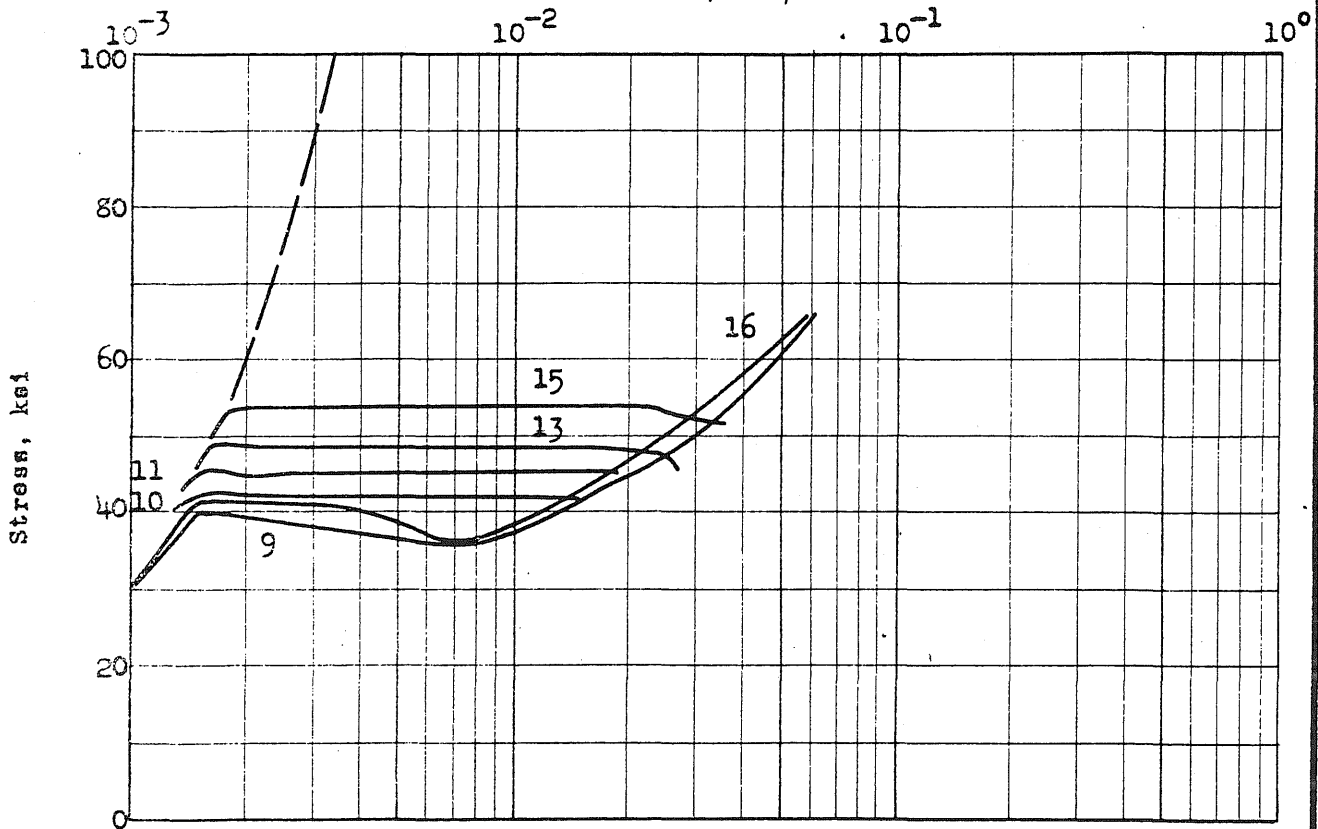
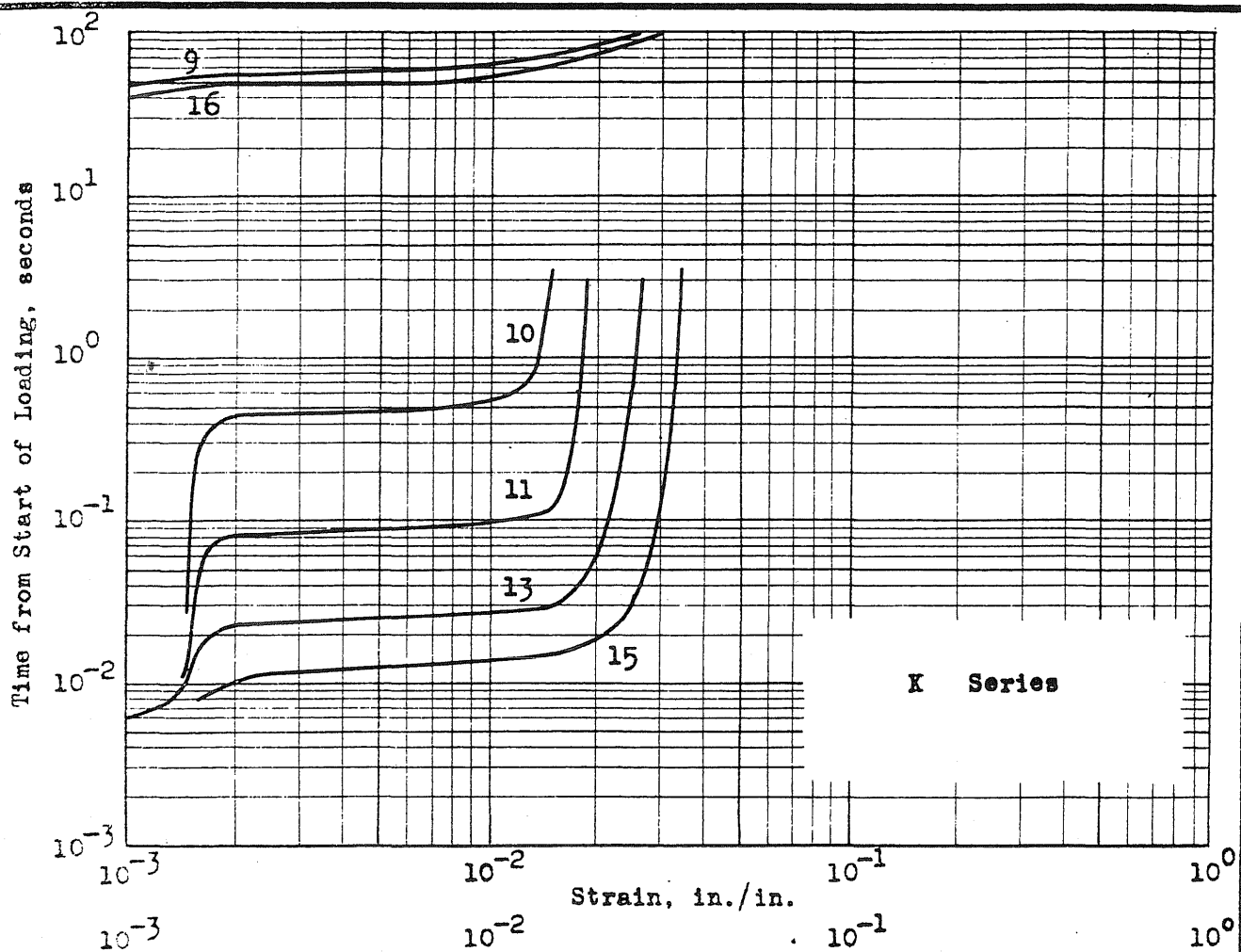


FIG. 21h STRESS-STRAIN AND STRAIN-TIME RELATIONSHIPS

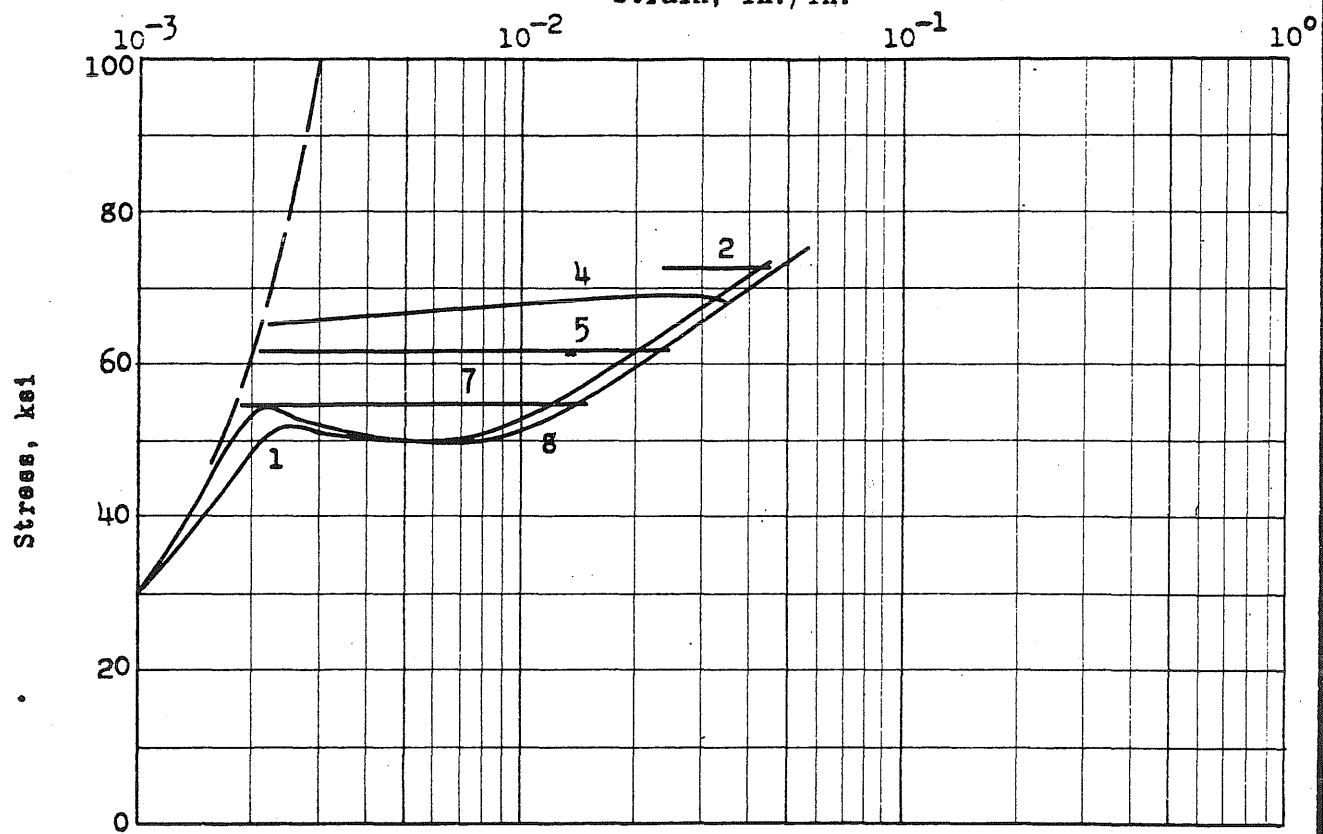
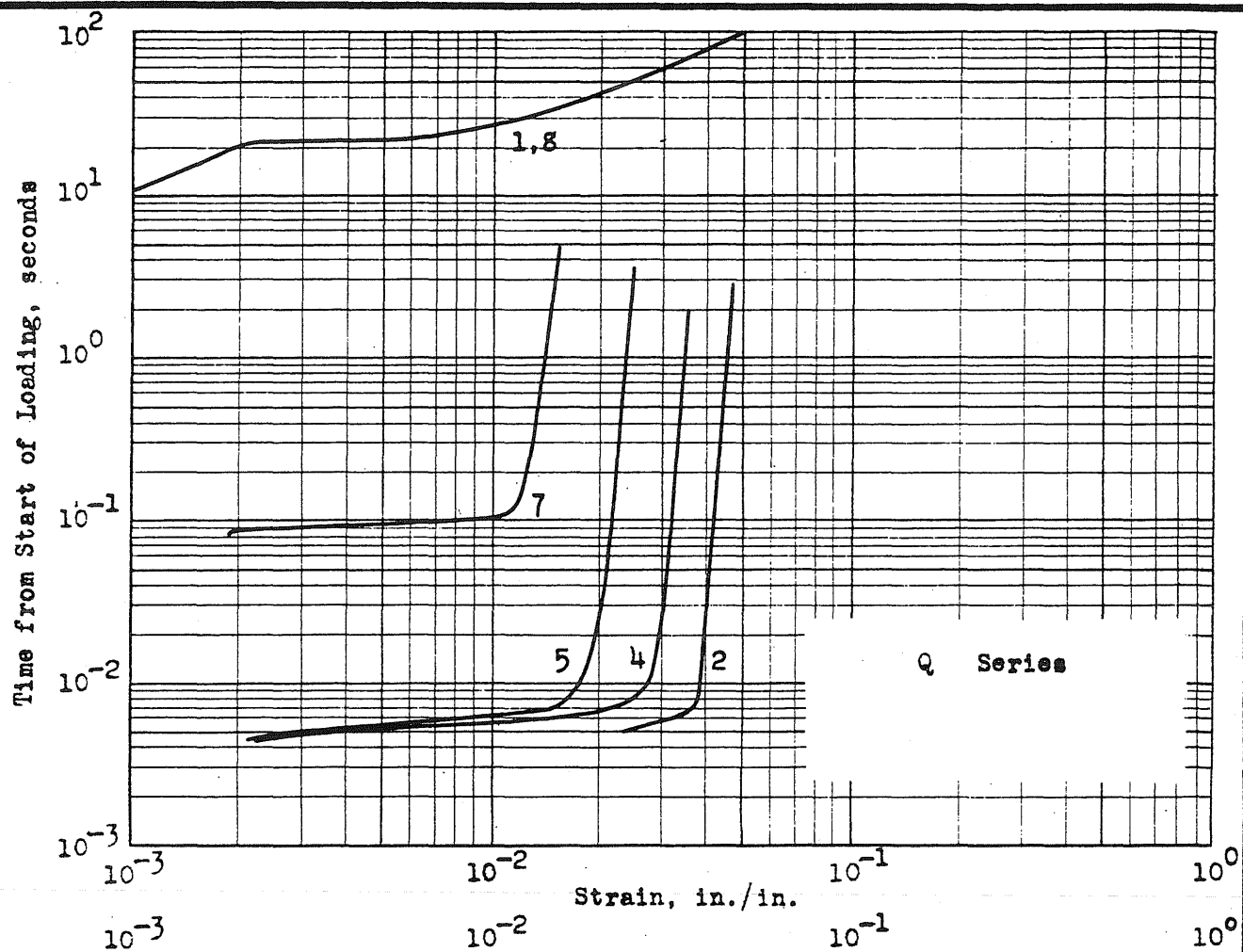


FIG. 211 STRESS-STRAIN AND STRAIN-TIME RELATIONSHIPS

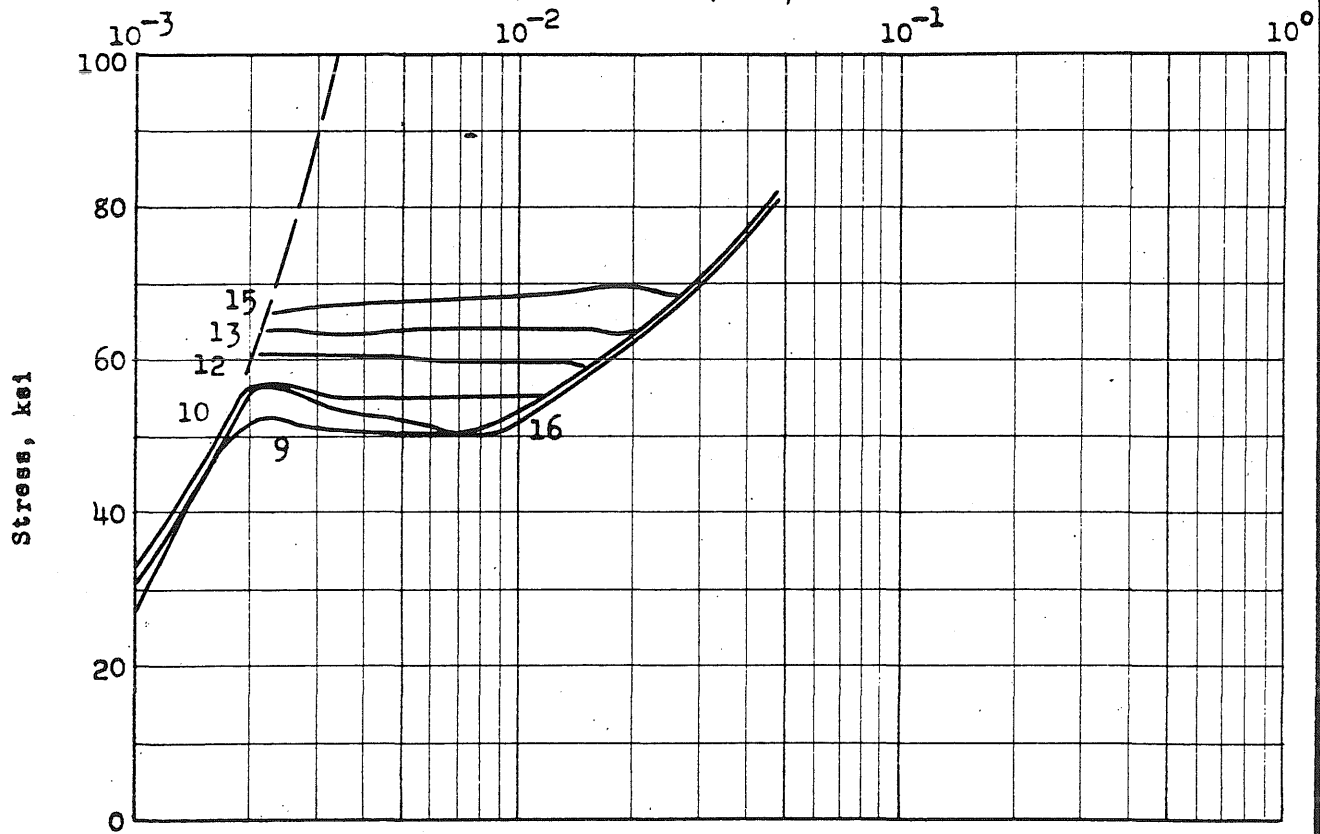
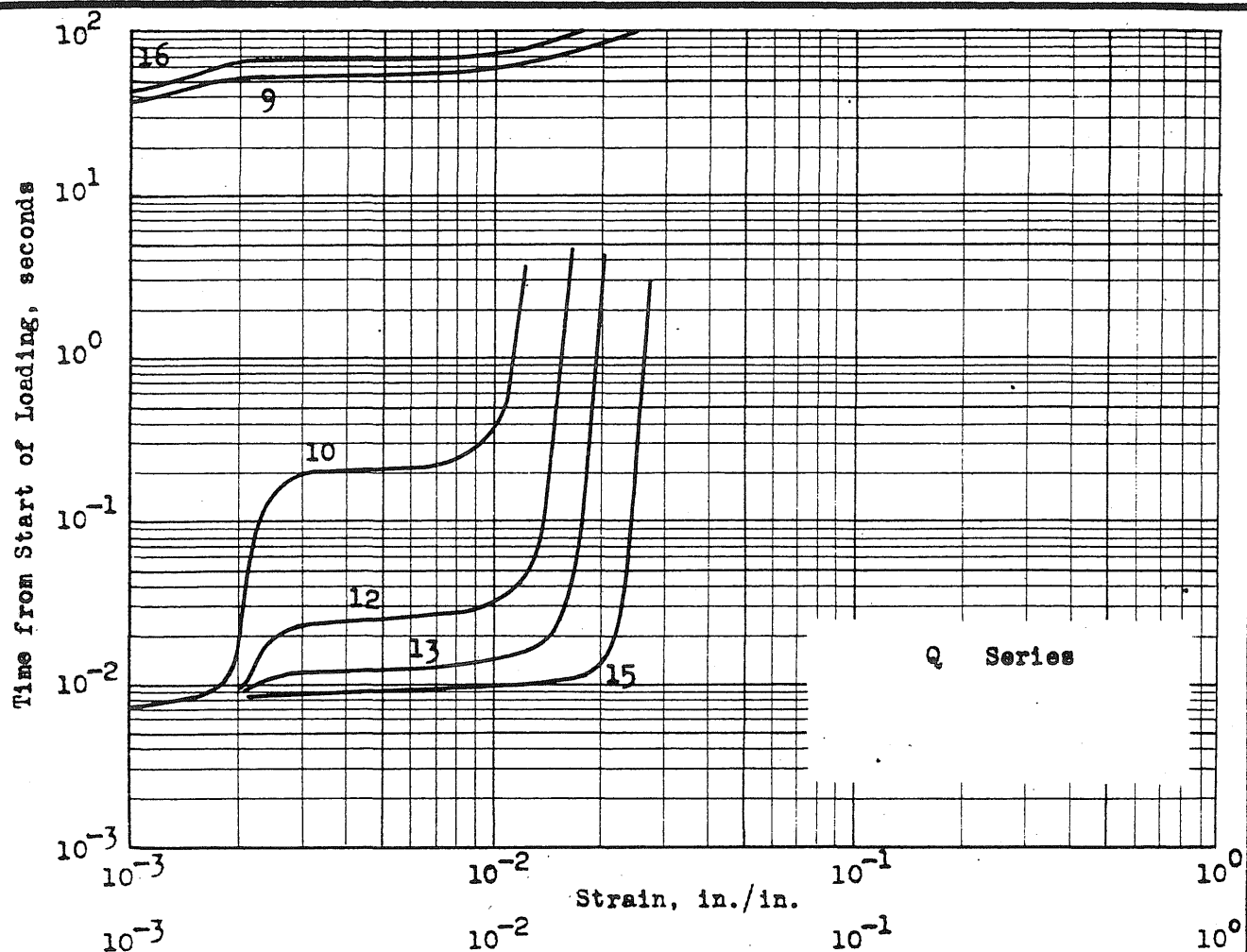


FIG. 21j STRESS-STRAIN AND STRAIN-TIME RELATIONSHIPS

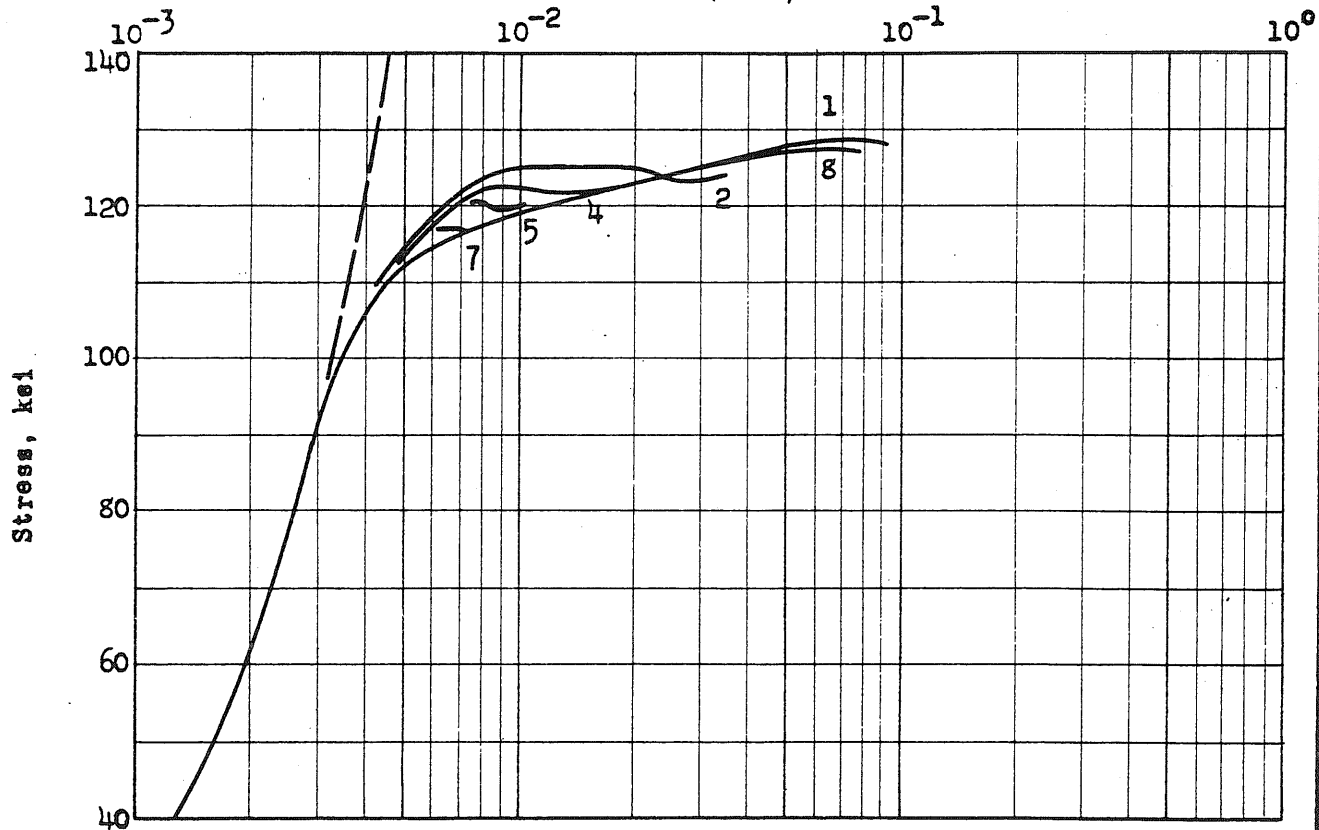
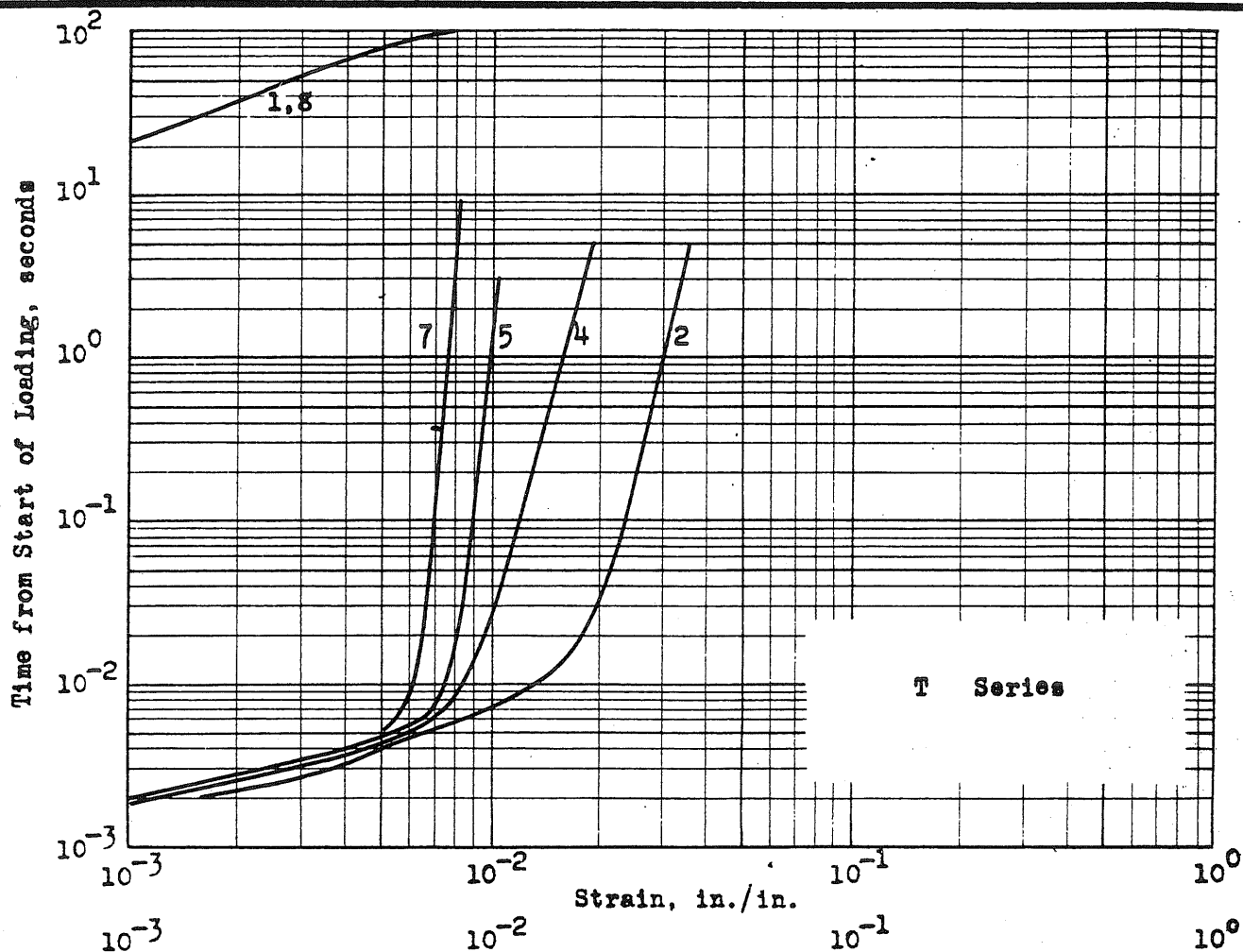


FIG. 21k STRESS-STRAIN AND STRAIN-TIME RELATIONSHIPS

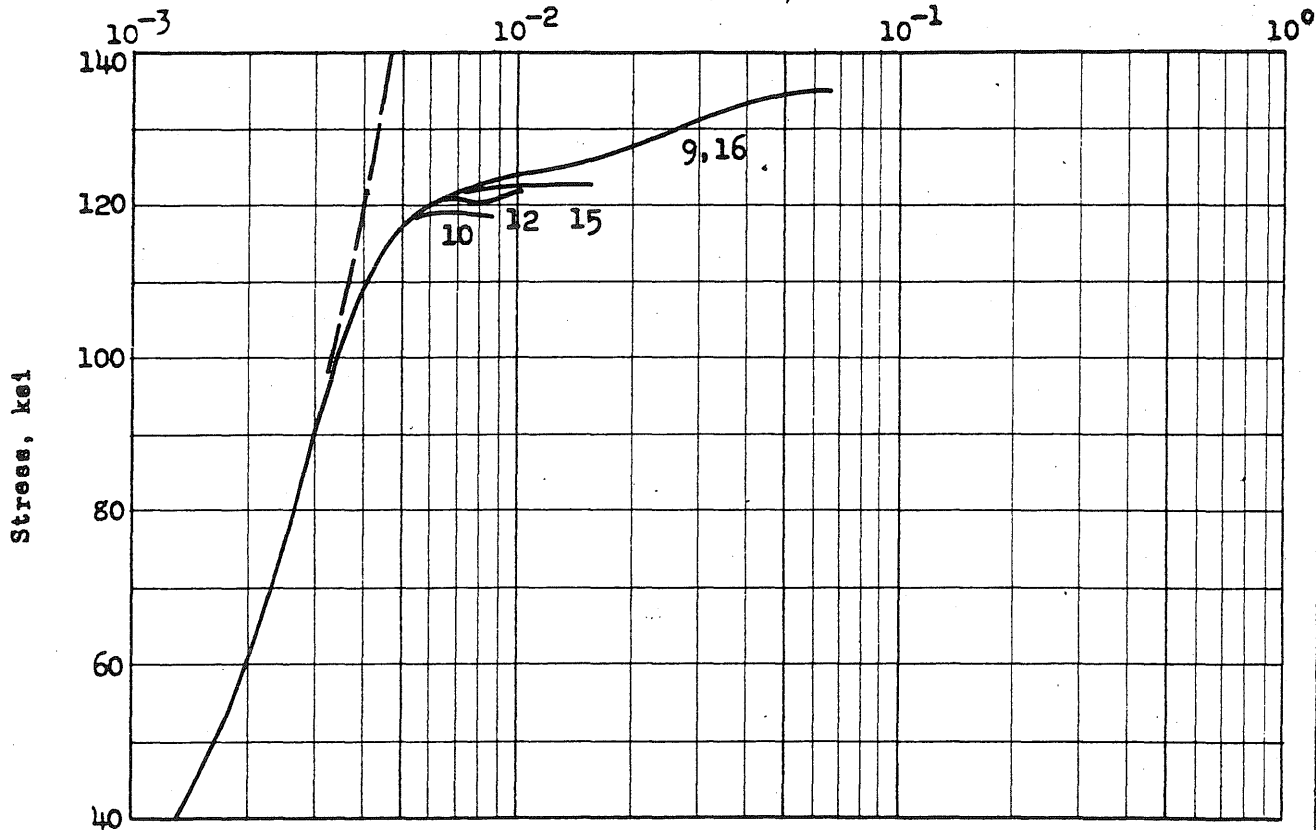
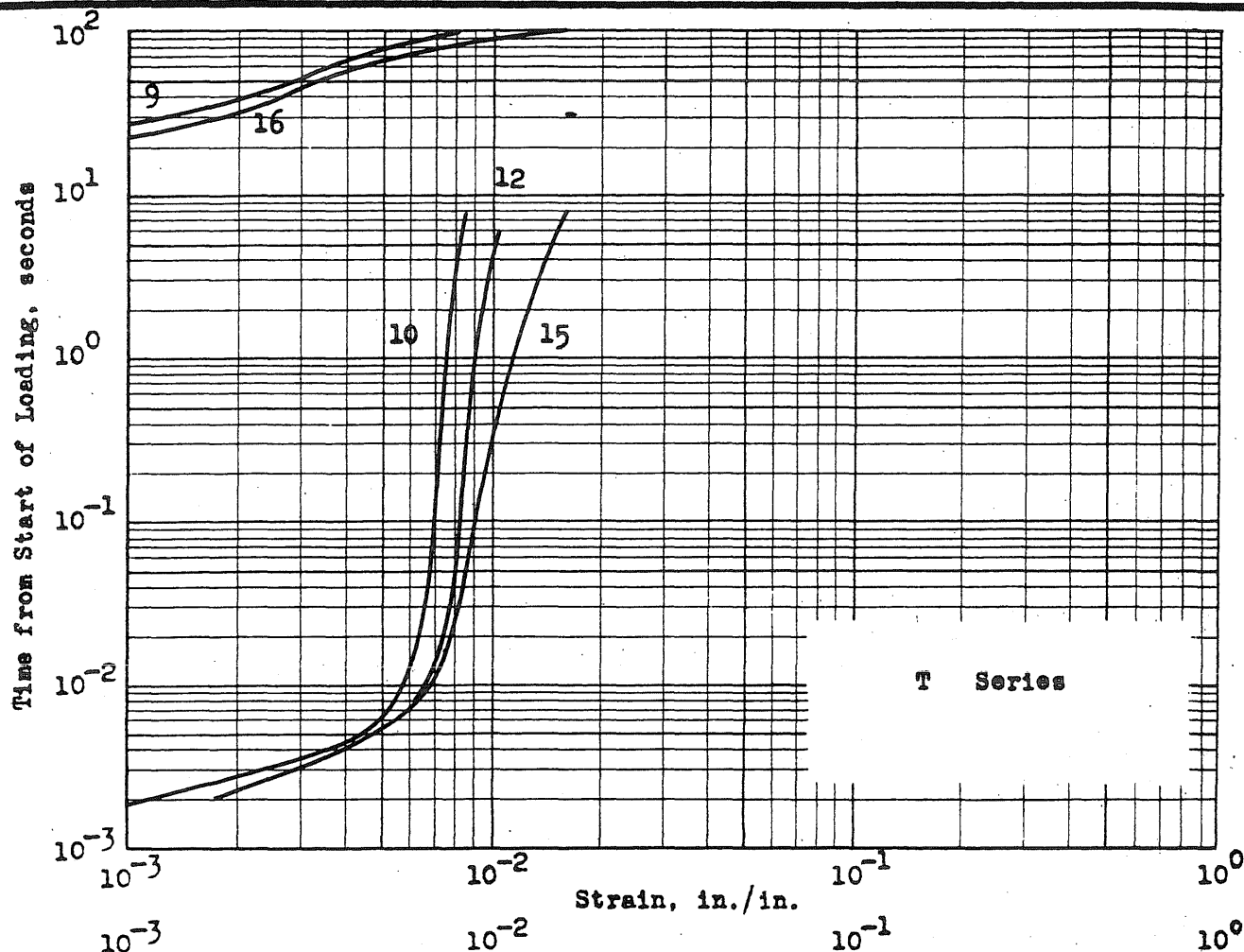


FIG. 211 STRESS-STRAIN AND STRAIN-TIME RELATIONSHIPS

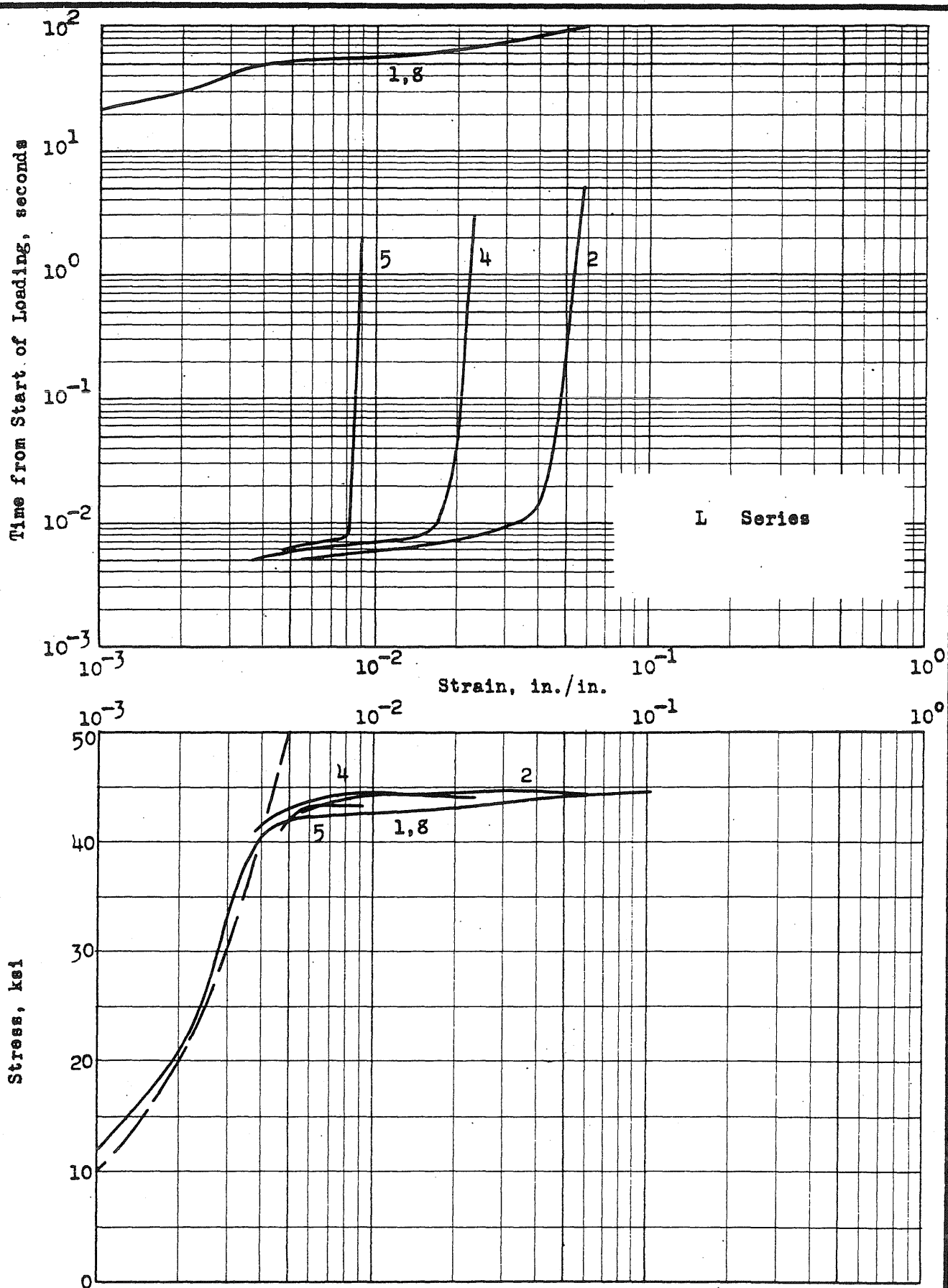


FIG. 21m STRESS-STRAIN AND STRAIN-TIME RELATIONSHIPS

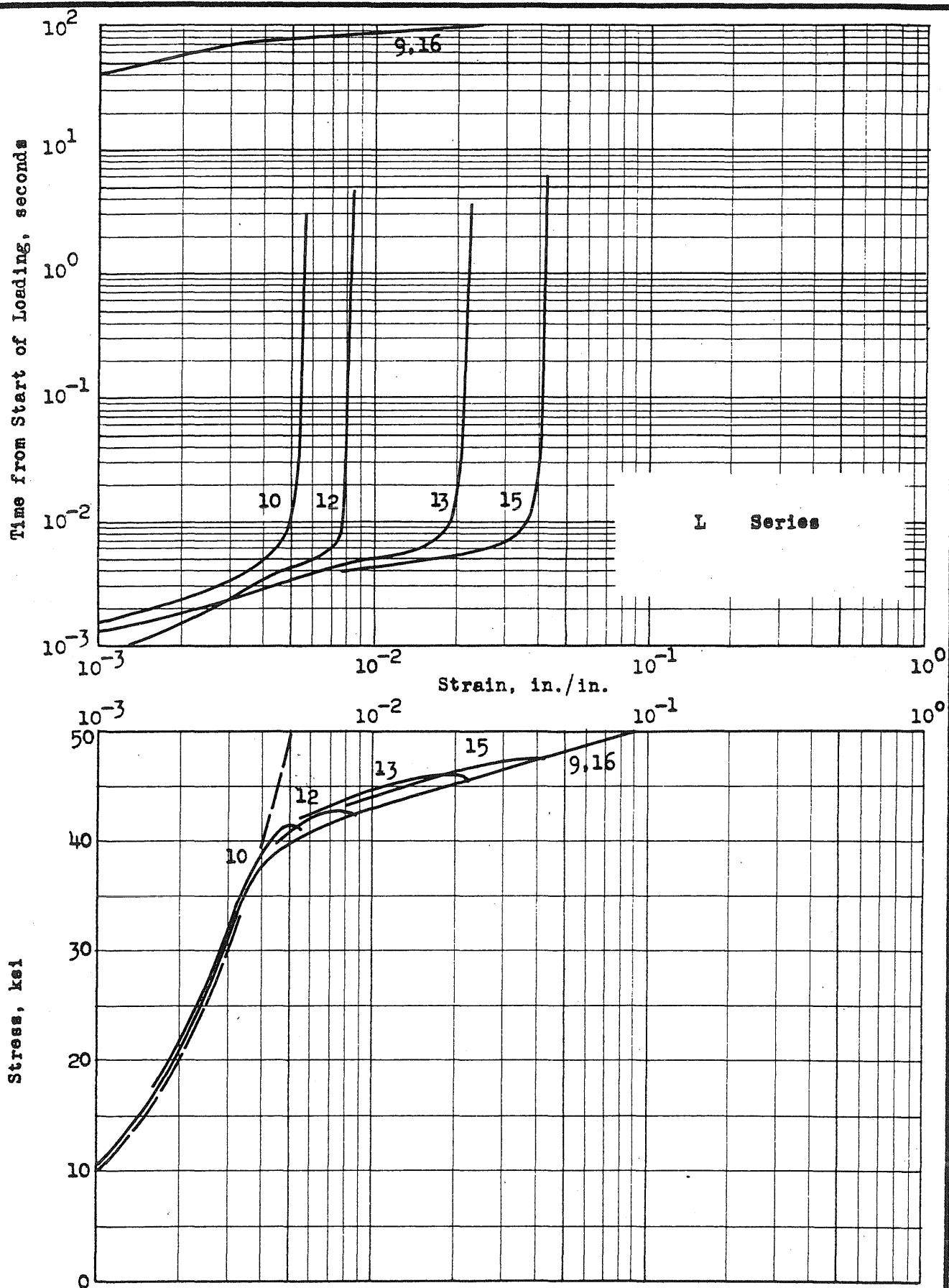


FIG. 2ln STRESS-STRAIN AND STRAIN-TIME RELATIONSHIPS

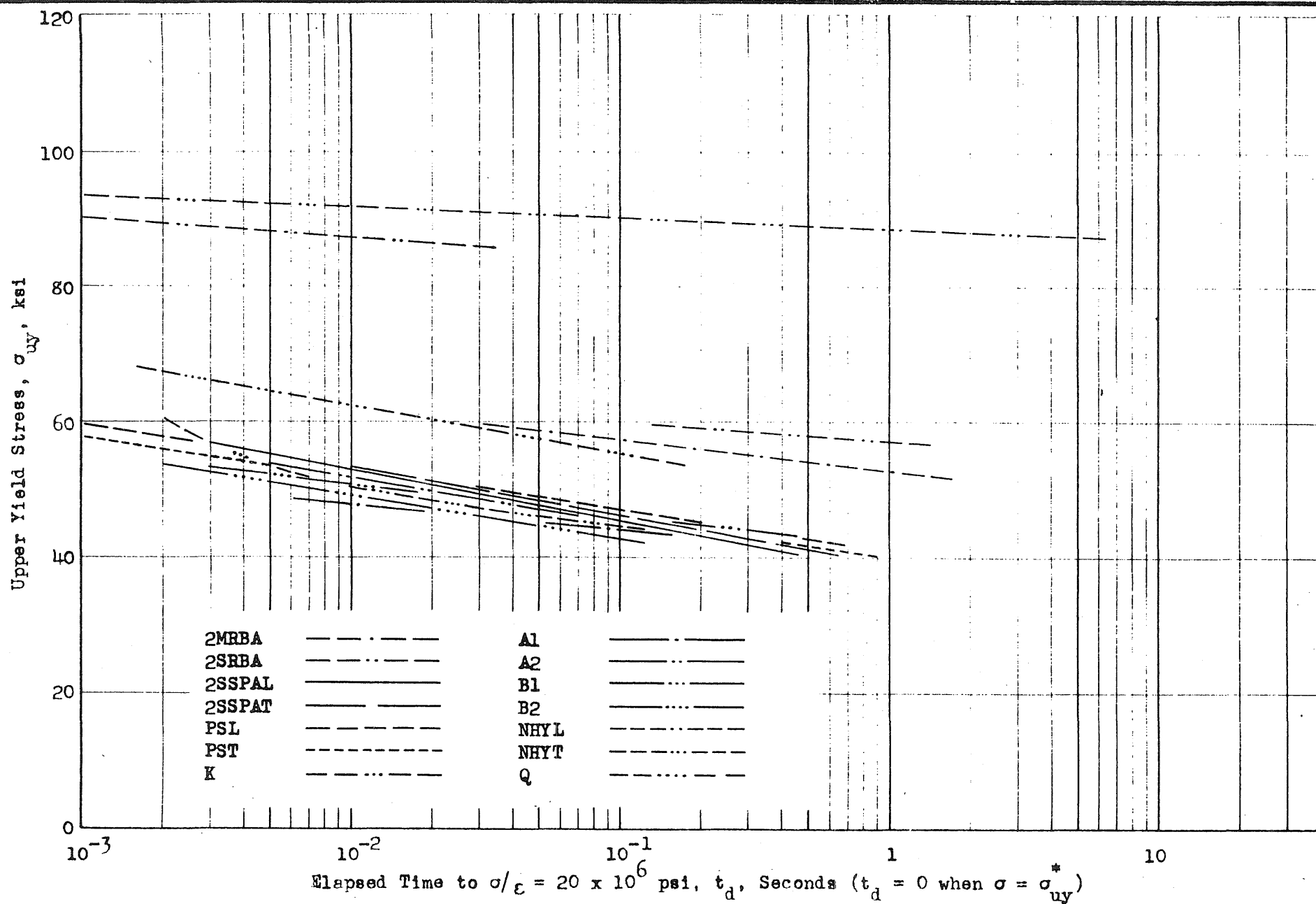


FIG. 22 UPPER YIELD STRESS - ELAPSED TIME TO $\sigma/\epsilon = 20 \times 10^6$

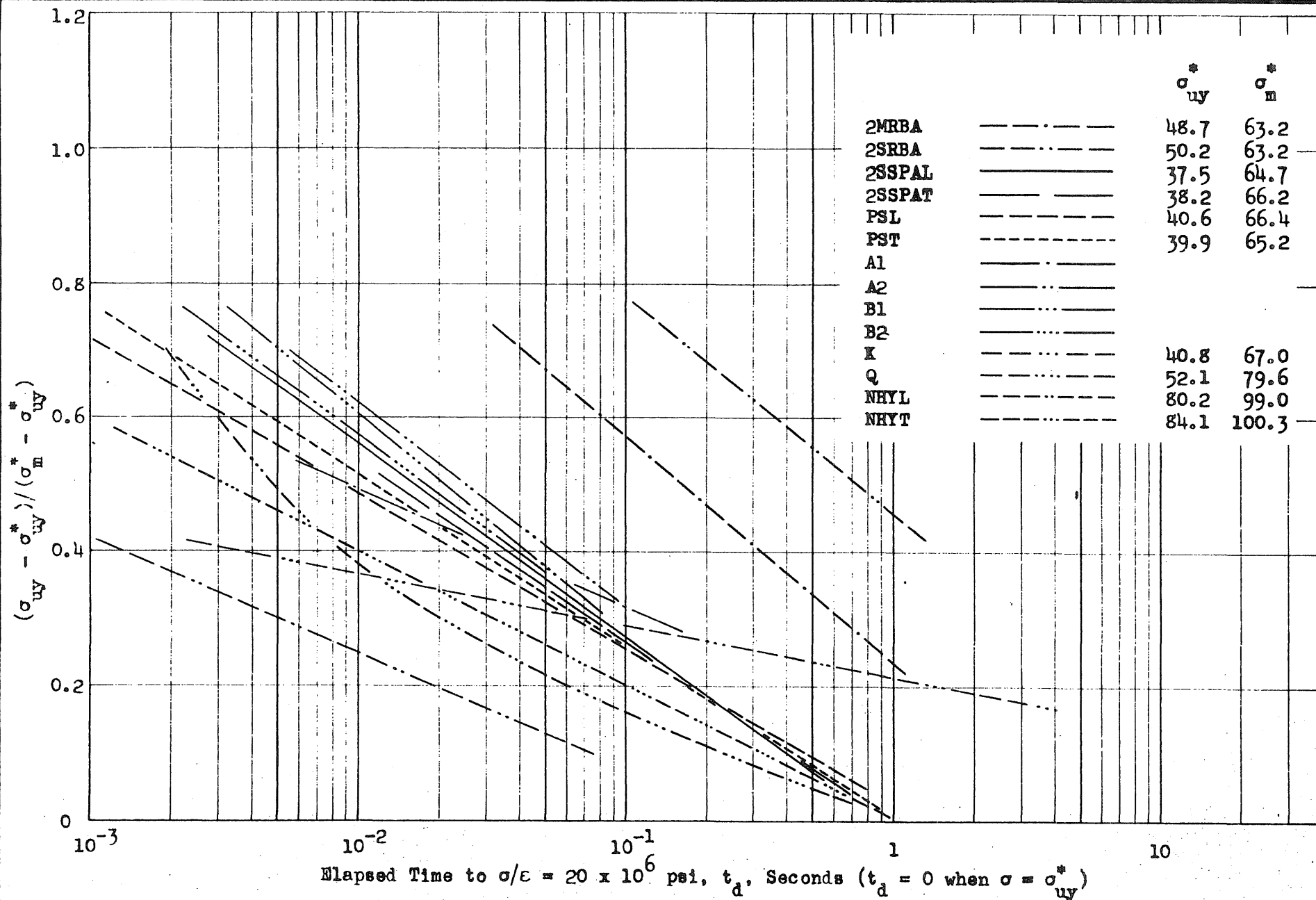


FIG. 23a UPPER YIELD STRESS PARAMETER - ELAPSED TIME TO $\sigma/\epsilon = 20 \times 10^6$ psi

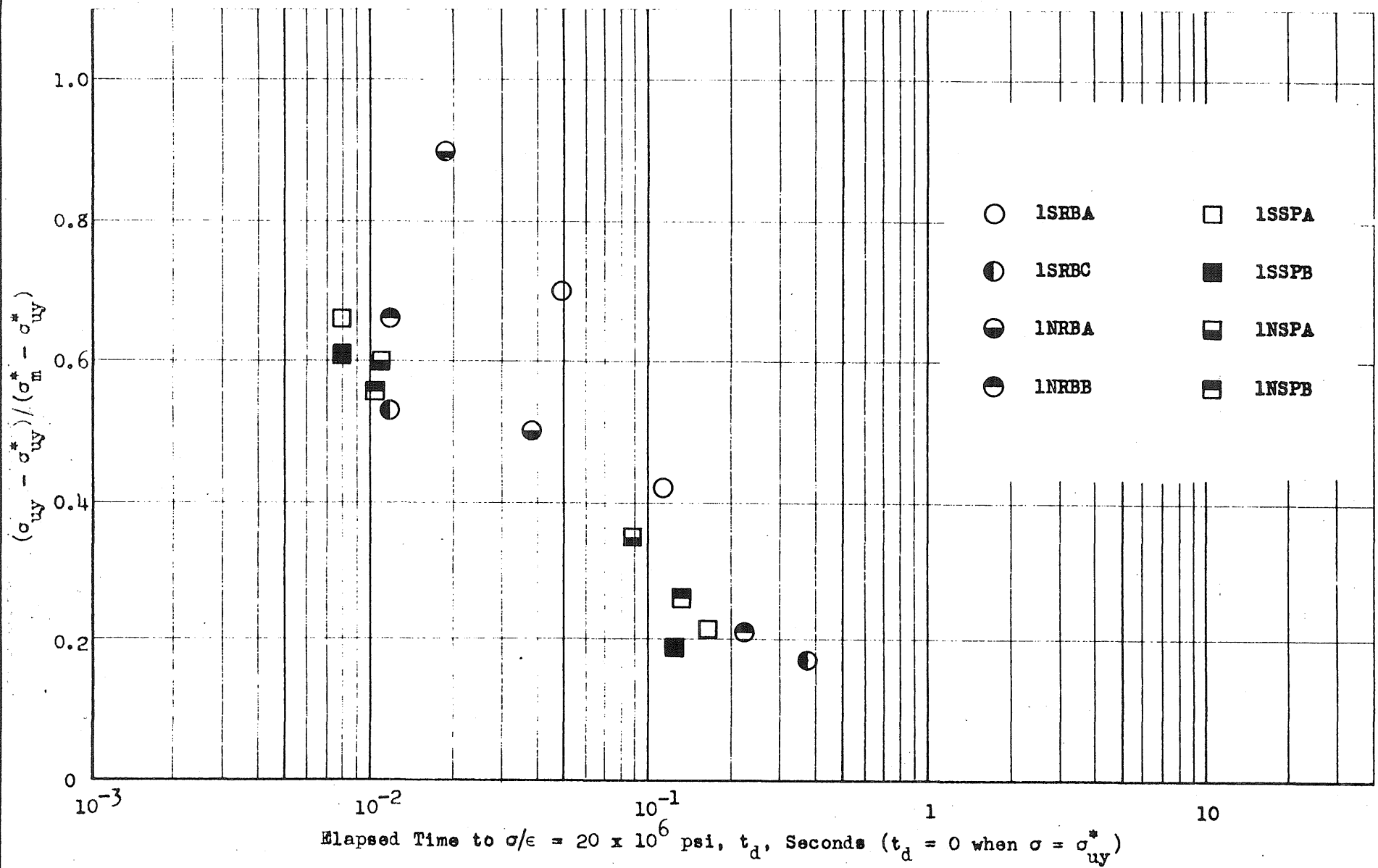


FIG. 23b YIELD STRESS PARAMETER -- ELAPSED TIME TO $\sigma/\epsilon = 20 \times 10^6$ psi

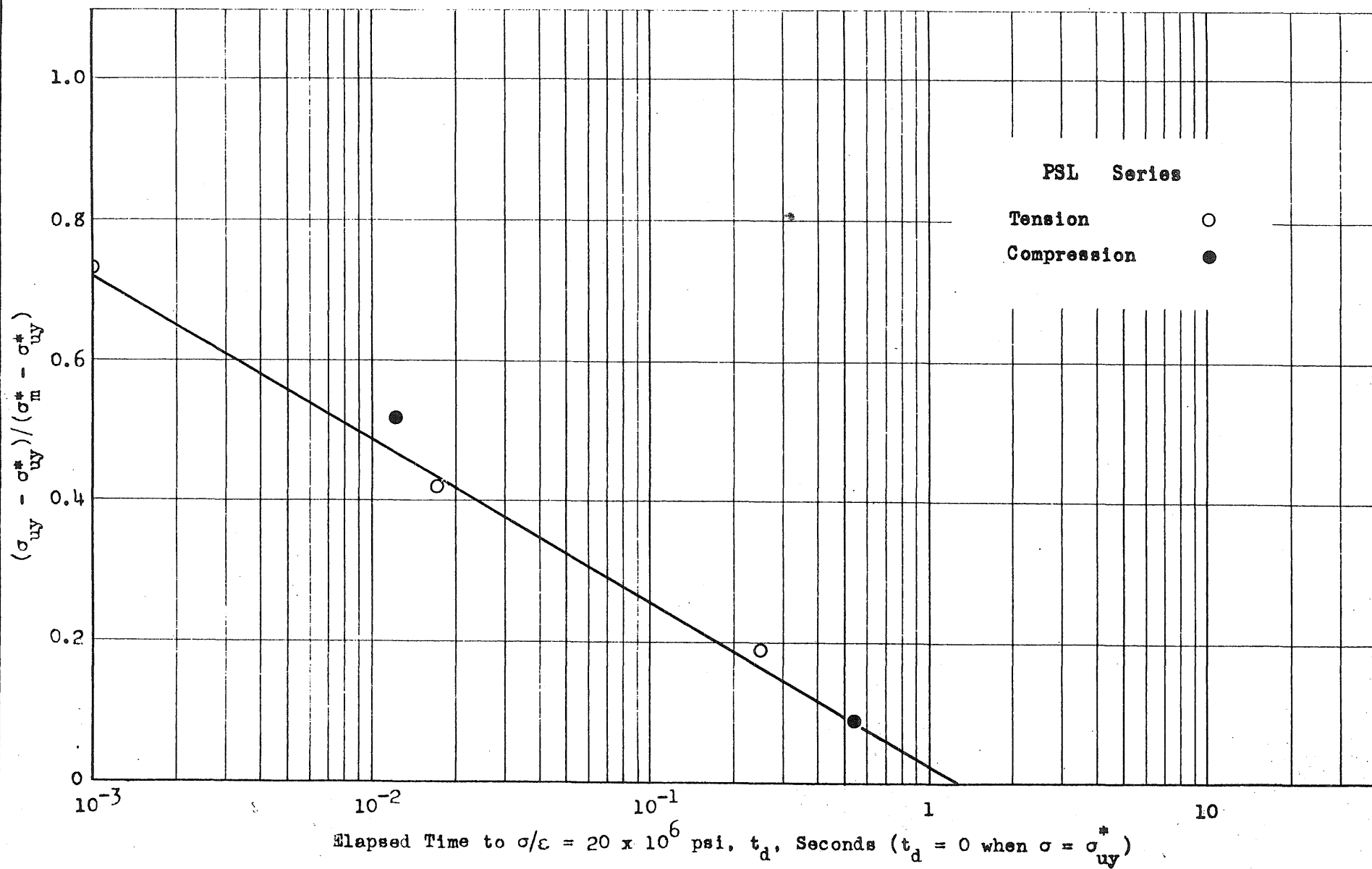


FIG. 23c YIELD STRESS PARAMETER - ELAPSED TIME TO $\sigma/\epsilon = 20 \times 10^6$ psi

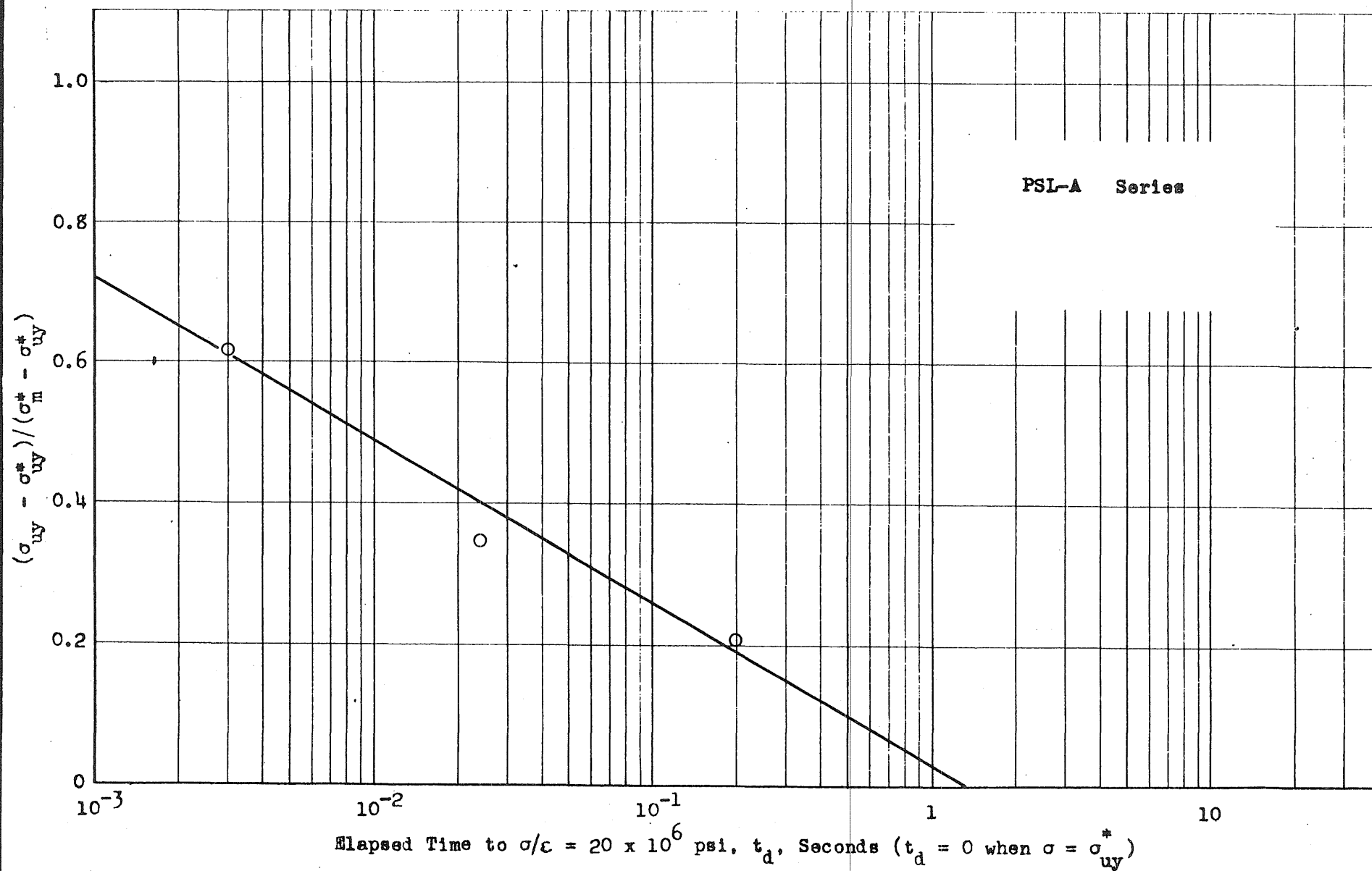


FIG. 23d YIELD STRESS PARAMETER - ELAPSED TIME TO $\sigma/\epsilon = 20 \times 10^6$ psi

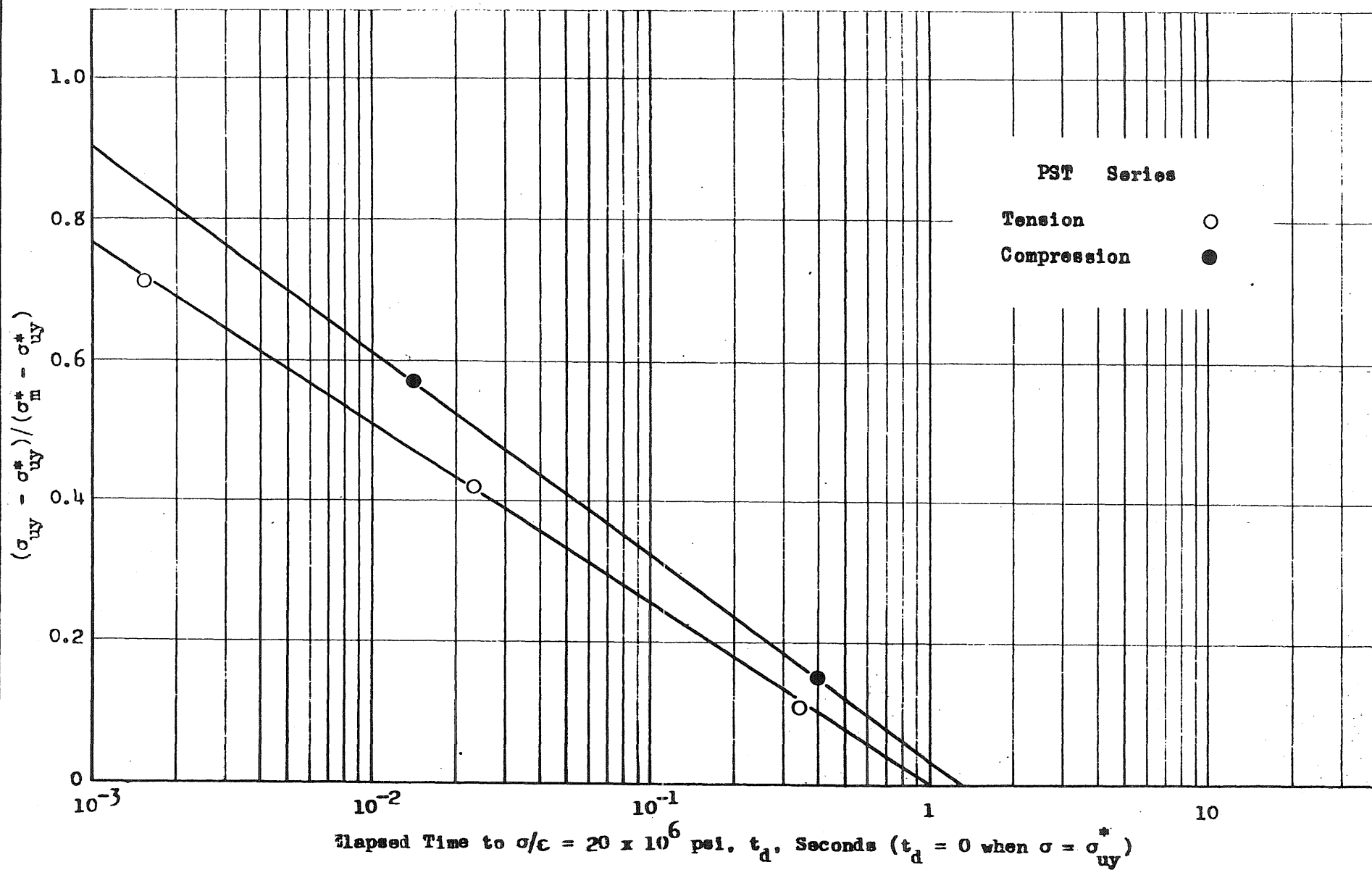


FIG. 23e YIELD STRESS PARAMETER - ELAPSED TIME TO $\sigma/\epsilon = 20 \times 10^6$ psi

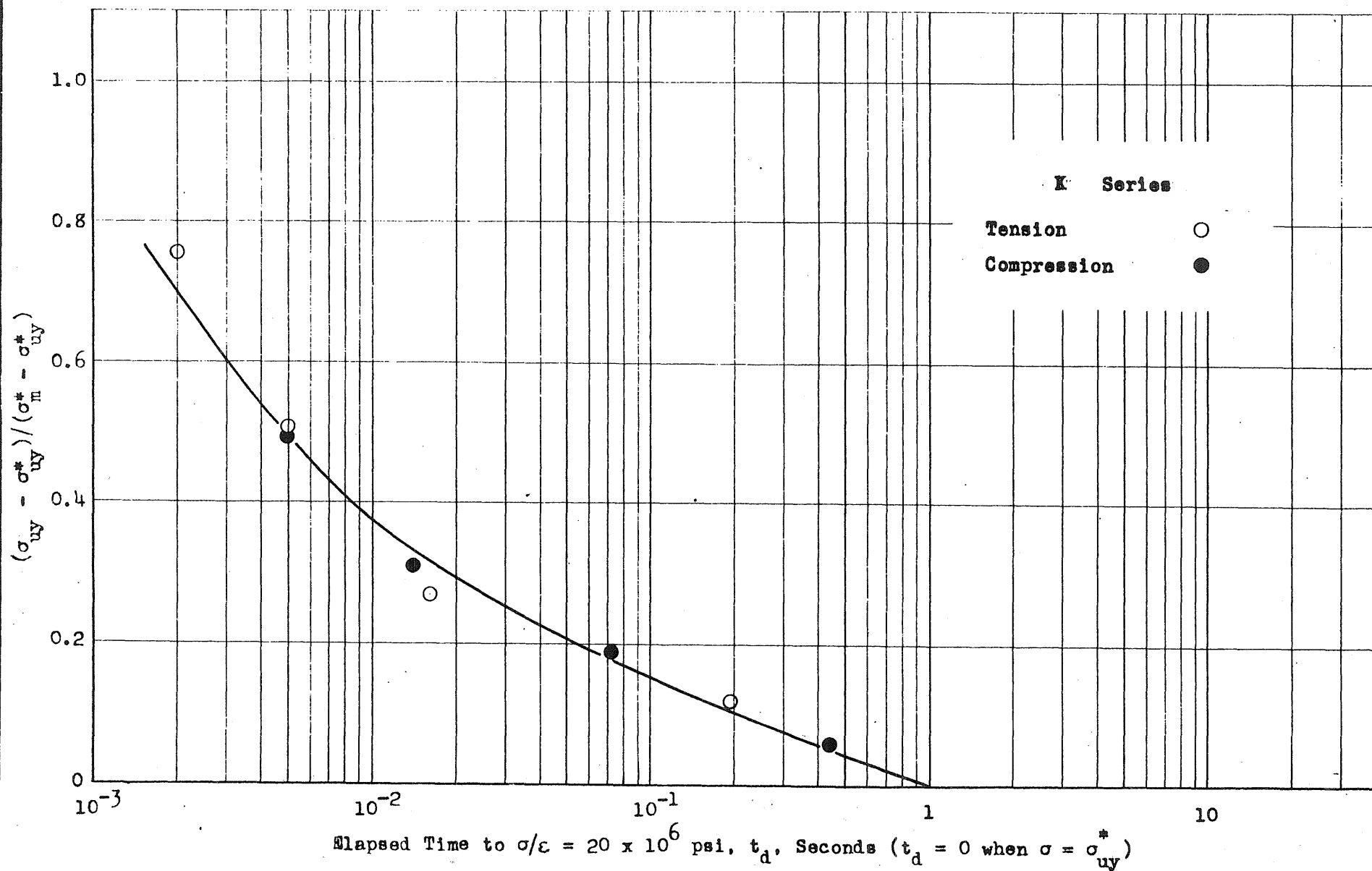


FIG. 23f YIELD STRESS PARAMETER - ELAPSED TIME TO $\sigma/\epsilon = 20 \times 10^6$ psi

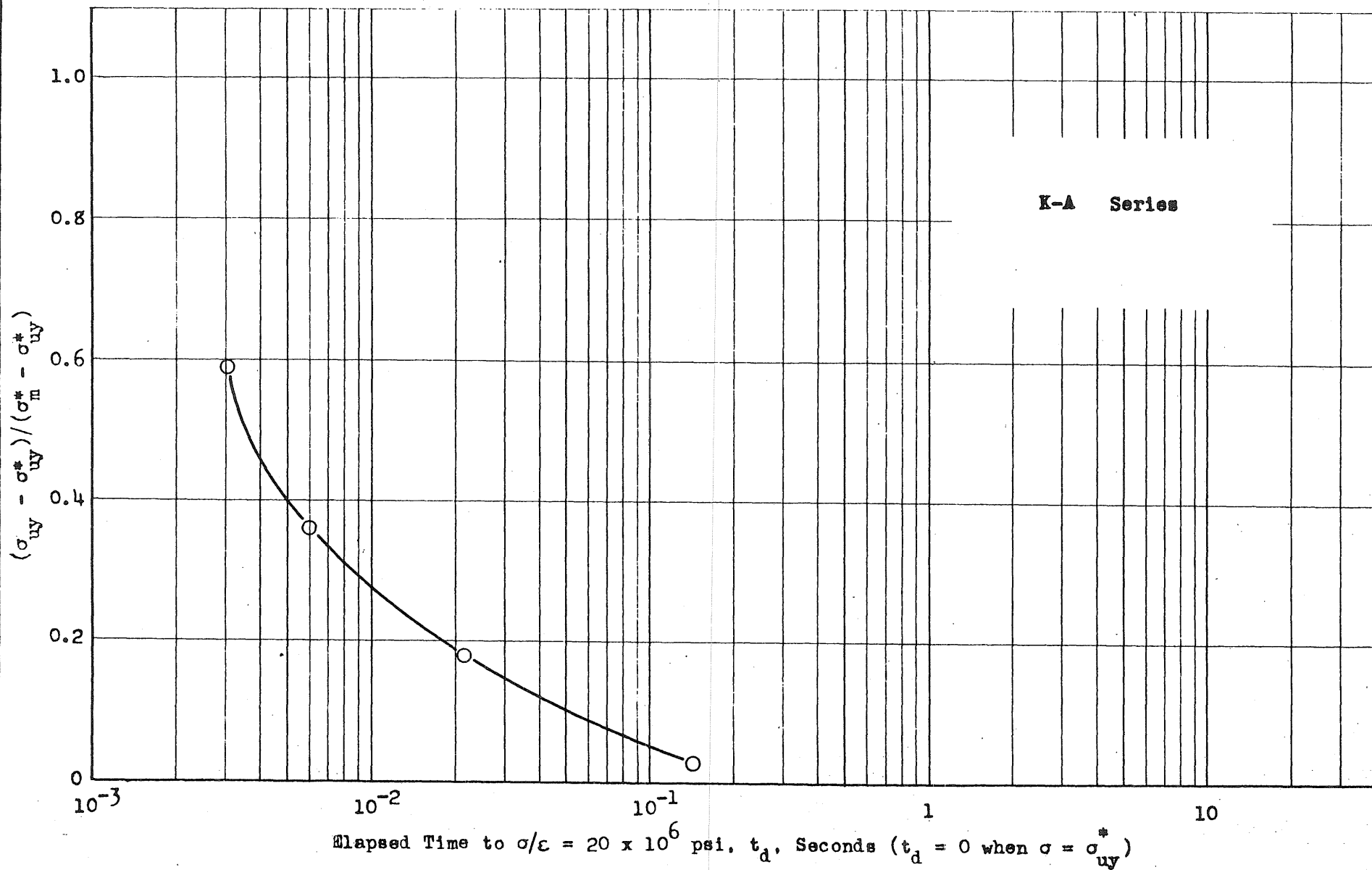


FIG. 23g YIELD STRESS PARAMETER - ELAPSED TIME TO $\sigma/\epsilon = 20 \times 10^6$ psi

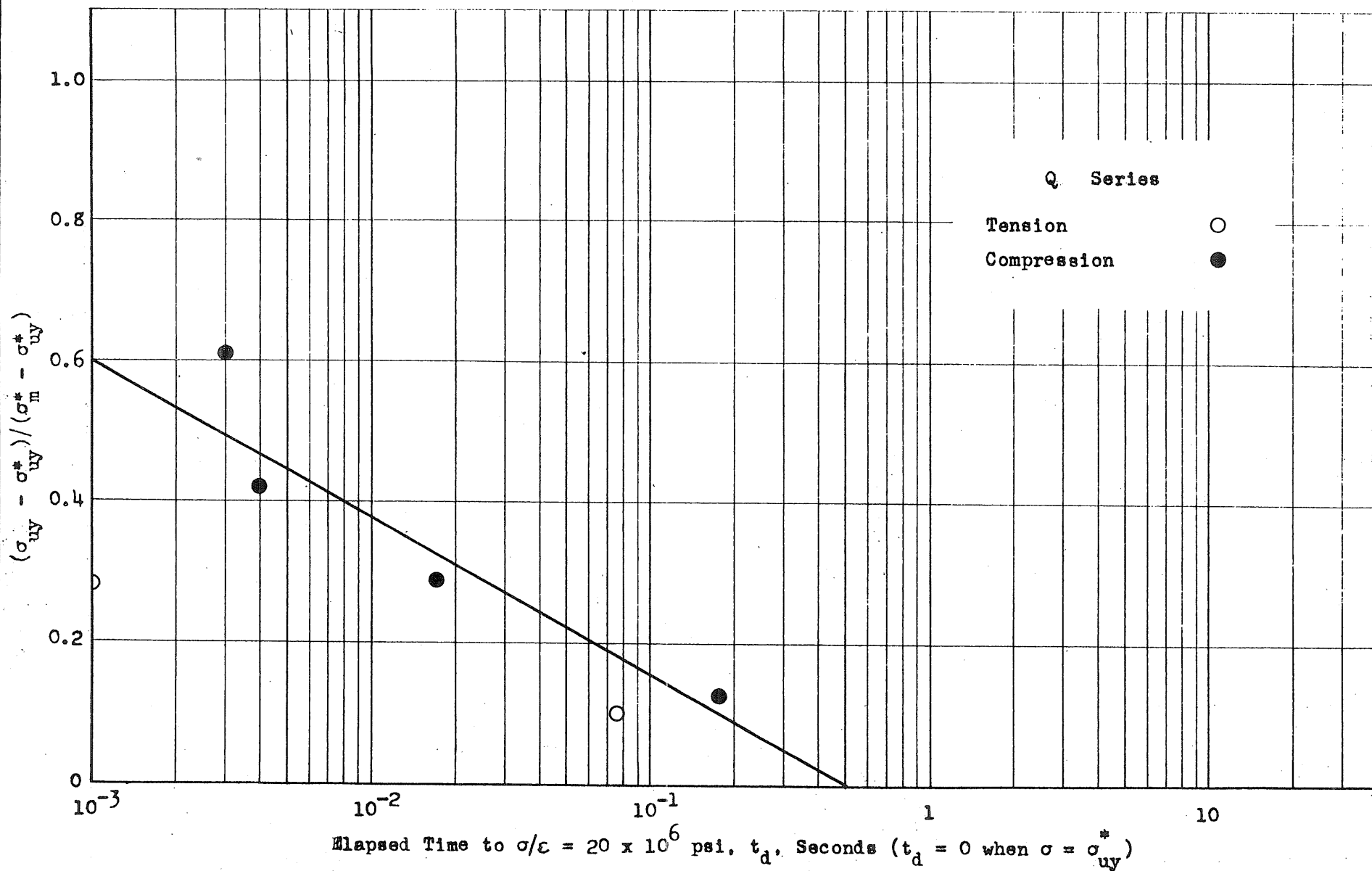


FIG. 23h YIELD STRESS PARAMETER - ELAPSED TIME TO $\sigma/\epsilon = 20 \times 10^6$ psi

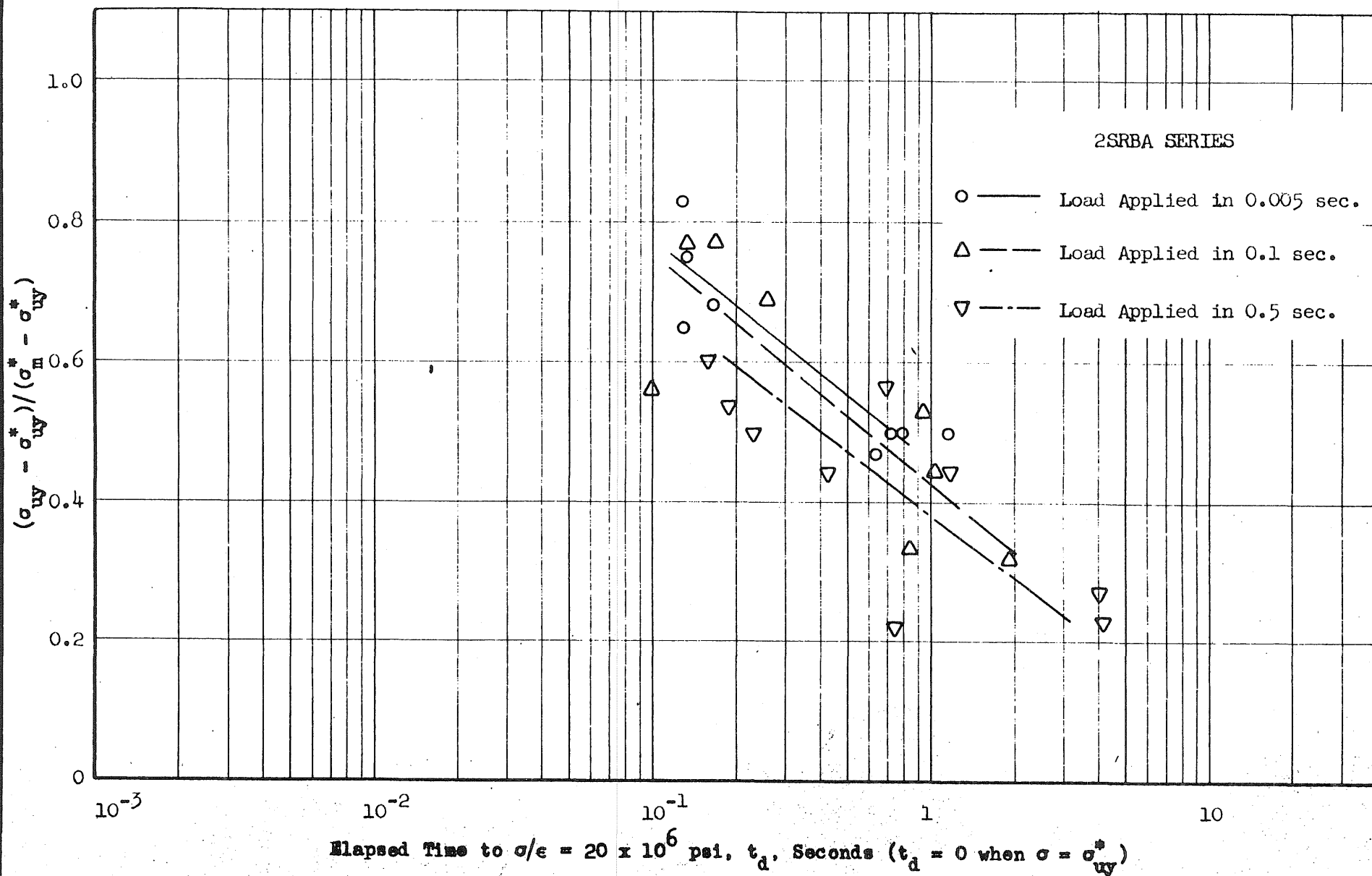


FIG. 24a YIELD STRESS PARAMETER - ELAPSED TIME TO $\sigma/\epsilon = 20 \times 10^6$ psi

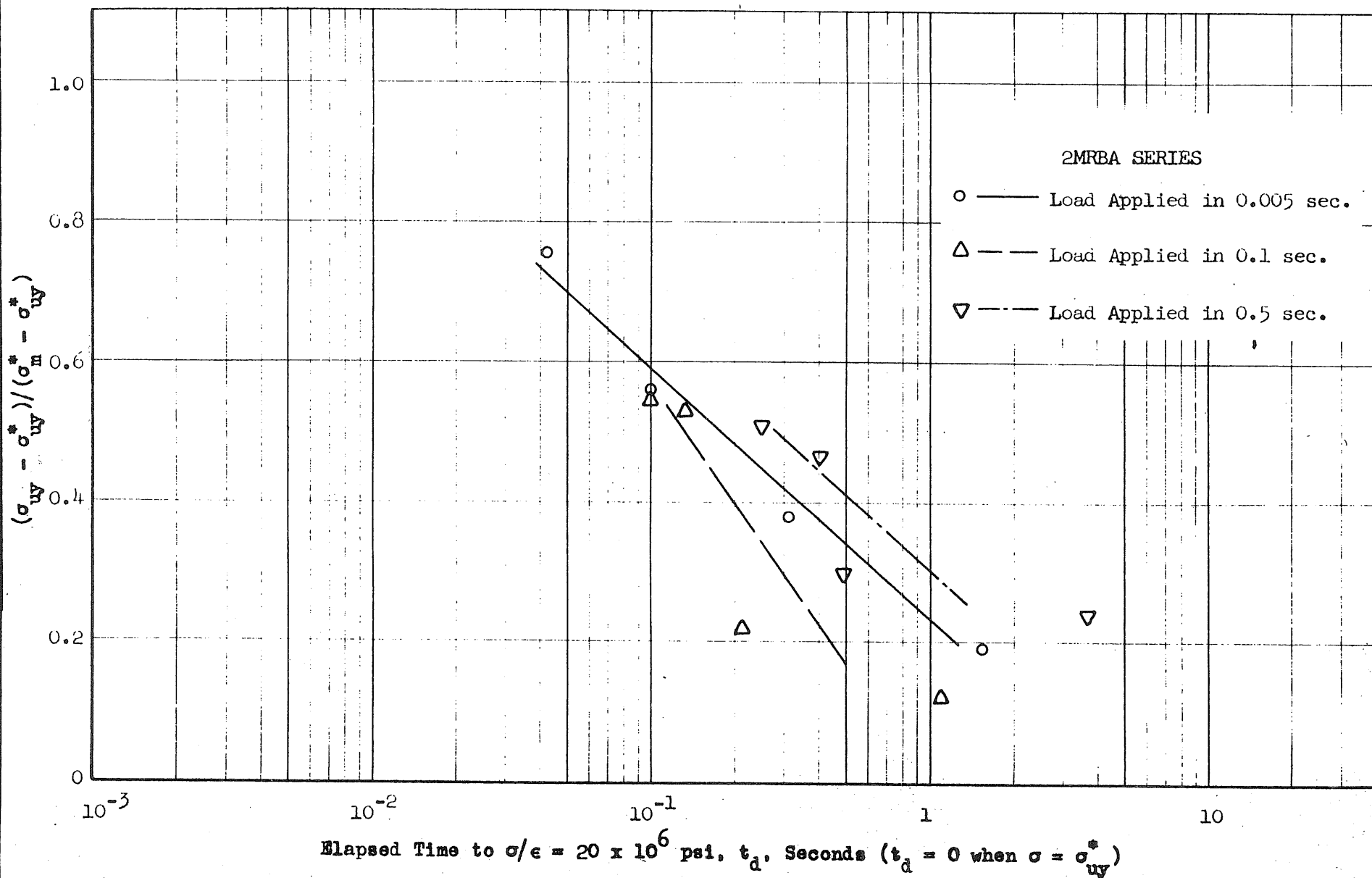


FIG. 24b YIELD STRESS PARAMETER - ELAPSED TIME TO $\sigma/\epsilon = 20 \times 10^6$ psi

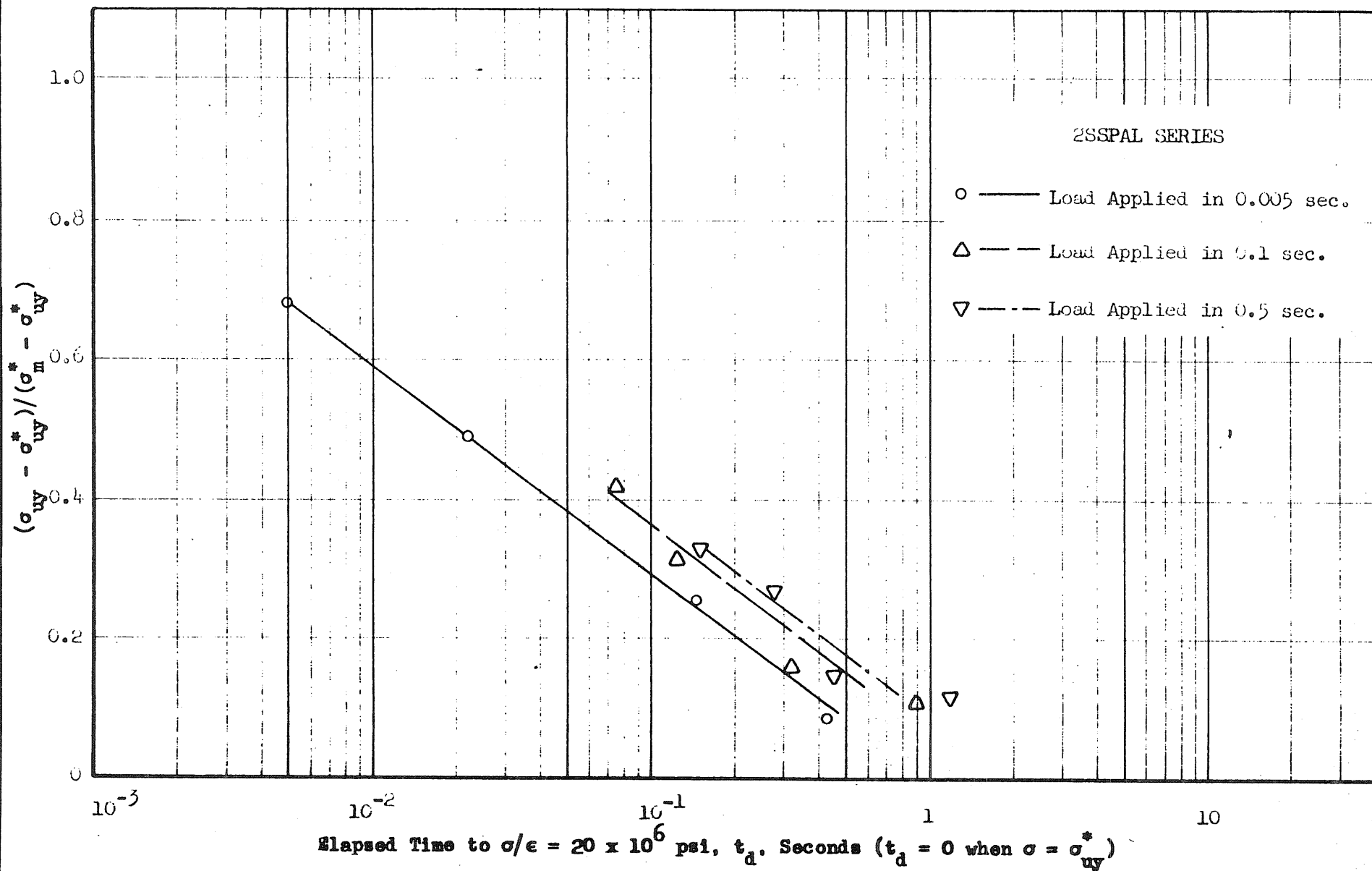


FIG. 24c YIELD STRESS PARAMETER - ELAPSED TIME TO $\sigma/\epsilon = 20 \times 10^6$ psi

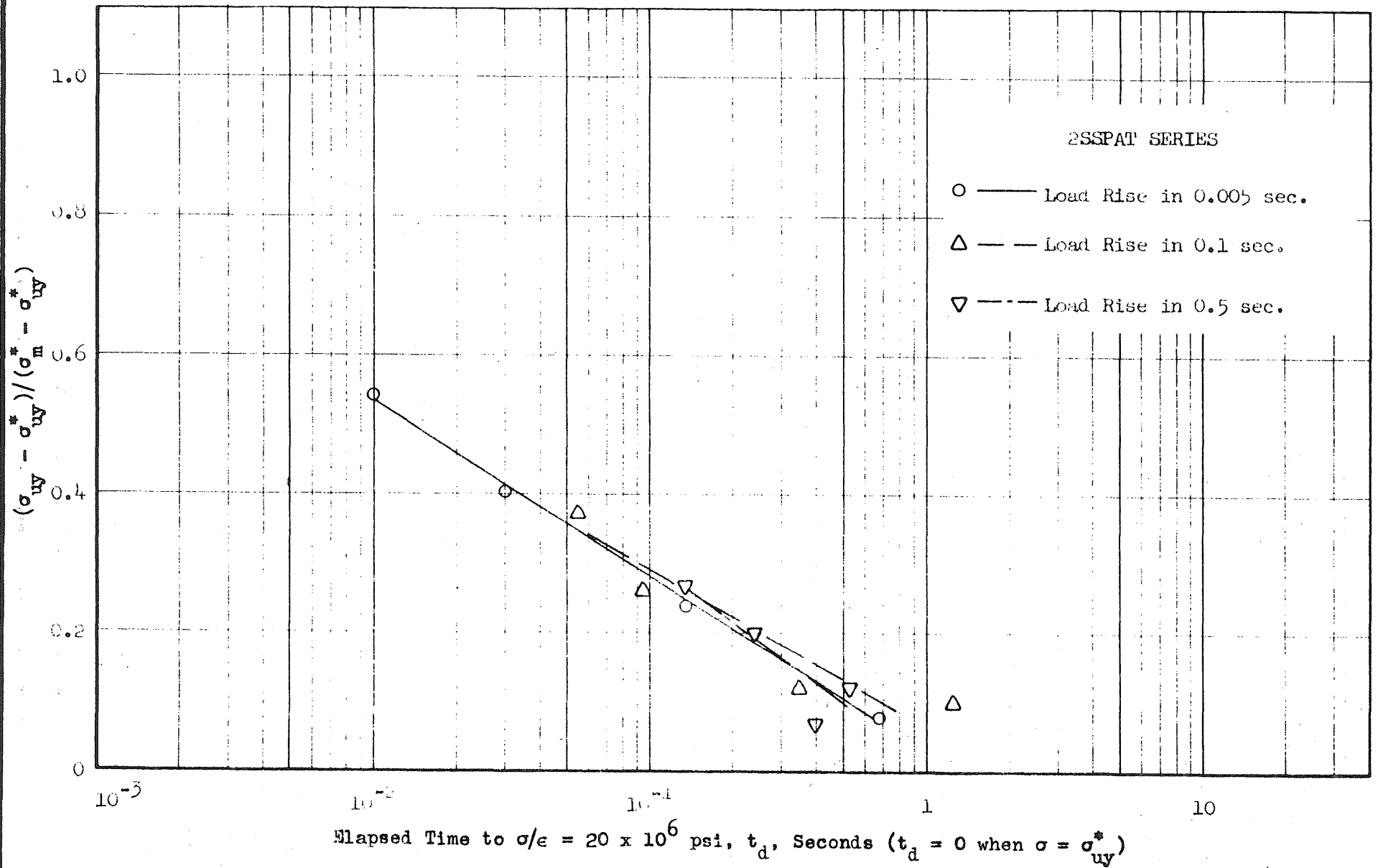


FIG. 24d YIELD STRESS PARAMETER - ELAPSED TIME TO $\sigma/\epsilon = 20 \times 10^6$ psi

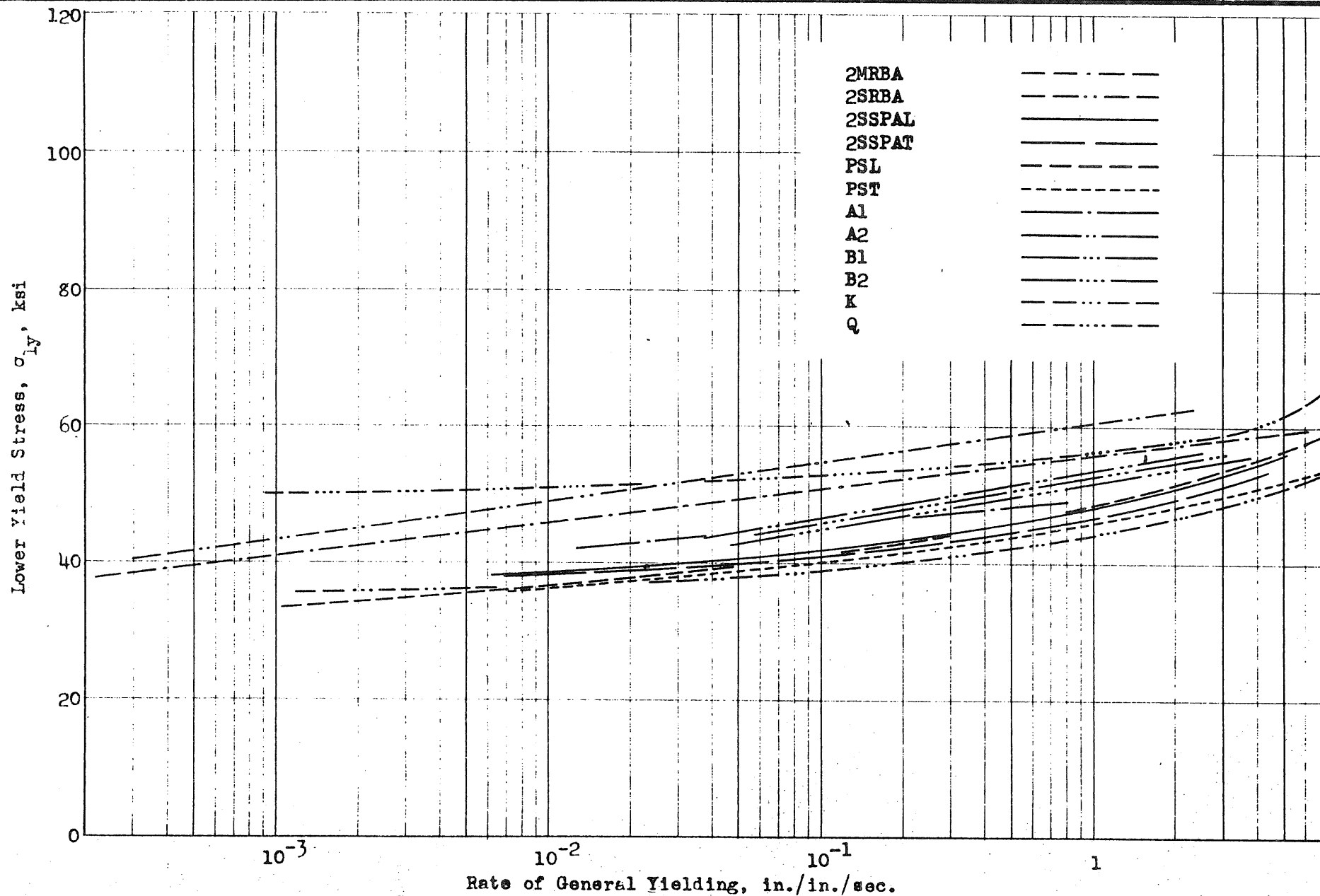


FIG. 25 LOWER YIELD STRESS - RATE OF GENERAL YIELDING

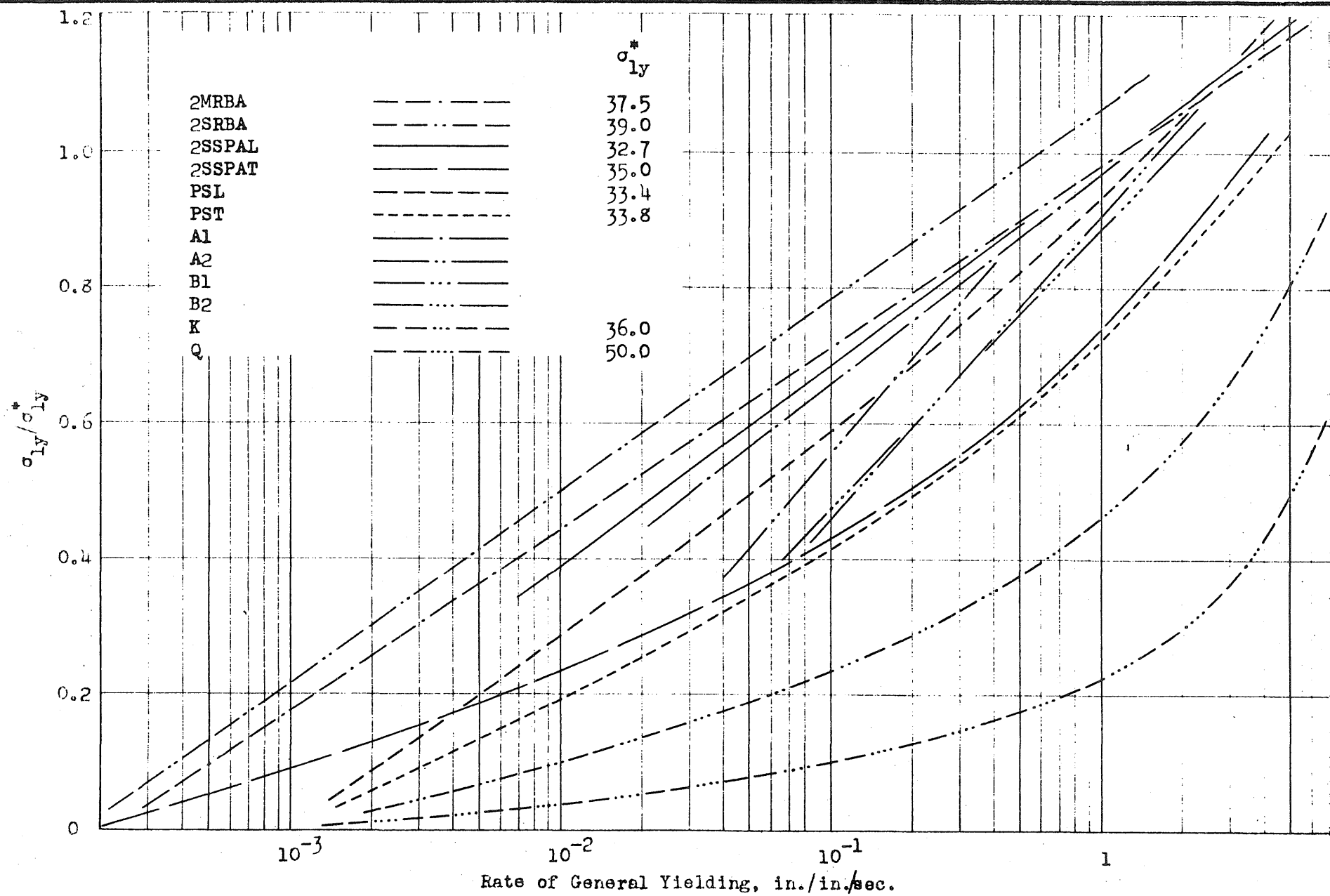


FIG. 26a LOWER YIELD STRESS PARAMETER - RATE OF GENERAL YIELDING

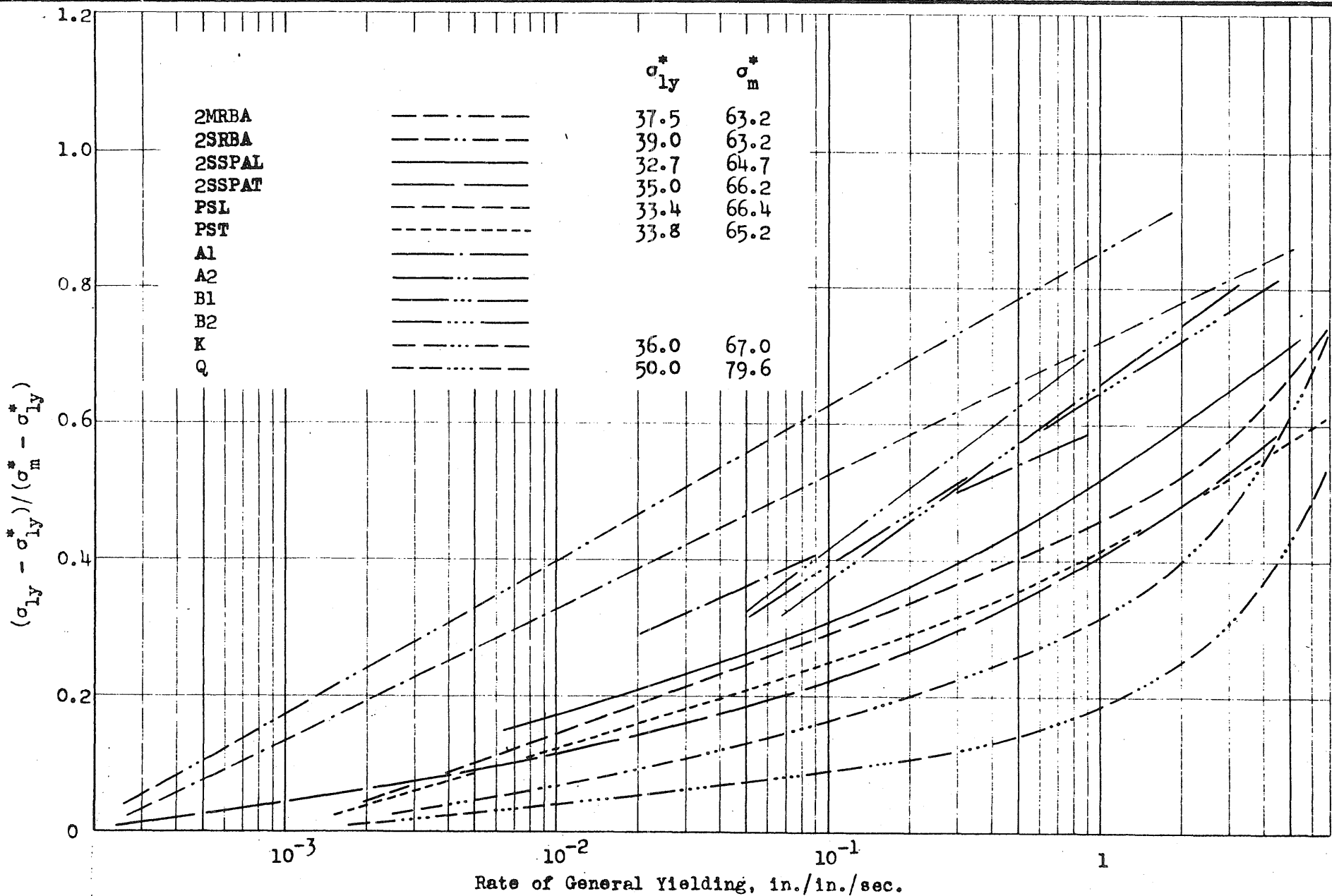


FIG. 26b LOWER YIELD STRESS PARAMETER - RATE OF GENERAL YIELDING

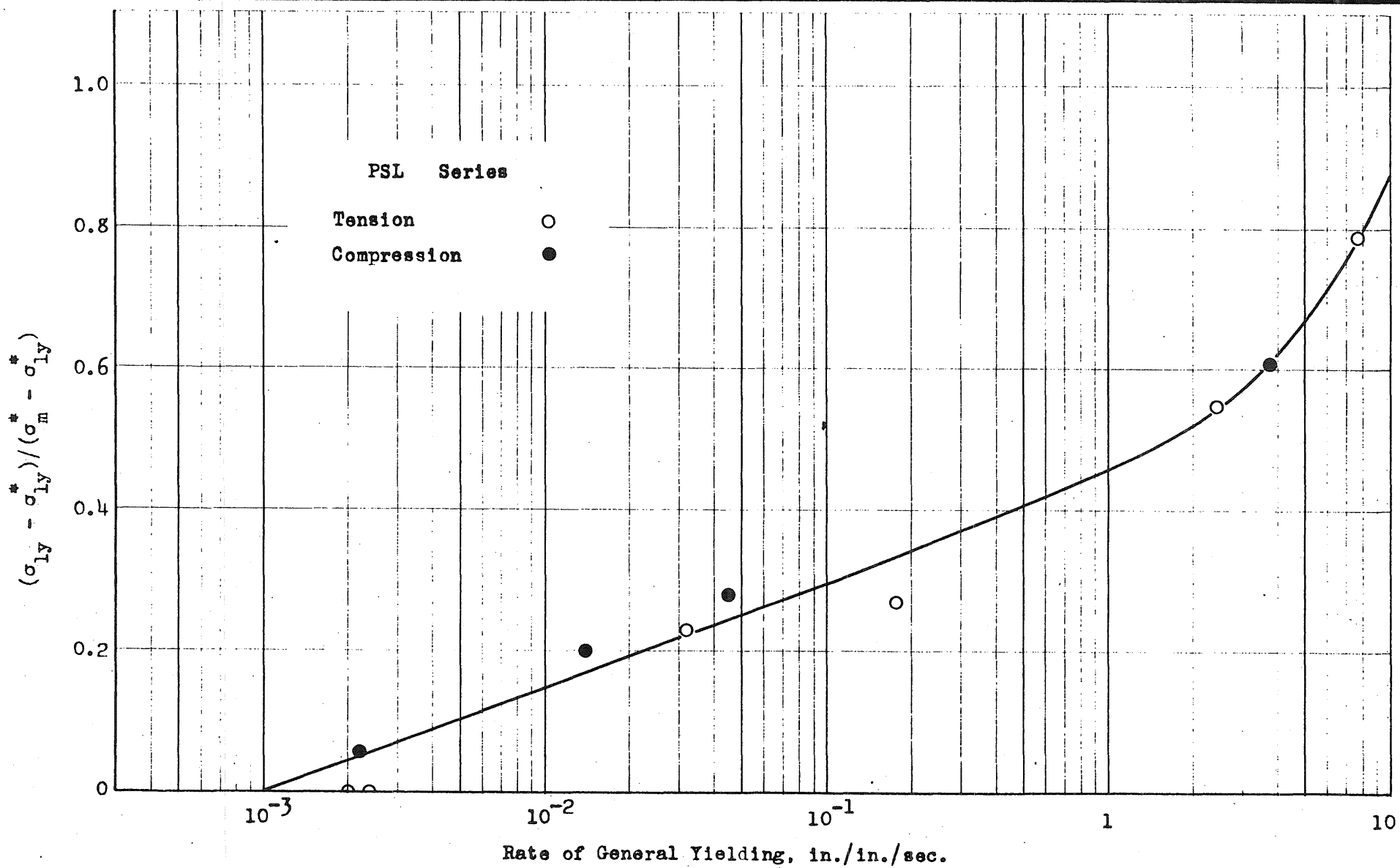


FIG. 26c YIELD STRESS PARAMETER - RATE OF YIELDING AT CONSTANT STRESS

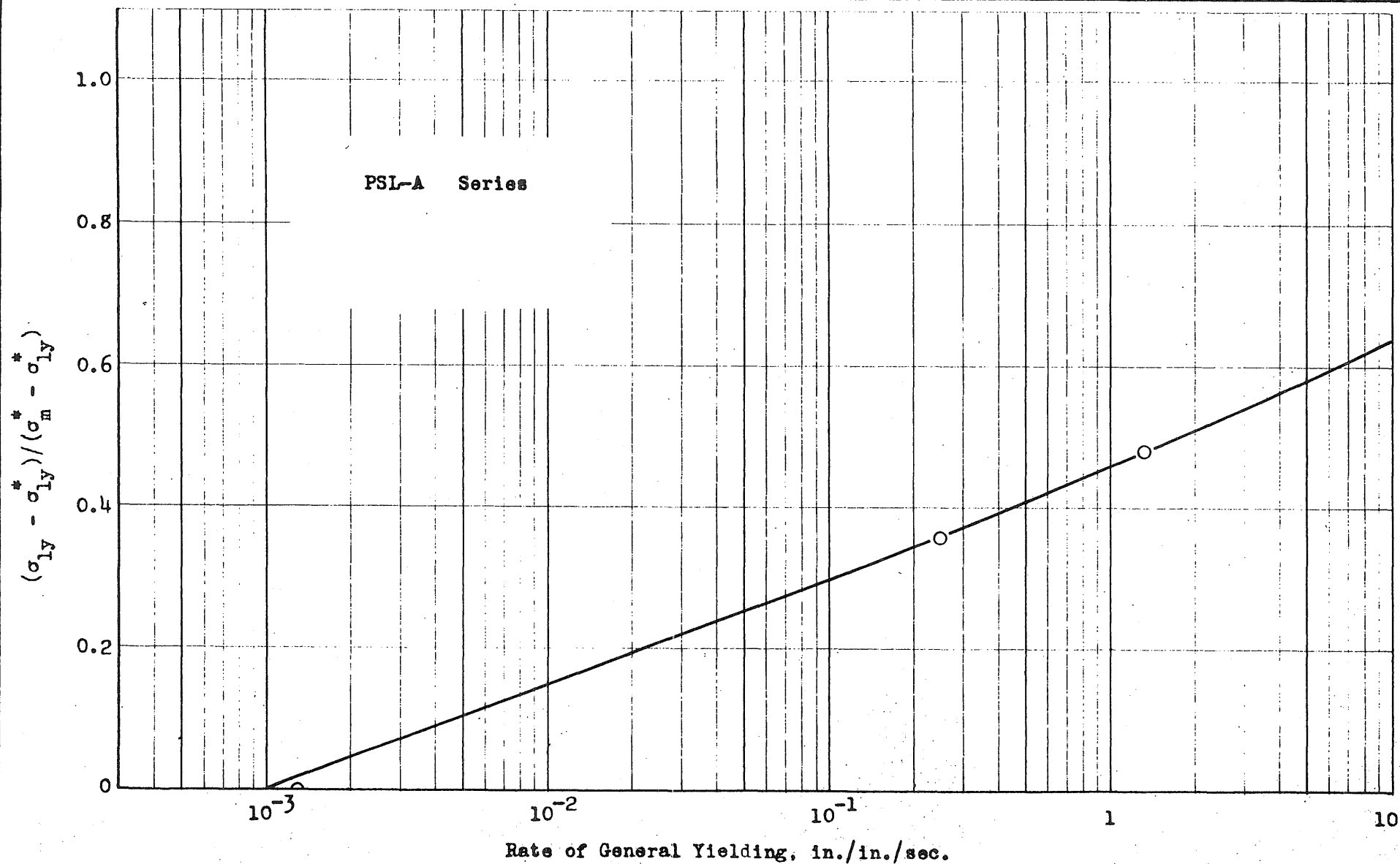


FIG. 26d YIELD STRESS PARAMETER - RATE OF YIELDING AT CONSTANT STRESS

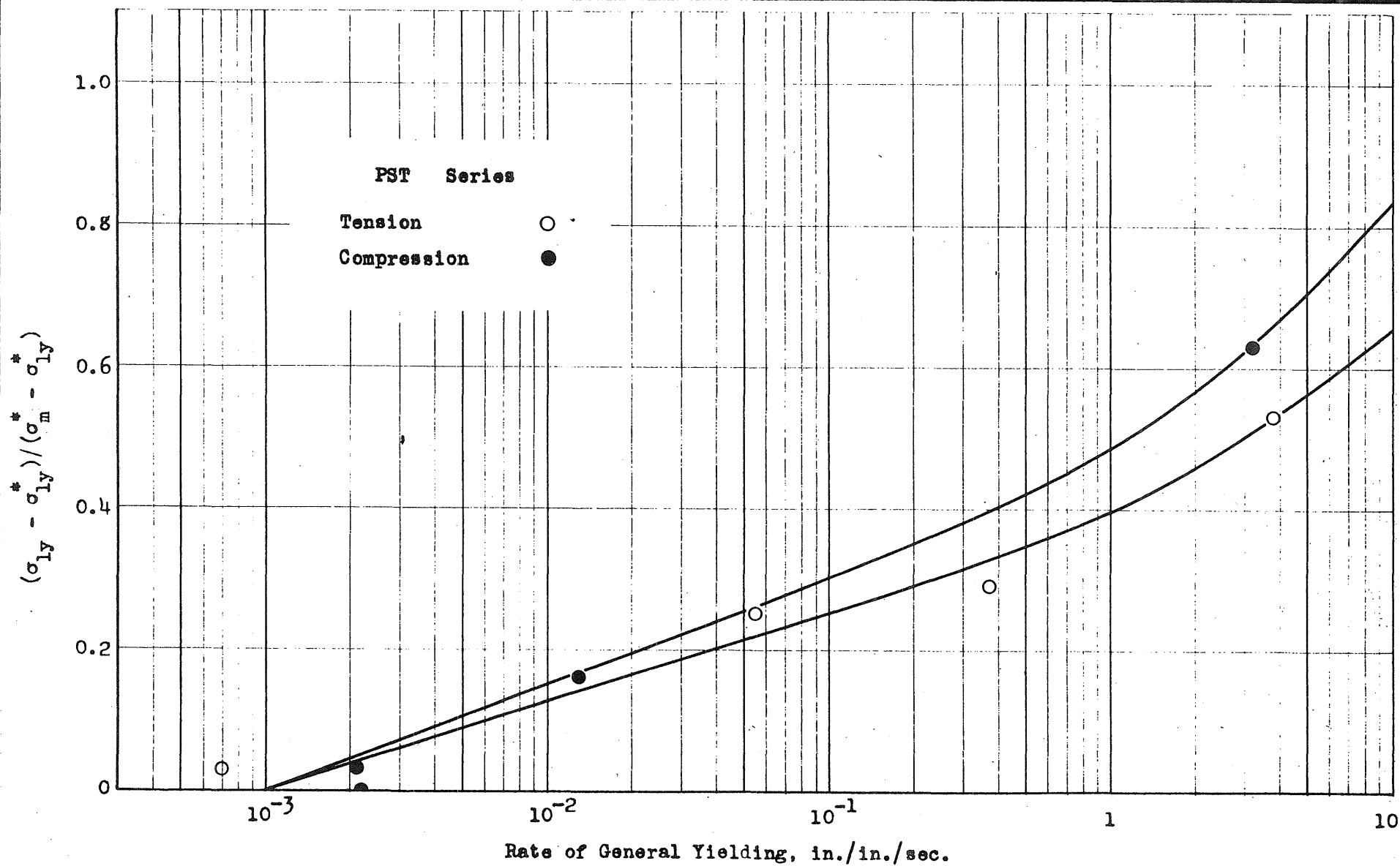


FIG. 26e YIELD STRESS PARAMETER - RATE OF YIELDING AT CONSTANT STRESS

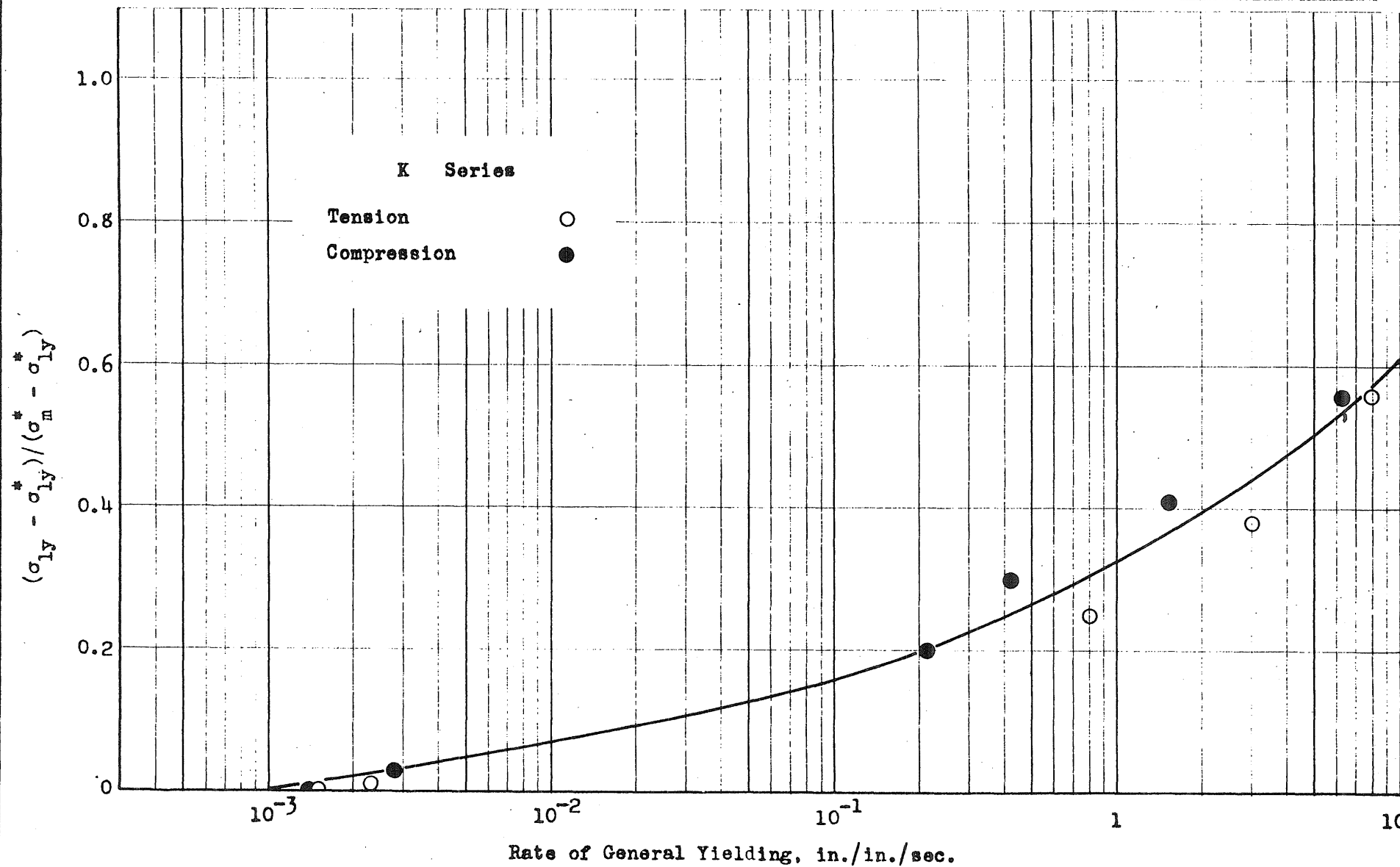


FIG. 26f YIELD STRESS PARAMETER - RATE OF YIELDING AT CONSTANT STRESS

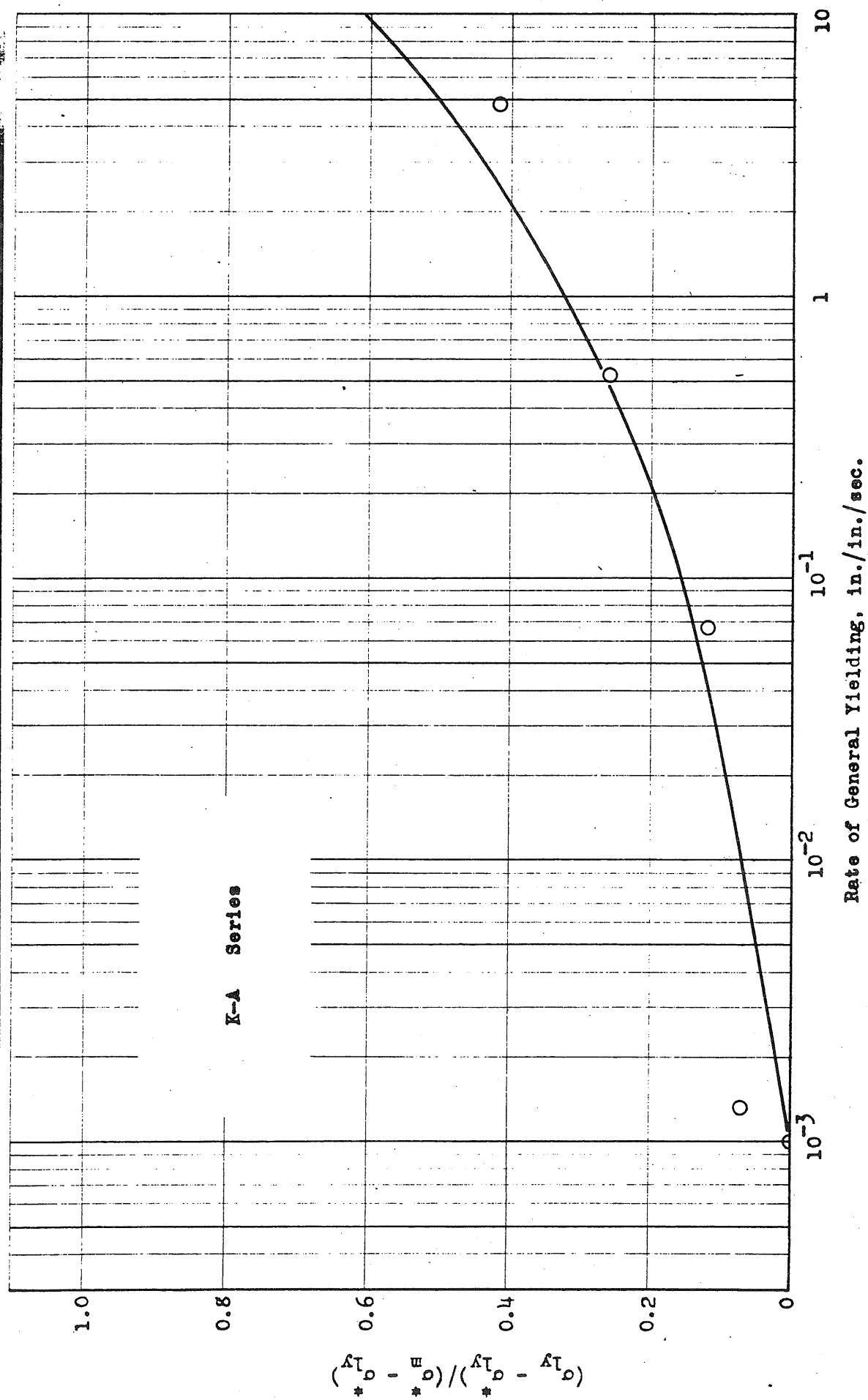


FIG. 26g YIELD STRESS PARAMETER - RATE OF YIELDING AT CONSTANT STRESS

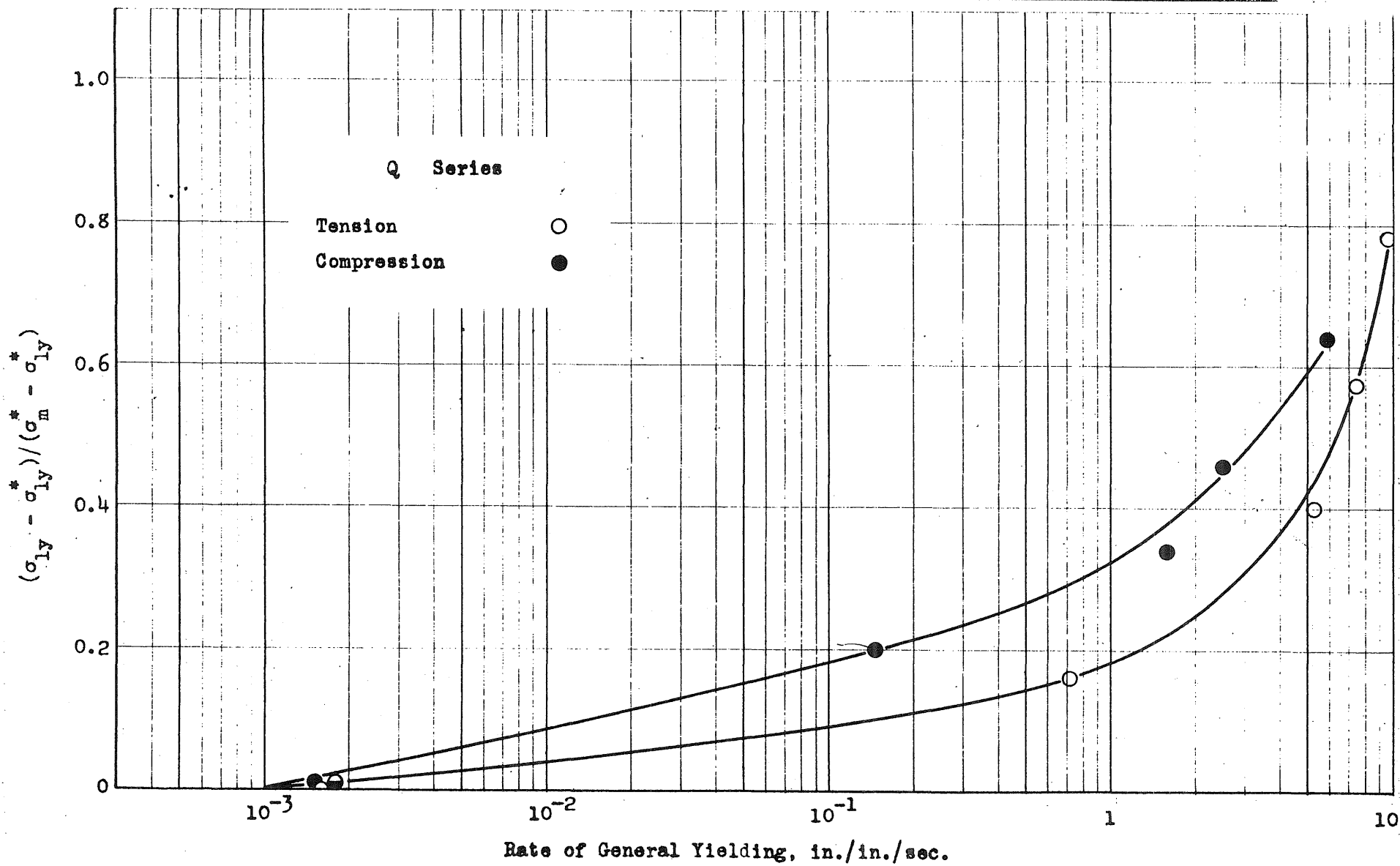


FIG. 26a YIELD STRESS PARAMETER - RATE OF YIELDING AT CONSTANT STRESS

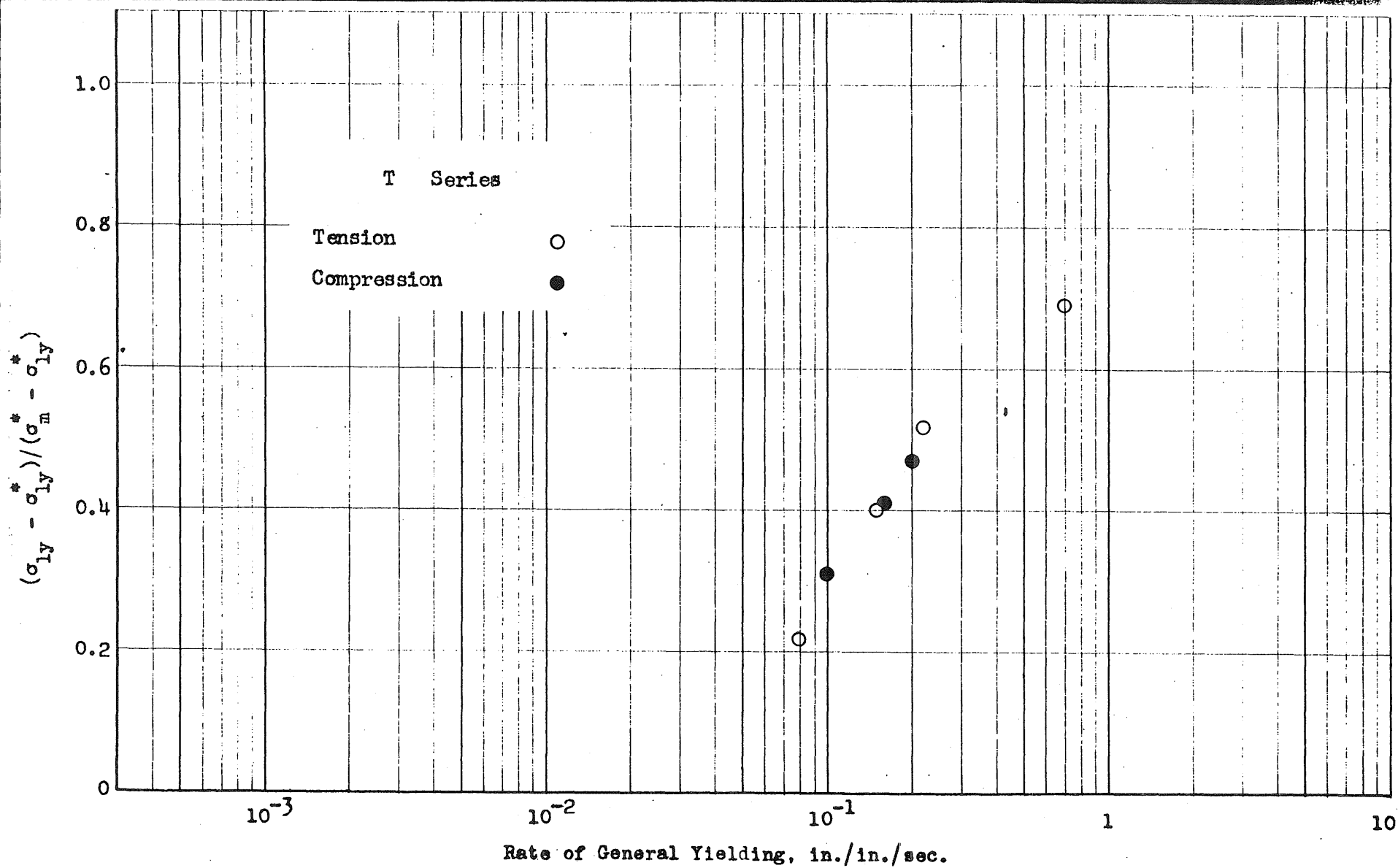


FIG. 261

YIELD STRESS PARAMETER - RATE OF YIELDING AT CONSTANT STRESS

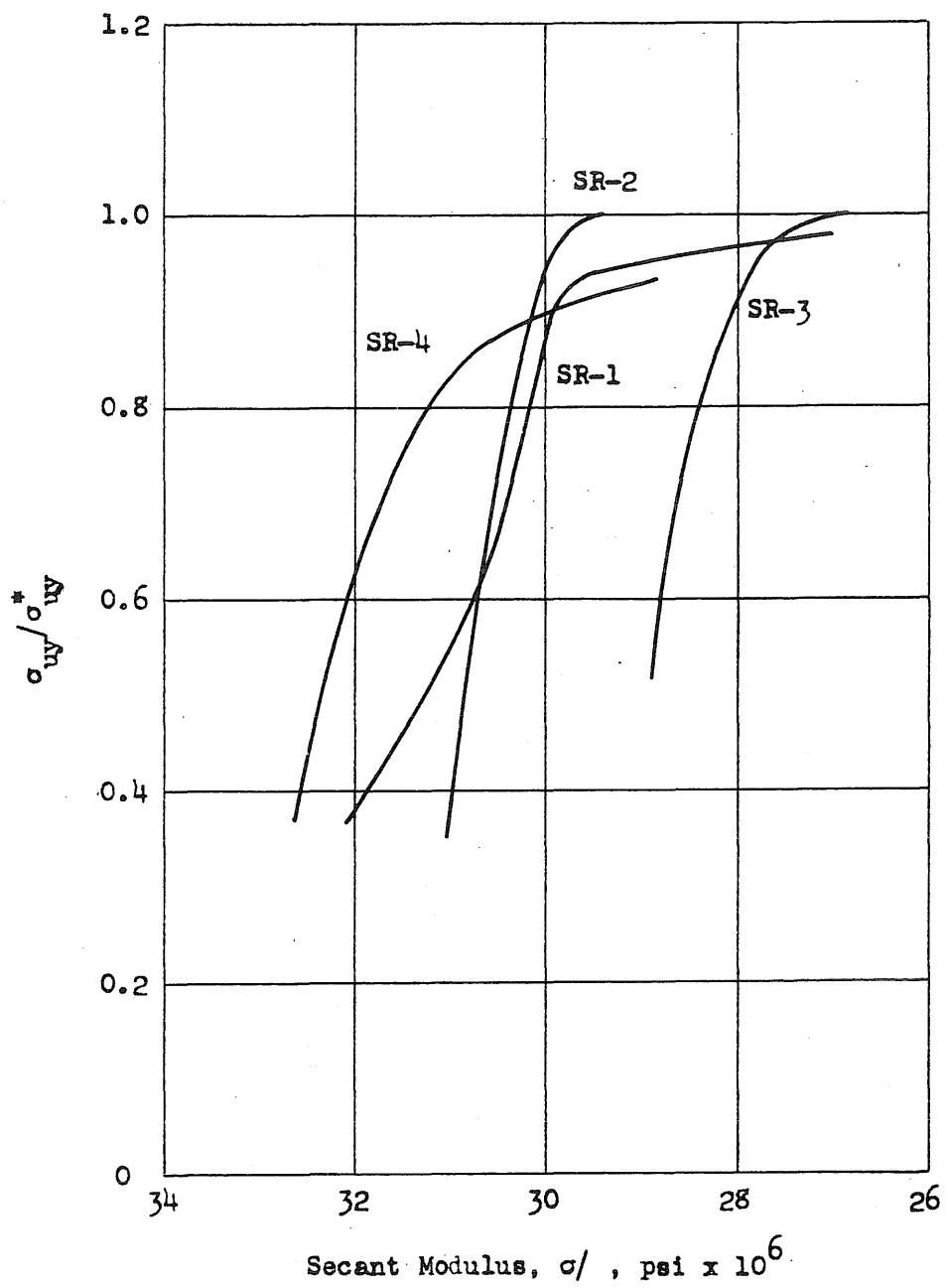


FIG. 27 UPPER YIELD STRESS PARAMETER - SECANT MODULUS

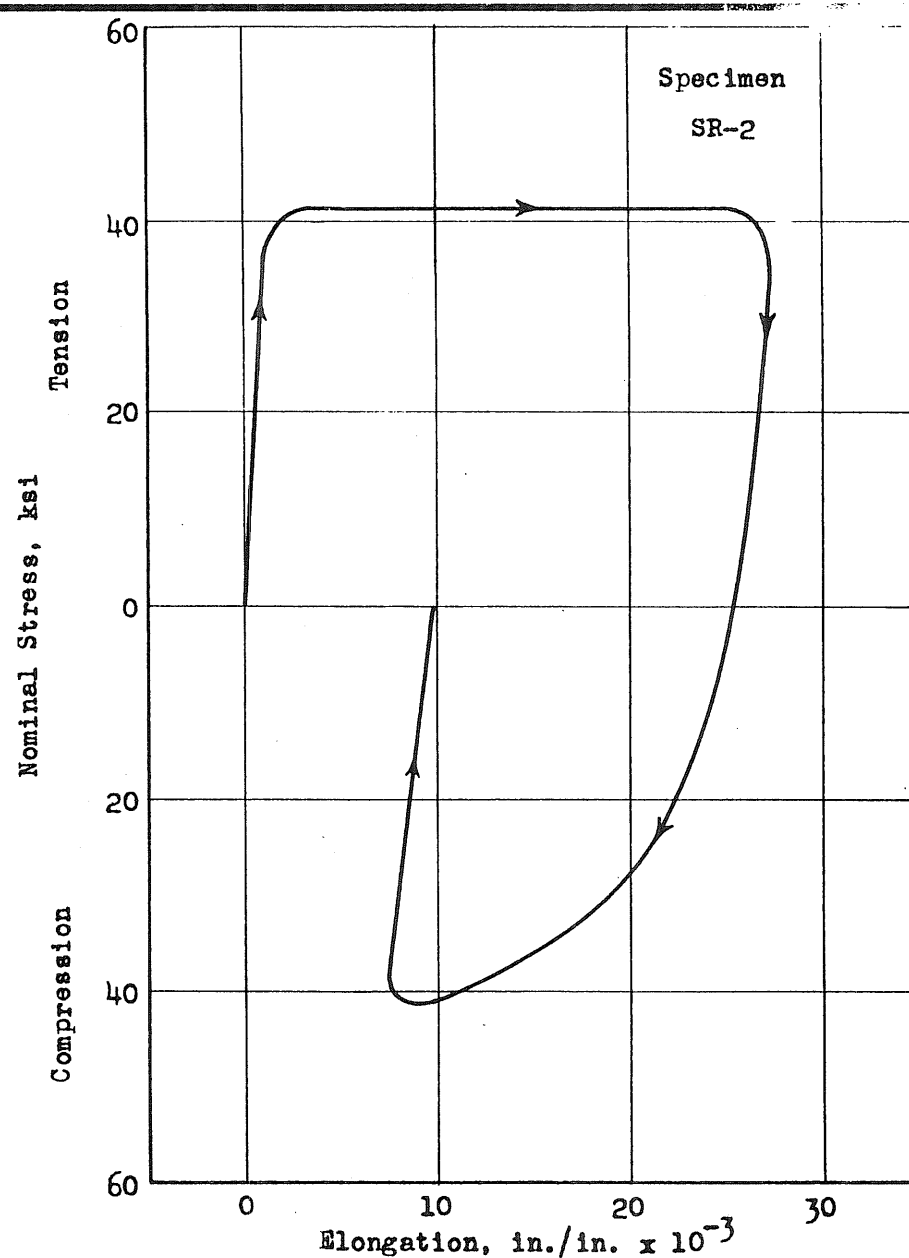
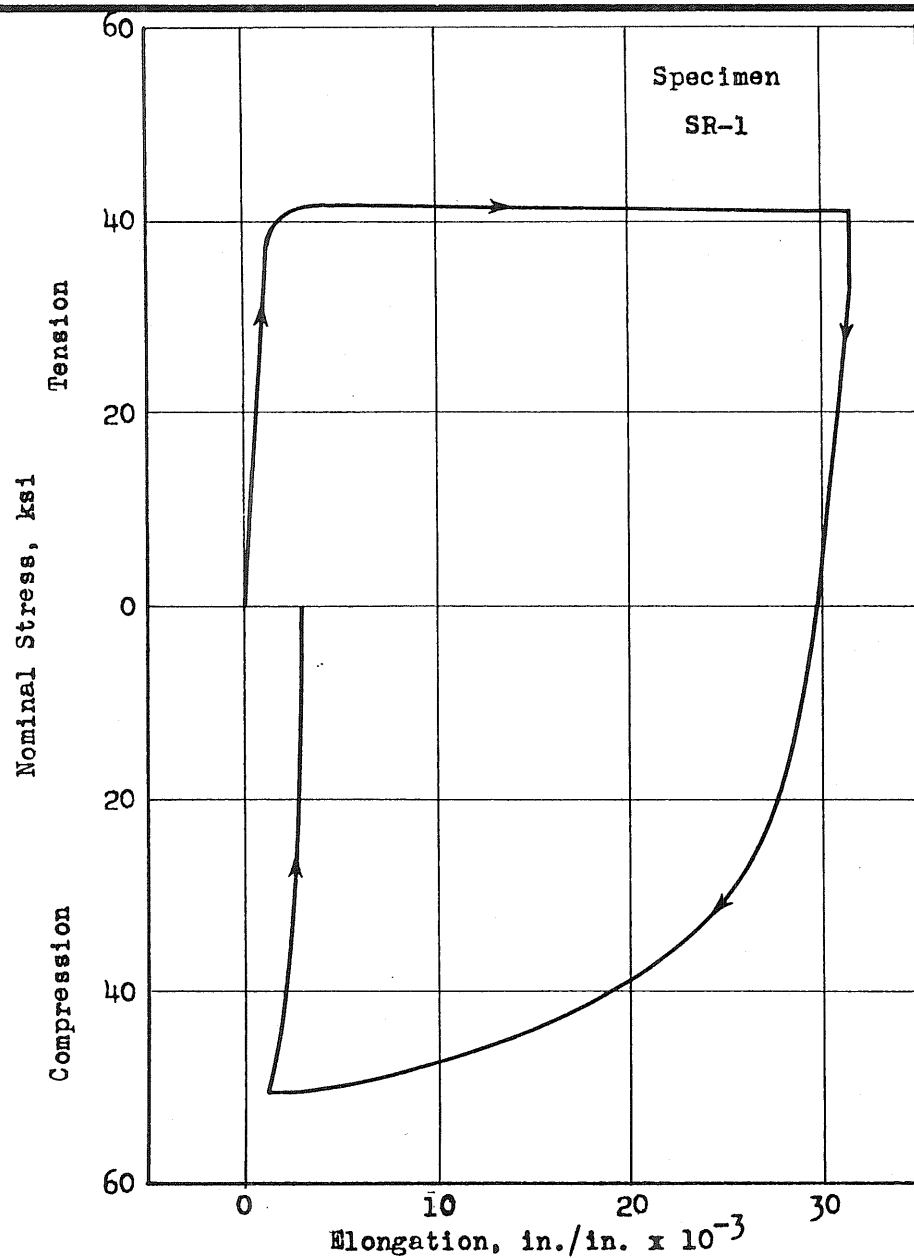


FIG. 28a NOMINAL STRESS - ELONGATION; SLOW LOADING WITH REVERSAL

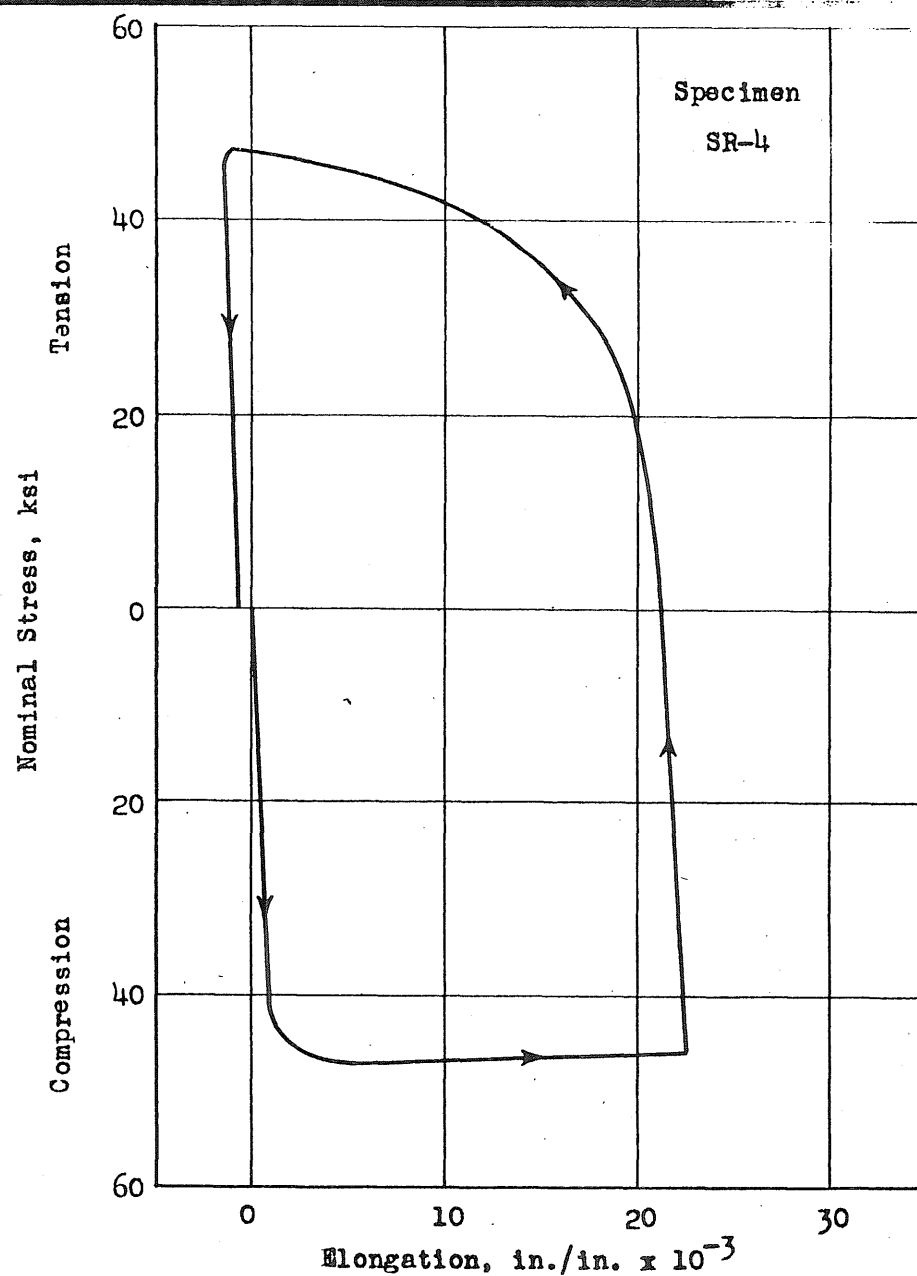
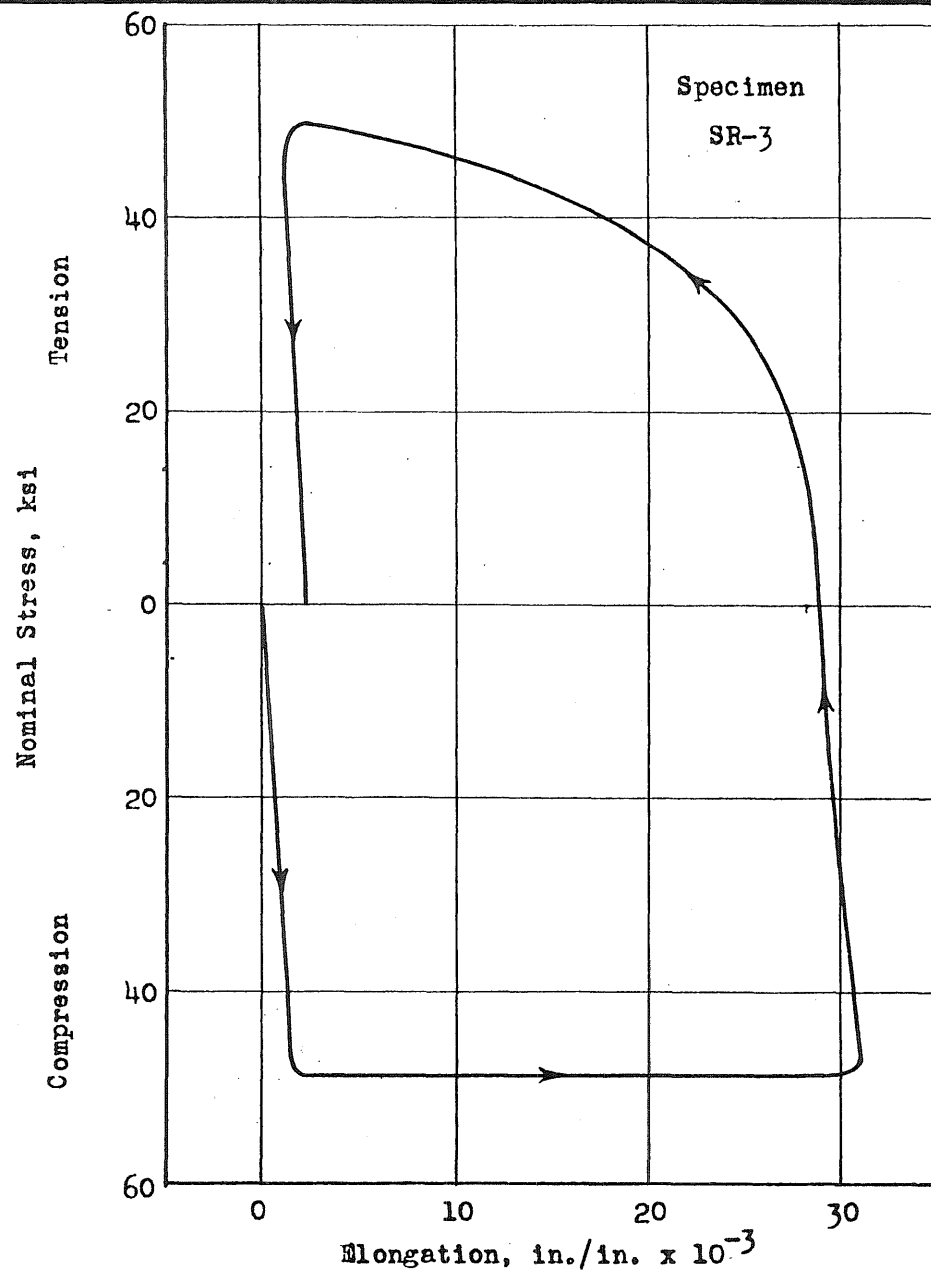


FIG. 28b NOMINAL STRESS - ELONGATION; SLOW LOADING WITH REVERSAL

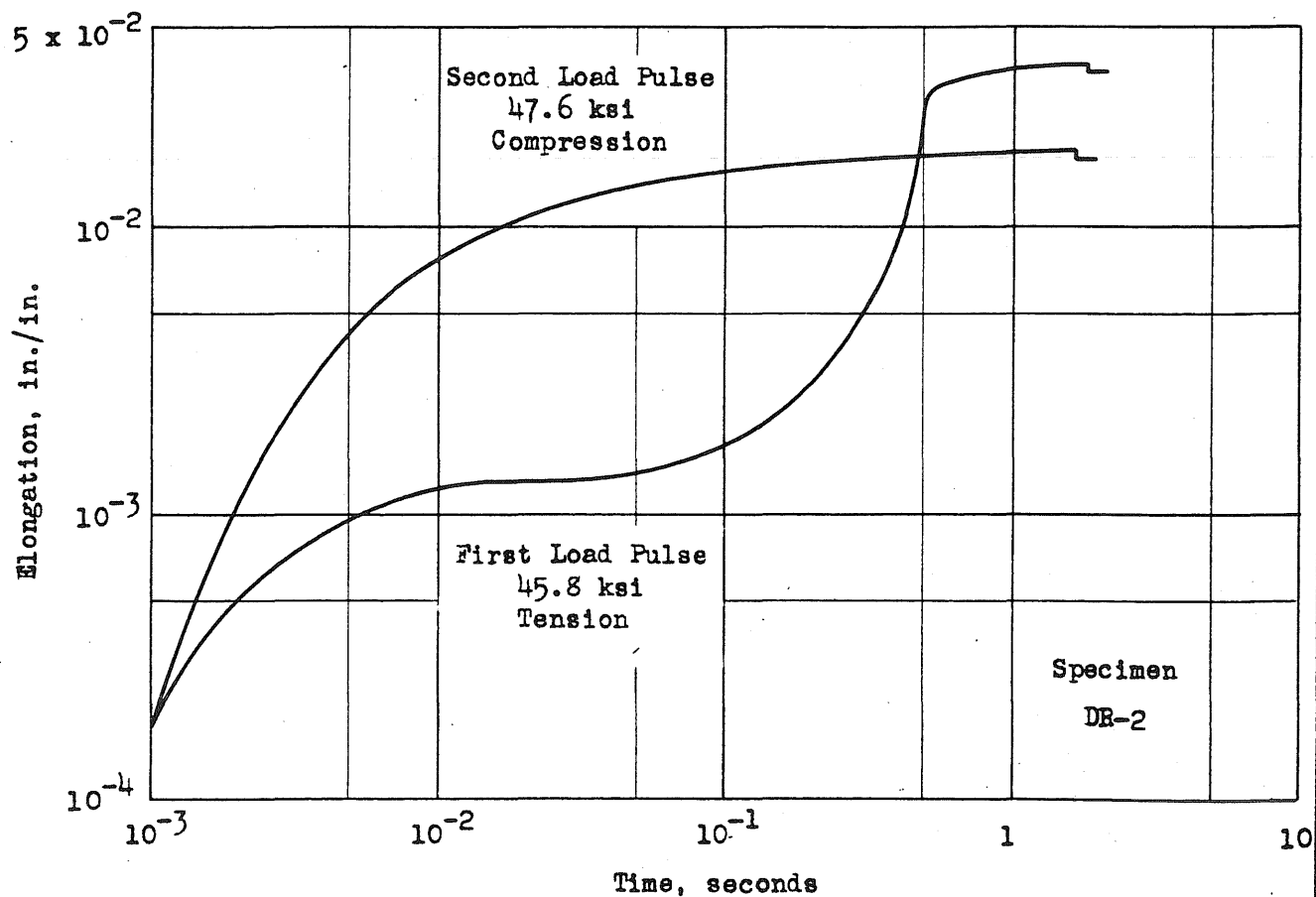
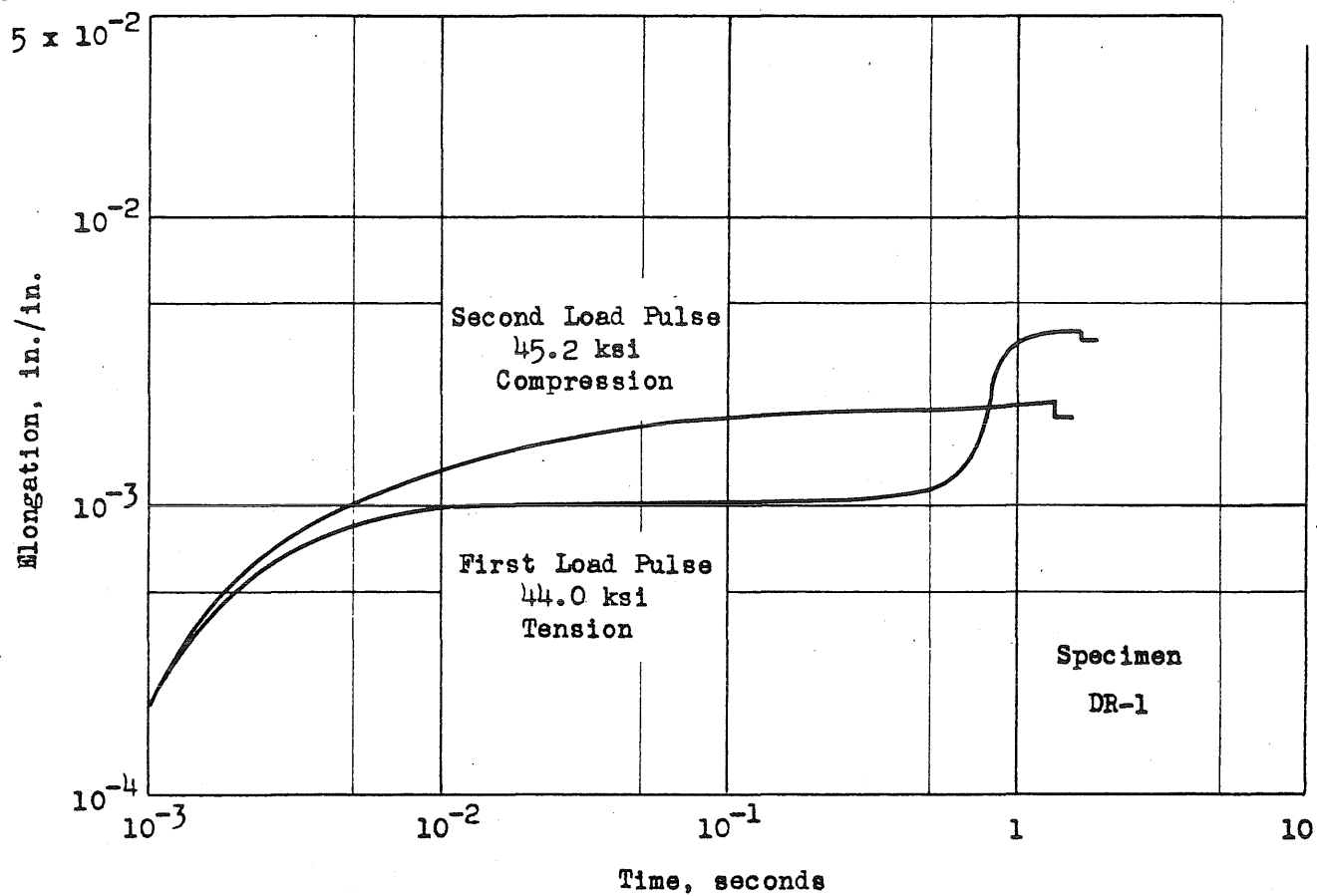


FIG. 29a ELONGATION - TIME; RAPID LOADING WITH REVERSAL

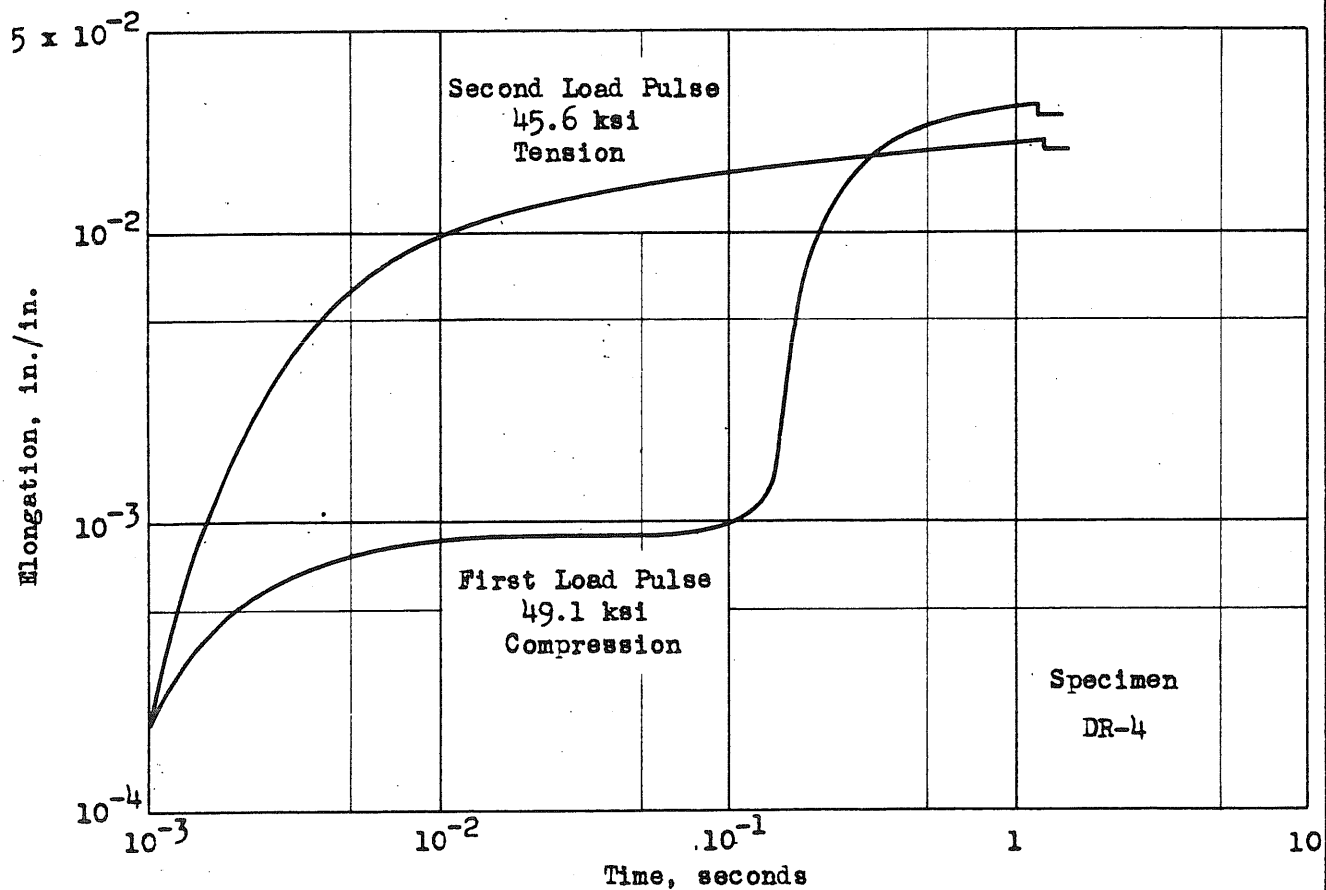
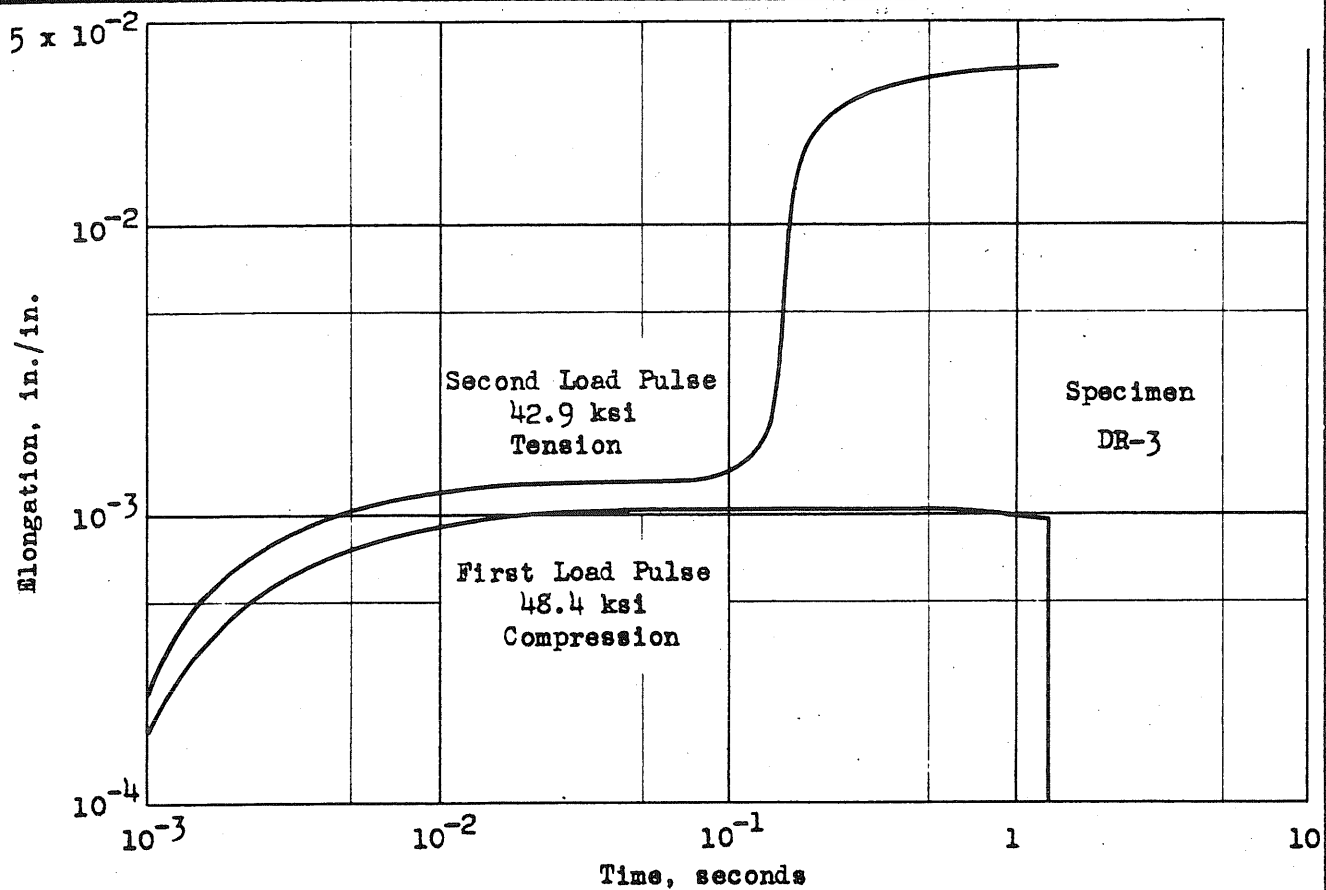


FIG. 29b ELONGATION - TIME; RAPID LOADING WITH REVERSAL

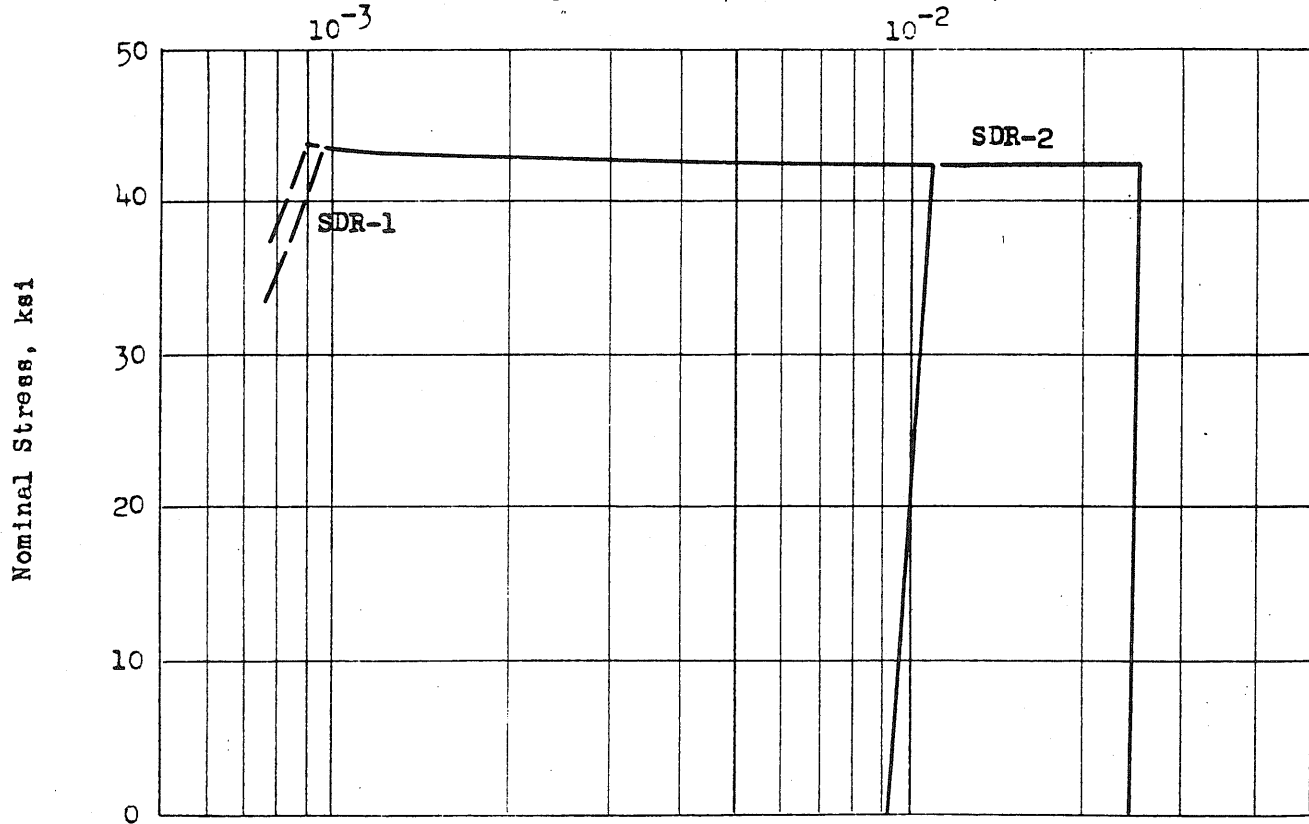
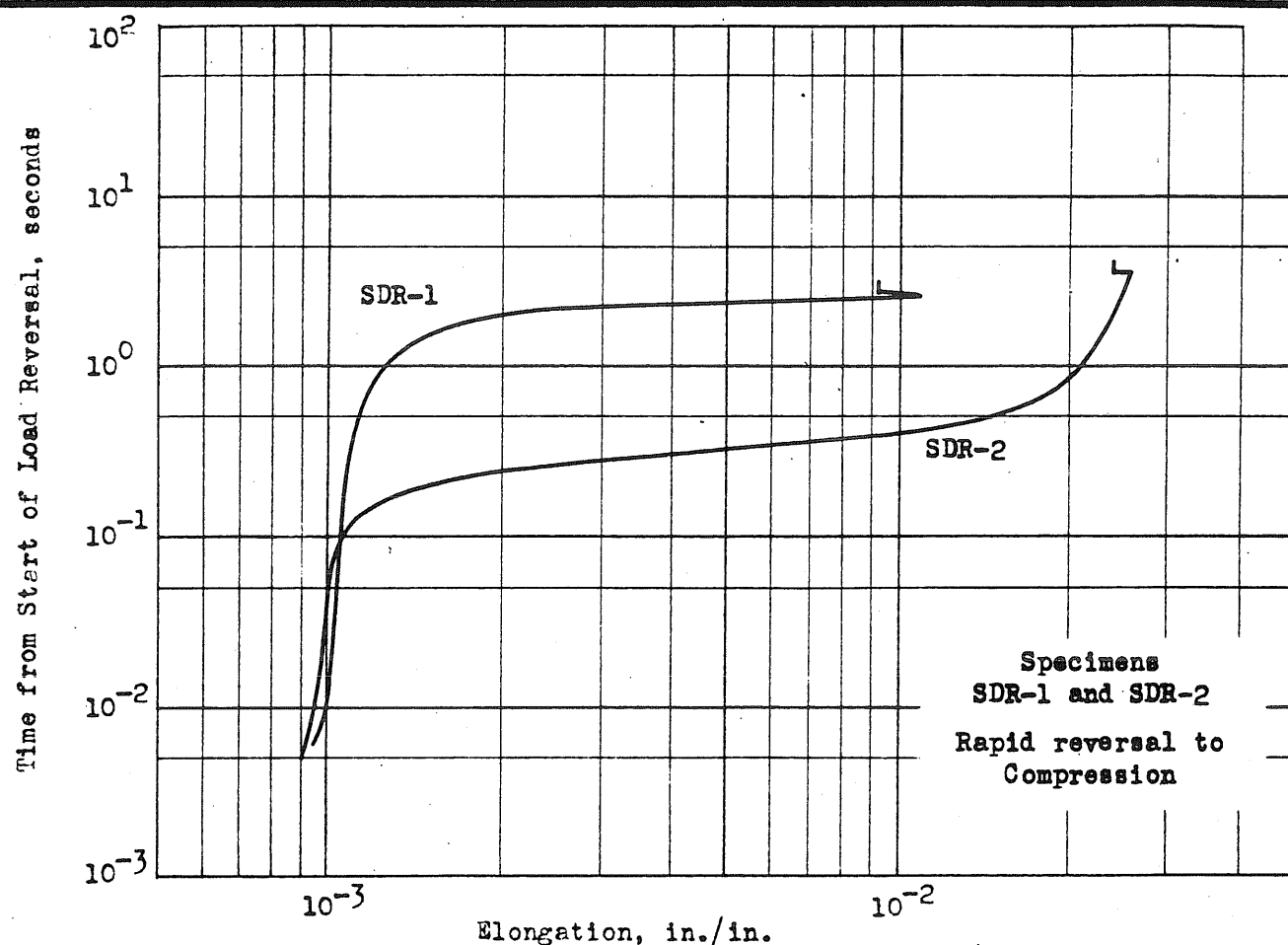


FIG. 30a

STRESS - ELONGATION AND ELONGATION - TIME;
RAPID REVERSAL FROM STATIC STRESS

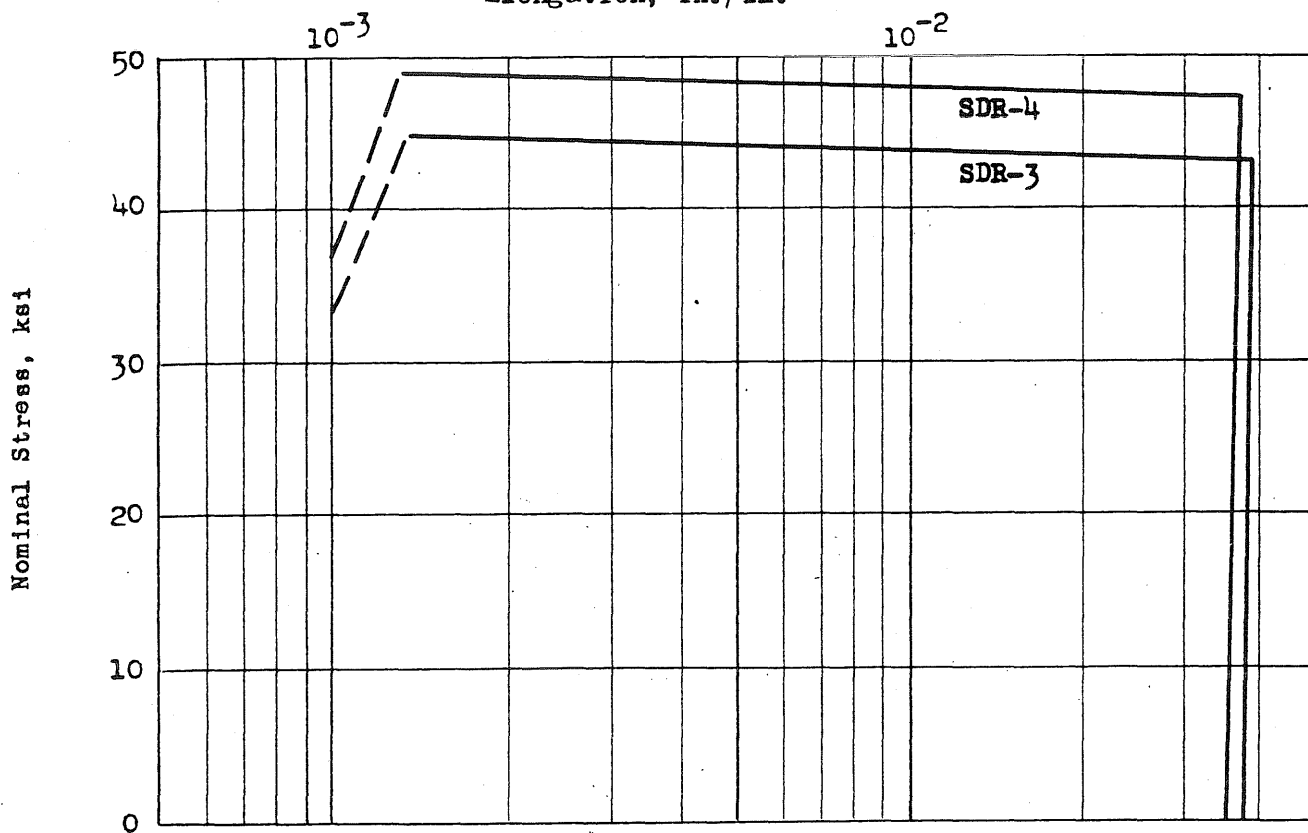
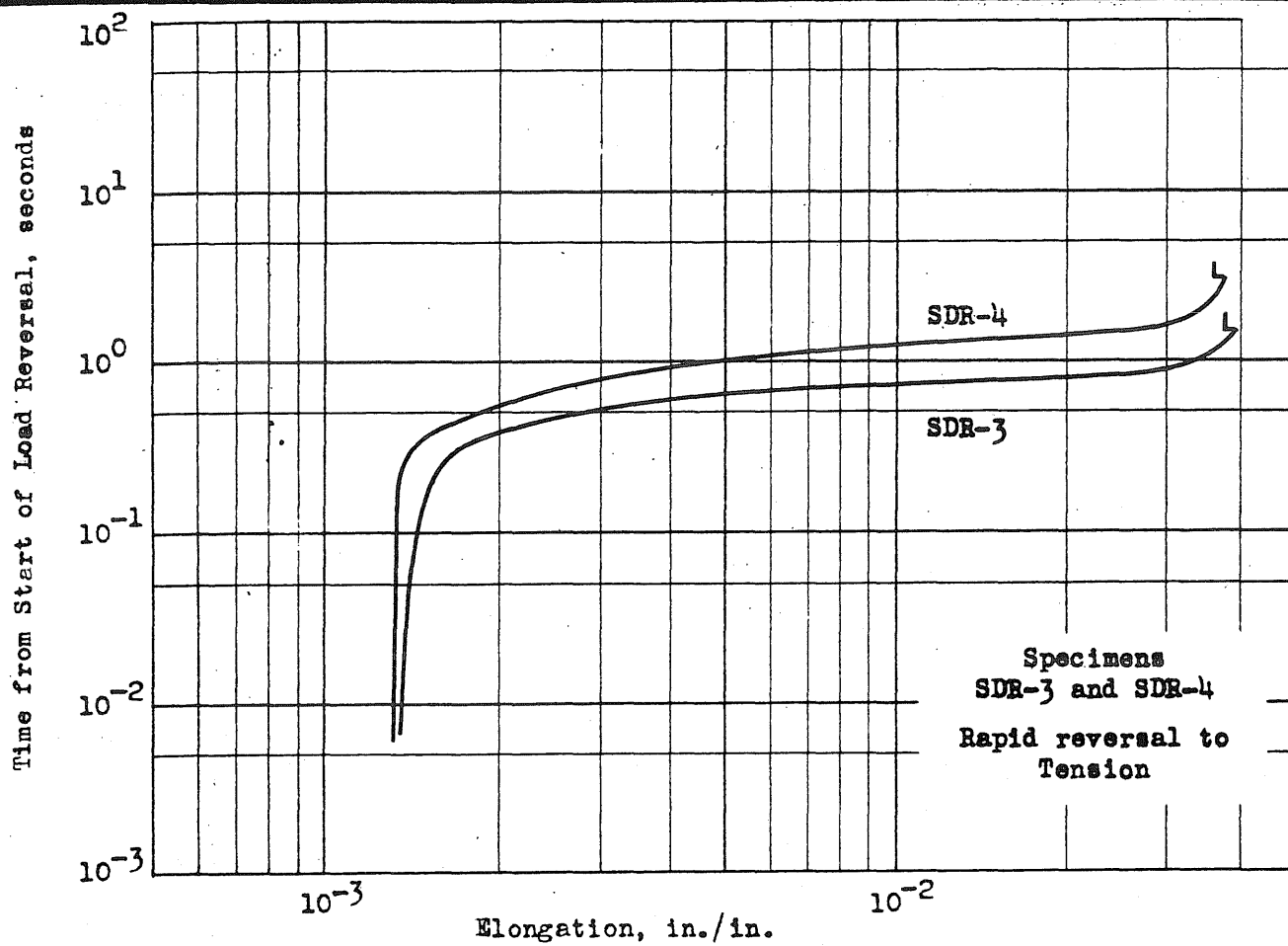


FIG. 30b

STRESS - ELONGATION AND ELONGATION - TIME;
RAPID REVERSAL FROM STATIC STRESS

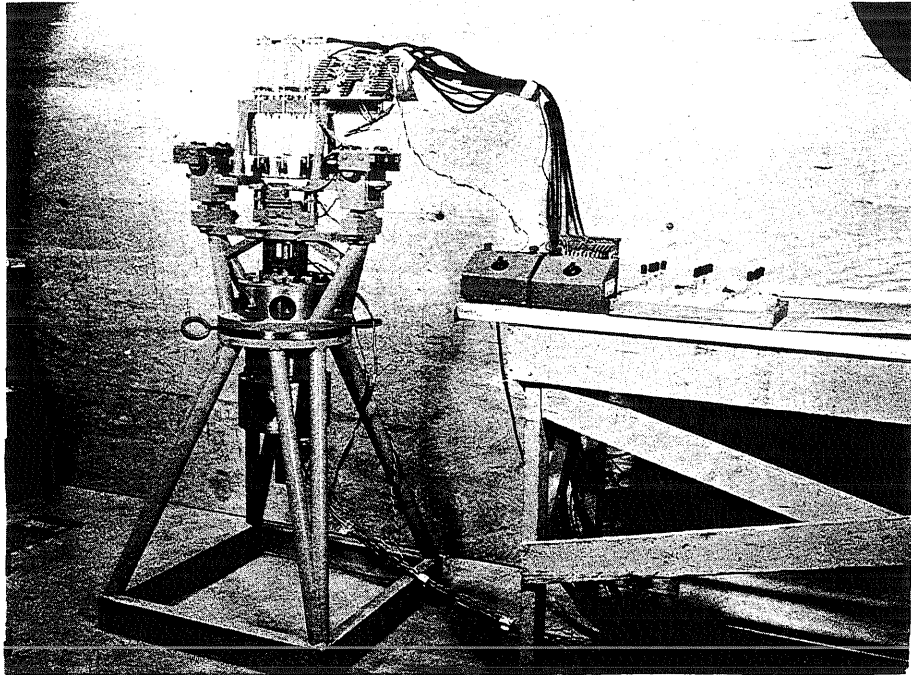


FIG. 31 OVERALL VIEW OF FLEXURAL TESTING EQUIPMENT

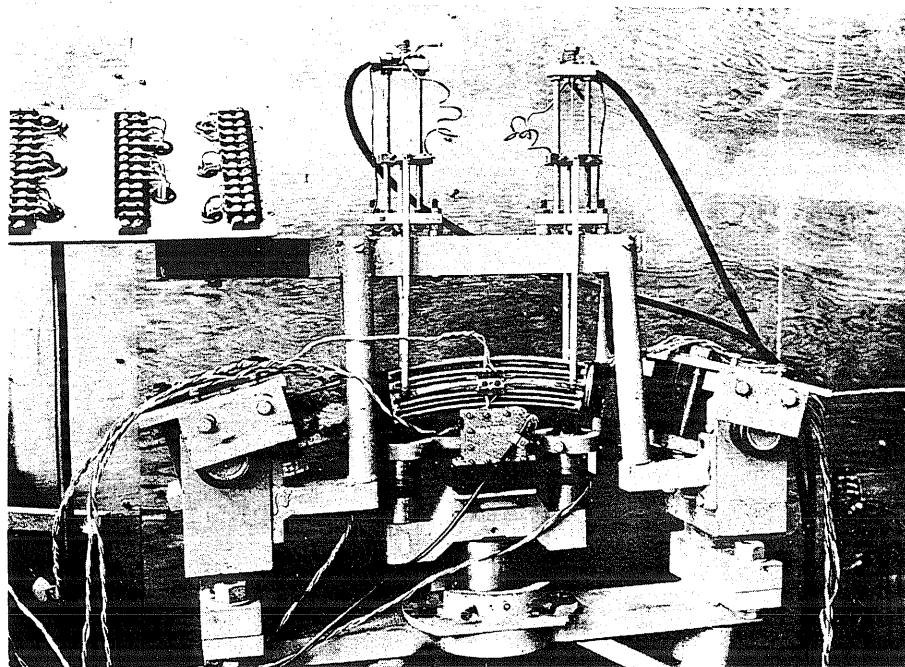


FIG. 32 ARRANGEMENT FOR TESTING SMALL BEAMS LOADED AT THE THIRD POINTS

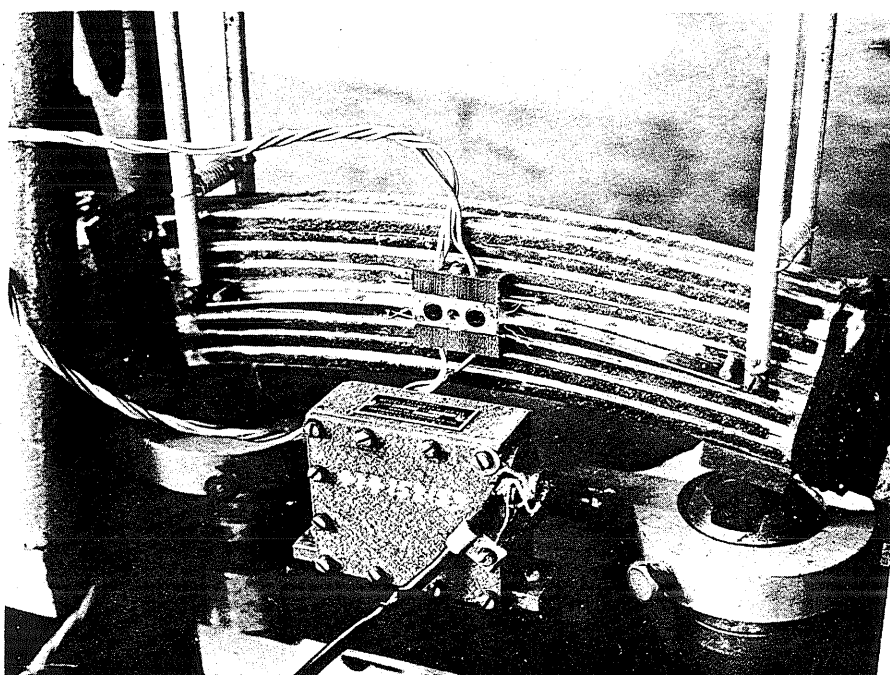
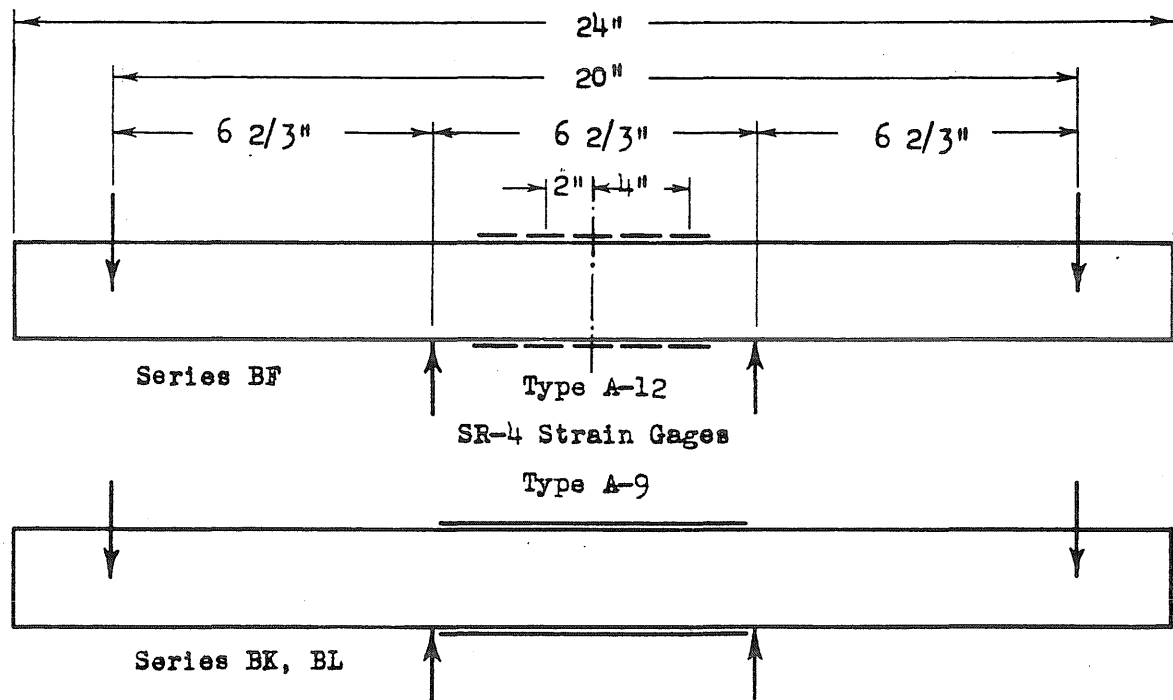
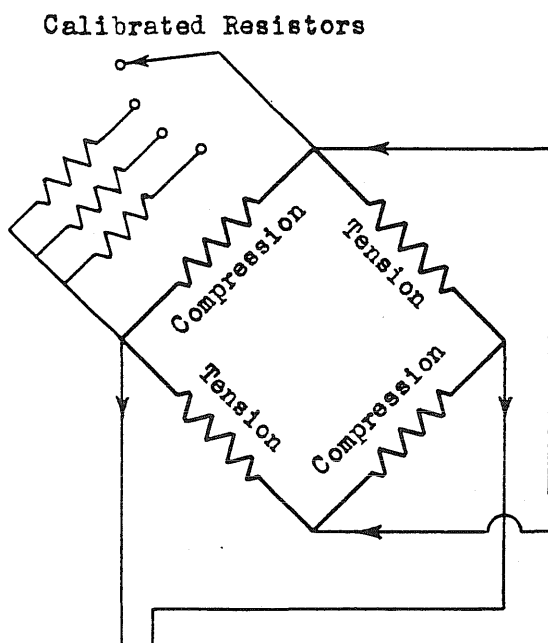


FIG. 33 VIEW OF PURE FLEXURE REGION INSTRUMENTED



Depth of Specimens:
2" all Series

Width of Specimens:
7/8" BF Series
0.665" BK Series
3/4" BL Series



This 4 arm bridge is typical of those used for dynamometers, curvature gages, and strain channels. In the bridge containing the 2 strain gages on the centre-line of the BF Series specimens, and that containing the top and bottom gages on the BK and BL Series specimens, 2 adjacent arms consist of dummy gages.

Hathaway MRC 18
Strain Measuring
System, Modified

Carrier
Filter
System

Hathaway S14-C
Oscillograph
(Hathaway
Group 23 OC-2
Galvanometers)

Standard Hathaway MRC 18 unit modified to reduce cross-talk between channels and to provide carrier supply oscillator with approximately 0.01% regulation.

FIG. 34

INSTRUMENTATION AND DIMENSIONS OF FLEXURAL SPECIMENS

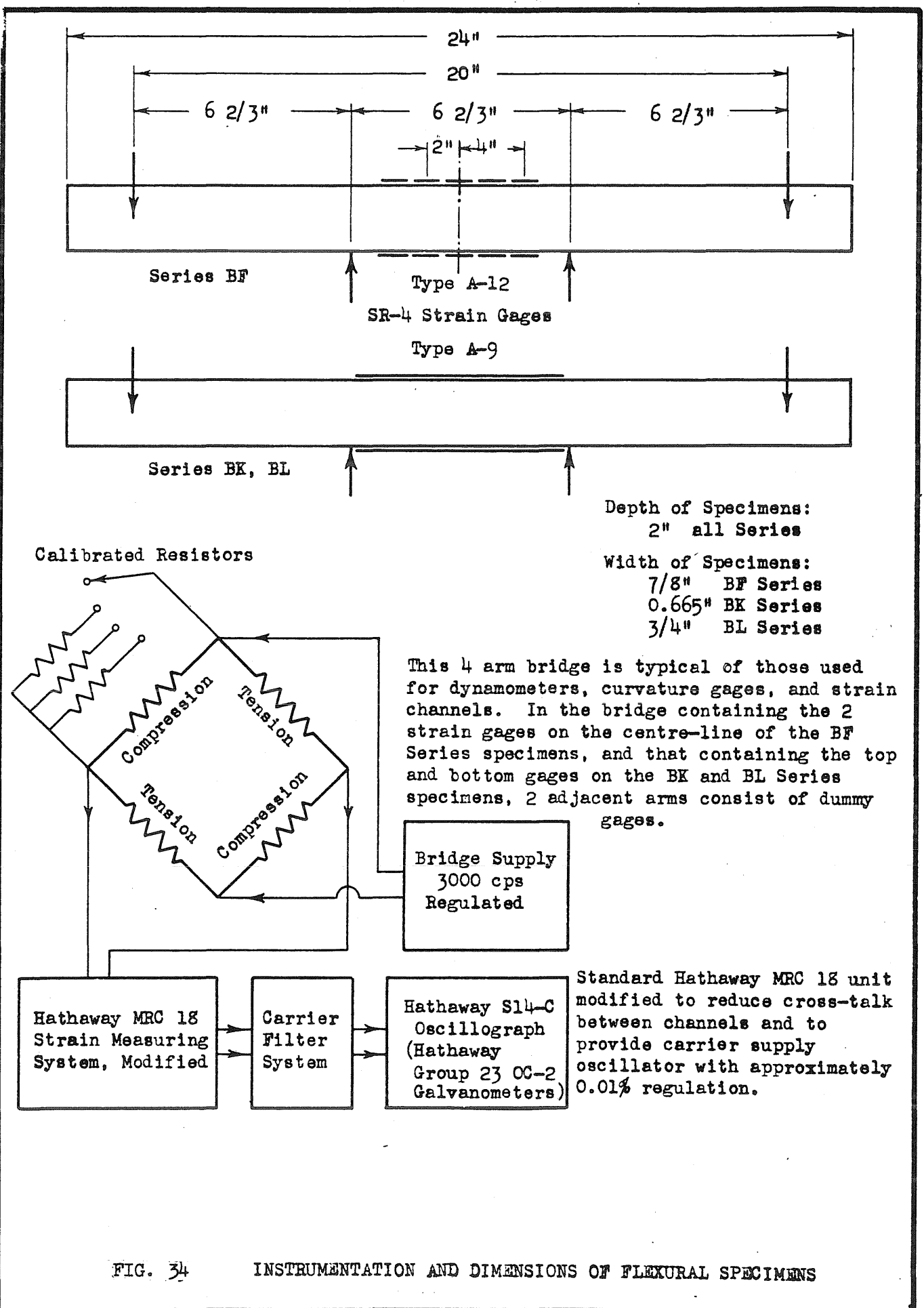
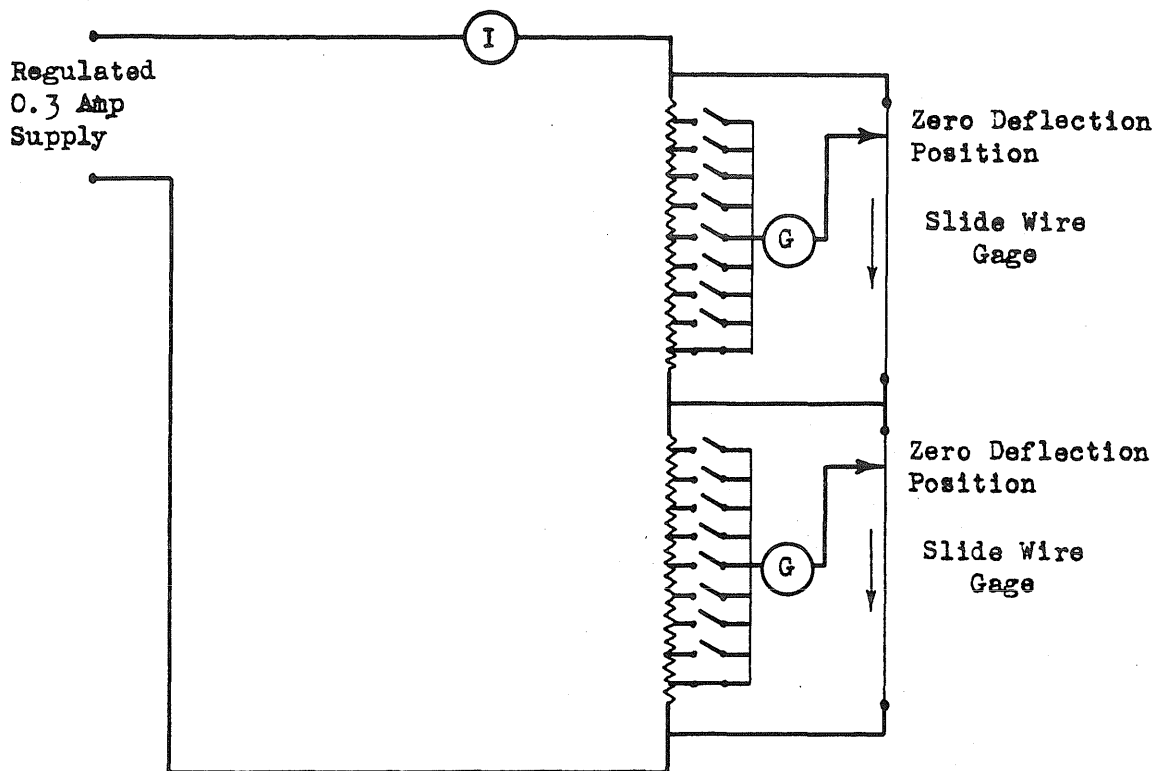


FIG. 34

INSTRUMENTATION AND DIMENSIONS OF FLEXURAL SPECIMENS



At zero deflection, bridge circuit had maximum unbalance. Both calibration switches and slide deflection move bridge towards balance.

The switches were used to set the sensitivity of the bridge circuit. When used as calibration switches, they are roughly equivalent to 2" of deflection each.

For BF Series specimens, one additional similar bridge was used.

"G" represents a galvanometer.

"I" represents an ammeter.

FIG. 35 DEFLECTION GAGE CIRCUITS

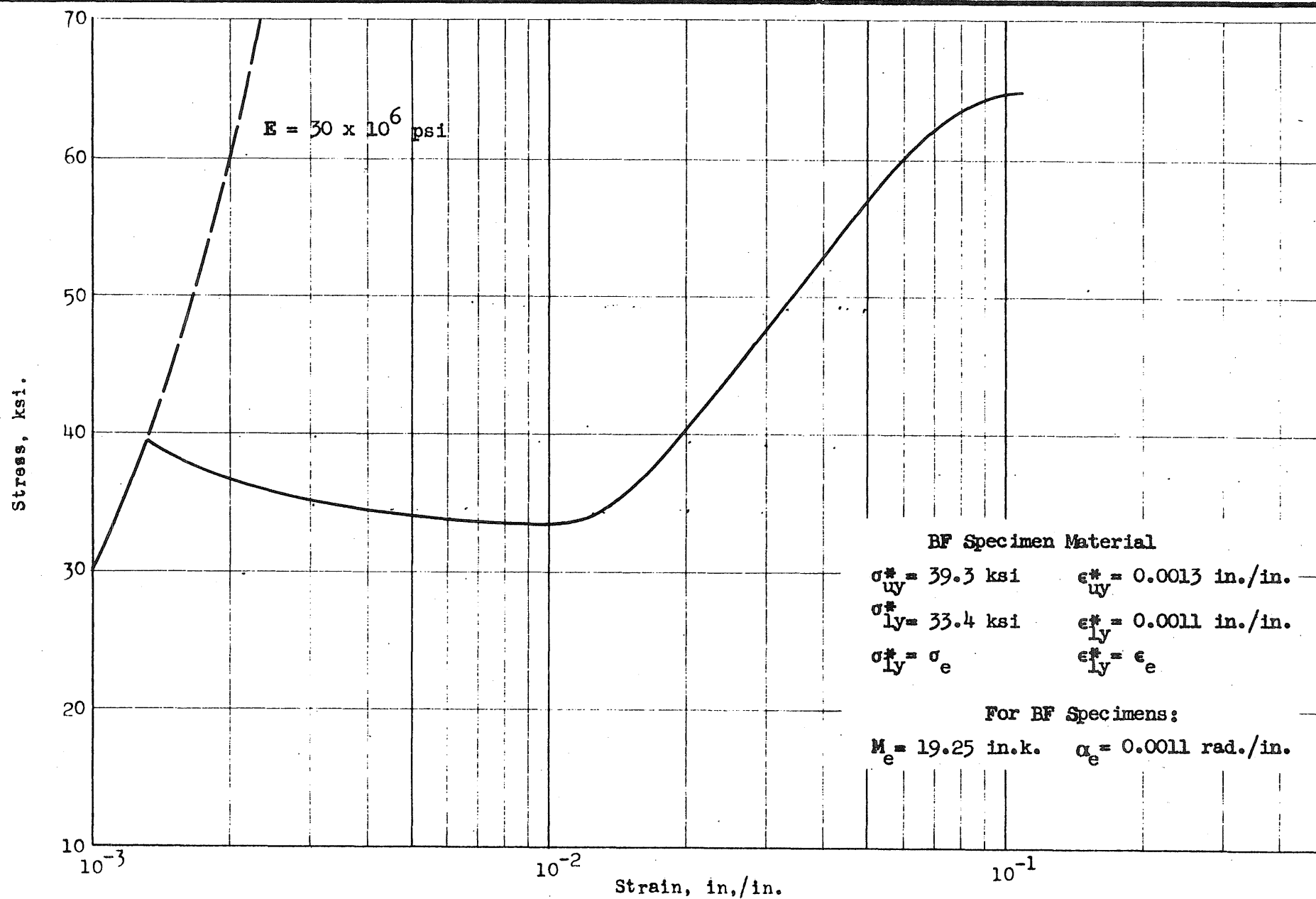
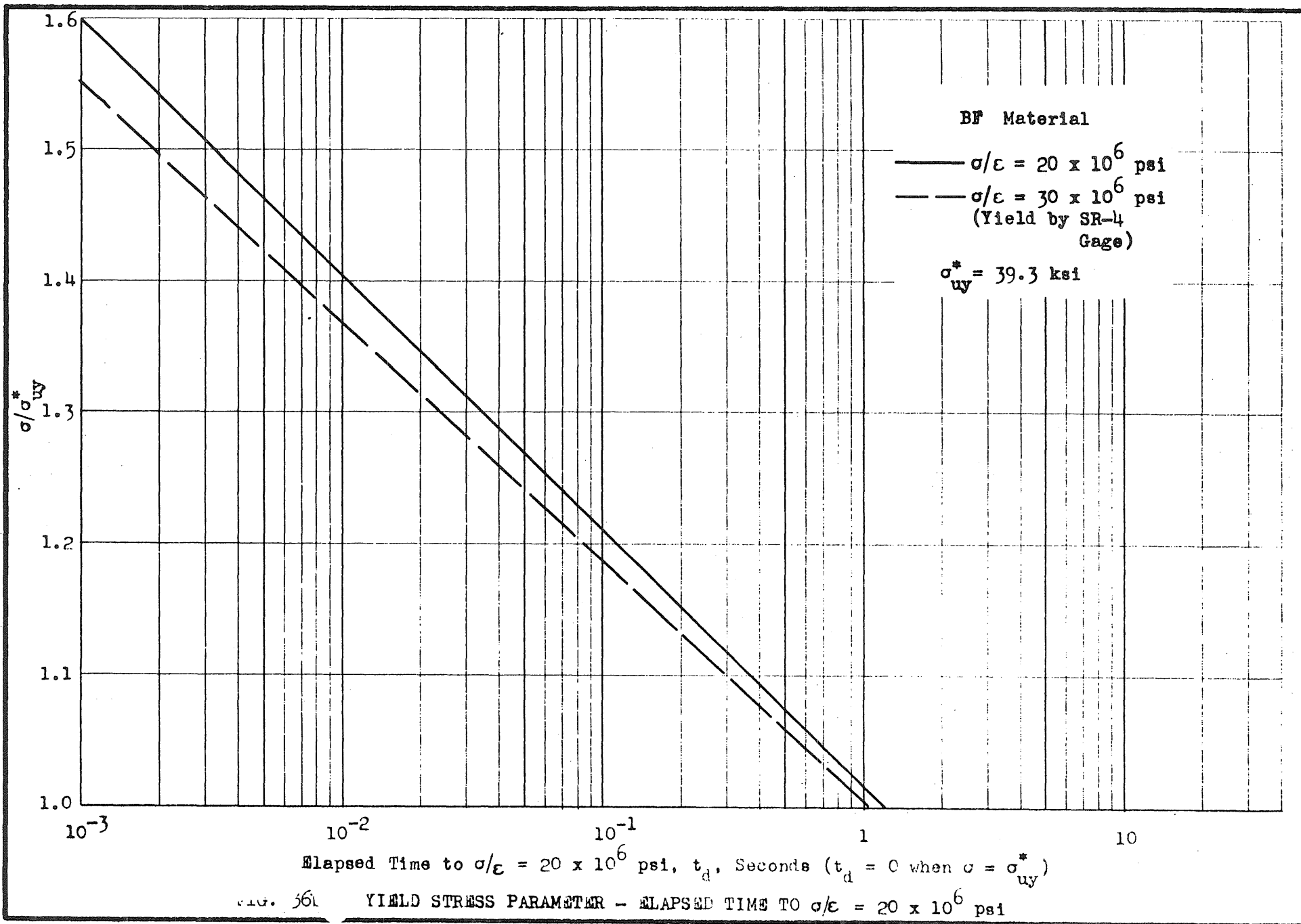


FIG. 36a STRESS - STRAIN



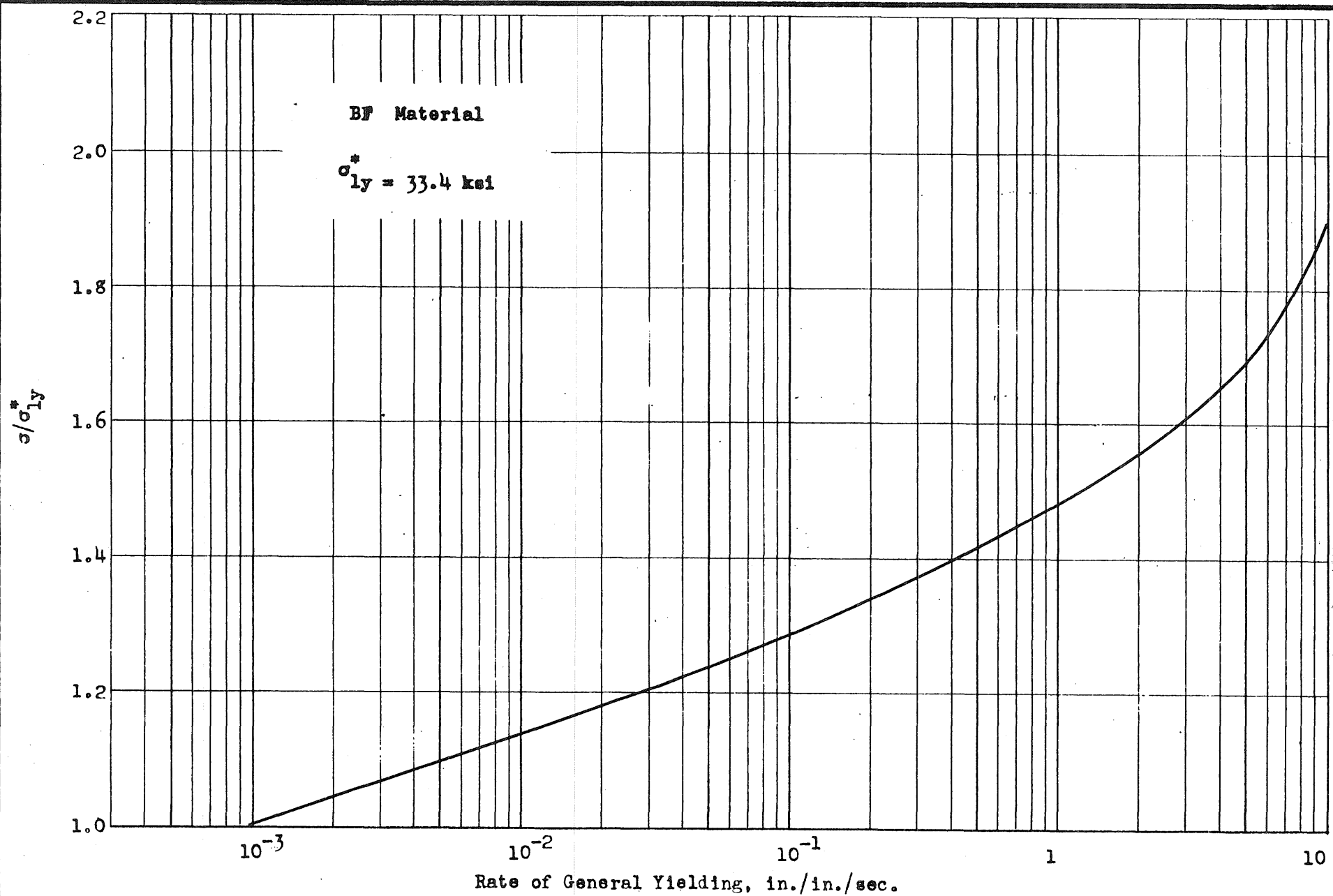


FIG. 36c

YIELD STRESS PARAMETER -- RATE OF YIELDING AT CONSTANT STRESS

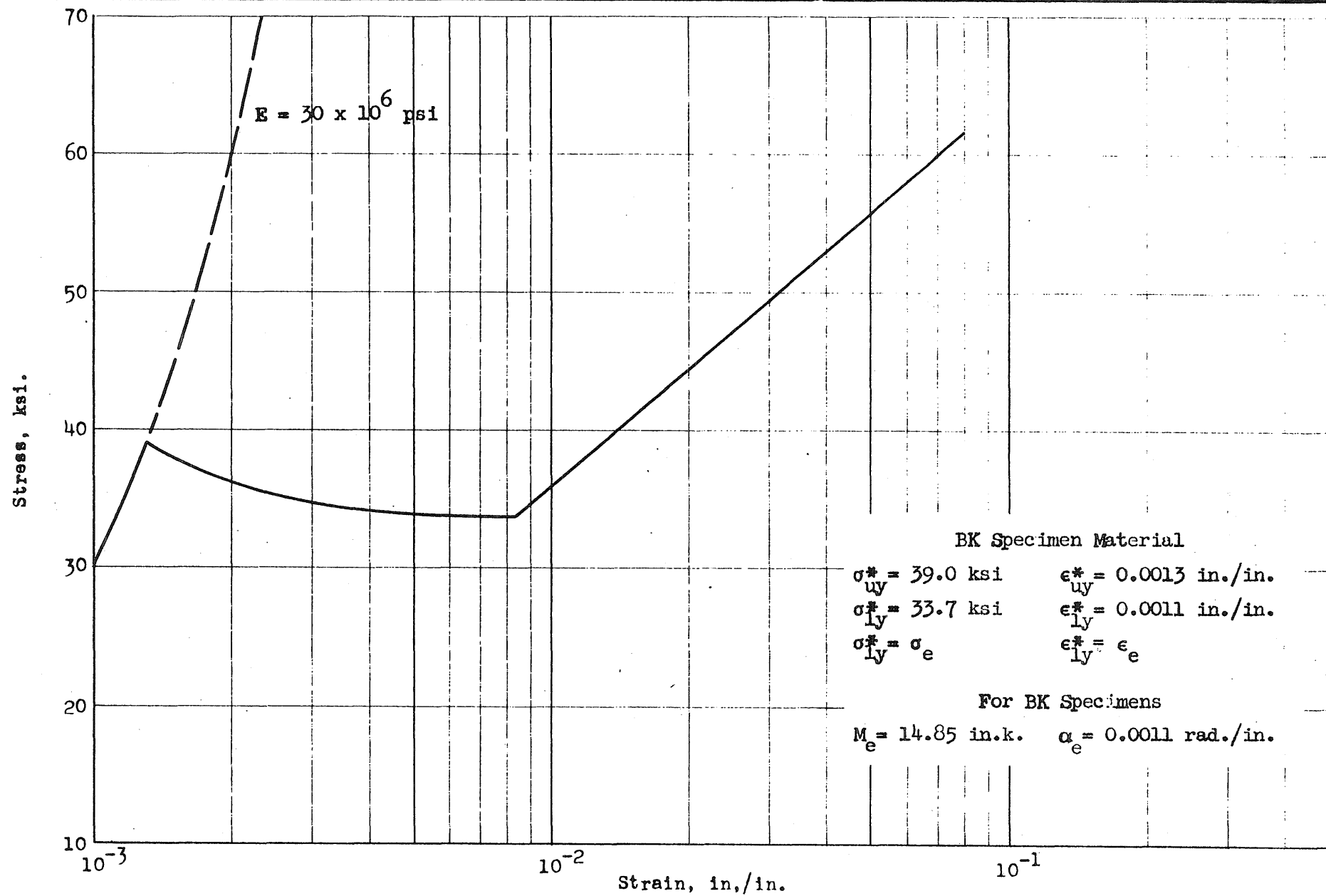
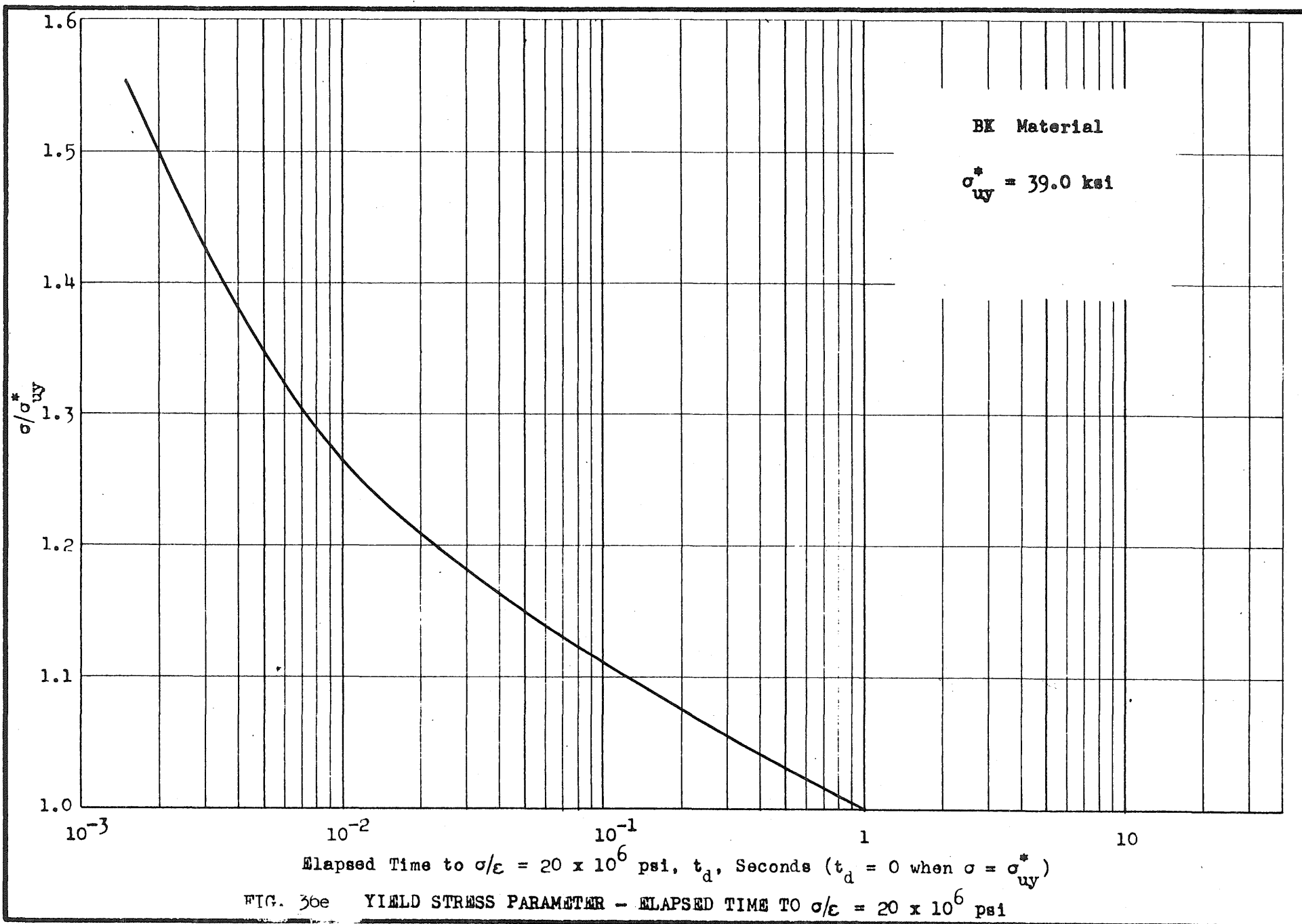


FIG. 36a STRESS - STRAIN



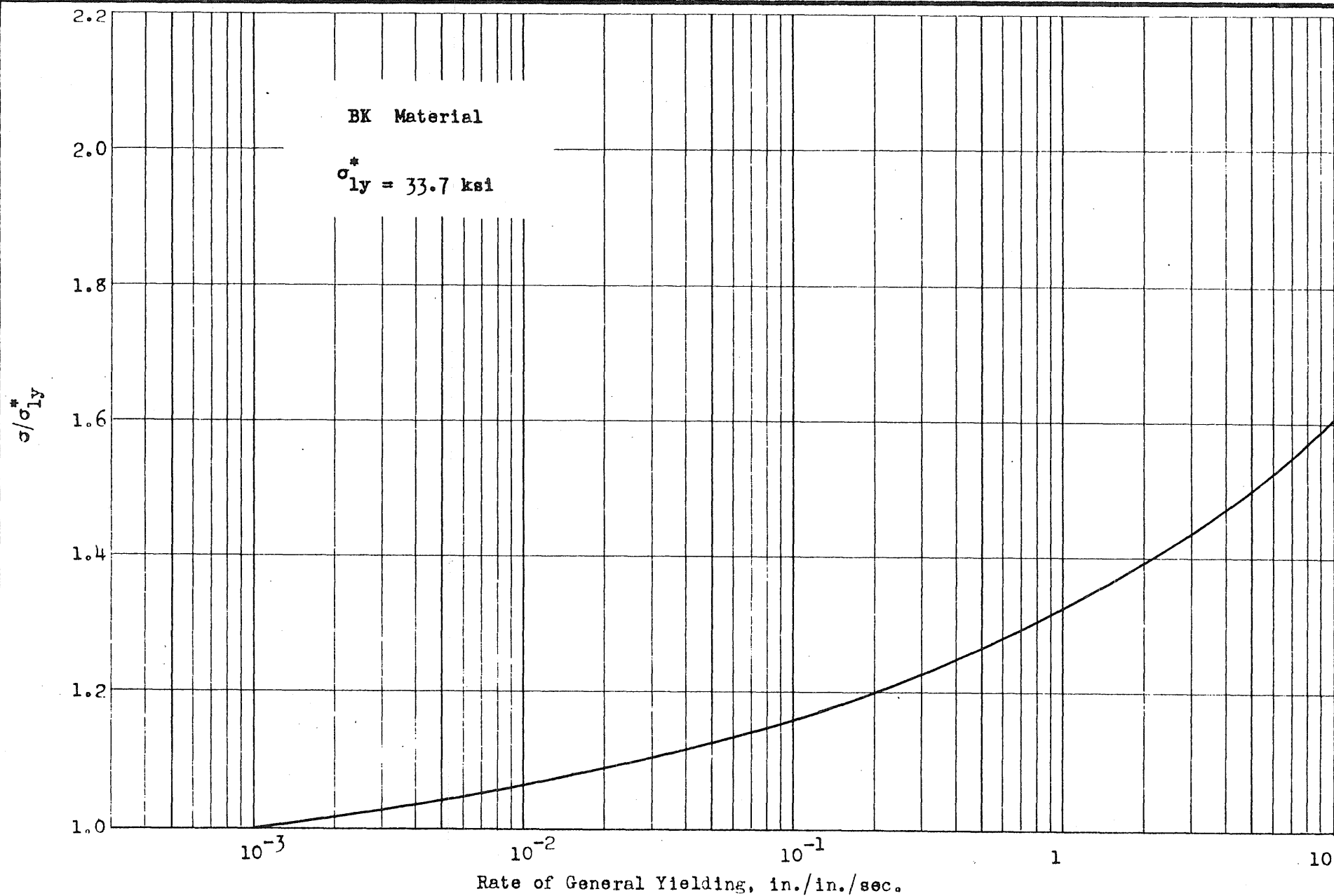


FIG. 36f YIELD STRESS PARAMETER - RATE OF YIELDING AT CONSTANT STRESS

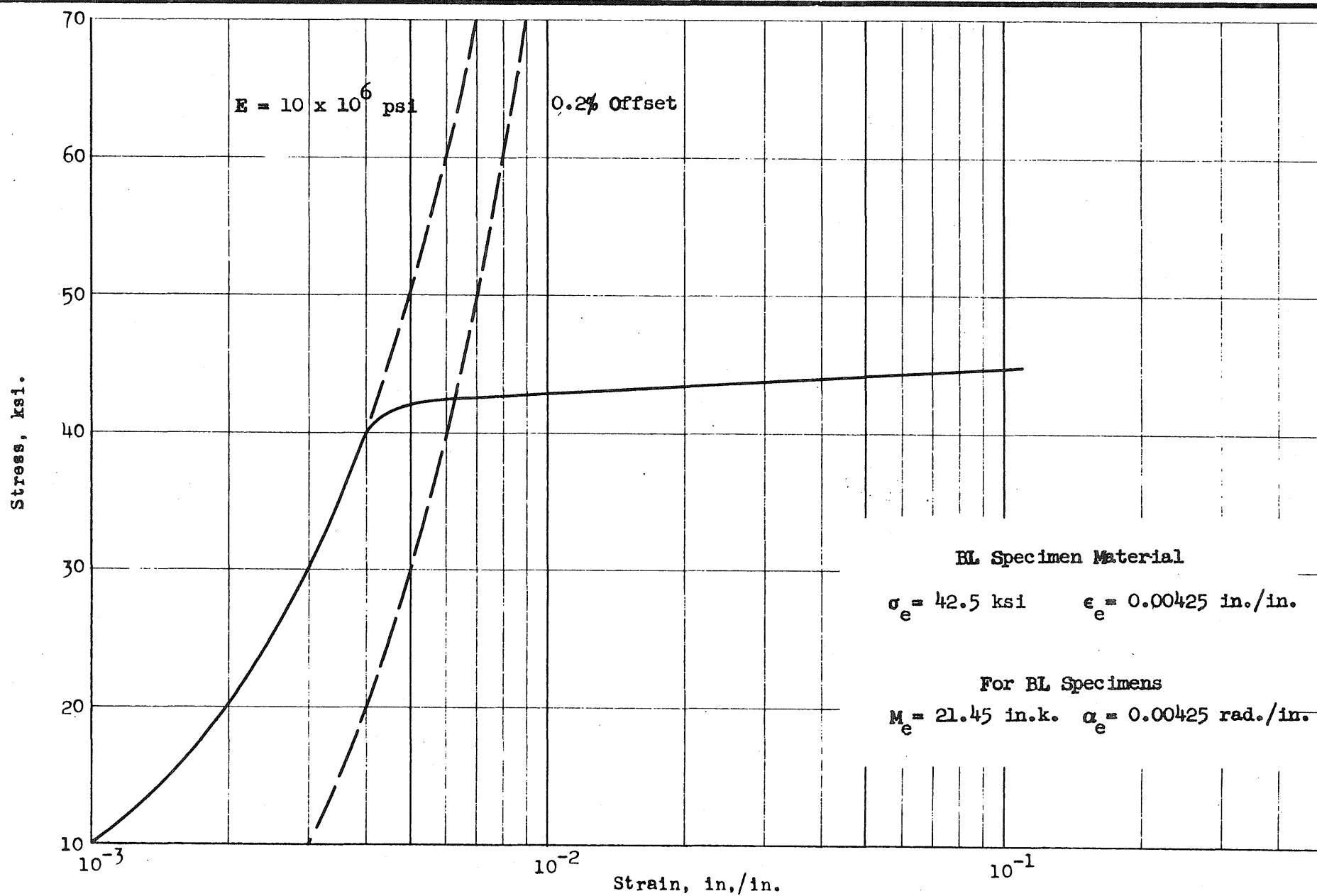


FIG. 36g STRESS - STRAIN

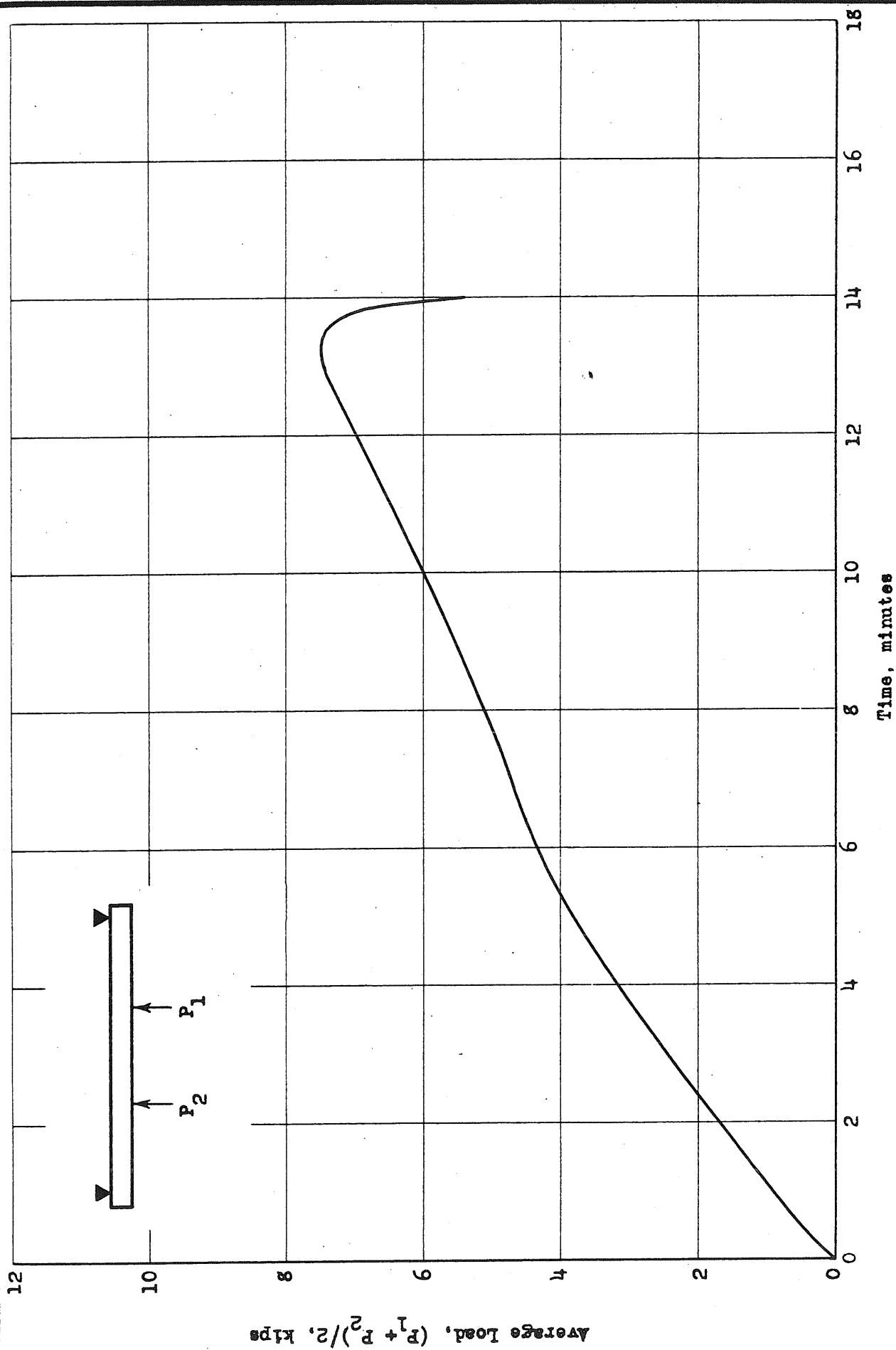


FIG 37a LOAD - TIME, SPECIMEN BJA-1

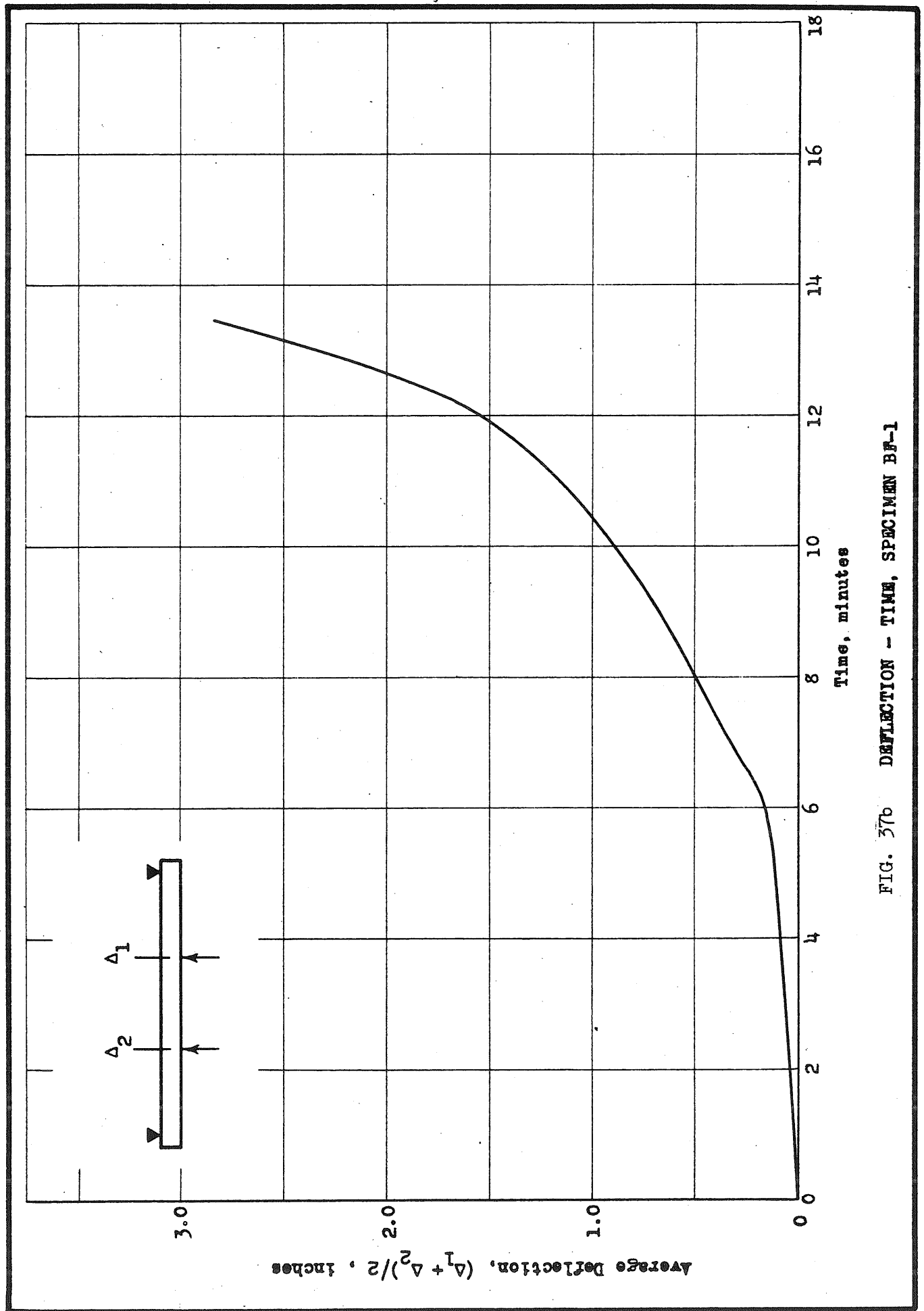


FIG. 37b DEFLECTION - TIME, SPECIMEN BF-1

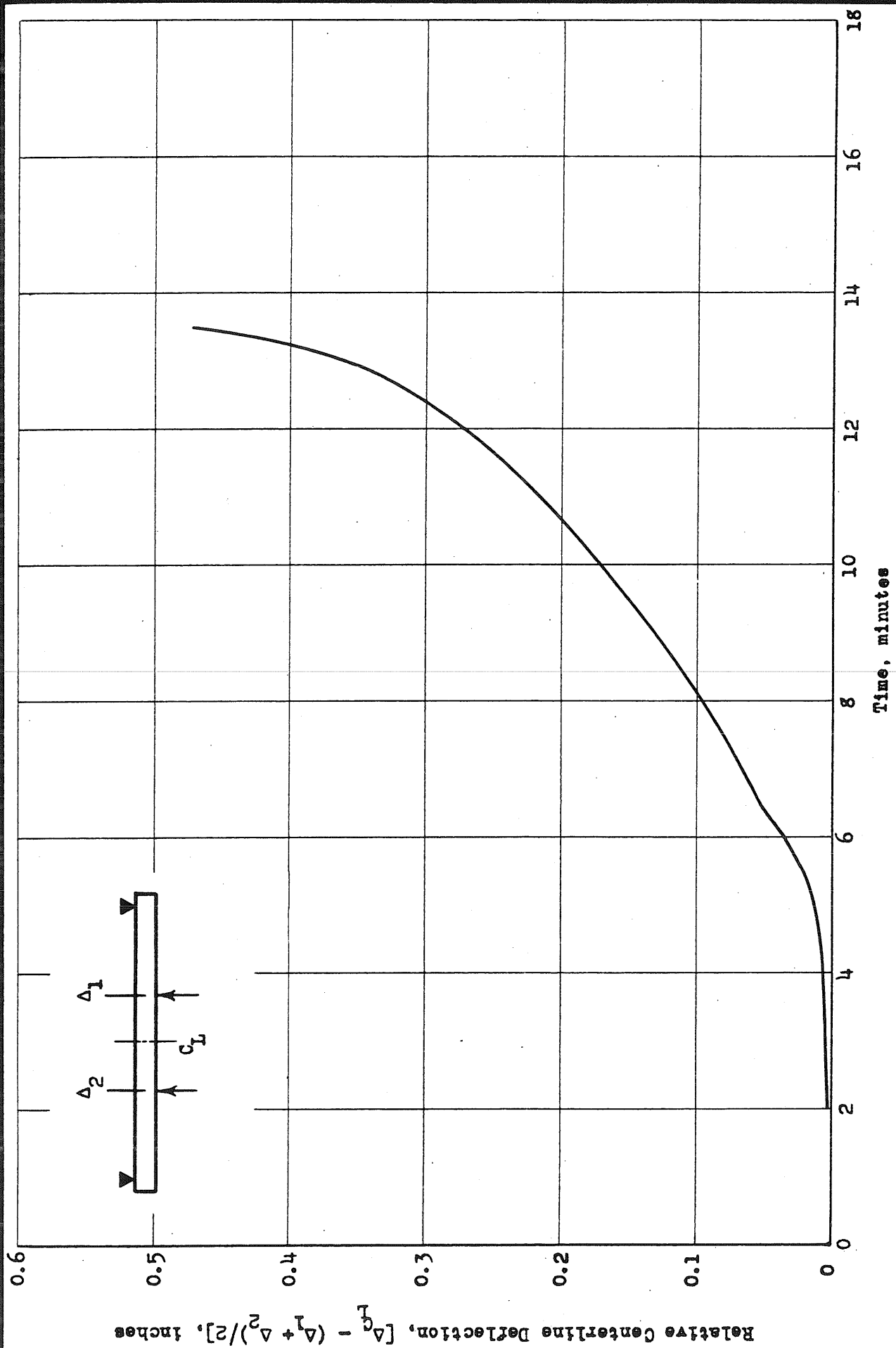
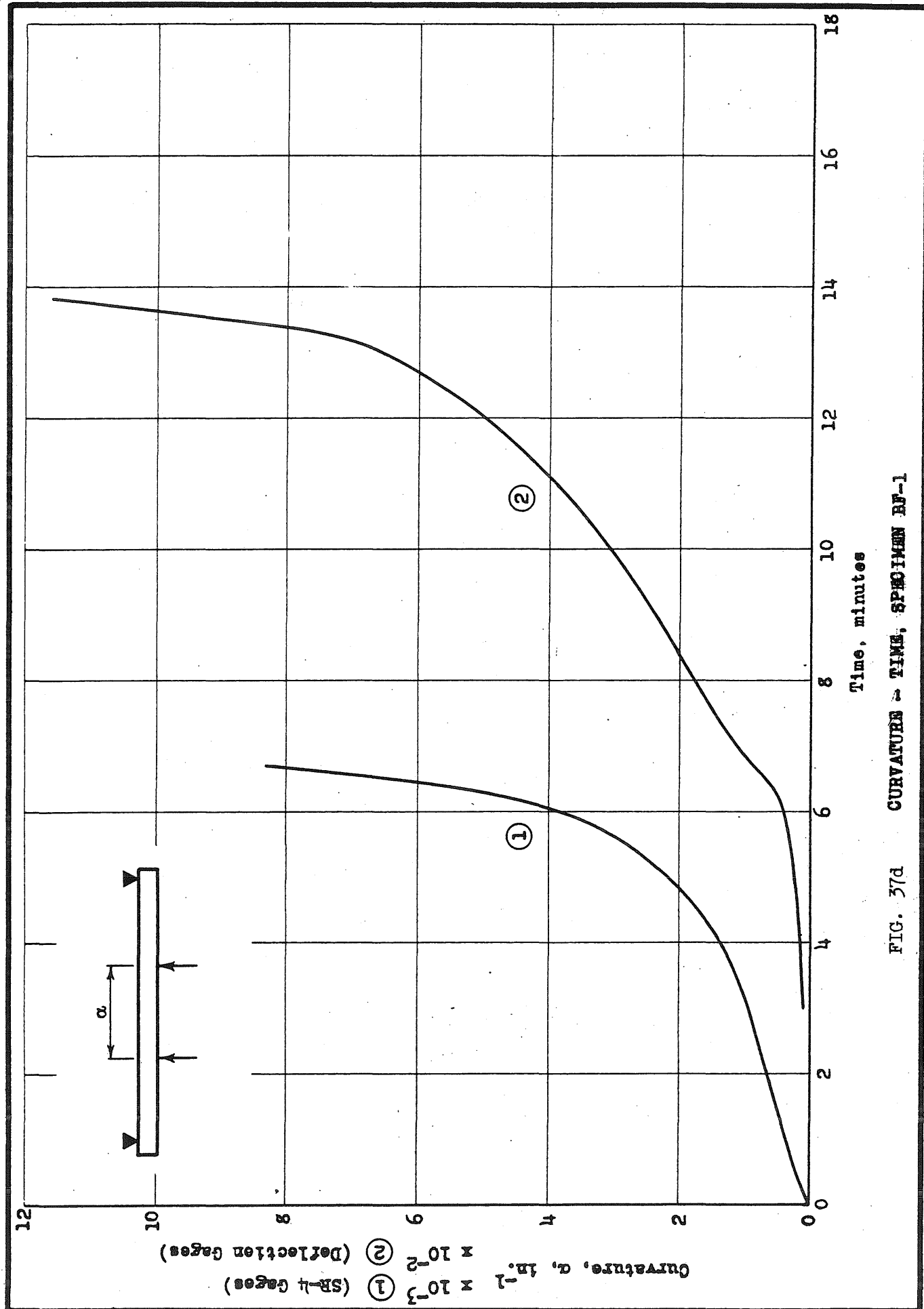


FIG. 37c RELATIVE CENTERLINE DEFLECTION - TIME, SPECIMEN BF-1



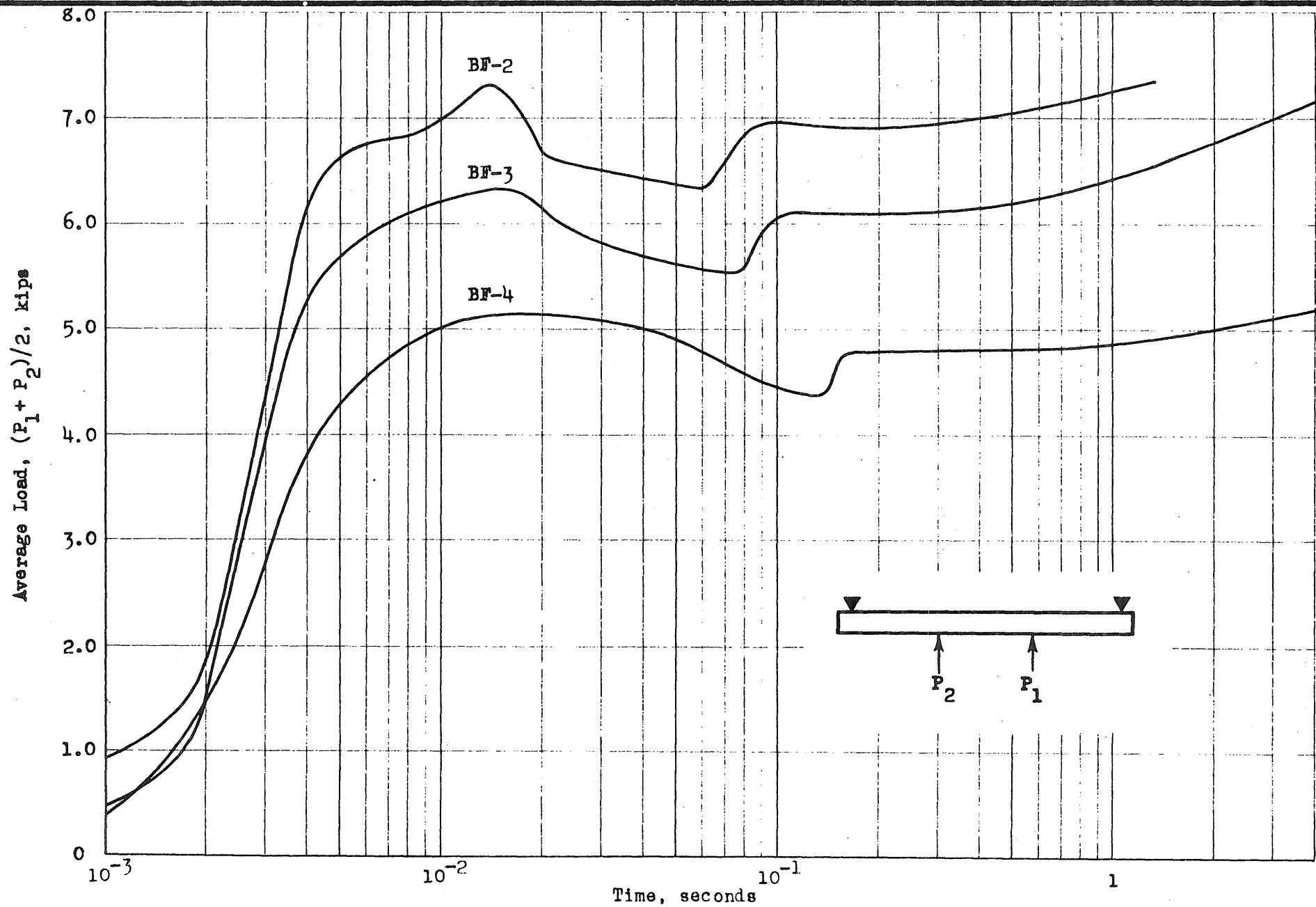


FIG. 37e

LOAD - TIME, SPECIMENS BF-2, BF-3, BF-4.

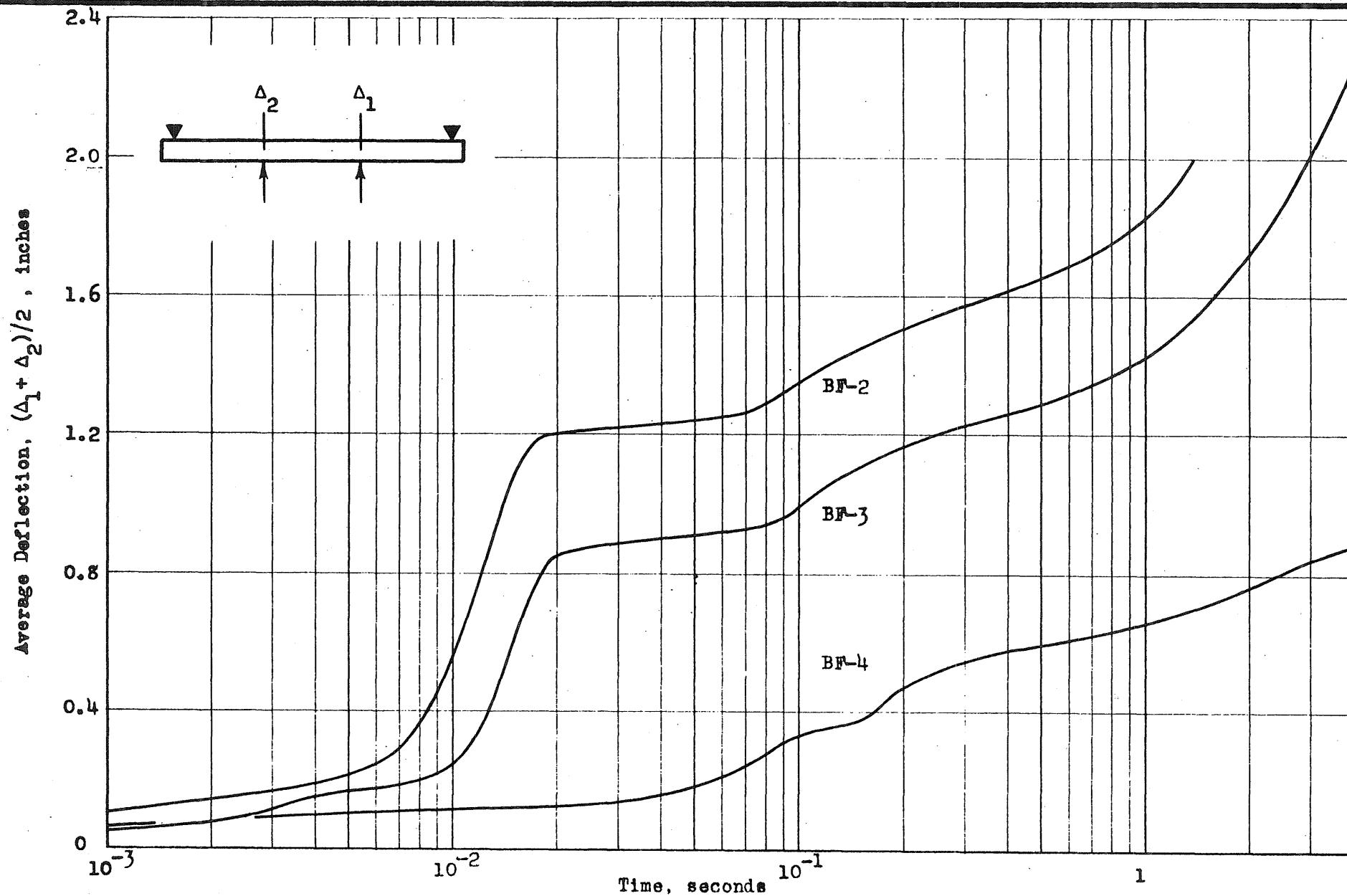


FIG. 37f DEFLECTION - TIME, SPECIMENS BF-2, BF-3, BF-4.

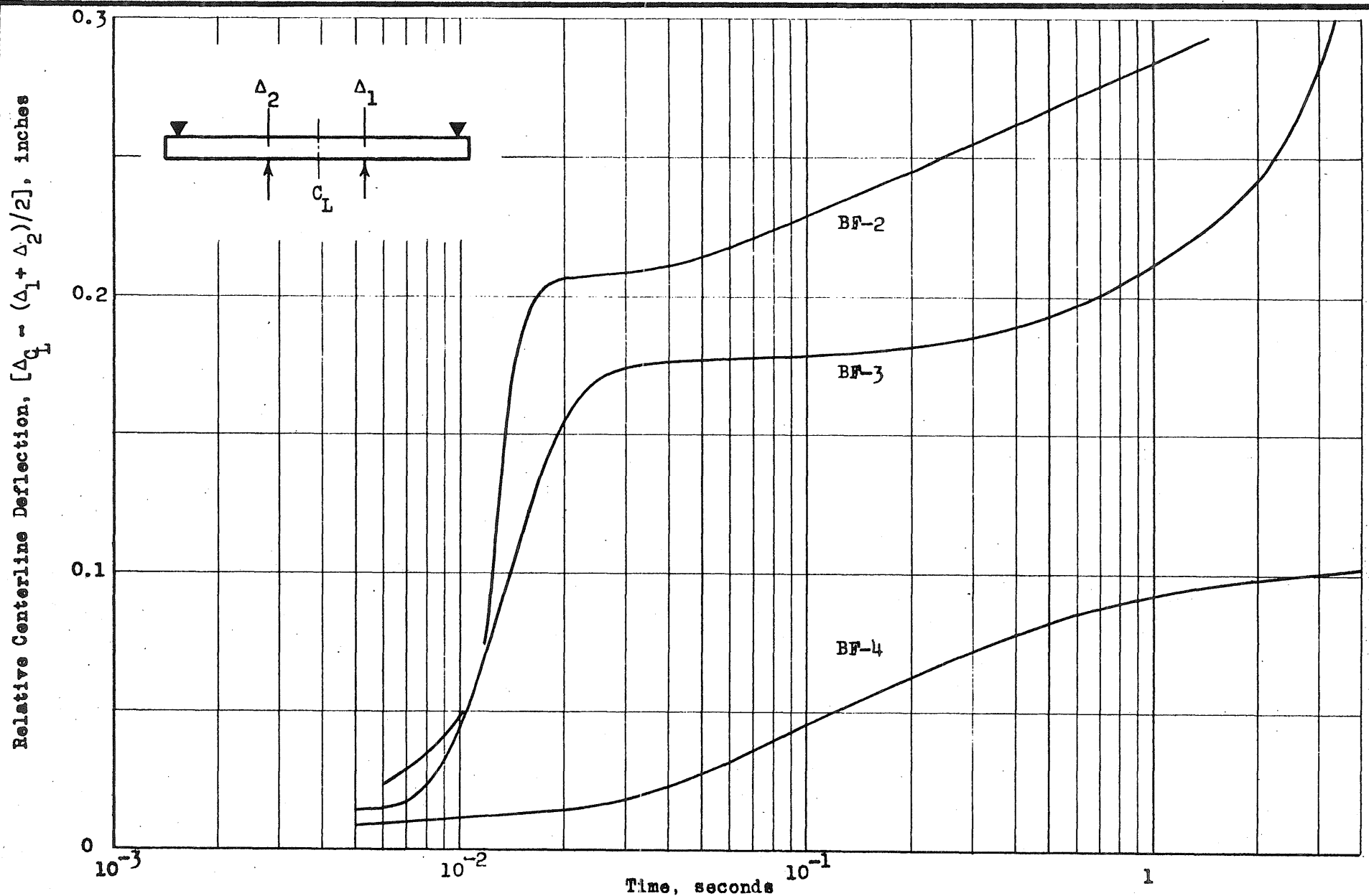


FIG. 37g

RELATIVE CENTERLINE DEFLECTION - TIME, SPECIMENS BF-2, BF-3, BF-4.

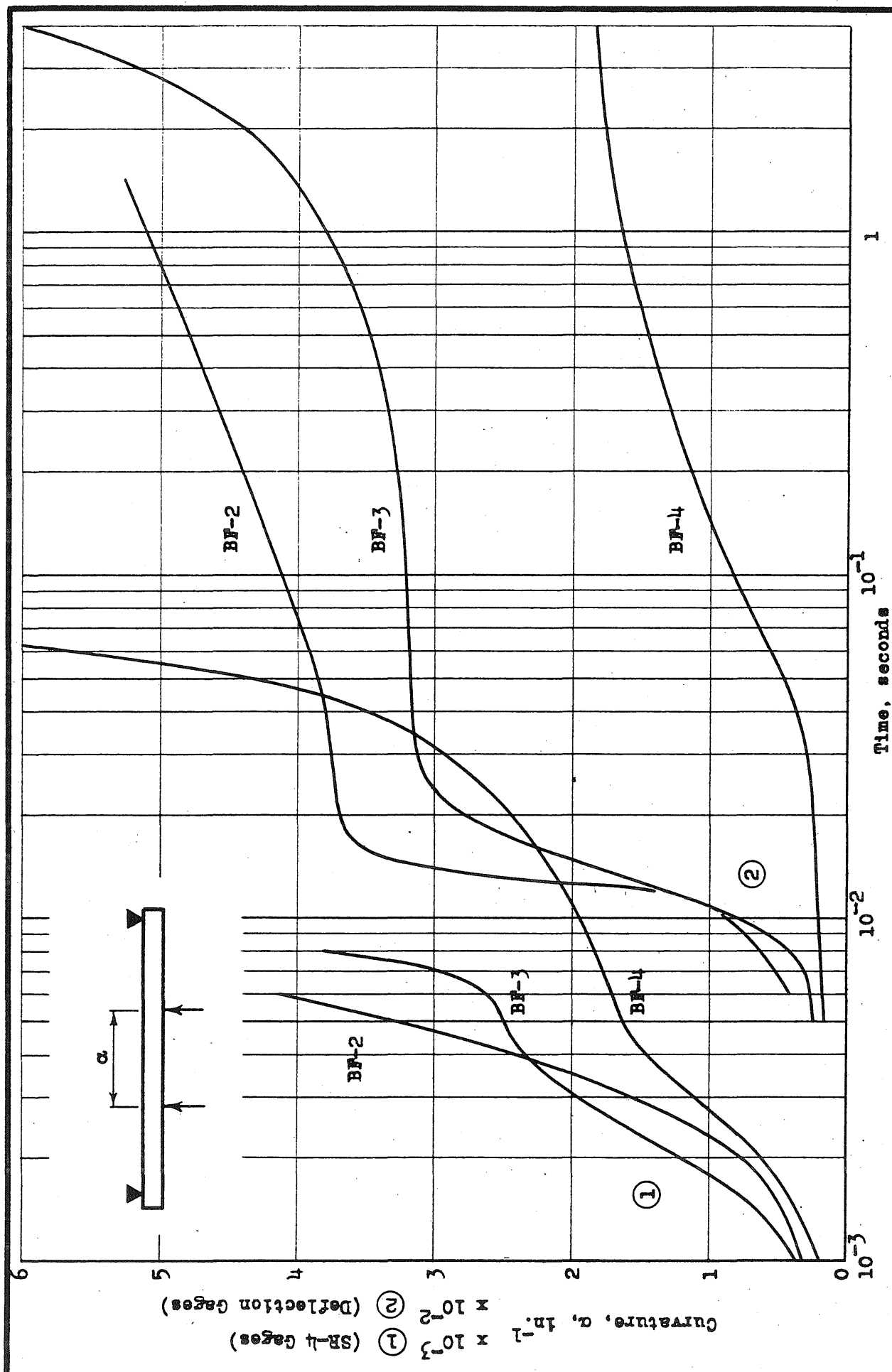


FIG. 37h CURVATURE - TIME, SPECIMENS BF-2, BF-3, BF-4.

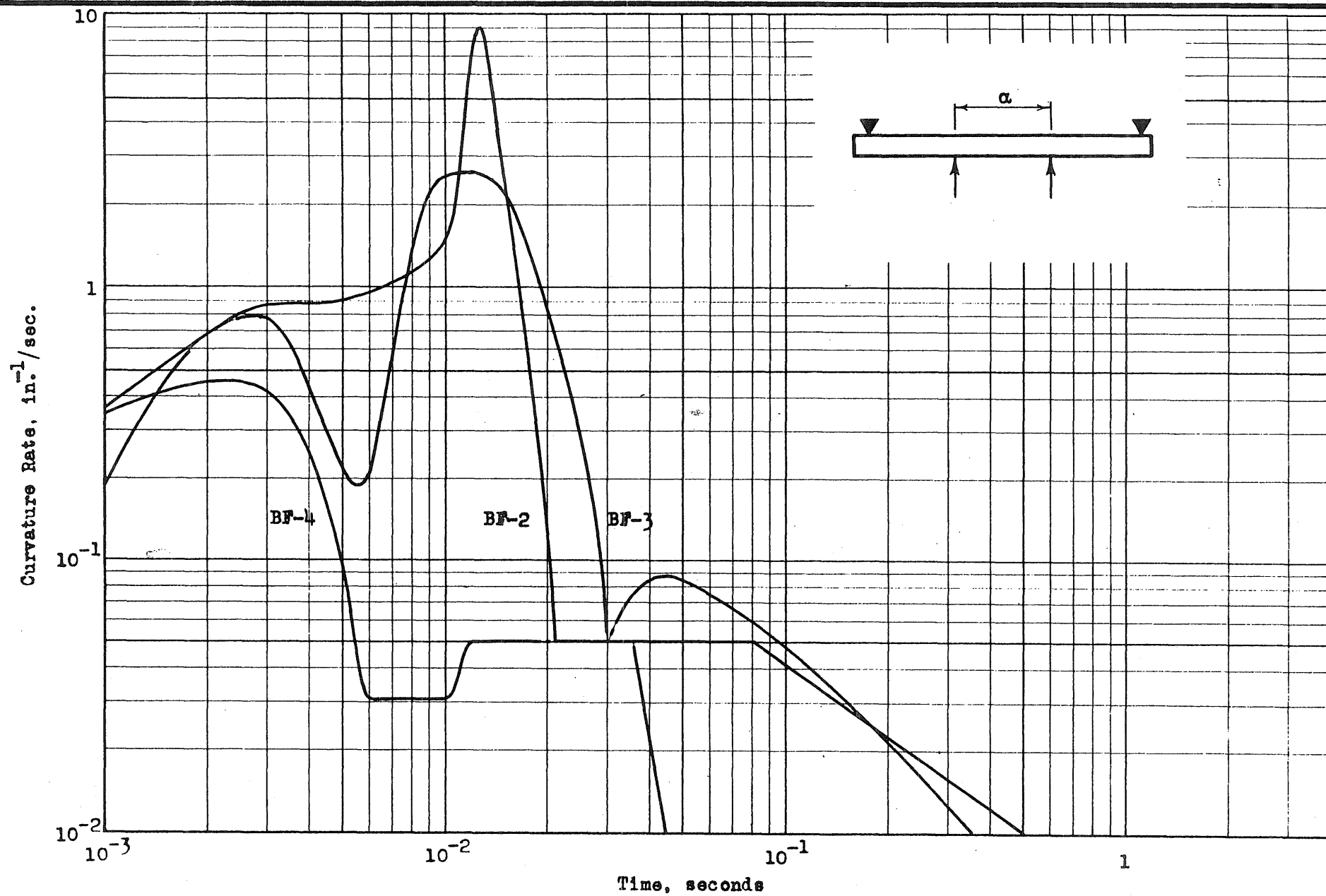


FIG. 371

CURVATURE RATE - TIME, SPECIMENS BF-2, BF-3, BF-4

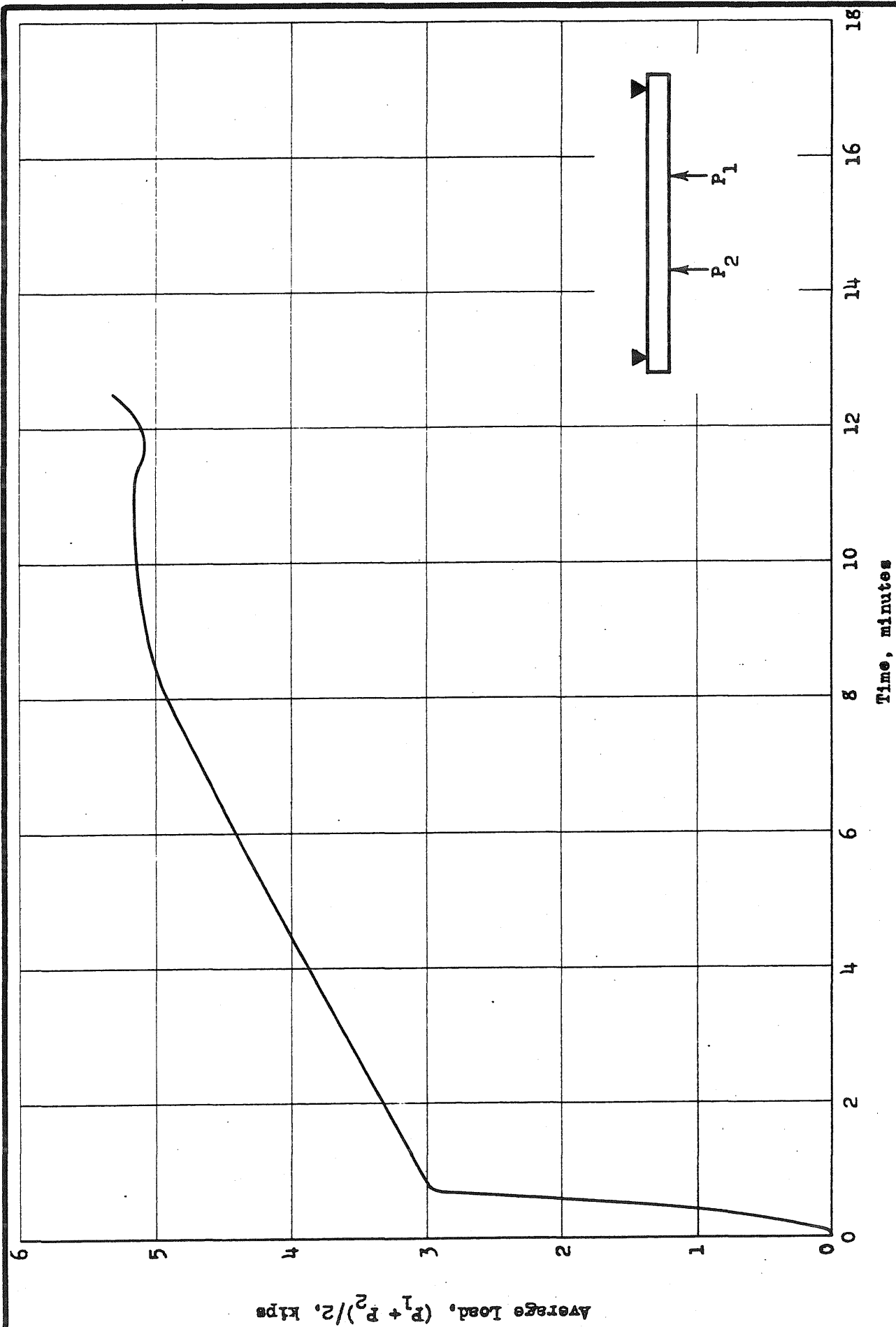


FIG. 38a LOAD - TIME, SPECIMEN BK-1

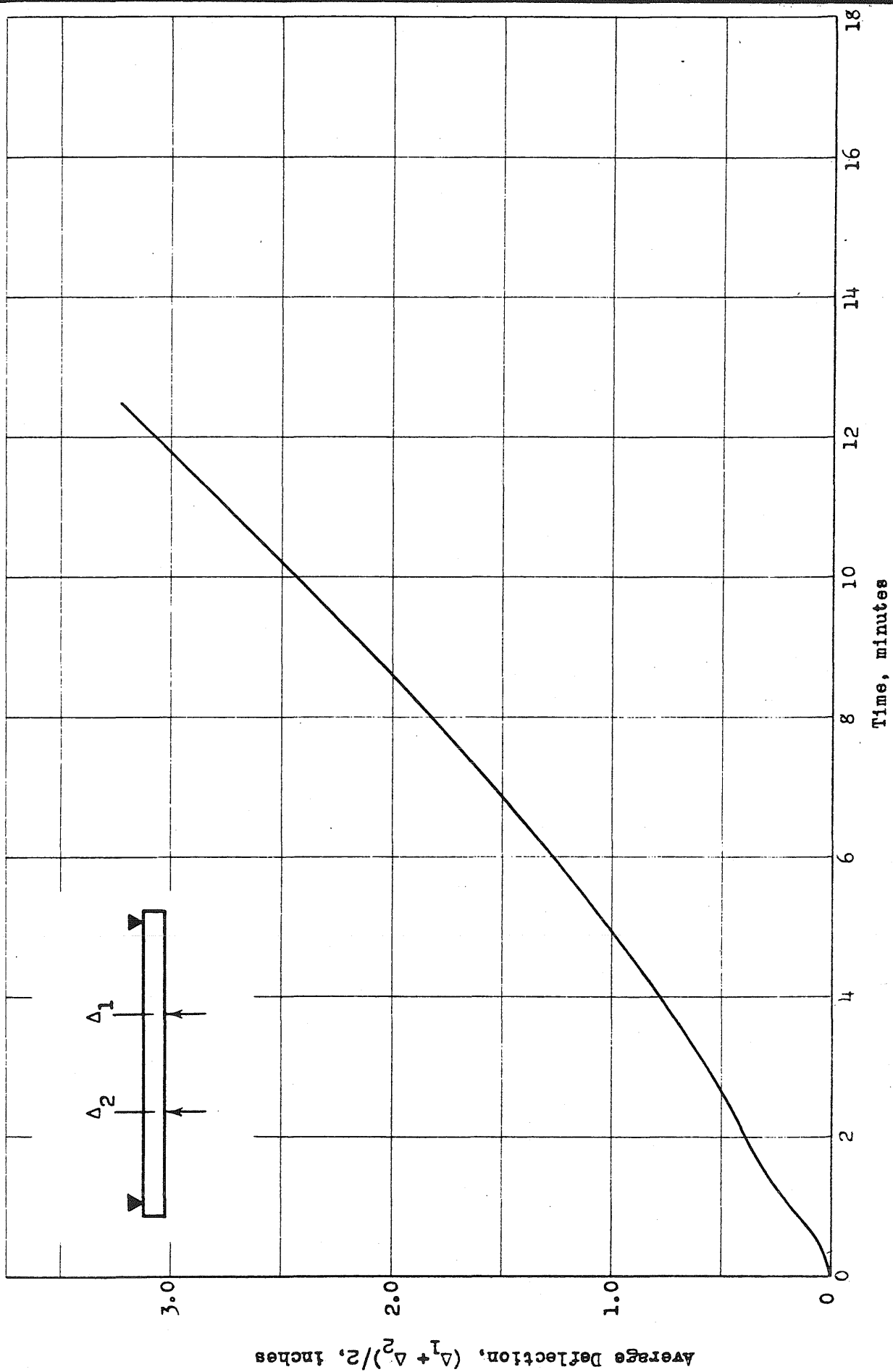


FIG. 38b DEFLECTION - TIME, SPECIMEN BK-1

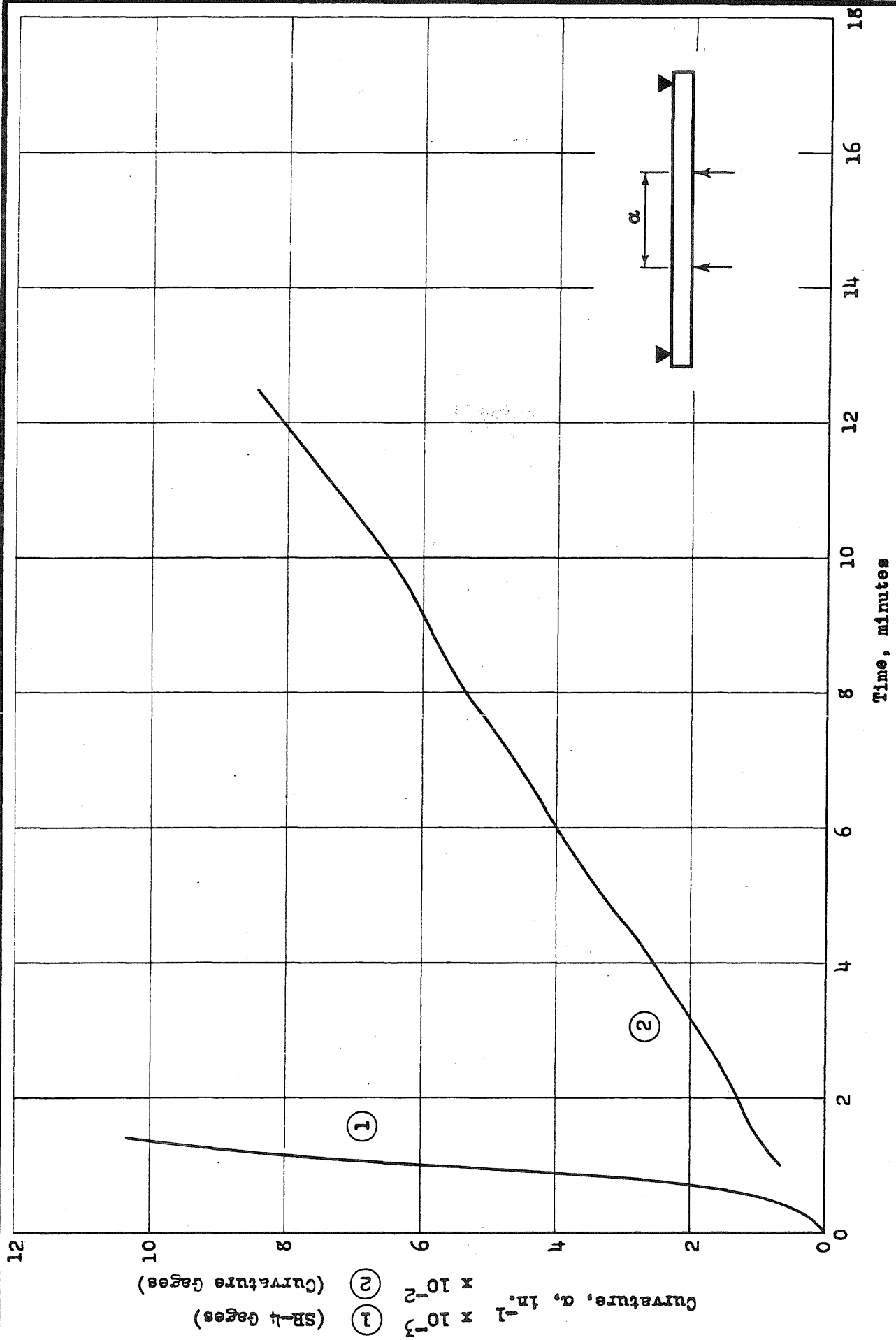


FIG. 38c CURVATURE - TIME, SPECIMEN BK-1

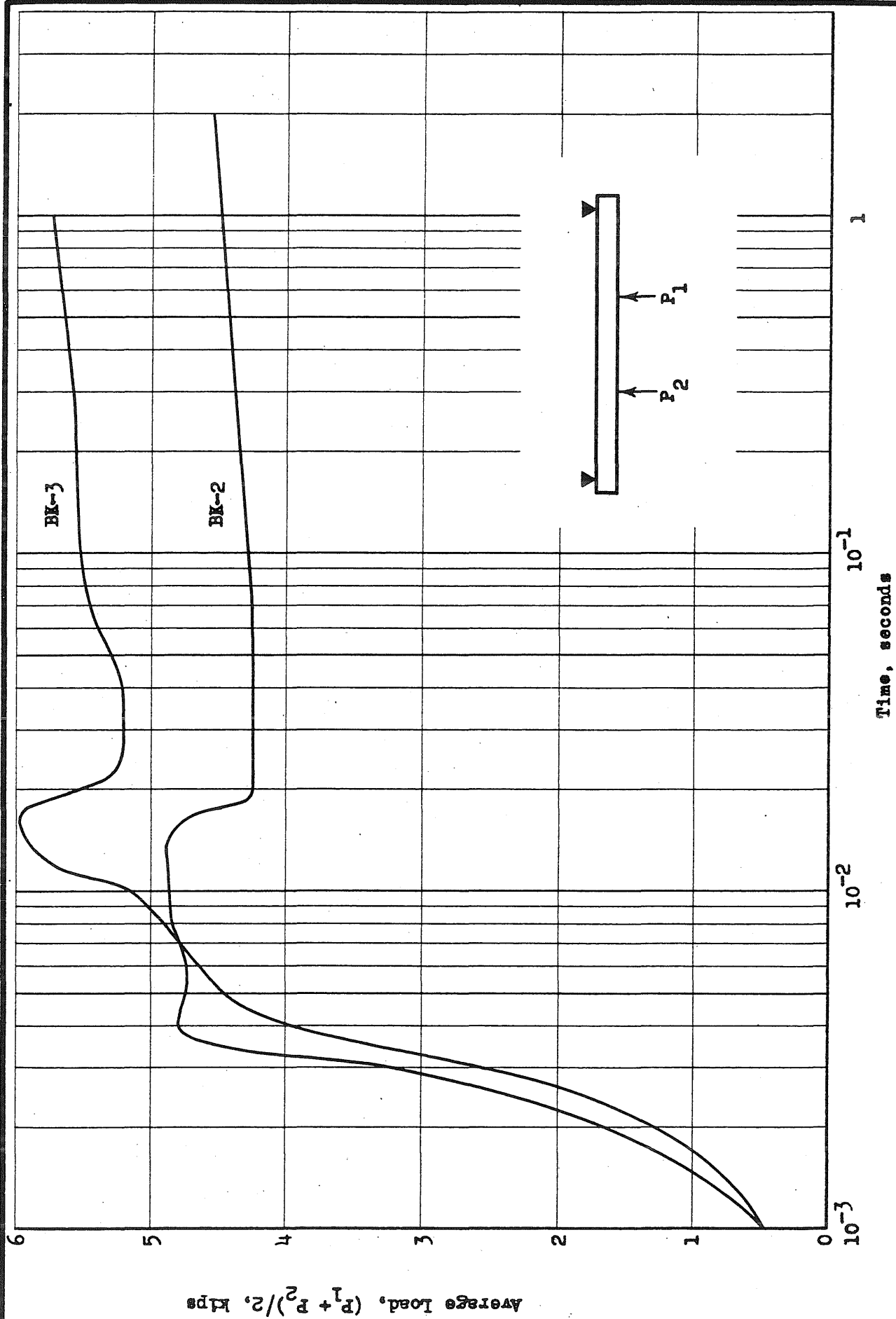


FIG. 38d LOAD - TIME, SPECIMENS BK-2, BK-3

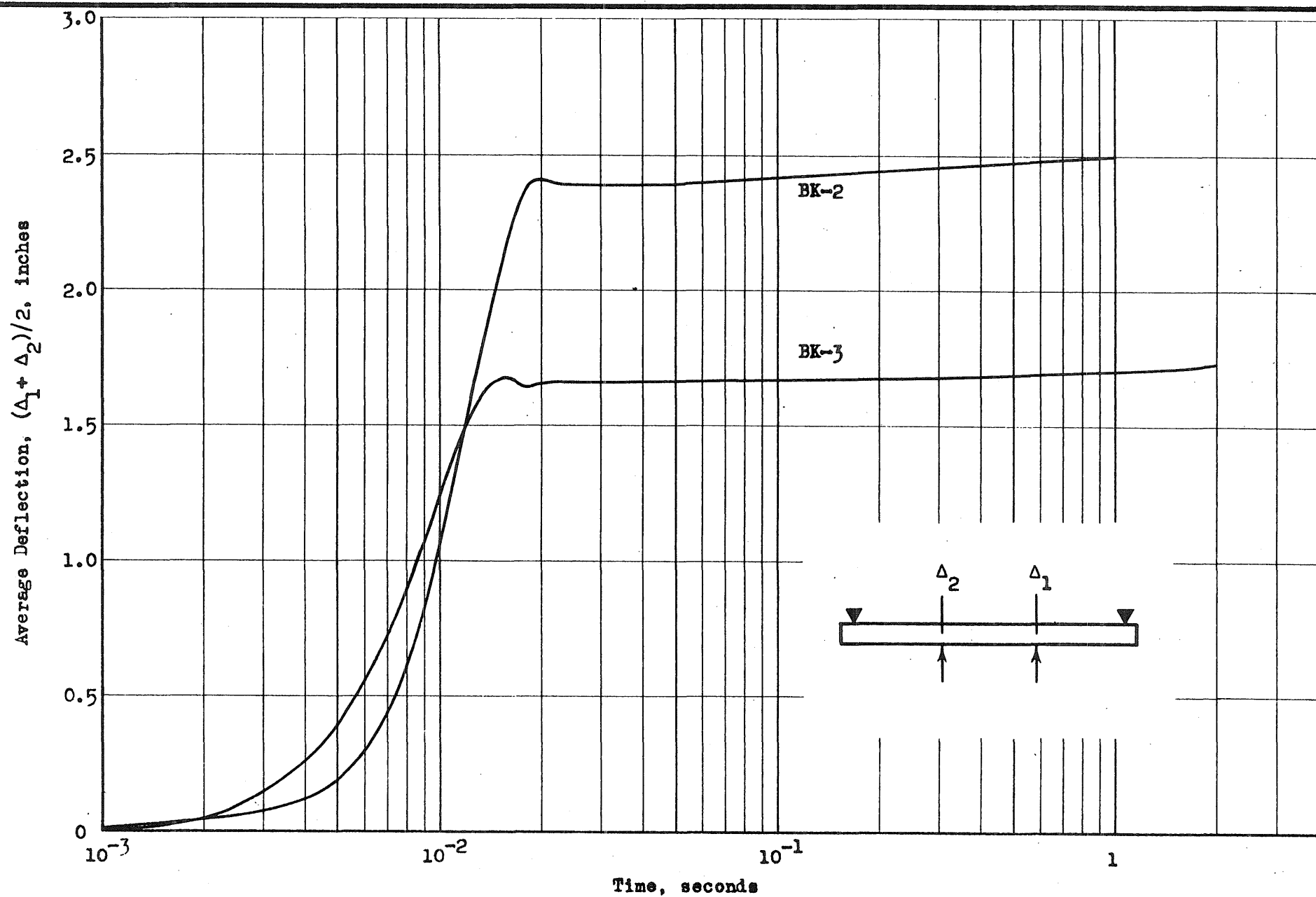
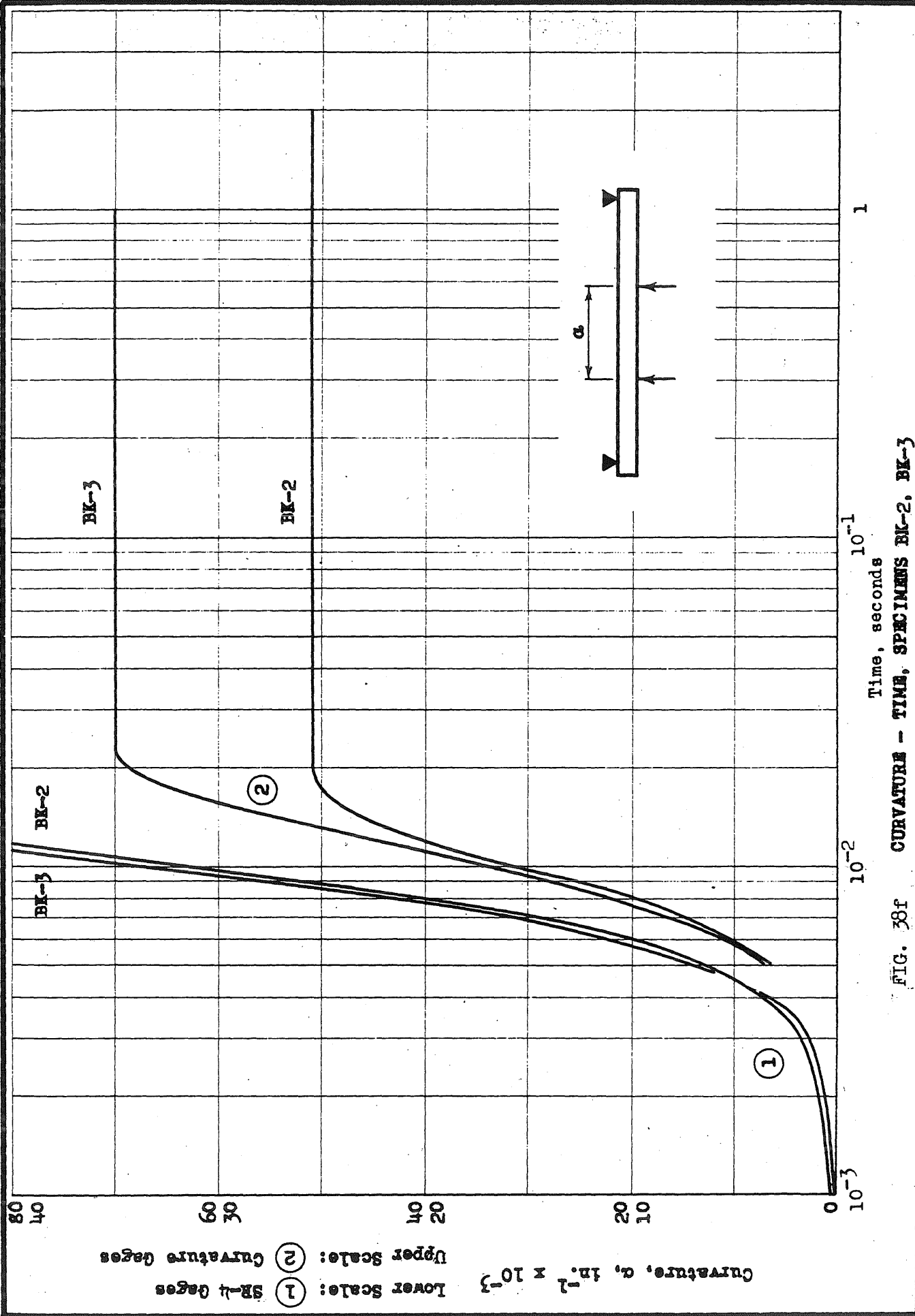
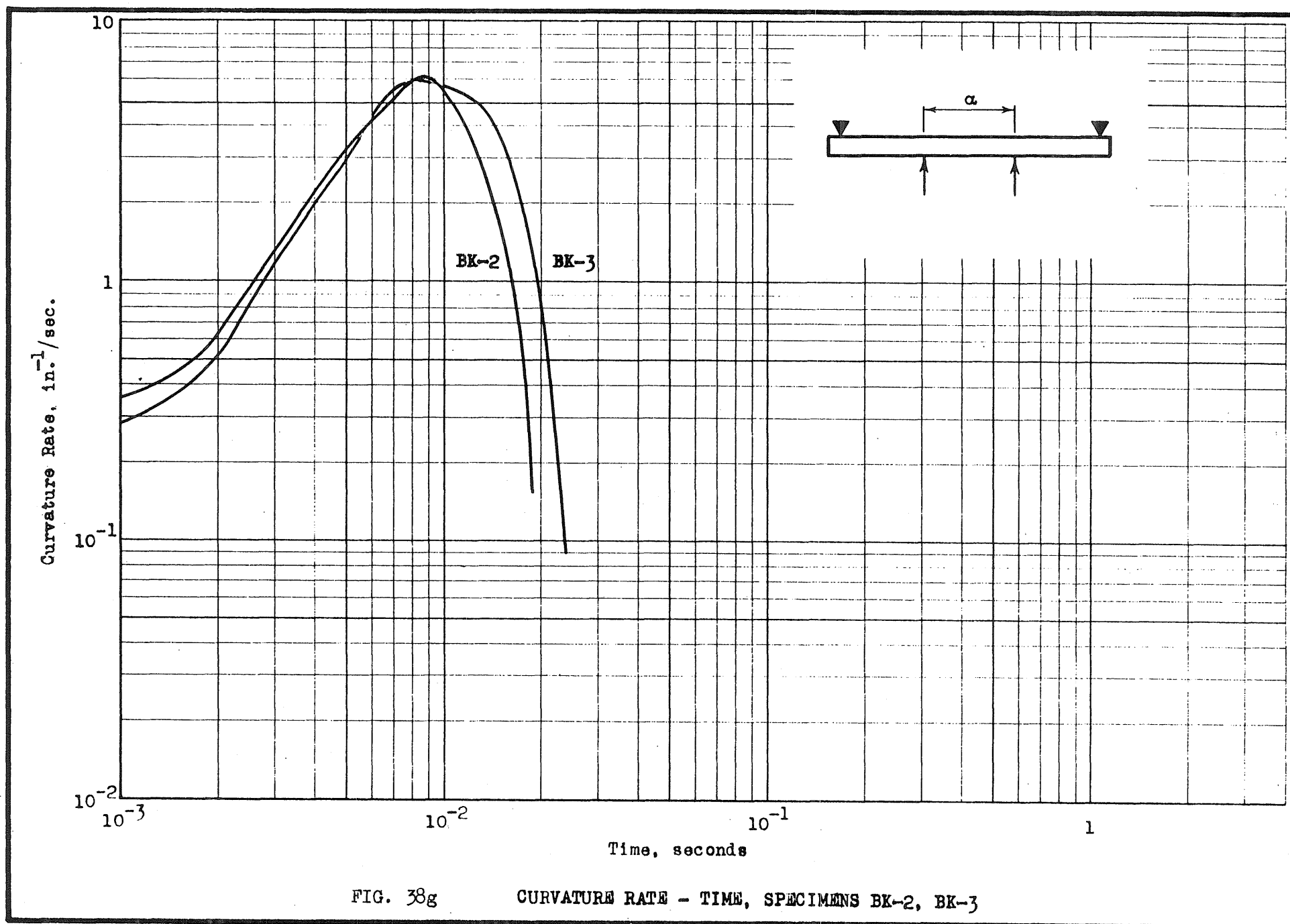


FIG. 38e DEFLECTION - TIME, SPECIMENS BK-2, BK-3





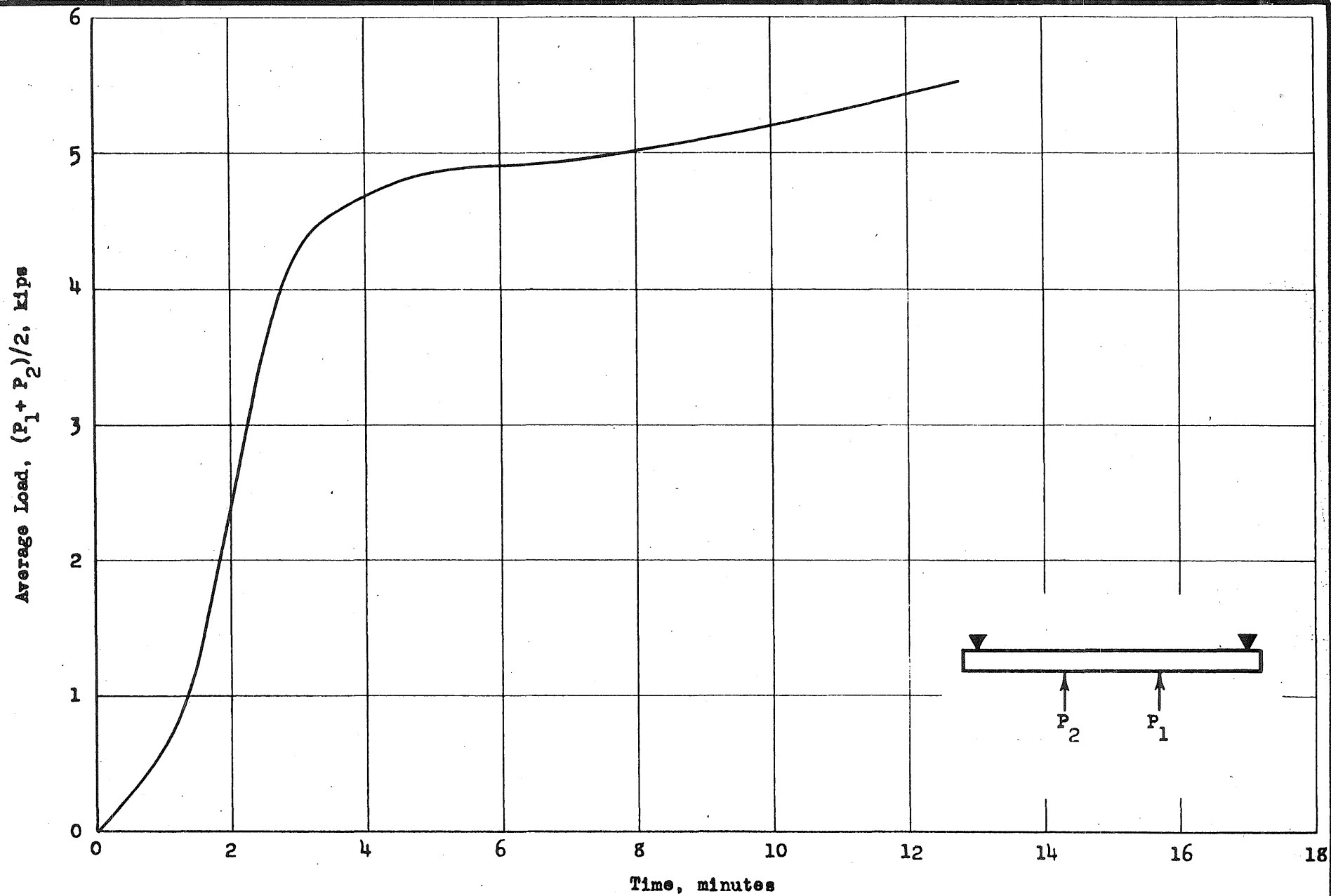


FIG. 39a LOAD - TIME, SPECIMEN BL-1

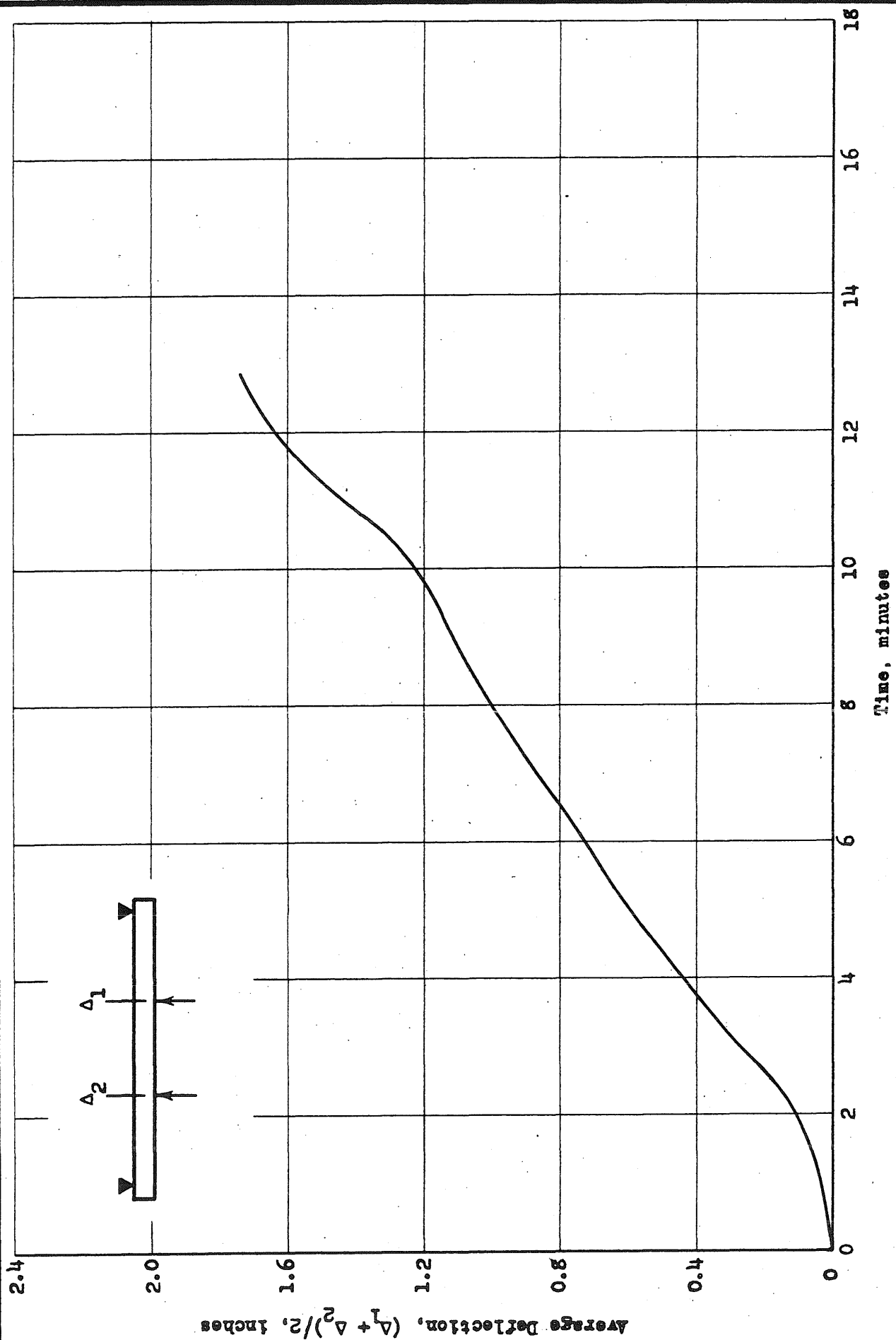


FIG. 39b DEFLECTION - TIME, SPECIMEN BL-1

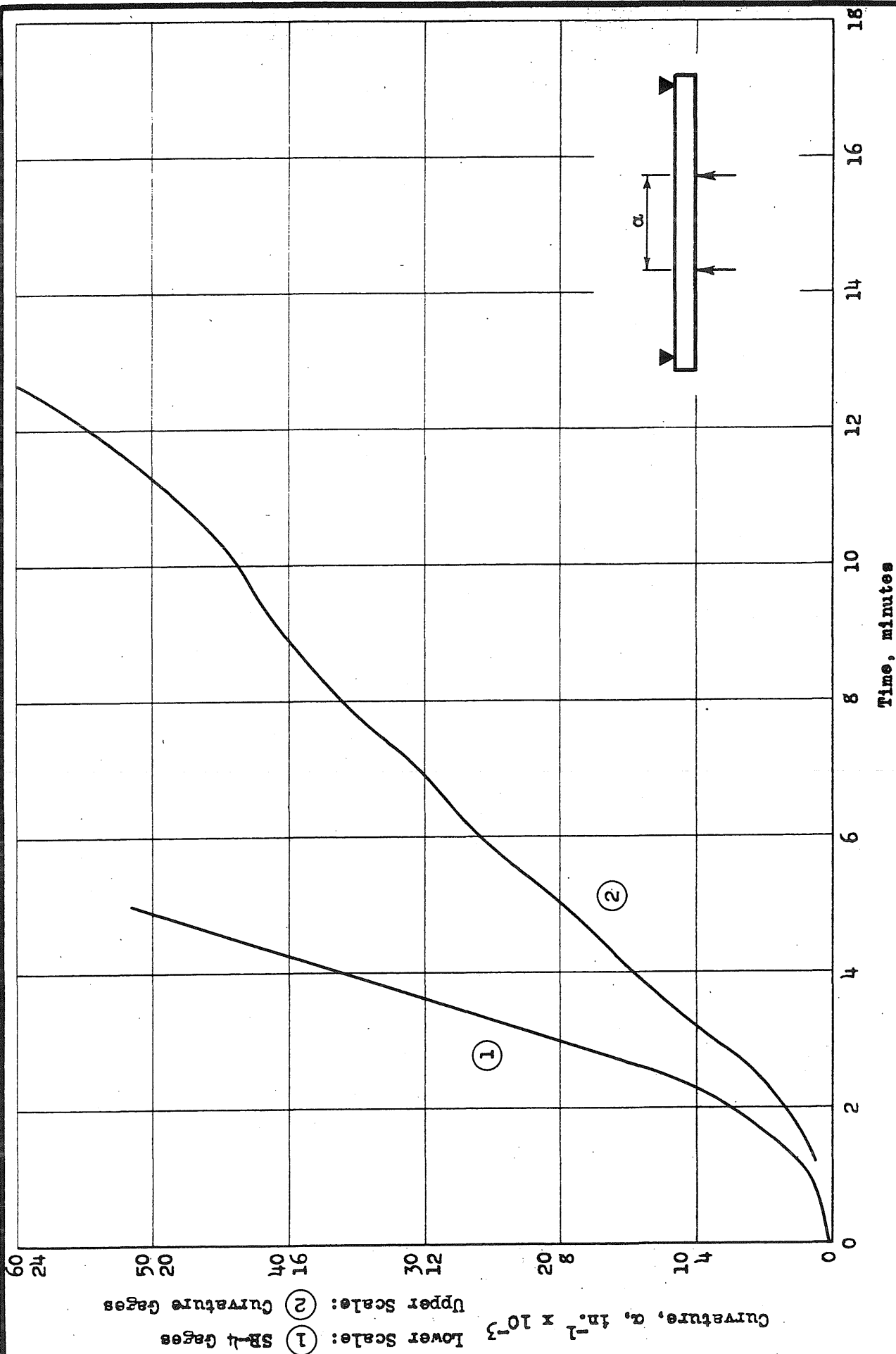


FIG. 39c CURVATURE - TIME, SPECIMEN BL-1

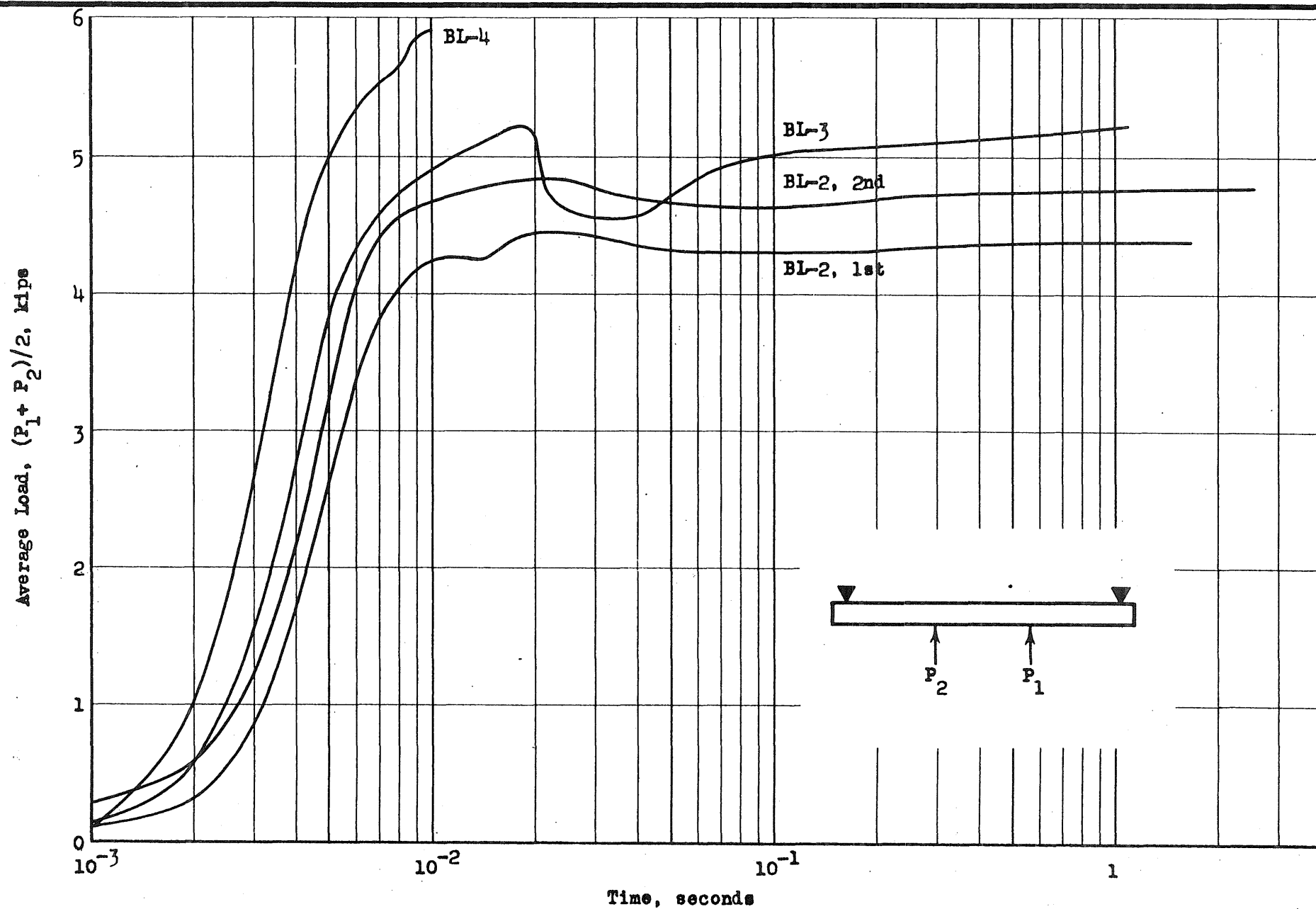


FIG. 59d LOAD - TIME, SPECIMENS BL-2, BL-3, BL-4

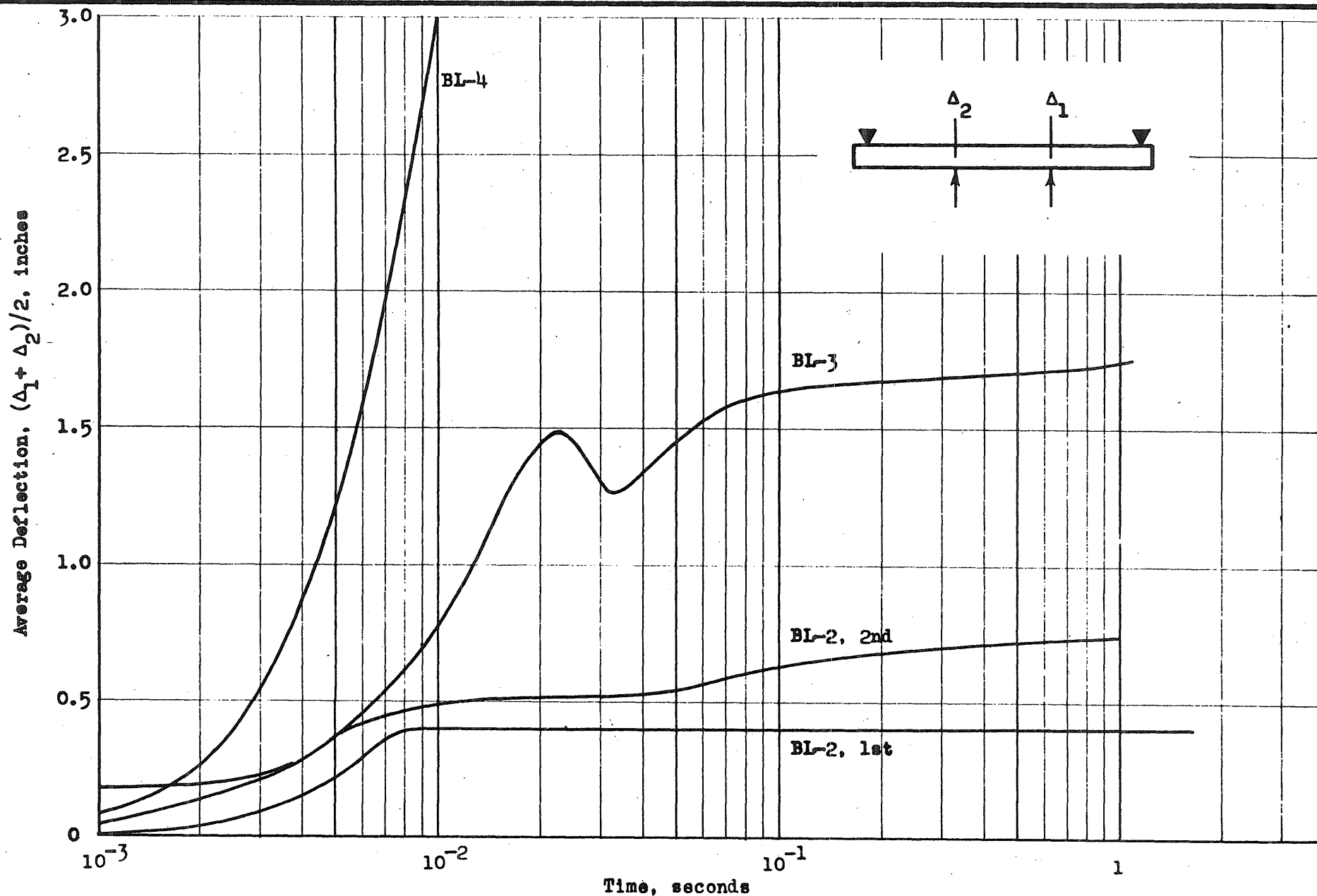


FIG. 39e DEFLECTION - TIME, SPECIMENS BL-2, BL-3, BL-4

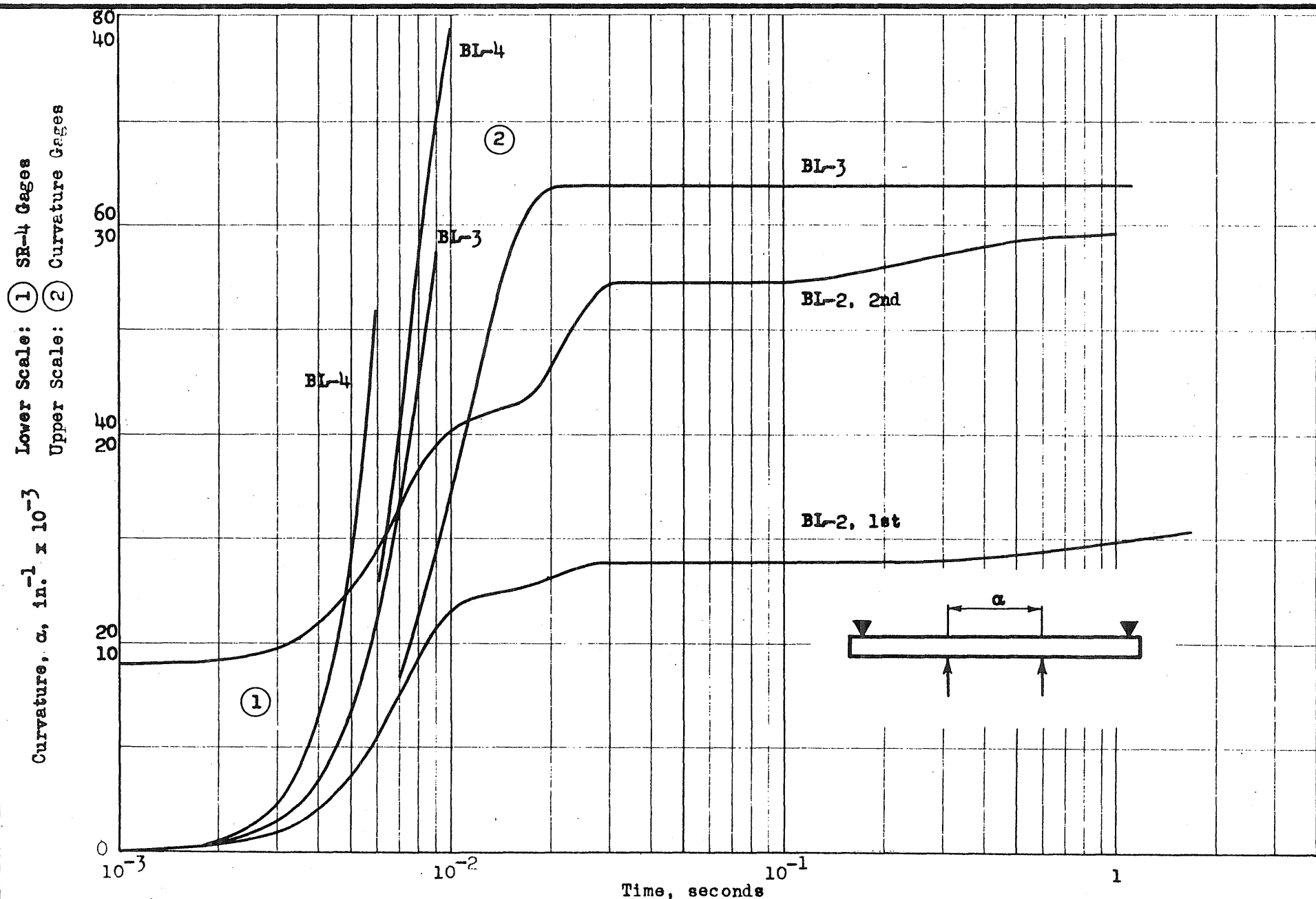


FIG. 39f

CURVATURE - TIME, SPECIMENS BL-2, BL-3, BL-4

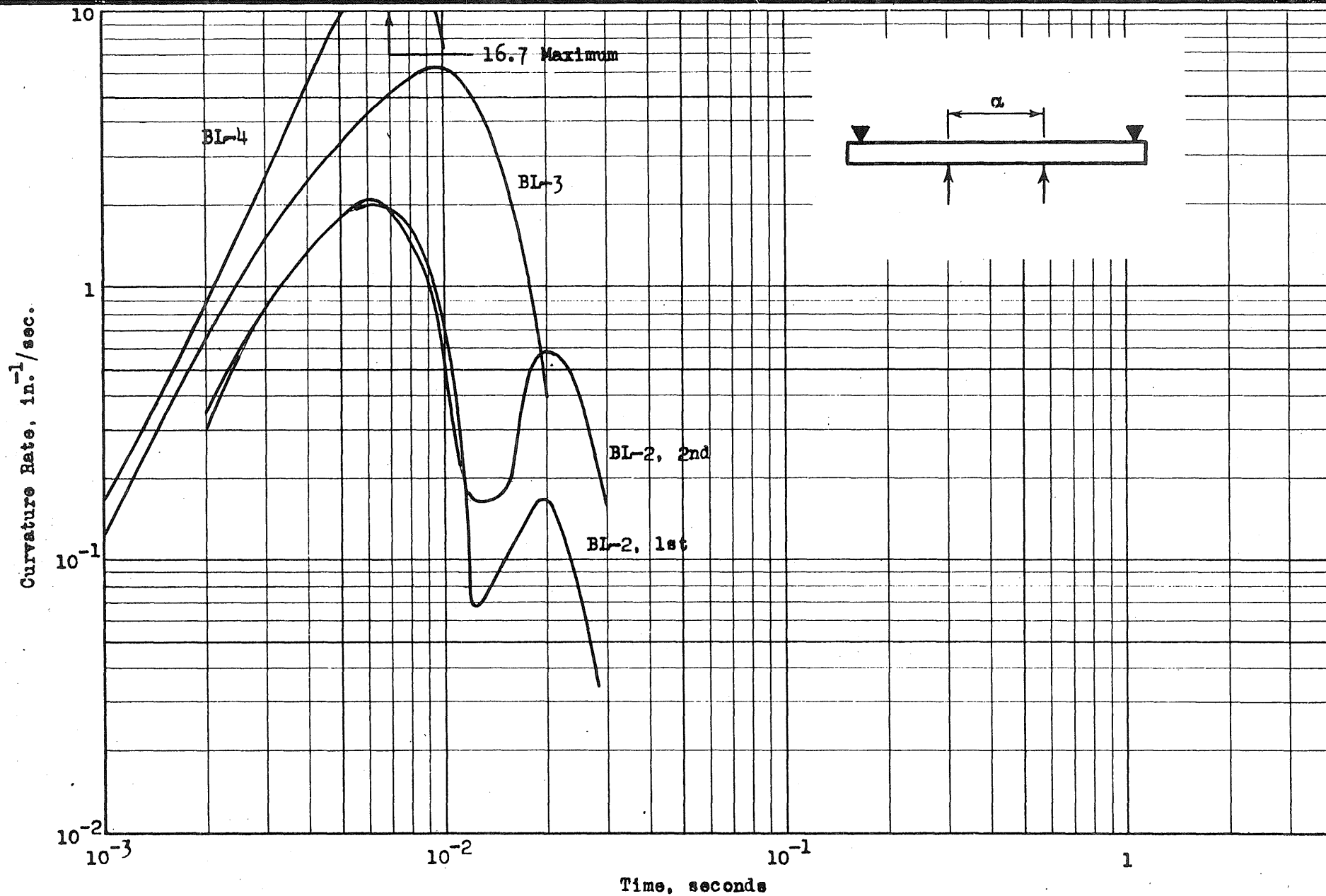


FIG. 39g CURVATURE RATE - TIME, SPECIMENS BL-2, BL-3, BL-4

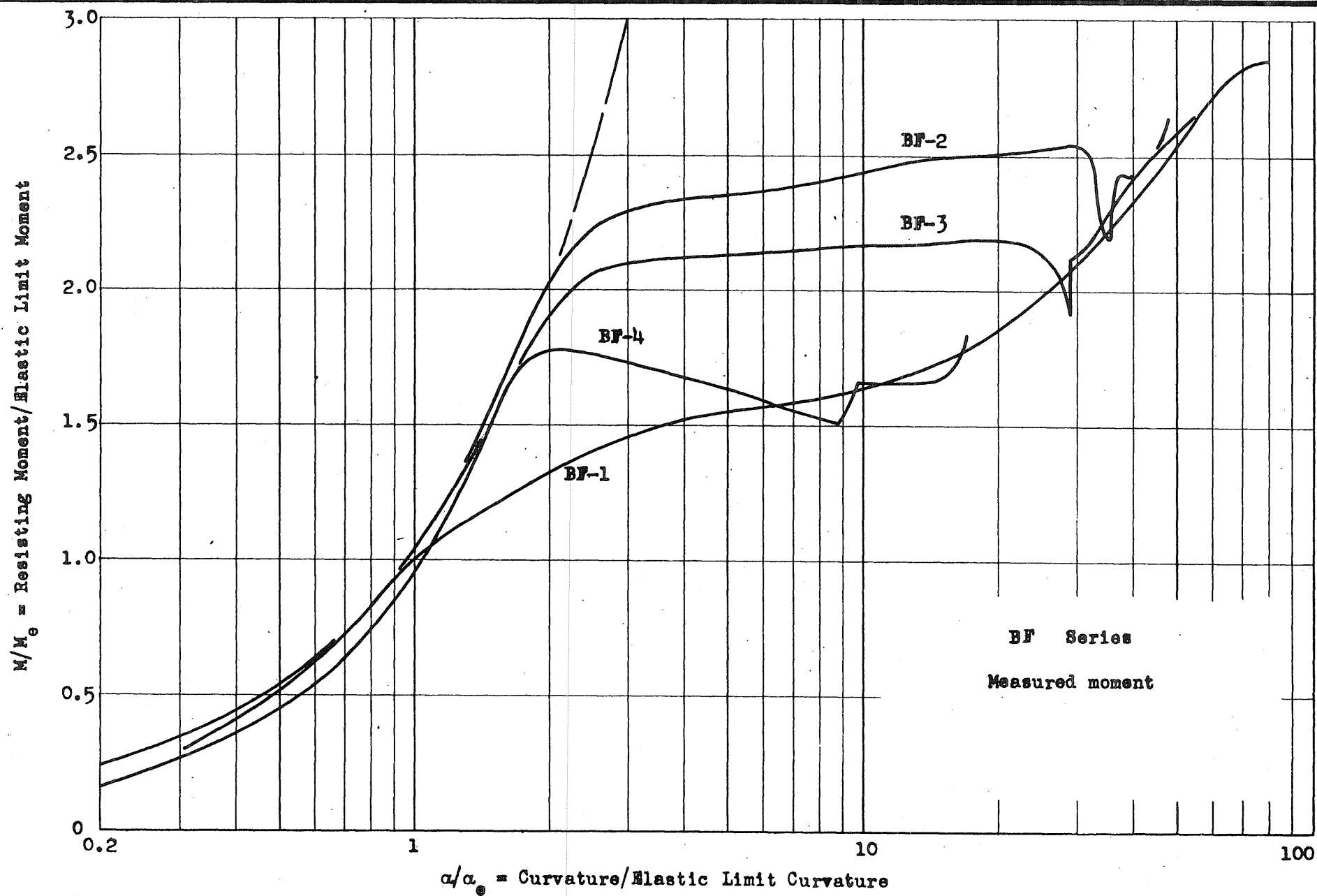


FIG. 40a

RESISTING MOMENT - CURVATURE

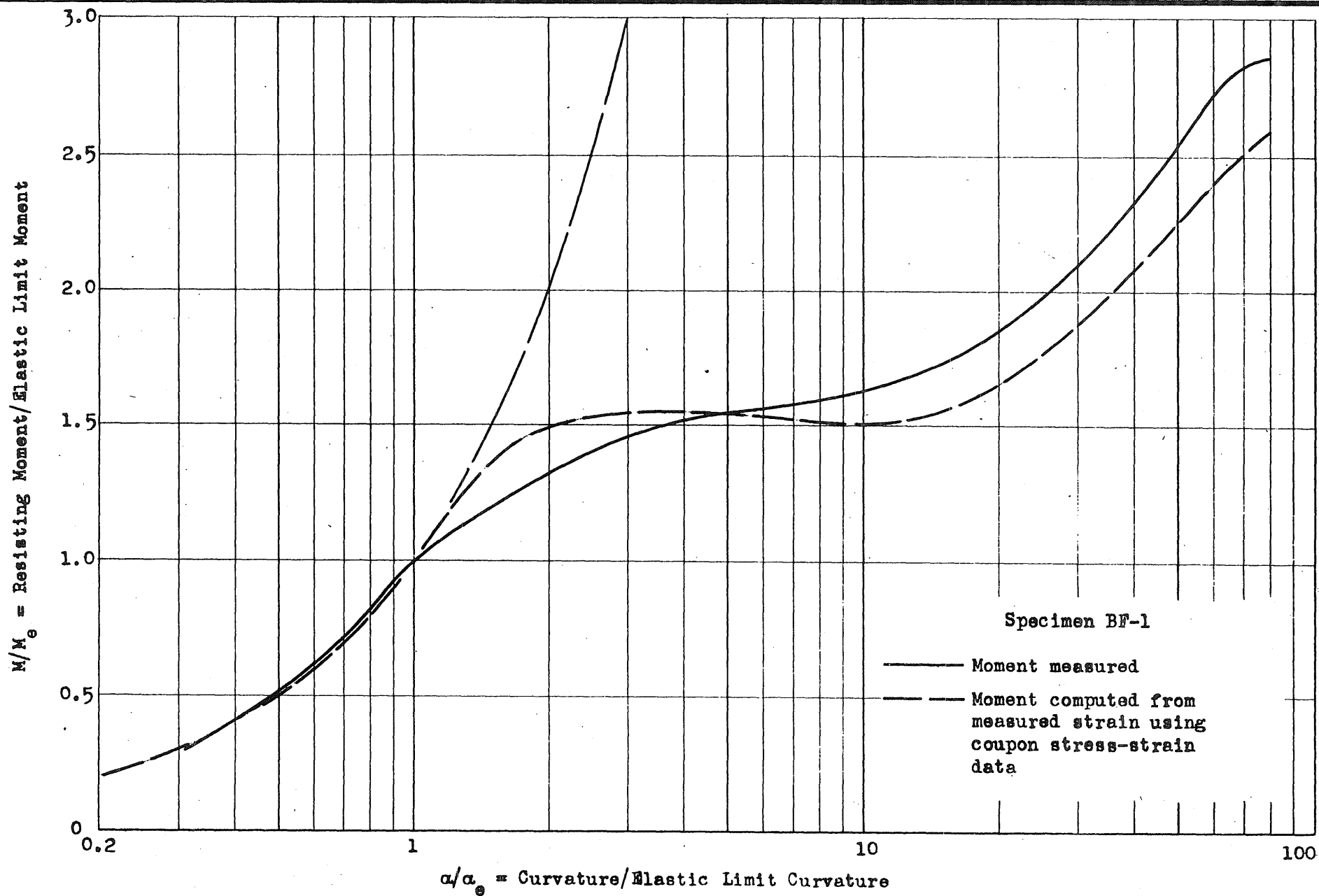


FIG. 40b RESISTING MOMENT - CURVATURE

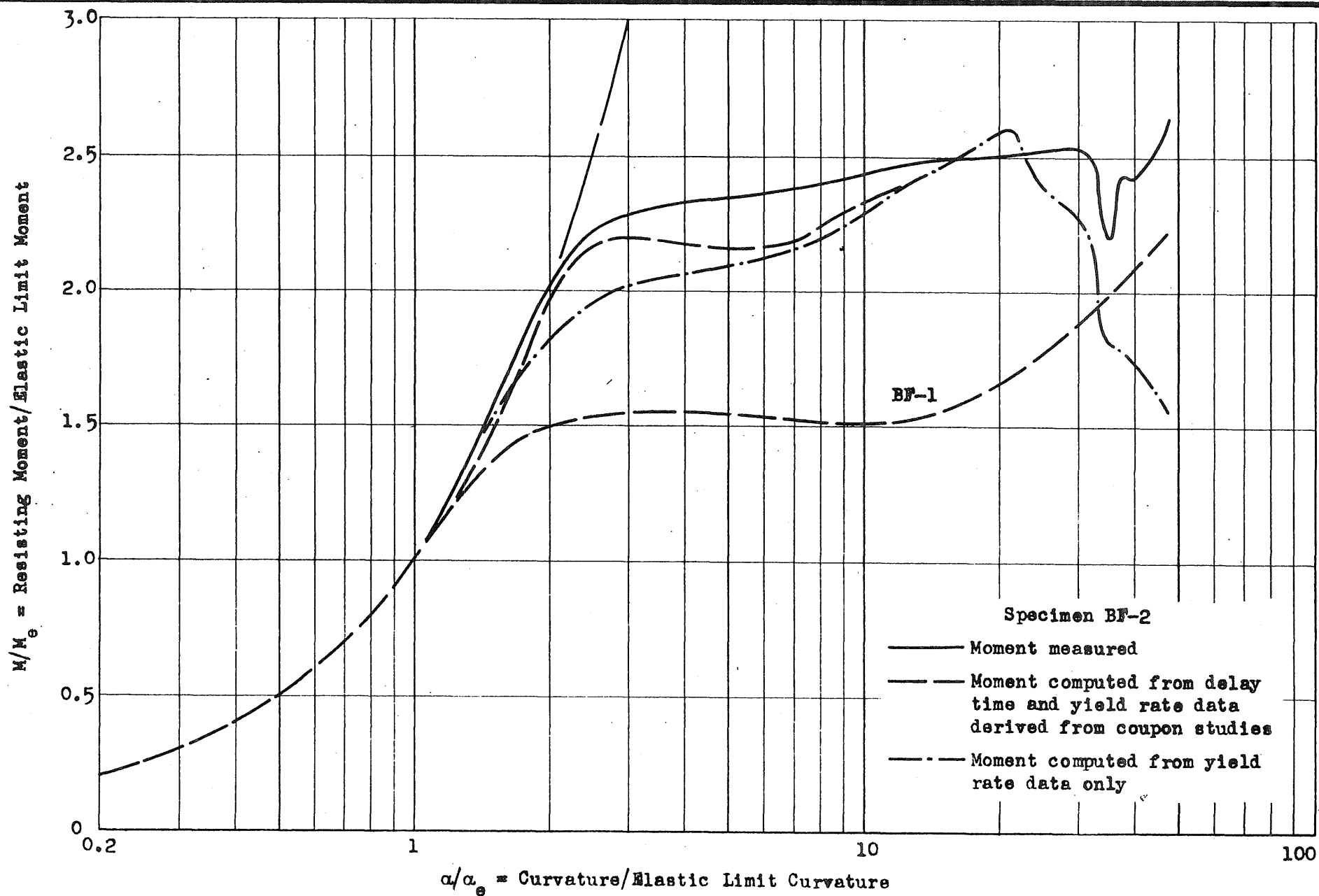


FIG. 40c RESISTING MOMENT - CURVATURE

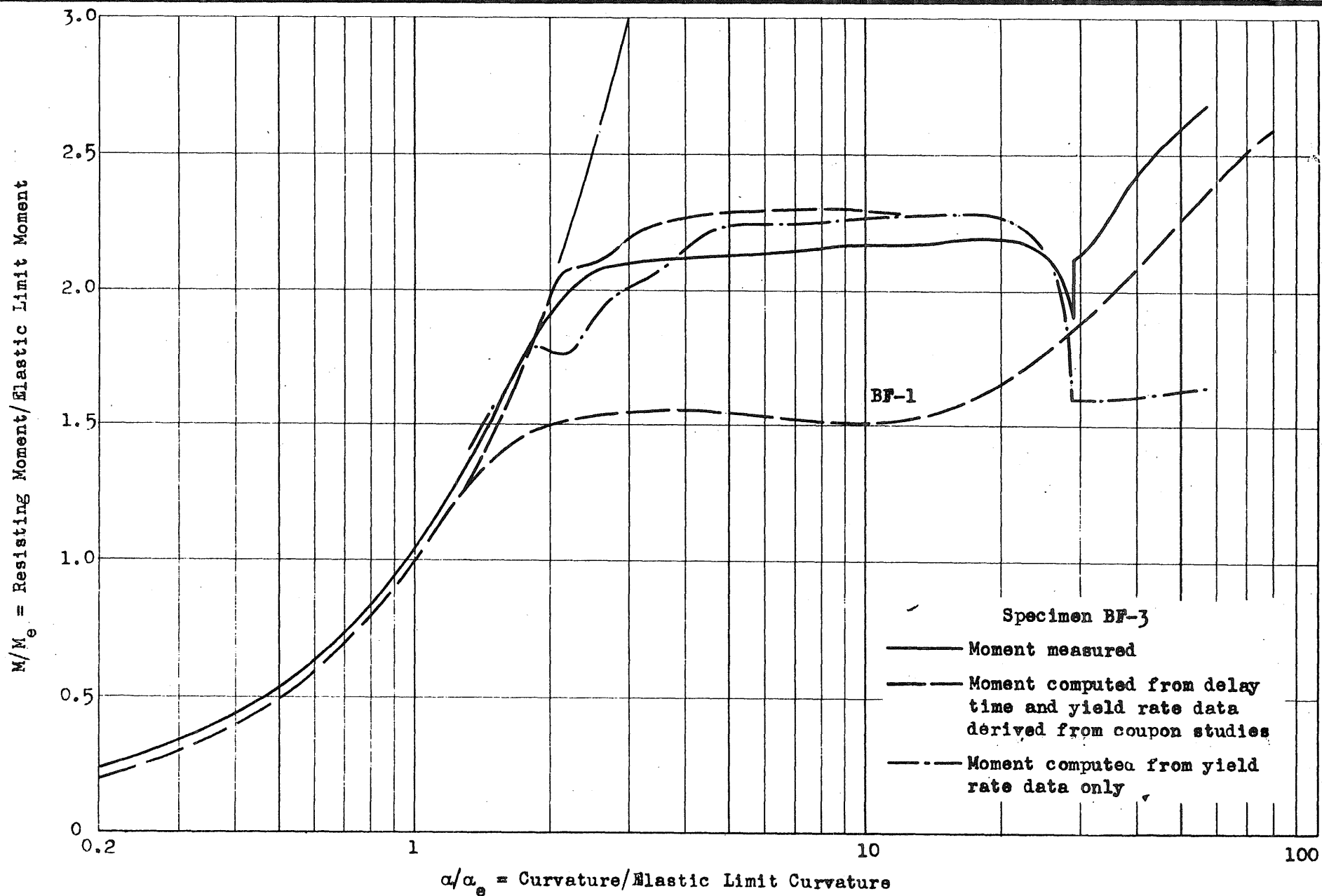


FIG. 40d

RESISTING MOMENT - CURVATURE

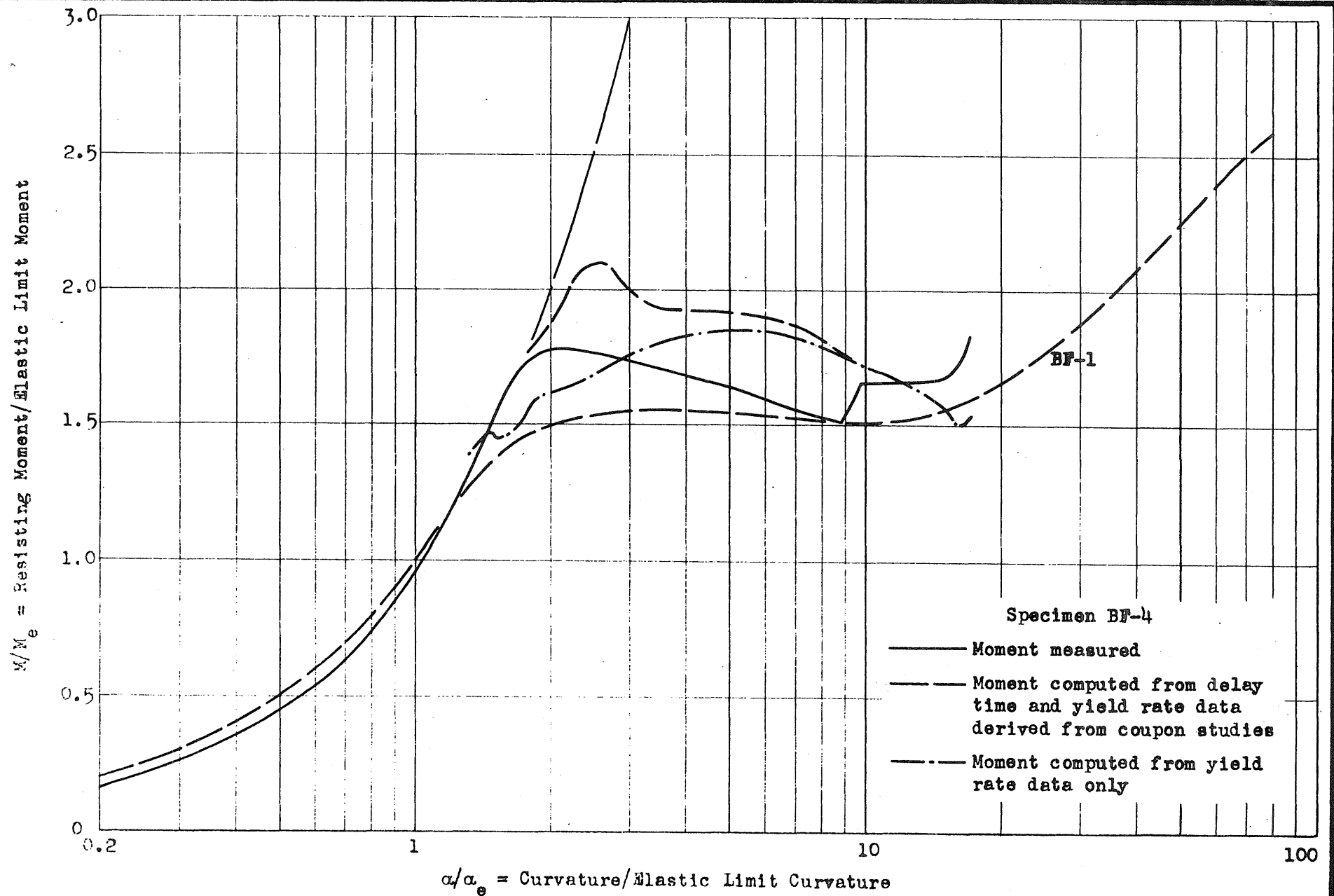


FIG. 40e RESISTING MOMENT - CURVATURE

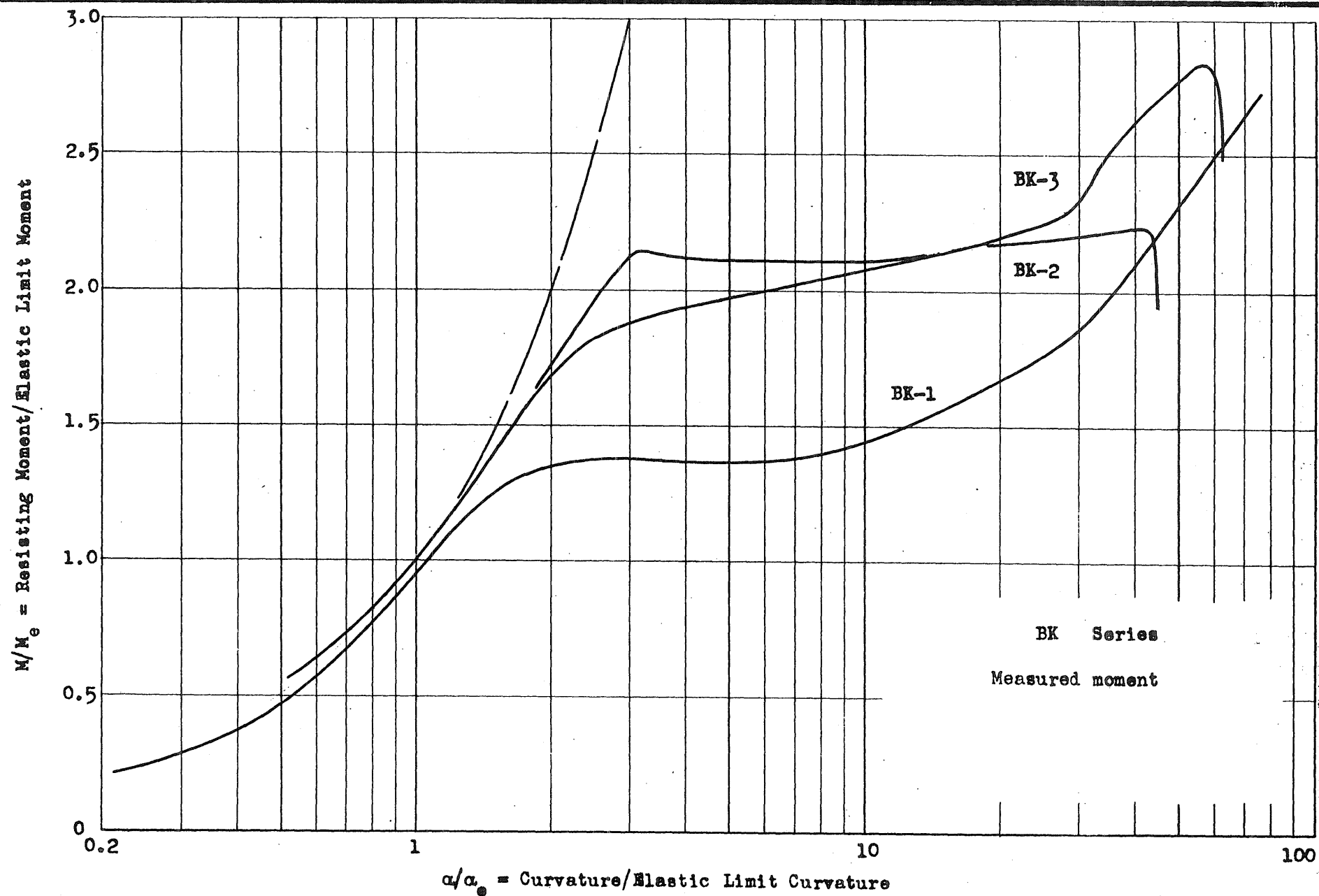


FIG. 41a RESISTING MOMENT - CURVATURE

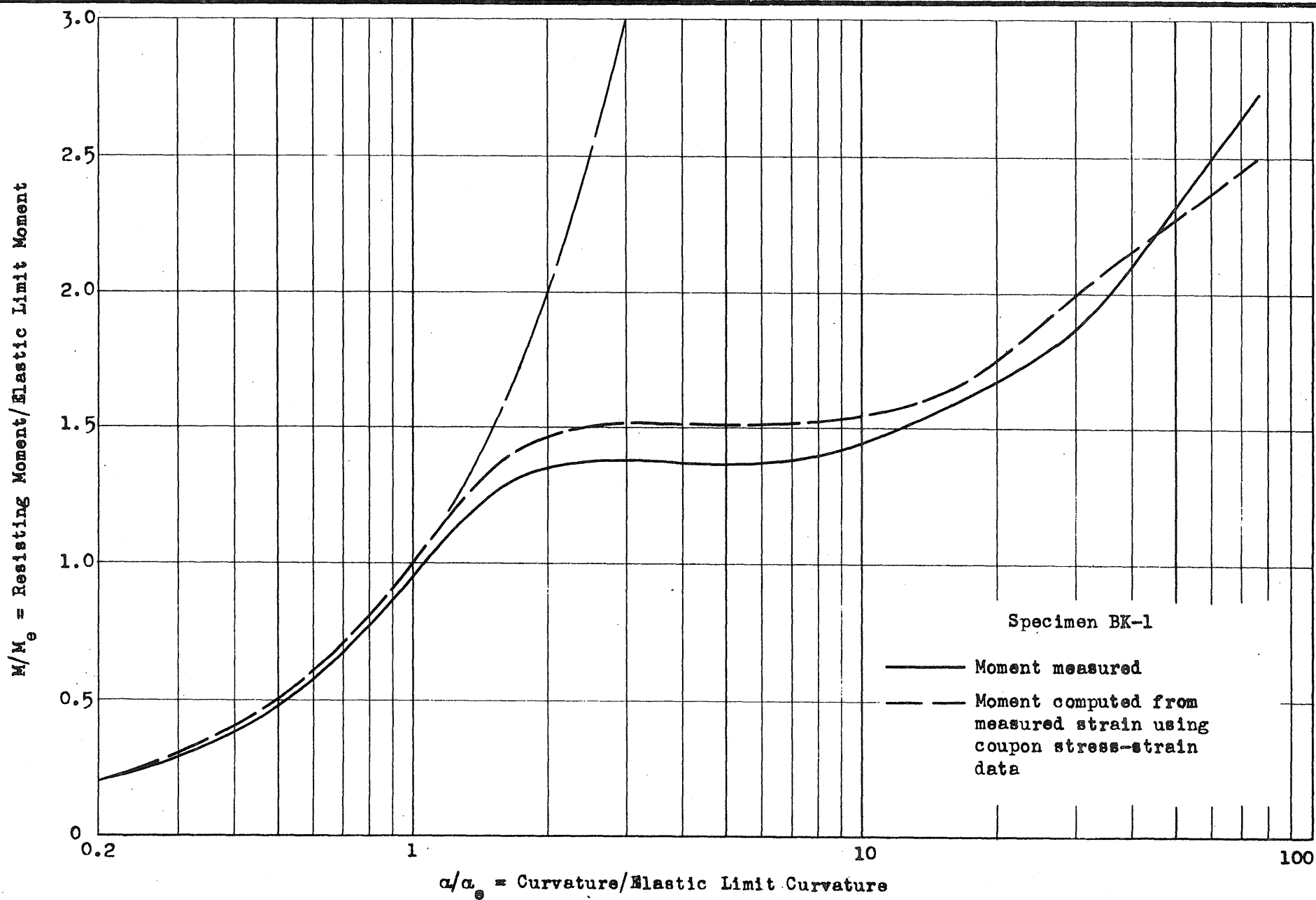


FIG. 41b

RESISTING MOMENT - CURVATURE

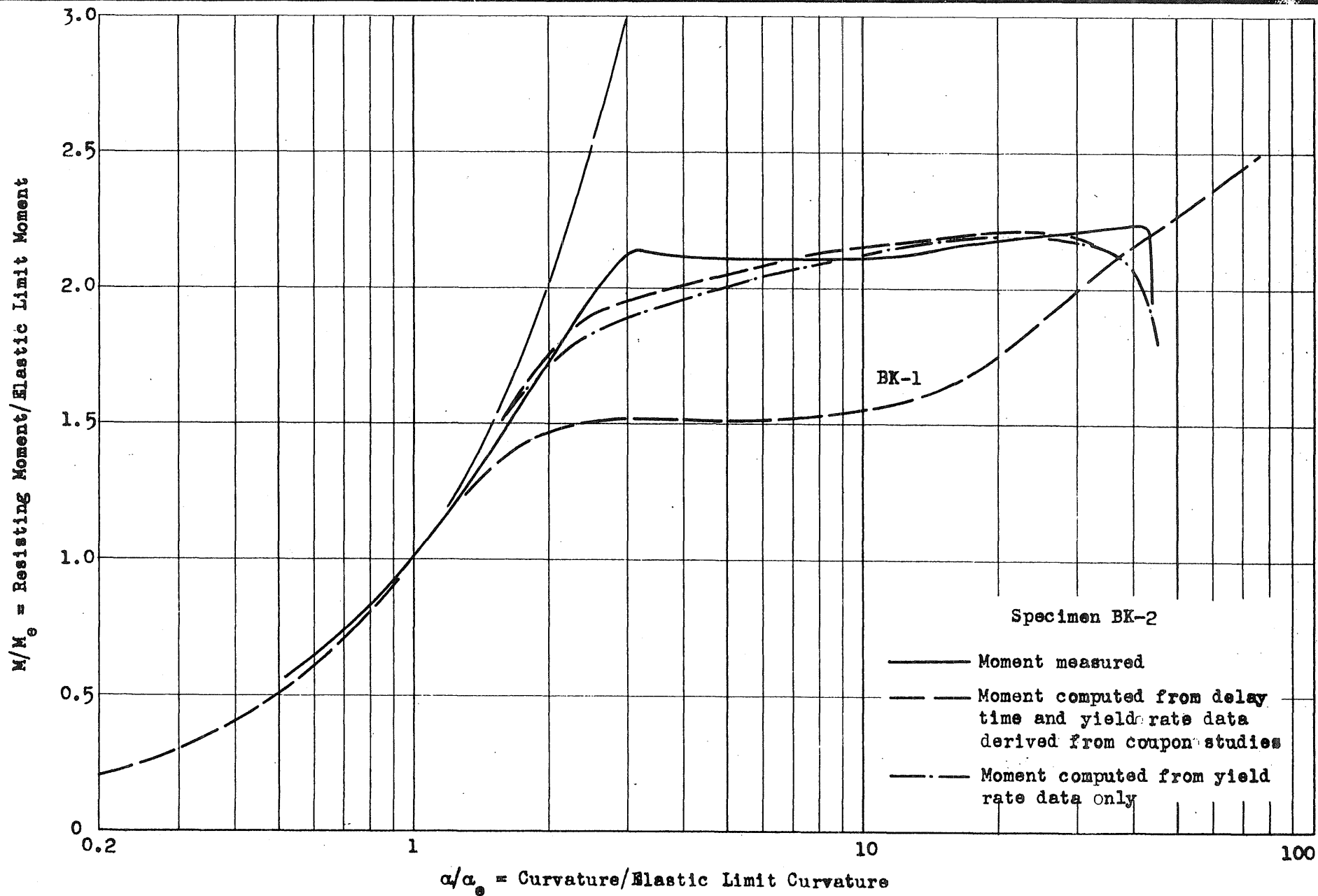


FIG. 41c

RESISTING MOMENT - CURVATURE

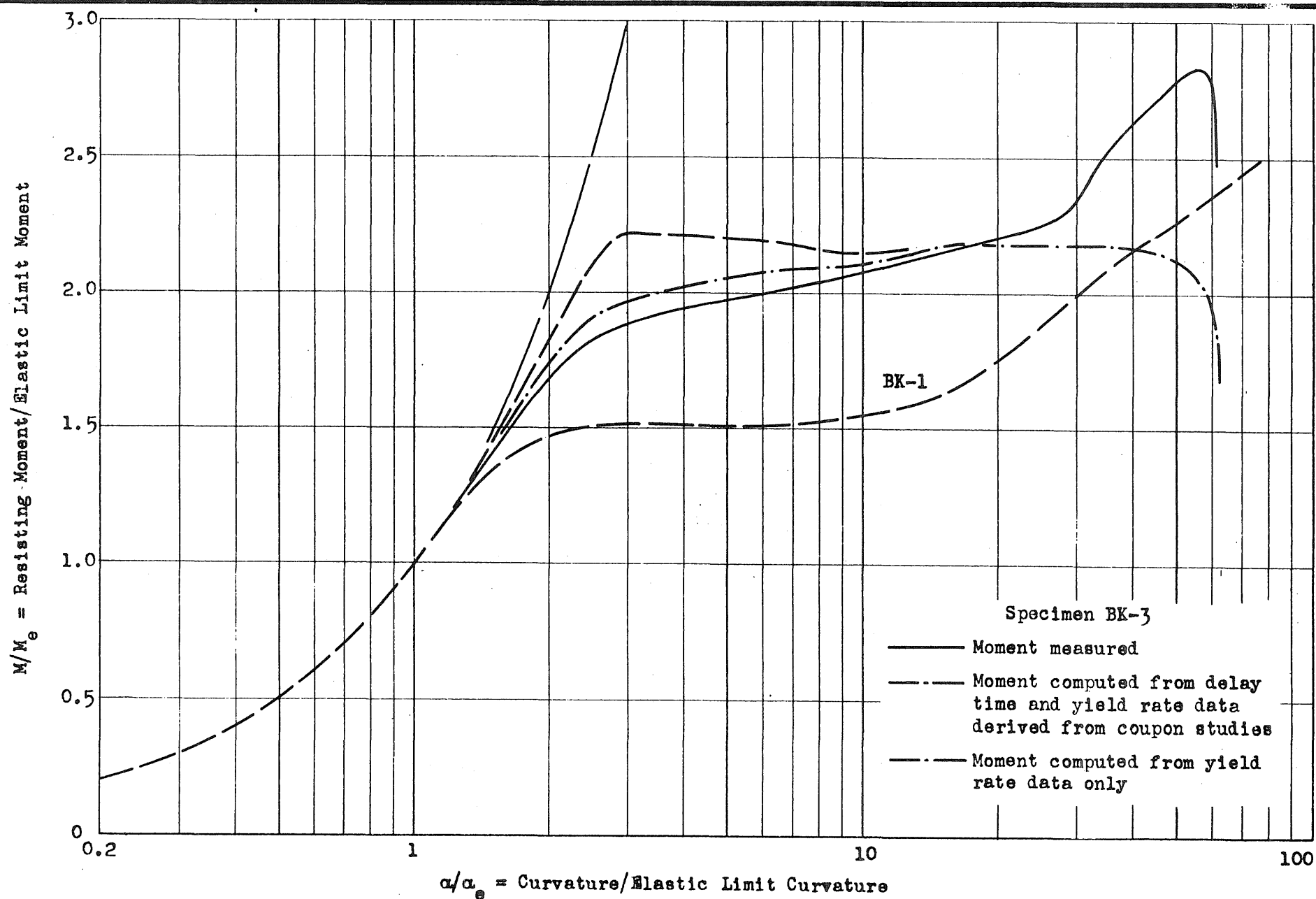


FIG. 41d

RESISTING MOMENT - CURVATURE

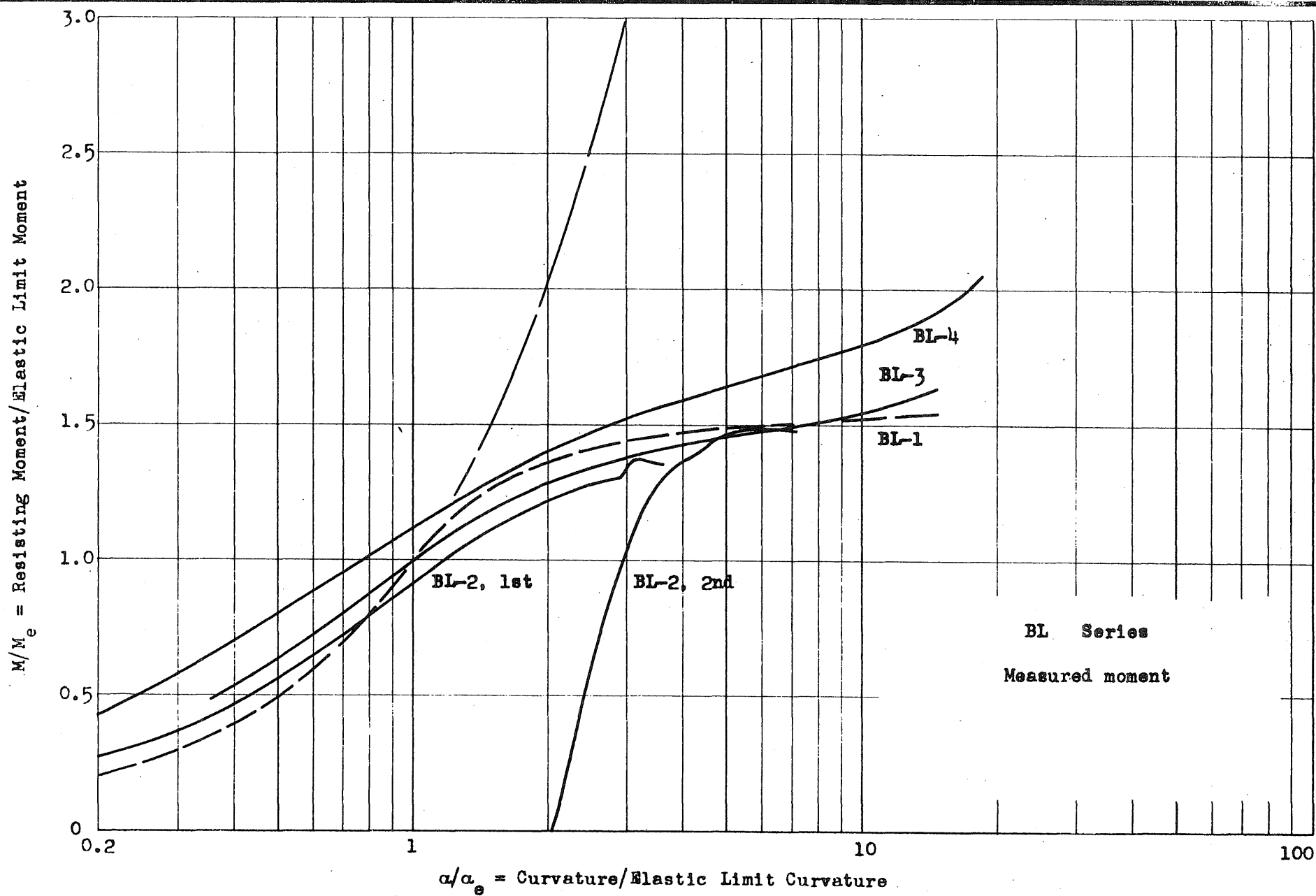


FIG. 42a

RESISTING MOMENT - CURVATURE

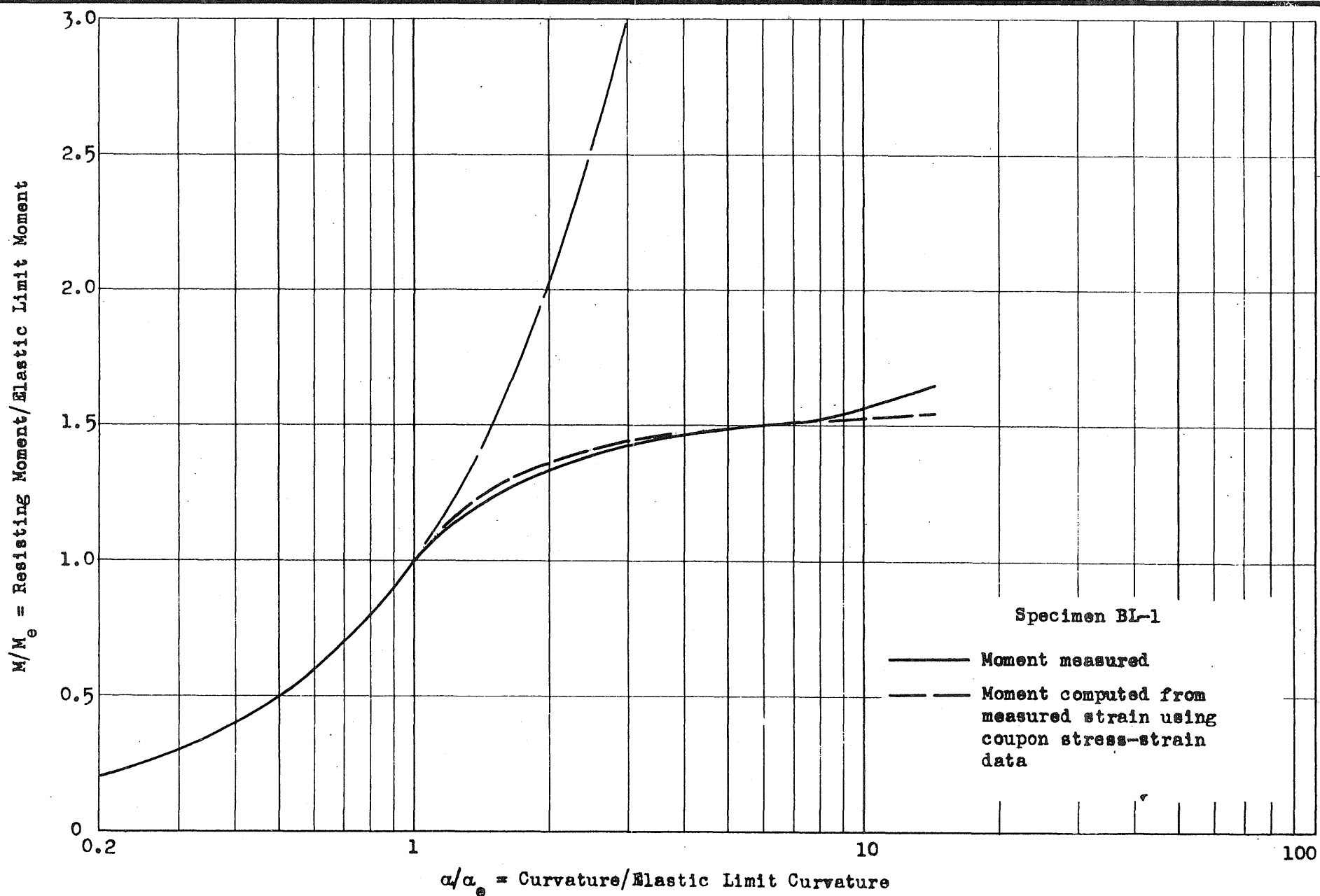


FIG. 42b

RESISTING MOMENT - CURVATURE

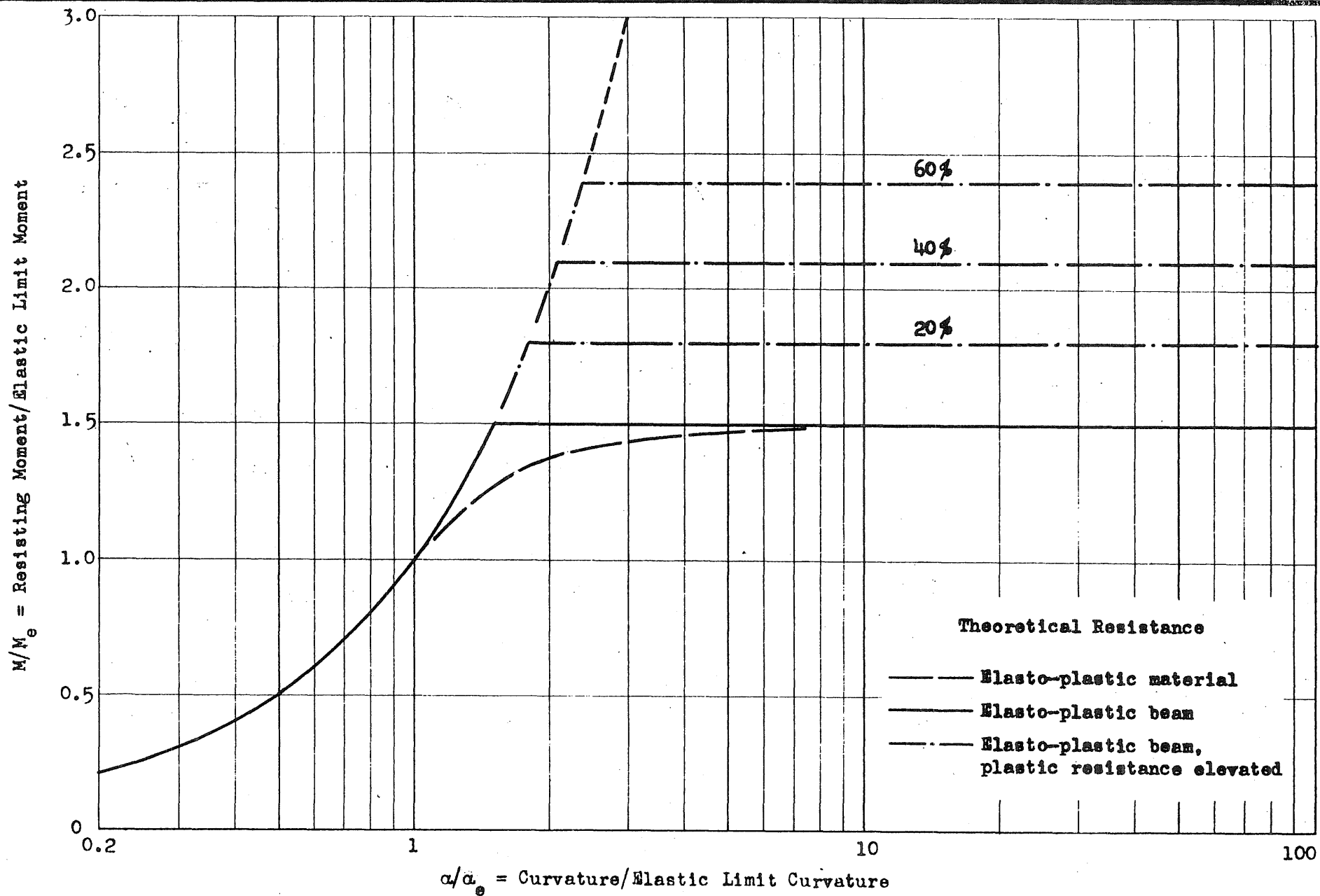


FIG. 45

RESISTING MOMENT - CURVATURE

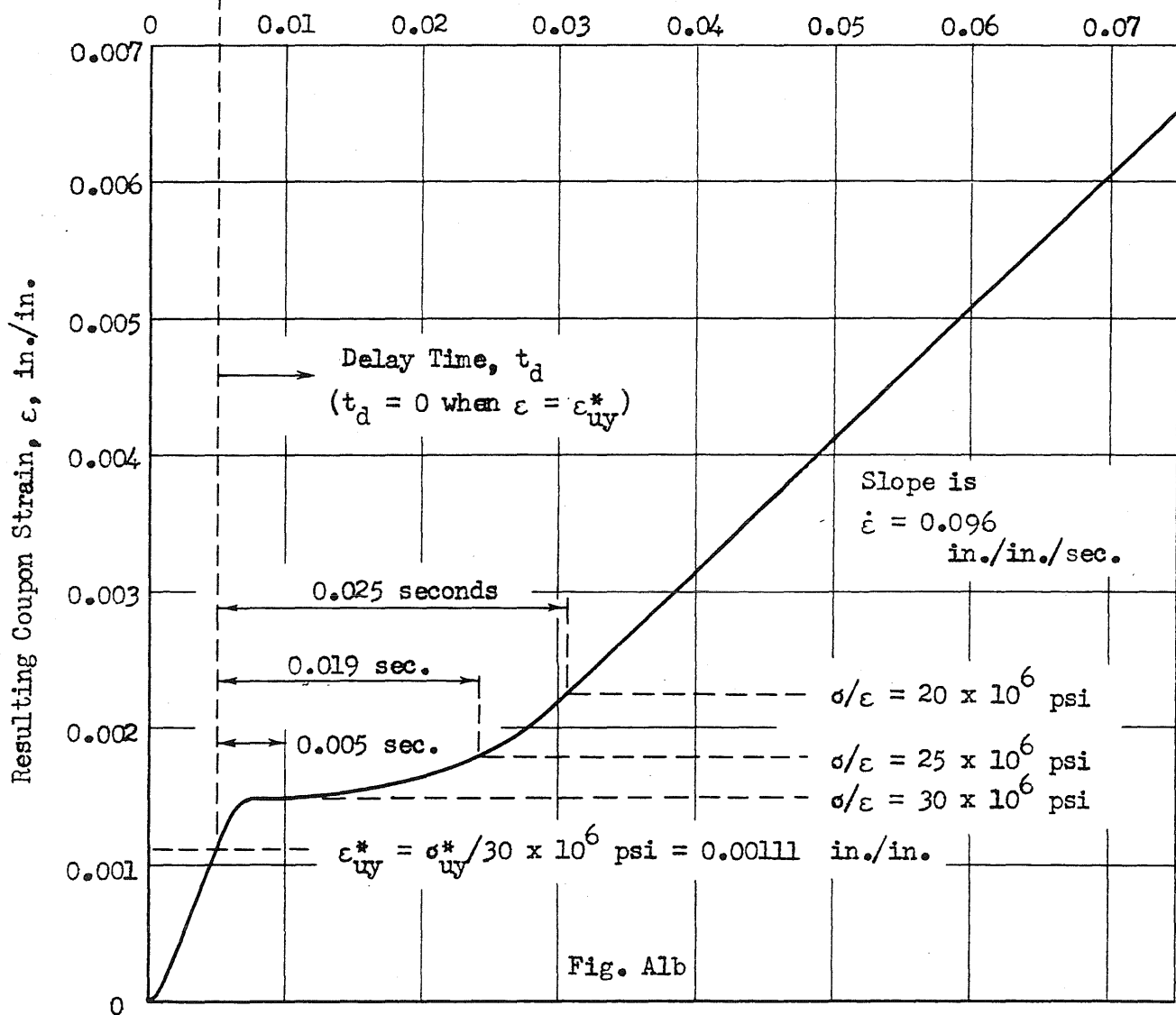
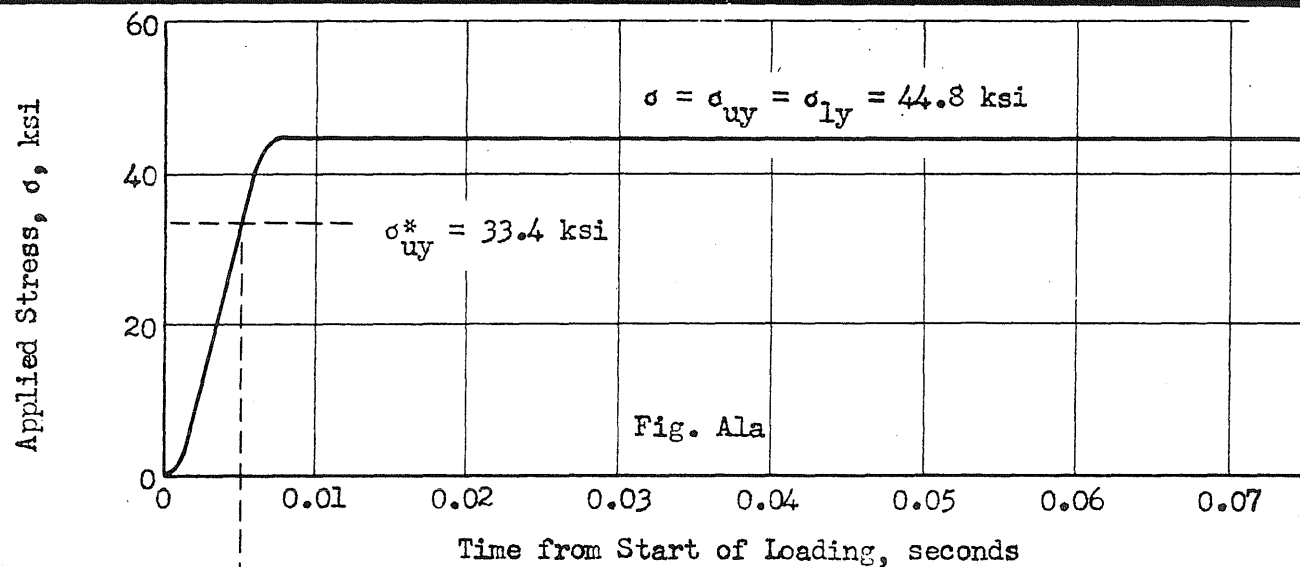


FIG. A1 TYPICAL RAPID COUPON TEST; APPLIED STRESS, RESULTING STRAIN

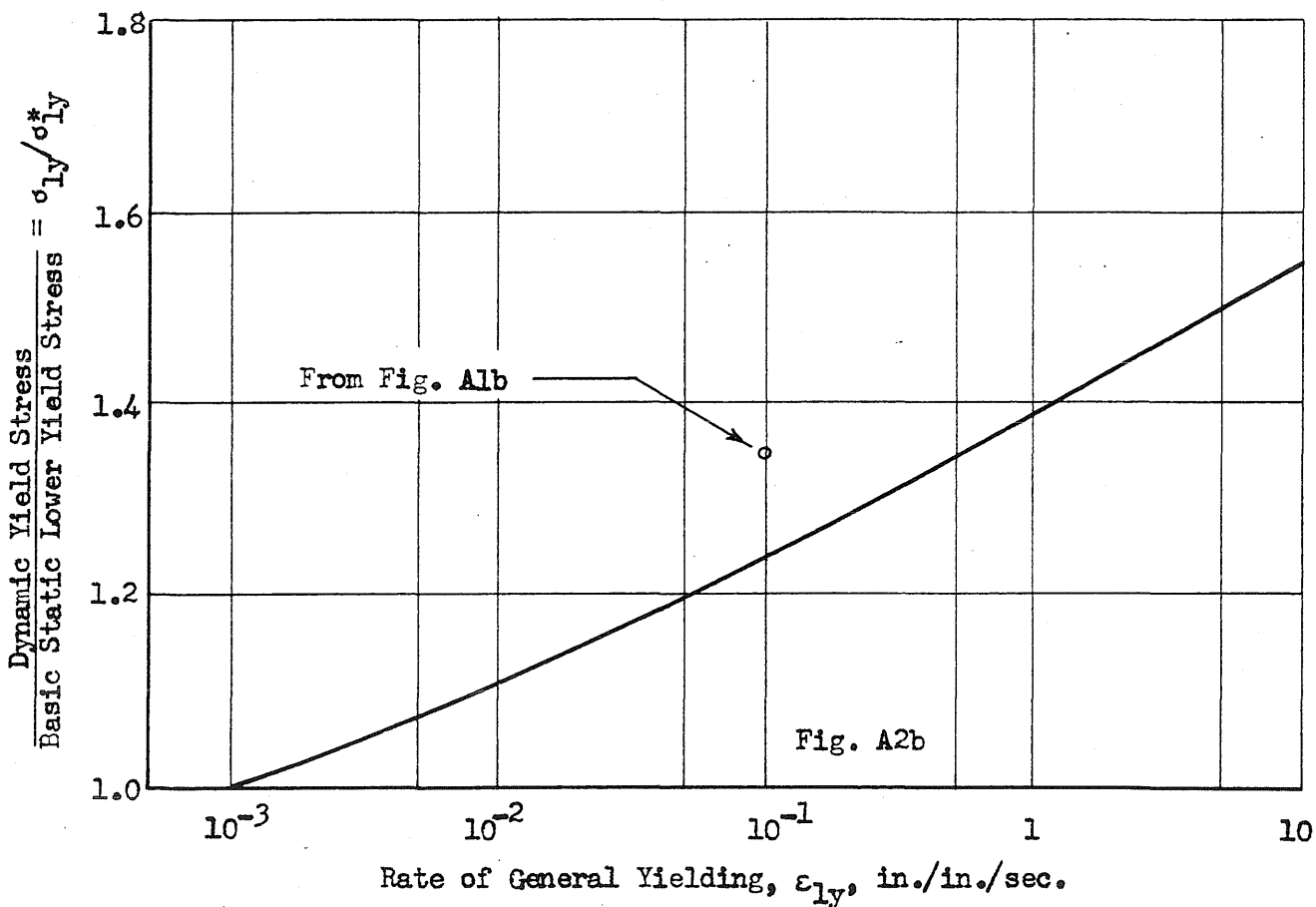
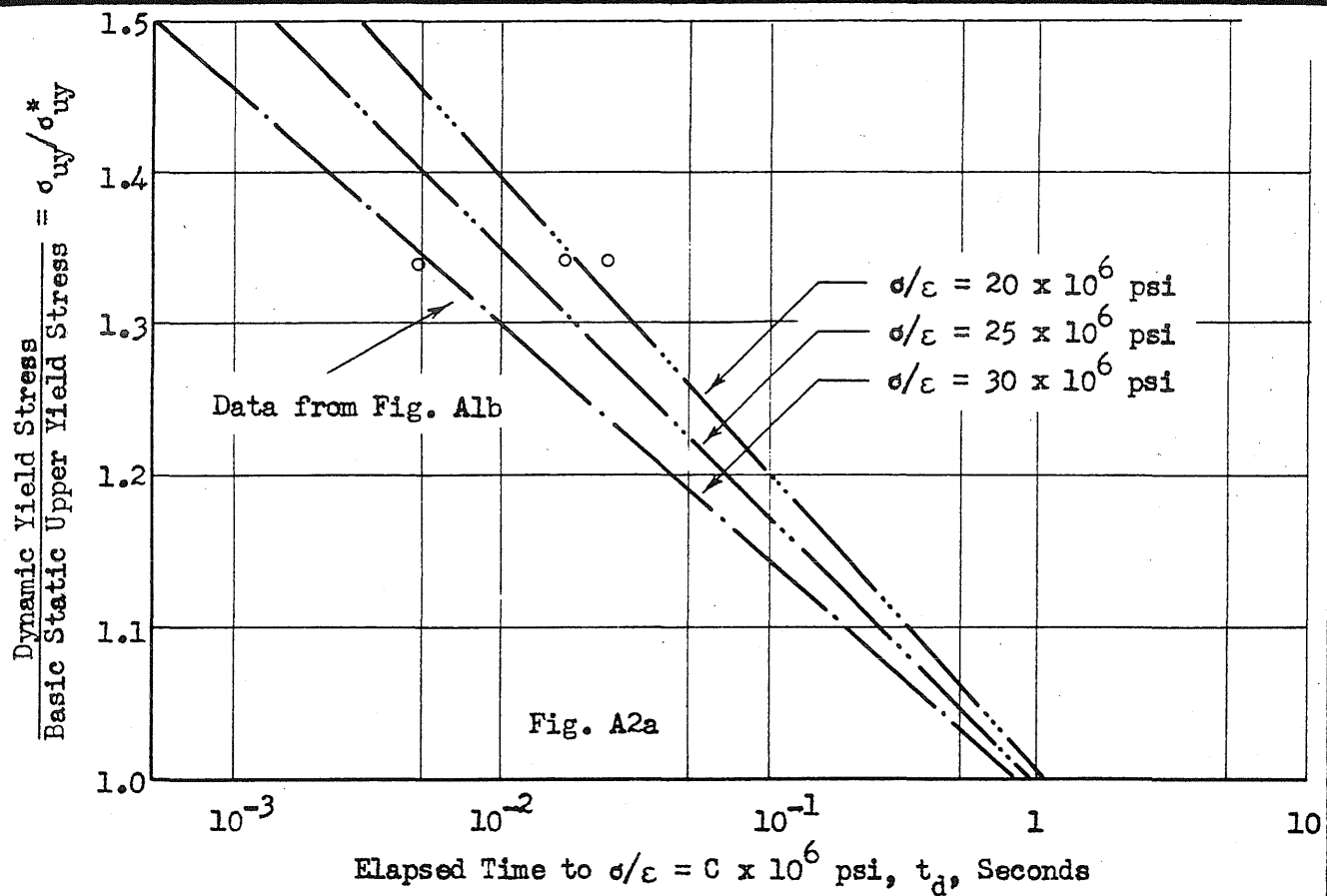


FIG. A2

DYNAMIC PROPERTIES OF BEAM MATERIAL

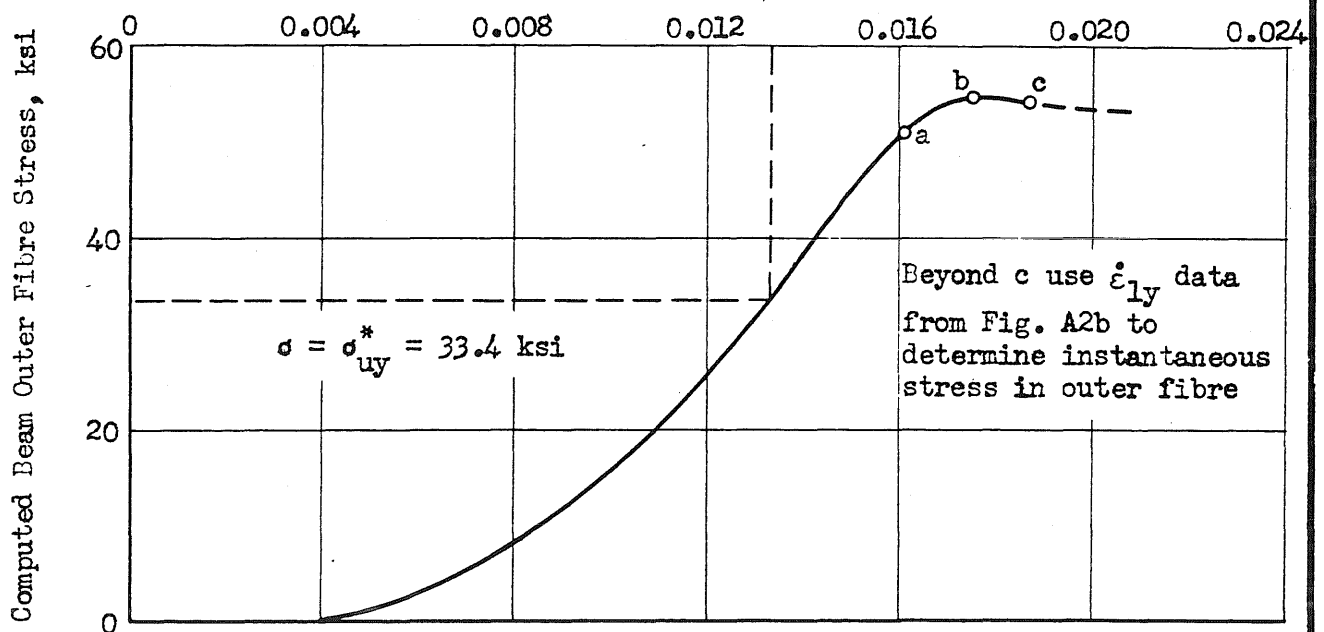
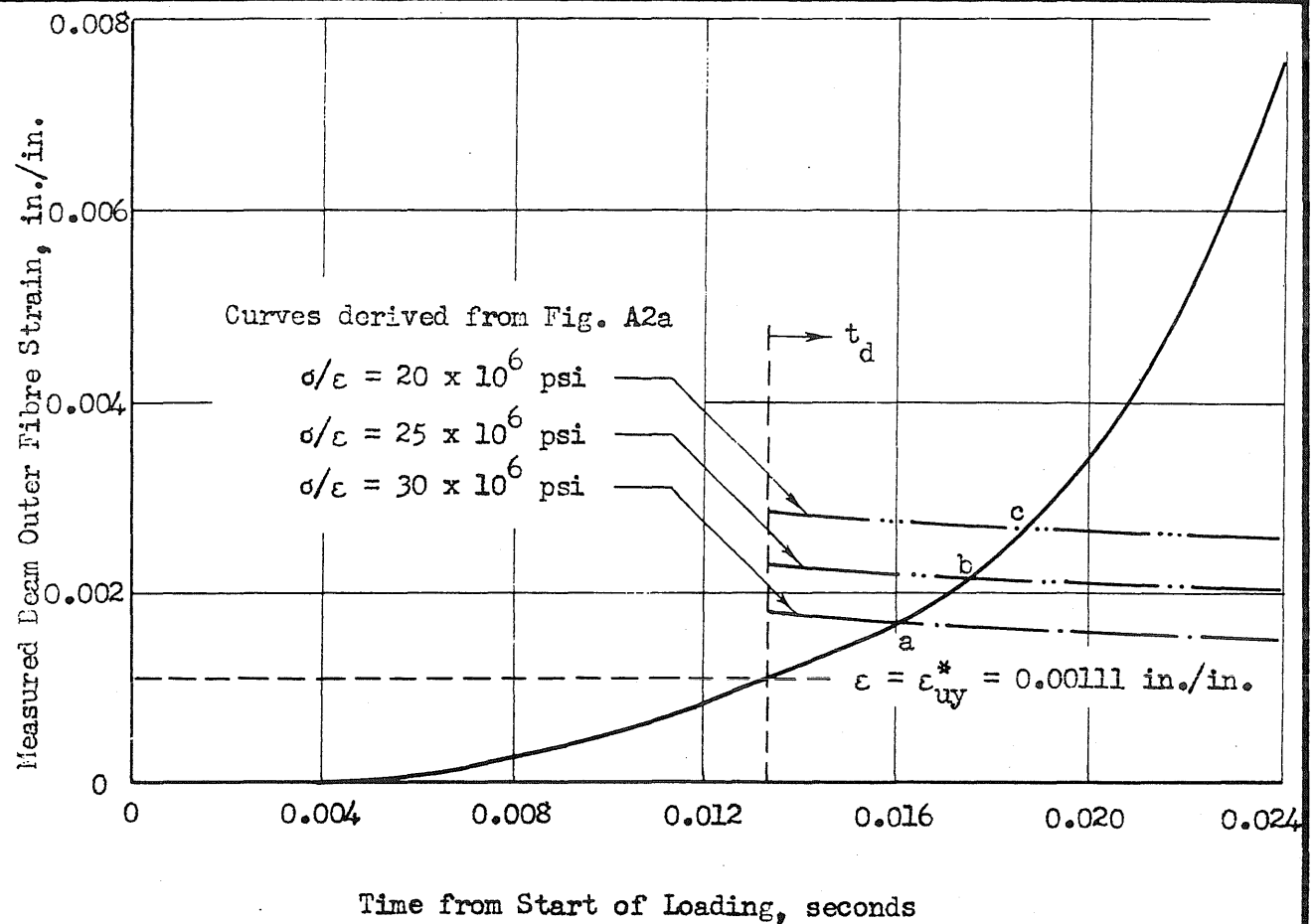


FIG. A3 DETERMINATION OF BEAM RESISTANCE FROM MEASURED STRAINS AND UNIAXIAL TIME DEPENDENT PROPERTIES OF MATERIALS

It is understood that if any of the above steps are not applicable for the time step under consideration, then that particular step is skipped. In order to determine the time-dependent effects during a time interval, the following procedure is followed:

10. Calculate the change in creep strains at the extreme top and bottom fibers of each section for this time interval. The procedure to be used will depend on whether experimentally determined specific creep curves, or specific creep curves generated by the C.E.B. recommendations (11) are used (see Sect. 3.2.4). The required stress histories are recorded at the extreme top and bottom fibers of each section. By accounting for the effects of elastic recovery of the concrete, the creep strains may be corrected. This calculation, furthermore, directly yields the change in prestressing force and the associated change in concrete stress due to the change in creep strain.
11. Find the free shrinkage strain of the concrete for this time interval. It is assumed to be uniformly distributed through the cross-section. This shrinkage strain is corrected by accounting for the effects of elastic recovery of the concrete. The change in prestressing force and concrete stress due to the change in shrinkage strain are also determined.
12. Calculate the loss of prestressing force in each tendon due to relaxation. This calculation is based on the steel stress existing at the beginning of the time interval, including the instantaneous elastic effects. By applying this loss of prestressing force as a tensile force acting on the section, the change in concrete stress and strain is corrected for the effects of elastic recovery of the concrete. The change in prestressing force resulting from this calculation must be added to the relaxation loss to yield the total change in

prestressing force due to stress relaxation of the steel, for this time interval.

13. The total change in concrete stresses and strains, as well as the total change in prestressing force due to the time-dependent effects for this time interval are found by summing the corrected changes in concrete stresses and strains as well as the changes in prestressing force due to the effects of creep, shrinkage and relaxation as determined in steps 10 through 12.
14. Update the total concrete stresses and strains by adding the total changes in these quantities due to the time-dependent effects for this time interval, as determined in step 13, to the total values, as determined in step 8.
15. Update the total prestressing force by adding the change in prestressing force due to the time-dependent effects for this time interval, as determined in step 13, to the total prestressing force, as determined in step 9.

The operations described by steps 1 through 15 are executed at each integration point, or section, along the span of each cantilever making up the double cantilever. The number of sections considered will depend on the total number of segments erected at the time corresponding to the beginning of the time interval under consideration.

The deflected shape of each cantilever at the end of the time interval can be calculated by repeating the following steps for each cantilever:

16. Calculate the total curvature at each section along the cantilever by making use of the total concrete strains, as determined in step 14.
17. Using the curvatures found in step 16 in conjunction with the Newmark numerical integration procedure given in Ref. 23, calculate the deflected shape of the cantilever.

The procedure, as defined by steps 1 through 17, is repeated for each time step up to the time that a closure segment is cast. From this time onwards, the calculation proceeds as follows:

18. If the cantilever to which the closure segment applies forms part of a side-span end, skip to step 20. It is assumed that, for this case, the closure segment is cast on false-work, so that its self-weight does not impose any loads on the structure at this stage.
19. Find the bending moment at each section of the cantilever to which the closure segment is added due to half the total weight of the segment. Subsequently calculate the concrete stresses and strains due to these moments. Correct these stresses and strains for the effects of elastic recovery of the concrete and find the resulting change in prestressing force.
20. If loads are to be applied or removed at the beginning of this time interval, calculate the concrete stresses and strains due to the moments resulting from these loads. These stresses and strains are subsequently corrected for the effects of elastic recovery, and the corresponding change in prestressing force determined.
21. Find the total change in the concrete stresses and strains as well as the total change in prestressing force that occurred at the beginning of the time interval by summing the appropriate quantities as determined in steps 19 and 20, when the closure segment is cast at this time. If the closure segment is not cast at this time, then the corrected changes in the concrete stresses and strains as well as the change in prestressing force determined in step 20 represents the total changes in these quantities that occurred at the beginning of the time interval.

22. Update the total concrete stresses and strains as well as the total prestressing force by adding the changes in these quantities, as determined in step 21, to the total values existing at the beginning of the time interval.
23. Find the total changes in concrete stresses and strains as well as the total change in prestressing force that take place during the time interval due to the effects of creep and shrinkage of the concrete, and relaxation of the steel. This step is executed exactly as indicated by steps 10 through 13.
24. Update the total concrete stresses and strains as well as the total prestressing force by adding the changes in these quantities due to the time-dependent effects for this time interval, as determined in step 23, to the total values determined in step 22.
25. Using the total concrete strains determined in step 24, the curvatures at each section are calculated, and subsequently the deflected shape of each cantilever, at the end of the time interval, is computed.

Steps 20 through 25 are repeated for each time interval up to the time that the tendons which establish continuity of this double cantilever with the structure to which it is joined are stressed. It should be noted that steps 18 through 25 are applied only to the first closure segment that applies to this double cantilever. When the closure segment on the opposite cantilever is cast, the structure must be changed from a double cantilever to an intermediate structure.

The procedure defined by steps 1 through 25 is repeated for each double cantilever until all these structures have been accounted for. Subsequently, each of the side-span ends is assembled. The numerical procedure followed is similar to that followed for the assembly of the double cantilevers. There are, however, some differences: It is assumed that no construction loads are imposed on the side-span end, the self-weight of the

closure segment is assumed not to impose any loads on the side-span end, and the boundary conditions for which moments and deflections are calculated correspond to a simply supported beam. All these assumptions are based on the fact that the side-span ends are assembled on false-work.

Once all the double cantilevers and side-span ends have been analyzed up to the point where the tendons that establish continuity between each of these structures and another structure are to be stressed, the numerical procedure is continued as follows for each of the resulting intermediate structures:

26. Find the prestressing force due to the stressing of the tendons that establish continuity of the new intermediate structure, accounting for friction and anchor-set losses. Calculate the concrete stresses and strains due to this force and apply the appropriate corrections due to the effects of elastic recovery of the concrete. The change in prestressing force in the already stressed tendons is also determined. By repeating the above calculations for each of the tendons in the sequence that they are stressed, the loss of prestress due to elastic shortening is correctly accounted for.
27. If the structure is statically determinate, skip to step 29.
28. Find all the elements of the flexibility matrix as it applies to the calculation of the unknown vertical reactions at each interior support. For this calculation the current value of the modulus of elasticity of the concrete for each segment is used, and the effects of elastic recovery of the concrete are properly accounted for. The exact procedure followed in finding the flexibility matrix is presented in Appendix A.5.
29. Calculate the change in deflected shape due to the stressing of the tendons by using the change in concrete strains found in step 26. For a statically determinate intermediate structure use the actual boundary conditions for this computation. If

the structure is statically indeterminate this calculation is based on the boundary conditions corresponding to a beam simply supported at the two outside supports, i.e. the internal supports are removed. This constitutes the equivalent statically determinate structure (see Appendix A.5).

30. If the structure is statically determinate, skip to step 36.
31. Find the vertical reactions at the interior supports by making use of the flexibility matrix and the deflected shape of the equivalent statically determinate structure, as determined in step 29 (see Appendix A.5).
32. Find the moments in the equivalent statically determinate structure due to the vertical reactions determined in step 31. This is done by applying these reactions as point loads on the equivalent statically determinate structure.
33. Find the concrete stresses and strains due to the moments found in step 32. By considering the effects of elastic recovery, these concrete stresses and strains may be corrected and the resulting change in prestressing force found.
34. Find the deflected shape of the equivalent statically determinate structure due to the strains found in step 33.
35. The concrete stresses and strains as well as the change in prestressing force found in step 33, and the deflected shape found in step 34 represent the corrections in these quantities due to the effects of continuity of the structure.
36. Find the total changes in the concrete stresses and strains as well as prestressing force due to stressing of the continuity tendons by summing the appropriate quantities found in steps 26 and 33. For statically determinate structures the total changes are given by the values found in step 26.
37. Find the total change in deflection due to stressing of the continuity tendons by superimposing the deflected shapes

calculated in steps 29 and 34. For statically determinate structures, the total change in deflection is given by the deflected shape found in step 29.

38. Update the total concrete stresses and strains as well as the total prestressing force by adding the changes in these quantities, as determined in step 36, to the values existing at the beginning of the time interval.
39. Update the total deflections by adding the change in deflection, as determined in step 37, to the total deflection existing at the beginning of the time interval.
40. Update the total bending moments by adding the change in bending moment due to the effects of continuity, as found in step 32, to the total bending moments existing at the beginning of the time interval.

If one of the structures forming this new intermediate structure is a side-span end, the effect of the self-weight of this side-span end now, for the first time, imposes loads on the structure. The effect of this weight is taken into account in the next few steps. For the case that neither component structure forming the new intermediate structure is a side-span end, the following steps are skipped and the numerical procedure continued from step 48.

41. Find the change in moments due to the self-weight of the side-span end as well as that of the closure segment. For the case of a statically indeterminate structure this calculation is based on the equivalent statically determinate structure.
42. Calculate the change in concrete stresses and strains due to the change in moments, found in step 41. Correct these concrete stresses and strains for the effects of elastic recovery, and find the associated change in prestressing force.
43. Calculate the change in deflected shape due to the self-weight of the side-span end by using the change in concrete strains,

found in step 42. For a statically indeterminate structure base this calculation on the equivalent statically determinate structure.

44. If the structure is statically determinate, skip to step 46.
45. Find the change in moment, the change in concrete stresses and strains, the change in prestressing force, and the change in deflected shape due to the effects of continuity of the intermediate structure. These operations are performed as indicated by steps 31 through 35, but are based on the deflected shape found in step 43.
46. Find the total change in moments, the total change in concrete stresses and strains as well as prestressing force, and the total change in deflection due to the self-weight of the side-span end by adding the changes in these quantities as found in steps 41, 42 and 43 to the appropriate changes due to the effects of continuity, as found in step 45. It is understood that for a statically determinate structure the changes found in steps 41, 42 and 43 constitute the total changes in the appropriate quantities.
47. Update the total bending moments, the total concrete stresses and strains, the total prestressing force, and the total deflections by adding the total change in these quantities, as found in step 46, to the total values existing after being updated in steps 38, 39 and 40.

For time steps up to the time that a closure segment is cast, the following procedure is followed for each time step:

48. Find the elements of the flexibility matrix. For this calculation use the current value of the modulus of elasticity of the concrete (see also step 28). If the intermediate structure is statically determinate, skip this step.
49. Determine the moments due to any loads that are applied or removed, as well as supports that are released, at the beginning of the time interval. For the case of a statically

indeterminate structure this calculation is based on the equivalent statically determinate structure. If neither of the above-mentioned operations are performed at the beginning of this time interval, ignore this step and skip to step 52.

50. Following the procedures outlined by steps 42 through 46, for the case of accounting for the self-weight of a side-span end, the total change in moments, the total change in concrete stresses and strains as well as prestressing force and the total change in deflection, due to the moments found in step 49, may be determined.
51. Update the total moments, the total concrete stresses and strains, the total prestressing force, and the total deflections, by adding the total change in these quantities, as found in step 50, to the total values existing prior to the execution of step 48.
52. Find the total changes in concrete stresses and strains as well as the total change in prestressing force that take place during the time interval due to the combined effects of creep and shrinkage of the concrete as well as relaxation of the steel. This step is executed exactly as outlined by steps 10 through 13.
53. Calculate the change in deflected shape due to the time-dependent effects for this time interval by using the total change in concrete strains found in step 52. For a statically indeterminate structure base this calculation on the equivalent statically determinate structure.
54. If the structure is statically determinate skip to step 56.
55. Find the change in moments, the change in concrete stresses and strains, the change in prestressing force, and the change in the deflected shape due to the continuity of the intermediate structure. This step is executed as outlined by steps 31 through 35, based on the deflected shape found in step 53.

56. Find the total change in concrete stresses and strains as well as prestressing force, and the total change in deflection due to the time-dependent effects, for this time interval, by adding the changes in these quantities as found in steps 52 and 53, to the appropriate changes due to the effects of continuity, as found in step 55. The change in moment as calculated in step 55 represents the total change in moment due to the time-dependent effects for this time interval. If the intermediate structure is statically determinate the changes found in steps 52 and 53 constitute the total changes in the above-mentioned quantities, and there is no change in moment due to the time-dependent effects.
57. Update the total moments, the total concrete stresses and strains, the total prestressing force, and the total deflections by adding the total change in these quantities, as found in step 56, to the total values existing before execution of step 52.

The procedure outlined by steps 48 through 57 is repeated for each time interval up to the time that the closure segment joining this intermediate structure to another structure, is cast. If the particular intermediate structure being considered is the final structure, the above procedure is repeated until the last time interval has been accounted for. At this point the analysis is halted.

If the next structure to be added to this intermediate structure is a side-span end, the self-weight of the closure segment is assumed not to impose any loads on the intermediate structure up to the time that the continuity tendons, which establish continuity of the intermediate structure and the side-span end, are stressed. In this case the numerical procedure is resumed from step 62. Otherwise, the self-weight of the closure segment must be included from the time of casting, and the numerical procedure is continued as follows:

58. Find the flexibility matrix based on the current value of the modulus of elasticity of the concrete (see also step 28).
If the intermediate structure is statically determinate, skip this step.
59. Find the moments in the intermediate structure due to half the self-weight of the closure segment. For the case of a statically indeterminate structure this calculation is based on the equivalent statically determinate structure.
60. Following the procedure as outlined in steps 42 through 46, for the case of the self-weight of a side-span end, the total change in moments, the total change in concrete stresses and strains as well as prestressing force, and the total change in deflection due to the bending moments found in step 59, may be determined.
61. Update the total moments, the total concrete stresses and strains, the total prestressing force, and the total deflected shape by adding the total change in these quantities, as found in step 60, to the total values existing prior to the execution of step 59.
62. Evaluate the behavior of the structure for each time interval up to the time that the next set of continuity tendons, that apply to this intermediate structure, are stressed. This is done by repeating the operations outlined in steps 48 through 57 for each time interval.

Once step 62 has been executed, the next intermediate structure can be analyzed, and the numerical procedure is resumed from step 26. This process is continued until all the intermediate structures, including the final structure, have been analyzed.

4. CALCULATED AND MEASURED DEFORMATIONS OF THE KISHWAUKEE RIVER BRIDGE

4.1 Introduction

It is a recognized fact that the prime contributors to the time-dependent behavior of prestressed concrete structures are the time-dependent material properties of concrete and steel. In the light of the discussions presented in Sections 2 and 3 it should be clear that this behavior will be influenced by numerous factors related to the surrounding environment and the composition of the concrete, as well as the stress history to which the constituent materials making up the structure are subjected. Of particular importance is the effect of the variations of the environmental factors on the time-dependent behavior of the concrete, since most real structures are not subjected to constant environments. It is, furthermore, of importance to note that the complex interaction of the creep and shrinkage of concrete as well as the relaxation of steel will have an influence on the time-dependent behavior of the structure.

It should be realized from the outset that it is virtually impossible to account exactly for the effects of all the above-mentioned contributory factors when conducting an analysis aimed at predicting the time-dependent behavior of a prestressed concrete structure. The difficulties involved in accounting for these effects primarily stem from the present lack of understanding of exactly how these factors affect the creep and shrinkage properties of the concrete as well as the lack of records which exactly describe the variable environmental conditions to which real structures are subjected. Nonetheless, such an analysis should in some measure attempt to account for most of these effects. For the particular case of prestressed concrete bridges built in segments by the cantilever method, the stresses are built up in a complex manner due to the nature of the construction procedure. This construction procedure should be reflected as accurately as possible in the analysis because of the

dependence of creep on the stress history to which the concrete is subjected.

In this work the time-dependent behavior of the Kishwaukee River Bridge was studied. The superstructure of this bridge is a five-span continuous box girder built in segments by the cantilever method. For details of the structure as well as the construction sequence, see Appendix B. This Appendix also provides the prestressing details.

An experimental program aimed at recording concrete strains at three different sections on the bridge itself, as well as determining the material properties of the concrete used in the bridge from laboratory stored specimens as well as specimens stored outdoors was conducted at the Construction Technology Laboratories of the Portland Cement Association (P.C.A.) (54). The locations of the instrumented segments were chosen such that records of concrete strain could be obtained in the support, quarter-span and mid-span regions of a particular span (see Figure 4.1 and B.1 b). These segments are designated SB1-N1, SB1-N9 and SB1-N16, respectively. Longitudinal concrete strains were measured by making use of Whittemore mechanical strain gauges, which measure surface concrete strain, and Carlson strain meters, which measure internal concrete strain. The locations of the Carlson strain meters at a particular section are given in Figure 4.2.

In this section analytically obtained concrete strains are compared to strains obtained from the Carlson strain meters. Three analyses were made, the differences lying in the material properties assigned to the concrete. For Analysis 1 the material properties determined experimentally from the outdoor stored concrete specimens were used. It was felt that these material properties would introduce into the analysis the effects on the time-dependent behavior of the variable environment to which the actual structure was subjected. Analysis 2 was conducted on the basis of concrete material properties determined experimentally from laboratory stored specimens. The procedure as proposed in Sect. 3.2.4 was used to calculate creep strains for the case of Analysis 1 and Analysis 2. For Analysis 3 the recommendations of the C.E.B. (11) were used to generate the concrete

material properties. For this particular analysis the method of superposition was used to estimate the creep of concrete. It was felt that Analysis 3 would represent the basis from which a designer would generally have to approach the solution of the problem at hand. It is very seldom that experimental data related to the creep and shrinkage properties of the concrete to be used in a structure is available at the time of design, so that Analysis 3 would serve as a useful indicator of the level of confidence with which the C.E.B. recommendations may be applied to the estimation of the time-dependent behavior of the type of structure under consideration herein. Following the recommendations of Hernandez and Gamble (28), creep was based on 50 percent relative humidity and shrinkage on 80 percent relative humidity in the case of Analysis 3.

4.2 Measured and Analytically Obtained Concrete Strains

The total concrete strains generated by Analysis 1, Analysis 2 and Analysis 3 are compared with the strains measured by means of the Carlson strain meters at the instrumented segments in Figures 4.3 through 4.11, Figures 4.12 through 4.20, and Figures 4.21 through 4.29, respectively. At each of the instrumented segments, measurements of strain were taken at three different levels through the depth of the segment (See Figure 4.2). It should be mentioned that gauge 1 was located slightly below gauges 2 and 8, and that gauge 5 was located slightly above gauges 4 and 6. The analytically obtained top and bottom fiber strains were reduced to levels 8 in., 56 in. and 131 in. (0.203 m, 1.422 m and 3.327 m) above the bottom fiber of the section so that these strains could directly be compared to the measured strains.

The time scales that apply to each of the above-mentioned plots were chosen such that day zero coincided with the day on which the particular segment being considered was erected. Thus, the origin of the time scales for the different instrumented segments do not fall on the same calendar day. The times at which some of the major construction activities

took place are marked in Figures 4.3, 4.6 and 4.9 for segments SB1-N1, SB1-N9 and SB1-N16, respectively. It should be mentioned that since total strain is being plotted as a function of time, the instantaneous elastic effects of the various construction activities are easily identified by obvious discontinuities in these plots.

For the correct interpretation of the measured strains, it is important to realize that there are no data points available for any of the strain meters for the time period extending from the time at which the continuity tendons for intermediate structure 9 were stressed to the time at which the closure segment for the final structure was cast. This means that the variations in concrete strain that took place during this time period are unknown.

4.2.1 Observations

Analysis 1 (see Figures 4.3 through 4.11): Bearing in mind the scatter inherent in the measured strains, the predicted strains compare very well with measured values. The shapes of the calculated curves as well as the magnitude of the calculated total time-dependent strains compare well with the measured quantities. As far as the shapes of the total concrete strain versus time curves are concerned it appears as if the trends of the measured curves are followed by the calculated curves for the first 250 days. Beyond the first 350 days the trends of the measured curves are not followed by the estimated curves, but it appears that a hint of these trends is present in the calculated curves in the vicinity of 300 days. The fluctuations of the time-dependent strain which characterize the trends referred to above seem to be amplified for segments further away from the pier, especially in the case of the calculated curves.

Analysis 2 (see Figures 4.12 through 4.20): For times beyond 300 days it appears that the magnitude and shape of the generated total concrete strain versus time curves closely

approximate the magnitude and shape of the measured curves. Once again, this comparison should be seen in the light of the scatter of the experimental data. Prior to 300 days the shapes of the generated curves do not agree with those of the measured curves. The time-dependent parts of the generated curves are, relatively speaking, smooth when compared to the experimentally determined curves as well as the curves generated by Analysis 1.

Analysis 3 (see Figures 4.21 through 4.29): The magnitudes of the calculated curves of total concrete strain versus time are consistently smaller than the experimentally determined curves. The time-dependent parts of the generated curves are smooth and do not reflect any of the fluctuations inherent in the curves obtained from the measurements of strain on the bridge.

Compared to the experimentally determined values of total strain it appears that Analysis 1 yielded the best values for total strain and Analysis 3 the worst.

At all stages Analysis 3 yielded values of concrete strain that were significantly lower than the values calculated by either one of the other analyses. A significant contributor to this observation appears to be the very high value of the concrete modulus of elasticity associated with the C.E.B. recommendations. When compared to the concrete modulus of elasticity used for Analysis 1 it is 36 percent higher at 28 days, and 54 percent higher at 360 days. For the case of Analysis 2, a similar comparison shows that the C.E.B. recommendations predict a concrete modulus of elasticity 34 percent higher at 28 days, and 50 percent higher at 360 days. This high value for the concrete modulus of elasticity led to rather low predicted values for instantaneous elastic strains. This point is clearly illustrated by comparing the magnitude of the total concrete strains obtained from Analysis 3 to the corresponding strains obtained from the other two analyses for the time period prior to the time at which the continuity tendons that establish continuity of intermediate structure 9

were stressed. During this time period the concrete strains in the instrumented segments are primarily due to instantaneous elastic effects.

In view of the very high value of the concrete modulus of elasticity predicted by the C.E.B. recommendations, it may be tempting to use the procedure outlined by these recommendations to calculate the creep and shrinkage properties of the concrete with an adjusted lower value for the modulus of elasticity. This would, however, be incorrect because the creep strain calculation is based on the initial instantaneous elastic strain which, in turn, directly involves the modulus of elasticity of the concrete. Consequently the multiplying factors that determine the creep factor (see Sect. 2.2.3.1) will implicitly reflect the high value of the modulus of elasticity prescribed by the C.E.B. recommendations.

The total time-dependent strain predicted by Analysis 3 is substantially lower than that predicted by either of the other two analyses. The difference in the total time-dependent strains predicted by Analysis 1 and Analysis 2 decreases as the section considered is located further from the pier. These trends are illustrated in Table 4.1. It should be noted that the values presented in Table 4.1 are based on the total change in top and bottom fiber concrete strains, excluding elastic effects, for the time period defined by the time at which the tendons that establish continuity of intermediate structure 9 are stressed and the time up to which the analysis is carried. During this time period the majority of the time-dependent deformation takes place.

4.2.2 Discussion

The shapes of the total concrete strain versus time curves for the case of the analysis of the Kishwaukee River Bridge highlight some important points that deserve special attention.

Comparing the shapes of the specific creep curves as well as the shrinkage curves used in Analysis 1 and Analysis 2 (see Figures B.5 through B.10) and bearing in mind that the creep and shrinkage curves as predicted

by the C.E.B. recommendations are smooth, it appears that the greatest differences in the shapes of these curves apply to the case of shrinkage. In particular, the shrinkage curve obtained from the outdoor stored specimens (see Figure B.10) shows a period of swelling (age 100-200 days) followed by a period of shrinkage (age 200-400 days). Since the tests for determining this shrinkage curve was started during the summer, the onset of the period of swelling was marked by the commencement of winter so that this swelling may have been associated with the increase of relative humidity that usually occurs during winter. It also appears as if the onset of another period of swelling is marked by a concrete age in the vicinity of 400 days. Unfortunately, there are no data points between a concrete age of 407 and 792 days to substantiate the above speculation. Bearing in mind that the instrumented segments were erected about 100 days after the end of curing (see Appendix B), the first "dip" in the shrinkage curve, described above, should correspond to the time period defined by the first 250 days after erection of the segments. Inspection of Figures 4.3 through 4.11 clearly indicates the profound influence that the shape of the shrinkage curve has on the time-dependent strains. The second "dip" in the shrinkage curve is also reflected in the results generated by Analysis 1. The implication that the shape of the shrinkage curve is an extremely important factor in establishing the trends followed by the time-dependent concrete strains is substantiated by consideration of the shapes of the total concrete strain versus time curves generated by Analysis 2 (see Figures 4.12 through 4.20). The trends present in the results generated by Analysis 1 are markedly absent in these curves primarily due to the fact that these trends are also absent in the shrinkage curve used for Analysis 2 (see Figure B.8). Furthermore, the "dip" near the end of the shrinkage curve for the laboratory stored specimens is reflected in the results generated by Analysis 2.

The effects of the shape of the shrinkage curve on the trends followed by the total strain appear to be more apparent for sections further away from the pier, especially in the case of Analysis 1. The reason for this most probably lies in the fact that the section close to the pier was

subjected to higher compressive stresses and consequently the component of the time-dependent deformation due to creep was greater in this region, thus offsetting the relative importance of the influence of shrinkage on the time-dependent strains. It is of interest to note that for the results of Analysis 2 the above trend does not really apply, because the slight "dip" in the shrinkage curve for this case takes place about 300 days after the segments were initially loaded. By that time the greatest portion of creep could have been expected to have taken place so that any changes in shrinkage taking place at that time may be expected to have had a major influence on the total time-dependent strain.

In the light of the above discussion it would thus appear that shrinkage has an extremely important influence on the total time-dependent strains to be expected in structures of the type under consideration here, where the segments are old when erected. Specifically, it was only the analysis that incorporated the shrinkage curve obtained experimentally from outdoor stored specimens that could correctly predict the seasonal fluctuations of the total concrete strains. It is quite obvious that these seasonal fluctuations cannot be correctly predicted when the material properties used in the analytical procedure are based either on results experimentally obtained from laboratory stored specimens or on the recommendations of the C.E.B. It should also be mentioned that the data obtained from the outdoor stored specimens inherently reflect the effect of the varying environmental factors, e.g. temperature and relative humidity, to which the structure was subjected on the time-dependent properties of the concrete. These effects cannot be reflected by the data obtained from the laboratory stored specimens or the C.E.B. recommendations. The data obtained from the laboratory stored specimens has the advantage over that obtained from the recommendations of the C.E.B. in that the influence of the intrinsic factors on the rheological properties of the concrete are more correctly determined.

For the particular case where the structure is built out of segments that are old at the time of erection, as is the case for the Kishwaukee River Bridge, the initial part of shrinkage has no structural effect because it takes place prior to erection of the segments. Thus, as

far as the structural analysis of the Kishwaukee River Bridge is concerned, it is only the part of the shrinkage curve beyond a concrete age of about 100 days that is of interest. If these portions of the shrinkage curves for the outdoor and laboratory stored specimens are compared (see Figures B.8 and B.10), it becomes clear that even though a major portion of the shrinkage at 800 days has developed at 100 days for both specimens, the behavior beyond 100 days differs greatly for the two specimens. The effects of these differences in the shrinkage curves on the structural behavior is of great importance, as has been illustrated above. It is thus suggested that when a shrinkage curve is obtained from outdoor specimens for use in an analysis such as that being performed in this study, measurements of shrinkage strain should be taken at time intervals that are short enough to include all the seasonal fluctuations in the shrinkage curve. This procedure should be followed for a time period of at least two years. This stands in opposition to the generally accepted practice employed in determining the shrinkage curve for laboratory stored specimens where the initial part of the curve is carefully determined and the later part determined on the basis of measurements of shrinkage strain taken at successively larger time intervals. The justification for each of the above procedures lies in the difference in shape of the shrinkage curves obtained from outdoor and laboratory stored specimens.

For the present analysis each segment in the entire structure was assigned the same material properties. Bearing in mind the fact that the various double cantilevers were not constructed at the same time of the year and that the segments were not cast at the same time, it becomes clear that for Analysis 1 the seasonal dependence of shrinkage is, strictly speaking, correctly reflected by the analysis only for the case of the instrumented cantilever. Judging by the agreement obtained between the time-dependent strains generated by Analysis 1 and the measured values for the instrumented segments, it would appear that for the particular structure under consideration herein, this effect was not of great importance on the calculated strains for the instrumented segments. Some of the effects of

starting the creep and shrinkage tests at the correct time may be illustrated by referring to Sect. 2.2.3.2 where it was pointed out that Hernandez and Gamble (28) found that the expected creep and shrinkage curves resulting from outdoor stored specimens could be satisfactorily approximated by using 50 percent relative humidity for creep and 80 percent relative humidity for shrinkage in conjunction with the C.E.B. recommendations. This was found not to be entirely true for the creep and shrinkage curves obtained from the outdoor specimens reported in the present study (see Figures 2.9 and 2.10). One important difference between the tests reported in Ref. 28 and those reported herein lies in the fact that the former tests were started during the winter while the latter ones were started during the summer. A suggestion for the possible solution to this problem would be to associate a particular shrinkage curve with the segments comprising a particular double cantilever, so that the seasonal effects are correctly accounted for in each double cantilever. It is, however, recommended that this matter be pursued in a further study.

Because the specimens used for experimentally determining creep and shrinkage curves were small when compared with the actual segments which comprise the structure, these curves had to be modified for use with Analysis 1 and Analysis 2 in order to account for the influence of size on shrinkage and creep. This effect was accounted for in the present study by multiplying the experimentally determined creep and shrinkage curves with multiplying factors. These multiplying factors were determined by making use of the C.E.B. multiplying factor K_e , which accounts for the effect of member size on creep and shrinkage (see Sect. 2.2.3 and Figures 2.5 and 2.8). For creep a value of K_e corresponding to the creep specimens and a value corresponding to the actual segments were determined. The multiplying factor used for adjusting the creep curves was subsequently found by calculating the ratio of the K_e value for the segments to the K_e value for the creep specimens. The multiplying factor applied to the shrinkage curves was determined as for the case of creep, the only difference being

that the K_e values that apply to shrinkage were used. Following the above procedure multiplying factors of 0.77 and 0.56 were derived for creep and shrinkage, respectively. These values were used for both Analysis 1 and Analysis 2. This procedure obviously only accounts for the influence of the size of the member on the magnitude of creep and shrinkage, but does not reflect the influence on the rates of creep and shrinkage. This procedure appears to be satisfactory when viewed in the light of the results of the comparisons of the total concrete strains generated by Analysis 1 and Analysis 2 with the measured strains.

For the particular case of Analysis 1, experimentally determined specific creep curves were available for only one particular age at loading, namely 28 days. This means that the method used in this analysis for evaluating creep strains reduced to the rate of creep method (see Sect. 3.2.4) for the case of Analysis 1. Because the majority of the segments were erected at least 100 days after being cast (some of the segments were substantially older than 100 days at the time of erection) it would appear reasonable to assume that the multiplying factor through which the specific creep curve was modified to introduce the influence of size on creep into the calculations should actually be interpreted as a factor that modifies the creep curve to include a combination of the effects of size as well as age at loading on creep. These remarks apply specifically to Analysis 1. As more experimentally determined specific creep curves corresponding to different ages at loading become available, the curves themselves properly reflect the effects of the age at loading on creep so that the multiplying factor, described in the previous paragraph, can be more correctly interpreted as reflecting the influence of the size of the member on creep. Analysis 2, where specific creep curves corresponding to three different ages at loading were available, is such a case. Thus, to summarize, the multiplying factor used to modify the experimentally determined specific creep curves used in the analysis should be interpreted as reflecting not only the influence of the size and shape of the member on creep but also the influence of the age at loading on creep. This will

depend on the number of experimentally determined specific creep curves available for the analysis as well as the differences between the ages at which the segments were erected and the ages at loading corresponding to the available specific creep curves.

Because of the substantial differences in the material properties used in the three analyses it is difficult to comment meaningfully on the relative merits of the procedure proposed in Sect. 3.2.4 for the calculation of creep strain in a situation where the concrete stress continually varies. On the basis of the comparison of the measured strains with the total concrete strains calculated in Analysis 2, where the proposed procedure was used in conjunction with three specific creep curves, it may be said that this procedure performed satisfactorily. It is, furthermore, of interest to note that the rate of creep method used with Analysis 1, as explained above, also yielded satisfactory results. In the case of Analysis 3 the method of superposition was used to calculate creep strains. When considering the time-dependent strains, it should be kept in mind that the creep strains calculated by each of the above-mentioned analyses inherently reflected the biases present in each of these methods, depending on whether the concrete stress was increasing or decreasing (see Sect. 3.2).

In conclusion, it would thus appear that the influence of the variable environment on creep and shrinkage had a profound effect on the long-time behavior of the structure. Indeed, for the structure under consideration here, it is imperative that the seasonal variations of the shrinkage strain be correctly included in the analysis in order to correctly forecast the time-dependent strains of the structure. If the structure is considered by the analysis as a filter that modifies the input parameters to yield the structural response, it is clear that the quality of the calculated response will directly reflect the quality of the input parameters. For the Kishwaukee River Bridge the relative importance of shrinkage in a variable environment was most probably amplified by the fact that the segments were old when erected so that the creep potential of the concrete was somewhat reduced.

4.3 Measured and Analytically Obtained Transverse Deflections

In addition to recording the concrete strains at segments SB1-N1, SB1-N9 and SB1-N16, measurements of the transverse deflection at each of these segments as well as at the corresponding segments in the opposite cantilever were taken. Ball-shaped reference points for level readings were installed on the underside of the top flange so that for each of the above-mentioned segments deflections could be measured at the centre of the cross-section and at 66 in. (1.676 m) off center. The pier segment was chosen as a fixed reference to which all measurements of deflection were referred.

The deflected shapes of the instrumented cantilever as generated by Analysis 1 at various stages of construction are presented in Figure 4.30. These deflected shapes serve to illustrate the opposing effects of the prestressing force and the self-weight of the structure on the deflection. For the cantilever the effect of the prestressing force is to produce an upward deflection while the effect of the self-weight is to produce a downward deflection. Judging by the deflected shapes presented in Figure 4.30, the prestressing force has the dominant effect during the initial construction stages, as indicated by the upward deflection of the cantilever. During the later construction stages the self-weight has the dominant effect on the deflected shape, as indicated by the net downward deflection of the cantilever for these stages of construction. These trends are to be expected when consideration is given to the increased moment due to the increased lever arm, and the decreased prestressing force due to a decreased number of tendons, during the later construction stages of the cantilever.

When segments were erected metal shims were used to correct alignments. This procedure may be expected to induce discontinuities in the slope of the cantilever at the interface of adjacent segments and, as such, induce vertical deflections. These components of deflection are of a rigid body nature and cannot be expected to induce any stresses in the structure. Since the magnitude of these corrections were unknown, they could not be included in the calculation of the deflected shapes given in Figure 4.30.

It would, however, be a simple matter to include these deflections in the calculated results if their magnitudes were known so that a direct comparison with measured deflections would be possible. No measurements of deflection were taken during the period of construction of the instrumented cantilever due to the tight construction schedule. Initial deflection measurements were started after completion of this cantilever.

The changes in the downward deflection of segment SB1-N16 which took place after the time of completion of the final structure as predicted by all three analyses are presented in Figure 4.31. For this figure the origin of the time scale coincides with the time at which the tendons which establish continuity of the final structure were stressed. The measured changes in deflection of segment SB1-N16 since the time of completion of the final structure are listed in Table 4.2. It is important to note that it is the change in transverse deflection that is being considered here and not the total deflection.

It should be pointed out that once a double cantilever was joined to an intermediate structure and the support released, this double cantilever was placed on permanent bearings at the prescribed elevation. This operation in general involved a transverse deflection of unknown magnitude. If the resulting intermediate structure was statically indeterminate this operation may be expected to modify the stresses in the structure to some extent. However, since the magnitude of these displacements were unknown it was not possible to account for these effects. In view of the excellent agreement that exists between the concrete strains generated by Analysis 1 and the measured strains it seems reasonable to assume that the effects of these operations were not very important. It should be realized that because of the unknown magnitude of the deflections induced in the structure by the corrections in alignment during construction of the cantilever, as well as by the seating of the double cantilevers on permanent bearings, the calculated deflections cannot be directly compared to the actual deflections of the structure. Because no construction activities took place once the final structure was completed, the calculated change in transverse deflection

which took place during this time period may be compared to the change in measured deflection.

Before the measured and calculated deflections are compared it is first necessary to mention the failure of a number of joints between the segments of the completed structure. The failure of these joints were discovered just after completion of the final structure and was evidently due to the fact that the epoxy in the joints between the affected segments did not properly harden (16). One of the results of this problem with the epoxy was that it could not have been counted on to transfer much shear force from one segment to the adjacent segment so that the shear was transferred primarily by the shear keys. Because these shear keys were reportedly designed to resist shear forces during erection only and not the total shear force after completion of the structure, it is not surprising that this weakness of the epoxy manifested itself in severe cracking and spalling of the concrete in the webs of the pier segments of double cantilever SB1. The joints affected by the defective epoxy included the instrumented segments. Evidently one corner of the bottom slab of segment SB1-N1 dropped 5/8 in. (15.9 mm) relative to the bottom slab of the pier segment SB1-N0 (16). The final structure was subsequently repaired by inserting stainless steel pins in the webs of the segments at the affected joints so that these pins acted as shear keys (16). Checks of the instrumentation in the bridge as carried out by the P.C.A. staff indicated that the Carlson strain meters were unaffected by the cracking which resulted from the failure of the joints, so that the measurements of concrete strain as obtained from these meters in the affected regions were still valid. It is, however, not reasonable to expect that the transverse deflections were unaffected by the failure of the joints.

For the first 91 days after completion of the final structure, the measured values of transverse deflection indicate that the downward deflection of segment SB1-N16 increased by 0.78 in. (19.8 mm) during this

time period (see Table 4.2). The results of Analysis 1 indicate an increase in the downward deflection of segment SB1-N16 of approximately 0.04 in. (1.0 mm) during this time period (see Figure 4.31). Since the time period considered above includes the time at which the failure of the joints were discovered, it seems reasonable to assume that the discrepancy in the measured and calculated change in the downward deflection of segment SB1-N16 during this time period is primarily due to the failure of the joints. For the following 200 days the values of the measured deflection indicate an increase in the downward deflection of segment SB1-N16 of 0.07 in. (1.8 mm) which compares rather well with the increase of approximately 0.05 in. (1.3 mm) as predicted by Analysis 1 for this time period (see Figure 4.31 and Table 4.2).

During the time period defined by 288 and 538 days after completion of the final structure the measured values of deflection indicate a net increase in the downward deflection of segment SB1-N16 of 0.53 in. (13.5 mm) (see Table 4.2). The results of Analysis 1 indicate an increase in the downward deflection of segment SB1-N16 of approximately 0.05 in. (1.3 mm) for the same time period (see Figure 4.31). Some preliminary calculations have indicated that this discrepancy between the measured and calculated change in deflection cannot be entirely explained in terms of the effects of the differential temperature distribution through the depth of the superstructure of the bridge. It, however, appears as if the measurements of deflection were taken under extremely adverse conditions and, as a result, cannot be expected to be as reliable as the measurements of concrete strain. Some of the sources to be blamed for the far from ideal conditions under which measurements of deflection were made appear to have been the poor light (measurements were taken inside the box girder) as well as the effects on the precise level of vibrations set up in the structure by the movement of heavy equipment across the bridge while measurements were taken.

Comparison of the magnitude of the changes of deflection of segment SB1-N16 as predicted by the three analyses for the time period associated with the final structure clearly illustrates that the magnitude of the deflections predicted by Analysis 3 is substantially smaller than those

predicted by the other two analyses (see Figure 4.31). This observation is in accordance with the relative magnitudes of the concrete strains predicted by the three analyses (see Sect. 4.2.1).

The curvatures at each of the instrumented segments as predicted by all three analyses are presented in Figures 4.32 through 4.34. A curvature corresponding to sagging is taken as positive. The small changes in curvature at the instrumented segments for the time period associated with the final structure serve to illustrate that a large portion of the time-dependent strain induced only an axial shortening of the final structure. The small change in transverse deflection in the final structure as predicted by all three analyses is the result of these small changes in curvature.

5. CALCULATED FORCES AND STRESSES OF THE KISHWAUKEE RIVER BRIDGE

5.1 Introduction

The deformations of a prestressed concrete member due to the time-dependent material properties of the concrete and steel will in general lead to a loss of prestressing force. These time-dependent strains will also tend to induce a time-dependent redistribution of bending moment for the specific case of a bridge constructed by the cantilever method. These time-dependent changes in prestressing force and bending moment will, in turn, combine to modify the concrete stresses in the structure. It should thus be clear that the prestressing force, concrete stresses and bending moments may be expected to change with time for the case of a prestressed concrete bridge built by the cantilever method. It should be pointed out that the time-dependent redistribution of bending moment will take place only after the structure becomes statically indeterminate.

The importance of having a knowledge of how these above-mentioned quantities change with time should be obvious. Consequently, the total prestressing force, concrete stresses and bending moments as predicted by Analysis 1, Analysis 2 and Analysis 3 (see Section 4.1) are presented and discussed in the following sections. As before, the results of Analysis 1 and Analysis 2 may be contrasted with each other in order to illustrate some of the effects of the variable outdoor environment on the time-dependent behavior of the structure. A comparison of the results of Analysis 2 and Analysis 3 may be used to illustrate the relative quality of the results which may be expected when the C.E.B. recommendations (11) instead of experimentally obtained data from laboratory stored specimens are used to predict the time-dependent material properties of the concrete.

The majority of the results presented herein apply to the instrumented segments, SB1-N1, SB1-N9 and SB1-N16.

During the course of the construction process of segmentally erected bridges a very strong possibility always exists that construction loads may be imposed on the structure. Indeed, for the case of the Kishwaukee River Bridge the launching girder was positioned in such a manner during the winter construction shutdown so as to impose loads on the uncompleted structure. These loads thus acted on the uncompleted structure for a time period of approximately 5 months. In order to illustrate some of the effects of the application and subsequent removal of the construction loads the structure was analyzed so as to include the application and removal of these loads. The material properties of concrete obtained experimentally from the outdoor stored specimens were used for the purposes of this analysis. This particular analysis was designated Analysis 4. The results predicted by Analysis 1 and Analysis 4 are compared in Sect. 5.5 in order to illustrate some of the effects on the time-dependent behavior of the structure of the construction loads.

Unless explicitly indicated otherwise, the origins of the time scales for each of the plots that apply to this chapter were taken as the day of erection of the particular segment to which the plot being considered applies. In order to identify the time periods associated with intermediate structure 9 and the final structure for segments SB1-N1, SB1-N9 and SB1-N16 reference should be made to Figures 4.3, 4.6 and 4.9, respectively. Appendix B also contains information about ages at time of erection.

5.2 Prestressing Force

As pointed out before, the general effect of the time-dependent concrete strain on the prestressing force in a prestressed concrete structure

is to reduce the prestressing force. There is a further loss of prestressing force associated with the stress relaxation of the steel which takes place in the absence of strain. Since the stress field that primarily resists the loads applied to a prestressed concrete structure is provided by the presence of the prestressing force, it is of importance to predict the total prestressing force with reasonable accuracy. In what follows the total prestressing forces predicted by the three analyses are presented and discussed. It should be pointed out that in addition to these time-dependent losses of prestressing force the immediate losses due to the effects of friction and anchor-set, as well as the elastic shortening of the member, were included in the analysis process. In this section, however, attention is focused primarily on the time-dependent character of the prestressing force.

Table 5.1 summarizes the time-dependent components of the prestress losses as predicted by each analysis for the time period from the time when the tendons which establish continuity of intermediate structure 9 were stressed, up to the last time interval considered. These losses are expressed as a percentage of the total prestressing force existing at the particular segment being considered just after the tendons that established continuity of intermediate structure 9 were stressed. Most of the time-dependent losses appear to have taken place during the time period described above. Clearly, the magnitude of the time-dependent component of the loss of prestressing force is very small. It should, however, be emphasized that the values presented in Table 5.1 only represent the time-dependent component of the prestress loss and that the instantaneous losses due to elastic shortening and friction losses are excluded. Time-dependent losses which occurred before continuity was established are also excluded. These losses were, of course, included in the analytical process and are consequently reflected in the magnitude of the predicted values of total prestressing force. The losses predicted by Analysis 1 are the largest while those predicted by Analysis 3 are the smallest at the segments considered. Furthermore, the losses predicted by Analysis 1 and Analysis

2 do not differ greatly while the losses predicted by Analysis 3 differ somewhat more significantly from those predicted by the other two analyses. These trends were to be more or less expected since they are consistent with the relative magnitudes of the concrete strains predicted by the three analyses.

It is, however, not the loss of prestressing force, per se, that is of importance in design practice but rather the total remaining prestressing force. As illustrated by Figures 5.1 through 5.3 as well as Table 5.1, the total remaining prestressing forces predicted by the three analyses do not differ significantly. The final values of prestressing force referred to in Table 5.1 are the predicted values at the time up to which the analyses were carried. This observation is rather significant, especially when viewed in the light of the substantial differences in the values of predicted concrete strain, especially for the case of Analysis 3. The reason for this apparent insensitivity of the total prestressing force to the concrete material properties most probably lies in the rather small loss of prestress exhibited by the structure. Even large differences in this small loss will reflect as small differences in the total prestressing force.

The shapes of the prestressing force versus time curves closely reflect the shapes of the concrete strain versus time curves. These trends are especially apparent in the results of Analysis 1 due to the degree of the fluctuations present in the concrete strain versus time curves generated by this particular analysis. The time-dependent strains generated by Analysis 1 are characterized by a period during which the strains develop at a reduced rate followed by a period during which the rate is substantially increased (see Figures 4.3 through 4.11). These trends take place during the first 250 days after erection of the instrumented segments. Inspection of Figures 5.1 through 5.3 will reveal that the period of reduced strain

is accompanied by a reduced rate of loss of prestress while the period of increased rate of strain is accompanied by an increased loss of prestress. As for the case of the total concrete strains, the observation that the magnitude of these fluctuations are increased for sections further from the pier is also applicable to the results of total prestressing force. The shapes of the curves of prestressing force versus time as predicted by Analysis 2 and Analysis 3 are smooth as are the curves of total concrete strain generated by these analyses. The fluctuations present in the curves of concrete strain versus time as generated by Analysis 2 (see Figures 4.12 through 4.20) are also properly reflected by the total prestressing force curves determined by this analysis. These observations serve to emphasize the inability of the analyses that do not make use of the concrete material properties obtained from outdoor stored specimens to predict the time-dependent behavior of the structure correctly. It should be kept in mind that, as mentioned before, the total prestressing forces predicted by the three analyses do not differ significantly, primarily due to the fact that the time-dependent loss of prestress is small.

The time-dependent behavior of concrete will induce a loss of prestressing force due to the resulting strain as distinguished from the effects of relaxation of the prestressing steel reinforcement, which will induce a loss of prestressing force in the absence of strain. The instantaneous elastic strains due to later applications of load, such as the erection of segments and the stressing of tendons, will also induce a change in the total prestressing force. It is thus clear that the time-dependent strains will to a large extent control the amount of prestress loss. It is important to realize that the magnitude of these time-dependent strains are in turn dependent on the prestress loss. The prestress loss induced in the first place by the time-dependent concrete strain will lead to a change of concrete stress. This change in concrete stress will in turn affect the rate at which creep of the concrete takes place, thus affecting the overall rate at which the time-dependent concrete strain

proceeds. A similar interaction exists between the development of the time-dependent concrete strains and the stress relaxation of the steel. These complex interactions are approximately accounted for in the analysis by discretising the analysis in the time domain and following the relevant basic assumptions outlined in Sect. 3.6.

The prestress losses due to the various time-dependent effects as predicted by the three analyses are summarized for each of the instrumented segments in Table 5.2. The losses presented in this table represent the total losses from erection of each segment due to each of the time-dependent effects including the corrections due to elastic recovery of the concrete. The effects of the moment redistribution due to each of these time-dependent effects on the prestressing force, although accounted for in the analytical procedure, are not included in these values.

Comparison of the time-dependent losses predicted by Analysis 2 with those predicted by Analysis 3 reveals that the sum of the losses due to shrinkage and creep are larger for the case of Analysis 2 while the losses due to relaxation are larger for the case of Analysis 3. This trend applies to all three segments considered and is most probably due to the fact that the higher losses due to creep and shrinkage as predicted by Analysis 2 led to lower steel stresses which in turn led to lower relaxation losses as compared to the values predicted by Analysis 3. The higher value of the concrete modulus of elasticity used for Analysis 3 also possibly contributed to this trend because it is associated with smaller concrete strains for instantaneous elastic effects which will lead to higher steel stresses and consequently higher relaxation losses. It is important to note that the total prestressing force, and consequently the steel stress, predicted by Analysis 2 is consistently lower than those predicted by Analysis 3 at all times. This may be verified by inspection of Figures 5.1 through 5.3.

A similar comparison of the prestress losses predicted by Analysis 1 with those predicted by Analysis 2 yields the somewhat surprising result that although the sum of the creep and shrinkage losses predicted by Analysis 1 are larger than those predicted by Analysis 2, the relaxation losses predicted by Analysis 1 are also larger. This trend, which applies to all three of the instrumented segments, apparently contradicts the trend established by the comparison of the results of Analysis 2 with those of Analysis 3. The explanation lies in the manner in which the prestress losses developed. Inspection of Figures 5.1 through 5.3 reveals that during the initial period under load the total predicted loss of prestressing force is somewhat less for the case of Analysis 1. This means that during this initial time period the steel stresses predicted by Analysis 1 were higher and consequently the predicted losses due to relaxation proceeded at a higher rate than for the case of Analysis 2. Because the greatest part of the expected relaxation loss takes place during the initial time period under load, it appears that the diminished rate at which the predicted prestress losses developed for the case of Analysis 1 was a prime contributor to the trend described above. It is of interest to note that since the reduced rate at which the predicted prestress losses developed for the case of Analysis 1 may be related to the manner in which the rheological properties of the concrete (specifically shrinkage) are affected by the varying outdoor environment to which the structure was actually subjected, the trends described above serve to illustrate some of the effects of the complex interaction of creep, shrinkage and relaxation on the time-dependent behavior of the structure. Although the differences in the predicted values of relaxation loss referred to above are small, the trends established by the comparisons are useful in explaining some of the aspects of the time-dependent losses of prestressing force.

5.3 Bending Moment

One of the features that characterizes the behavior of segmental prestressed concrete bridges built by the cantilever method is the time-dependent redistribution of bending moment. References (41) and (46) point out that for the case of a continuous prestressed concrete bridge cast in-situ on falsework creep will not induce any time-dependent redistribution of bending moment because the creep strains in the structure are allowed to develop in a stress field that corresponds to the original boundary conditions of the structure. In general, this statement is true only when the restraining effect of the steel reinforcement is ignored. In the present study this restraining effect is accounted for by the procedure followed to account for the effects of elastic recovery. For the case of bridges built by the cantilever method the stress field set up by the self-weight of the structure obeys the boundary conditions that correspond to a cantilever. When adjacent cantilevers are joined to form new intermediate structures the original boundary conditions are altered so that creep will then develop under a stress field that does not correspond to the original boundary conditions. The resulting creep deflections must, however, satisfy the current boundary conditions. In order to meet this requirement in statically indeterminate intermediate structures, bending moments are generally induced in the structure. The same reasoning may be applied to the explanation of the development of the time-dependent redistribution of bending moment due to creep resulting from stresses induced in the structure by loads applied to intermediate structures that do not constitute the final structure. Examples of such loads are the secondary moments due to stressing of continuity tendons of statically indeterminate intermediate structures and the change in moment resulting from the release of supports.

In the above, the creep effects due to different causes were artificially separated for purposes of illustration. In the real structure these effects take place simultaneously and interact with one another. The

effects of shrinkage and relaxation will also in general induce a time-dependent redistribution of bending moment. Once again, it should be kept in mind that creep, shrinkage and relaxation interact with one another with regard to the development of the redistribution of bending moment.

The structural mechanism whereby the change in bending moment due to the time-dependent effects develops may readily be illustrated as follows. Assume that the time-dependent concrete strains of a statically indeterminate intermediate structure develops independently of the boundary conditions. The structure is then rendered statically determinate by artificially removing all the interior supports so that the boundary conditions correspond to those of a simply supported beam. Using these boundary conditions and the time-dependent strains described above, the deflected shape of the structure may be determined. In general, the deflection of this statically determinate structure at the positions of the various interior supports will not be zero so that point loads must be applied at these positions to restore the geometric boundary conditions. The total bending moments induced in the equivalent statically determinate structure by these point loads constitute the change in bending moment due to the time-dependent effects.

Inspection of Figures 5.4 through 5.9 will reveal that the effect of the time-dependent properties of concrete and steel is to induce time-dependent changes in bending moment that are positive everywhere in the structure. That is, the magnitudes of the negative bending moments decrease with time while the magnitudes of the positive bending moments increase with time. The bending moments at the interior supports and in the mid-span regions of the interior spans at the time at which the final structure was completed and at the last time interval of these analyses are summarized in Tables 5.3 and 5.4. These tables also present the percentage change in predicted bending moment that takes place during the time period defined by the times at which the bending moments are presented. The percentage change

was based on the value of bending moment existing at the time at which the final structure was completed. It should be noted that the total values of bending moment include the secondary moments due to the stressing of the continuity tendons of statically indeterminate intermediate structures.

The results of all three analyses indicate that the percentage changes in bending moment in the support regions are small when compared to the percentage changes that take place in the mid-span regions. The results of Analysis 1 indicate an 11 percent decrease in moment at pier 1 and a 42 percent increase in the mid-span moment of span 2. It is of interest to note that for each analysis the bending moments at the different piers tend to more or less the same value with the passage of time. A similar trend may be observed for the mid-span moments of the interior spans. Percentage-wise, the largest change in support moment takes place at pier 1 and the largest change in positive moment occurs in span 2. The trend is consistently established by the results of all three analyses. Tables 5.3 and 5.4 as well as Figures 5.7 through 5.9 clearly show that at the time of completion of the final structure the negative bending moment at pier 1 is larger than those at the remaining piers and that the positive mid-span moment of span 2 is less than those of the other interior spans.

Seen in the light of the tendency of the time-dependent redistribution of bending moment to equalize the negative bending moments at the piers and to equalize the positive mid-span moments of the interior spans, as well as the tendency to induce changes of moment that are positive everywhere in the structure, it may be expected that the greatest change in bending moment would take place in the regions identified above for the time period under consideration. It should be realized that prior to the time at which the final structure was completed the bending moments in the component structures constituting intermediate structure 9 were subjected to redistribution.

It should be noted that up to the time that the continuity of intermediate structure 9 was established, all three analyses predict the same value of bending moment at each of the three instrumented segments and no redistribution of moment was predicted during this time period (see Figures 5.4 through 5.6). These results are due to the fact that during this time period the instrumented segments formed part of the double cantilever SB1, a structure that is statically determinate. Further inspection of Figures 5.4 through 5.6 will also reveal that for the time period during which the instrumented segments formed part of intermediate structure 9 the rate of change of bending moment was somewhat less than that associated with the time period during which the segments formed part of the final structure. This observation is generally true for the results generated by all three analyses. Because this trend is somewhat contrary to what may be expected when the shapes of the specific creep and shrinkage curves as well as the rate at which relaxation proceeds are considered, the explanation for this trend should in part be sought in the change of boundary conditions of the structure associated with the construction procedure. The manner in which the time-dependent bending moment varies along the structure is also of importance in this regard.

At a particular point in time the time-dependent change in bending moment must vary linearly along each span in order to satisfy the conditions of static equilibrium. Thus for the side-spans the time-dependent change in moment varies linearly from a non-zero positive value at the interior support to zero at the outer support. For the interior spans the time-dependent change in moment varies linearly from a positive value at one support to another positive value at the other support. It should thus be clear that since the change in moment does not approach zero anywhere along an interior span as for the case of a side-span, the change in moments at sections along an interior span should be larger than those for sections along a side-span, especially as the section considered approaches the outer

support where no change in moment takes place. This is substantiated by inspection of the bending moment diagrams presented in Figures 5.7 through 5.9. For intermediate structure 9 the instrumented segments formed part of a side-span while for the final structure they were contained in an interior span so that during the time period associated with intermediate structure 9 the time-dependent changes of bending moment at the instrumented segments were smaller than those that took place during the time period associated with the final structure. This argument is supported by the observation that the above-mentioned trend becomes more pronounced as the segment considered is located closer to pier 1 (see Figures 5.4 through 5.6). Specifically for the case of segment SB1-N1, which is located very close to pier 1, a negligible amount of moment redistribution was predicted for the time period associated with intermediate structure 9 (see Figure 5.4). From a designer's point of view it is of interest to note that the greatest time-dependent change in shear force most probably takes place in the side-spans due to the fact that the greatest variation of the time-dependent change in moment with distance appears to take place within these spans.

The time-dependent change of bending moment predicted by Analysis 1 was consistently larger than the changes predicted by the other two analyses for the time period associated with the final structure. Comparing the total negative bending moments at pier 1 at the time up to which the analyses were carried, Analysis 2 and Analysis 3 yielded values that were 3.5 and 2.2 percent larger than the value predicted by Analysis 1, respectively. A similar comparison of the mid-span moment of span 2 shows that Analysis 2 and Analysis 3 yielded values that were 9.8 and 9.5 percent smaller than the values predicted by Analysis 1, respectively. Bearing in mind the large difference in the values of total concrete strain predicted by Analysis 3 as compared to the results of the other two analyses, the differences in the bending moments at the supports predicted by the three

analyses are very small. It is, however, important to note that for the case of the positive mid-span moments the differences in the values predicted by Analysis 1 as compared to the values predicted by Analysis 2 and Analysis 3 are not negligible. For purposes of design it is the growth of positive moment that is of prime importance when accounting for the effects of the time-dependent moment redistribution so that it would appear that the effects of the outdoor environment on the time-dependent material properties of concrete are of some importance as far as the time-dependent increase of positive moment is concerned.

Inspection of Tables 5.3 and 5.4 reveals that for the time period associated with the final structure the percentage change in bending moment predicted by Analysis 3 was greater than the change predicted by Analysis 2 for the support as well as the mid-span regions. This trend is also present in the instrumented segments as illustrated by Figures 5.4 through 5.6. In fact, for segments SB1-N1 and SB1-N9 the total negative bending moments at the time up to which the analyses were carried as predicted by Analysis 2 are larger than those predicted by Analysis 3. The positive bending moment at segment SB1-N16 as predicted by Analysis 2 is less than the value predicted by Analysis 3. These observations are surprising, especially when viewed in the light of the substantially greater time-dependent concrete strains predicted by Analysis 2 as compared to the magnitude of the strains predicted by Analysis 3. Bearing in mind the structural mechanism whereby the change in bending moment due to the time-dependent effects develop, it is clear that the magnitude of this change in bending moment is dependent not only on the time-dependent deformations but also on the modulus of elasticity of the concrete. For given time-dependent deformations a higher value of the modulus of elasticity of the concrete will lead to greater time-dependent changes in bending moment. As previously indicated, the value of the modulus of elasticity of the concrete used with Analysis 3 was substantially greater than the value used with

Analysis 2. It would, therefore, appear that as far as the time-dependent redistribution of bending moment is concerned, the effects of the greater time-dependent concrete strains predicted by Analysis 2 was offset by the effects of the lower value used for the modulus of elasticity of concrete, as compared to the case of Analysis 3.

It should be pointed out that the explanation given above belies the extremely complicated nature of the various interactions that influence the development of the time-dependent change in bending moment. The changes in bending moment induce changes in concrete and steel stress which, in turn, influence the rate at which the time-dependent strains develop. Bearing in mind that it was these time-dependent strains which originally induced the change in bending moment it should be clear that these interactions are not simple and do not readily lend themselves to a simple explanation of observed behavior.

The time-dependent redistribution of bending moment is of importance in the design of prestressed concrete bridges constructed in segments by the cantilever method. Specifically, the relatively large increase of the positive moments in the mid-span regions is important. In the quarter-span regions the sense of the bending moment may even change (see Figures 5.7 through 5.9). It is necessary to account for these effects in the design of the type of structure under consideration herein by providing either tensioned or non-tensioned reinforcement to resist the increase of positive bending moment, otherwise, unwanted cracking may develop in the affected regions. Such cracks have, in fact, been found to develop in structures similar to the one under consideration herein, where no provision was made for the substantial time-dependent increase in positive bending moment (41).

5.4 Concrete Stress

The effect of the time-dependent material properties of the concrete and steel is to induce a loss in prestressing force as well as a redistribution of bending moment in the structure. Generally, these effects lead

directly to a time-dependent change in concrete stress in the structure. In this section the concrete stresses predicted by the three analyses are presented and discussed. Unless explicitly stated otherwise, all stresses referred to herein are compressive concrete stresses.

The stress histories for the extreme top and bottom fibers of each of the instrumented segments as predicted by each of the three analyses are presented in Figures 5.10 through 5.15. The concrete stresses at each of the instrumented segments at the time at which the final structure was completed and at the time up to which the analyses were carried are presented in Table 5.5. The percentage change of these stresses, based on the value of stress at the time of completion of the final structure, that took place during the time period associated with the final structure is also summarized.

The general trends indicated by the figures and table referred to above are that the stresses in the top fibers increase with time while the stresses in the bottom fibers decrease with time. The only exception to these trends is to be found in the stress history of segment SB1-N1 for the time period corresponding to intermediate structure 9, during which the top fiber stress decreases with time and no significant change in the bottom fiber stress takes place.

In order to explain these observed trends it is necessary to indicate how the time-dependent changes in prestressing force and bending moment each affect the stress in the extreme fibers of a particular segment. Because the effect of the time-dependent redistribution of bending moment is to induce a change in moment that is positive everywhere in the structure (see Sect. 5.3), the effect of the time-dependent change in bending moment will be to increase the compressive stresses in the top fibers and to decrease the compressive stresses in the bottom fibers. Furthermore, a given change in bending moment at a particular section will tend to induce a change in stress of greater magnitude in the bottom fiber than in the top fiber. The reason for this lies in the fact that the bottom fiber of all the

sections in the bridge being analyzed is located at a greater distance from the centroid of the section than the top fiber. According to beam theory, the magnitude of the stress at any fiber due to an applied moment is linearly related to the distance of the fiber to the centroid of the section.

Within the realm of ordinary beam theory the total change of stress due to a loss of prestressing force may be considered as the superposition of the changes of stress due to two effects. The first effect is associated with the change in axial thrust. This stress is uniformly distributed through the depth of the section and corresponds to the stress resulting from a force of magnitude equal to the change in prestressing force applied at the centroid of the section. The second effect accounts for the location of the tendons relative to the centroid of the section. This stress is linearly distributed through the depth of the section and corresponds to the stress resulting from a moment applied at the centroid of the section. The magnitude of this moment is equal to the product of the change in prestressing force and the eccentricity of the tendons measured from the centroid of the section. When these two stress distributions are superimposed it should be clear that for the extreme fiber on one side of the section centroid they will be additive while for the extreme fiber on the opposite side of the centroid they will oppose each other so that the sense of the resulting stress will depend on the relative magnitudes of the stresses set up by the thrust and moment effects.

Since the three instrumented segments were not similarly reinforced, it is necessary to consider the effects of the loss of prestressing force on the extreme fiber stresses separately for each segment. For the case of segment SB1-N1 the majority of the tendons were located in the top flange so that a loss of prestressing force would be accompanied by a decrease in the top fiber stress and a much smaller decrease in bottom fiber stress. The change in bottom fiber stress could possibly have been an increase in stress depending on the relative magnitudes of the stresses due to the thrust and moment effects, as explained above. For the case of

segment SB1-N16 the majority of the tendons were located in the bottom flange so that the effects of the loss of prestressing force at this segment may be expected to be opposite to those associated with segment SB1-N1. Thus, at segment SB1-N16 the loss of prestressing force may be expected to induce a decrease in the bottom fiber stress. Depending on the relative magnitudes of the stresses due to the thrust and moment effects, the associated change of the top fiber stress will be a smaller decrease in stress than for the case of the bottom fiber, or may even be an increase in stress. At segment SB1-N9 the tendons are divided between the top and bottom flanges in such a manner that an equal loss of prestressing force in each tendon will lead to a more or less equal decrease in stress in the top and bottom fibers. It is, however, not reasonable to expect that the magnitude of the loss of prestressing force in each tendon will be the same so that the decrease in stress at the extreme fibers due to loss of prestress are most probably not equal. The difference in the change of extreme fiber stresses is most probably smaller for the case of segment SB1-N9 than for the case of either segment SB1-N1 or segment SB1-N16 so that segment SB1-N9 represents an intermediate case relative to the other two segments.

The combined effects of the time-dependent change in bending moment and loss of prestressing force on the extreme fiber concrete stresses may best be illustrated by consideration of the appropriate stress histories of segment SB1-N1 (see Figures 5.10 and 5.11). For this particular segment the stresses due to the loss in prestressing force tend to oppose those due to the change in bending moment. For the time period associated with intermediate structure 9, segment SB1-N1 was located close to the outer support of a side-span so that no significant time-dependent change in bending moment may be expected to have taken place at this segment during this time period (see also Sect. 5.3). It would thus appear that for this time period the concrete stress at segment SB1-N1 was primarily influenced by the prestress loss. This means that the top fiber concrete stresses may be

expected to have decreased while the bottom fiber stresses may be expected not to have changed substantially during this time period. Inspection of Figures 5.10 and 5.11 will reveal that the predicted extreme fiber stresses indeed follow these trends for the time period under consideration.

For the time period associated with the final structure, segment SB1-N1 formed part of an interior span so that the time-dependent change in bending moment during this time period was no longer negligible here (see Sect. 5.3). Thus, for this time period the loss of prestressing force as well as the time-dependent change in bending moment simultaneously influence the stress at the extreme fibers of the section under consideration. Furthermore, as pointed out before, the influence of these effects will oppose each other. Figures 5.10 and 5.11 clearly indicate that for this time period the effects on the extreme fiber stresses associated with the time-dependent change in bending moment was dominant; i.e., the top fiber stress increased with time while the bottom fiber stress decreased with time. This observation is further substantiated by the fact that the magnitude of the stress change in the extreme bottom fiber is greater than that of the stress change in the extreme top fiber (for segment SB1-N1 the extreme bottom fiber is located further from the centroidal axis than the extreme top fiber).

For segments SB1-N9 and SB1-N16 the percentage increase in top fiber stress as well as the percentage decrease in bottom fiber stress for the time period associated with the final structure are both substantially larger than for the case of segment SB1-N1 (see Table 5.5). For segment SB1-N9 this trend was most probably due to the fact that the effects of the loss of prestressing force on the concrete stress were, to a greater extent than in the case of segment SB1-N1, of secondary importance relative to the effects of the time-dependent change in bending moment. In the case of segment SB1-N16 the effects of the loss of prestressing force on the concrete stress added to the effects of the time-dependent change in bending moment.

It thus seems reasonable to conclude that the effects of the time-dependent change of bending moment were of prime importance as far as the

magnitude of the concrete stress was concerned, while the effects of the loss of prestressing force were, relatively speaking, of secondary importance.

Comparing the magnitudes of the stresses predicted by each of the analyses at the time up to which they were carried, it appears as if Analysis 1 predicted the largest top fiber stresses and the smallest bottom fiber stresses. The only exception to this observation is the case of the top fiber stresses of segment SB1-N1 where Analysis 3 predicted the largest stresses (see Figures 5.10 through 5.15 and Table 5.5). This trend is most probably due to the fact that the loss of prestressing force as well as the time-dependent change in bending moment as predicted by Analysis 1 were larger than the values predicted by the other two analyses.

Comparing the final stresses predicted by Analysis 2 and Analysis 3 with the values predicted by Analysis 1, the largest percentage difference in the top fiber stresses appear to be at segment SB1-N16 where Analysis 2 and Analysis 3 both predict values that are 10 percent smaller than the value predicted by Analysis 1. A similar comparison of the predicted bottom fiber stresses indicates that the largest percentage difference for the case of Analysis 2 is at segment SB1-N9 and for the case of Analysis 3 is at segment SB1-N16 where the predicted values are 15 and 17 percent larger than the values predicted by Analysis 1, respectively. These comparisons only apply to the instrumented segments. It is furthermore of interest to note that at section SB1-N1, where the concrete stresses in both the extreme top and bottom fibers were larger than at the other instrumented segments, the final top and bottom fiber stresses predicted by Analysis 2 and Analysis 3 were less than 5.5 percent different from the values predicted by Analysis 1.

Finally, the close agreement of the concrete stresses predicted by Analysis 2 and Analysis 3 is of interest from the point of view of design, especially when viewed in the light of the substantial differences in the concrete strains predicted by these two analyses. It thus appears that for the specific case of the Kishwaukee River Bridge the concrete stresses may be satisfactorily determined by making use of the recommendations of the C.E.B.

construction loads were applied to the structure the presence of these loads decreased the top fiber stresses while it increased the bottom fiber stresses at segment SB1-N1 (see Figure 5.18). In the light of this behavior of the concrete stresses it appears reasonable to assume that the residual decrease in the top fiber concrete strain was primarily due to the diminished creep associated with the decreased top fiber concrete stress during this time period. Similarly, the residual increase in the bottom fiber concrete strain appears to have been primarily due to the increased creep associated with the increased bottom fiber concrete stress during this time period.

For times greater than the time at which the construction loads were removed the development of the concrete strains at both extreme fibers of segment SB1-N1 seem to have been essentially unaffected by the previous presence of the construction loads (see Figure 5.17). For this time period the only effect on the time-dependent strains appears to have been the residual strains developed during the time period during which the construction loads were applied to the structure. These observations are substantiated by the fact that for times greater than the time of removal of the construction loads the concrete strain versus time curves predicted by Analysis 1 and Analysis 4 for segment SB1-N1 are more or less parallel for both the top and bottom fiber strains (see Figure 5.17).

It should be kept in mind that both Analysis 1 and Analysis 4 made use of the rate of creep method to predict the creep of concrete under a variable state of stress because specific creep curves corresponding to only one age at loading were available for the outdoor stored specimens. It should thus be pointed out that the insensitivity of the behavior of the time-dependent strains to the previous presence of the construction loads for times beyond the time at removal of these loads should be seen partly in the light of the property of the rate of creep method to ignore the previous stress history as discussed in Sect. 3.2.2.

magnitude of the concrete stress was concerned, while the effects of the loss of prestressing force were, relatively speaking, of secondary importance.

Comparing the magnitudes of the stresses predicted by each of the analyses at the time up to which they were carried, it appears as if Analysis 1 predicted the largest top fiber stresses and the smallest bottom fiber stresses. The only exception to this observation is the case of the top fiber stresses of segment SB1-N1 where Analysis 3 predicted the largest stresses (see Figures 5.10 through 5.15 and Table 5.5). This trend is most probably due to the fact that the loss of prestressing force as well as the time-dependent change in bending moment as predicted by Analysis 1 were larger than the values predicted by the other two analyses.

Comparing the final stresses predicted by Analysis 2 and Analysis 3 with the values predicted by Analysis 1, the largest percentage difference in the top fiber stresses appear to be at segment SB1-N16 where Analysis 2 and Analysis 3 both predict values that are 10 percent smaller than the value predicted by Analysis 1. A similar comparison of the predicted bottom fiber stresses indicates that the largest percentage difference for the case of Analysis 2 is at segment SB1-N9 and for the case of Analysis 3 is at segment SB1-N16 where the predicted values are 15 and 17 percent larger than the values predicted by Analysis 1, respectively. These comparisons only apply to the instrumented segments. It is furthermore of interest to note that at section SB1-N1, where the concrete stresses in both the extreme top and bottom fibers were larger than at the other instrumented segments, the final top and bottom fiber stresses predicted by Analysis 2 and Analysis 3 were less than 5.5 percent different from the values predicted by Analysis 1.

Finally, the close agreement of the concrete stresses predicted by Analysis 2 and Analysis 3 is of interest from the point of view of design, especially when viewed in the light of the substantial differences in the concrete strains predicted by these two analyses. It thus appears that for the specific case of the Kishwaukee River Bridge the concrete stresses may be satisfactorily determined by making use of the recommendations of the C.E.B.

(11) to establish the material properties of the concrete for use with the time-dependent analysis of the structure.

5.5 Influence of Construction Loads

One of the unique features of the launching girder used for the erection of the segments comprising the Kishwaukee River Bridge was that it did not normally impose significant loads on the structure. However, just after the completion of intermediate structure 9 the launching girder was placed in such a position so that it imposed major loads on the structure. The magnitude and position of these loads are indicated by Figure 5.16. The girder remained in this position until just prior to the time at which the closure segment of span 1 was cast. It thus appears that intermediate structure 9 was subjected to these construction loads for a period of approximately 5 months.

It is of some interest to study the influence of these construction loads on the time-dependent behavior of the structure. In order to achieve this aim the structure was analyzed taking into account the loads illustrated by Figure 5.16. For purposes of analysis these loads were applied at the time at which the tendons which establish continuity of intermediate structure 9 were stressed. The loads were removed at the time of casting of the closure segment of span 1. The material properties obtained experimentally from the outdoor stored specimens were assigned to the concrete. The results of this analysis, designated as Analysis 4, may therefore be directly compared to the results of Analysis 1 in order to illustrate some of the effects of the presence of the construction loads on the time-dependent behavior of the structure.

The percentage differences in the results predicted by Analysis 1 and Analysis 4 at the time up to which the analyses were carried are presented for each of the instrumented segments in Table 5.6. These percentages are based on the final values predicted by Analysis 1. Inspection of this

table will reveal that the differences in the predicted values, and consequently the effects of the construction loads on the time-dependent behavior of the structure, are of negligible importance for practical purposes. Of the quantities considered in Table 5.6 it appears as if the concrete strains are affected to the greatest extent by the presence of the construction loads, the maximum difference in predicted final concrete strain being less than 3.3 percent at the sections considered. The concrete strains in the extreme top fibers are decreased while the strains in the bottom fibers are increased by the effects of the construction loads. For the final concrete stresses at the extreme fibers this trend is reversed, i.e. the top fiber stresses are increased while the bottom fiber stresses are decreased by the presence of the construction loads. The total prestressing force is increased at segments SB1-N1 and SB1-N9, while it is decreased at segment SB1-N16 by the application and removal of the construction loads. For the case of Analysis 4 as compared with Analysis 1, the magnitude of the bending moments at the instrumented segments is greater in the negative moment region while it is less in the positive moment region. It would thus appear that the time-dependent moment redistribution was slightly inhibited by the application of the construction loads.

The development of the concrete strains at the extreme fibers of segment SB1-N1 as predicted by Analysis 1 and Analysis 4 is illustrated in Figure 5.17. For the time period associated with the application of the construction loads it appears as if the greatest part of the decrease in top fiber strain and increase in the bottom fiber strain as predicted by Analysis 4 was a result of the elastic response of the concrete to the increase in negative moment at this section caused by the application of the construction loads. However, when the construction loads are removed from the structure a residual decrease in the top fiber strains and a residual increase in bottom fiber strains are predicted by Analysis 4 relative to the results predicted by Analysis 1. For the time period during which the

construction loads were applied to the structure the presence of these loads decreased the top fiber stresses while it increased the bottom fiber stresses at segment SB1-N1 (see Figure 5.18). In the light of this behavior of the concrete stresses it appears reasonable to assume that the residual decrease in the top fiber concrete strain was primarily due to the diminished creep associated with the decreased top fiber concrete stress during this time period. Similarly, the residual increase in the bottom fiber concrete strain appears to have been primarily due to the increased creep associated with the increased bottom fiber concrete stress during this time period.

For times greater than the time at which the construction loads were removed the development of the concrete strains at both extreme fibers of segment SB1-N1 seem to have been essentially unaffected by the previous presence of the construction loads (see Figure 5.17). For this time period the only effect on the time-dependent strains appears to have been the residual strains developed during the time period during which the construction loads were applied to the structure. These observations are substantiated by the fact that for times greater than the time of removal of the construction loads the concrete strain versus time curves predicted by Analysis 1 and Analysis 4 for segment SB1-N1 are more or less parallel for both the top and bottom fiber strains (see Figure 5.17).

It should be kept in mind that both Analysis 1 and Analysis 4 made use of the rate of creep method to predict the creep of concrete under a variable state of stress because specific creep curves corresponding to only one age at loading were available for the outdoor stored specimens. It should thus be pointed out that the insensitivity of the behavior of the time-dependent strains to the previous presence of the construction loads for times beyond the time at removal of these loads should be seen partly in the light of the property of the rate of creep method to ignore the previous stress history as discussed in Sect. 3.2.2.

The concrete stresses and bending moments at segment SB1-N1 as predicted by both Analysis 1 and Analysis 4 are presented in Figures 5.18 and 5.19. These figures clearly demonstrate that the time-dependent component of the concrete stresses at both the top and bottom fibers, as well as the time-dependent component of the bending moment are essentially unaffected by the application and removal of the construction loads. Considering the extreme fiber concrete stresses and the bending moment, the only significant difference in the results predicted by Analysis 1 and Analysis 4 appears to occur during the time period during which the construction loads were applied to the structure. The decrease in top fiber stress and the increase in bottom fiber stress at segment SB1-N1, due to the application of the construction loads, are consistent with the increase in negative moment here, due to these loads. Once the construction loads are removed, the results predicted by Analysis 1 and Analysis 4 are the same for all practical purposes.

It is of some interest to investigate some of the effects of the application of the construction loads on the vertical deflection of the structure. The downward transverse deflections of the free cantilever tip (segment SB1-S17) of intermediate structure 9 as predicted by Analysis 1 and Analysis 4 at the times of application and removal of the construction loads are presented in Table 5.7. This cantilever eventually formed part of span 1 of the final structure. It should be pointed out that these deflections cannot be directly compared to the actual deformations of the structure due to the unknown magnitude of the corrections in vertical alignment that were made during the construction process. The differences in the deflections at the time of application of the construction loads and at the time of removal of these loads may, however, be expected to be comparable to the change in actual deflection that took place during this time period.

Considering the change in downward deflection of the free cantilever tip of intermediate structure 9 for the time period during which the construction loads were applied to the structure, Analysis 1 predicted a

change in downward deflection of 1.609 in. (40.9 mm) while Analysis 4 predicted a change in deflection of 2.005 in. (50.9 mm). It may thus be concluded that the effect of the application of the construction loads on the downward deflection of the free cantilever tip for the time period described above is to increase this deflection by 0.396 in. (10.0 mm). A similar comparison of the deflections of segment SB1-N16 as predicted by Analysis 1 and Analysis 4 reveals that for the time period during which the construction loads were applied to the structure the upward deflection of this segment was increased by 0.073 in. (1.9 mm) by the presence of these loads. It is of interest to note that for the time period associated with the final structure the previous application and removal of the construction loads appear to have decreased the downward change in deflection of segment SB1-N16 that takes place during this time period by 0.07 percent.

In conclusion, it would thus appear, that as far as the time-dependent components of the concrete stresses, prestressing force and bending moments are concerned, the effects of the presence of the construction loads are negligible for practical purposes. The concrete strains and, consequently, the transverse deflections seem to be affected to a greater extent than the quantities mentioned above. It furthermore appears as if most of this effect on the deformations takes place during the time period during which the construction loads are applied to the structure and that once these loads are removed the time-dependent behavior of the deformations seems to be essentially unchanged. The elastic effects associated with the application of the construction loads are not small and should be accounted for in the design process.

6. CONCLUSIONS AND RECOMMENDATIONS FOR FURTHER STUDY

The conclusions and recommendations for further study presented in the following section are based on the results of the various analyses of the Kishwaukee River Bridge as well as the results of the comparison of measured deformations of the actual structure with computed deformations. The differences in the analyses of the Kishwaukee River Bridge lie in the material properties assigned to the concrete. Concrete material properties experimentally obtained from outdoor stored and indoor stored specimens, as well as those prescribed by the C.E.B. recommendations, were used in the different analyses. The conclusions drawn herein apply, strictly speaking, only to the Kishwaukee River Bridge so that generalizations to include other structures of a similar type should be made with the utmost care.

Based on the comparison of measured deformations of the Kishwaukee River Bridge with the analytically obtained deformations, the following conclusions and recommendations for further study may be made:

1. The analytical procedure used for the time-dependent analysis of the structure performed satisfactorily. This is particularly apparent when consideration is given to the excellent agreement of the measured and computed concrete strains for the case where the concrete material properties obtained experimentally from outdoor stored specimens were used in the analytical procedure.
2. The procedure introduced during the course of this study for the estimation of the creep of concrete subjected to a varying state of stress appears to have performed satisfactorily. In this regard it is important to note that the rate of creep method yielded satisfactory results. The proposed procedure for estimating the creep of concrete reduces to the rate of creep method where specific creep curves corresponding

to only one particular age at loading are available, as was the case for the analysis that utilized the concrete material properties obtained experimentally from outdoor stored specimens.

3. Compared with the measured strains, the analysis that made use of concrete material properties obtained experimentally from outdoor stored specimens yielded the best results. In this regard the analysis that made use of the concrete material properties as prescribed by the C.E.B. recommendations yielded results that were poor, with the predicted strains being smaller than the measured values. The magnitude of the strains predicted by the analysis that made use of the material properties obtained from the laboratory stored specimens compared well with the measured values at the time up to which the analyses were carried.
4. For the particular structure under consideration herein the development of the total time-dependent strains was governed to a large extent by the manner in which the shrinkage of concrete developed and this was partly due to the fact that the segments were relatively old when erected. Because the shrinkage curve obtained from the outdoor specimens was the only one which reflected the seasonal fluctuations that characterize the shrinkage of concrete subjected to a variable outdoor environment, the analysis which made use of the material properties obtained from outdoor stored specimens was the only one which correctly predicted the development of the total time-dependent concrete strains. This particular conclusion serves to emphasize the necessity of using material properties obtained from outdoor stored specimens in order to correctly predict the behavior of the time-dependent concrete strains for structures of the type under consideration herein. These material properties may be expected to reflect the effects of the variable outdoor

environment to which the structure is subjected on the rheological properties of the concrete.

5. For the analysis which employed the concrete material properties obtained from outdoor stored specimens the seasonal dependence of shrinkage was, strictly speaking, correctly included only for the instrumented double cantilever because the same shrinkage curve was used for all the segments. This effect, however, did not appear to significantly influence the behavior of the segments studied. It is strongly recommended that this matter be made the topic of a further study which would involve the use of different shrinkage curves each of which would be associated with a different cantilever so that the seasonal effects are correctly accounted for. It should be mentioned that it appears as if the season during which the concrete is cast has an influence on the subsequent development of shrinkage. Thus, a study such as the one mentioned above would involve a substantial experimental effort because shrinkage curves would have to be determined separately to correctly account for the seasons during which the segments for the different double cantilevers are cast. Measures should be taken to insure that the seasonal fluctuations of shrinkage are carefully recorded, especially at later ages, when determining the shrinkage curves for outdoor stored specimens.
6. The procedure used in this study to modify the experimentally obtained creep and shrinkage curves to include the effects of the size and shape of the member on creep and shrinkage performed satisfactorily. There is, however, a great need for further study in this regard especially as far as experimental work is concerned. It is strongly recommended that a study of this nature should include the effects of size and shape on the creep and shrinkage of members stored outdoors.

7. An extensive comparison of calculated and measured deflections was not possible as a result of the effects of the failure of certain joints between adjacent segments on the completed structure and the questionable reliability of the measured values due to the extremely adverse conditons under which they were taken. The sense of the time-dependent changes of deflection at the instrumented segments were the same for both the measured and calculated values. The magnitudes of the time-dependent changes in transverse deflection of the completed structure are extremely small while the relative magnitudes of the time-dependent change in deflection as predicted by the three analyses are consistent with the relative magnitudes of the predicted concrete strains. In order to predict the actual deflections of the structure correctly, it is necessary to account for deflections induced in the structure by certain construction activities such as alignment corrections and the seating of the double cantilevers on permanent bearings. It appears as if a major portion of the time-dependent strain induced an axial shortening of the completed structure.

Based on a consideration of the prestressing force, bending moments and concrete stresses predicted by the analyses of the Kishwaukee River Bridge the following conclusions may be drawn:

8. The magnitude of the total time-dependent loss of prestressing force is small and the development of this loss of prestressing force with time closely reflects the manner in which the total time-dependent concrete strains develop. The total loss of prestress due to relaxation is slightly less than that due to creep, while the loss due to shrinkage is substantially less than the losses due to either creep or relaxation. The relatively small time-dependent loss of prestressing force is in part due to the reduced time-dependent concrete strain which goes hand-in-hand with the relatively great age at which the segments were erected.

9. The time-dependent redistribution of bending moment tends to reduce the magnitude of the negative bending moments and to increase the magnitude of the positive bending moments in the structure. The tendency is for the negative bending moments at the interior supports to approach the same value. A similar tendency is exhibited by the positive mid-span bending moments of the interior spans. The percentage change of the negative bending moments at the interior supports are relatively small when compared with the large percentage change of the positive mid-span bending moments of the interior spans. This large change in positive bending moment is important and must be accounted for in the design of the type of structure under consideration herein. The rate at which the time-dependent change of bending moment proceeds at a particular section of the structure depends on the construction sequence.
10. The effect of the time-dependent behavior of the concrete and steel on the extreme fiber concrete stresses in the completed structure is to increase the top fiber compressive stresses and to decrease the bottom fiber compressive stresses with time. The magnitude of the decrease in bottom fiber stress is greater than the magnitude of the increase in top fiber stress. Both the loss of prestressing force and the time-dependent change of bending moment induce changes of concrete stress. Of the two contributory effects, the time-dependent change in bending moment seems to be the more important. When the intermediate structure being considered is statically determinate no time-dependent change of bending moment takes place and consequently the time-dependent change of concrete stress for this case is governed by the loss of prestressing force. A similar situation arises in a statically indeterminate intermediate structure when the segment considered is located close to an outer support.

11. Generally the magnitudes of the total prestressing force, bending moments and concrete stresses as predicted by the analyses that make use of the concrete material properties obtained experimentally from laboratory stored specimens and those prescribed by the C.E.B. recommendations do not differ significantly. This conclusion is of significance when viewed in the light of the great difference that exists in the magnitude of the concrete strains predicted by these two analyses. The predicted deformations of the structure thus seem to be much more sensitive to the material properties assigned to the concrete than the predicted prestressing force, bending moments and concrete stresses. Since approximate procedures for determining the rheological properties of concrete are usually used in the design of these structures and since the time-dependent behavior of these structures is primarily a problem of serviceability, it is suggested that the time-dependent deformations of the structure be emphasized as a design criterion when considering the serviceability requirements of the structure.
12. The final magnitudes of the prestressing force, bending moments and concrete stresses as predicted by the analysis that makes use of the concrete material properties obtained experimentally from the outdoor stored specimens differ somewhat from the values predicted by the other two analyses.

Based on the analysis that includes the effects of the construction loads applied to the structure, the following conclusions may be drawn:

13. The time-dependent deformations of the structure are influenced to a much greater extent than the stresses and forces by the presence of the construction loads. This influence is, however, very small and appears to take place during the time of application of the loads. Once the loads are removed, the

time-dependent component of the behavior of the structure remains essentially unaffected. The effects of the construction loads on the time-dependent behavior of the prestressing force, bending moments and concrete stresses are, for practical purposes, negligible. Most of the effects of the construction loads on the structure are elastic in nature. These elastic effects are not small and should be accounted for in the design process.

The following general conclusions and recommendations may be made:

14. Generalizations in the type of bridge under consideration herein are very difficult because of the dependence of the time-dependent response of these structures on the construction history. A parametric study is, nonetheless, recommended. It is suggested that a simpler structure be considered for such a study.
15. The continuation of obtaining field data in terms of both measurements of the deformations of actual structures as well as obtaining material properties of concrete from outdoor stored specimens is strongly recommended.

LIST OF REFERENCES

1. ACI Committee 209, Subcommittee I, "Effects of Concrete Constituents, Environment, and Stress on Creep and Shrinkage of Concrete," ACI SP-27, Designing for Effects of Creep, Shrinkage, and Temperature in Concrete Structures, Detroit, 1971, pp. 1-42.
2. ACI Committee 209, Subcommittee II, "Prediction of Creep, Shrinkage and Temperature Effects in Concrete Structures," ACI SP-27, Designing for Effects of Creep, Shrinkage, and Temperature in Concrete Structures, Detroit, 1971, pp. 51-93.
3. Ali, I., and Kesler, C. E., "Mechanics of Creep in Concrete," ACI SP-9, Symposium on Creep of Concrete, Houston, 1964, pp. 35-57.
4. Anderson, T. C., Houdeshell, D. M., and Gamble, W. L., "Construction and Long Term Behaviour of 1/8th Scale Prestressed Concrete Bridge Components," Structural Research Series No. 384, Civil Engineering Studies, University of Illinois, Urbana, October 1972.
5. Ballinger, C. A., Podolny, W., and Abrahams, M. J., "A Report on the Design and Construction of Segmental Prestressed Concrete Bridges in Western Europe - 1977," U. S. Department of Transportation, Federal Highway Administration, Report No. FHWA-RD-78-44, July 1978.
6. Bazant, Z. P., "Prediction of Concrete Creep Effects using Age-Adjusted Effective Modulus Method," ACI Journal, Proc., Vol. 69, April 1972, pp. 212-217.
7. Belmain, M., and Le Bourdelles, Y., "Etude du Retrait et des Deformations de Flange dans un Pont en Beton Precontraint Construit par Encorbellement," Annales des Ponts et Chaussees, No. II, 1971, pp. 81-103.
8. Bennett, E. W., and Loat, D. R., "Shrinkage and Creep of Concrete as Affected by the Fineness of Portland Cement," Magazine of Concrete Research, Vol. 22, No. 71, June 1970, pp. 69-78.
9. Breen, J. E., Cooper, R. L., and Gallaway, T. M., "Minimizing Construction Problems in Segmentally Precast Box Girder Bridges," Research Report 121-6F, Center for Highway Research, University of Texas at Austin, Aug. 1975.
10. Brown, R. C., Burns, N. H., and Breen, J. E., "Computer Analysis of Segmentally Erected Precast Prestressed Box Girder Bridges," Research Report 121-4, Center for Highway Research, University of Texas at Austin, Nov. 1974.

11. C. E. B. (European Concrete Committee), "International Recommendations for the Design and Construction of Concrete Structures, Principles and Recommendations," June 1970.
12. Danon, J. R., and Gamble, W. L., "Time-Dependent Deformations and Losses in Concrete Bridges Built by the Cantilever Method," Structural Research Series No. 437, Civil Engineering Studies, University of Illinois, Urbana, January 1977.
13. Davies, R. D., "Some Experiments on the Applicability of the Principle of Superposition to the Strains of Concrete Subjected to Changes of Stress, with Particular Reference to Prestressed Concrete," Magazine of Concrete Research, Vol. 9, No. 27, Nov. 1957, pp. 161-172.
14. Davis, R. E., Davis, H. E., and Brown, E. H., "Plastic Flow and Volume Changes of Concrete," Proceedings, ASTM 37, 1937, Part II, pp. 317-330.
15. Dilger, W., Ghali, A., Kountouris, C., "Time Dependent Forces Induced by Settlement in Continuous Prestressed Concrete Structures," Symposium, International Association for Bridge and Structural Engineering, Madrid, 1970, pp. 89-98.
16. Engineering News Record, "Twin box girder bridges develop cracks in joints," 31 May 1979, pp. 8-9; "Epoxy blamed for crack in bridge," 26 July 1979, p. 13; "Cracked bridge cured by pins through joints," 22 May 1980, p. 41.
17. England, G. L., and Ross, A. D., "Reinforced Concrete under Thermal Gradients," Magazine of Concrete Research, Vol. 14, No. 40, March 1962, pp. 2-12.
18. Fadi, A. I., and Gamble, W. L., "Time-Dependent Behavior of Noncomposite and Composite Post-Tensioned Concrete Girder Bridges," Structural Research Series No. 430, Civil Engineering Studies, University of Illinois, Urbana, October 1976.
19. Ghali, A., Neville, A. M., and Jha, P. C., "Effects of Elastic and Creep Recoveries of Concrete on Loss of Prestress," ACI Journal, Proc., Vol. 64, No. 12, Dec. 1967, pp. 802-810.
20. Ghali, A., Sisodiya, R. G., and Tadros, G. S., "Computer Program for Displacements and Losses in Multi-Stage Prestressed Members," Research Report, Civil Engineering Department, The University of Calgary, Calgary, Alberta, Canada, 1973.
21. Ghali, A., Sisodiya, R. G., and Tadros, G. S., "Displacements and Losses in Multistage Prestressed Members," Proc. ASCE, Journal of the Structural Division, Vol. 100, No. ST11, Nov. 1974, pp. 2307-2322.

22. Glodowski, R. J., and Lorenzetti, J. J., "A Method for Predicting Prestress Losses in a Prestressed Concrete Structure," PCI Journal, Vol. 17, No. 2, March/April 1972, pp. 17-31.
23. Godden, W. G., "Numerical Analysis of Beam and Column Structures," Prentice Hall Inc., London, 1965.
24. Greenspan, D., "Introduction to Numerical Analysis and Applications," Markham Publishing Company, Chicago, 1971.
25. Guyon, Y., "Limit State Design of Prestressed Concrete," Vol. 2, Halsted Press and John Wiley and Sons, 1974.
26. Hansen, T. C., and Mattock, A. H., "Influence of Size and Shape of Member on the Shrinkage and Creep of Concrete," ACI Journal, Proc., Vol. 63, No. 2, Feb. 1966, pp. 267-290.
27. Henneberger, W., and Breen, J. E., "First Segmental Bridge in the U. S.," Civil Engineering Magazine, ASCE, June 1974, pp. 54-57.
28. Hernandez, H. D., and Gamble, W. L., "Time-Dependent Prestress Losses in Pretensioned Concrete Construction," Structural Research Series No. 417, Civil Engineering Studies, University of Illinois, Urbana, May 1975.
29. Huang, T., "Anchorage Take-up Loss in Post-Tensioned Members," PCI Journal, Vol. 14, No. 8, Aug. 1969, pp. 30-35.
30. Illinois Department of Transportation, "Private Communication to W. L. Gamble and V. Marshall," March 1980, Aug. 1980, Sept. 1980 and Nov. 1980.
31. Illston, J. M., "The Delayed Elastic Deformation of Concrete as a Composite Material," International Conference on the Structure of Concrete, London, Cement and Concrete Association, 1965, pp. 24-36.
32. Kabir, A. F., "Nonlinear Analysis of Reinforced Concrete Panels, Slabs and Shells for Time-Dependent Effects," Report No. UC SESM 76-6, University of California at Berkeley, Dec. 1976.
33. Kashima, S., and Breen, J. E., "Construction and Load Tests of a Segmental Precast Box Girder Bridge Model," Research Report 121-5, Center for Highway Research, University of Texas at Austin, Feb. 1975.
34. Keijer, U., "Long-Term Deflections of Cantilever Prestressed Bridges," Symposium, International Association for Bridge and Structural Engineering, Madrid, 1970, pp. 27-34.

35. Khachaturian, N., and Gurfinkel, G., "Prestressed Concrete," McGraw-Hill Book Company, 1969.
36. Khalil, M. S. A., "Time-Dependent Non-Linear Analysis of Prestressed Concrete Cable-Stayed Girders and Other Concrete Structures," Ph.D. Thesis, University of Calgary, Calgary, Alberta, Canada, 1979.
37. Kokubu, M., Goto, Y., Ozaka, Y., Okamura, H., and Momoshima, S., "Measurements of Creep and Shrinkage in Actual Prestressed Concrete Bridges," Symposium, International Association for Bridge and Structural Engineering, Madrid, 1970, pp. 19-26.
38. Lacey, G. C., and Breen, J. E., "Long Span Prestressed Concrete Bridges of Segmental Construction, State of the Art," Research Report 121-1, Center for Highway Research, University of Texas at Austin, May 1969.
39. Lacey, G. C., and Breen, J. E., "The Design and Optimization of Segmentally Precast Prestressed Box Girder Bridges," Research Report 121-3, Center for Highway Research, University of Texas at Austin, Aug. 1975.
40. Leonhardt, F., "Prestressed Concrete: Design and Construction," W. Ernst, Berlin, 1964.
41. Libby, J. R., "Segmental Box Girder Bridge Superstructure Design," ACI Journal, Proc., Vol. 73, No. 5, May 1976, pp. 279-290.
42. Magura, D. D., Sozen, M. A., and Siess, C. P., "A Study of Stress Relaxation in Prestressing Reinforcement," PCI Journal, Vol. 9, No. 2, April 1964, pp. 13-57.
43. McHenry, D., "A New Aspect of Creep in Concrete and its Application to Design," Proc., ASTM, Vol. 43, 1943, pp. 1069-1084.
44. Mossiossian, V., "Mechanisms of Creep and Shrinkage in Plain, Reinforced and Prestressed Concrete," Department of Civil Engineering, University of Illinois, Urbana, May 1970.
45. Mossiossian, V., and Gamble, W. L., "Time-Dependent Behavior of Noncomposite and Composite Prestressed Concrete Structures under Field and Laboratory Conditions," Structural Research Series No. 385, Civil Engineering Studies, University of Illinois, Urbana, May 1972.
46. Muller, J., "Long-Span Precast Prestressed Concrete Bridges Built in Cantilever," ACI SP-23, First International Symposium on Concrete Bridge Design, 1969, pp. 705-740.

47. Muller, J., "Ten Years of Experience in Precast Segmental Construction," PCI Journal, Vol. 20, No. 1, Jan./Feb. 1975, pp. 28-61.
48. Nasser, K. W., and Neville, A. M., "Creep of Concrete at Elevated Temperatures," ACI Journal, Proc., Vol. 62, No. 12, Dec. 1965, pp. 1567-1579.
49. Neville, A. M., and Meyers, B. L., "Creep of Concrete: Influencing Factors and Prediction," ACI SP-9, Symposium on Creep of Concrete, Houston, 1964, pp. 1-31.
50. Neville, A. M., "Creep of Concrete: Plain, Reinforced, and Prestressed," North-Holland Publishing Company, Amsterdam, 1970.
51. Neville, A. M., "Properties of Concrete," 2nd Edition, Pitman Publishing Company, 1977.
52. Portland Cement Association, "Private Communication to W. L. Gamble," June 1979, May 1980, May 1980, Sept. 1980, Oct. 1980, and Nov. 1980.
53. Ross, A. D., "Creep of Concrete Under Variable Stress," ACI Journal, Proc., Vol. 54, No. 9, March 1958, pp. 739-758.
54. Shiu, K. N., Russel, H. G., Marshall, V., and Gamble, W. L., "Time-Dependent Behaviour of Segmental Cantilever Concrete Bridges," Portland Cement Association Report to State of Illinois, Department of Transportation, Oct. 1979 (limited circulation).
55. "Standard Method of Test for Creep of Concrete in Compression," C512-69, American Society for Testing and Materials, Philadelphia, Pa.
56. "Standard Test Method for Compressive Strength of Cylindrical Concrete Specimens," C39-72, American Society for Testing and Materials, Philadelphia, Pa.
57. Troxell, G. E., Raphael, J. M., and Davis, R. E., "Long-Time Creep and Shrinkage Tests of Plain and Reinforced Concrete," Proceedings, ASTM 58, 1958, pp. 1101-1120.
58. van Zyl, S. F., "Analysis of Curved Segmentally Erected Prestressed Concrete Box Girder Bridges," Report No. UC SESM78-2, University of California at Berkeley, Jan. 1978.
59. Zienkiewicz, O. C., and Watson, M., "Some Creep Effects in Stress Analysis with Particular Reference to Concrete Pressure Vessels," Nuclear Engineering and Design, No. 4, 1966, pp. 406-412.

Table 4.1: Comparison of the Time-Dependent Change of Concrete Strain Predicted by the Three Analyses

Segment	Position of Fiber	Analysis 1	Analysis 2	Analysis 3
SB1-N1	Top	1	0.77	0.55
	Bottom	1	0.83	0.53
SB1-N9	Top	1	0.88	0.61
	Bottom	1	0.93	0.58
SB1-N16	Top	1	1.02	0.67
	Bottom	1	0.98	0.64

Note: The time period considered above corresponds to the time period defined by the time at which continuity of intermediate structure 9 was established up to the time up to which the analyses were carried.

All changes of strain are expressed as fractions of the changes predicted by Analysis 1.

Table 4.2: Measured Change in Deflection of Segment SB1-N16

Time (Days)	Deflection of Segment SB1-N16 (in.)
0	0
13	0.40
91	0.78
174	0.72
260	0.84
288	0.85
538	1.38

Note: All changes in deflection are taken relative to the deflection at day 0.

Day 0 corresponds to the time at which the final structure was completed.

The failure of the joints between the segments was discovered just prior to day 13.

1 in. = 25.4 mm.

Table 5.1: Total Prestressing Force and Prestress Loss as Predicted by Analysis 1, Analysis 2 and Analysis 3

Segment	Analysis	Prestress Loss (%)	Final Prestress Force as a Fraction of the Value Calculated by Analysis 1	
SB1-N1	1	8.7	1	(11,068 kips)*
	2	7.1	1.01	
	3	5.6	1.04	
SB1-N9	1	8.6	1	(6,020 kips)*
	2	7.9	1.01	
	3	6.1	1.03	
SB1-N16	1	9.6	1	(5,628 kips)*
	2	9.4	1.00	
	3	7.4	1.03	

Note: The prestress losses refer to the time-dependent component of prestress loss that occurred during the time period defined by the time at which the continuity tendons for intermediate structure 9 were stressed up to the time up to which the analyses were carried. These losses are expressed as percentages of the values that existed just after the continuity tendons for intermediate structure 9 were stressed.

The final values of prestressing force refer to the values existing at the time up to which the analyses were carried.

* Final Force from Analysis 1.

1 kip = 4.448 kN.

Table 5.2: Total Prestress Losses Due to Shrinkage,
Creep and Relaxation

Segment	Analysis	Prestress Loss Due To:		
		Shrinkage (kips)	Creep (kips)	Relaxation (kips)
SB1-N1	1	183	587	403
	2	241	440	398
	3	143	303	418
SB1-N9	1	100	292	223
	2	137	226	219
	3	80	157	226
SB1-N16	1	80	374	208
	2	123	308	203
	3	73	213	214

Note: 1 kip = 4.448 kN

Table 5.3: Redistribution of Support Moments for the Time Period Corresponding to the Final Structure

Pier	Analysis	Bending Moment (k-ft)		Change in Bending Moment (%)
		Time at Completion of Final Structure	Time up to which Analysis was Carried	
1	1	81,352	72,394	11.0
	2	81,247	74,926	7.8
	3	81,125	73,957	8.8
2	1	76,880	72,459	5.8
	2	76,724	74,371	3.1
	3	79,130	75,205	5.0
3	1	78,461	73,095	6.8
	2	77,776	74,975	3.6
	3	79,582	75,360	5.3
4	1	76,520	72,105	5.8
	2	77,402	74,958	3.2
	3	78,779	75,059	4.7

Note: The analysis was continued for 600 days after the final structure was completed.

1 k-ft = 1.356 kN-m

Table 5.4: Redistribution of Mid-Span Moments for the Interior Spans for the Time Period Corresponding to the Final Structure

Span	Analysis	Bending Moment (k-ft)		Change in Bending Moment (%)
		Time at Completion of Final Structure	Time up to which Analysis was Carried	
2	1	15,994	22,706	42.0
	2	16,124	20,478	27.0
	3	14,982	20,547	37.1
3	1	17,441	22,328	28.0
	2	17,864	20,435	14.4
	3	15,753	19,823	25.8
4	1	17,605	22,509	27.9
	2	17,505	20,135	15.0
	3	15,910	19,891	25.0

Note: The analysis was continued for 600 days after the final structure was completed.

1 k-ft = 1.356 kN-m

Table 5.5: Change of Concrete Stress for the Time Period
Corresponding to the Final Structure

Segment	Analysis	Concrete Stress (ksi)				Change in Stress (%)	
		Time at Completion of Final Structure		Time up to which Analysis was Carried		Top Fiber	Bottom Fiber
		Top Fiber	Bottom Fiber	Top Fiber	Bottom Fiber		
SB1-N1	1	0.49	1.36	0.55	1.17	12.2	14.0
	2	0.47	1.36	0.52	1.23	10.6	9.6
	3	0.51	1.35	0.58	1.20	13.7	11.1
SB1-N9	1	0.40	0.81	0.52	0.53	30.0	34.6
	2	0.39	0.80	0.47	0.61	20.5	23.8
	3	0.39	0.82	0.50	0.60	28.2	26.8
SB1-N16	1	0.26	0.96	0.39	0.65	50.0	32.3
	2	0.26	0.93	0.35	0.73	34.6	21.5
	3	0.24	0.99	0.35	0.76	45.8	23.2

Note: All the stresses are compressive.

The analysis was continued for 600 days after the final structure was completed.

$$1 \text{ ksi} = 6.895 \text{ N/mm}^2.$$

Table 5.6: Percentage Difference in the Final Results Predicted by Analysis 1 and Analysis 4

Segment	Concrete Strain		Concrete Stress		Prestressing Force	Bending Moment
	Top Fiber	Bottom Fiber	Top Fiber	Bottom Fiber		
SBI-N1	- 3.28	2.45	0.73	- 0.09	0.27	- 0.06
SBI-N9	- 2.75	3.29	0.19	- 0.19	0.03	- 1.14
SBI-N16	- 0.84	0.59	0.00	- 0.15	- 0.05	- 0.01

Note: The final results refer to the predicted results at the time up to which the analyses were carried.

A negative sign indicates a decrease in the particular quantity as predicted by Analysis 4 relative to the result predicted by Analysis 1.

All percentages are based on the final values predicted by Analysis 1.

Table 5.7: Effect on Free Cantilever Tip Deflection Due to Application and Removal of Construction Loads

Time	Deflection Predicted by Analysis 1 (in.)	Deflection Predicted by Analysis 4 (in.)
Just prior to application of construction loads	1.626	1.626
Just after application of construction loads	1.626	2.272
Just prior to removal of construction loads	3.235	4.277
Just after removal of construction loads	3.235	3.607

Note: Downward deflections are taken positive.

1 in. = 25.4 mm.

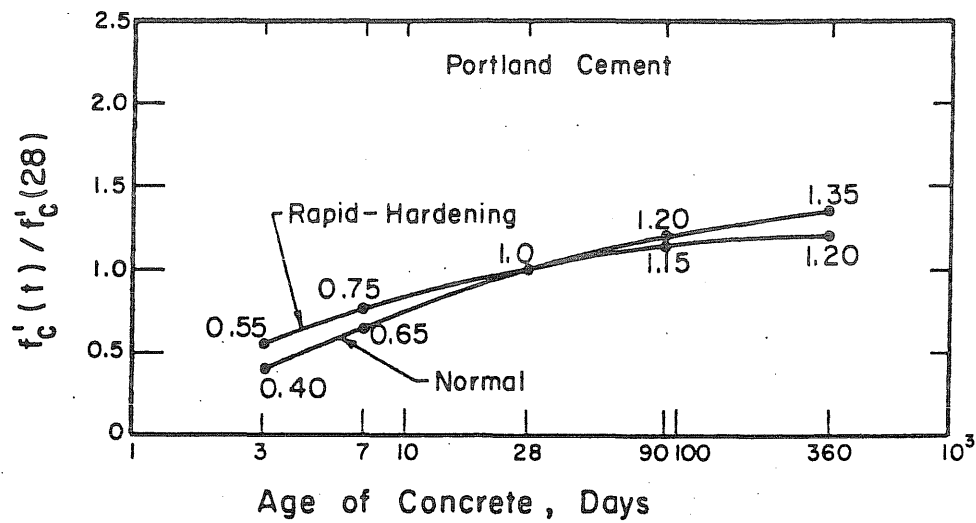


Fig. 2.1 Ratio of Compressive Strength at Age t to that at 28 Days According to European Concrete Committee

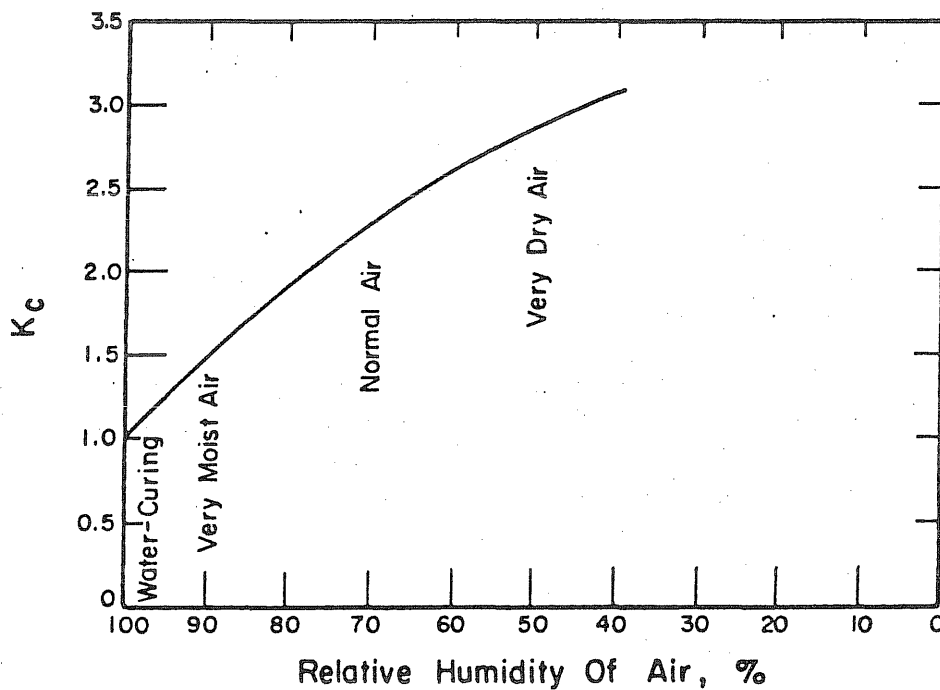


Fig. 2.2 European Concrete Committee Creep Prediction Factor Coefficient K_c vs. Relative Humidity

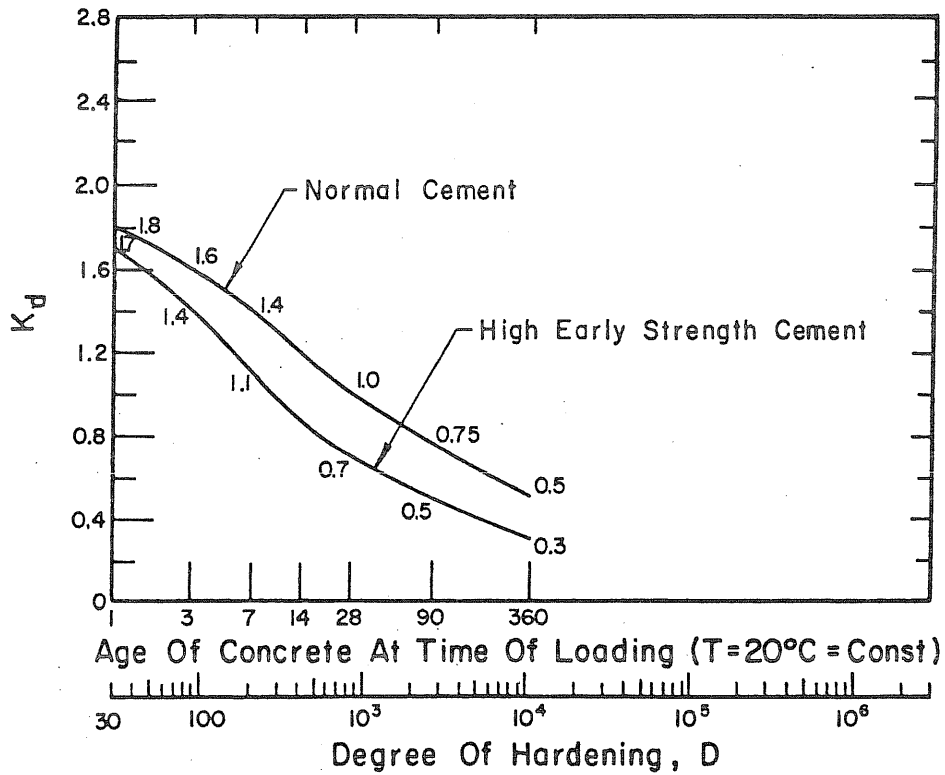


Fig. 2.3 European Concrete Committee Creep Prediction Factor Coefficient K_d vs. Age at Loading

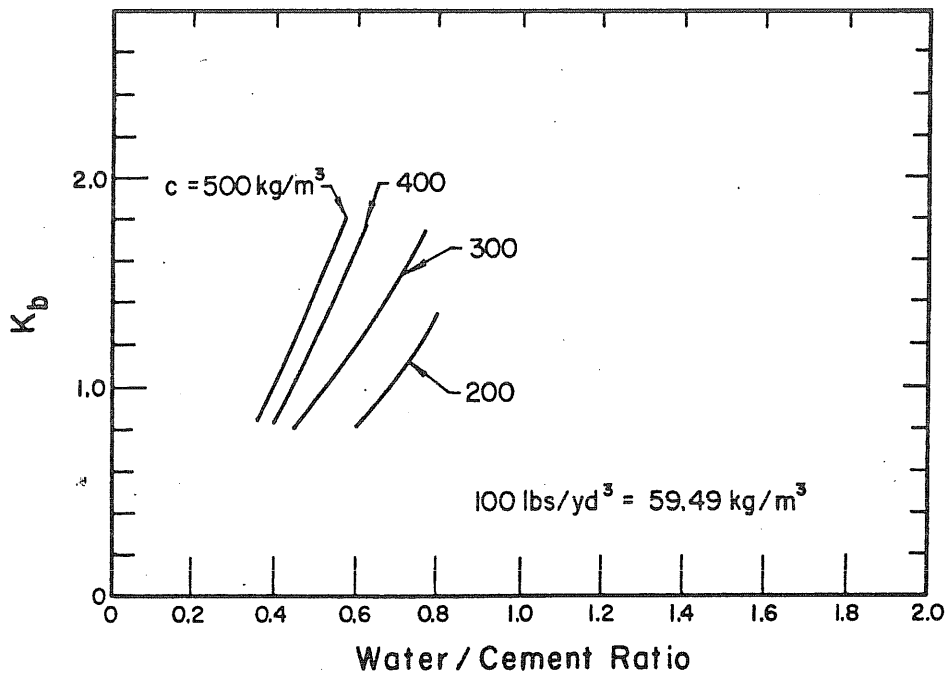


Fig. 2.4 European Concrete Committee Creep Prediction Factor Coefficient K_b vs. Mix Properties

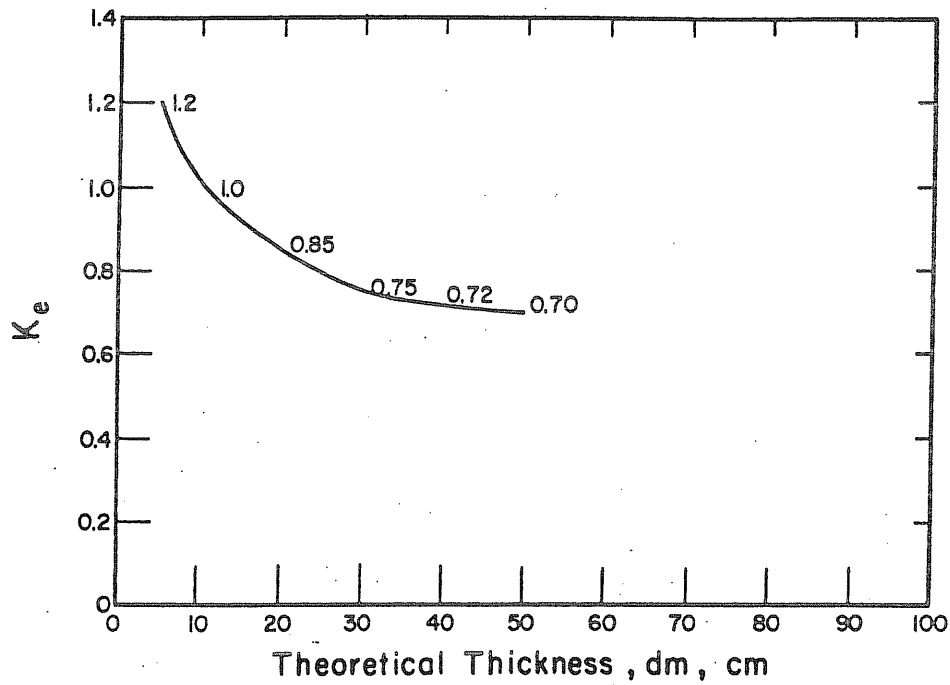


Fig. 2.5 European Concrete Committee Creep Prediction Factor Coefficient K_e vs. Theoretical Thickness

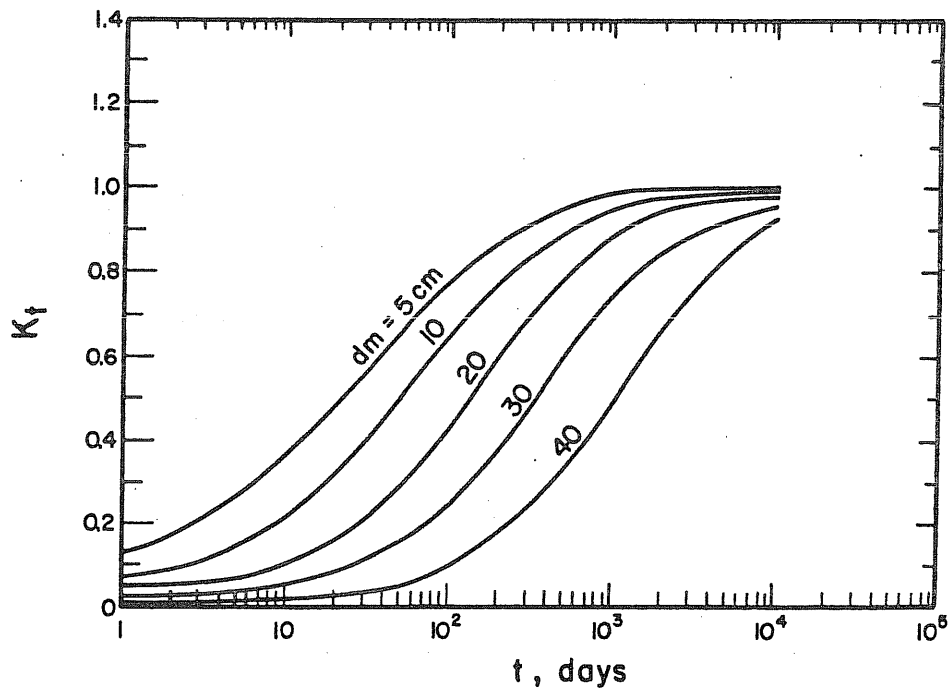


Fig. 2.6 European Concrete Committee Creep Prediction Factor Coefficient K_t vs. Time

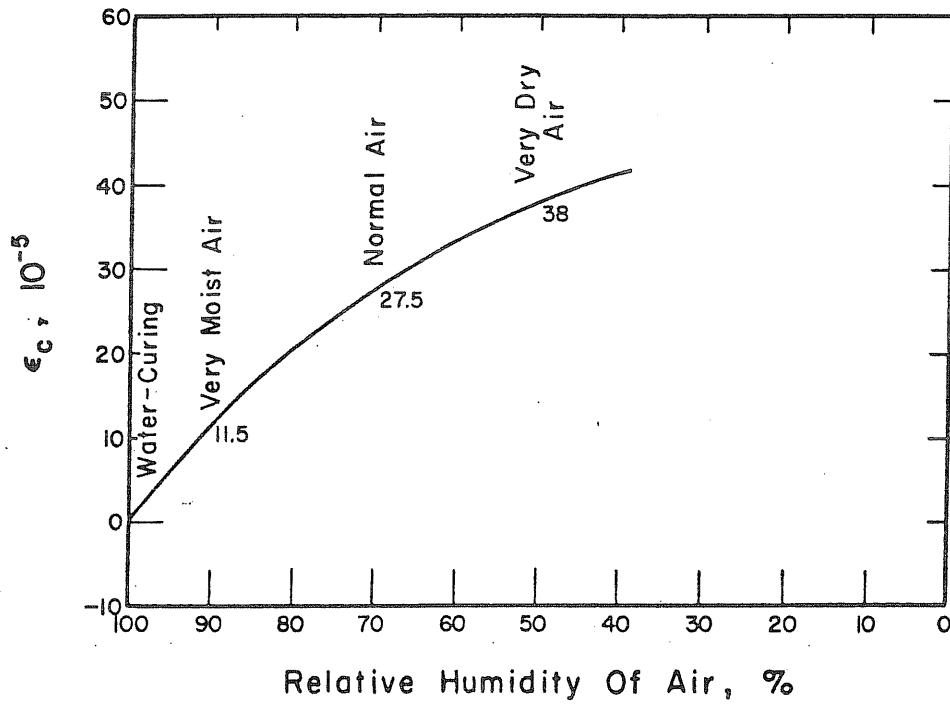


Fig. 2.7 European Concrete Committee Shrinkage Prediction Factor Coefficient ϵ_c vs. Relative Humidity

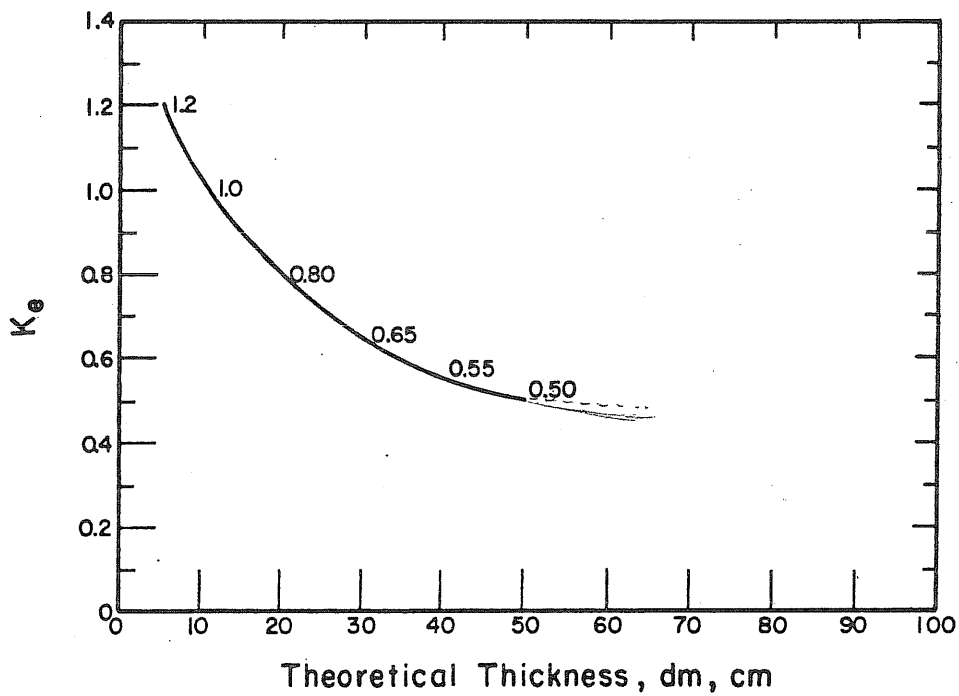


Fig. 2.8 European Concrete Committee Shrinkage Prediction Factor Coefficient K_e vs. Theoretical Thickness

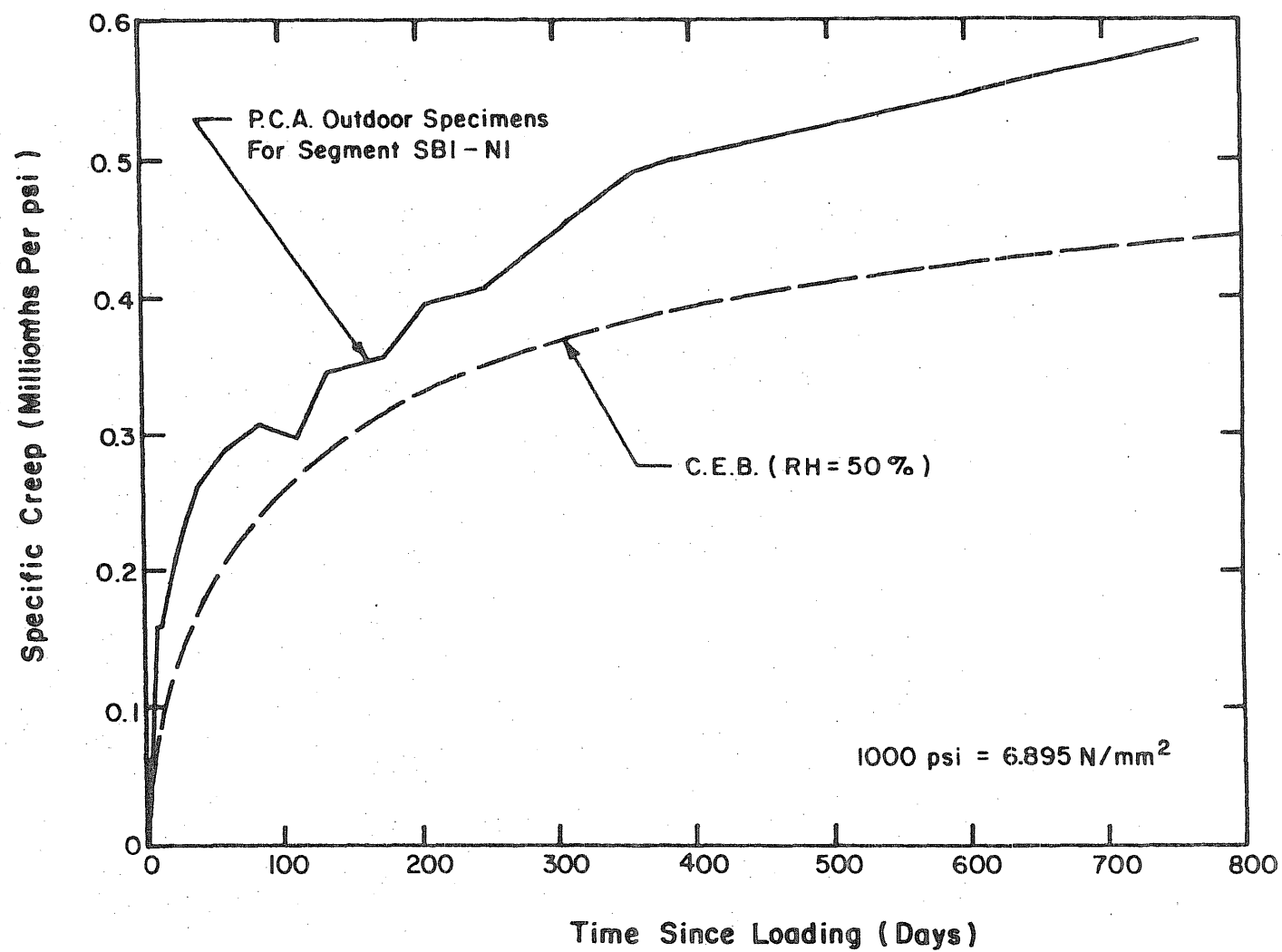


Fig. 2.9 Measured and Predicted Specific Creep Curves for Outdoor Stored Creep Specimens (Segment SBI-N1)

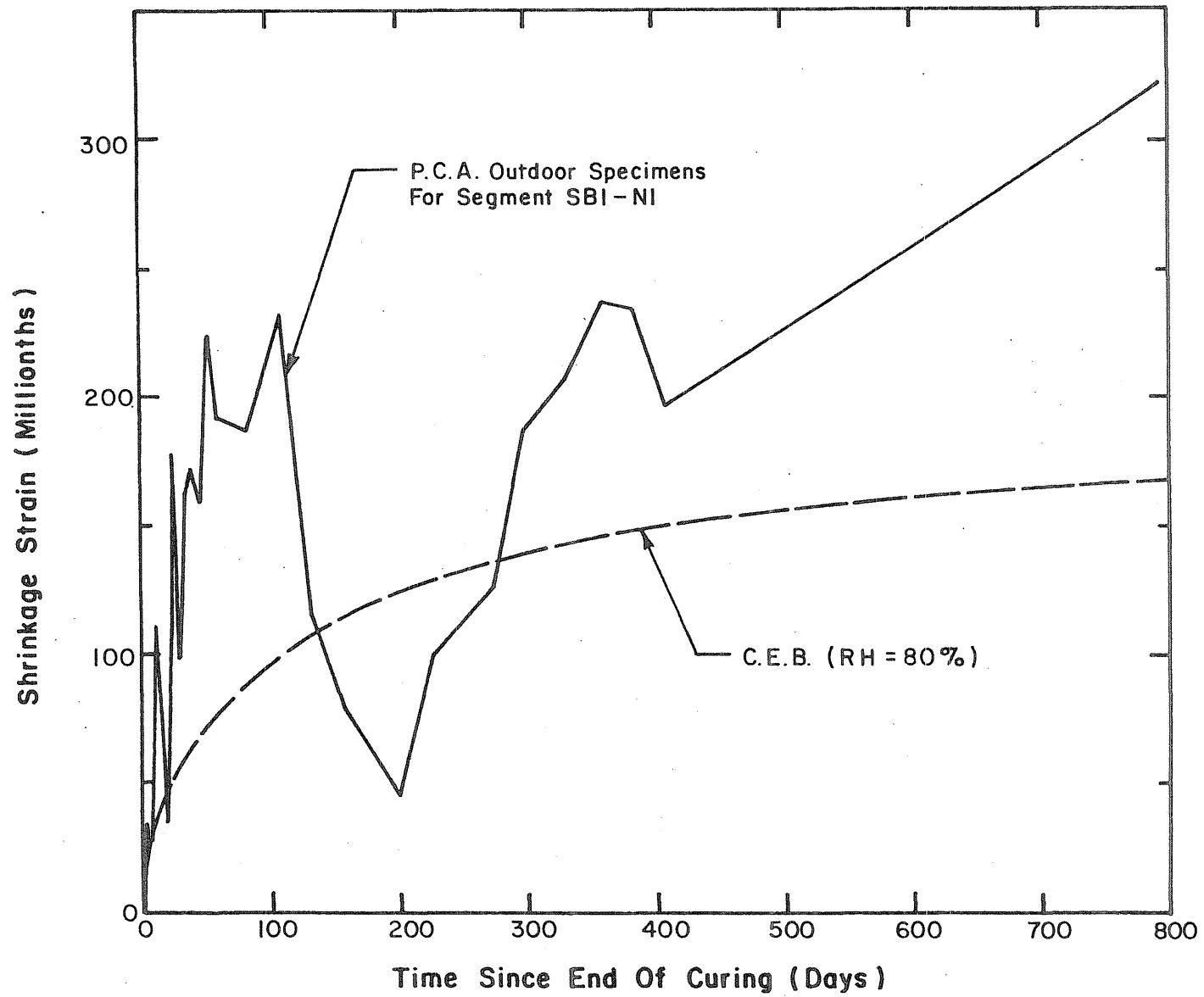


Fig. 2.10 Measured and Predicted Shrinkage Curves for Outdoor Stored Shrinkage Specimens (Segment SB1-N1)

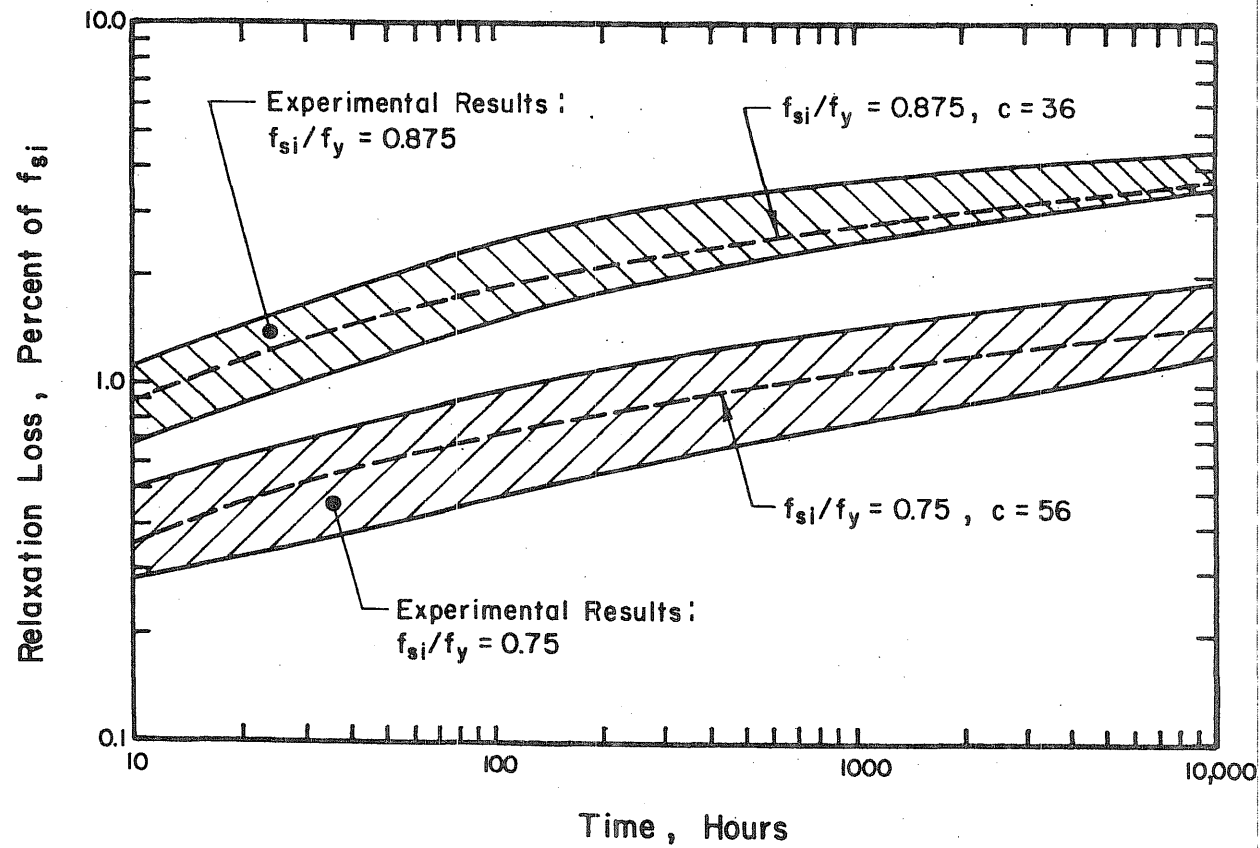


Fig. 2.11 Fit of Eq. 2.9 to Experimentally Obtained Relaxation Data for Dywidag Bars

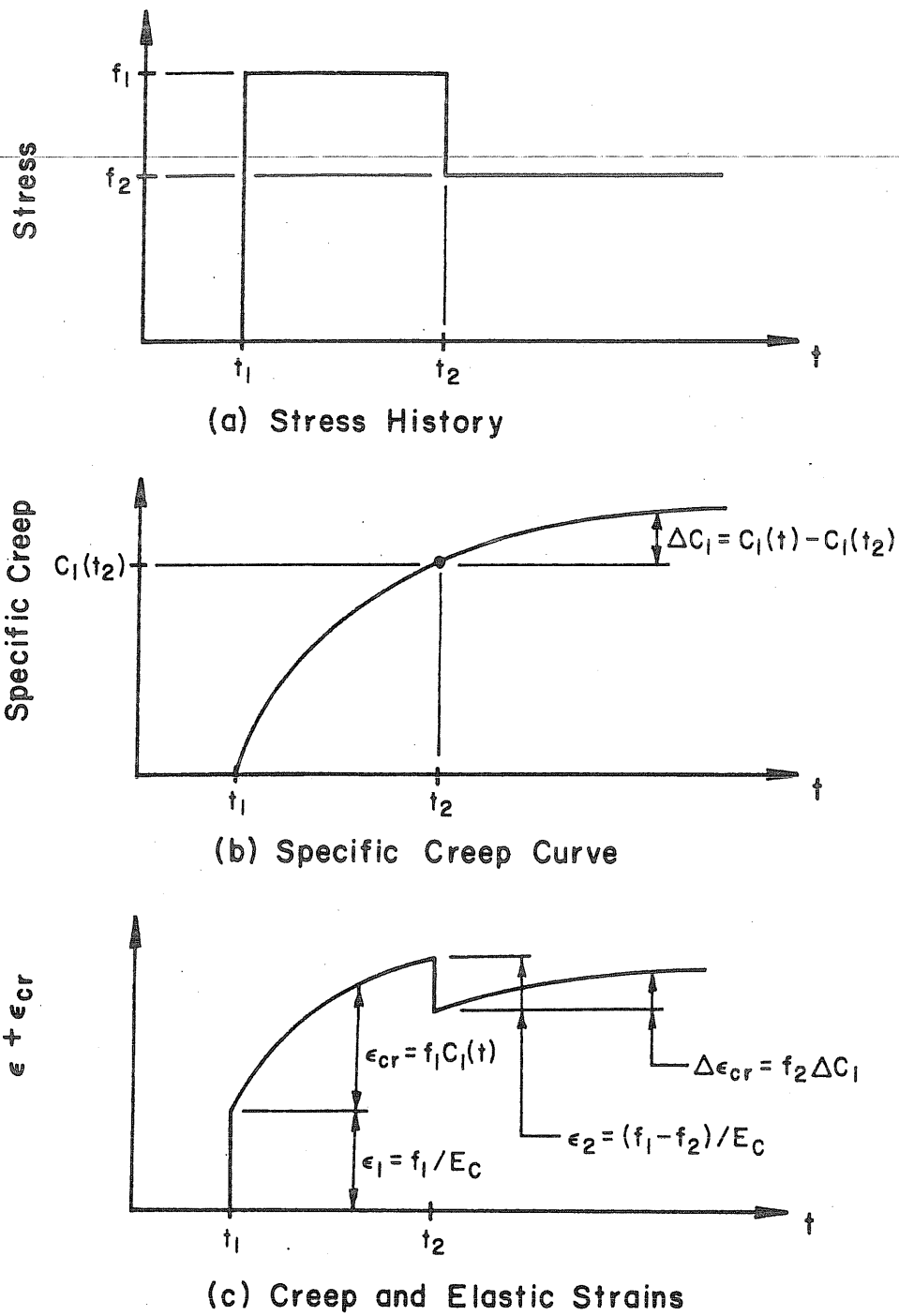


Fig. 3.1 Prediction of Creep Under Variable Stress According to the Rate of Creep Method

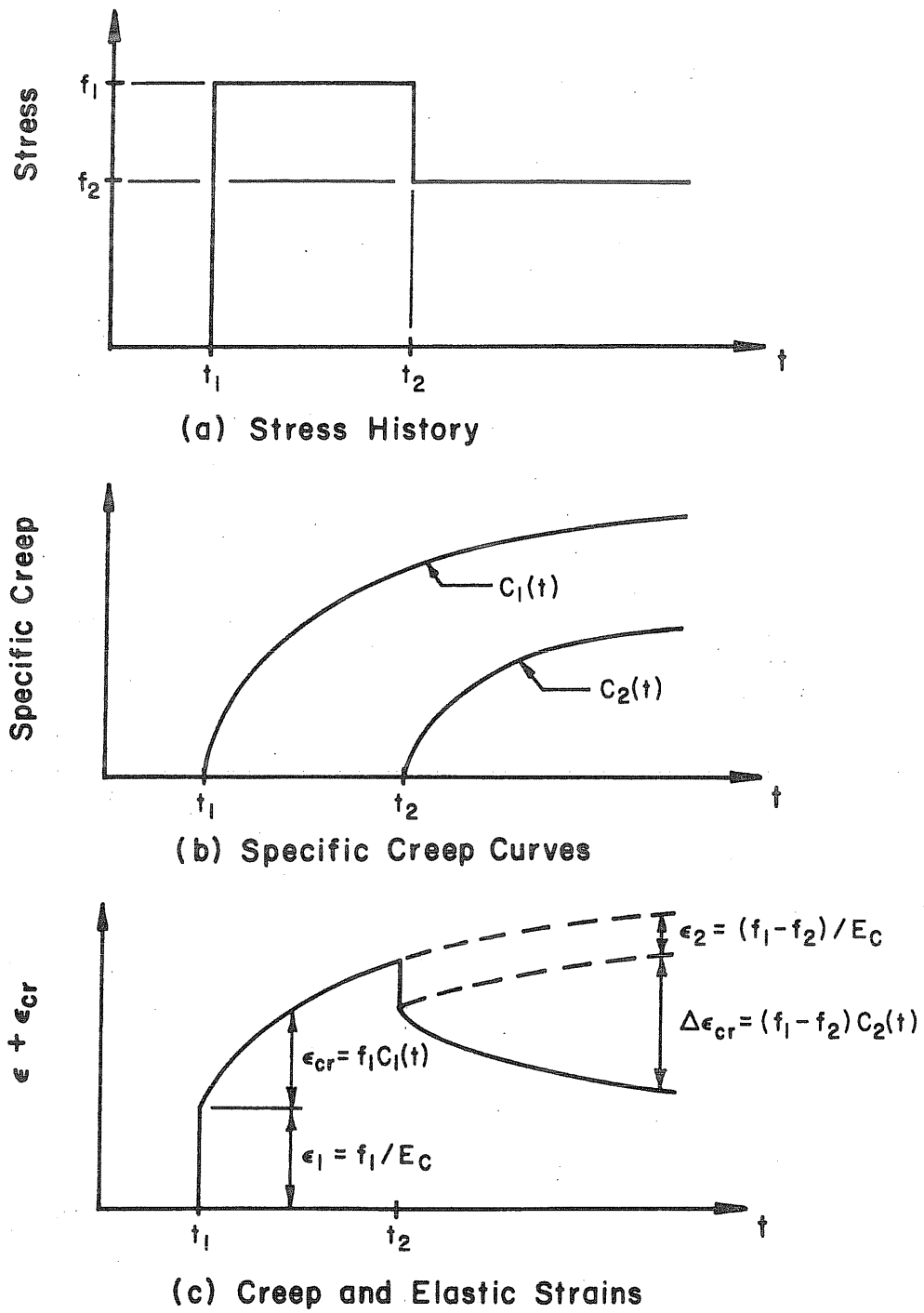
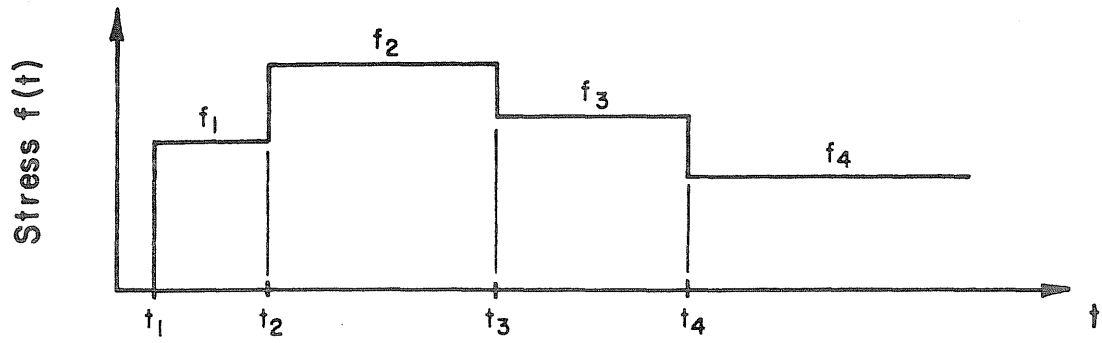
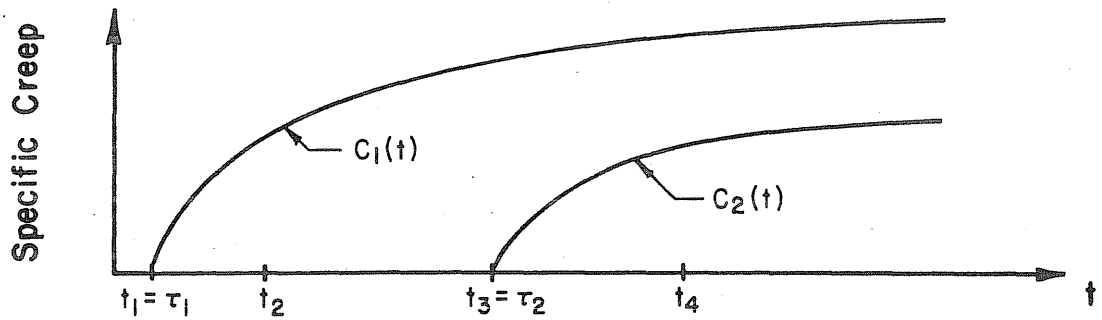


Fig. 3.2 Prediction of Creep under Variable Stress According to the Method of Superposition



(a) Stress History



(b) Specific Creep Curves

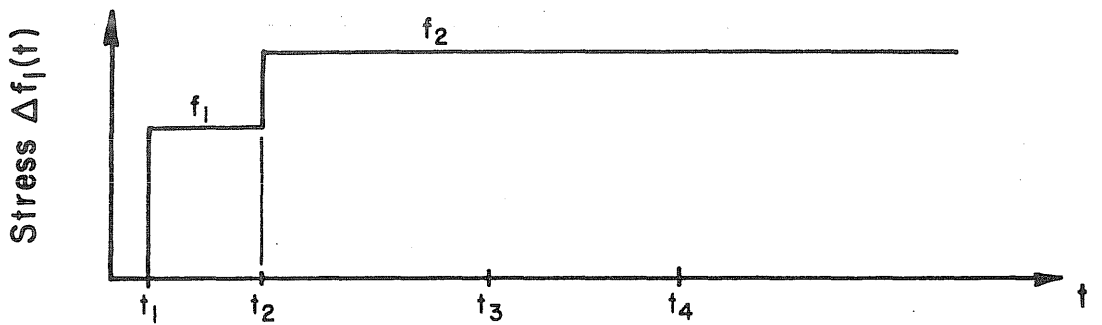
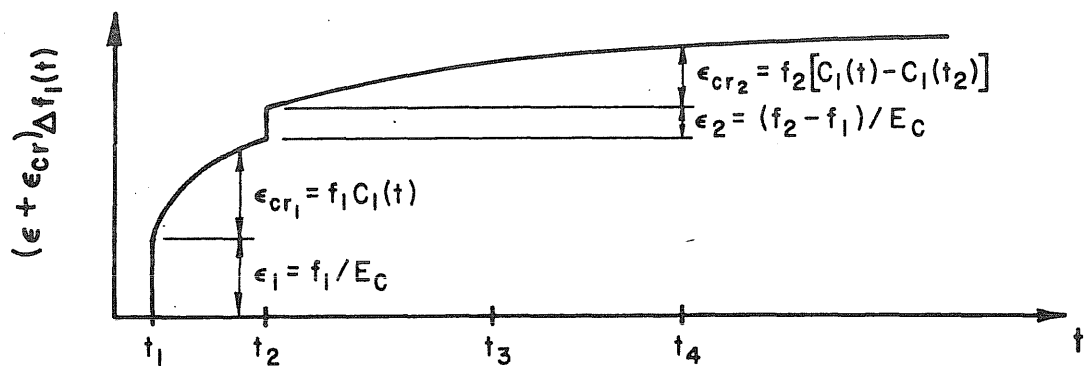
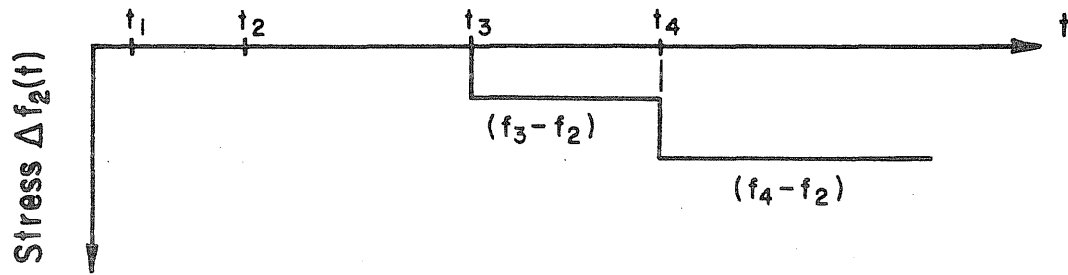
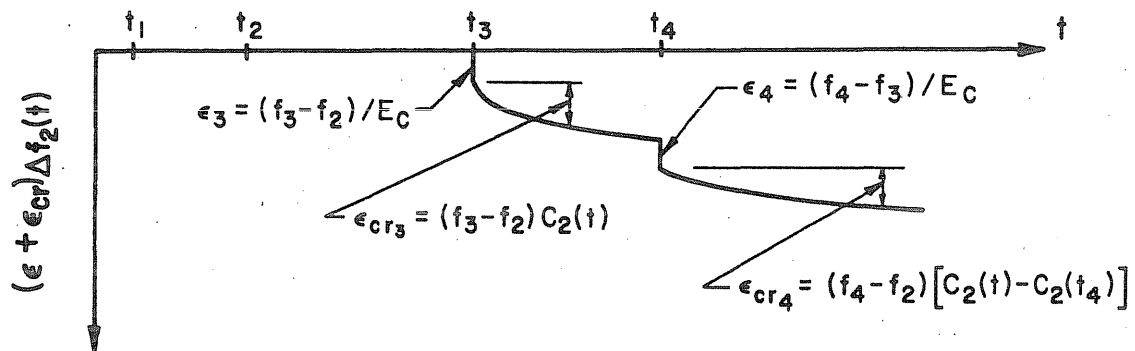
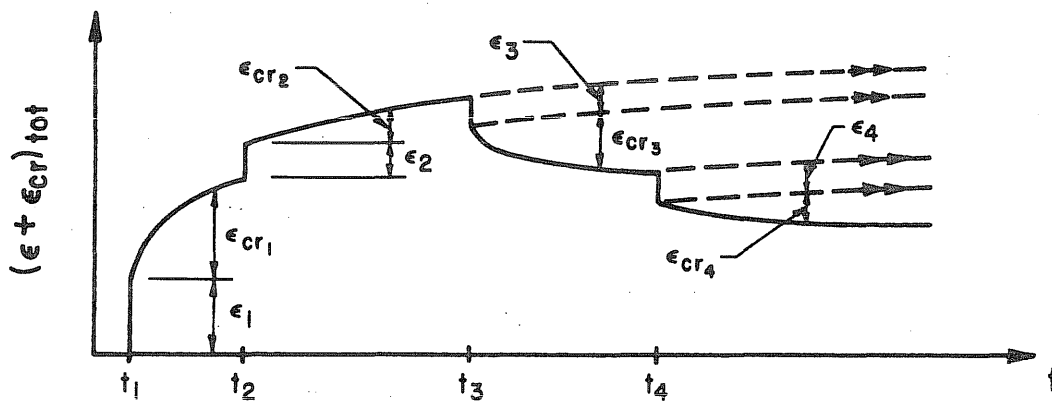
(c) Sub-History $\Delta f_1(t)$ (d) Elastic and Creep Strains Due To Sub-History $\Delta f_1(t)$

Fig. 3.3 Prediction of Creep under Variable Stress According to the Method Proposed in this Study

(e) Sub-History $\Delta f_2(t)$ (f) Elastic and Creep Strains Due To Sub-History $\Delta f_2(t)$ 

(g) Total Elastic and Creep Strains

Fig. 3.3 (Continued)

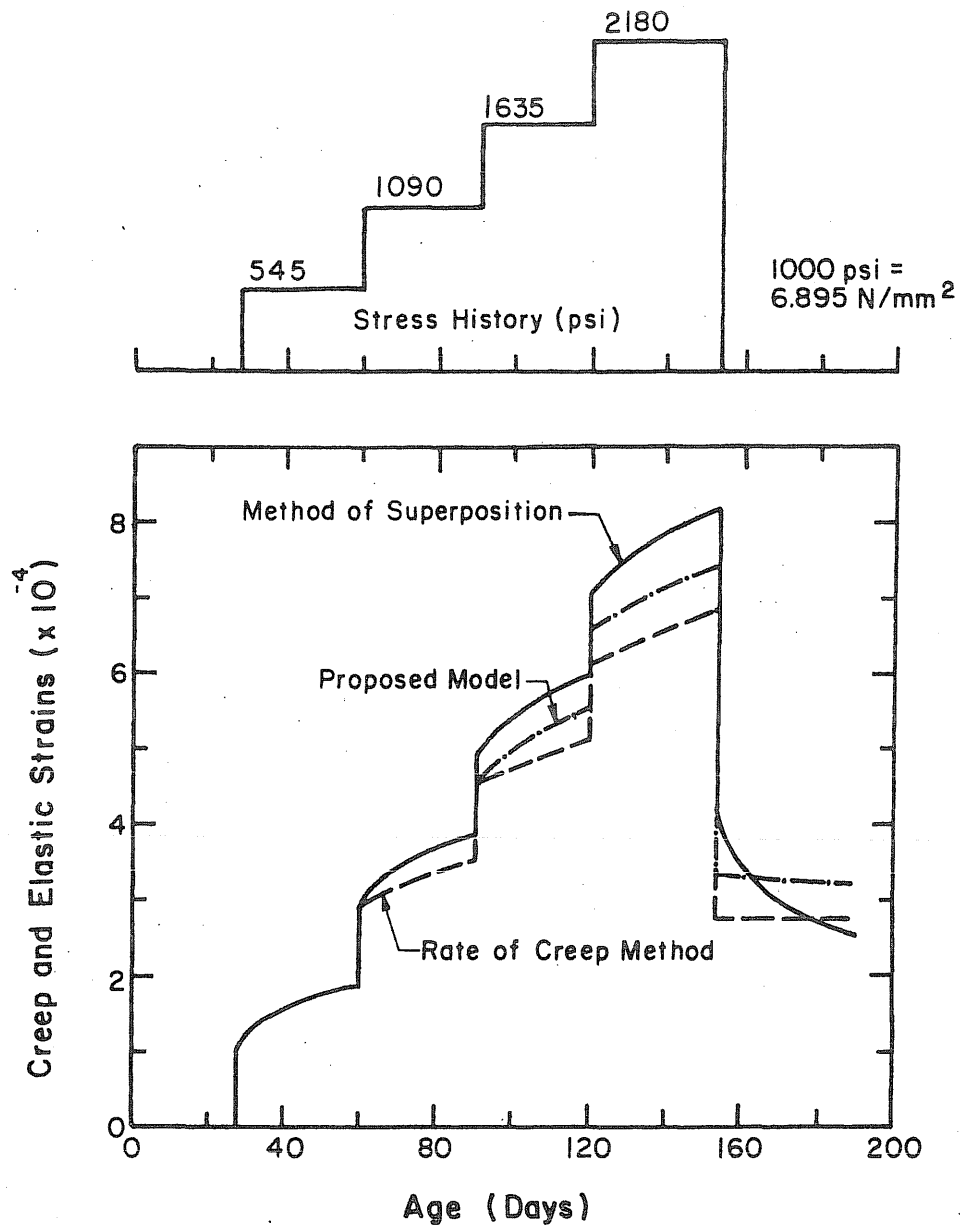


Fig. 3.4 Creep of Concrete Subjected to an Increasing Stress History as Predicted by the Rate of Creep Method, the Method of Superposition and the Method Proposed in this Study

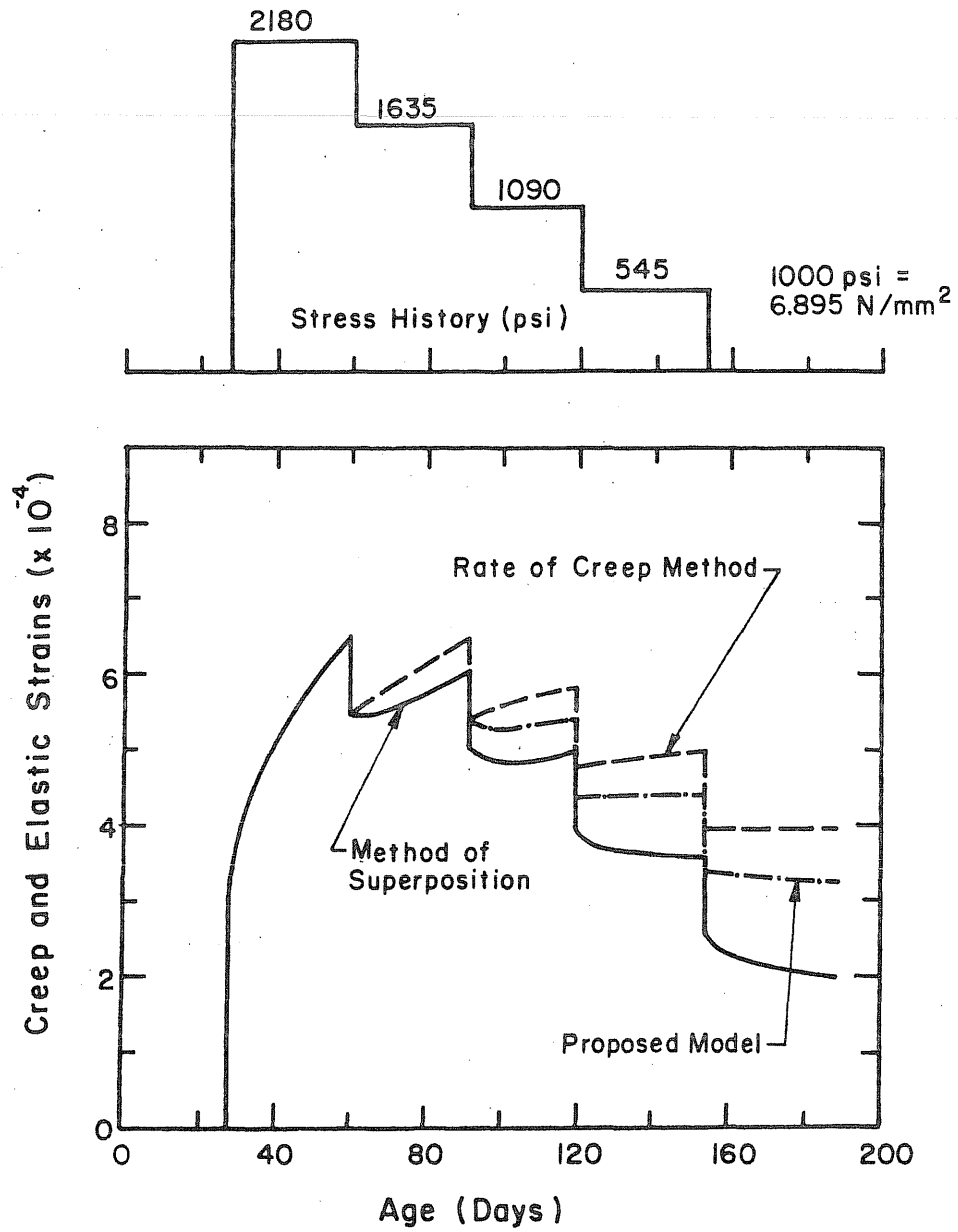


Fig. 3.5. Creep of Concrete Subjected to a Decreasing Stress History as Predicted by the Rate of Creep Method, the Method of Superposition and the Method Proposed in this Study

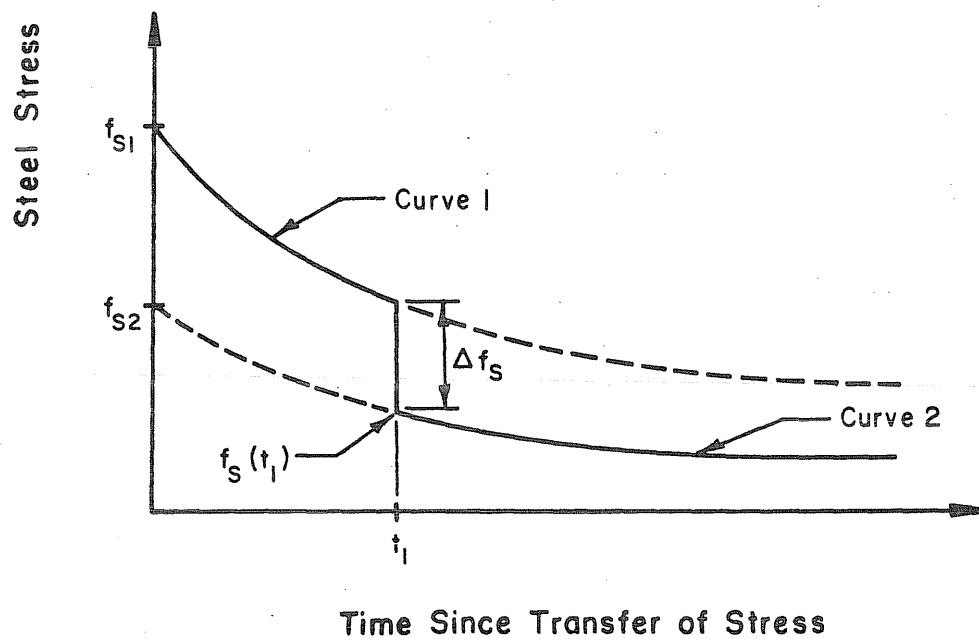


Fig. 3.6 Prediction of Steel Relaxation under a Variable State of Strain

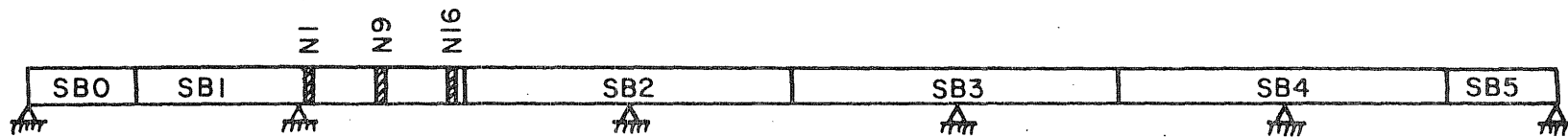


Fig. 4.1 Location of Instrumented Segments

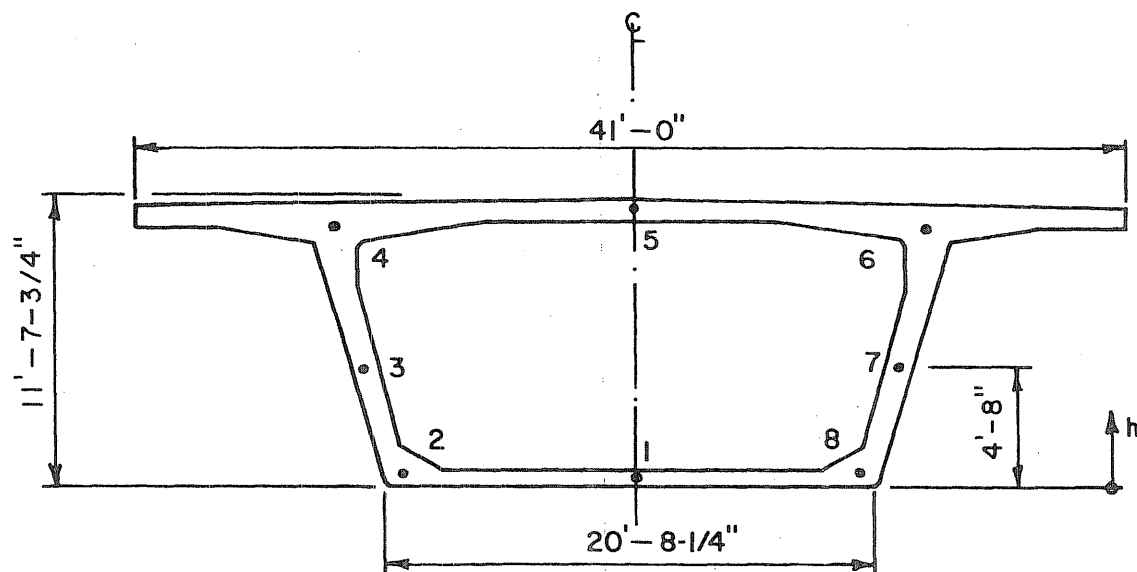


Fig. 4.2 Location of Carlson Strain Meters

1 in. = 25.4 mm
1 ft = 304.8 mm

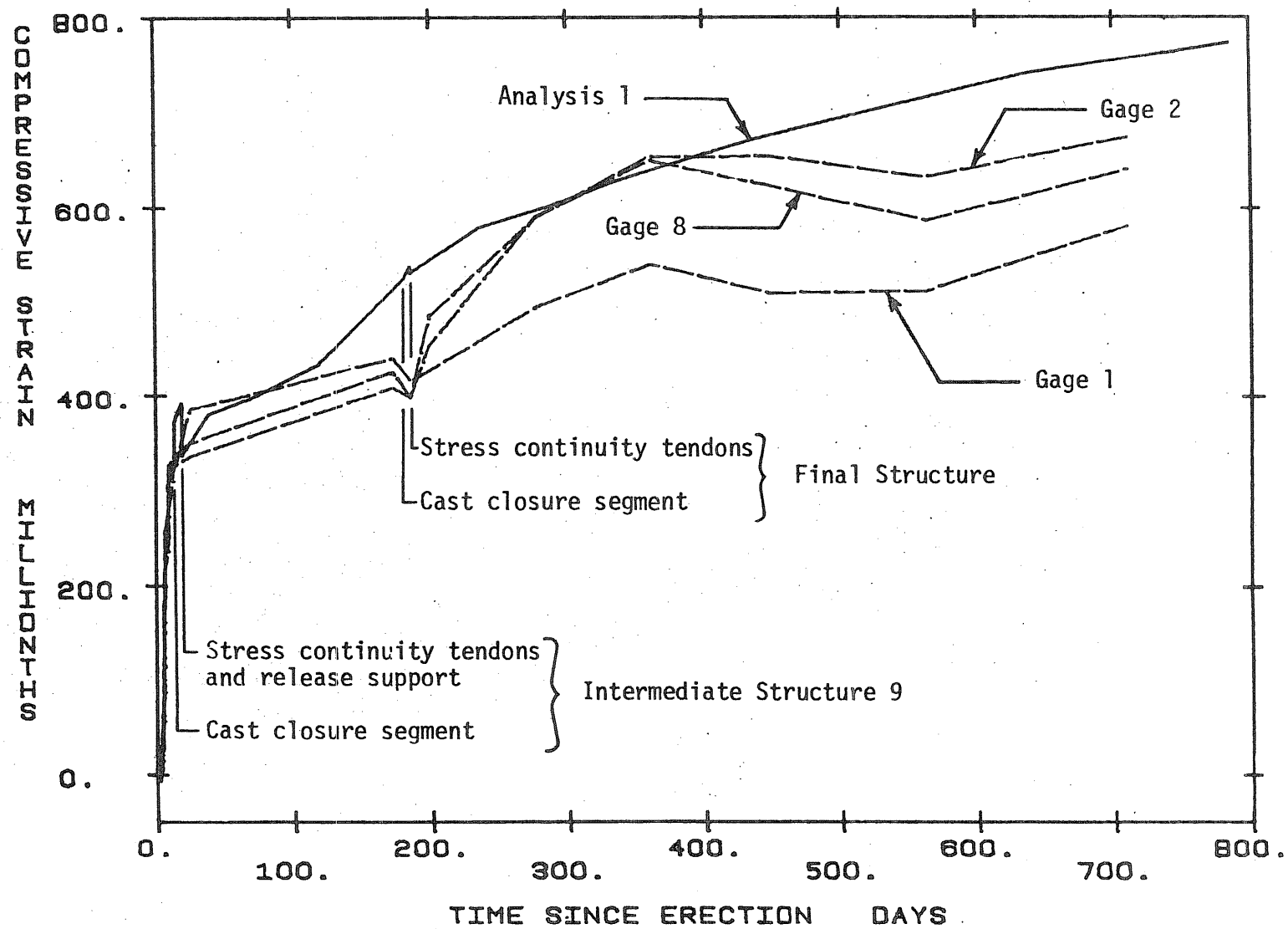


Fig. 4.3 Comparison of Measured and Calculated Concrete Strains in Bottom Flange of Segment SB1-N1 (Analysis 1, $h = 8$ in.)

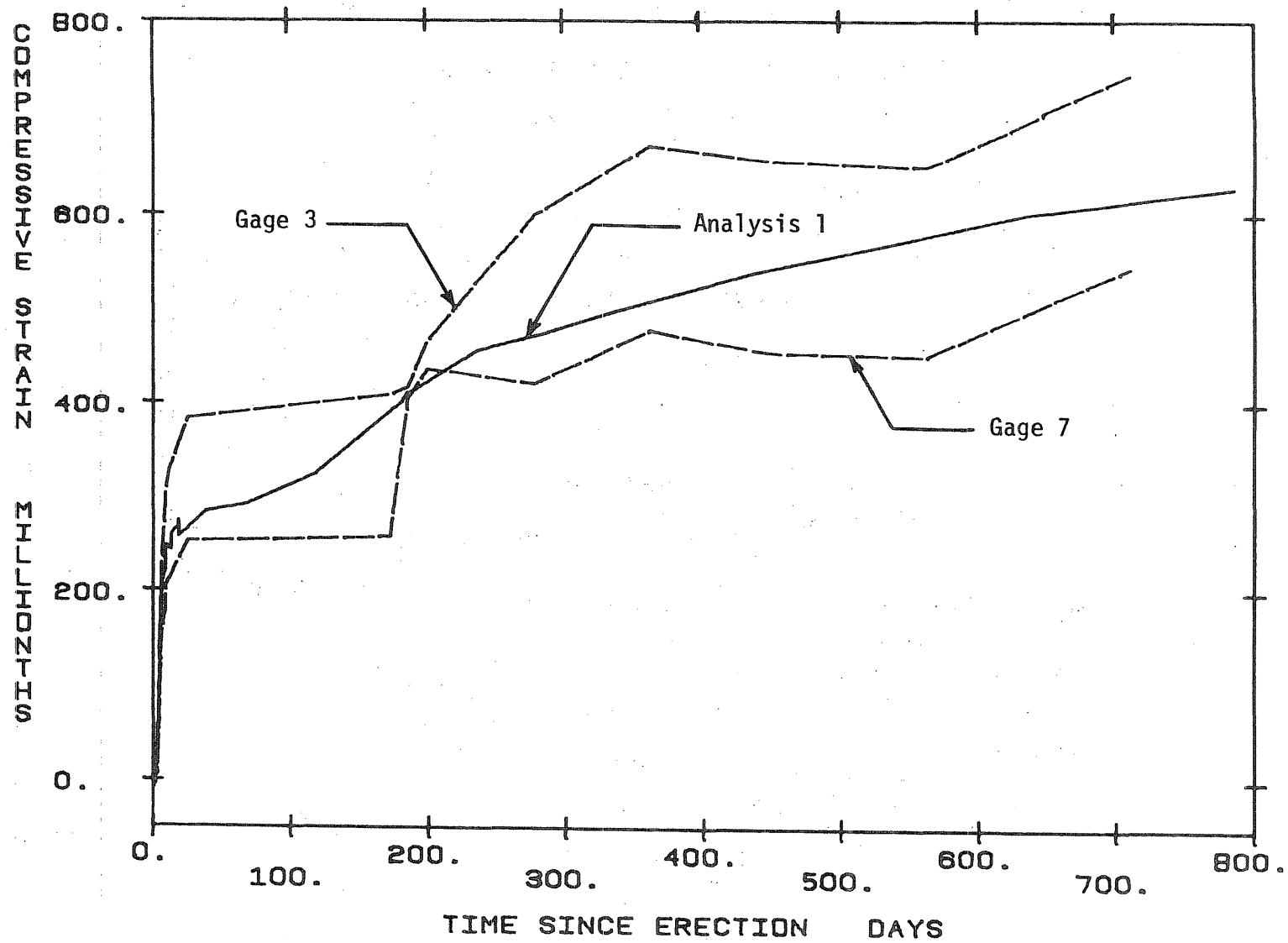


Fig. 4.4 Comparison of Measured and Calculated Concrete Strains in Webs of Segment SB1-N1 (Analysis 1, $h = 56$ in.)

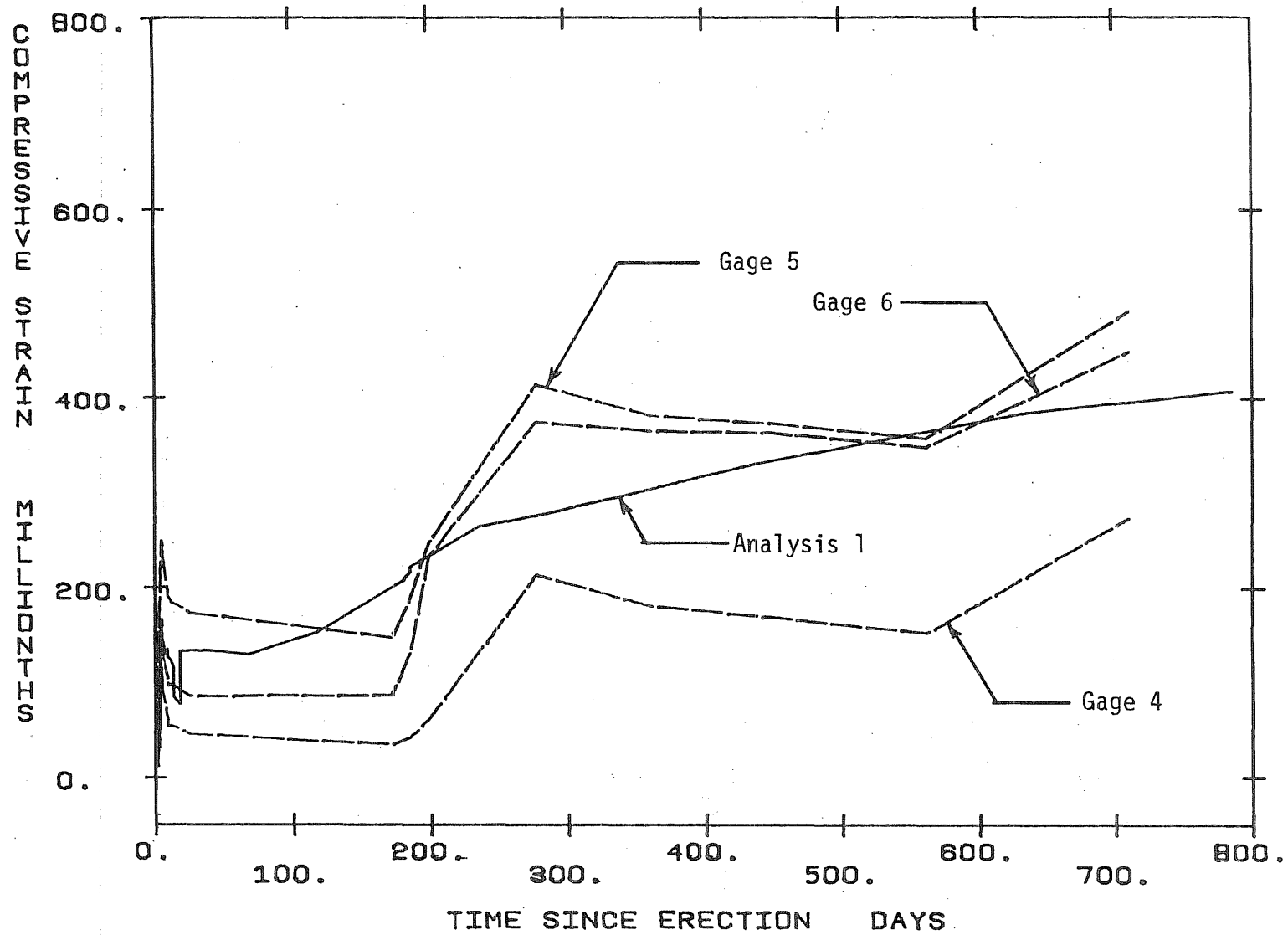


Fig. 4.5 Comparison of Measured and Calculated Concrete Strains in Top Flange of Segment SB1-N1 (Analysis 1, $h = 131$ in.)

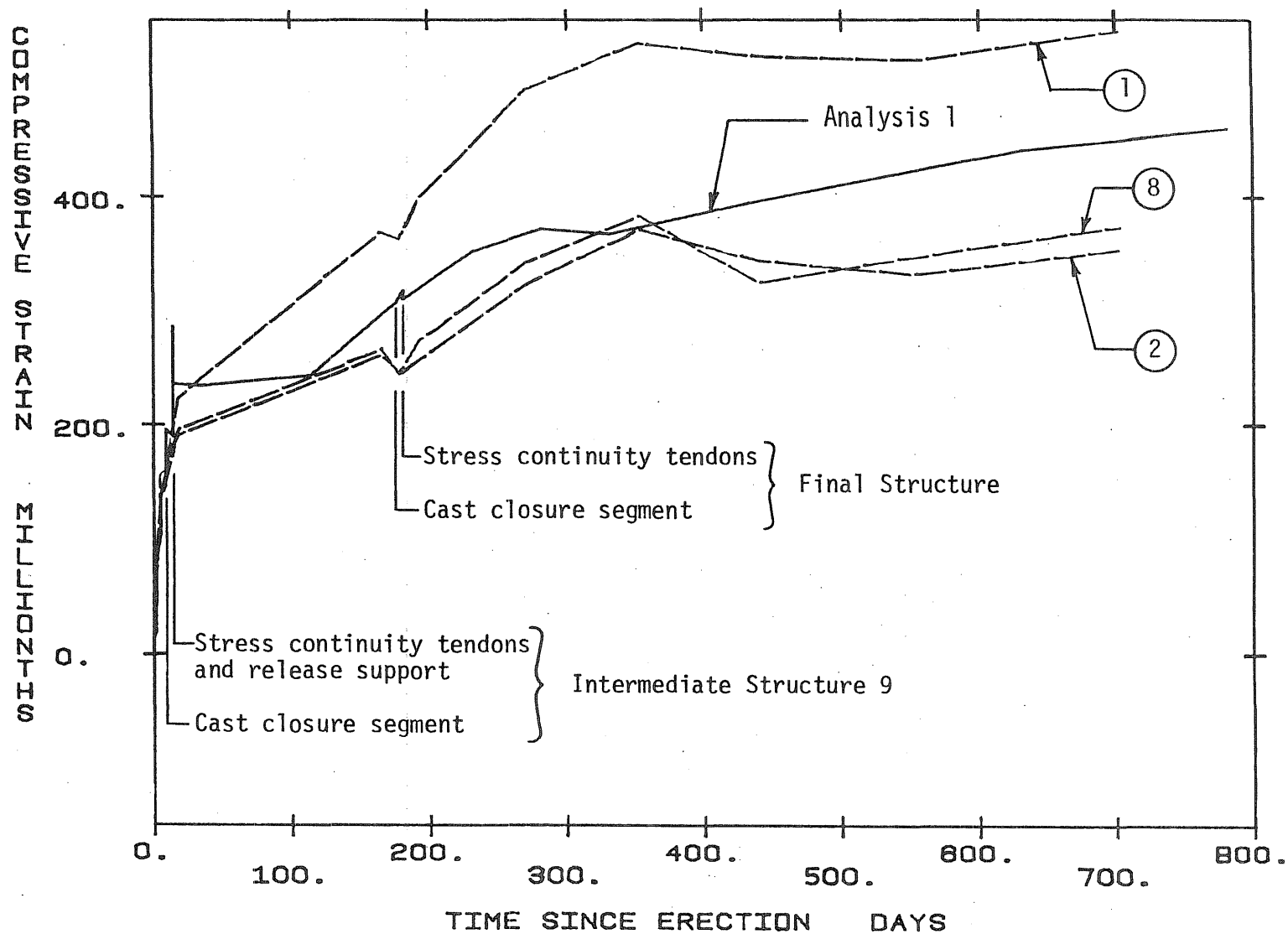


Fig. 4.6 Comparison of Measured and Calculated Concrete Strains in Bottom Flange of Segment SB1-N9 (Analysis 1, $h = 8$ in.)

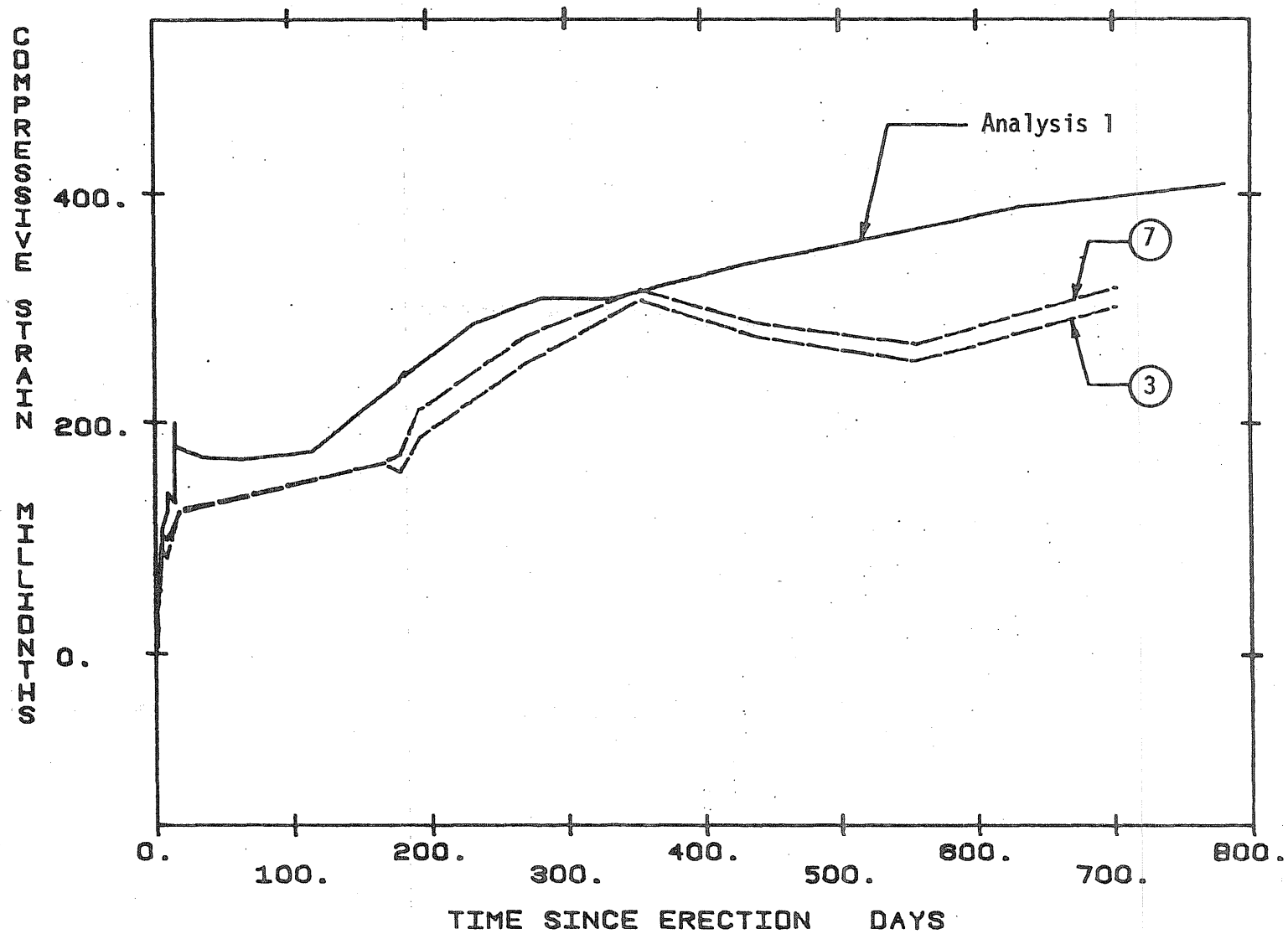


Fig. 4.7 Comparison of Measured and Calculated Concrete Strains in Webs of Segment SB1-N9. (Analysis 1, $h = 56$ in.)

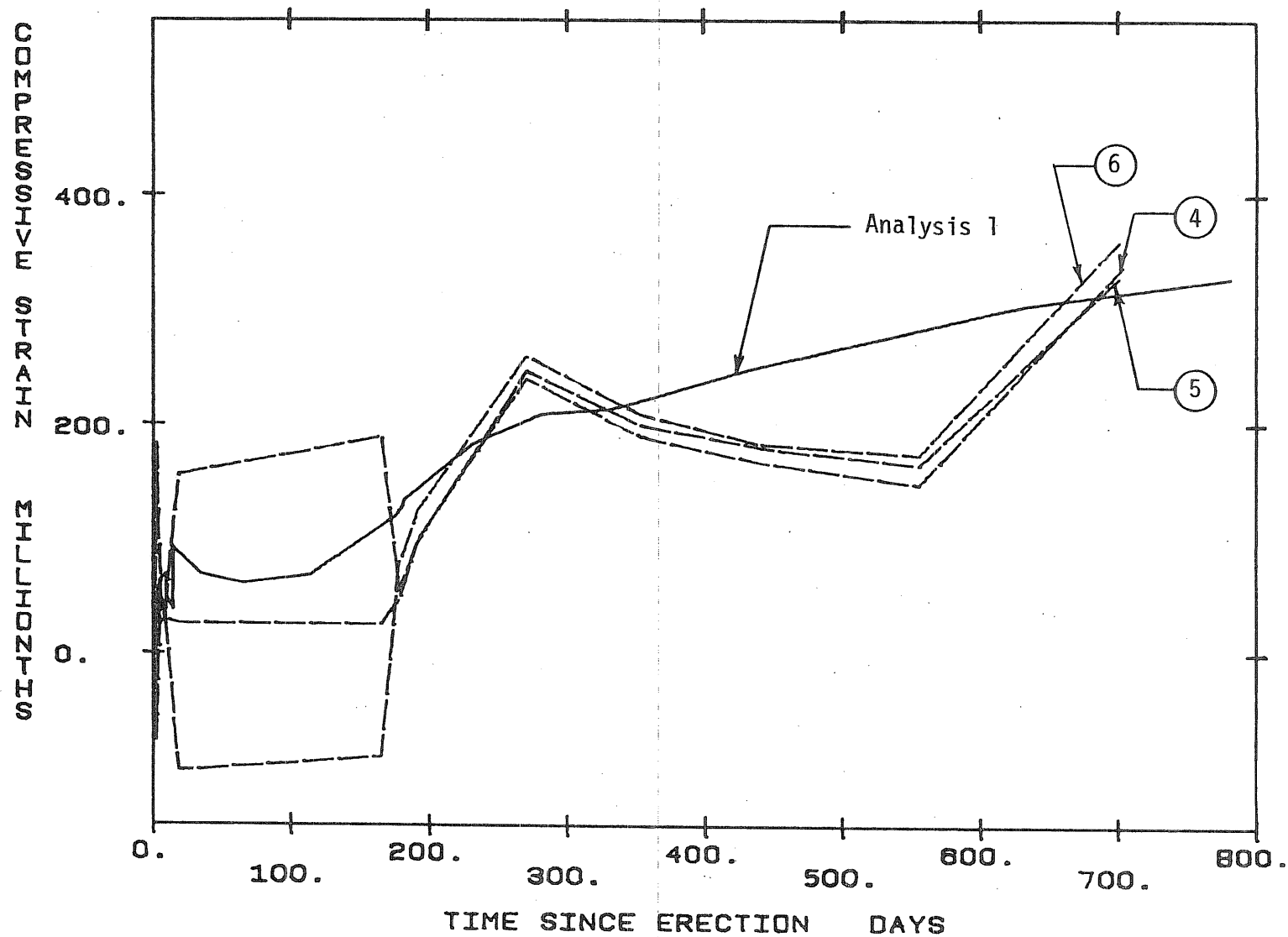


Fig. 4.8 Comparison of Measured and Calculated Concrete Strains in Top Flange of Segment SBI-N9 (Analysis 1, $h = 131$ in.)

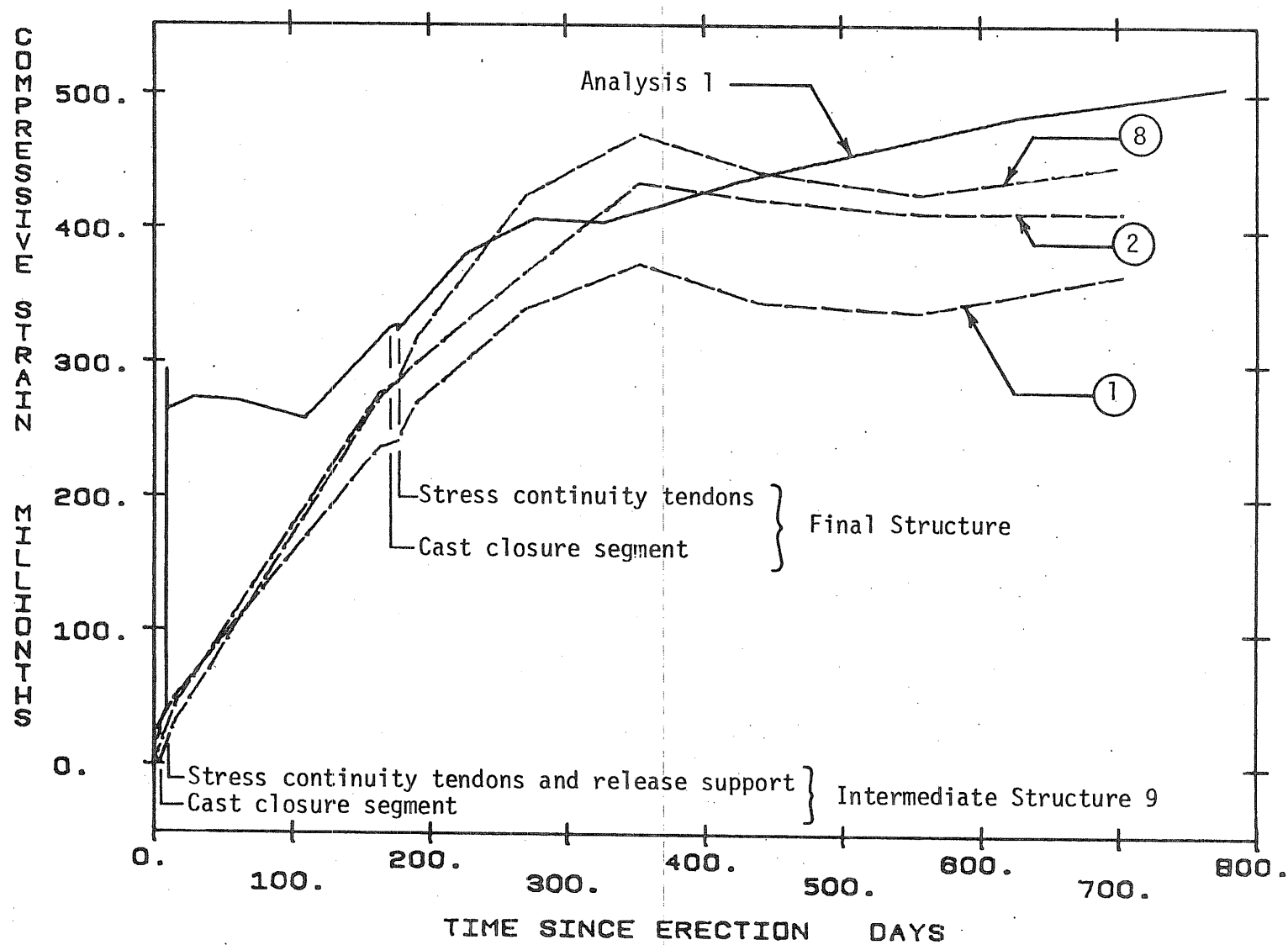


Fig. 4.9 Comparison of Measured and Calculated Concrete Strains in Bottom Flange of Segment SB1-N16 (Analysis 1, $h = 8$ in.)

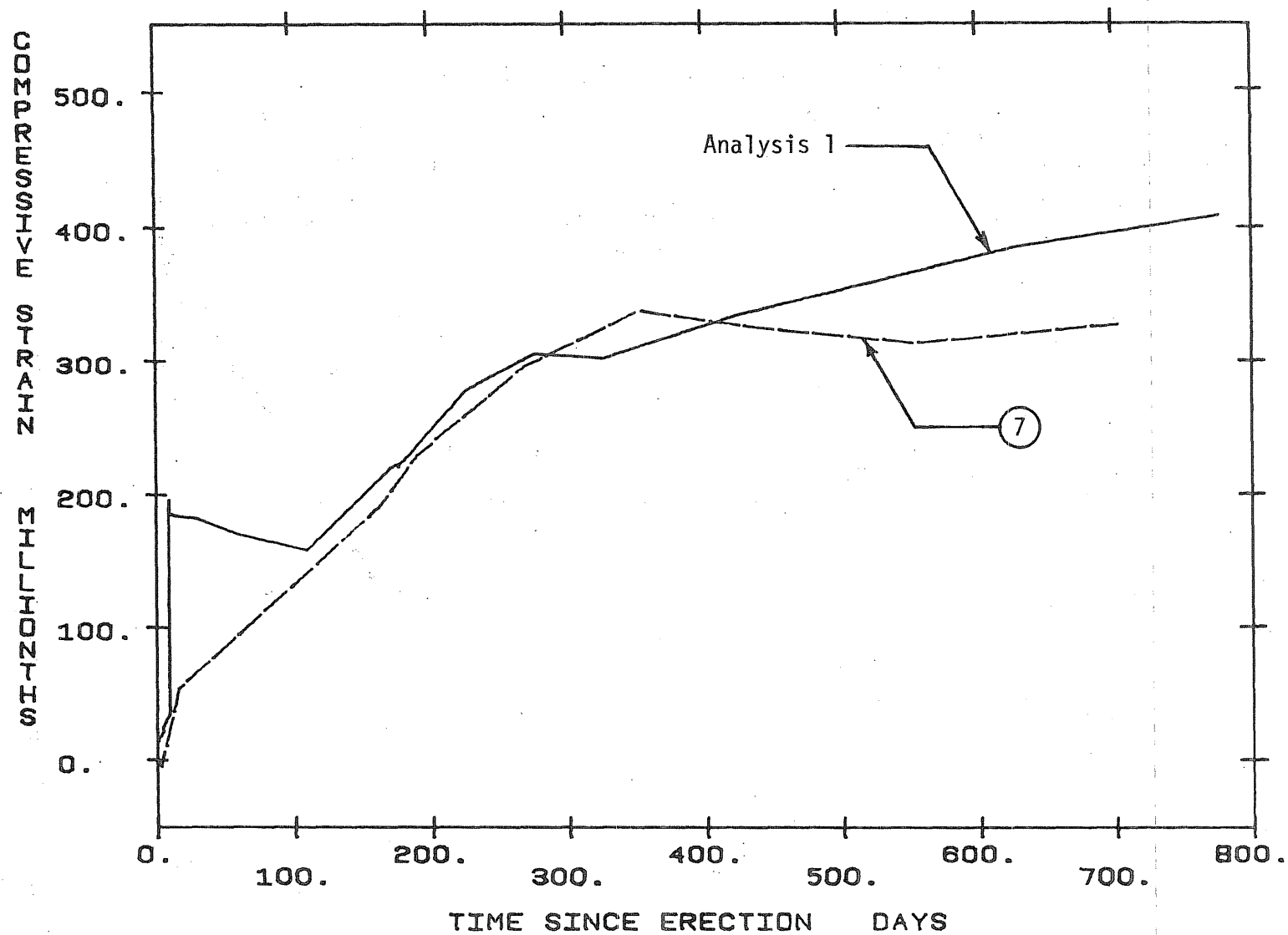


Fig. 4.10 Comparison of Measured and Calculated Concrete Strains in Webs of Segment SB1-N16 (Analysis 1, $h = 56$ in.)

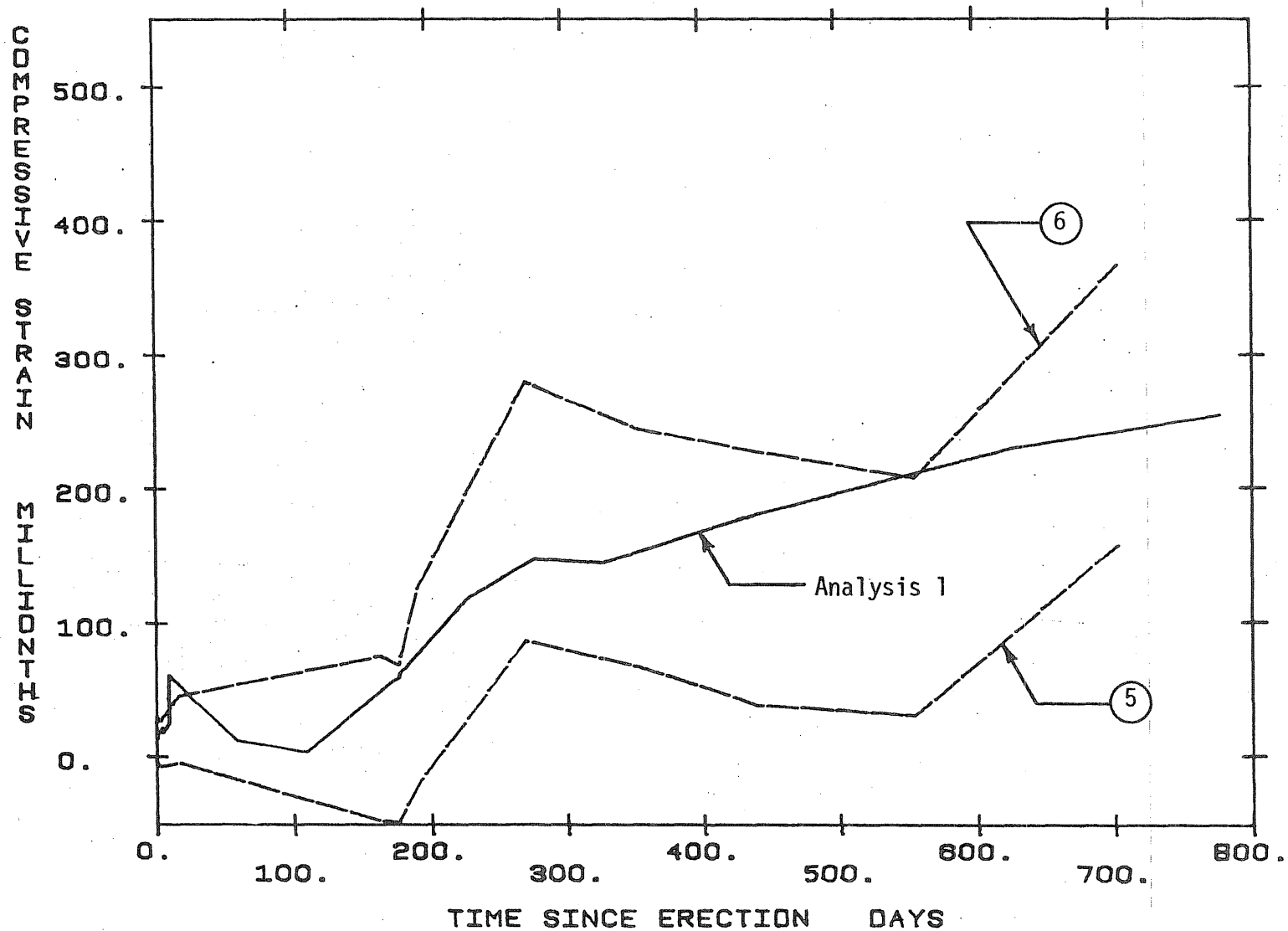


Fig. 4.11 Comparison of Measured and Calculated Concrete Strains in Top Flange of Segment SB1-N16 (Analysis 1, $h = 131$ in.)

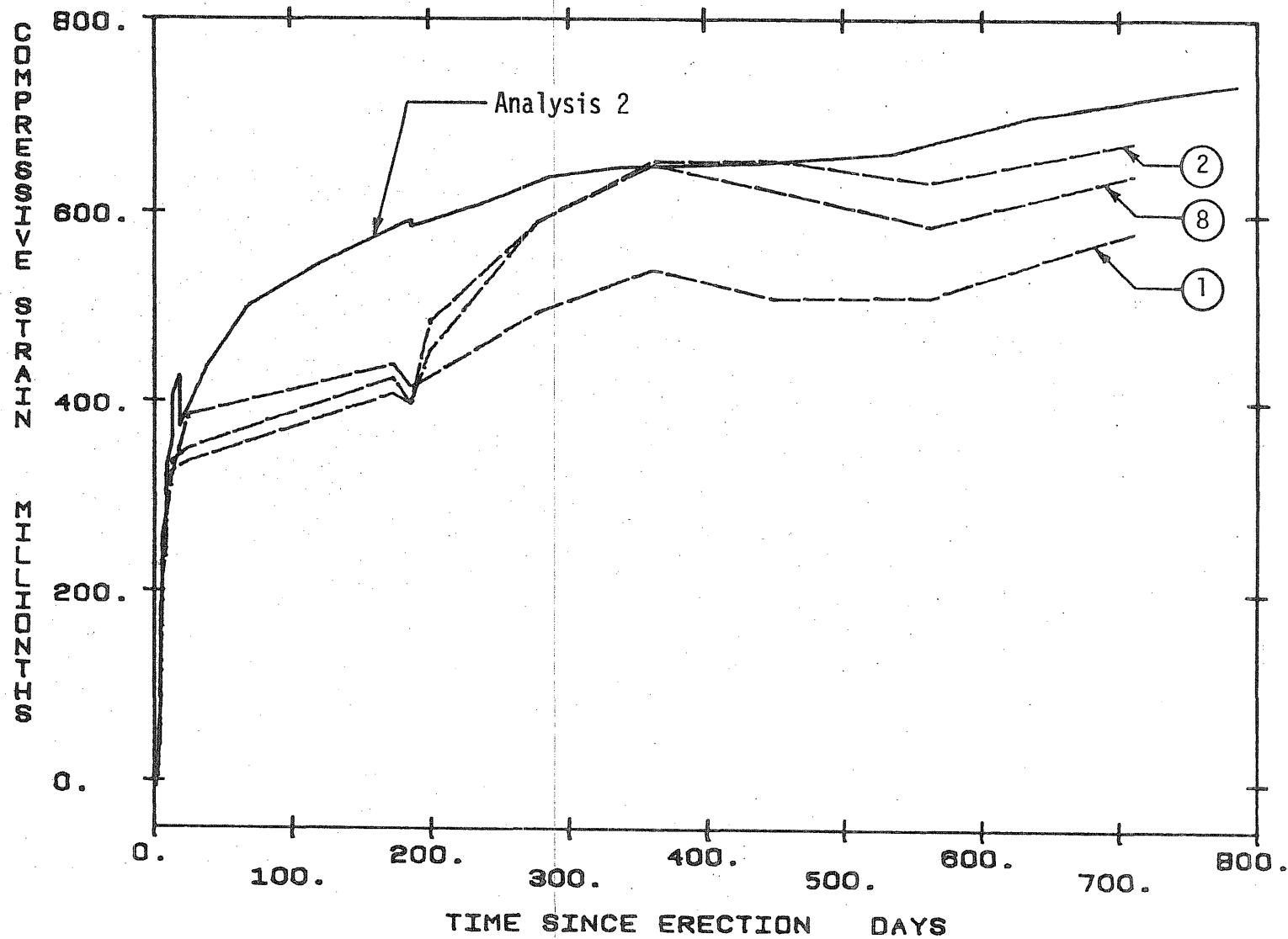


Fig. 4.12 Comparison of Measured and Calculated Concrete Strains in Bottom Flange of Segment SB1-N1 (Analysis 2, $h = 8$ in.)

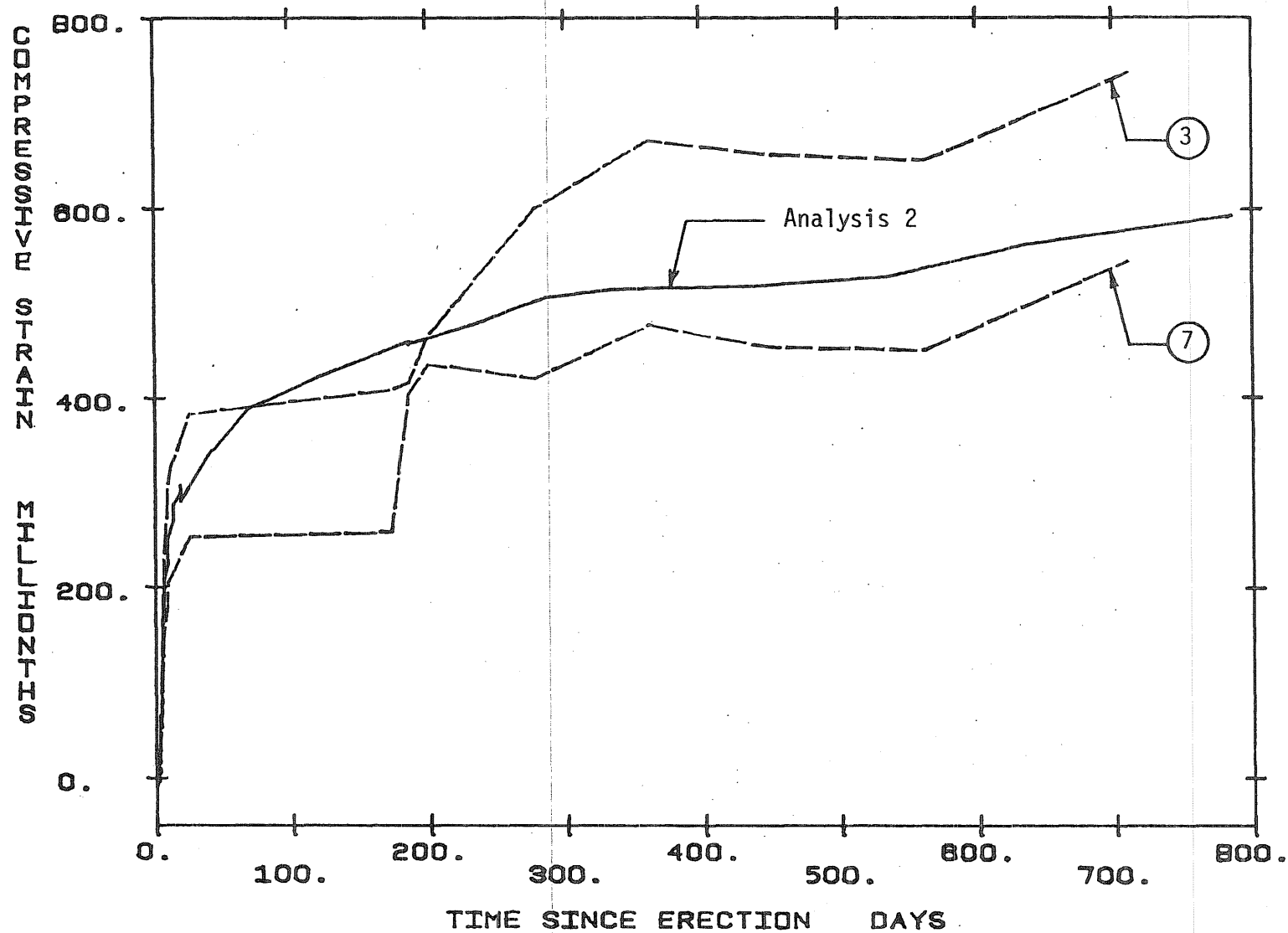


Fig. 4.13 Comparison of Measured and Calculated Concrete Strains in Webs of Segment SB1-N1 (Analysis 2, $h = 56$ in.)

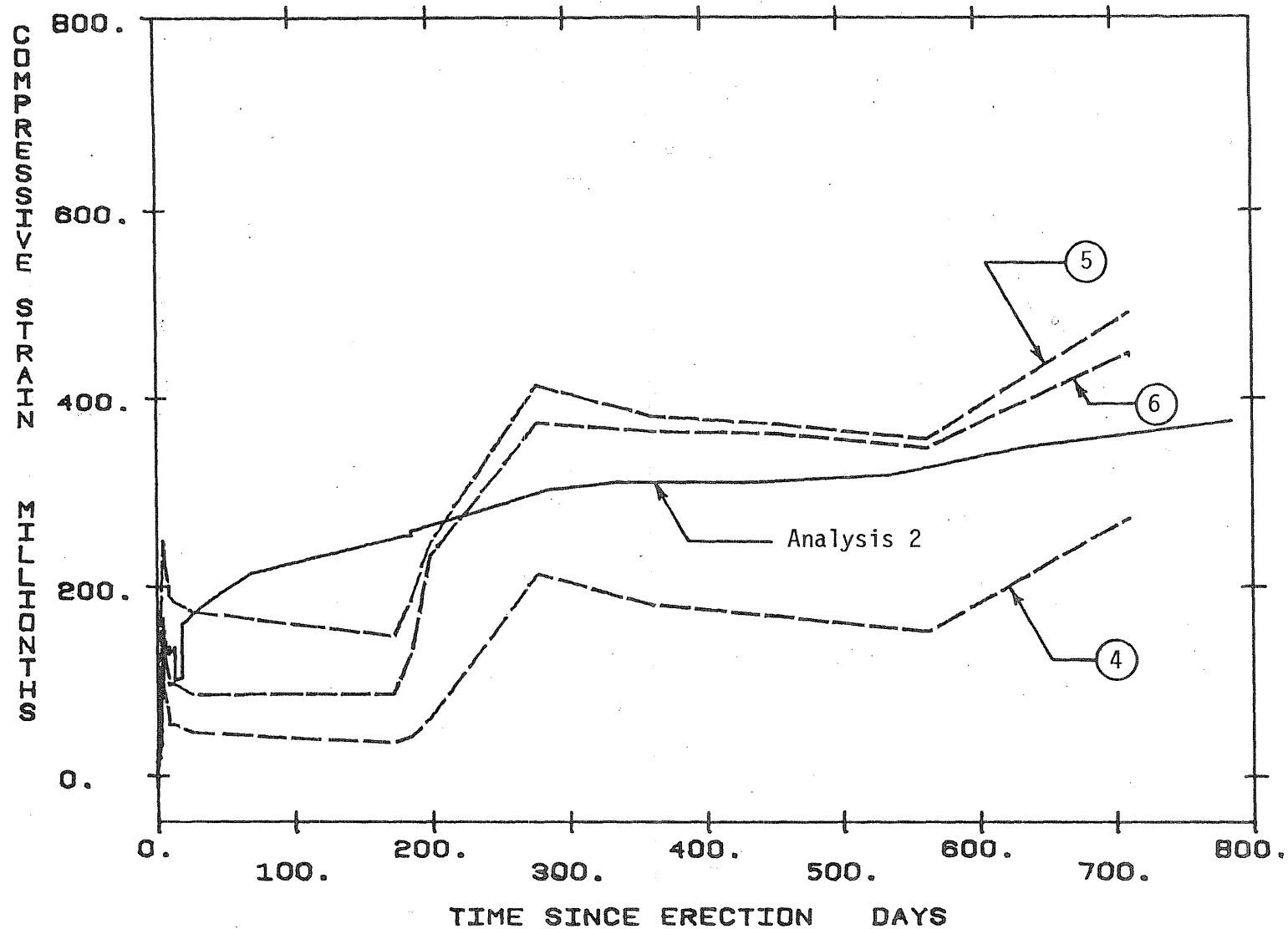


Fig. 4.14 Comparison of Measured and Calculated Concrete Strains in Top Flange of Segment SB1-N1 (Analysis 2, $h = 131$ in.)

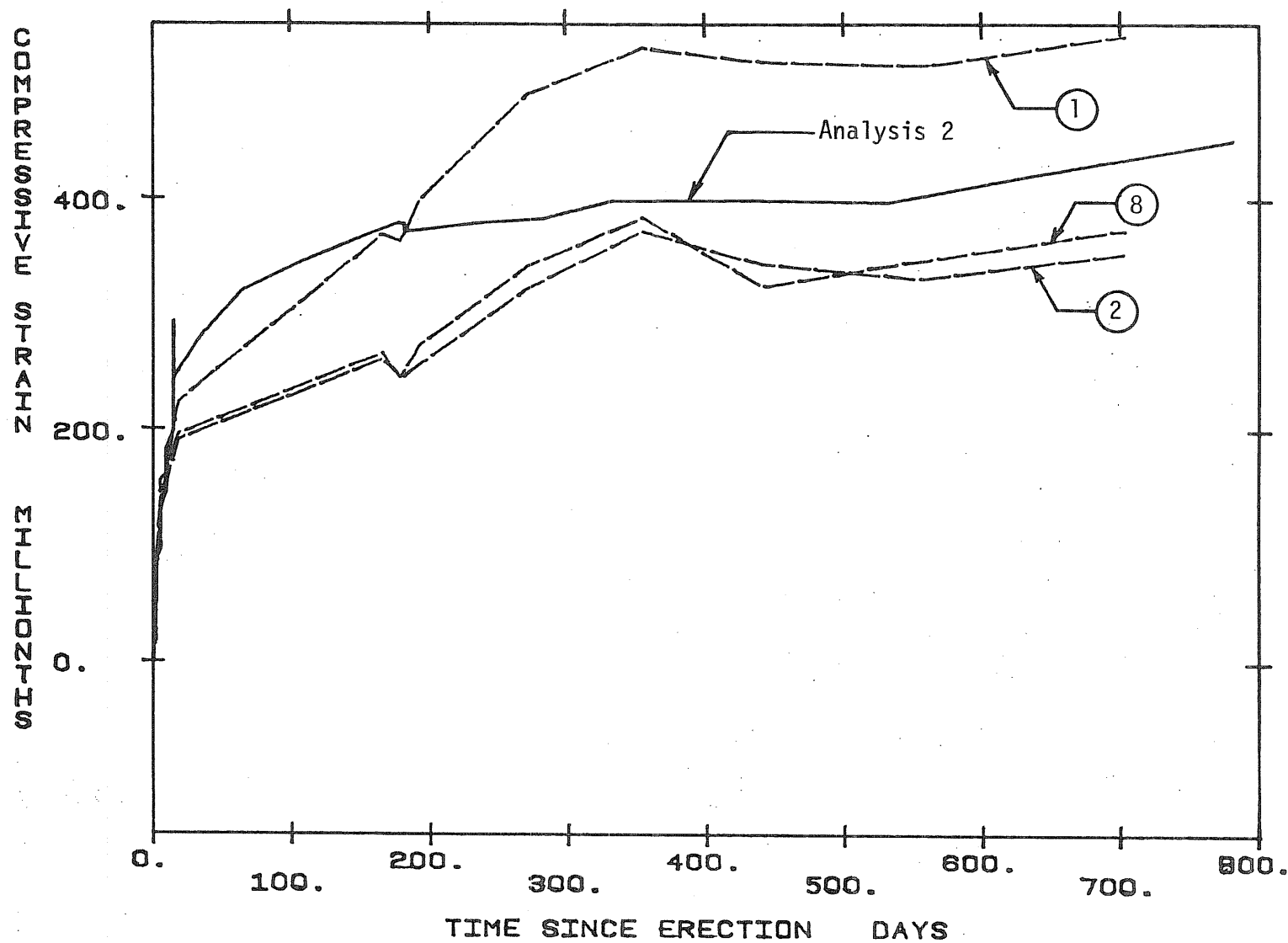


Fig. 4.15 Comparison of Measured and Calculated Concrete Strains in Bottom Flange of Segment SB1-N9 (Analysis 2, $h = 8$ in.)

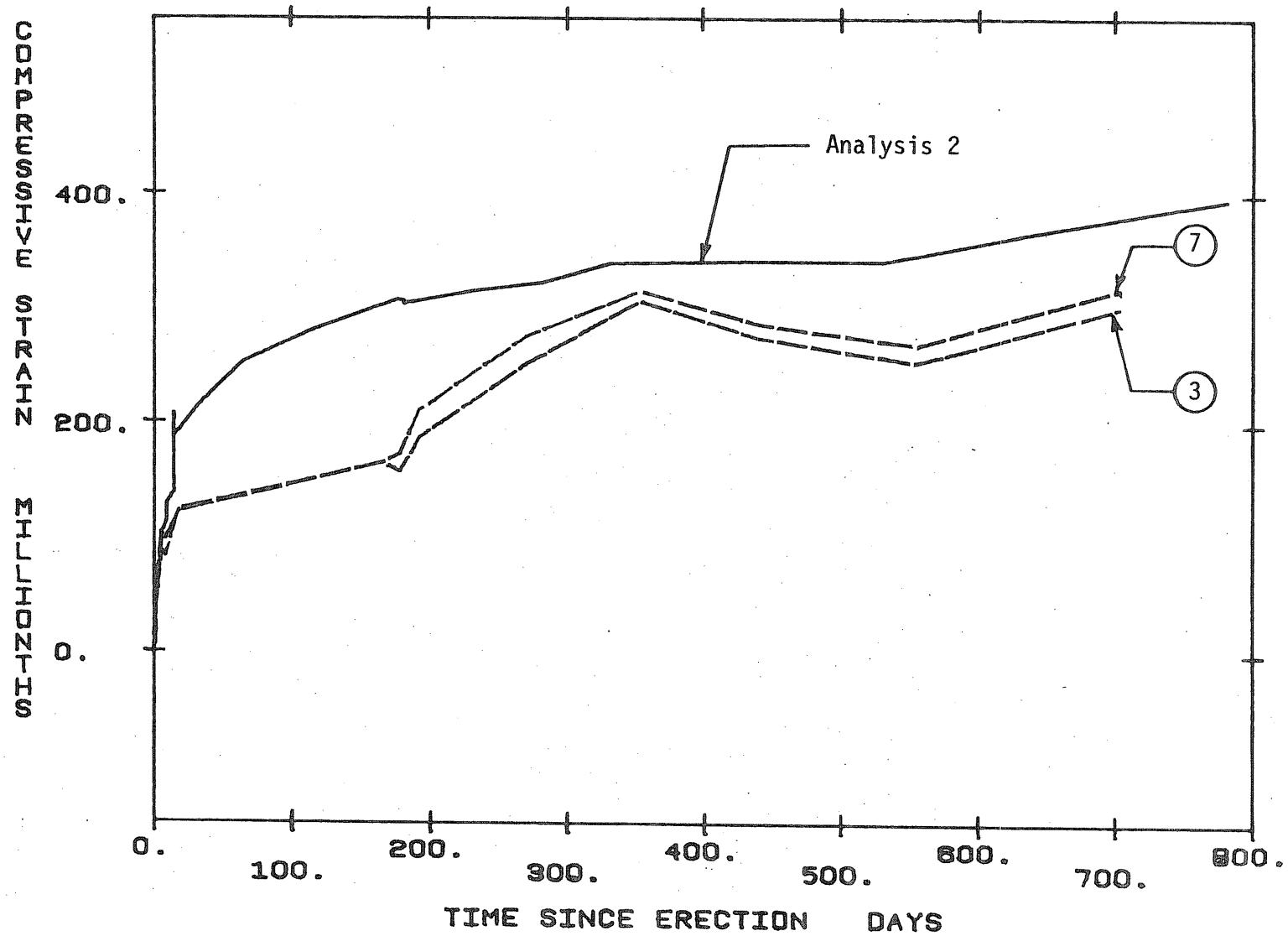


Fig. 4.16 Comparison of Measured and Calculated Concrete Strains in Webs of Segment SB1-N9 (Analysis 2, $h = 56$ in.)

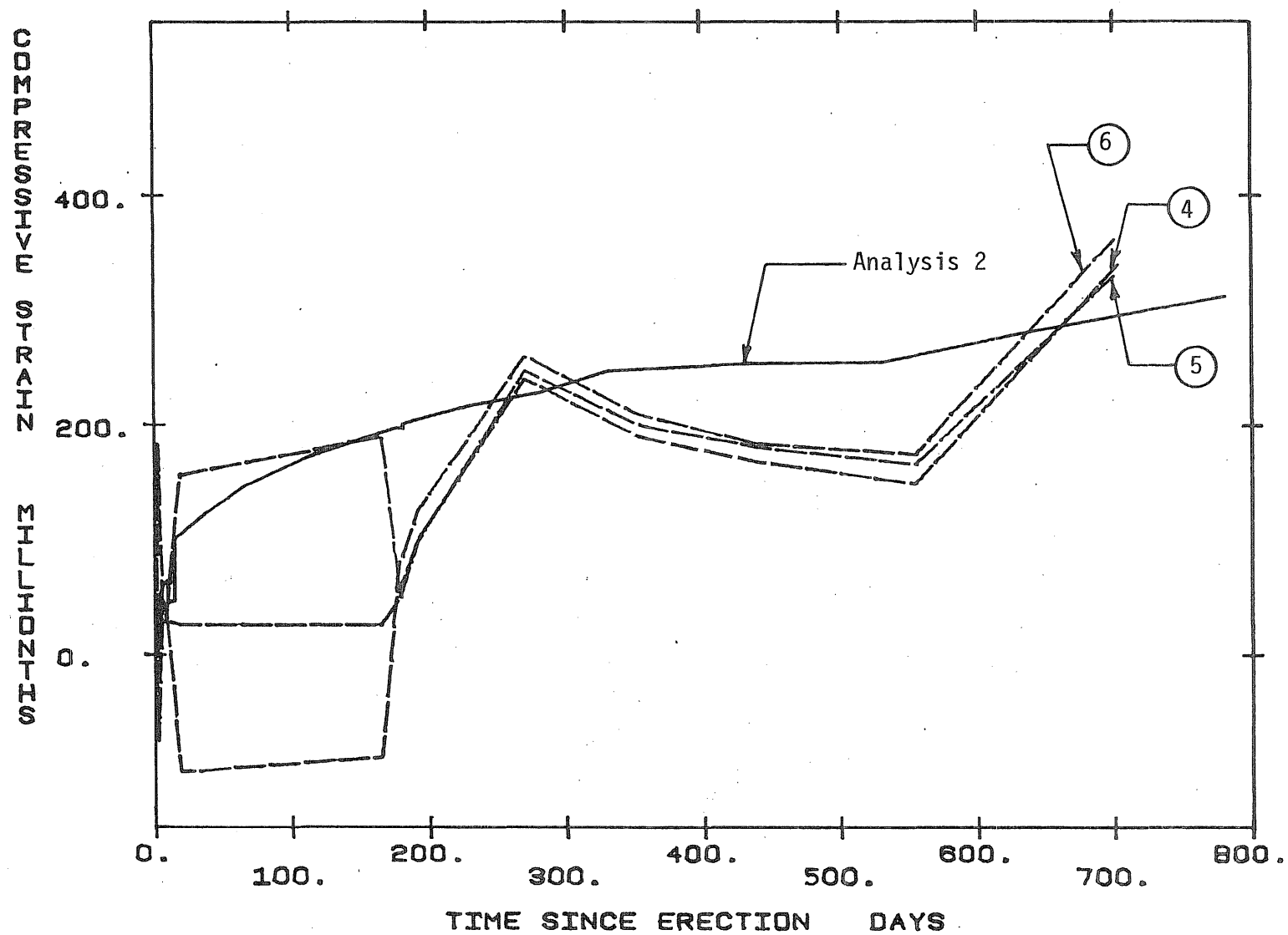


Fig. 4.17 Comparison of Measured and Calculated Concrete Strains in Top Flange of Segment SB1-N9 (Analysis 2, $h = 131$ in.)

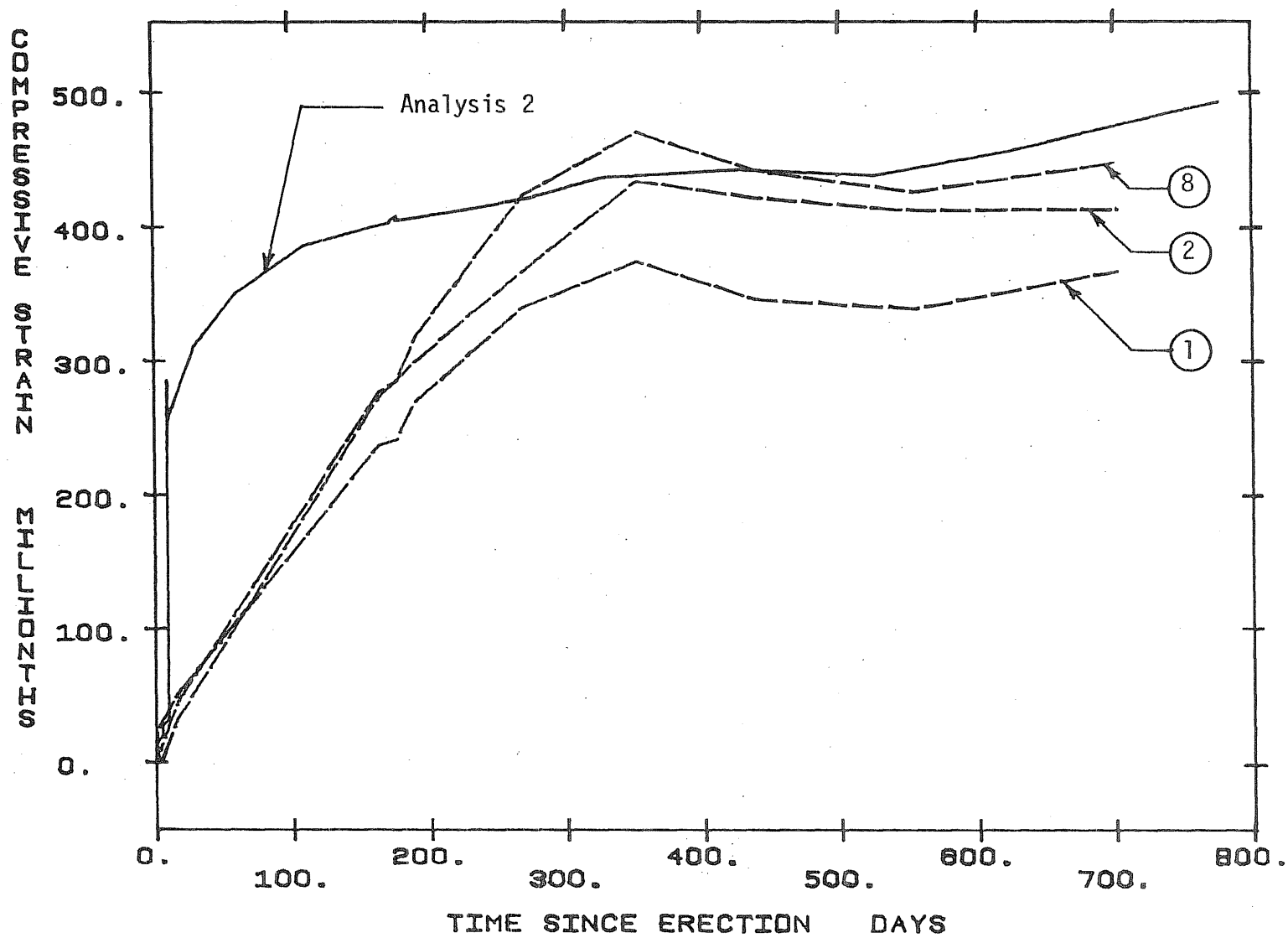


Fig. 4.18 Comparison of Measured and Calculated Concrete Strains in Bottom Flange of Segment SB1-N16 (Analysis 2, $h = 8$ in.)

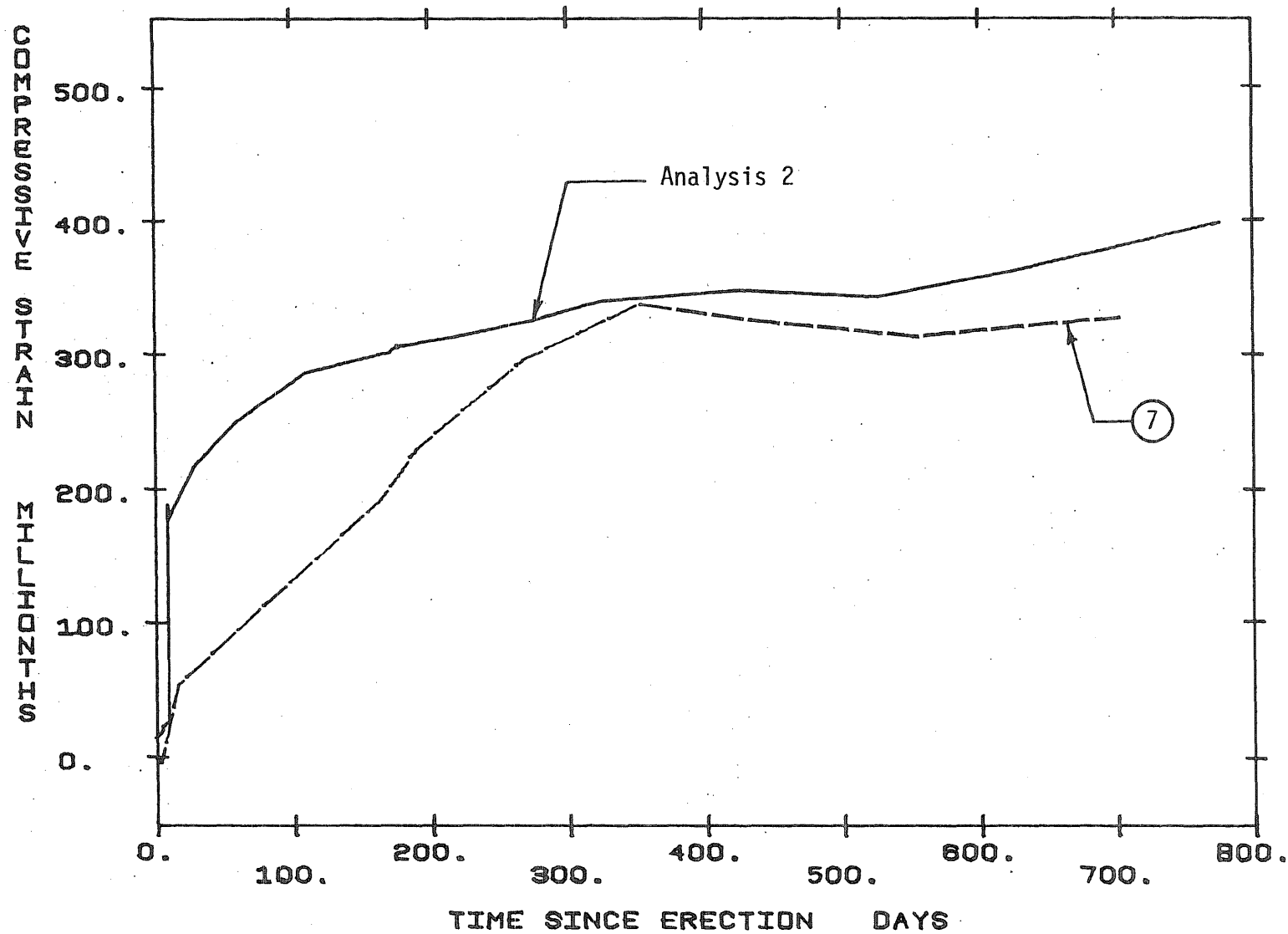


Fig. 4.19 Comparison of Measured and Calculated Concrete Strains in Webs of Segment SB1-N16 (Analysis 2, $h = 56$ in.)

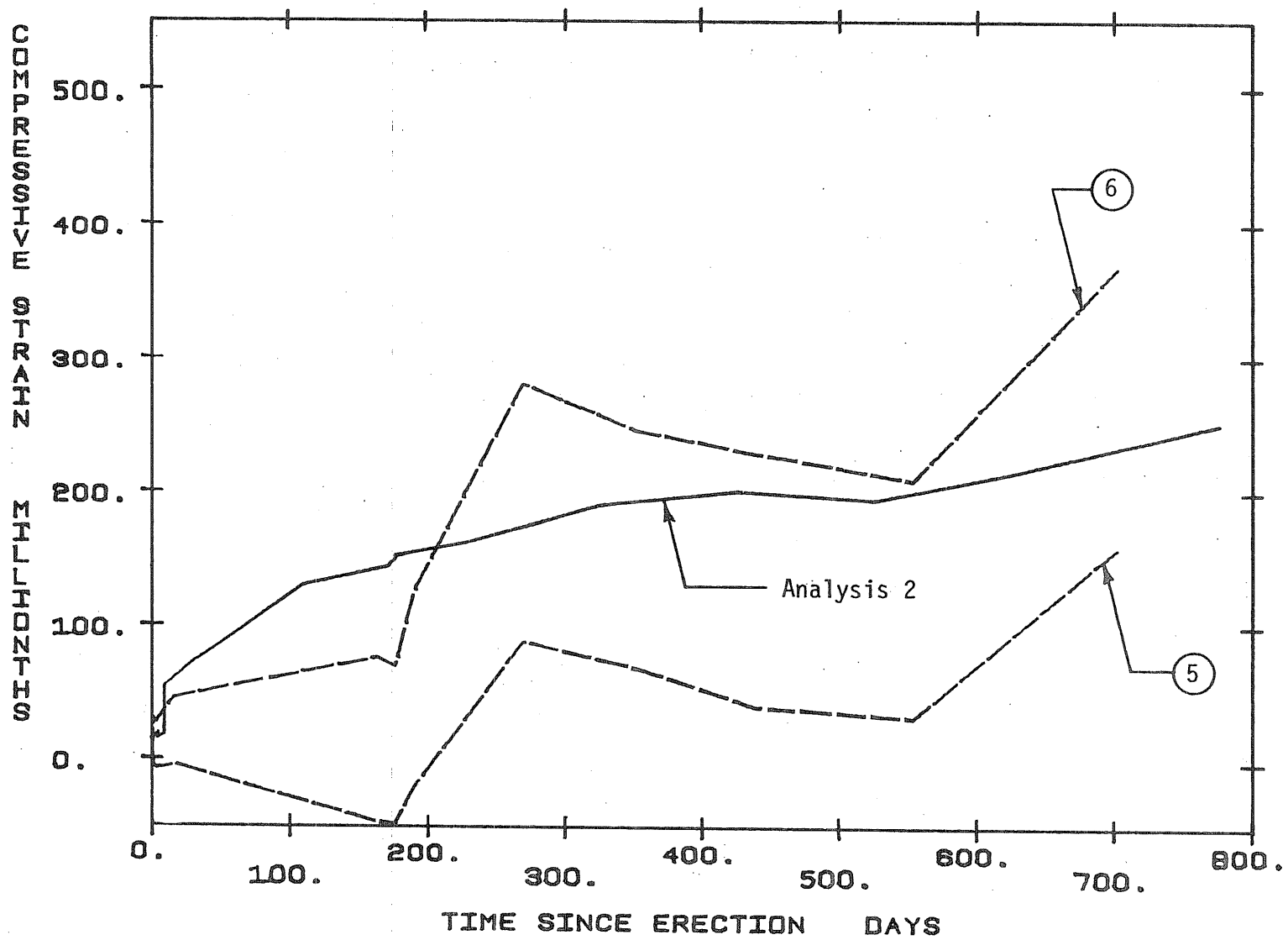


Fig. 4.20 Comparison of Measured and Calculated Concrete Strains in Top Flange of Segment SB1-N16 (Analysis 2, $h = 131$ in.)

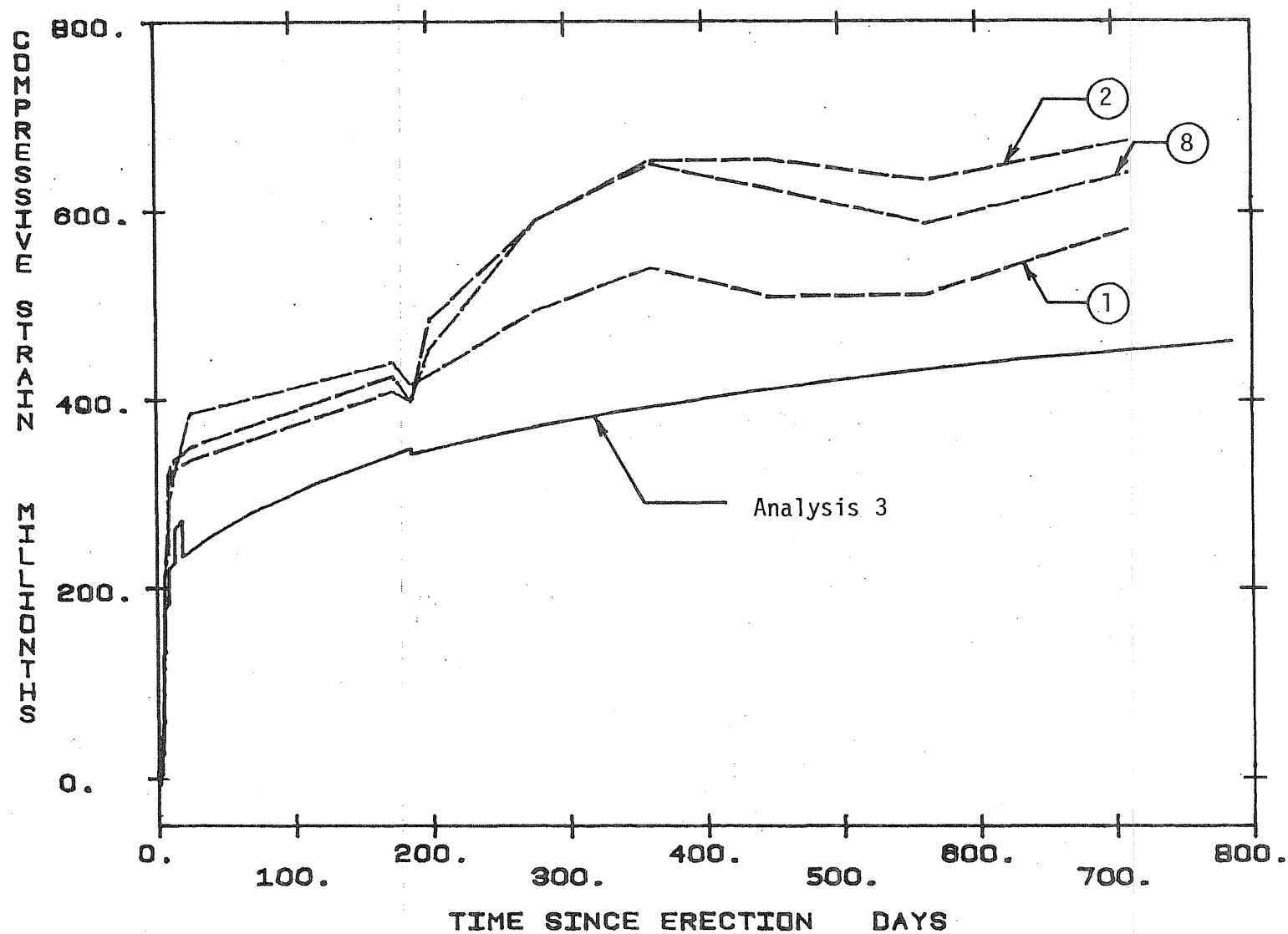


Fig. 4.21 Comparison of Measured and Calculated Concrete Strains in Bottom Flange of Segment SB1-N1 (Analysis 3, $h = 8$ in.)

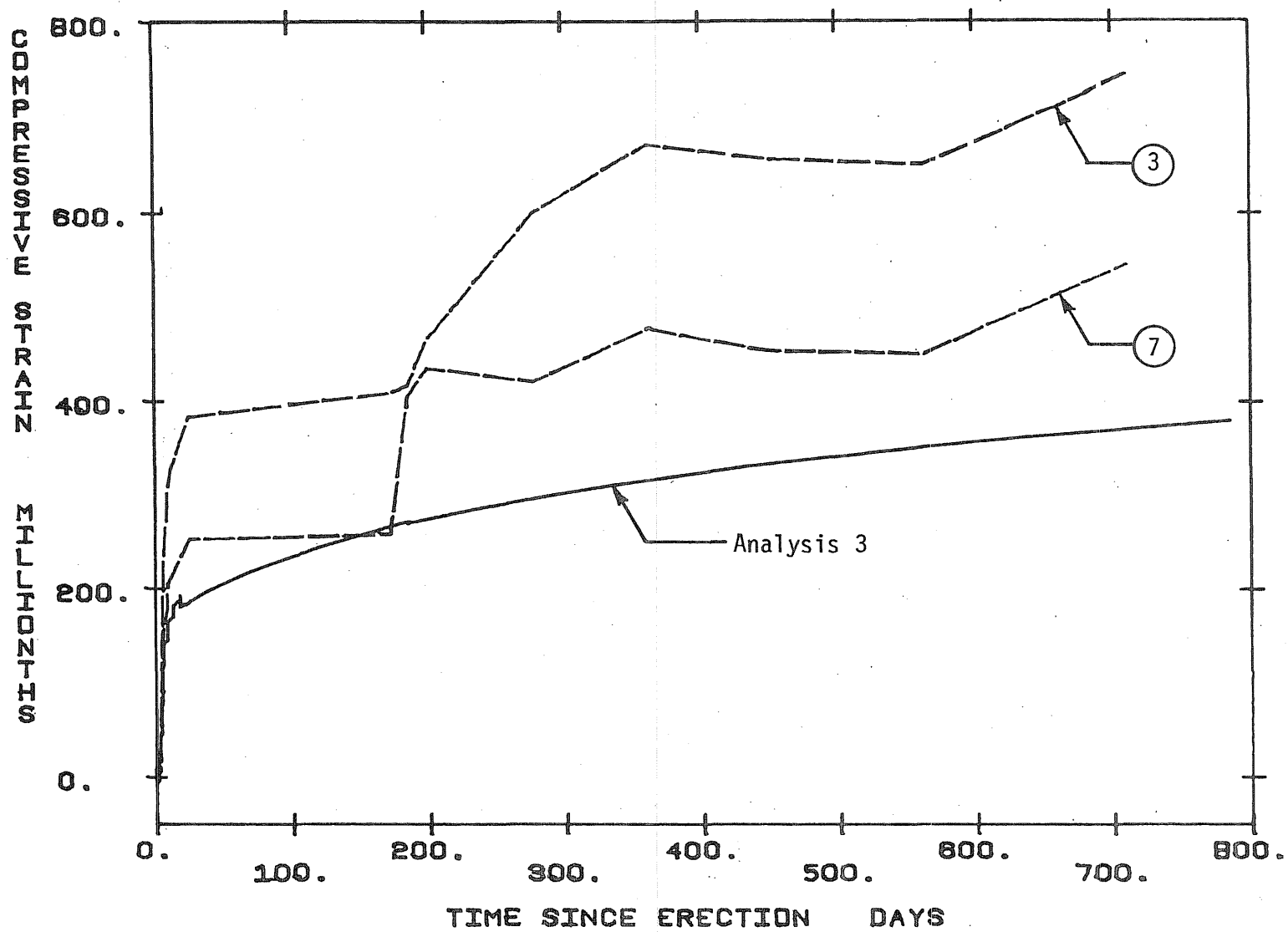


Fig. 4.22 Comparison of Measured and Calculated Concrete Strains in Webs of Segment SB1-N1 (Analysis 3, $h = 56$ in.)

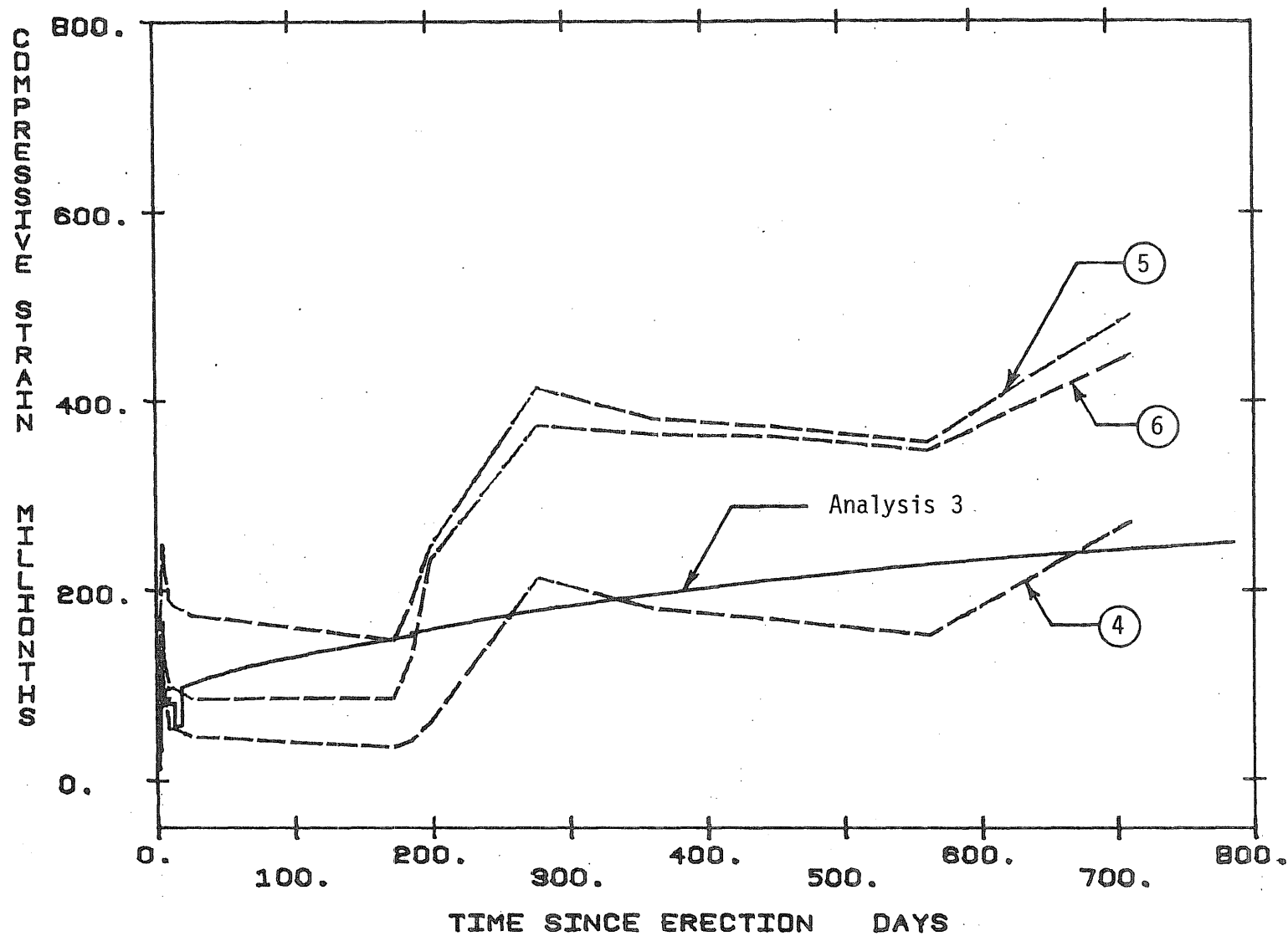


Fig. 4.23 Comparison of Measured and Calculated Concrete Strains in Top Flange of Segment SB1-N1 (Analysis 3, $h = 131$ in.)

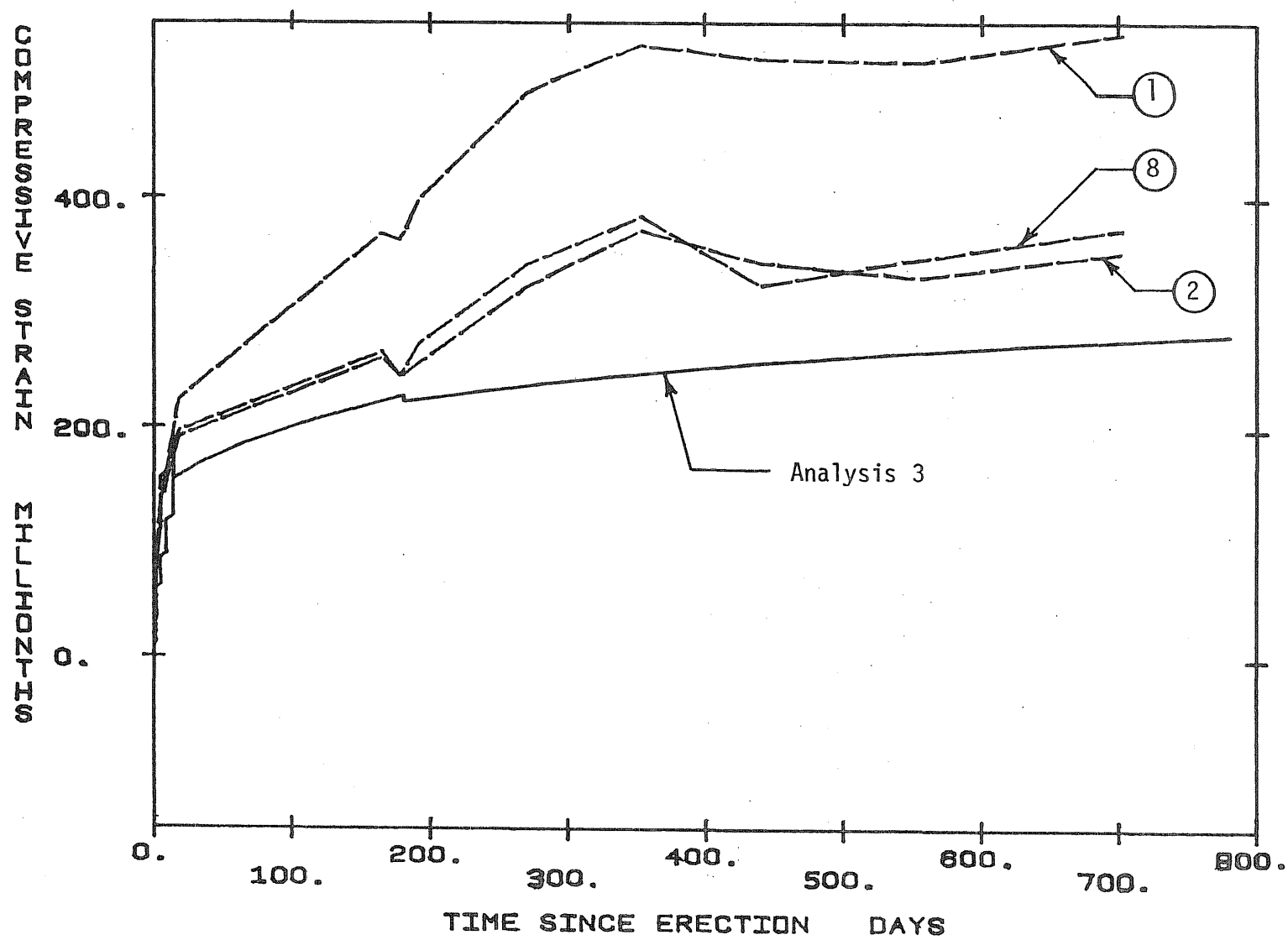


Fig. 4.24 Comparison of Measured and Calculated Concrete Strains in Bottom Flange of Segment SB1-N9 (Analysis 3, $h = 8$ in.)

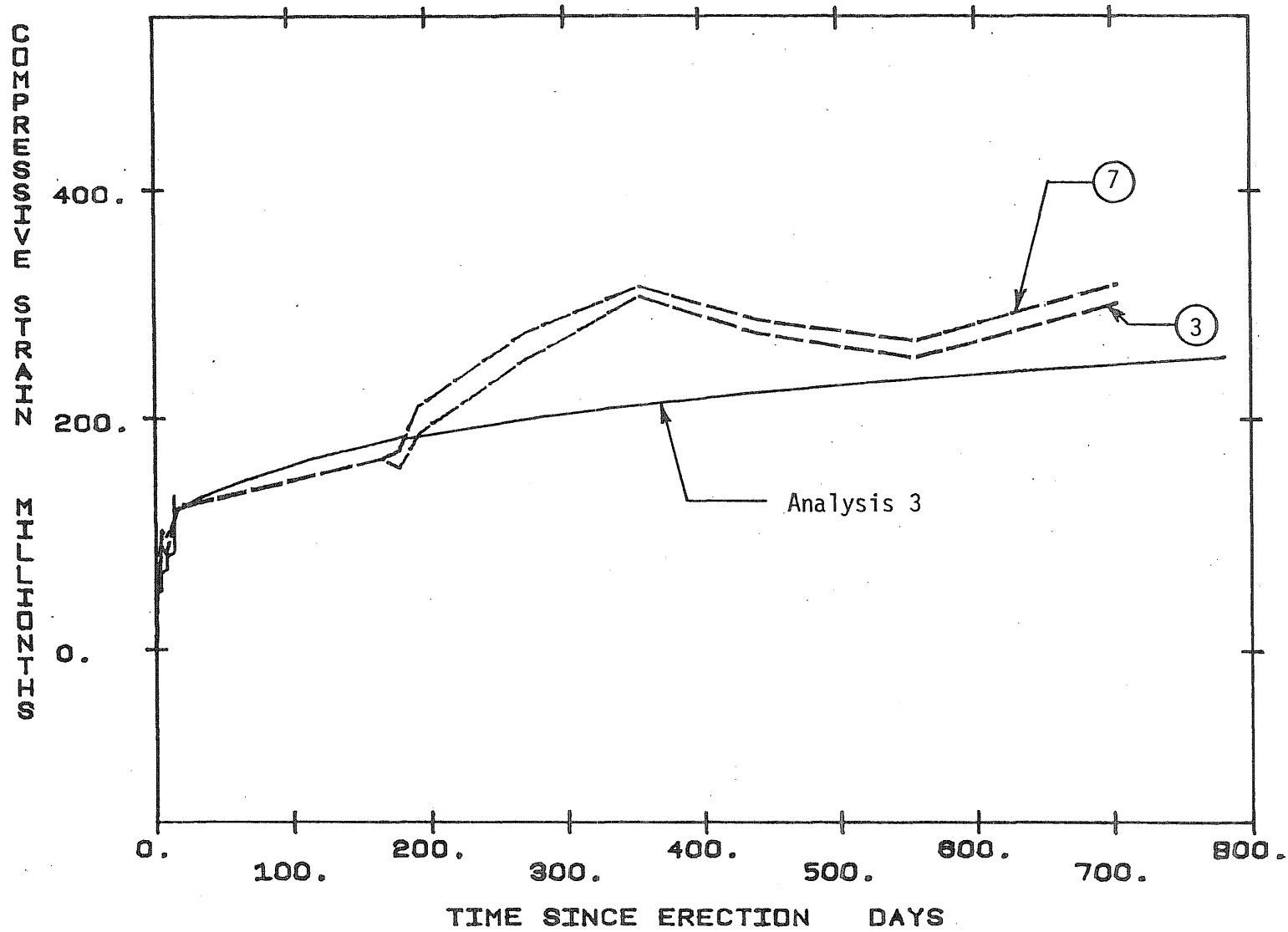


Fig. 4.25 Comparison of Measured and Calculated Concrete Strains in Webs of Segment SB1-N9 (Analysis 3, $h = 56$ in.)

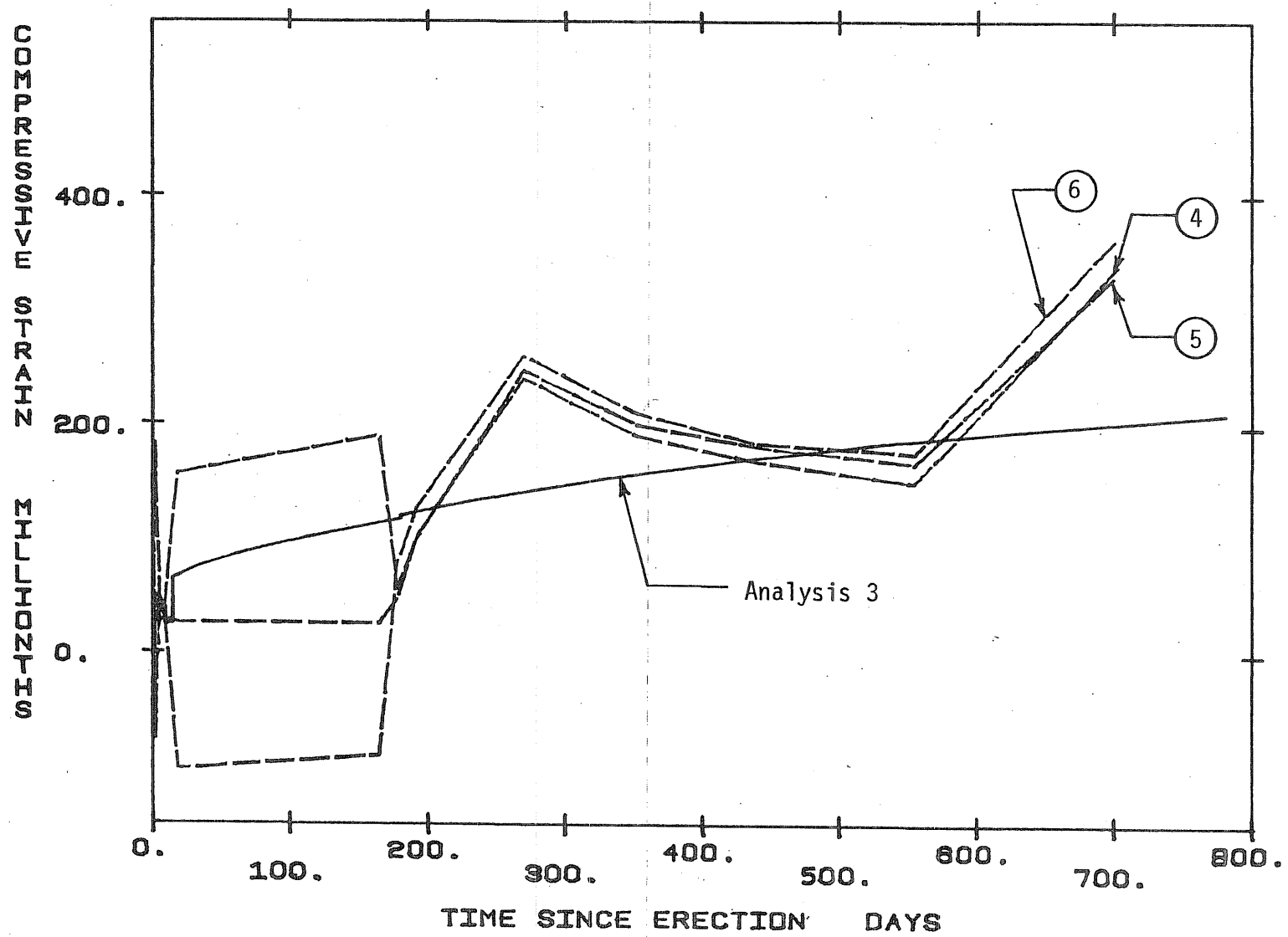


Fig. 4.26 Comparison of Measured and Calculated Concrete Strains in Top Flange of Segment SB1-N9 (Analysis 3, $h = 131$ in.)

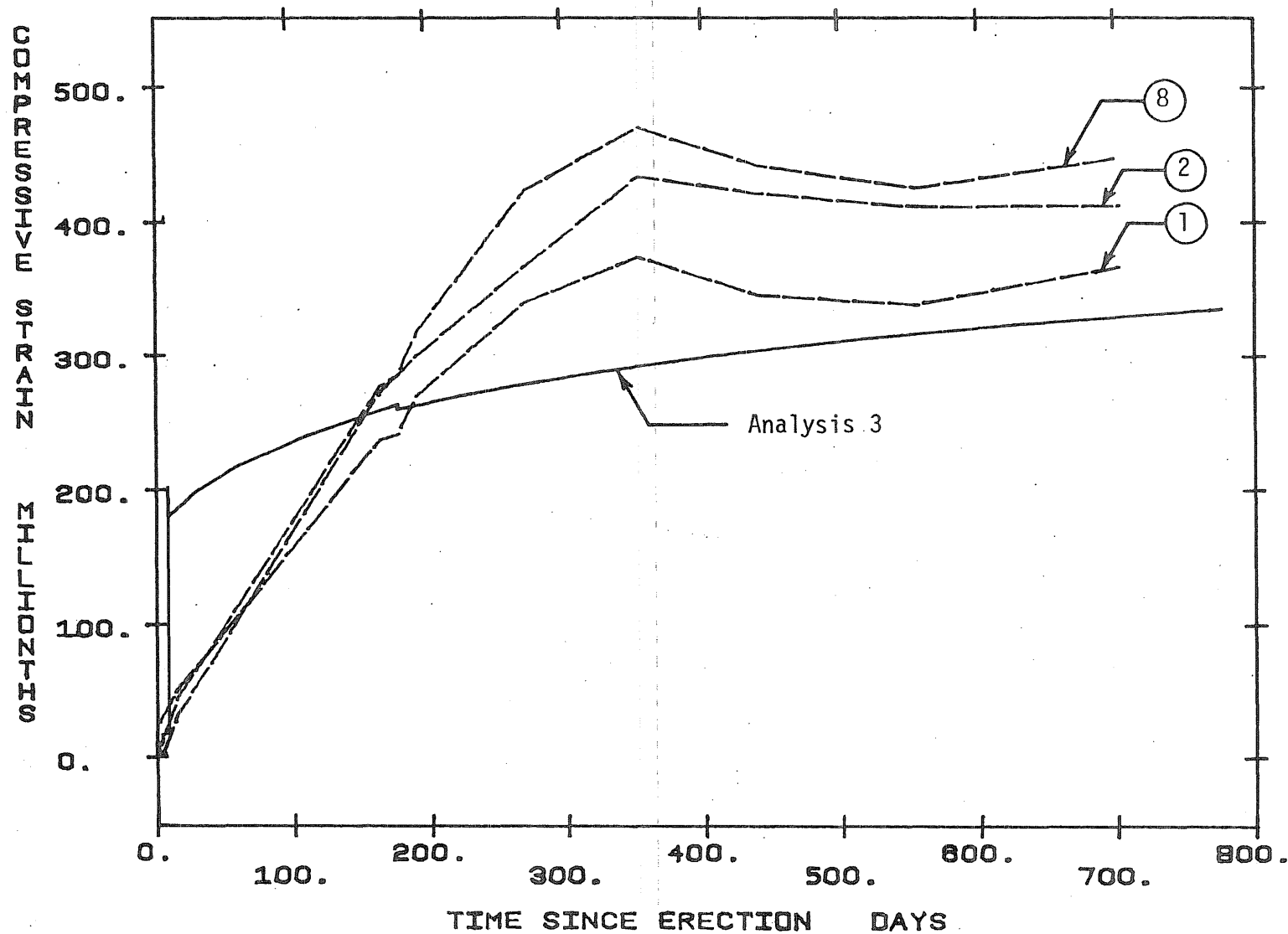


Fig. 4.27 Comparison of Measured and Calculated Concrete Strains in Bottom Flange of Segment SB1-N16 (Analysis 3, $h = 8$ in.)

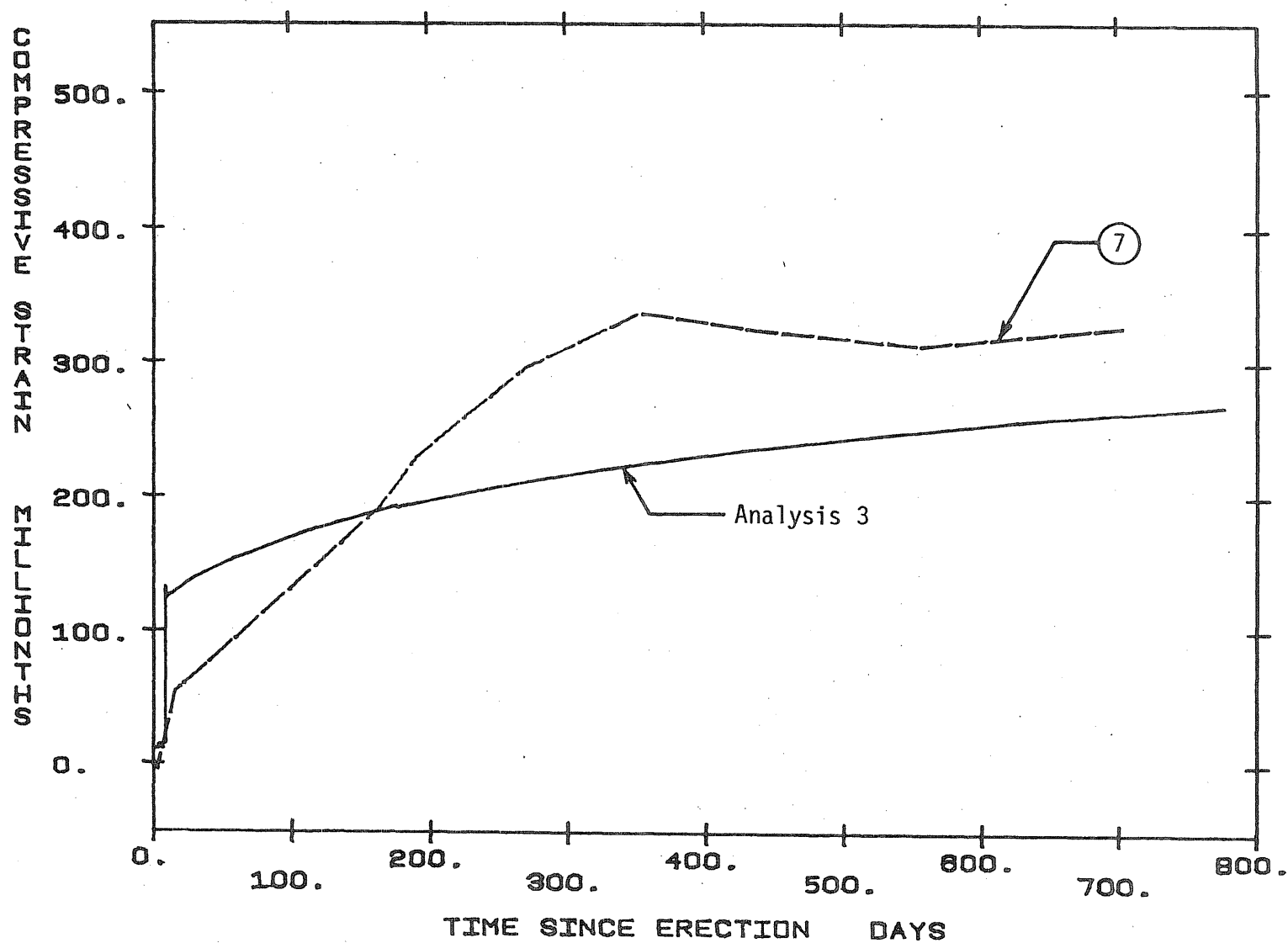


Fig. 4.28 Comparison of Measured and Calculated Concrete Strains in Webs of Segment SB1-N16 (Analysis 3, $h = 56$ in.)

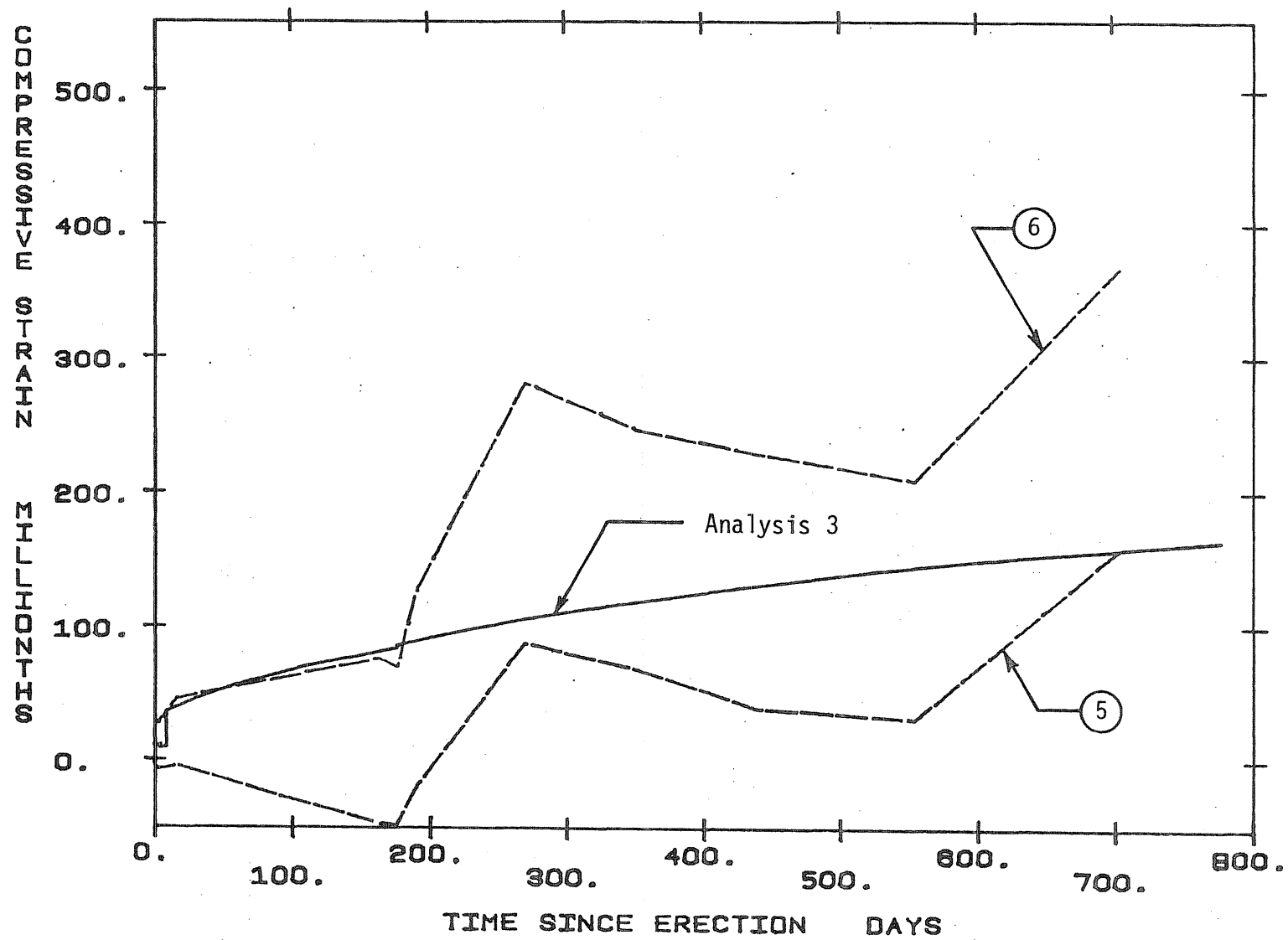


Fig. 4.29 Comparison of Measured and Calculated Concrete Strains in Top Flange of Segment SB1-N16 (Analysis 3, $h = 131$ in.)

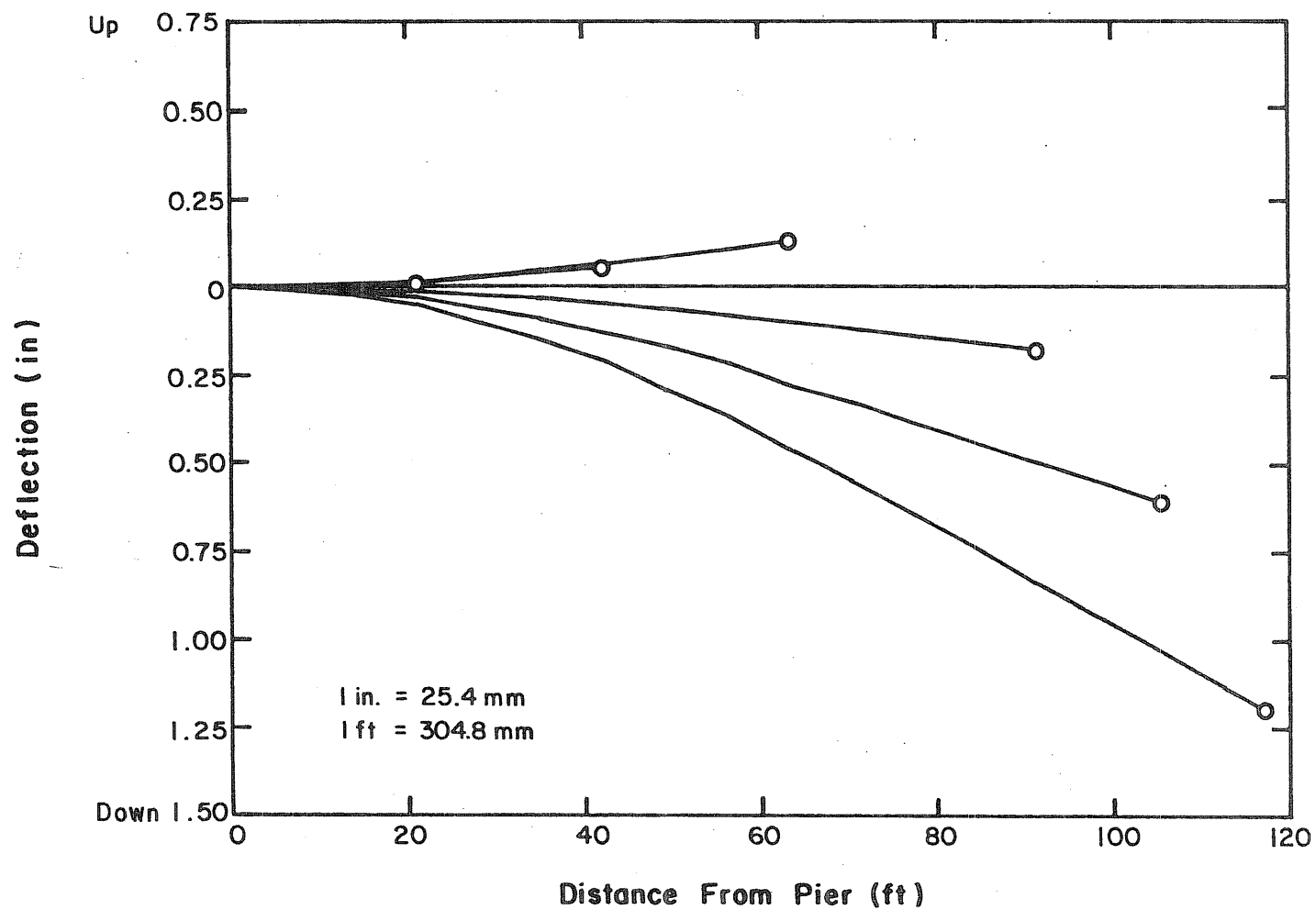


Fig. 4.30 Deflected Shape of Instrumented Cantilever During Construction as Predicted by Analysis 1

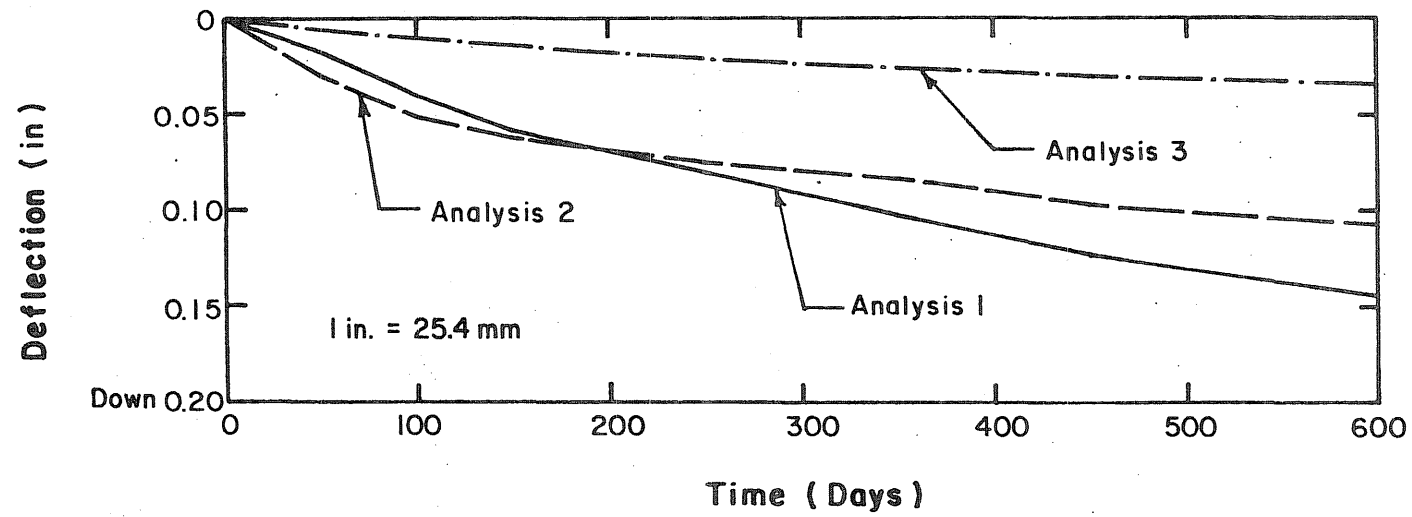


Fig. 4.31 Calculated Change in Deflection of Segment SB1-N16 Since Completion of Final Structure

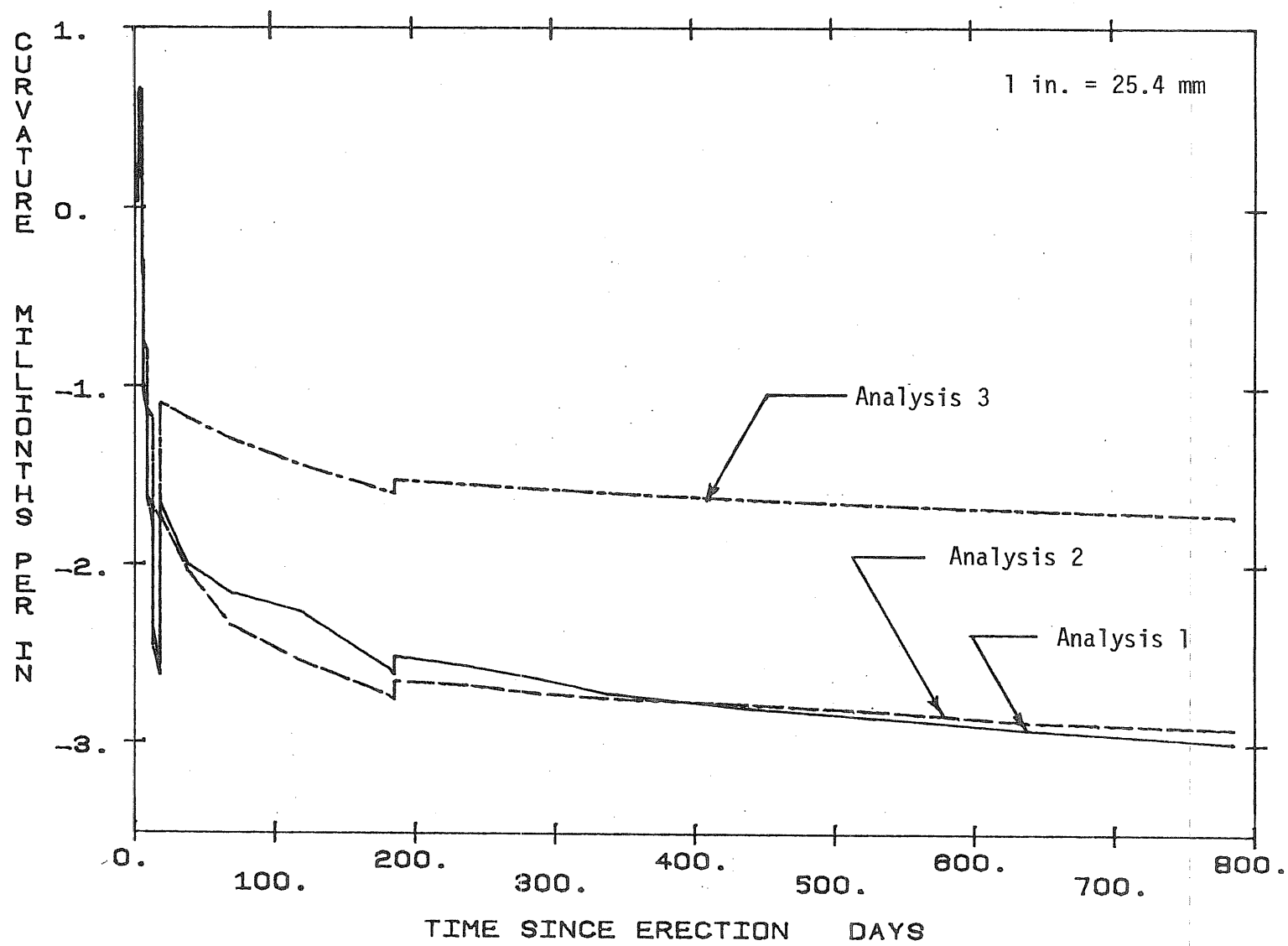


Fig. 4.32 Calculated Curvatures for Segment SB1-N1

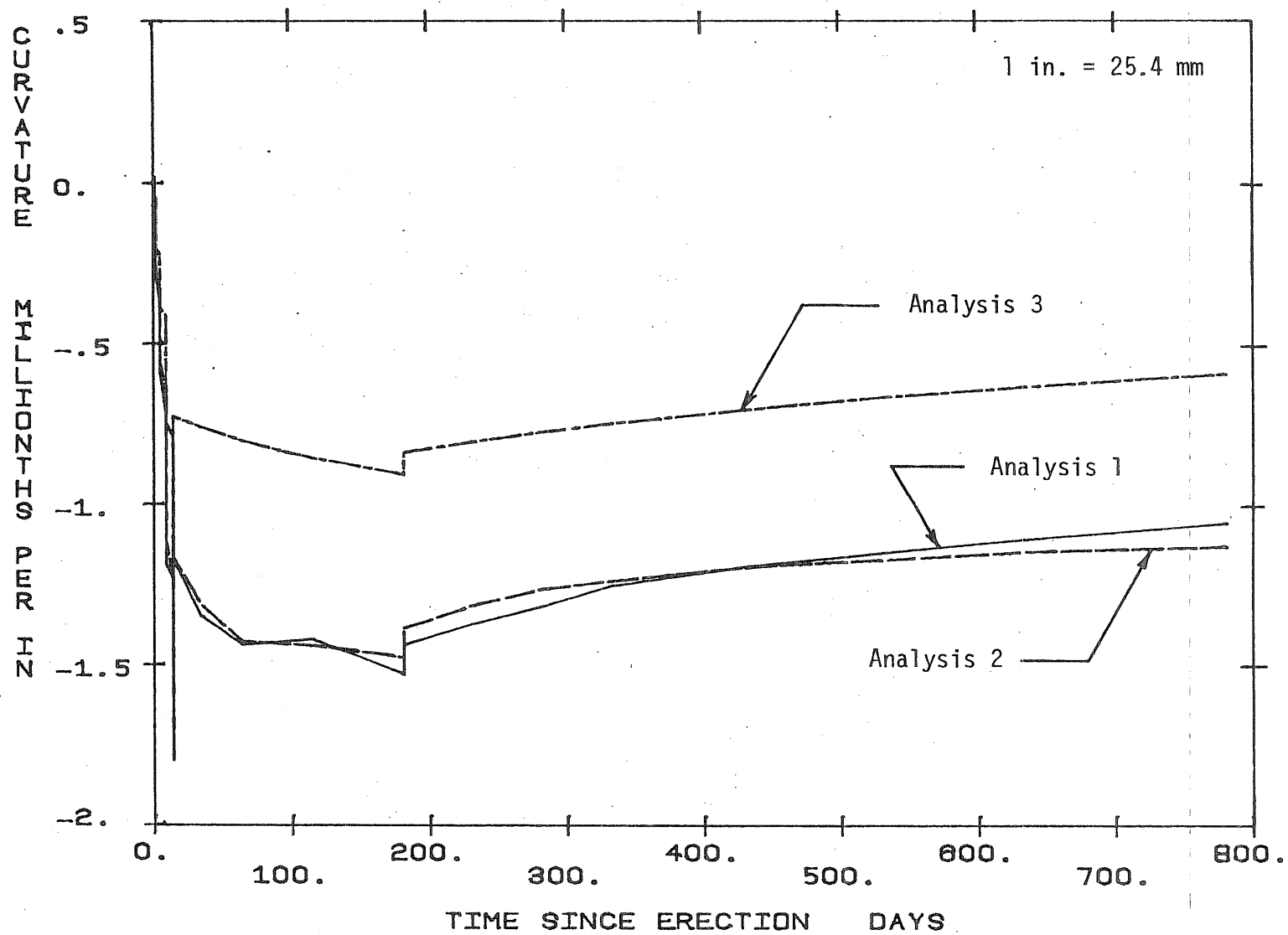


Fig. 4.33 Calculated Curvatures for Segment SB1-N9

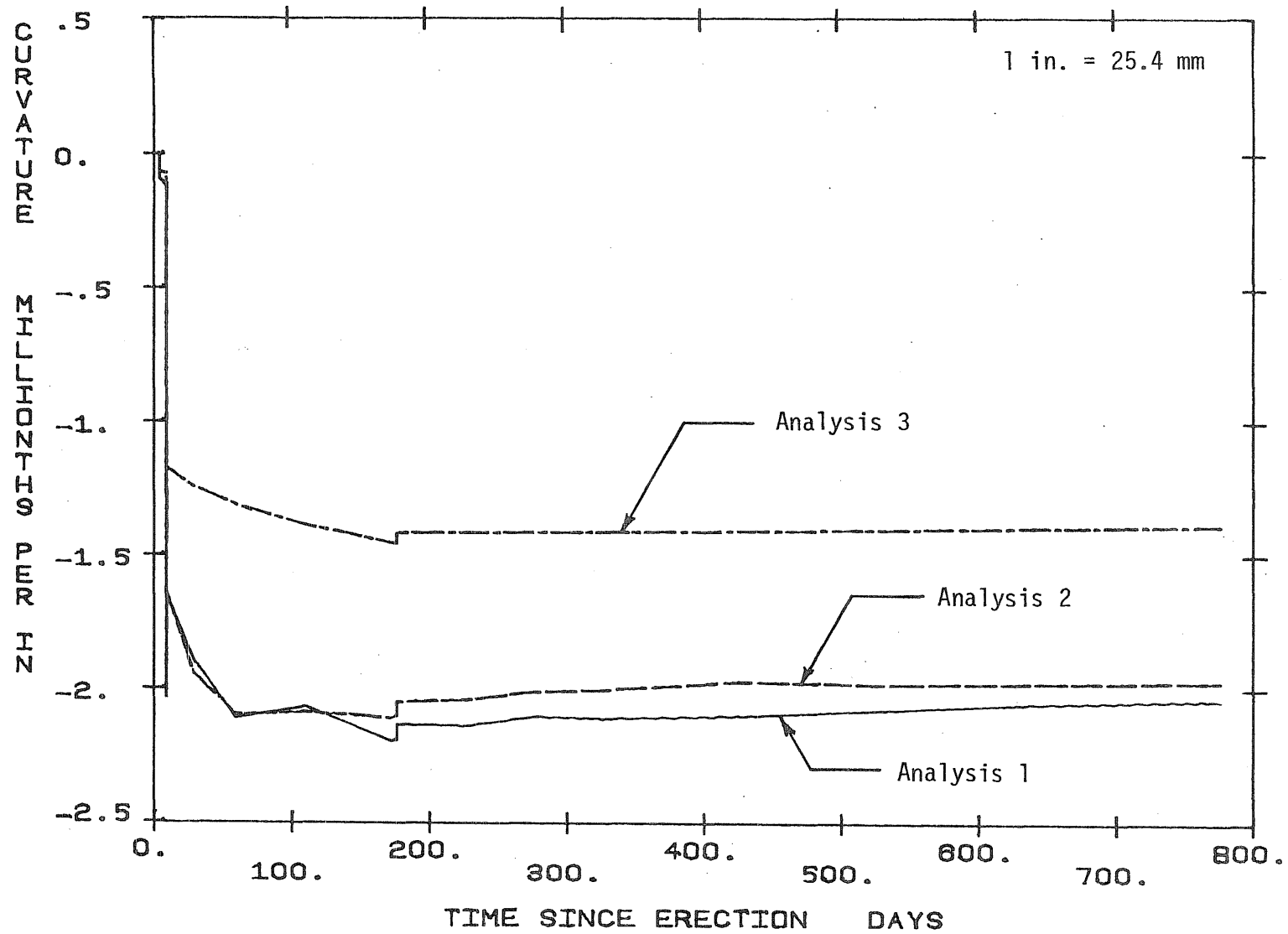


Fig. 4.34 Calculated Curvatures for Segment SB1-N16

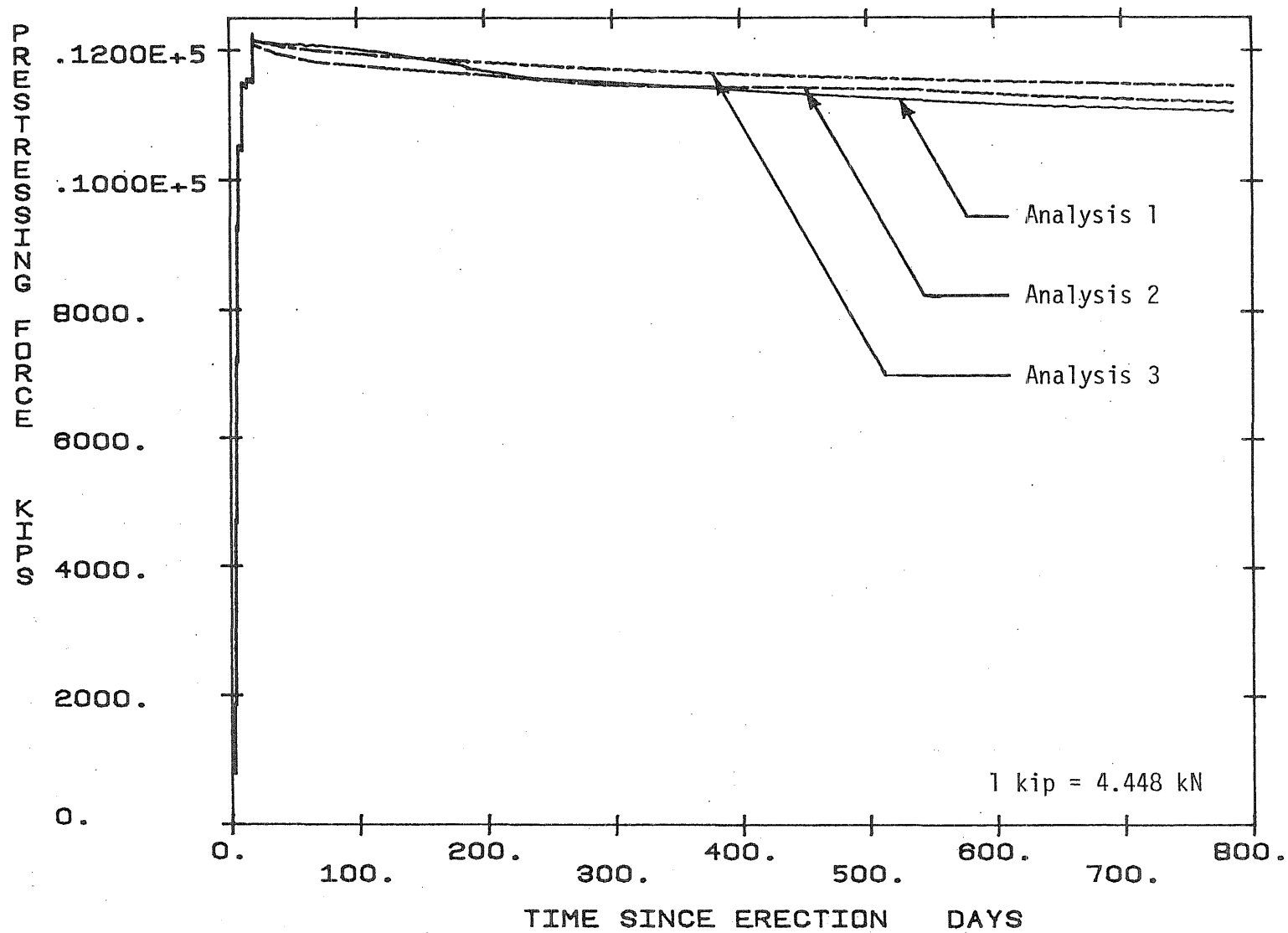


Fig. 5.1 Calculated Total Prestressing Force at Segment SB1-N1

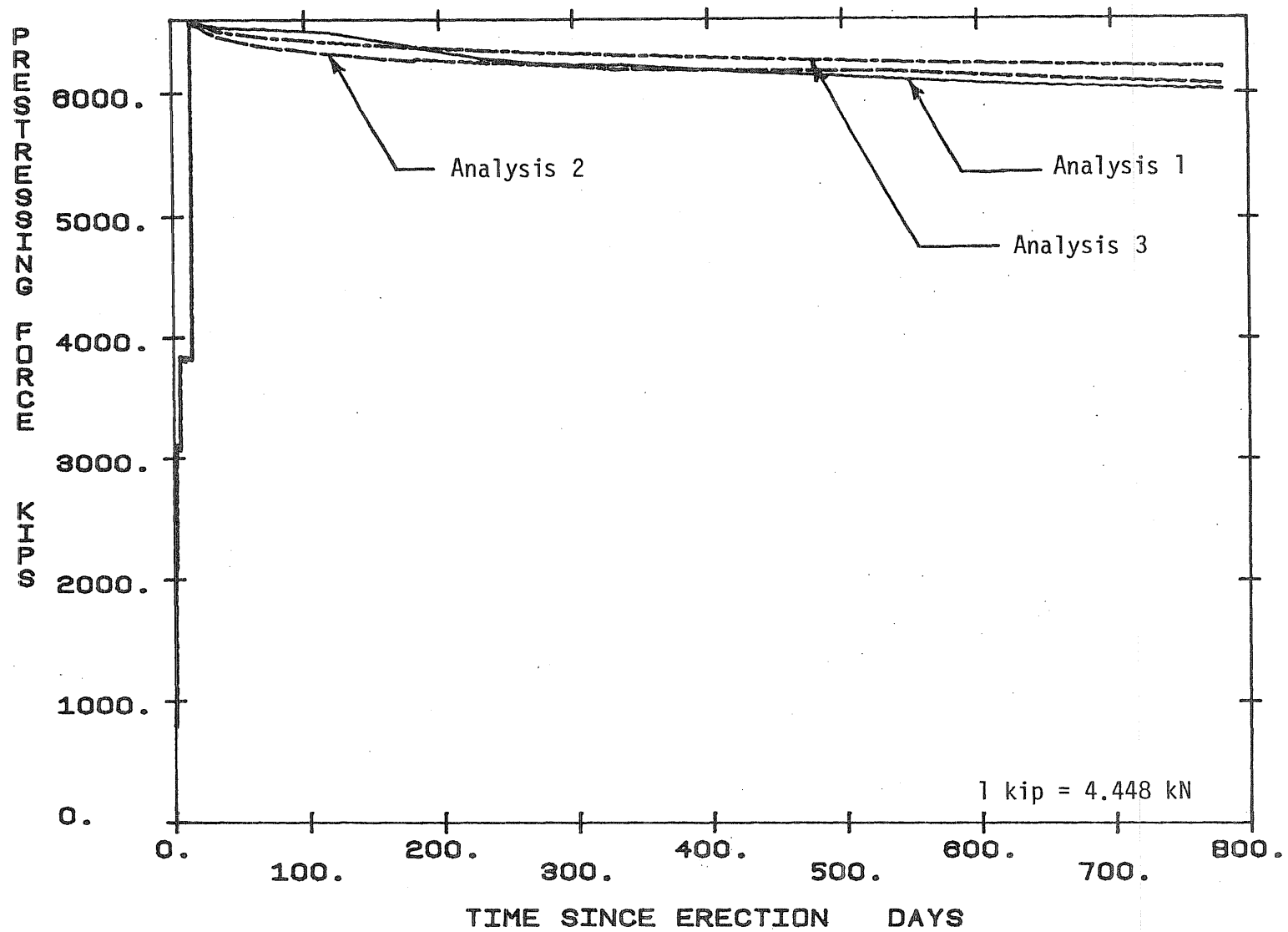


Fig. 5.2 Calculated Total Prestressing Force at Segment SB1-N9

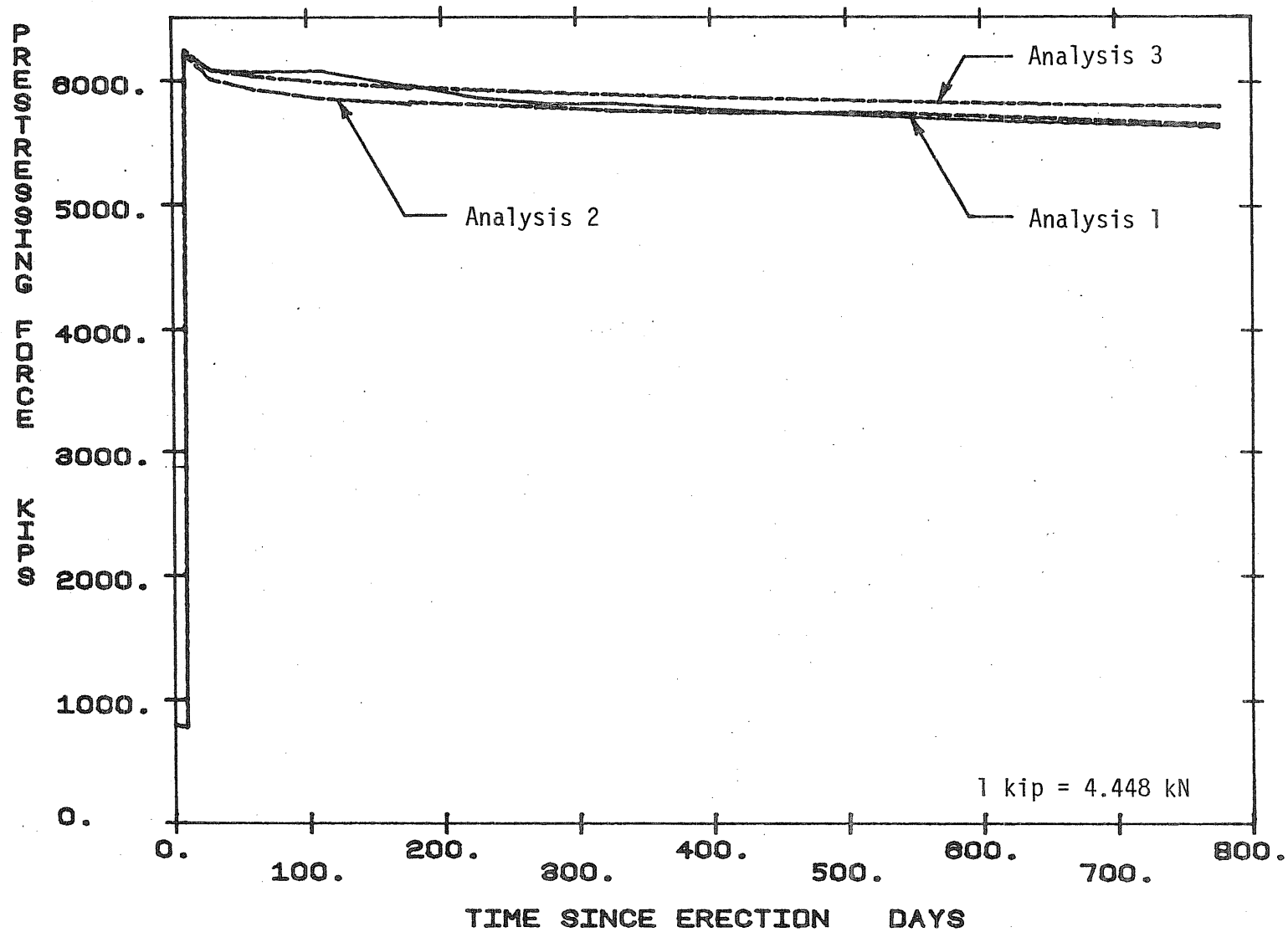


Fig. 5.3 Calculated Total Prestressing Force at Segment SB1-N16

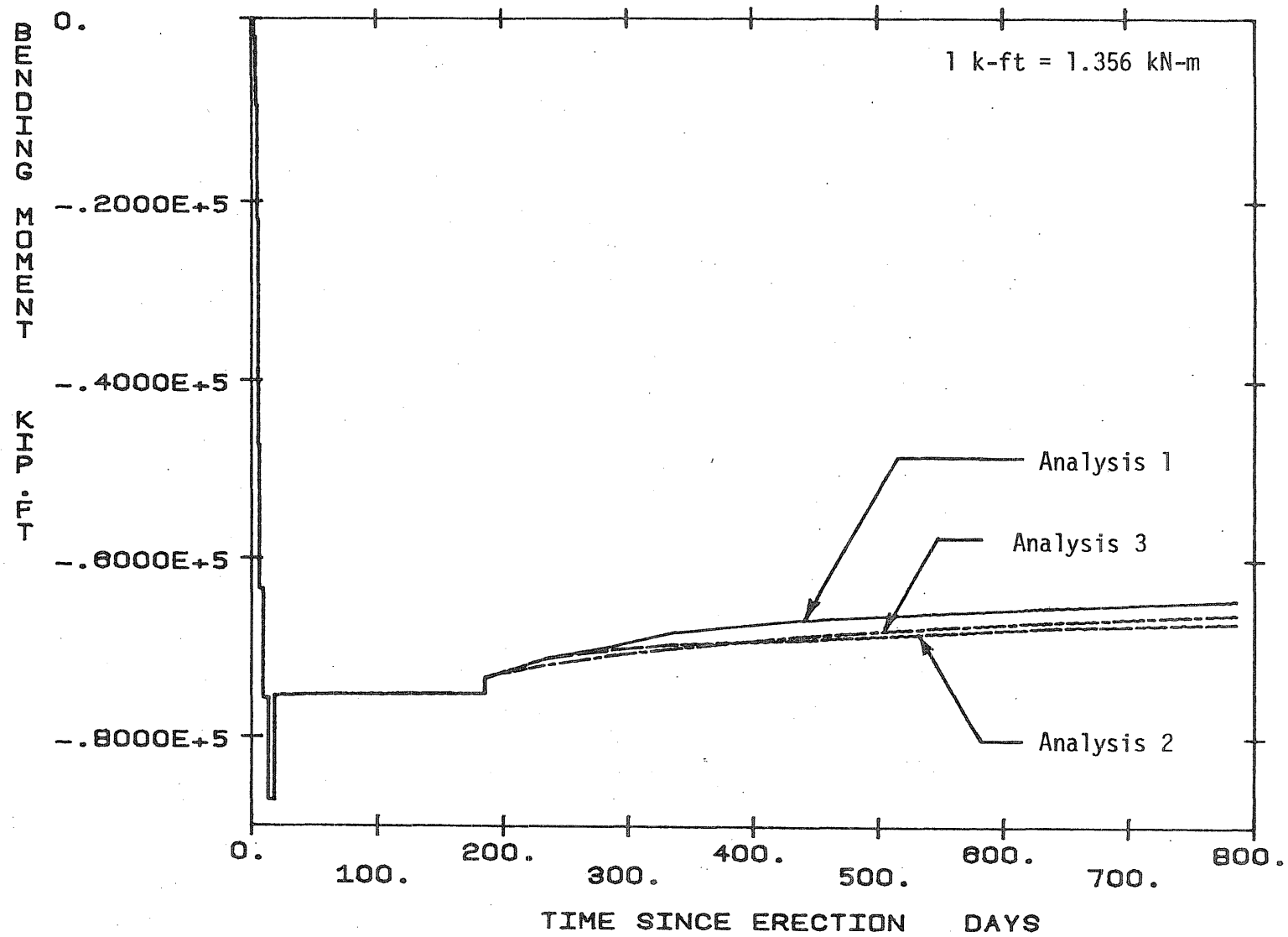


Fig. 5.4 Calculated Bending Moment at Segment SB1-N1

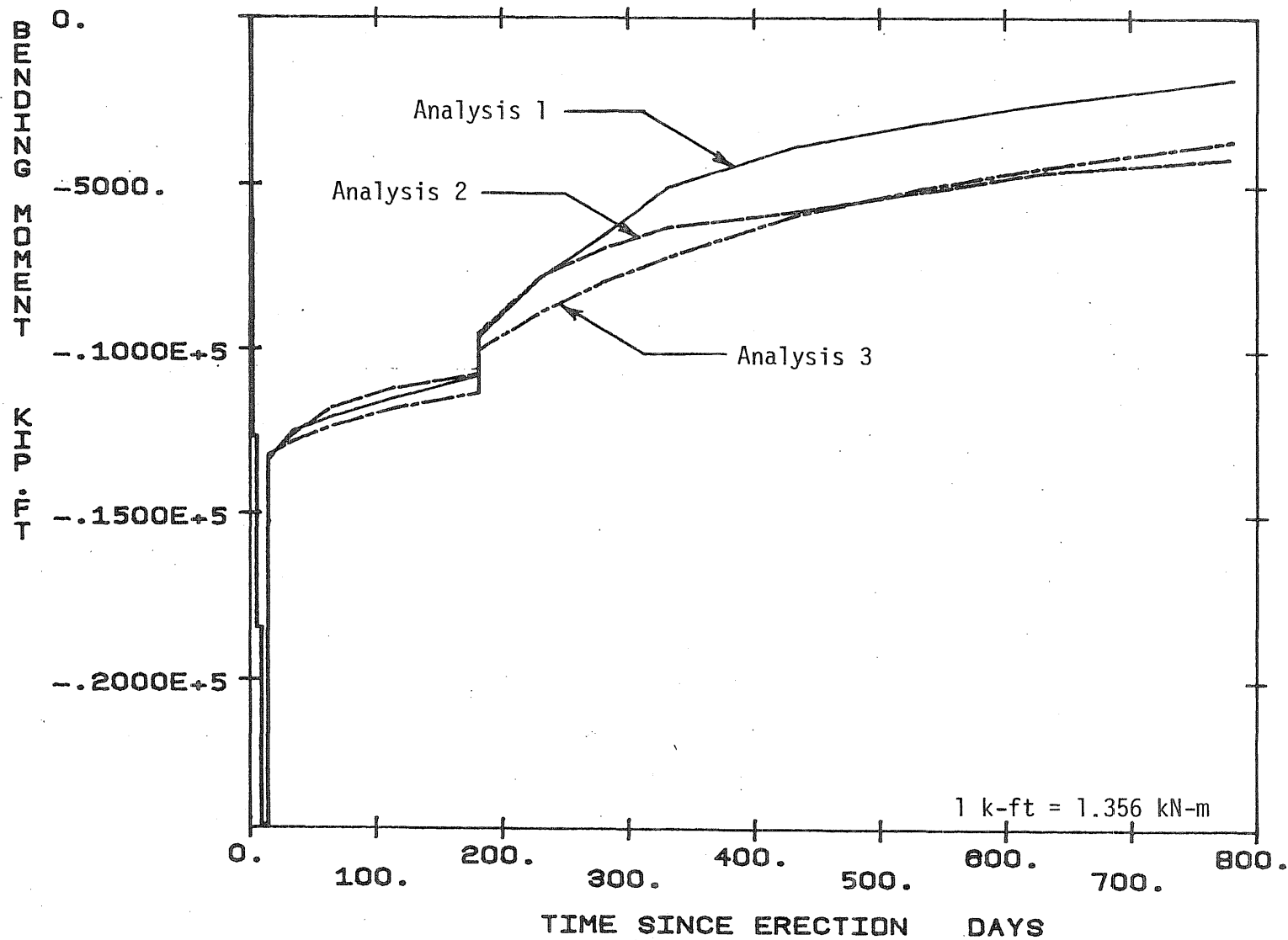


Fig. 5.5 Calculated Bending Moment at Segment SB1-N9

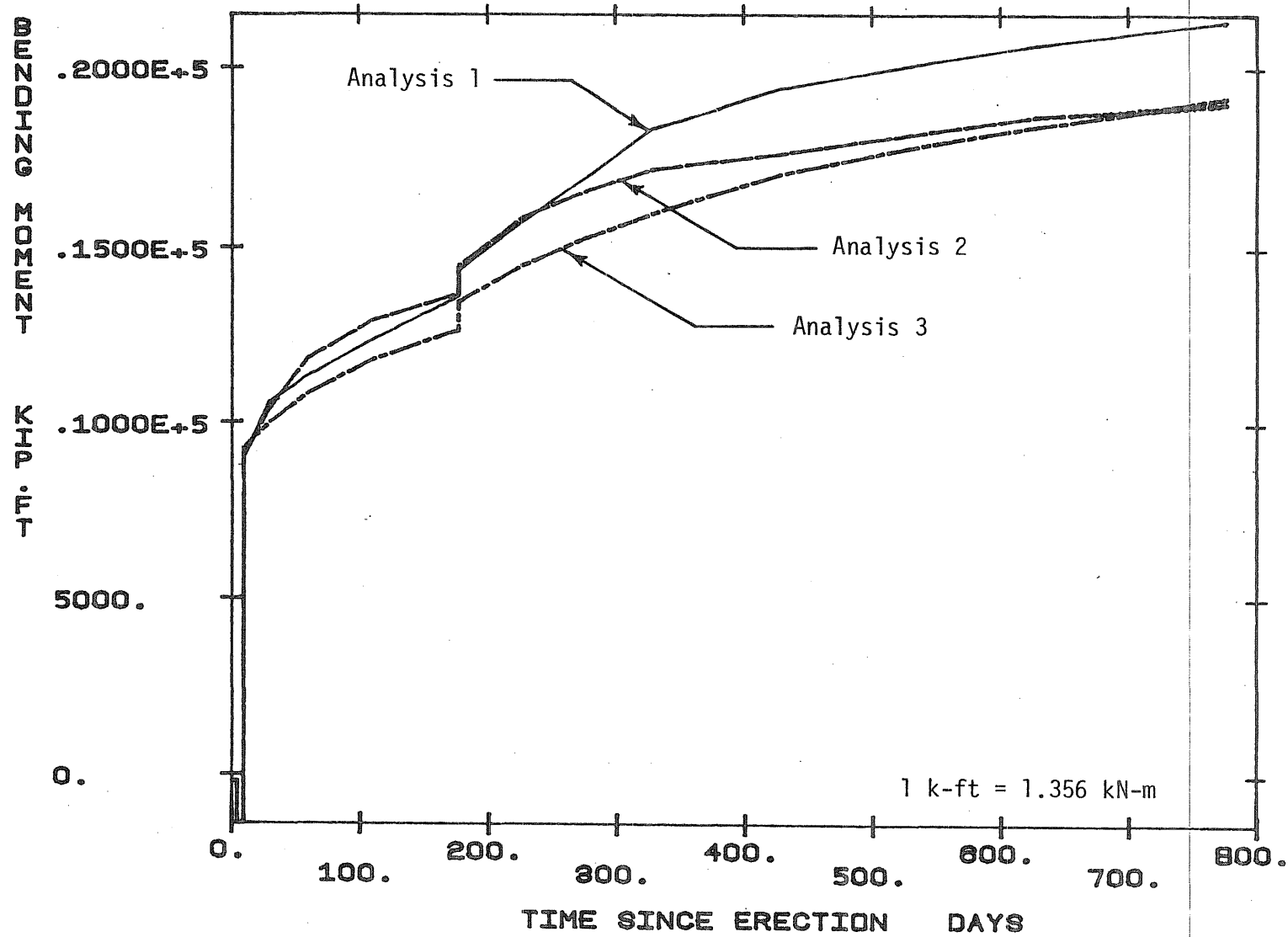


Fig. 5.6 Calculated Bending Moment at Segment SB1-N16

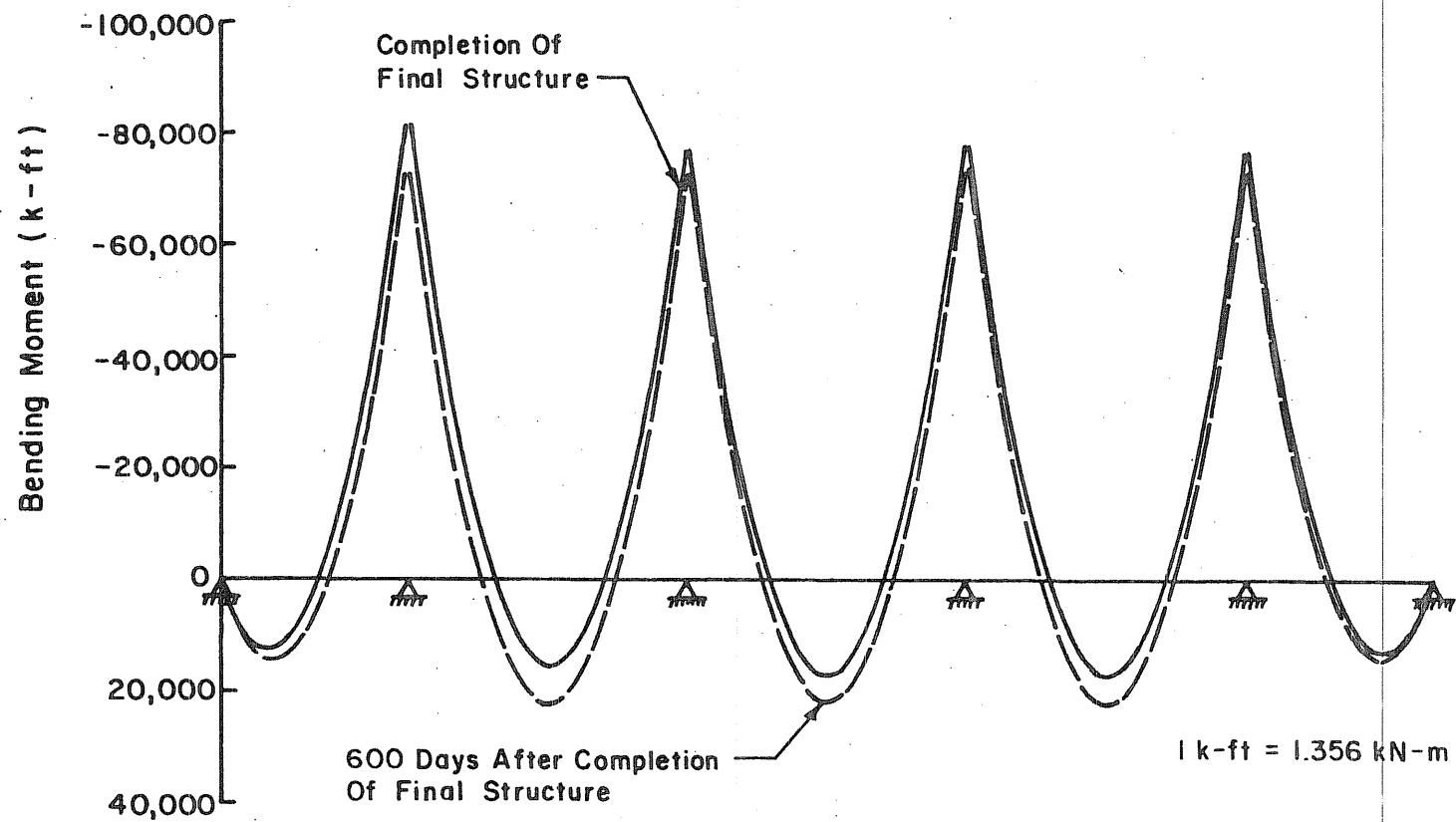


Fig. 5.7 Redistribution of Bending Moment in the Final Structure as Predicted by Analysis 1

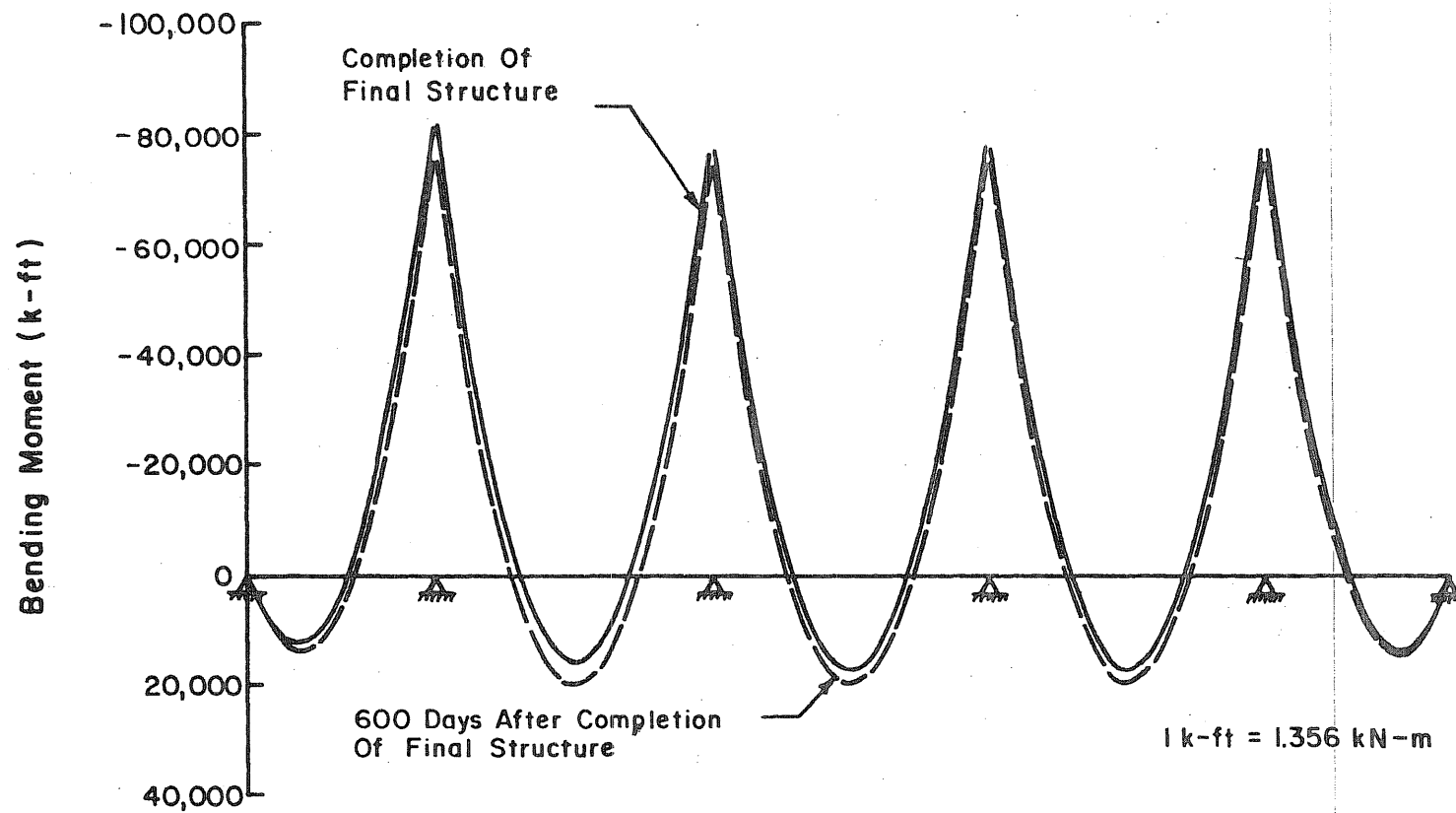


Fig. 5.8 Redistribution of Bending Moment in the Final Structure as Predicted by Analysis 2

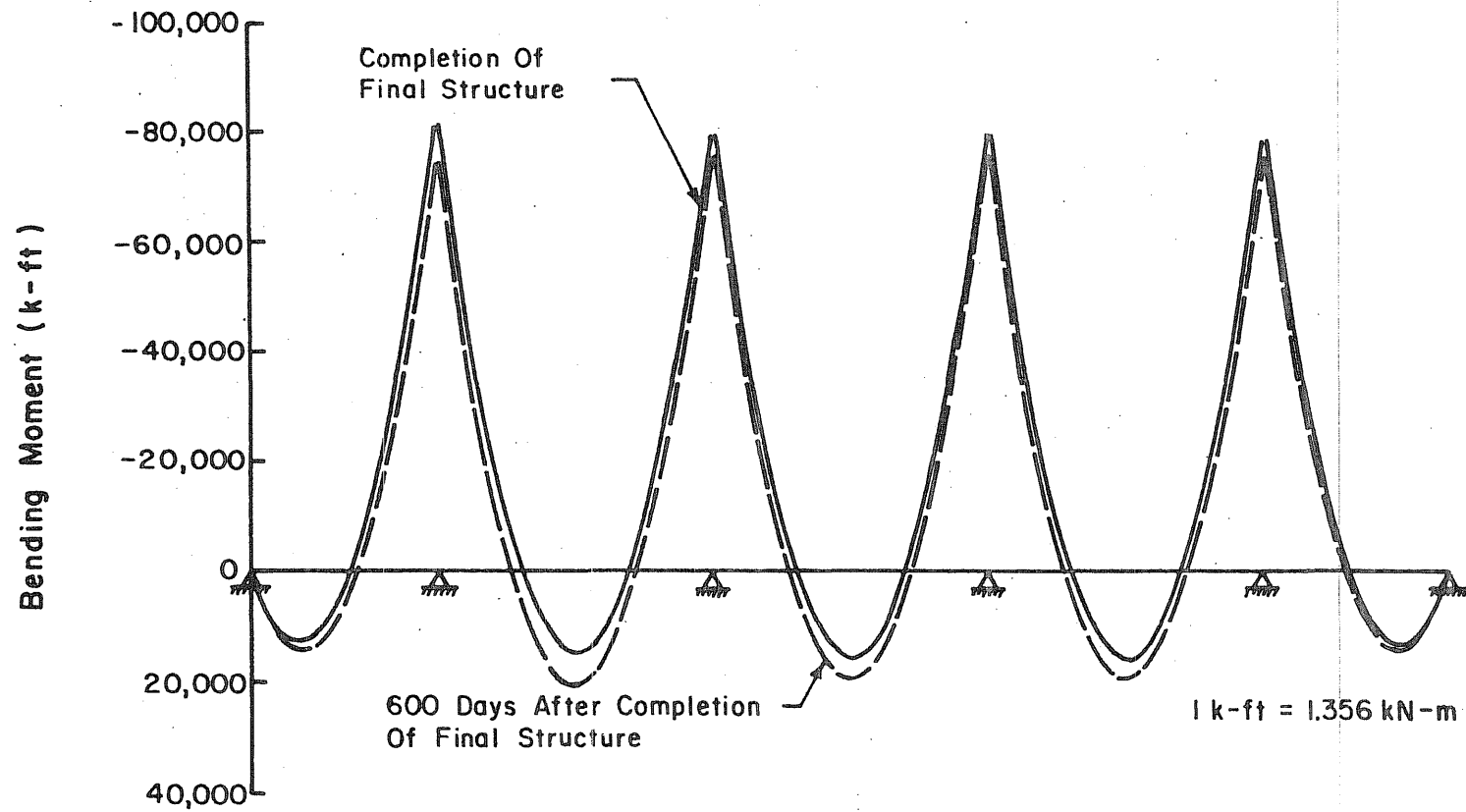


Fig. 5.9 Redistribution of Bending Moment in the Final Structure as Predicted by Analysis 3

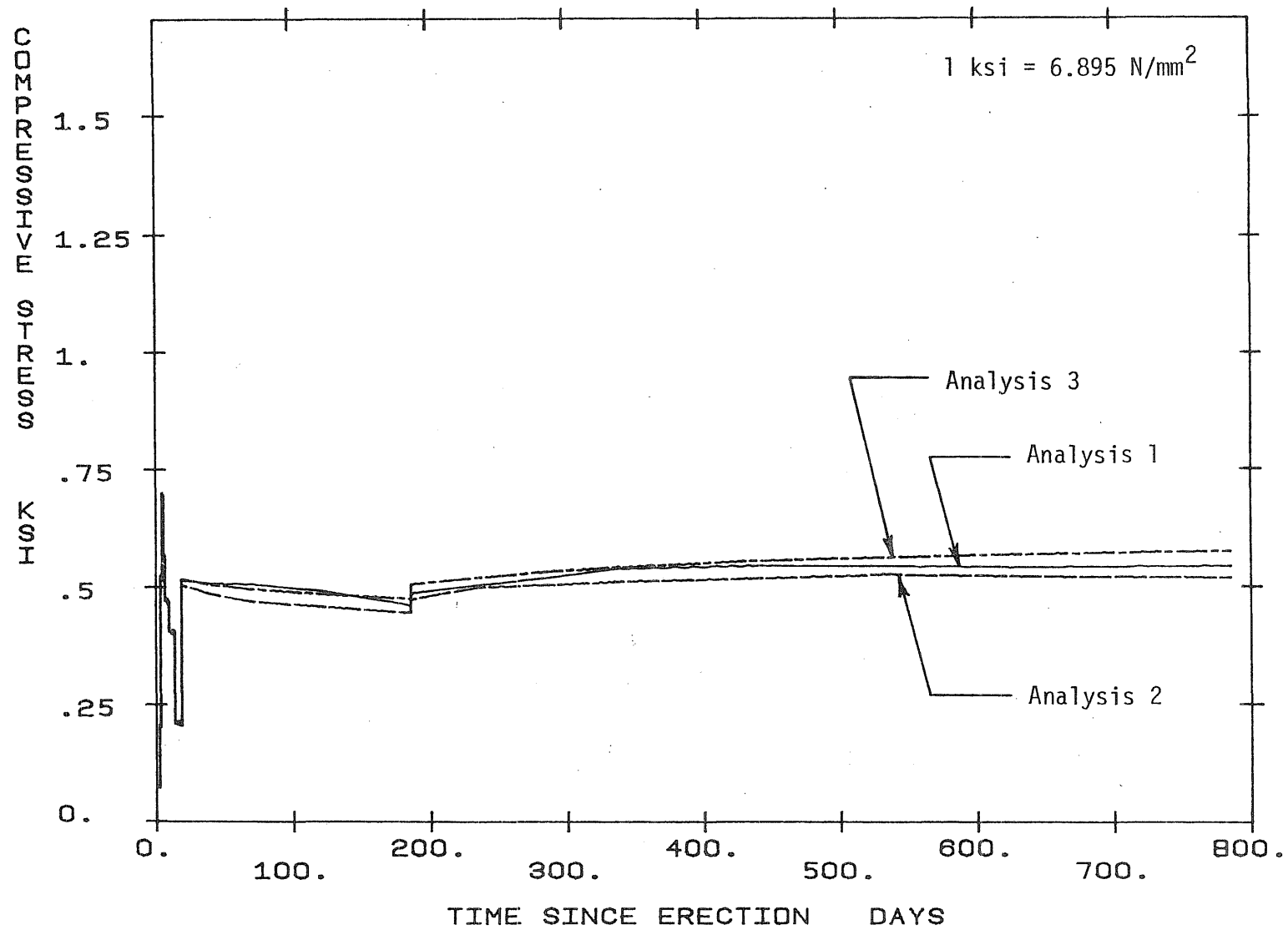


Fig. 5.10 Calculated Top Fiber Concrete Stress at Segment SB1-N1

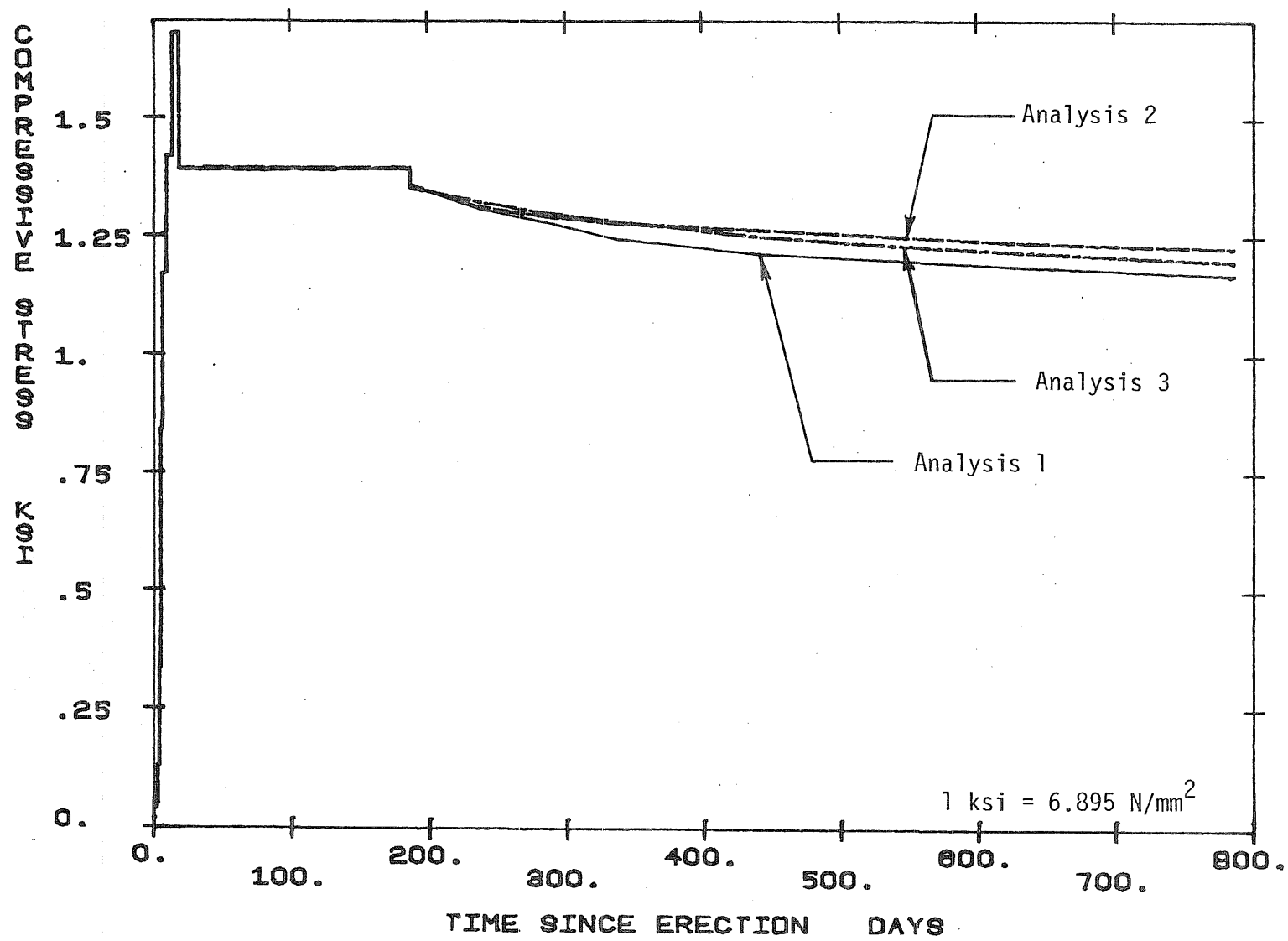


Fig. 5.11 Calculated Bottom Fiber Concrete Stress at Segment SB1-N1

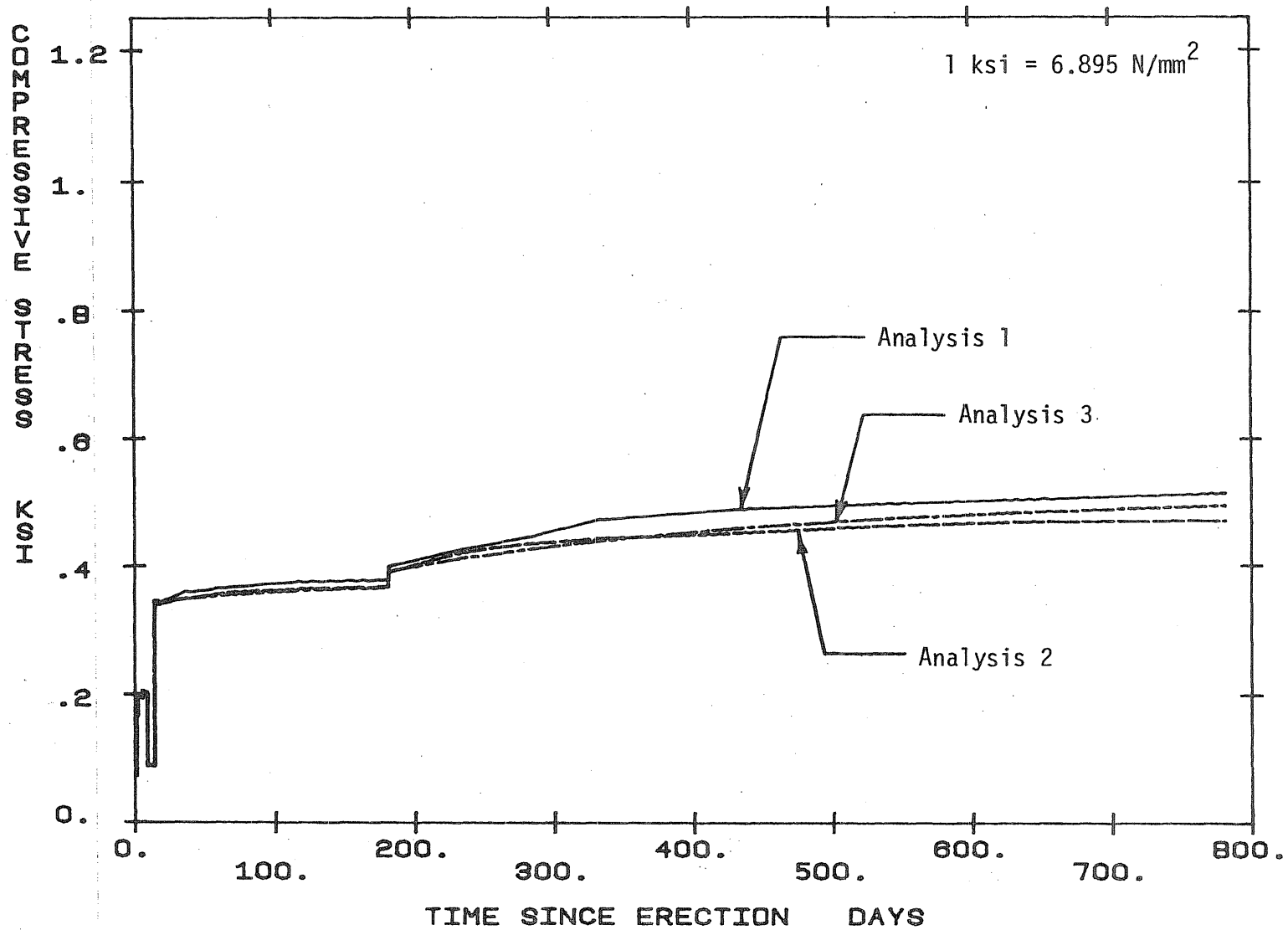


Fig. 5.12 Calculated Top Fiber Concrete Stresses at Segment SB1-N9

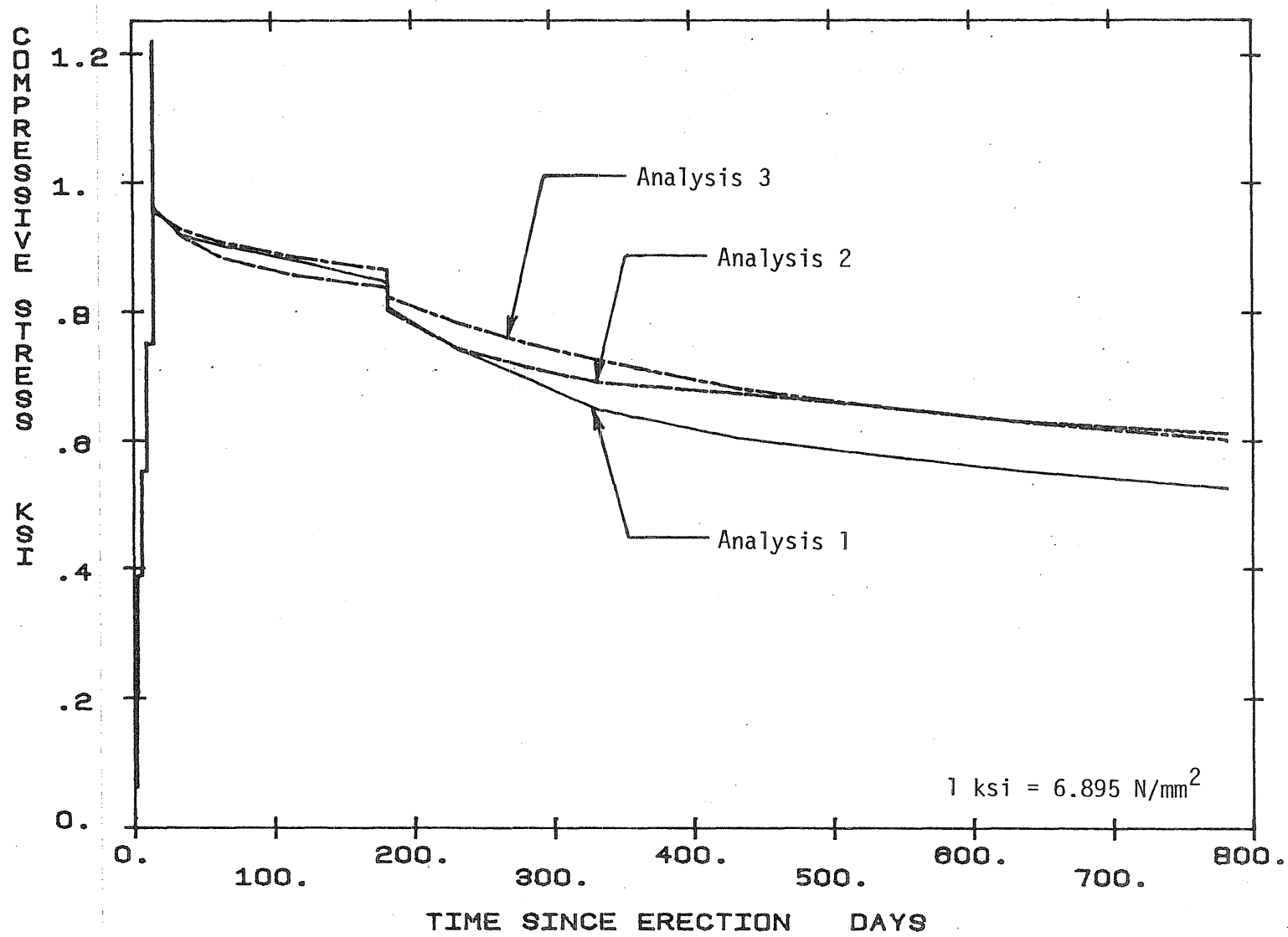


Fig. 5.13 Calculated Bottom Fiber Concrete Stresses at Segment SB1-N9

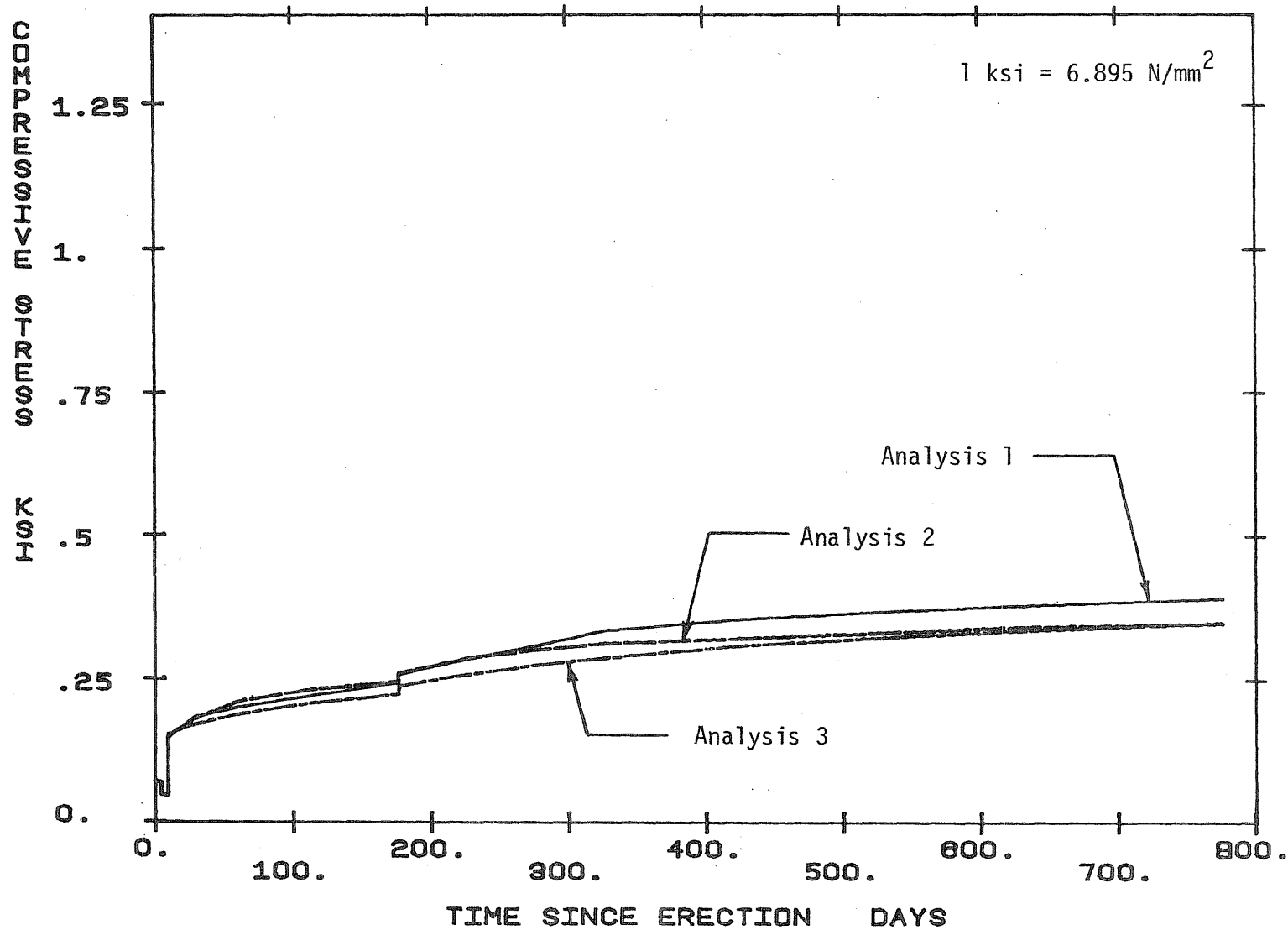


Fig. 5.14 Calculated Top Fiber Concrete Stresses at Segment SB1-N16

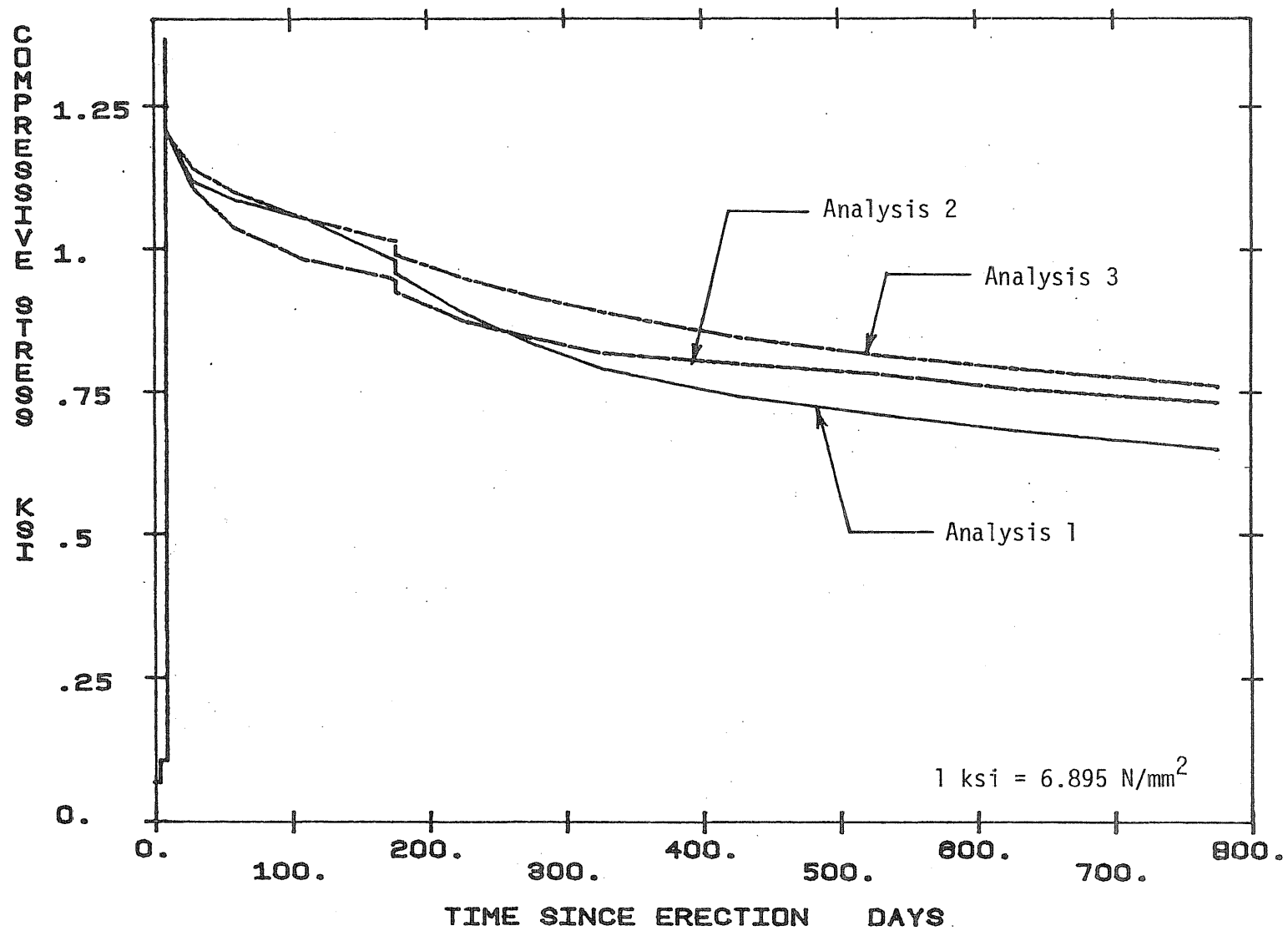


Fig. 5.15 Calculated Bottom Fiber Concrete Stresses at Segment SB1-N16

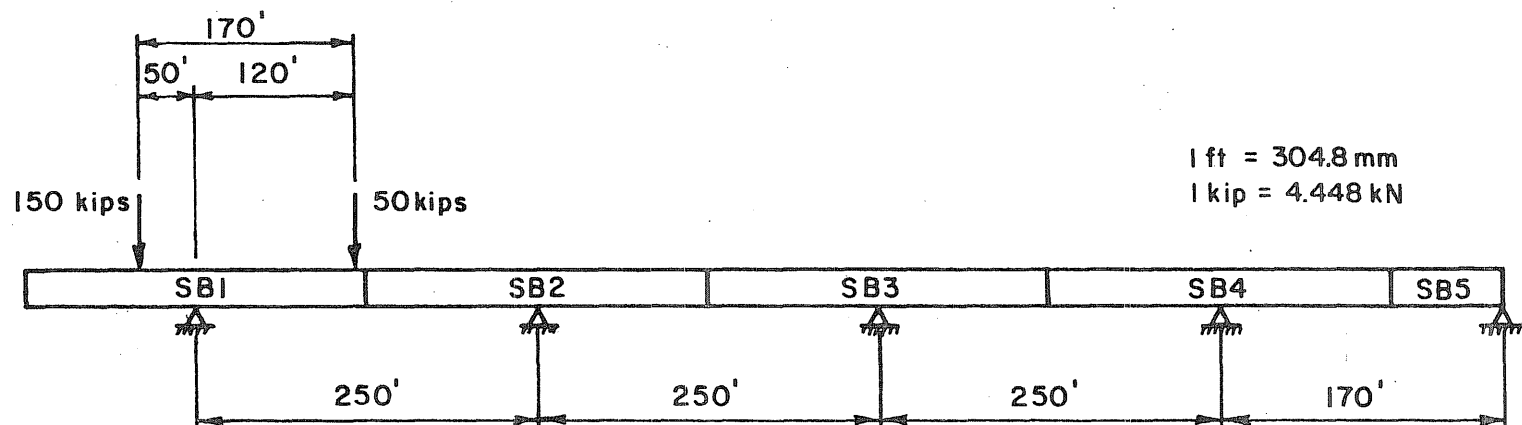


Fig. 5.16 Construction Loads Applied to Intermediate Structure 9

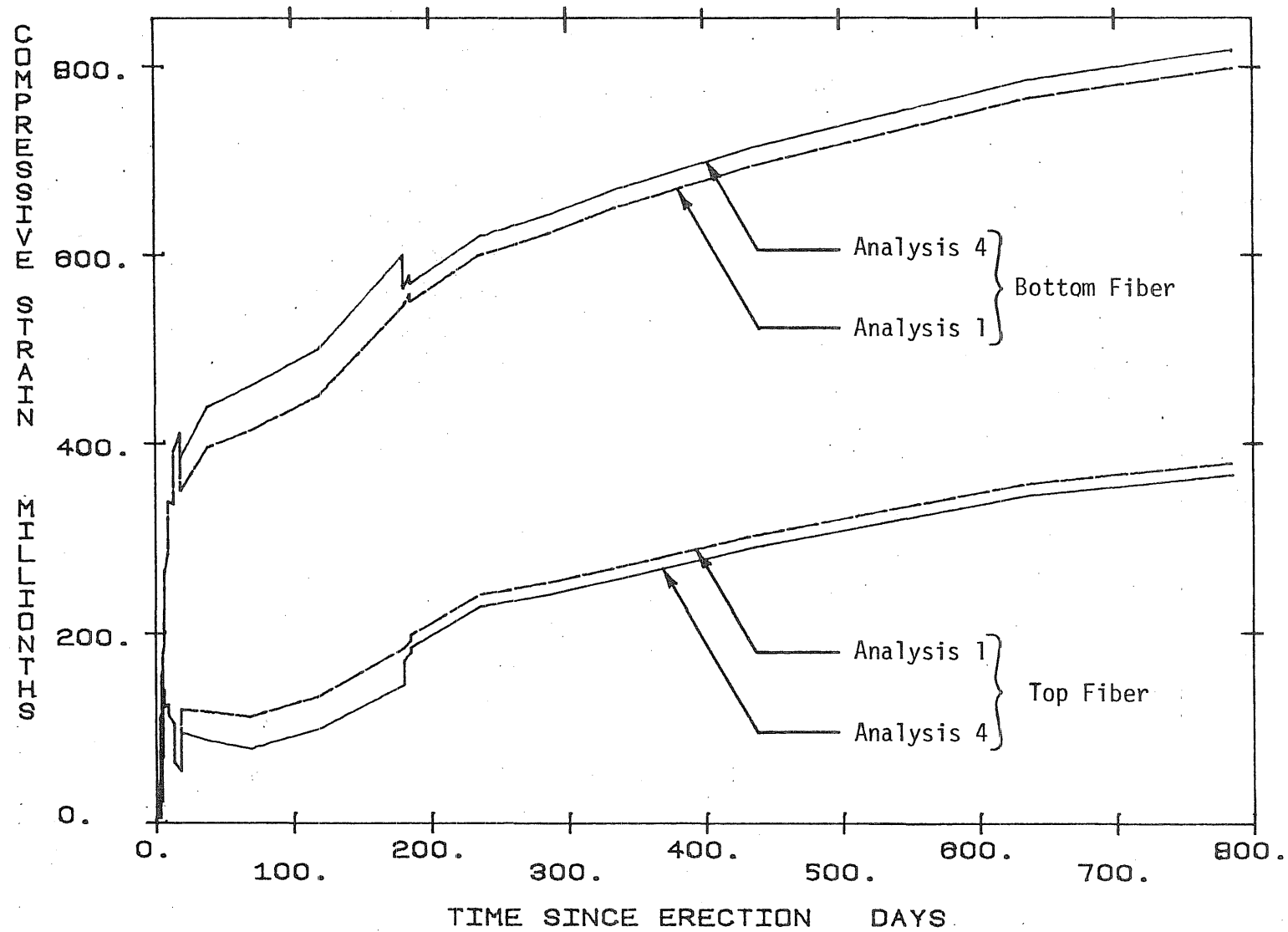


Fig. 5.17 Effects of the Construction Loads on the Extreme Fiber Concrete Strains at Segment SB1-N1

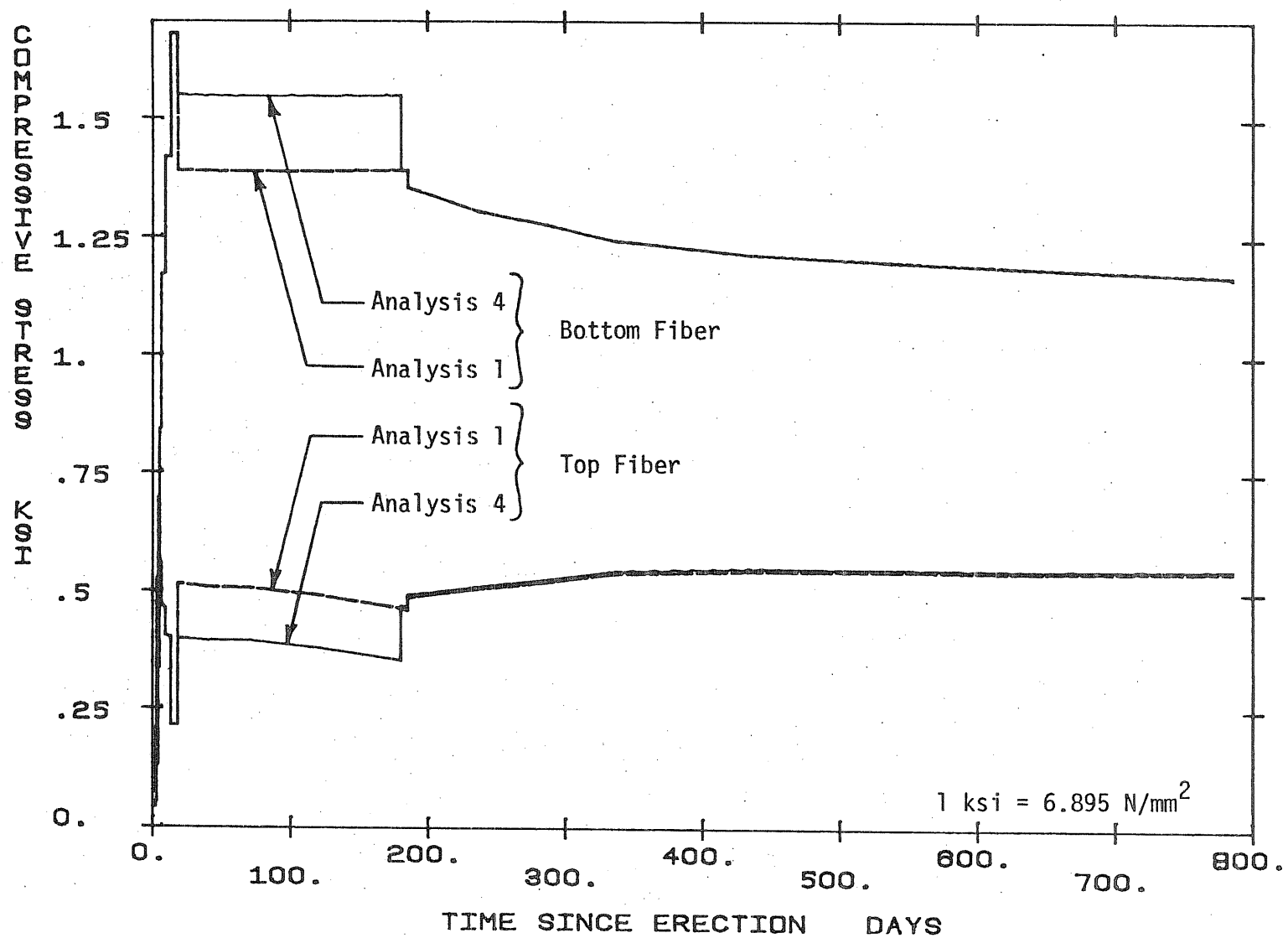


Fig. 5.18 Effects of the Construction Loads on the Extreme Fiber Concrete Stresses at Segment SB1-N1

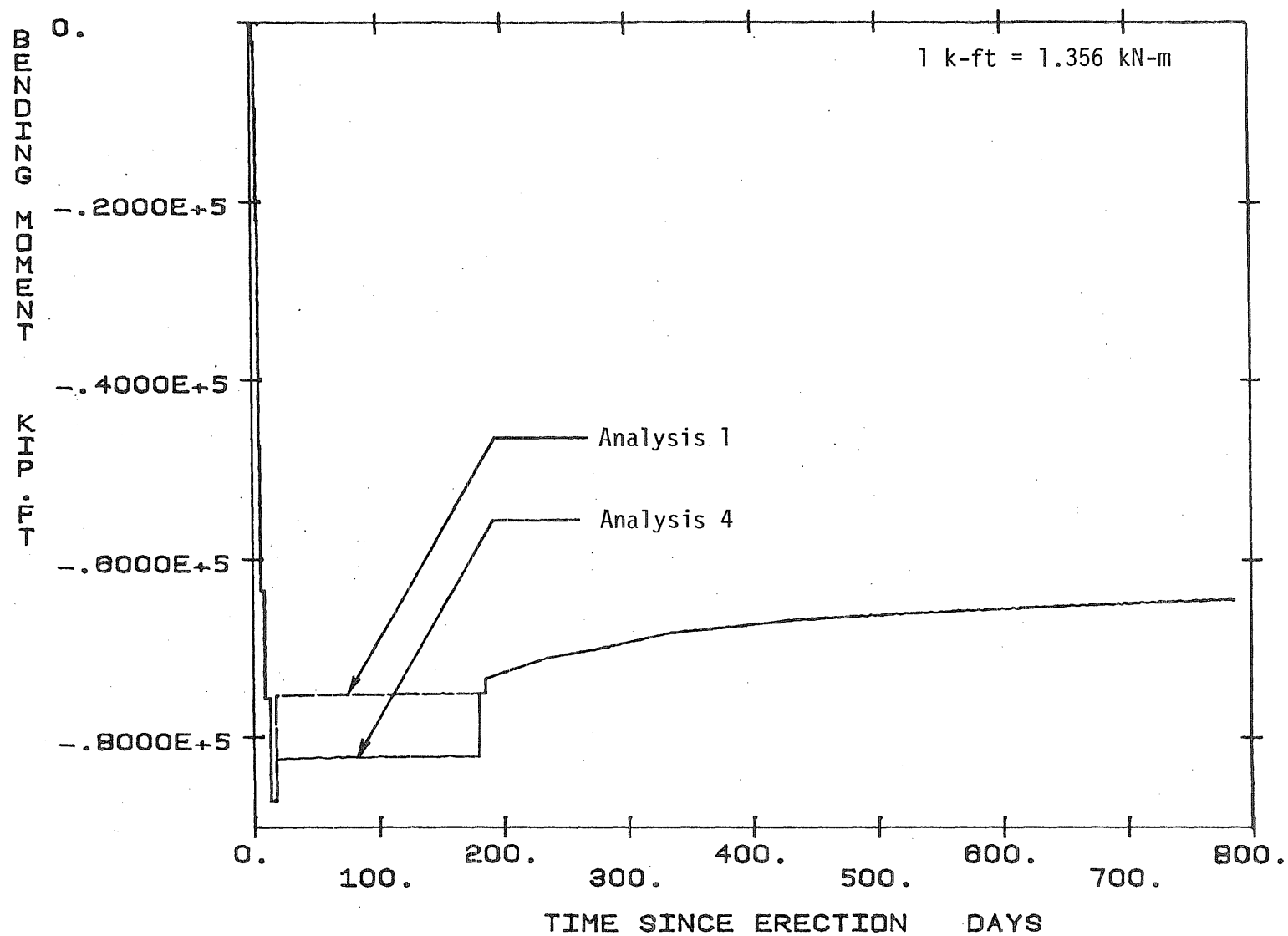


Fig. 5.19 Effects of the Construction Loads on the Bending Moment at Segment SB1-N1

APPENDIX A

DERIVATION OF EXPRESSIONS USED IN THE ANALYTICAL PROCEDURE

A.1 Creep Expressions According to the C.E.B. Recommendations

A.1.1 Expressions for C.E.B. Factors, K_t and K_d

When the time-dependent behavior of the structure was determined on the basis of creep and shrinkage properties as determined by the C.E.B. recommendations (11), the creep strains were estimated by making use of the method of superposition. For this particular case the computations were simplified by deriving mathematical expressions for the C.E.B. creep factors K_t and K_d , where K_t describes the time-dependence of creep and K_d reflects the effects of the concrete age at loading on creep. These multiplying factors are given by the C.E.B. in graphical form.

K_t was assumed to be described by the following exponential expression:

$$K_t = (1 - e^{-\alpha t^\beta}) \quad (A.1.1)$$

where: t = time in days, since the concrete was initially loaded and
 α and β = coefficients to be determined by fitting expression A.1.1 to the curves given by the C.E.B. recommendations for K_t .

Consideration of Fig. 2.6 reveals that K_t is also a function of theoretical thickness, d_m . A different set of values for α and β was derived for each K_t curve given by the C.E.B., i.e. for values of

$d_m = 5, 10, 20, 40$ and 80 cm. The values of α and β as derived by a curve fitting procedure for the above values of d_m are listed in Table A.1.

The values of α and β were determined as follows: First of all, rewrite Eq. A.1.1 as follows:

$$\ln [-\ln (1 - K_t)] = \beta \ln t + \ln \alpha \quad (\text{A.1.2})$$

For a particular value of d_m , the appropriate curve for K_t as given by the C.E.B. recommendations may be used to plot values of $\ln [-\ln (1 - K_t)]$ versus $\ln t$. If these values plot as a straight line then the functional form assumed by Eq. A.1.1 for K_t , is correct because Eq. A.1.2 represents the equation of a straight line in a $\ln [-\ln (1 - K_t)]$ versus $\ln t$ system of axes. Figure A.1 reveals that the above assumption was correct because the $\ln [-\ln (1 - K_t)]$ versus $\ln t$ values almost lie on a straight line. This plot applies to values of K_t for $d_m = 5$ cm.

The least squares fitting procedure (24) was then used to fit a straight line through these points. The intercept of this line on the $\ln [-\ln (1 - K_t)]$ axis yields $\ln \alpha$, from which α is readily determined. The slope of this line yields β .

K_d was assumed to be described by the following hyperbolic expression:

$$K_d = \frac{1}{A + B \tau^n} \quad (\text{A.1.3})$$

where: τ = concrete age at loading, in days and
 A, B , and n = coefficients to be determined by fitting expression A.1.3 to the curves given by the C.E.B. recommendations for K_d .

Curves of K_d for normal portland cement and high early strength cement are given (see Fig. 2.3). A set of values of A, B and n had to be

derived for each curve. The same basic procedure was followed to fit Eq. A.1.3 to the curves given by the C.E.B. recommendations for K_d , as for the case of K_t :

Rewrite Eq. A.1.3 as follows:

$$\frac{1}{K_d} = B \tau^n + A \quad (A.1.4)$$

The non-linear expression given by Eq. A.1.4 can be linearized by assuming a value for n . Using the least squares procedure a straight line was fitted to values of $1/K_d$ and τ^n , as determined by using the curves given by the C.E.B. recommendations. The intercept on the $1/K_d$ axis and the slope directly yield the values of B and A , respectively. Following this procedure a set of values for A and B may be determined for a particular value of n . Each of these fitted curves were then compared to the K_d values given by the C.E.B. recommendations, by finding the sum of the squares of the errors at a number of specific values of τ . The values of A , B and n corresponding to the fitted curve that yielded the smallest value of the sum of the squares of the errors, as found above, were used.

The following expressions were used for K_d :

Normal portland cement

$$K_d = \frac{1}{0.402 + 0.152 \tau^{0.4}} \quad (A.1.5)$$

High early strength cement

$$K_d = \frac{1}{0.309 + 0.284 \tau^{0.4}} \quad (A.1.6)$$

These expressions are compared to the values of K_d given by the C.E.B. recommendations in Fig. A.2.

A.1.2 Calculation of the Change in Creep Strain During a Time Interval

In what follows an expression is derived for the calculation of the change in creep strain over a time interval. This expression applies specifically to the case where the creep properties of the concrete are based on the C.E.B. recommendations. As explained before, the method of superposition was used to predict the creep response of concrete when the C.E.B. creep properties were used.

According to the C.E.B. recommendations the creep strain may be expressed as follows:

$$\epsilon_{cr}(t) = \frac{f_c}{E_{b28}} K_c K_b K_e K_d K_t \quad (A.1.7)$$

where: f_c = constant sustained concrete stress,
 E_{b28} = secant modulus of elasticity of the concrete at 28 days and
 K_c, K_b, K_e, K_d, K_t = multiplying factors that reflect the effect of intrinsic and environmental factors on the magnitude of creep (see Sect. 2.2.3.1).

This expression may be rewritten as follows:

$$\epsilon_{cr}(t) = \frac{f_c}{E_{b28}} \xi K_d(\tau) K_t(t - \tau) \quad (A.1.8)$$

where: $\xi = K_c K_d K_e$,
 $K_d(\tau) = \frac{1}{A + B \tau^n}$,

$K_t(t-\tau) = [1 - e^{-\alpha(t-\tau)^\beta}]$ and

τ = age at which the concrete was initially loaded.

Applying the method of superposition in conjunction with Eq. A.1.8, the creep strain at time t_m is given by

$$\epsilon_{cr}(t_m) = \frac{\xi}{E_{b28}} \left\{ \sum_{i=1}^{m-1} \Delta f_{ci} K_d(t_i) [1 - e^{-\alpha(t_m-t_i)^\beta}] \right\} \quad (A.1.9)$$

where: Δf_{ci} = change in concrete stress at time t_i .

Notice that ξ/E_{b28} is written outside the summation due to the fact that this quotient is independent of time.

Similarly, the creep strain at time t_{m+1} is given by

$$\epsilon_{cr}(t_{m+1}) = \frac{\xi}{E_{b28}} \left\{ \sum_{i=1}^m \Delta f_{ci} K_d(t_i) [1 - e^{-\alpha(t_{m+1}-t_i)^\beta}] \right\} \quad (A.1.10)$$

The change of creep strain during the m -th time interval is given by

$$\Delta \epsilon_{cr}(\Delta t_m) = \epsilon_{cr}(t_{m+1}) - \epsilon_{cr}(t_m) \quad (A.1.11)$$

Substitution of expressions A.1.9 and A.1.10 into the above expression yields:

$$\Delta \epsilon_{cr}(\Delta t_m) = \frac{\xi}{E_{b28}} \left\{ \sum_{i=1}^m \Delta f_{ci} K_d(t_i) [e^{-\alpha(t_m-t_i)^\beta} - e^{-\alpha(t_{m+1}-t_i)^\beta}] \right\} \quad (A.1.12)$$

The above expression clearly illustrates that the calculation of creep strains at a given time requires a record of the previous stress history.

A.2 Elastic Recovery

As pointed out in Sect. 3.4, the elastic and creep recoveries associated with the change in prestressing force during the lifetime of a prestressed concrete member must be accounted for, otherwise the total prestress loss will be overestimated. Essentially, the elastic recovery of the concrete represents the effect of the restraint offered by the prestressing steel to concrete deformation. Therefore, the approach followed in deriving an expression for the estimation of elastic recovery of the concrete was based on a process of reestablishing compatibility of the strains of the concrete and steel, at the level of the steel, when a strain was imposed on the concrete cross-section. The other requirement that must always be satisfied is that of equilibrium.

In what follows, a procedure is presented for the calculation of the effects of elastic recovery of the concrete when a linearly varying strain distribution is imposed on the concrete cross-section. No restriction is placed on the number of different tendons or the positions of the individual tendons over the depth of the cross-section. It is important to note that for all the derivations that follow, stresses and strains are taken negative for compression and positive for tension.

Firstly, stiffness matrices associated with the axial strain (i.e. strain at the centroid of the section) and the curvature of the section are derived for both the concrete and steel.

For the steel:

$$[K_s] \begin{Bmatrix} \epsilon_s \\ \phi_s \end{Bmatrix} = \begin{Bmatrix} P_s \\ M_s \end{Bmatrix} \quad (A.2.1)$$

The stiffness matrix for the steel is given by

$$[K_S] = E_S \begin{bmatrix} \sum A_i & \sum A_i e_i \\ \sum A_i e_i & \sum A_i e_i^2 \end{bmatrix} \quad (A.2.2)$$

- where: E_S = modulus of elasticity of the steel,
 A_i = cross-sectional area of tendon i ,
 e_i = eccentricity of tendon i measured from the centroidal axis of the section, taken positive when the tendon is below the centroidal axis, and negative when above,
 ϵ_S = strain associated with the steel, at the centroid of the section (see Fig. A.3),
 ϕ_S = curvature associated with the steel strain (see Fig. A.3),
 P_S = resultant of the forces in all the tendons, applied at the centroid of the section (see Fig. A.3) and
 M_S = resultant of the moments of the forces in all the tendons, about the centroid of the section (see Fig. A.3).

It is understood that the indicated summations in Eq. A.2.2 include all the tendons in the section.

For the concrete:

$$[K_C] \begin{Bmatrix} \epsilon_C \\ \phi_C \end{Bmatrix} = \begin{Bmatrix} P_C \\ M_C \end{Bmatrix} \quad (A.2.3)$$

The stiffness matrix for the concrete is given by

$$[K_C] = E_C \begin{bmatrix} A_C & 0 \\ 0 & I_C \end{bmatrix} \quad (A.2.4)$$

where: E_C = modulus of elasticity of the concrete,
 A_C = cross-sectional area of the concrete section,
 I_C = moment of inertia of the concrete section about the centroidal axis,
 ϵ_C = concrete axial strain (see Fig. A.4),
 ϕ_C = curvature of concrete section (see Fig. A.4),
 P_C = resultant force acting on the concrete section, applied at the centroid (see Fig. A.4) and
 M_C = resultant moment acting on the concrete section, about the centroid (see Fig. A.4).

The elements of each column of the above stiffness matrices were evaluated by setting the degree of freedom corresponding to the particular column to unity, while the other is set to zero. The forces required for equilibrium correspond to the elements of the particular column of the stiffness matrix. This process is illustrated for steel and concrete in Figs. A.3 and A.4, respectively.

Consider the case where a linearly varying strain is imposed on the concrete section. The strain distribution is defined by the strains at the extreme top and bottom fibers of the section, $\Delta\epsilon_t$ and $\Delta\epsilon_b$, respectively (see Fig. A.5). This strain clearly violates the compatibility assumption, i.e. that the change of strain in the steel is equal to the change of strain in the concrete at the same level. In order to restore compatibility, forces must be applied to the steel as well as the concrete. The resultant of the steel forces, P_S , is applied at the centroid of the section. The resultant of the moments of the steel forces about the centroid is designated by M_S . The resultant concrete force, P_C , is applied at the centroid, while the resultant moment about the centroid, acting on the concrete, is designated by M_C (see Fig. A.5).

Horizontal and moment equilibrium yields:

$$\begin{Bmatrix} P_s \\ M_s \end{Bmatrix} + \begin{Bmatrix} P_c \\ M_c \end{Bmatrix} = \begin{Bmatrix} 0 \\ 0 \end{Bmatrix} \quad (\text{A.2.5})$$

Compatibility of strains yield:

$$\begin{aligned} \epsilon_{st} - \epsilon_{ct} &= \Delta\epsilon_t \\ \epsilon_{sb} - \epsilon_{cb} &= \Delta\epsilon_b \end{aligned} \quad (\text{A.2.6})$$

See Fig. A.5 for the definition of the strains involved in Eq. A.2.6. These above expressions may be manipulated in order to express the compatibility requirements in terms of strains at the level of the centroid of the section and curvatures:

$$\begin{aligned} \epsilon_s - \epsilon_c &= \Delta\epsilon \\ \phi_s - \phi_c &= \Delta\phi \end{aligned} \quad (\text{A.2.7})$$

where: ϵ_s , ϵ_c and $\Delta\epsilon$ are defined in Fig. A.5, and ϕ_s , ϕ_c and $\Delta\phi$ are the curvatures as defined by

$$\begin{aligned} \phi_s &= \frac{\epsilon_{sb} - \epsilon_{st}}{d} \\ \phi_c &= \frac{\epsilon_{cb} - \epsilon_{ct}}{d} \\ \Delta\phi &= \frac{\Delta\epsilon_b - \Delta\epsilon_t}{d} \end{aligned}$$

Substitution of Eqs. A.2.1 and A.2.3 into A.2.5 yields

$$[K_S] \begin{Bmatrix} \epsilon_S \\ \phi_S \end{Bmatrix} + [K_C] \begin{Bmatrix} \epsilon_C \\ \phi_C \end{Bmatrix} = \begin{Bmatrix} 0 \\ 0 \end{Bmatrix}$$

Equations A.2.7 are used to eliminate ϵ_C and ϕ_C from the above expression. By performing this substitution and after rearrangement the following expression is obtained:

$$[K_C]^{-1} [K_S] + [I] \begin{Bmatrix} \epsilon_S \\ \phi_S \end{Bmatrix} = \begin{Bmatrix} \Delta\epsilon \\ \Delta\phi \end{Bmatrix}$$

where: I is a 2 x 2 identity matrix.

Upon substitution of the appropriate arrays and subsequent simplification

$$\begin{bmatrix} \left(1 + \frac{n \sum A_i e_i}{A_c}\right) & \frac{n \sum A_i e_i}{A_c} \\ \frac{n \sum A_i e_i}{I_c} & \left(1 + \frac{n \sum A_i e_i^2}{I_c}\right) \end{bmatrix} \begin{Bmatrix} \epsilon_S \\ \phi_S \end{Bmatrix} = \begin{Bmatrix} \Delta\epsilon \\ \Delta\phi \end{Bmatrix} \quad (A.2.8)$$

where: $n = E_S/E_C =$ modular ratio.

Equation A.2.8 can be solved to yield ϵ_S and ϕ_S . Once these quantities are known, they can be used to find the change in steel force (prestressing force) associated with the imposed concrete strain, as well

as the corrections that must be applied to the imposed concrete strain to yield the final concrete strain.

The change in steel force in the i-th tendon is given by:

$$P_{si} = (\epsilon_s + \phi_s e_i) A_i E_s \quad (A.2.9)$$

The corrections that must be applied to the imposed concrete strains at the top and bottom fibers of the section are given by:

$$\begin{aligned} \epsilon_{ct} &= (\epsilon_s - \phi_s y_t) - \Delta\epsilon_t \\ \epsilon_{cb} &= (\epsilon_s + \phi_s y_b) - \Delta\epsilon_b \end{aligned} \quad (A.2.10)$$

where: y_t and y_b are the distances of the centroid to the extreme top and bottom fibers, respectively.

The total corrected concrete strains at the extreme top and bottom fibers of the section, are given by:

$$\begin{aligned} \epsilon'_{ct} &= \Delta\epsilon_t + \epsilon_{ct} \\ \epsilon'_{cb} &= \Delta\epsilon_b + \epsilon_{cb} \end{aligned} \quad (A.2.11)$$

The changes in concrete stress, associated with the change in steel force are obtained as follows:

$$\begin{aligned} f_{c_{top}} &= \frac{P_c}{A_c} - \frac{M_c y_t}{I_c} \\ f_{c_{bot}} &= \frac{P_c}{A_c} + \frac{M_c y_b}{I_c} \end{aligned} \quad (A.2.12)$$

The values to be used for P_c and M_c in Eq. A.2.12 are obtained from Eqs. A.2.1 and A.2.5:

$$\begin{Bmatrix} P_c \\ M_c \end{Bmatrix} = - \begin{Bmatrix} P_s \\ M_s \end{Bmatrix} = - [K_s] \begin{Bmatrix} \epsilon_s \\ \phi_s \end{Bmatrix}$$

A.3 Calculation of Changes in Concrete Stress and Strain and Prestressing Force

As previously pointed out, the effects of creep, shrinkage and relaxation were assumed to be independent during a particular time interval. Thus, the effects of each of these phenomena could be determined separately during a time interval and then superimposed at the end of that time interval.

Each of these time-dependent effects as well as externally applied loads lead to a change in prestressing force, which goes hand in hand with an elastic change in concrete stress and strain. In what follows an outline is given of how the expressions given in Sect. A.2 were applied to account for the above-mentioned effects.

The change in free shrinkage strain that takes place at a particular section during a time interval may be readily determined. This strain is assumed to be uniformly distributed across the cross-section. By applying this strain distribution to the cross-section, Eq. A.2.8 may be used to find ϵ_s and ϕ_s . Subsequently, Eq. A.2.9 yields the change in prestressing force in each tendon and Eqs. A.2.12 yield the associated change in concrete stress, due to the change in shrinkage strain. The final corrected change in shrinkage strain for the time interval is obtained by using Eqs. A.2.11 in conjunction with Eqs. A.2.10.

The unrestrained change in creep strain during a time interval is determined at the extreme top and bottom fibers of the concrete section

using the procedure outlined in Sect. 3.2.4 or the method of superposition, depending on whether or not experimentally determined creep properties are being used. This change in creep strain is linearly distributed through the depth of the cross-section because linear creep theory is assumed to be applicable. The exact procedure outlined for the case of shrinkage is applied to the strain distribution determined above in order to find the change in prestressing force in each tendon as well as the change in concrete stress due to the change in creep strain for the time interval. This procedure simultaneously yields the final corrected change in creep strain that takes place during the time interval.

The procedure outlined in Sect. 3.3 is used to determine the change in prestressing force due to relaxation in each tendon during a particular time interval. Once these changes in prestressing force are known, beam theory may be used to calculate the associated changes in concrete stress and strain. The procedure outlined for the case of shrinkage is applied to this strain distribution to find the changes in prestressing force and concrete stress due to the elastic recovery of concrete. The corrected concrete strains thus obtained represent the final corrected change in concrete strain due to relaxation for the time interval. By adding the changes in prestressing force and concrete stress due to relaxation to the change in these quantities due to elastic recovery of concrete, as calculated above, the final corrected changes in prestressing force and concrete stress due to relaxation for the time interval are determined.

When loads are imposed on the structure, such as the effect of the self weight of a newly erected segment or the stressing of new tendons, the resulting concrete stresses and strains may be calculated at each section by making use of beam theory. The change in prestressing force and the associated change in concrete stress due to elastic recovery of the concrete are calculated by applying the procedure as outlined for the case of shrinkage to the above concrete strain distribution. The change in prestressing force, and corrected total change in strain thus obtained, represent the final values of these quantities due to application of the load.

The final corrected change in concrete stress is found by adding the change in concrete stress due to application of the load, to the change in concrete stress due to elastic recovery. For the particular case in which a new tendon is being stressed, it should be noted that this particular tendon is excluded from the calculations which account for the effects of elastic recovery.

For the case of applied loads, the concrete stresses and strains predicted by the above procedure, used in conjunction with the net section properties, will be the same as those predicted by using the transformed section properties. The general proof of this statement is rather tedious and consequently not presented here. Finally, it should be pointed out that the net concrete section properties should, in the strict sense, be used in the analytical procedure. In this study, the gross section properties were used.

A.4 Initial Prestressing Force

For post-tensioned systems, the initial prestressing force will generally vary along the length of a tendon due to instantaneous losses in force arising from friction and anchor-set. For such systems the following expression is commonly used for the estimation of friction losses (35):

$$f_s(x) = f_{s0} e^{-(kx + \mu\alpha)} \quad (\text{A.4.1})$$

where: $f_s(x)$ = steel stress at a distance x from the jacking end,
 f_{s0} = steel stress at the jacking end,
 e = base of Napierian logarithms,
 k = wobble friction coefficient per unit length,
 μ = curvature friction coefficient,
 α = total angular change of the tendon profile measured from the jacking end to the point at a distance x from this end and

x = distance from the jacking end to the point on the tendon being considered.

It is understood that the steel stresses in Eq. A.4.1 apply to the time immediately following the stressing operation but prior to anchoring.

Methods for finding the prestress losses associated with anchor-set may be found in Refs. 18, 29 and 40. The iterative approach given by Leonhardt (40) accounts for the effects of the actual tendon profile, and furthermore makes provision for the possibility that the reverse coefficient of friction may be unequal to the coefficient of friction associated with stressing of the tendon. In general the reverse coefficient of friction is larger than the coefficient associated with stressing of the tendon. When the above approach is applied to straight tendons, closed-form expressions may be derived for the total initial prestressing force.

In what follows, expressions are developed for the calculation of the initial prestressing force in straight tendons. These expressions account for the instantaneous loss of prestressing force associated with friction and anchor-set.

Considering Fig. A.6, it may be seen that the effect of anchor-set is to reduce the steel stress from $f_s(x)$ to $f_s^*(x)$. The distance over which anchor-set affects the prestressing force extends over a distance b from the live anchor. This distance will be referred to as the slip length. Considering an element dx of the tendon situated a distance x from the jacking end, the change in its length $d\Delta$ due to anchor set may be written

$$d\Delta = \frac{1}{E_s} [f_s(x) - f_s^*(x)] dx \quad (A.4.2)$$

The total change in length that takes place in the tendon over the slip length b must be equal to the amount that the tendons slip at the

anchor Δ due to anchor set. The total slip may be obtained by integration of Eq. A.4.2:

$$\Delta = \frac{1}{E_s} \int_0^b [f_s(x) - f_s^*(x)] dx = \frac{1}{E_s} (\text{Area ABC}) \quad (\text{A.4.3})$$

Thus, the area ABC is linearly related to the slip that takes place at the anchor.

Applying Eq. A.4.1 to the case of straight tendons (i.e. $\alpha = 0$), $f_s(x)$ and $f_s^*(x)$ may be expressed as (see Fig. A.6):

$$f_s(x) = f_{so} e^{-kx} \quad (\text{A.4.4})$$

$$f_s^*(x) = f_{sb} e^{-k(b-x)} = f_{so} e^{-2kb} e^{kx} \quad (\text{A.4.5})$$

Substitution into Eq. A.4.3 and performing the indicated integration yields:

$$\Delta = \frac{f_{so}}{kE_s} [1 - e^{-kb}]^2 \quad (\text{A.4.6})$$

Eq. A.4.6 is now solved for the slip length b :

$$b = -\frac{1}{k} \ln \left[1 - \sqrt{\frac{\Delta k E_s}{f_{so}}} \right] \quad (\text{A.4.7})$$

where: \ln = Napierian logarithm.

Once the slip length, b , is known, the initial steel stress can be calculated by using Eq. A.4.5 over the interval $0 \leq x \leq b$ and Eq. A.4.4 over the rest of the tendon. These expressions may be written in terms of prestressing force simply by replacing the steel stresses by appropriate values of steel force. It must be confirmed that the slip length, b , is less than or equal to the tendon length.

In the case of segmentally constructed post-tensioned bridges, some of the prestressing tendons may be very short. In these short tendons it is possible that the slip length may extend over the entire length of the tendon. Consideration of Fig. A.7 will reveal that knowledge of $f_s(L)$, the steel stress at the dead-end anchor, will enable one to estimate the steel stress everywhere in the tendon.

Referring to Fig. A.7:

$$f_s^*(x) = f_s(L) e^{-k(L-x)} \quad (A.4.8)$$

where: L = total length of the tendon.

Eq. A.4.4 for $f_s(x)$ is, of course, still valid. Bearing in mind that the slip that takes place at the anchor is related to $1/E_s$ (Area ABCD),

$$\Delta = \frac{1}{E_s} \int_0^L [f_s(x) - f_s^*(x)] dx = \frac{1}{E_s} (\text{Area ABCD}) \quad (A.4.9)$$

Substituting Eqs. A.4.4 and A.4.8 into the above expression, performing the integration and solving for $f_s(L)$, the following expression is obtained:

$$f_s(L) = f_{so} + \frac{\Delta k E_s}{(e^{-kL} - 1)} \quad (A.4.10)$$

Once $f_s(L)$ is known, the initial steel stress in the tendon may be calculated from Eq. A.4.8.

For tendons stressed from both ends, the procedures outlined above may be followed to determine the initial prestressing force. If the slip length is less than or equal to half the tendon length, the first set of equations is used independently at both ends of the tendon. If the slip length exceeds half the tendon length, the second set of equations may be used, with L set equal to half the length of the tendon. For this particular case only one half of the tendon need be considered because the variation of prestressing force will be symmetrical about the middle of the tendon.

A.5 Effects of Static Indeterminacy

For statically indeterminate structures, the equations of equilibrium do not yield enough information to enable one to determine the stresses that arise in the structure due to the application of load. Thus, the material properties need to be included in the solution of such a problem. Furthermore, the time-dependent deformations of statically indeterminate prestressed concrete structures may be expected to lead to time-dependent changes in stress distribution. Specifically, for statically indeterminate prestressed concrete beams this means that a time-dependent redistribution of bending moment may be expected to take place due to the combined effects of shrinkage, creep and relaxation.

In this study, the effects of static indeterminacy were treated by a flexibility approach. In order to outline the approach followed, consider the beam continuous over n supports, as illustrated in Fig. A.8a. Firstly, the structure is made statically determinate by removing all the interior supports, as shown in Fig. A.8b. In general, the imposed load system or time-dependent strains, whichever is being considered, will impose non-zero deflections in the equivalent statically determinate beam at the locations of the interior supports.

From this point on the object is to find a set of point loads that will satisfy the original boundary conditions, when they are applied to the equivalent statically determinate structure at the positions of the supports. These point loads correspond to the unknown interior reactions. This objective is accomplished by calculating the deflections of the equivalent statically determinate structure at the positions of the interior supports due to a unit point load applied, in turn, at the locations of each interior support. Figure A.8c defines these deflections for the unit point load applied at support j . By making use of the principle of superposition and the fact that the vertical deflection at each support is zero, the following expressions may be written:

$$\begin{array}{rcl}
 R_2 \delta_{22} & + R_3 \delta_{23} & + \dots + R_{(n-1)} \delta_{2(n-1)} + \Delta_2 = 0 \\
 R_2 \delta_{32} & + R_3 \delta_{33} & + \dots + R_{(n-1)} \delta_{3(n-1)} + \Delta_3 = 0 \\
 - & - & - \\
 - & - & - \\
 - & - & - \\
 R_2 \delta_{(n-1)2} & + R_3 \delta_{(n-1)3} & + \dots + R_{(n-1)} \delta_{(n-1)(n-1)} + \Delta_{(n-1)} = 0
 \end{array}$$

(A.5.1)

where: Δ_i = deflection of the equivalent statically determinate structure at the location of support i due to the effects of applied loads or time-dependent effects, whichever is being considered,

δ_{ij} = deflection of the equivalent statically determinate structure at the location of support i due to a unit point load applied at the location of support j and

R_i = vertical reaction at support i .

The positive directions of the above quantities are defined in Fig. A.8. Equations A.5.1 represent $(n-2)$ simultaneous equations in $(n-2)$ unknowns. This system of equations may be cast in matrix form as follows:

$$\begin{bmatrix} \delta_{22} & \delta_{23} & - & - & - & \delta_{2(n-1)} \\ \delta_{32} & \delta_{33} & - & - & - & \delta_{3(n-1)} \\ - & - & & & & - \\ - & - & & & & - \\ - & - & & & & - \\ \delta_{(n-1)2} & \delta_{(n-1)3} & - & - & - & \delta_{(n-1)(n-1)} \end{bmatrix} \begin{Bmatrix} R_2 \\ R_3 \\ - \\ - \\ - \\ R_{(n-1)} \end{Bmatrix} = \begin{Bmatrix} - \Delta_2 \\ - \Delta_3 \\ - \\ - \\ - \\ - \Delta_{(n-1)} \end{Bmatrix} \quad (\text{A.5.2})$$

This expression may be represented in a more compact notation as:

$$[F] \{R\} = - \{\Delta\} \quad (\text{A.5.3})$$

This system of equations may readily be solved to yield $\{R\}$, the unknown reactions at the interior supports. Once these reactions are known, they may be applied to the equivalent statically determinate structure as point loads and the resulting moments, stresses, strains and deflections calculated. It should be noted that for the case of a tendon being stressed, the moments thus calculated are the so-called secondary, or parasitic, moments due to prestressing. The total of the moments, stresses, strains and deflections due to the applied actions or deformations is obtained by superimposing the results obtained above on the results obtained by applying the actual action or deformations to the equivalent statically determinate structure.

In the light of the above derivation, it should be clear that the elements of a particular column of the flexibility matrix $[F]$ may be generated by finding the deflection of the equivalent statically determinate structure at the locations of each of the interior supports, due to the application of a unit point load at the location of the support to which this particular column of the flexibility matrix applies (see Eqs. A.5.2 and A.5.3 and Fig. A.8c).

Finally, the numerical integration procedure as outlined by Godden (23) was used for the calculation of deflections in this study.

Table A.1: Coefficients for the Expression for the C.E.B. Creep and Shrinkage Factor, K_t

Theoretical Thickness (cm)	α	β
5	0.139	0.515
10	0.0709	0.574
20	0.0331	0.608
40	0.0103	0.713
80	0.00101	0.934

Note: These coefficients are for use with the following expression:

$$K_t = (1 - e^{-\alpha t^\beta})$$

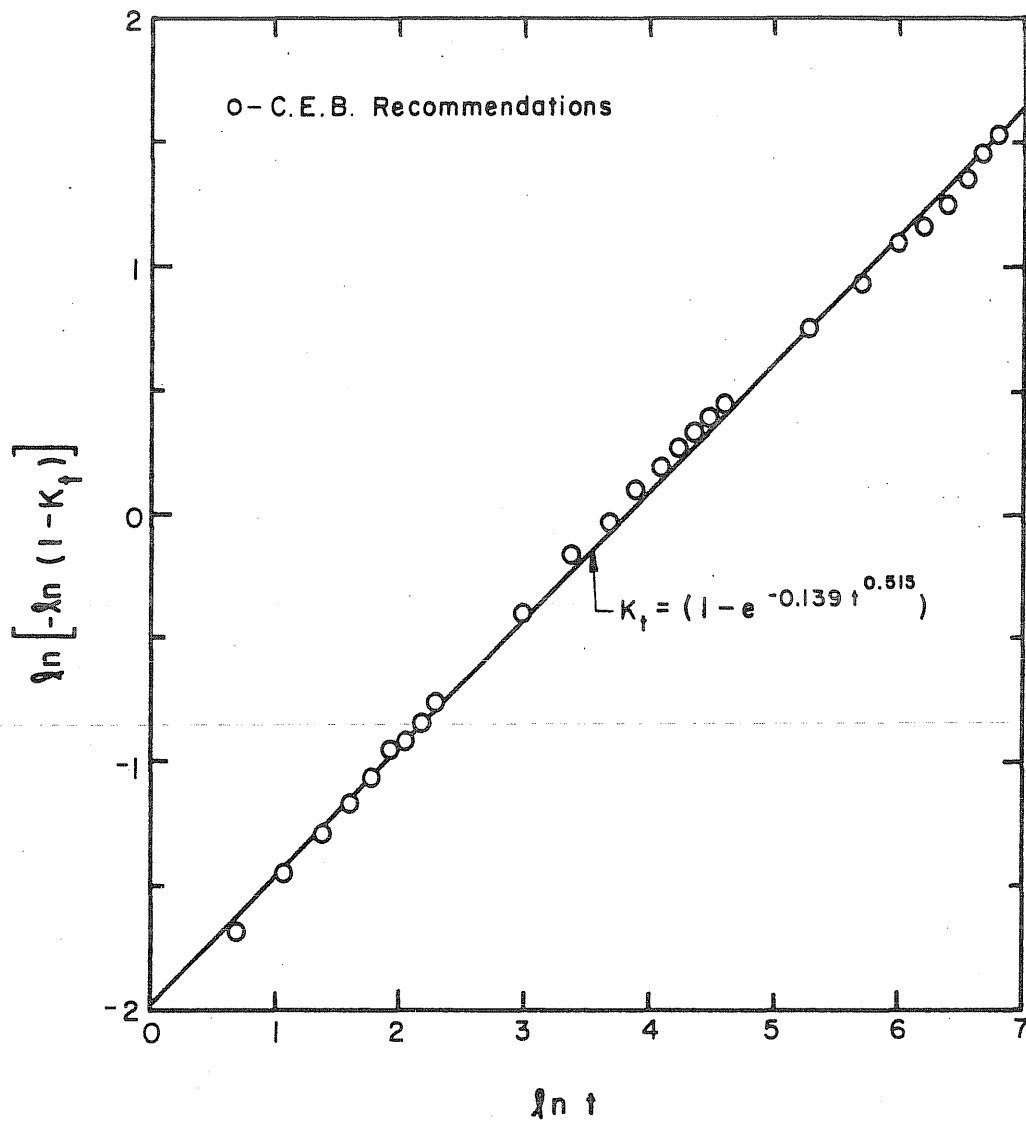


Fig. A.1 Fitted Expression for C.E.B. Creep Factor K_t ,
Theoretical Thickness = 5 cm

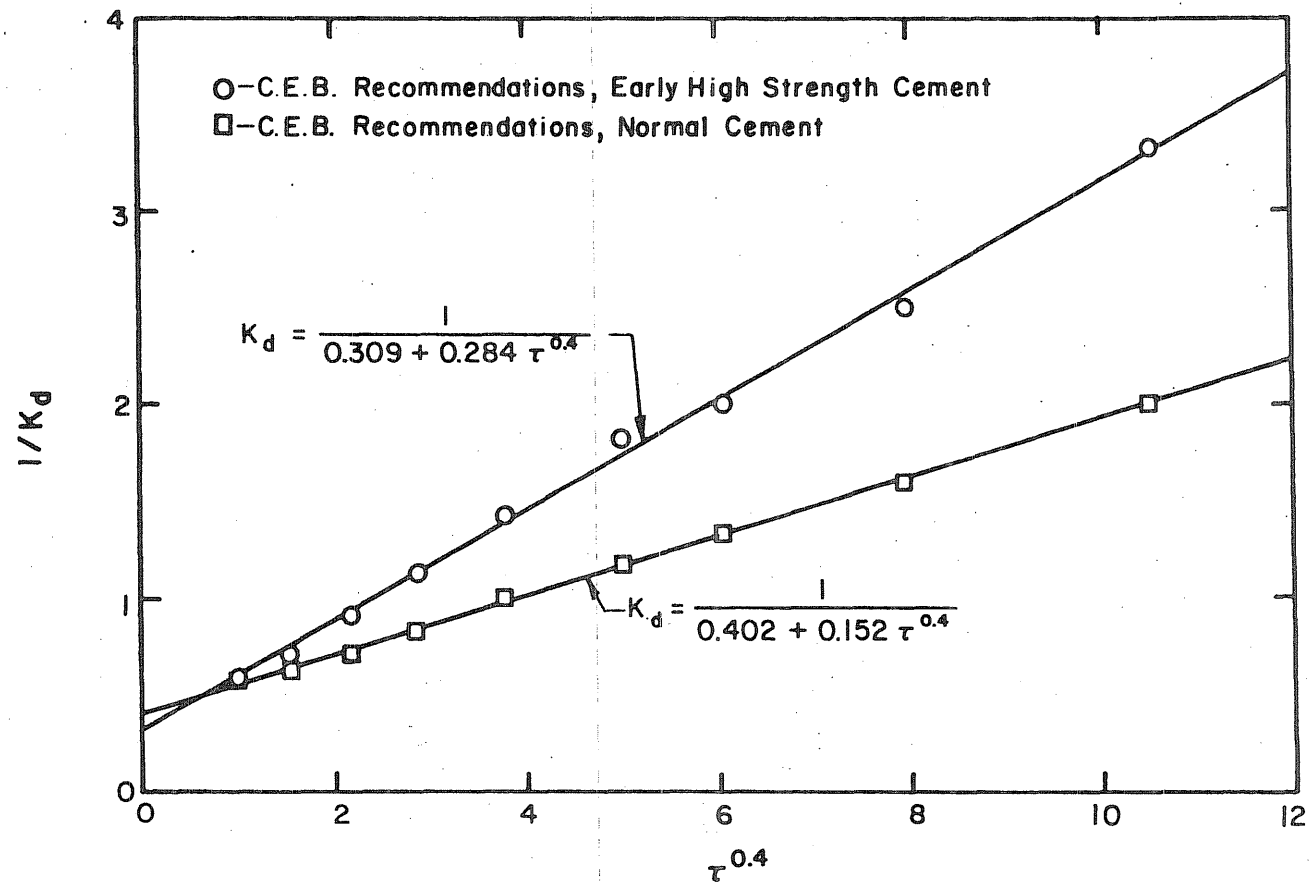
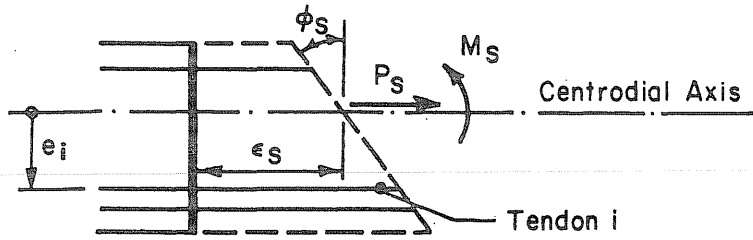
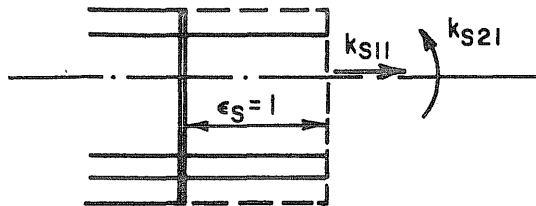


Fig. A.2 Fitted Expressions for C.E.B. Creep Factor K_d



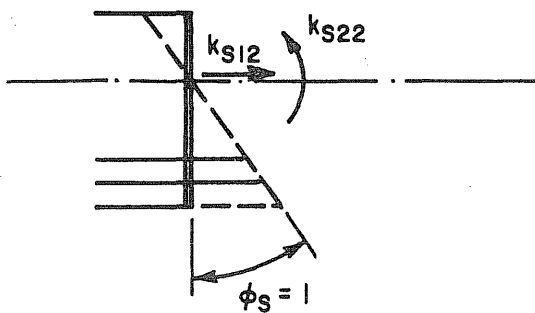
(a) Degrees of Freedom and Associated Forces



$$k_{S11} = E_S \Sigma A_i$$

$$k_{S21} = E_S \Sigma A_i e_i$$

(b) First Column of Stiffness Matrix ($\epsilon_S = 1$ and $\phi_S = 0$)

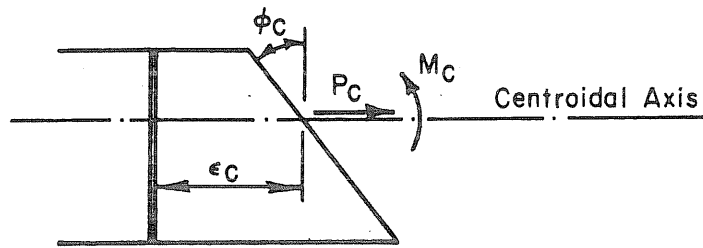


$$k_{S12} = E_S \Sigma A_i e_i$$

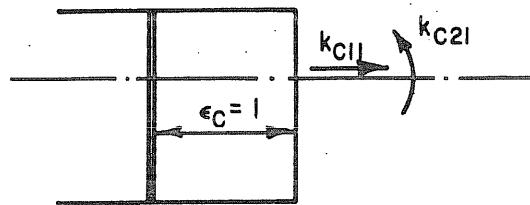
$$k_{S22} = E_S \Sigma A_i e_i^2$$

(c) Second Column of Stiffness Matrix ($\epsilon_S = 0$ and $\phi_S = 1$)

Fig. A.3 Derivation of the Stiffness Matrix Corresponding to the Prestressing Steel Reinforcement at a Section



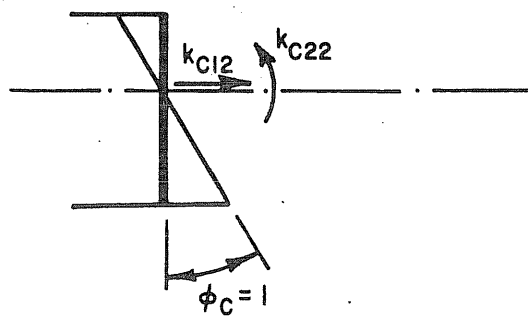
(a) Degrees of Freedom and Associated Forces



$$k_{C11} = E_C A_C$$

$$k_{C21} = 0$$

(b) First Column of Stiffness Matrix ($\epsilon_C = 1$ and $\phi_C = 0$)



$$k_{C12} = 0$$

$$k_{C22} = E_C I_C$$

(c) Second Column of Stiffness Matrix ($\epsilon_C = 0$ and $\phi_C = 1$)

Fig. A.4 Derivation of the Stiffness Matrix Corresponding to the Concrete Section

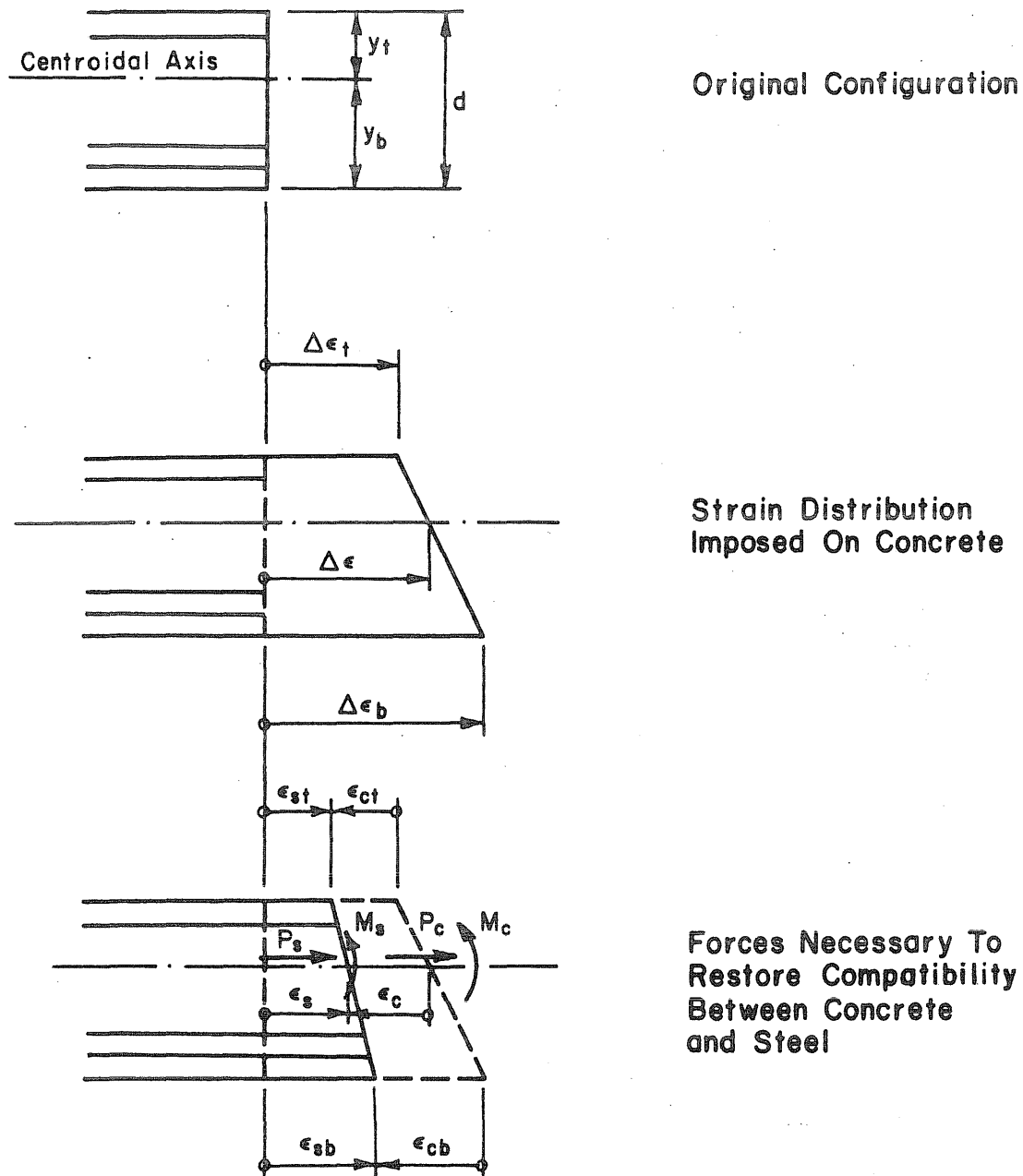


Fig. A.5 Calculation of Elastic Recovery Resulting from a Linear Strain Distribution Applied to the Concrete at a Section

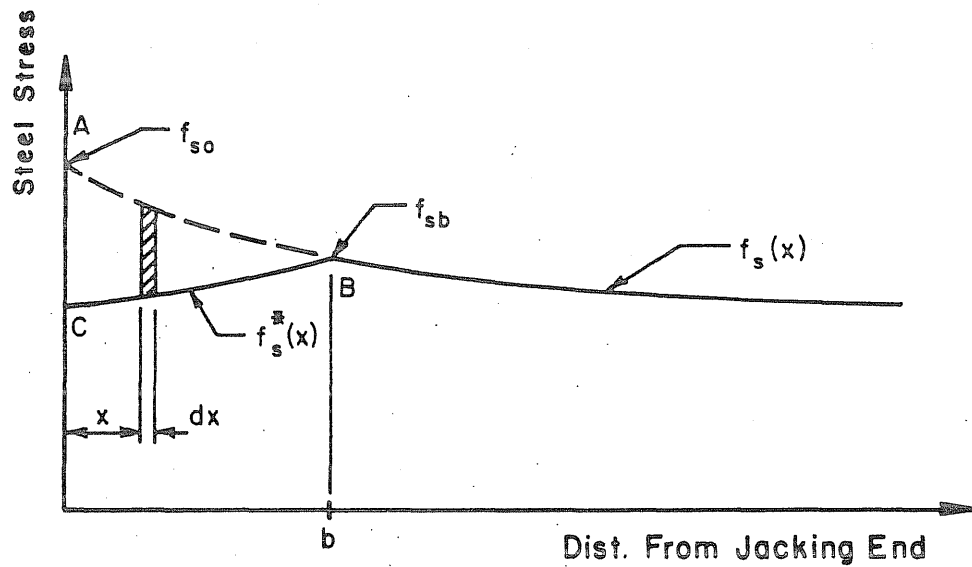


Fig. A.6 Variation of Initial Steel Stress Along Tendon when Slip Length is Less than Tendon Length

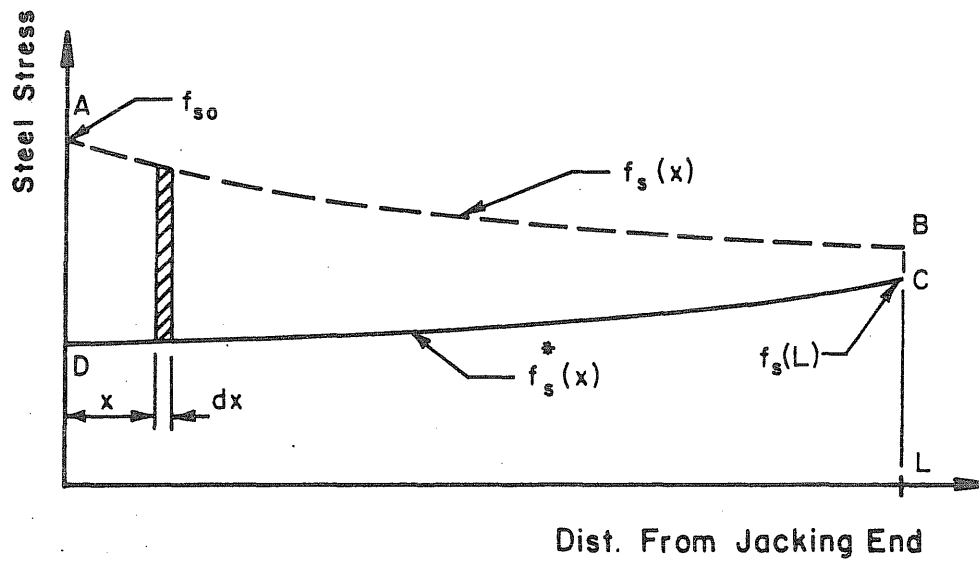
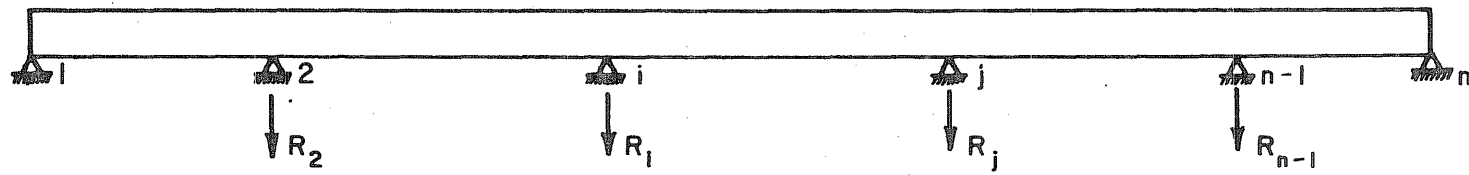
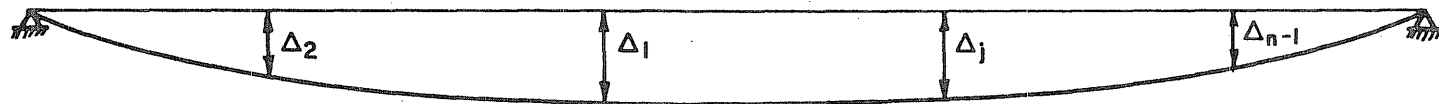


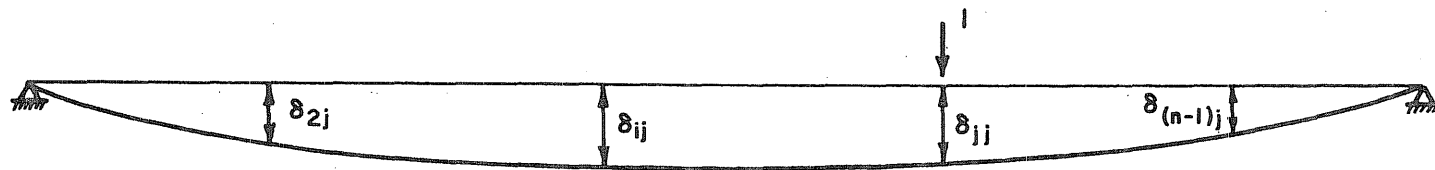
Fig. A.7 Variation of Initial Steel Stress Along Tendon when Slip Length is Equal to Tendon Length



(a) Original Structure



(b) Equivalent Statically Determinate Structure



(c) Structure and Loading System For Generating
The i -th Column Of The Flexibility Matrix

Fig. A.8 Derivation of Flexibility Matrix for Statically Indeterminate Intermediate Structures

APPENDIX B

THE KISHWAUKEE RIVER BRIDGE AND EXPERIMENTALLY DETERMINED CONCRETE MATERIAL PROPERTIES

The Kishwaukee River Bridge is located in Winnebago County, about four miles south of Rockford, Illinois. The structure spans over the heavily wooded Kishwaukee River Valley and, consequently, one of the primary considerations for selecting a particular construction procedure was the preservation of the environment. In order to achieve this aim the segmental cantilever construction procedure was a natural choice because this method eliminates the use of heavy construction false-work and temporary supports.

The contents of this Appendix are devoted to a description of the structure itself as well as a presentation of the experimentally determined material properties of the concrete used in the bridge. These material properties were determined by tests conducted at the laboratories of the Portland Cement Association (P.C.A.). All the information presented in this Appendix was supplied by either the P.C.A. or the Illinois Department of Transportation (30,52).

It is important to note that the origin of the time scale which is used to define the points in time at which each construction activity took place has arbitrarily been chosen as the day prior to which the first segment was cast. Thus, the day on which the first segment was cast is designated as day one.

B.1 The Kishwaukee River Bridge

B.1.1 General Description

The Kishwaukee River Bridge comprises two identical parallel bridges, each bridge having three 250 ft (76.2 m) interior spans and two 170 ft (51.8 m) side spans for an overall length of 1090 ft (332.2 m). The final structure is continuous over all five spans. An elevation of the structure as well as the designation assigned to each segment is shown in Figure B.1a. Each double cantilever is made up of 34 precast segments, while the side-span ends each comprise 6 segments. Adjacent double cantilevers are joined to each other by means of a cast in-situ closure segment (see Figure B.1b).

Typically each segment has a constant depth of 11 ft 4 in (3.454 m), a top width of 41 ft (12.50 m), and a length of 7 ft (2.134 m). The overall dimensions of such a segment is given in Figure B.2. Note that, in a double cantilever, the bottom flange thickness varies continually from 8 in. to 18 in. (0.203 m to 0.457 m) over the first six segments on each side of the pier (see Figure B.1b). The section properties of each particular segment to be found in a double cantilever or side-span end are listed in Tables B.1 and B.2, respectively. The pier segments were each provided with a diaphragm, the effect of which was ignored in the analytical procedure. The instrumented segments are designated SB1-N1, SB1-N9 and SB1-N16.

B.1.2 Erection Sequence

The bridge was erected by the segmental cantilever construction procedure. Following this procedure, a double cantilever was progressively constructed by adding segments to each side of the pier. Once the erection of a particular double cantilever was completed, it was joined to an adjacent double cantilever by providing a cast in-situ closure segment. Continuity between the two structures was finally established by stressing the so-called continuity prestressing tendons.

In order to restrict to a minimum the unbalanced moment that will

occur at the pier during the construction of a double cantilever, segments were added alternately to cantilevers on opposite sides of the pier. Vertical prestressing and suitably placed flat jacks were provided at the pier to resist the unbalanced moment. Once the double cantilever was joined to the rest of the structure and the continuity tendons stressed, the moment resisting part of the support was destroyed by releasing the vertical prestressing tendons at the pier and placing the double cantilever on the bearings. From that time onward, the support functions as a simple support. This operation is termed release of the support.

Segments were erected by making use of a steel launching girder. After the segment to be erected was in position, epoxy was applied to mating surfaces and the segment subsequently post-tensioned to the cantilever. During this erection procedure metal shims were used to correct alignments as needed. This operation is of importance when interpreting the measured vertical deflection of the bridge. In order to insure that adjacent segments match properly, the segments were precast using the short-line method of match-casting.

The casting and erection times of each segment are given in Tables B.3 and B.4, respectively. Each of the precast segments was assumed to have been cured for 2 days, while the in-situ closure segments were cured for 7 days. It should be noted that for the purposes of analysis the actual erection sequence was used for the instrumented double cantilever, SB1. In order to save some computational time, the erection sequences used for the purposes of the analysis of the other double cantilevers were somewhat modified by erecting more segments at fewer time steps than was the case for the actual structure. This step is justified by the relatively great age at which these segments were erected. It should also be mentioned that the modifications to the actual erection sequence were minimal. The actual casting sequence of all the segments was used by the analysis.

The sequence in which the double cantilevers and side-span ends were joined to each other is given in Figure B.3. This figure also gives the

times at which each of the in-situ closure segments was cast as well as the times at which the different sets of continuity tendons were stressed to their final value. It should be mentioned that prior to being stressed to this final value, the continuity tendons were stressed to 40 percent of the final value one day after the closure segment was cast.

For the purposes of the analysis it was assumed that the interior supports were released at the times at which the continuity tendons were stressed. In the actual structure this operation usually took place two days after these tendons were stressed. It was, however, felt that the discrepancy introduced into the calculation of creep strain would be negligible due to the relatively great age of most of the segments by the time this operation was performed. For this very reason it was assumed that the continuity tendons were directly stressed to their final value at the times given in Figure B.3.

It should be noted that both side-span ends were erected on falsework.

B.1.3 Prestressing Details

During the construction of each double cantilever, tendons were provided primarily to resist the negative moments induced by the self-weight of the structure. These tendons were located in the top flange of the beam. Two tendons were provided in the bottom flange to facilitate the erection of segments. The tendons that established continuity of two adjacent cantilevers were primarily located in the bottom flange of the beam in order to provide some measure of positive moment resistance. The locations of the tendons in the top and bottom flanges are indicated by Figure B.2.

All prestressing tendons used in the Kishwaukee River Bridge were $1\frac{1}{4}$ in. (31.8 mm) diameter Dywidag-Threadbar. Each of these tendons were stressed to 145 kips (645 kN) and anchored at 136 kips (605 kN). All

tendon profiles were straight. The variation of the number of tendons along the bridge is summarized in Figure B.4.

For the construction of a double cantilever the times at which the tendons were stressed were dictated by the erection sequence of the segments. The stressing times of the continuity tendons are summarized in Figure B.3.

For the purposes of analysis a wobble coefficient of 0.0007/ft (0.0023/m) and an anchor-set of 0.01 in. (0.25 mm) was assumed.

B.2 Material Properties of the Concrete

At the time that each of the instrumented segments were cast, thirty-five 6 x 12 in. (150 x 300 mm) concrete cylinders, per segment, were prepared in the precasting plant. These cylinders were steam cured for several hours and then shipped to the P.C.A. laboratories in Skokie, Illinois, for testing. Some of the cylinders were cured in the laboratories under constant environmental conditions at 73°F (23°C) and 50 percent relative humidity, while others were subjected to the outdoor environment. It was felt that the exposed specimens would be subjected to about the same environmental conditions as the bridge itself. In what follows, a brief description of the concrete material properties as determined by tests on these specimens is given. A more extensive report will be published in the near future.

The variation of the concrete compressive strength and the modulus of elasticity was determined by conducting tests which conform to the ASTM Specification C-39 (56). These properties of the concrete at different ages are summarized in Table B.5.

Shrinkage measurements on both the indoor and outdoor specimens were started 7 days after casting. There were three sets of laboratory stored creep specimens, each set being loaded at a different age. The ages at loading were 28, 90 and 180 days. All the outdoor creep specimens were loaded at an age of 28 days. All creep tests were conducted in

compliance with the ASTM Specification C-512 (55), each specimen being subjected to a constant stress of 2000 psi (13.8 N/mm^2). The experimentally obtained specific creep curves for the different ages at loading as well as the shrinkage curves for all three of the instrumented segments are given in Figures B.5 through B.8 for the laboratory stored specimens, and in Figures B.9 and B.10 for the outdoor specimens.

For the purposes of the analytical procedure followed in this study, the material properties were assumed to be the same for each segment. Thus, the values of compressive strength and modulus of elasticity used in the analysis were obtained by taking the average of the appropriate quantities at each age. The specific creep and shrinkage curves used by the analysis procedure were not obtained by averaging appropriate curves, but rather by selecting curves corresponding to particular segments. The specific creep curves as well as the shrinkage curves used in the analysis are listed in Table B.6.

For the particular case where the recommendations of the C.E.B. (11) were used to generate the material properties of the concrete, the average 28-day compressive strengths for the outdoor specimens were used in the analysis. The creep and shrinkage multiplying factor reflecting the dependence of these phenomena on the composition of the concrete, K_b , deserves some special attention here (see Sect. 2.2.3.1). During the course of the casting of the prefabricated segments the mix proportions of the concrete were changed several times. The water-cement ratio and the cement content used in three different mixes are listed in Table B.7. Each of these combinations yielded a different value for K_b . These values of K_b were then averaged and the result used in the analysis.

Table B.1: Section Properties of Segments in the Double Cantilevers

Segment	Length	Cross- Sectional Area	Moment of Inertia	Distance of Top Fiber to Centroidal Axis	Distance of Bottom Fiber to Centroidal Axis	Weight
	(in.)	(in. ²)	(in. ⁴)	(in.)	(in.)	(k/ft)
S0 and N0	42.000	13,692	42,115,000	62.762	76.988	14.263
S1 and N1	84.625	13,465	41,297,000	61.758	77.992	14.026
S2 and N2	84.625	13,022	39,537,000	59.650	80.100	13.565
S3 and N3	84.625	12,595	37,607,000	57.408	82.342	13.120
S4 and N4	84.625	12,183	35,502,000	55.031	84.719	12.691
S5 and N5	84.625	11,787	33,216,000	52.521	87.229	12.278
S6 through S16 N6 through N16	84.625	11,595	32,005,000	51.216	88.534	12.078
S17 and N17	28.625	11,595	32,005,000	51.216	88.534	12.078
Closure Segment	150.750	14,845	45,510,000	67.150	72.600	15.464

Note: 1 in. = 25.4 mm

1 k/ft = 14.594 kN/m

Table B.2: Section Properties of Segments in the Side-Span Ends

Segment	Length (in.)	Cross- Sectional Area (in. ²)	Moment of Inertia (in. ⁴)	Distance of Top Fiber to Centroidal Axis (in.)	Distance of Bottom Fiber to Centroidal Axis (in.)	Weight (k/ft)
S0 and N0	36.000	11,595	32,005,000	51.216	88.534	12.078
S1 through S4 N1 through N4	90.000	11,595	32,005,000	51.216	88.534	12.078
S5 and N5	51.313	11,595	32,005,000	51.216	88.534	12.078

Note: 1 in. = 25.4 mm

1 k/ft = 14.594 kN/m

Table B.3: Casting Times of the Segments
Days after 6 August 1977

Segment	Double Cantilever				Side-Span Ends SB0 and SB5
	SB1	SB2	SB3	SB4	
S17	446	298	244	189	-
S16	445	294	243	187	-
S15	444	293	242	185	-
S14	441	292	241	181	-
S13	440	290	238	179	-
S12	439	290	237	173	-
S11	438	287	236	164	-
S10	437	287	235	161	-
S9	434	285	230	154	-
S8	433	284	229	152	-
S7	432	283	228	147	-
S6	432	280	227	138	-
S5	370	279	224	133	70
S4	369	278	223	130	67
S3	368	277	222	122	62
S2	367	276	221	119	60
S1	364	272	220	116	55
S0	322	7	19	22	42
N0	311	1	11	14	319
N1	339	248	193	76	322
N2	341	249	195	82	326
N3	342	250	196	85	327
N4	343	251	199	88	328
N5	346	252	201	90	322
N6	347	255	202	91	-
N7	348	256	203	94	-
N8	349	256	206	95	-
N9	350	258	207	96	-
N10	353	259	208	97	-
N11	355	262	209	98	-
N12	355	263	210	101	-
N13	356	264	213	102	-
N14	357	265	214	103	-
N15	360	266	215	104	-
N16	361	269	216	105	-
N17	362	270	217	110	-

Note: Day 1 corresponds to the day on which the first segment was cast.

Table B.4: Erection Times of the Segments
Days after 6 August 1977

Segment	Double Cantilevers				Side-Span Ends SB0 and SB5
	SB1	SB2	SB3	SB4	
S17	458	437	412	362	-
S16	458	437	412	361	-
S15	455	437	411	361	-
S14	455	435	411	360	-
S13	455	434	411	360	-
S12	454	434	410	357	-
S11	454	434	410	357	-
S10	454	433	409	356	-
S9	453	433	409	356	-
S8	453	432	406	355	-
S7	453	432	406	354	-
S6	453	432	406	354	-
S5	452	431	402	353	94
S4	452	431	402	353	91
S3	452	431	399	349	91
S2	451	430	398	348	91
S1	449	428	397	347	90
S0	448	427	392	340	63
N0	448	427	396	341	468
N1	449	428	397	346	615
N2	451	430	398	348	615
N3	451	430	399	349	615
N4	452	431	399	350	615
N5	452	431	402	353	615
N6	452	432	402	353	-
N7	453	432	406	354	-
N8	453	432	406	354	-
N9	453	432	409	355	-
N10	454	433	409	356	-
N11	454	433	410	356	-
N12	454	434	410	357	-
N13	454	434	410	360	-
N14	455	434	411	360	-
N15	455	435	411	361	-
N16	458	437	412	361	-
N17	458	437	412	362	-

Note: Day 1 corresponds to the day on which the first segment was cast.

Table B.5: Compressive Strength and Modulus of Elasticity of Concrete

Segment	Curing Environment	Age (Days)	Compressive Strength (psi)	Modulus of Elasticity (ksi)
SB1-N1	Controlled	28	5680	4320
		180	6240	4490
	Outdoor	28	5750	4200
		180	6460	4530
SB1-N9	Controlled	28	6190	4470
		90	6070	4630
		180	6450	4760
	Outdoor	28	6080	4620
		90	6510	4720
		180	6450	4580
SB1-N16	Controlled	28	5740	4420
		90	6130	4750
		180	6290	4410
	Outdoor	28	4670	4190
		180	6200	4240

Note: 1 ksi = 6.895 N/mm²

1 ksi = 1000 psi

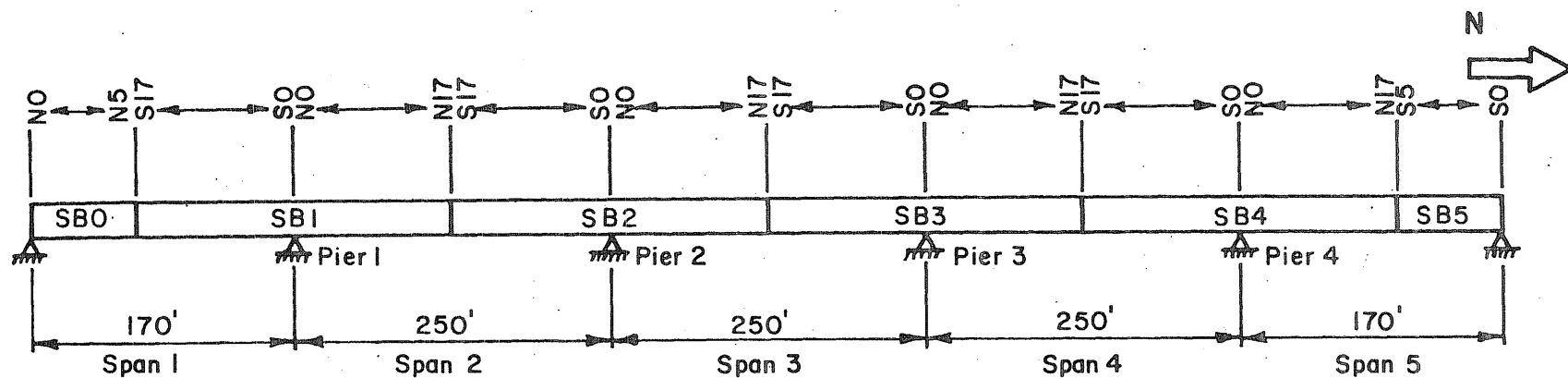
Table B.6: Specific Creep and Shrinkage Curves
Used in the Analyses

Curing Environment	Specific Creep Age at Loading (Days)			Shrinkage
	28	90	180	
Controlled	SB1-N1	SB1-N9	SB1-N1	SB1-N1
Outdoor	SB1-N1	-	-	SB1-N1

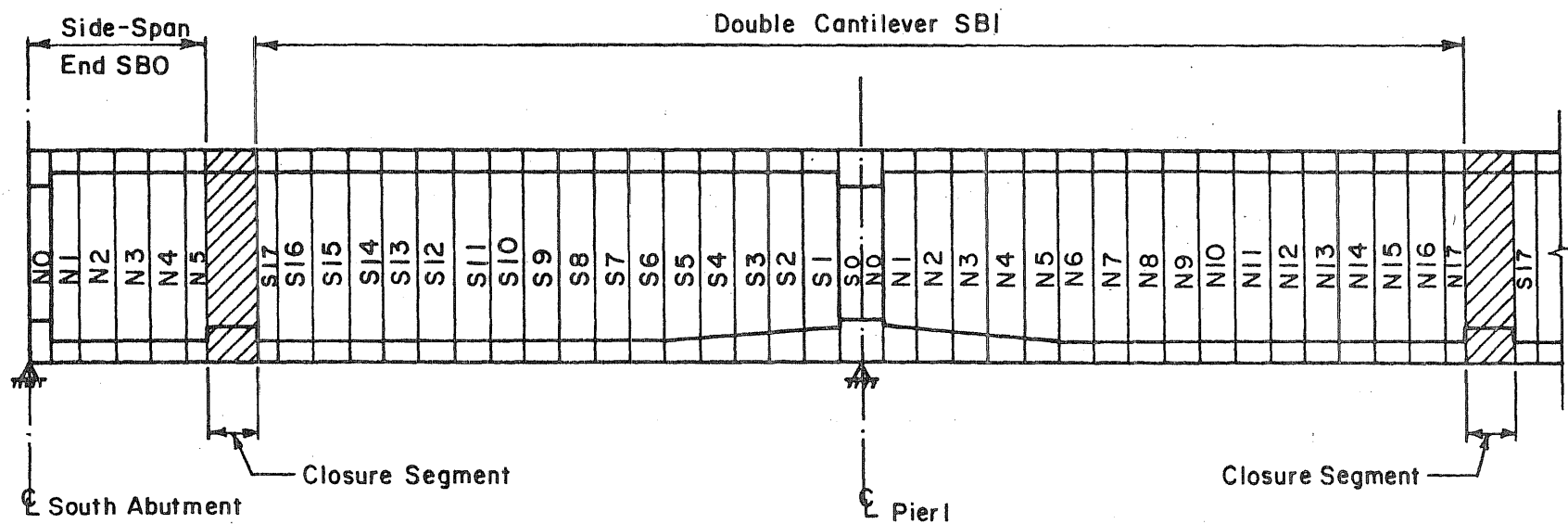
Table B.7: Cement Content and Water-Cement Ratios
for Different Concrete Mixes

Cement Content (lbs/yd ³)	Water-Cement Ratio
658	0.46
658	0.44
705	0.44

Note: 1 lb/yd³ = 0.593 kg/m³



(a) Elevation



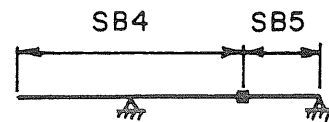
(b) Longitudinal Section

1 ft = 304.8 mm

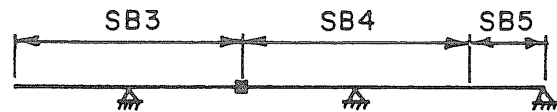
Fig. B.1 Elevation and Designation of the Various Segments of the Kishwaukee River Bridge



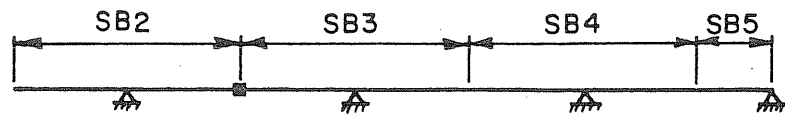
Fig. B.2 Cross-Section of a Typical Segment



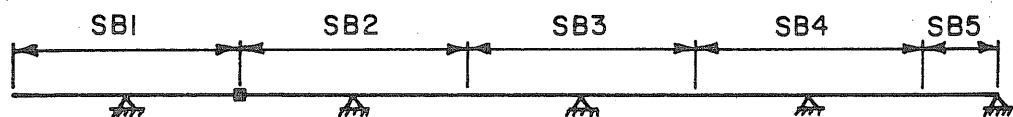
(a) Intermediate Structure 6



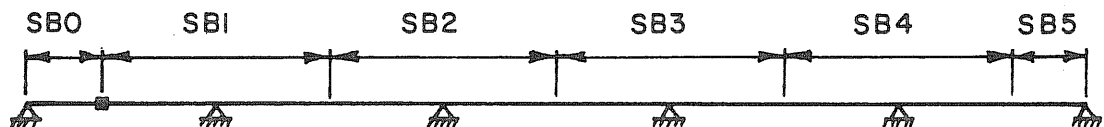
(b) Intermediate Structure 7



(c) Intermediate Structure 8



(d) Intermediate Structure 9



(e) Final Structure

Substructure	Time At Which Closure Segment Is Cast	Time At Which Continuity Tendons Are Stressed
6	382	387
7	419	424
8	441	446
9	462	467
10	629	634

Note : Times Are In Days Since 6 Aug. 1977

Fig. B.3 Sequence in which Double Cantilevers were Joined to Form Final Structure

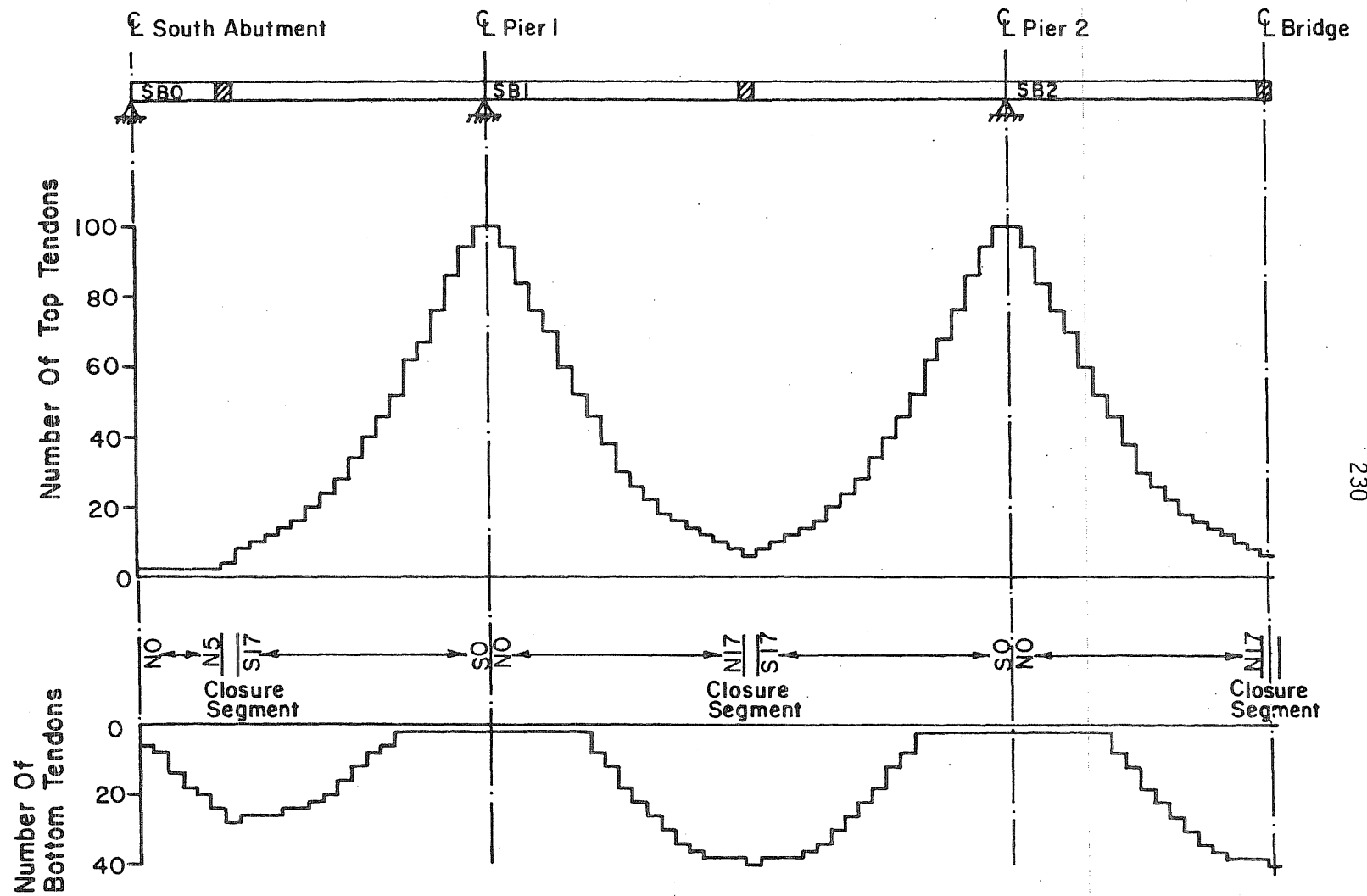


Fig. B.4 Distribution of Prestressing Tendons along the Bridge

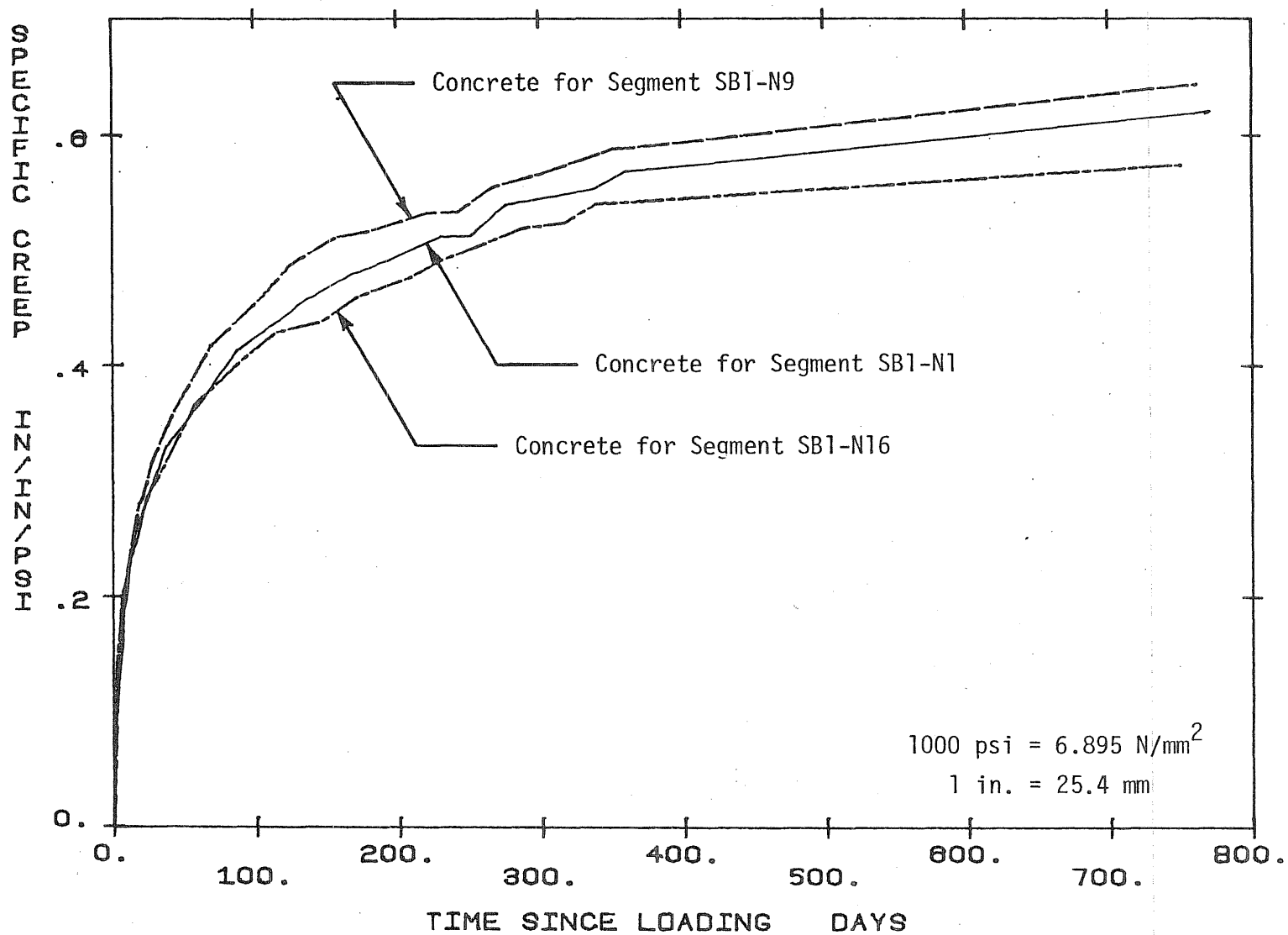


Fig. B.5 Specific Creep Curves for Laboratory Stored Specimens Loaded at an Age of 28 Days

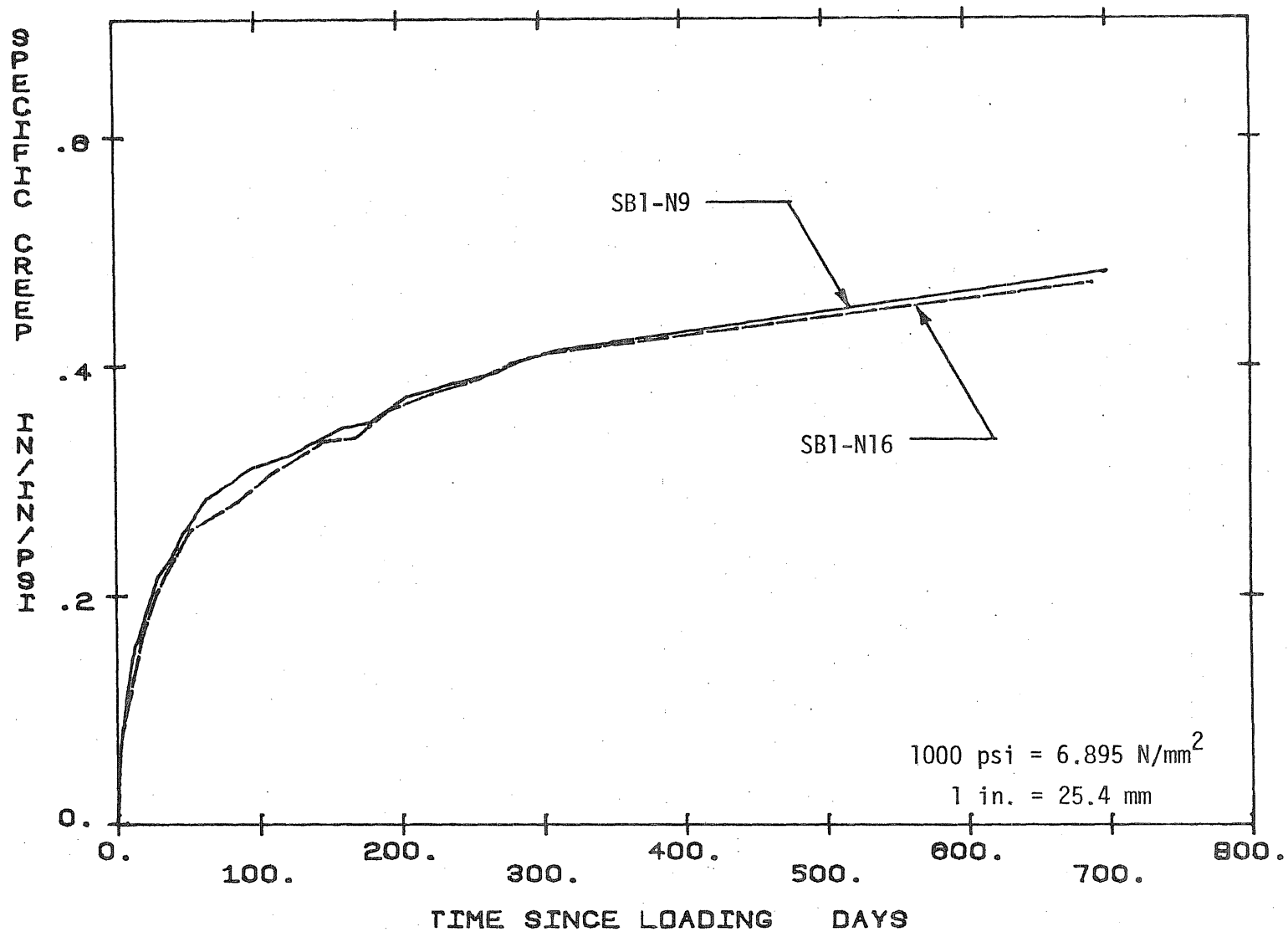


Fig. B.6 Specific Creep Curves for Laboratory Stored Specimens Loaded at an Age of 90 Days

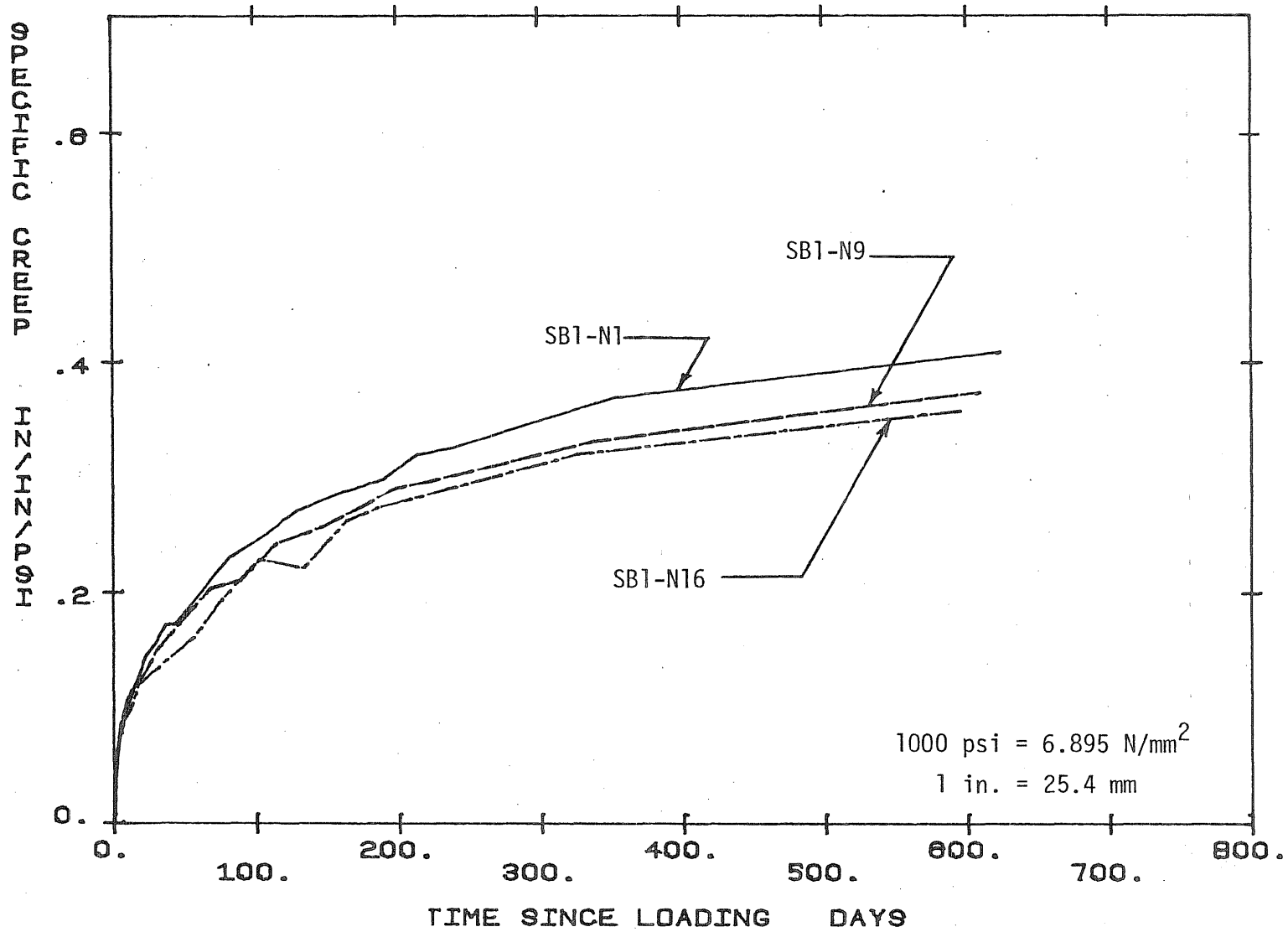


Fig. B.7 Specific Creep Curves for Laboratory Stored Specimens Loaded at an Age of 180 Days

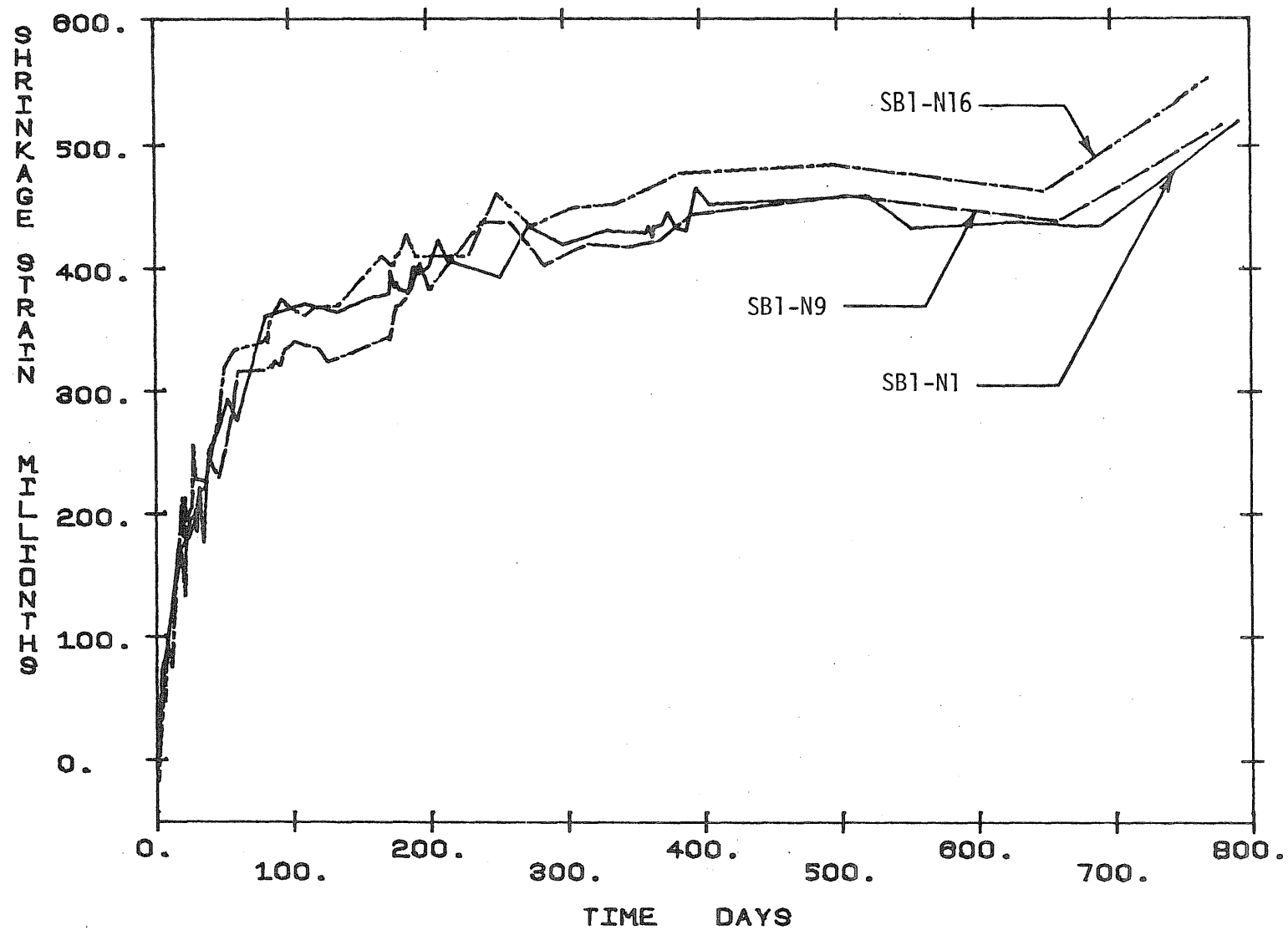


Fig. B.8 Shrinkage Curves for Laboratory Stored Specimens

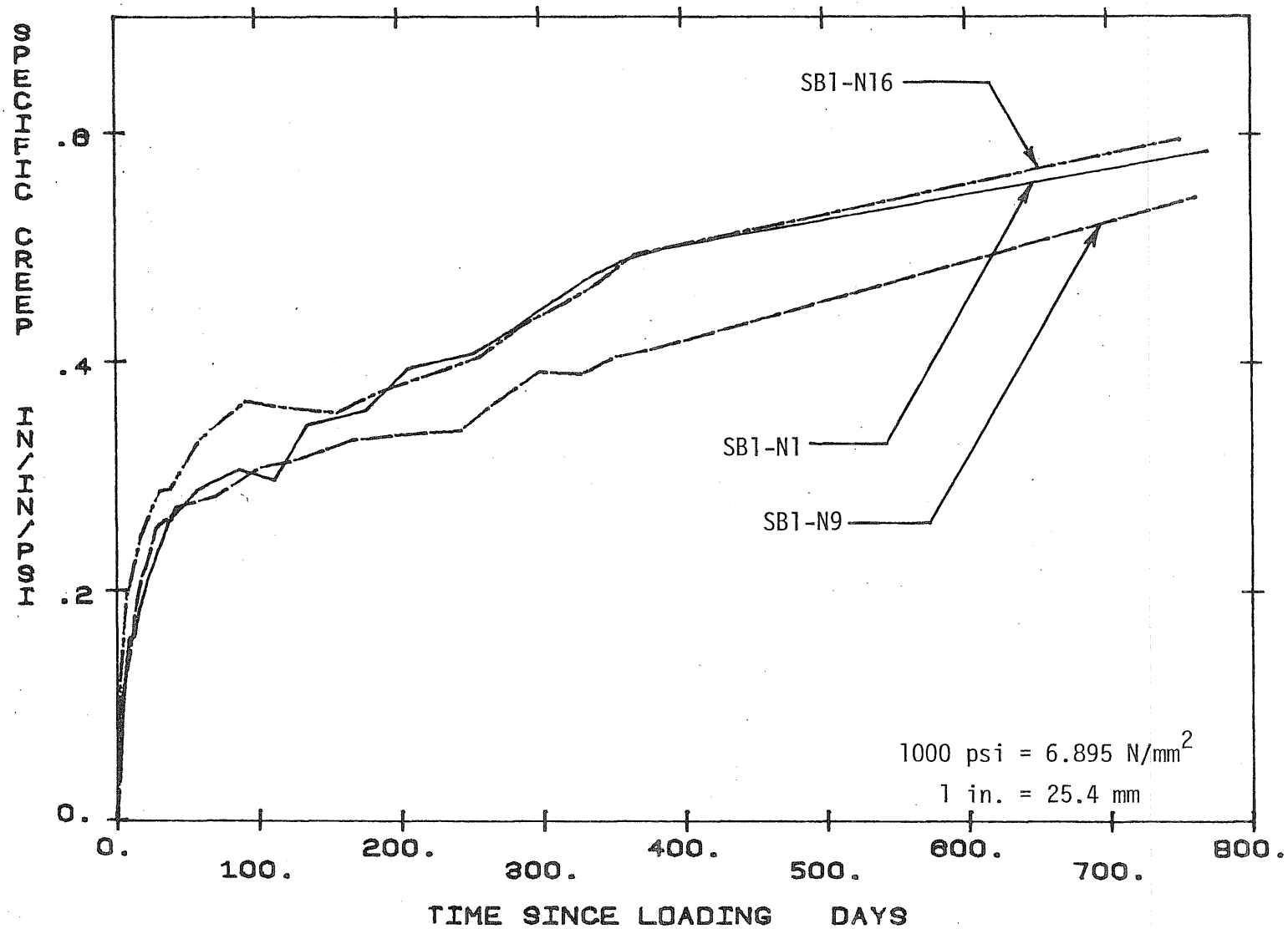


Fig. B.9 Specific Creep Curves for Outdoor Stored Specimens Loaded at an Age of 28 Days

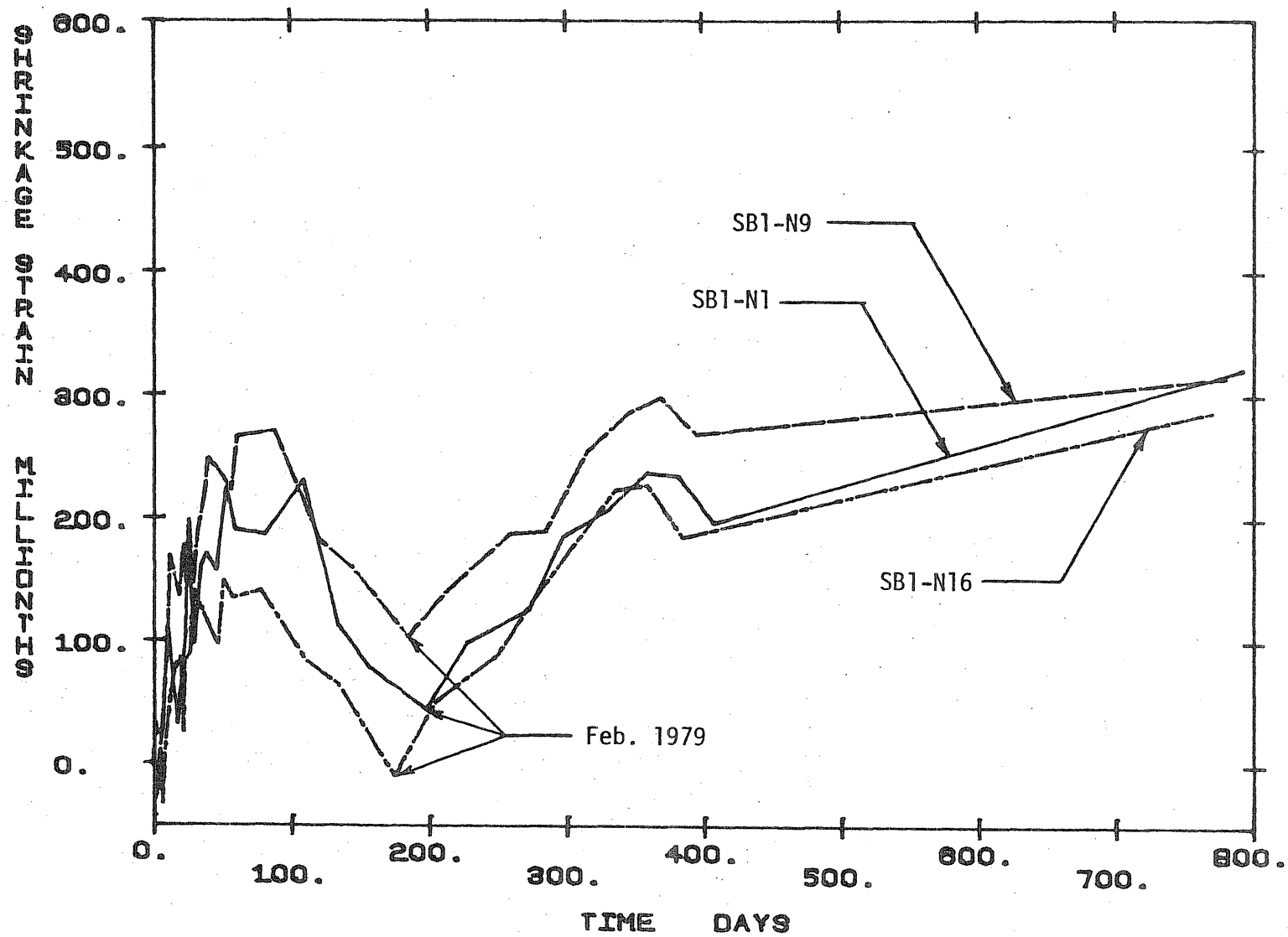


Fig. B.10 Shrinkage Curves for Outdoor Stored Specimens

APPENDIX C

NOTATION

The symbols used throughout this study are defined as they first appear. For convenience they are summarized in what follows:

$a_i(\tau)$	=	aging parameters, for use with the Dirichlet series representation of specific creep
A	=	coefficient used in the expression for K_d , as given in Appendix A, Sect. A.1.1
A_c	=	cross-sectional area of the concrete section
A_i	=	cross-sectional area of tendon i
b	=	distance over which anchor-set affects the prestressing force, measured from the jacking end
B	=	coefficient used in the expression for K_d , as given in Appendix A, Sect. A.1.1
c	=	relaxation constant, depending on the type of prestressing strand
$C_i(t)$	=	specific creep at time t , for concrete loaded at age t_i
$C_r(t_i)$	=	specific creep at time t_i , for concrete initially loaded at age τ_r
$C_\tau(t)$	=	specific creep at time t , for concrete initially loaded at age τ
d_m	=	theoretical thickness of member, as defined by the C.E.B. recommendations
D	=	degree of hardening of the concrete at the time of loading

e_i	=	eccentricity of tendon i measured from the centroidal axis of the section, taken positive when the tendon is below the centroidal axis, and negative when above
E_{b28}	=	secant modulus of elasticity of the concrete at an age of 28 days
$E_c, E_c(t)$	=	modulus of elasticity of the concrete at time t
$E'_c(t)$	=	effective modulus of the concrete at time t , as defined in Sect. 3.2.1
E_s	=	modulus of elasticity of the steel
f_c	=	constant sustained concrete stress
$f_c(t)$	=	concrete stress as a function of time
$f_i, f(t_i)$	=	concrete stress at time t_i
$f_{c_{top}}$	=	concrete stress in extreme top fiber of cross-section
$f_{c_{bot}}$	=	concrete stress in extreme bottom fiber of cross-section
$f'_c(t)$	=	cylinder compressive strength of concrete as a function of time since casting
$f_s(t)$	=	steel stress at time t
f_{si}	=	initial steel stress
f_{so}	=	steel stress at the jacking end, just prior to anchoring of the tendon
$f_s(x)$	=	steel stress at a distance x from the jacking end, just prior to anchoring of the tendon
f_y	=	yield stress of steel, measured at an offset strain of 0.001
$[F]$	=	flexibility matrix, as defined in Appendix A, Sect. A.5
I_c	=	moment of inertia of the concrete section about the centroidal axis
k	=	wobble friction coefficient, per unit length

- K_b = factor expressing the dependence of creep and shrinkage on the composition of the concrete mix, defined in Sect. 2.2.3.1
- K_c = factor expressing the dependence of creep on relative humidity, defined in Sect. 2.2.3.1
- K_d = factor expressing the dependence of creep on the concrete age at the time of loading, defined in Sect. 2.2.3.1
- K_e = factor expressing the dependence of creep and shrinkage on the member size and shape, defined in Sect. 2.2.3.1 and Sect. 2.2.3.2
- K_p = factor including the restraining effect of the longitudinal reinforcement on shrinkage, defined in Sect. 2.2.3.2
- K_t = factor expressing the time dependence of creep and shrinkage, defined in Sect. 2.2.3.1
- $[K_c]$ = stiffness matrix for the concrete cross-section, associated with the axial strain and curvature of the section
- $[K_s]$ = stiffness matrix for the prestressing steel, associated with the axial strain and curvature of the section
- \ln = natural or Napierian logarithm
- \log = logarithm to the base 10
- L = tendon length
- M_c = resultant moment of the concrete force about the section centroid necessary to restore compatibility of steel and concrete strains when a strain is imposed on the cross-section
- M_s = resultant moment of the steel forces about the section centroid necessary to restore compatibility of steel and concrete strains when a strain is imposed on the cross-section

n	=	E_s/E_c , modular ratio; also used as a coefficient in the expression for K_d , as given in Appendix A, Sect. A.1.1
p	=	percentage longitudinal steel
P_c	=	resultant concrete force necessary to restore compatibility of steel and concrete strains when a strain is imposed on the cross-section
P_s	=	resultant steel force necessary to restore compatibility of steel and concrete strains when a strain is imposed on the cross-section
P_{si}	=	change in force in the i -th tendon due to the effects of elastic recovery
R	=	ratio of specific creep recovery to specific creep
R_i	=	vertical reaction at support i of an intermediate structure
$\{R\}$	=	column vector containing the reactions at the interior supports of a statically indeterminate intermediate structure
t, t_i	=	time
T	=	temperature
x	=	distance from the jacking end to the point on the tendon being considered
y_b	=	distance of the section centroid to the extreme bottom fiber of the section
y_t	=	distance of the section centroid to the extreme top fiber of the section
α	=	coefficient used in the expression for K_t , as given in Appendix A, Sect. A.1.1; elsewhere it represents the total angular change of the tendon profile between the jacking end and any point x along the span, in radians
β	=	coefficient used in the expression for K_t , as given in Appendix A, Sect. A.1.1

δ_{ij}	=	deflection of the equivalent statically determinate structure, as defined in Appendix A, Sect. A.5, at the location of support i due to a unit point load applied at the location of support j
Δ	=	anchor set
Δ_i	=	deflection of the equivalent statically determinate structure, as defined in Appendix A, Sect. A.5, at the location of support i due to the effects of applied loads or time-dependent effects
Δ_t	=	number of days at which hardening of the concrete took place at T°C
$\{\Delta\}$	=	column vector containing the Δ_i 's which apply to the interior supports of a statically indeterminate intermediate structure
$\Delta f_{ci}, \Delta f(t_i)$	=	change in concrete stress at time t_i
Δf_s	=	change in steel stress due to causes other than relaxation
$\Delta \epsilon$	=	imposed axial strain on concrete cross-section, defined in Appendix A, Sect. A.2
$\Delta \epsilon_b$	=	imposed strain in extreme bottom fiber of concrete cross-section, defined in Appendix A, Sect. A.2
$\Delta \epsilon_{cr}(\Delta t_m)$	=	change of creep strain during the m-th time interval
$\Delta \epsilon_t$	=	imposed strain in extreme top fiber of concrete cross-section, defined in Appendix A, Sect. A.2
$\Delta \phi$	=	imposed curvature of concrete cross-section, defined in Appendix A, Sect. A.2
ϵ	=	instantaneous elastic strain
ϵ_c	=	basic shrinkage strain as a function of relative humidity, defined in Sect. 2.2.3.2; also used as axial strain of the concrete section as defined in Appendix A, Sect. A.2
$\epsilon_{cb}, \epsilon_{ct}$	=	concrete strains involved in the calculation of the effects of elastic recovery, defined in Appendix A, Sect. A.2

$\epsilon_{cr}, \epsilon_{cr}(t)$	=	total creep strain at time t
ϵ_s	=	strain associated with the steel, at the centroid of the section, defined in Appendix A, Sect. A.2
$\epsilon_{sb}, \epsilon_{st}$	=	hypothetical steel strains involved in the calculation of the effects of elastic recovery, defined in Appendix A, Sect. A.2
ϵ_{sh}	=	shrinkage strain at time t
ϵ_{cb}^i	=	concrete strain in the extreme bottom fiber corrected for the effects of elastic recovery
ϵ_{ct}^i	=	concrete strain in the extreme top fiber corrected for the effects of elastic recovery
λ_i	=	retardation times, for use with the Dirichlet series representation of specific creep
μ	=	curvature friction coefficient
ξ	=	creep coefficient independent of time and concrete age at loading, defined in Appendix A, Sect. A.1.2
τ	=	concrete age at loading
τ_i	=	concrete age at loading corresponding to the i -th specific creep curve
$\phi(T)$	=	temperature shift function, for use with the Dirichlet series representation of specific creep
ϕ_c	=	curvature of concrete section as defined in Appendix A, Sect. A.2
ϕ_s	=	curvature associated with the steel strain as defined in Appendix A, Sect. A.2
ϕ_t	=	creep coefficient, expressed as the product of five partial factors